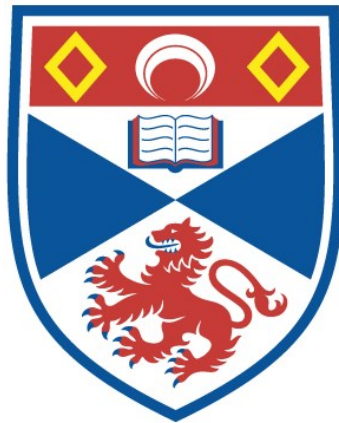


AN INVESTIGATION OF MOLECULAR OPACITIES FOR LATE-TYPE STARS

Christopher Martin Sharp

**A Thesis Submitted for the Degree of PhD
at the
University of St Andrews**



1981

**Full metadata for this item is available in St Andrews Research
Repository
at:**

<http://research-repository.st-andrews.ac.uk/>

Please use this identifier to cite or link to this item:

<http://hdl.handle.net/10023/11103>

This item is protected by original copyright

An Investigation of Molecular Opacities for Late-Type Stars

by

Christopher Martin Sharp

A thesis submitted for the Degree of Doctor of Philosophy at the
University of St. Andrews, October 1981.



Dedicated to my Mother and Father

CERTIFICATE

I certify that C.M.Sharp has spent nine terms in research in the Department of Astronomy, University of St.Andrews, that he has fulfilled the conditions of Ordinance General No. 12 and Senate Regulations under Resolution of the University Court, 1967, No. 1, and that he is qualified to submit the accompanying thesis in application for the degree of Ph.D.

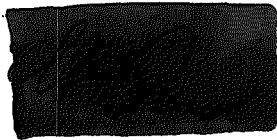


T.R.Carson

Supervisor

DECLARATION

Except where reference is made to the work of others, the research described in this thesis and the composition of the thesis are my own work. No part of this work has been previously submitted for another degree. I was admitted to the Faculty of Science of the University of St. Andrews as a research student, under Ordinance General No. 12, and accepted as a candidate for the degree of Ph.D., under Resolution of the University Court, 1967, No. 1, on 1st October 1974.

A rectangular area of the document has been completely blacked out, obscuring the signature of the author.

C.M. Sharp

ACKNOWLEDGEMENTS

I am sincerely grateful to my supervisor Dr.T.R.Carson for the help and guidance he has given me in the course of my research. I would sincerely like to thank Professor D.W.N.Stibbs, Director of the University Observatory, for his help and the facilities he has provided. Thanks are also due to the other members of the staff and the research students over the years, and to Mrs. Rhona McNeill for helping me with the diagrams.

I am most grateful to Professor P.A.Wayman, Director of Dunsink Observatory, Co.Dublin, for providing me with facilities during my period of research there, and the other members of the staff, in particular Miss Mary Callanan for helping me with references. Thanks are also due to the staff of the Physics Department of University College Dublin for useful discussions and providing me with library facilities.

I would also like to thank the staff of the Computing Laboratory of the University of St.Andrews for the facilities used for producing the results in this thesis, together with the thesis itself. Thanks are also due to the Central Data Processing Services of the Irish government, Kilmainham, Dublin, whose computing facilities were also used. Finally, I wish to thank my parents for proof reading this thesis.

This work has received support from the Science Research Council and the Dublin Institute for Advanced Studies.

ABSTRACT

This work investigates molecular opacities under conditions appropriate to the atmospheres of late-type stars. Given a specified initial abundance of the chemical elements, the equations of atomic ionization and molecular dissociation are solved by iteration for various temperatures and densities. With the abundances of the atomic and molecular species so determined at a particular temperature and density, the continuous absorption coefficient due to a number of processes is first computed, then the molecular band absorption coefficient is computed line-by-line superimposed for diatomic and triatomic molecules considered separately. The band calculations for the diatomic molecules include all possible isotopic variants, but computing resources did not permit this degree of detail for triatomic molecules, nor diatomic and triatomic molecules to be considered together. These calculations are performed for a number of different temperatures and densities.

The theory for calculating the spectral lines due to molecules is discussed in some detail, with various methods being investigated for computing opacities including the contributions from these spectral lines. With the computing resources available, the best method for the calculation of the opacity due to the molecular absorption is found to be that of opacity sampling, provided the frequency of sampling is adequate.

From the results presented in this thesis, a number of important conclusions can be drawn. At low temperatures and high densities, pressure-induced absorption due to molecular hydrogen is an important source of continuous opacity. Isotopic variants of at least diatomic molecules have to be considered in any calculations, as they can significantly affect the contribution that diatomic molecules make to the Rosseland mean opacities. Also at low temperatures, water is a major source of absorption. Finally, tables of some thermodynamic quantities for the molecular gas are given for a number of temperatures and densities.

CONTENTS

1	INTRODUCTION	
1.1	Introduction to Stellar Opacities	1
1.2	Summary of this Work	4
1.3	Brief Literature Survey	9
2	DETERMINATION OF EQUILIBRIUM ABUNDANCES	
2.1	Introduction	14
2.2	Determination of Atomic and Ionic Partition Functions and Equilibrium Constants	18
2.3	Iterative Process for Determining Equilibrium Abundances of Atoms and Ions	24
2.4	Introduction to Diatomic Molecules	31
2.5	Determination of Rotational Partition Functions of Diatomic Molecules	35
2.6	Determination of Vibrational Partition Functions of Diatomic Molecules	45
2.7	Determination of the Electronic and Total Partition Functions and Equilibrium Constants of Diatomic Molecules	47
2.8	Isotopic Shifts of Rotational and Vibrational Constants of Diatomic Molecules	50
2.9	Introduction to Triatomic Molecules	53
2.10	Determination of Rotational Partition Functions of Triatomic Molecules	57
2.11	Determination of Vibrational Partition Functions of Triatomic Molecules	59

2.12	Determination of Total Partition Functions and Equilibrium Constants of Triatomic Molecules	62
2.13	Rotational Isotopic Shifts of Triatomic Molecules	65
2.14	Vibrational Isotopic Shifts of Triatomic Molecules	69
2.15	Molecular and Grand Iteration Scheme for Determining Equilibrium Abundances	87
2.16	The Inclusion of Molecules with more than Three Atoms and Solid Particles	109
3	DETERMINATION OF SCATTERING AND CONTINUOUS OPACITY	
3.1	Introduction	113
3.2	Electron and Rayleigh Scattering	119
3.3	Free-Free and Bound-Free Sources of Opacity	126
3.4	Other Sources of Continuous Opacity	133
4	COMPUTING THE BAND SPECTRA OF DIATOMIC MOLECULES	
4.1	Introduction	140
4.2	Rotational Fine Structure of Bands	145
4.3	Vibrational Energy Levels and Matrix Elements	168
4.4	Determination of Absolute Line Strengths	185
5	COMPUTING THE BAND SPECTRA OF TRIATOMIC MOLECULES	
5.1	Introduction	191
5.2	Vibration-Rotation Spectra of Linear Molecules	196
5.3	Vibration-Rotation and Pure Rotation Spectra of Non-Linear Molecules	207
5.4	Equilateral Triangle Molecules	228

6	METHODS OF COMPUTING OPACITIES DUE TO MANY LINES	
6.1	Introduction	232
6.2	The Independent Line Method	235
6.3	The Partial Overlap of Two Gaussian Profiles	250
6.4	The Line Smear Method	265
6.5	The Opacity Sampling Method	277
7	PRESENTATION AND DISCUSSION OF RESULTS	
7.1	Introduction	282
7.2	Abundances and Continuous Opacities	284
7.3	Some Examples of Computing Band Absorption	313
7.4	Some Tests and Timings of Computing Band Opacities with Bins	335
7.5	Results of Some Computed Total Opacities with Continuum and Molecular Bands	358
7.6	Comparisons of Abundances and Opacities and Tables of Thermodynamic Quantities	401
8	SUMMARY	420
	APPENDICES	
A	Determination of the Principal Moments of Inertia for any Triatomic Molecule	428
B	Determination of Vibrational Partition Functions and some other Vibrational Properties	442
C	Data for Determining Sources of Continuous Opacity	452
D	Adopted Core Statistical Weights of Atoms and Ions	471
E	Hönl-London Factors for Doublets and Triplets	475
F	The Isotropic Plane Harmonic Oscillator	483

G	Line Strengths and Energy Level Diagram of the Asymmetric Top	494
H	Sources of Molecular Oscillator Strengths and Transition Moments	502
I	Determination of the Internal Energies and Adiabatic Exponents of a Gas of Electrons, Atoms, Ions and Molecules	507
J	Abundances of Elements and Isotopes	520
	REFERENCES	525

INDEX OF TABLES

<u>Tab.</u>	<u>Sec.</u>	<u>Subject</u>	
2.1	2.9	Molecular Point Groups	53
2.2	2.9	Possible Isotopic Substitutions	54
2.3	2.14	Methods for Obtaining Isotopic Frequencies	84
5.1	5.3	Rotational Sublevels of Asymmetric Top with J=5	210
5.2	5.3	Rotational Selection Rules of Asymmetric Top	217
5.3	5.3	Subbranches Considered of Asymmetric Top	220
6.1	6.3	Overlap Parameters for Different Relative Line Strengths	262
7.1	7.2	Log RMO & Log PMO for Continuum	288
7.2	7.2	Abundances at Log T = 3.2 & Log R = -8.0	301
7.3	7.2	" " " 3.3 " "	302
7.4	7.2	" " " 3.4 " "	303
7.5	7.2	" " " 3.5 " "	304
7.6	7.2	" " " 3.6 " "	305
7.7	7.2	" " " 3.7 " "	306
7.8	7.2	" " " 3.8 " "	307
7.9	7.2	Sources and Sinks of Electrons	308
7.10	7.3	Franck-Condon Factors of the Swan System	315
7.11	7.3	r-Centroids of the Swan System	316
7.12	7.3	Hönl-London Factors of the 0-0 Swan Band	319
7.13	7.3	Comparisons of the Sums of Hönl-London Factors	320
7.14	7.3	CO Band Strengths in cm ² /sec/absorber	327
7.15	7.3	CO Band Strengths in (cm sec) ⁻¹ at 2000 ^o K	327
7.16	7.3	Some Transitions of Water 001 ←← 000 Band	332
7.17	7.4	Different Sampling Intervals	340

7.18	7.4	Some Tests on a Sample of Bins	341
7.19	7.4	CPU Timing Runs and Sums Over Bins	346
7.20	7.5	Isotopic Abundances of CO at Log T = 3.3 & Log R = -8	360
7.21	7.5	Isotope Effect of CO	360
7.22	7.5	Isotopic Abundances of HCl at Log T = 3.3 & Log R = -8	376
7.23	7.5	Isotope Effect of HCl	376
7.24	7.5	Isotopic Abundances of TiO at Log T = 3.5 & Log R = -8	378
7.25	7.5	Isotope Effect of TiO alpha-System	378
7.26	7.5	Reduced Band Strengths of Water	390
7.27	7.5	Reduced Band Strengths of Carbon Dioxide	396
7.28	7.5	Conversions between u and lambda in Microns	400
7.29	7.6	Log RMO & Log PMO for Continuum + Diatomic Molecules	405
7.30	7.6	Comparison of Log RMO for some Grid Points	406
7.31	7.6	Comparison of Log PMO for some Grid Points	406
7.32	7.6	Pressure & Internal Energy	407
7.33	7.6	CP & CV	409
7.34	7.6	Gamma0 & Gamma1	411
7.35	7.6	Gamma2 & Gamma3	413
7.36	7.6	Chi T & Chi R	415

<u>Table</u>	<u>Subject</u>	
A.1	I_p/I_q for some C_{2v} Molecules	440
C.1	Rayleigh Scattering Coefficients	453
C.2	H^- Free-Free & Bound-Free Absorption Coefficients	456
C.3	He^- Free-Free Absorption Coefficients	458
C.4	Li^- " " " "	460
C.5	C^- " " " "	460
C.6	N^- " " " "	461

C.7	O ⁻	"	"	"	"	461
C.8	Ne ⁻	"	"	"	"	461
C.9	Na ⁻	"	"	"	"	462
C.10	Cl ⁻	"	"	"	"	462
C.11	Ar ⁻	"	"	"	"	463
C.12	Kr ⁻	"	"	"	"	463
C.13	Xe ⁻	"	"	"	"	464
C.14	Cs ⁻	"	"	"	"	464
C.15	Hg ⁻	"	"	"	"	464
C.16	H ₂ ⁻	"	"	"	"	465
C.17	N ₂ ⁻	"	"	"	"	465
C.18	O ₂ ⁻	"	"	"	"	466
C.19	CO ⁻	"	"	"	"	466
C.20	H ₂ O ⁻	"	"	"	"	466
C.21	CO ₂ ⁻	"	"	"	"	467
C.22	OH Bound-Free	"	"	"	"	467
C.23	CH	"	"	"	"	468
C.24	Bound-Free Absorption Coefs. for Several Neg. Ions					469
C.25	Quasi-H ₂ Absorption Coefficients					470
D.1	Core Statistical Weights					473
G.1	Relative Line Strengths in A-Type Bands					497
G.2	"	"	"	"	"	498
G.3	"	"	"	"	"	499
G.4	"	"	"	"	B-Type Bands	499
G.5	"	"	"	"	"	500
G.6	"	"	"	"	"	500
H.1	Molecular Oscillator Strengths & Transition Moments					505
J.1	Abundances of Elements & Isotopes					521

INDEX OF FIGURES

<u>Fig.</u>	<u>Sec.</u>	<u>Subject</u>	
2.1	2.13	Notation of Bonds & Force Consts. of Triatomic Molecules	66
6.1	6.3	Idealized Curve of Partl. Ovlp. of two Gaussian Profiles	253
6.2	6.3	Partl. Ovlp. of two Equal Strength Gaussian Profiles	254
6.3	6.3	Partl. Ovlp. of two Unequal Strength Gaussian Profiles	255
6.4	6.3	Total Ovlp. of two Unequal Strength Gaussian Profiles	260
6.5	6.4	Rectangular Smear	266
6.6	6.4	Triangular Smear	266
6.7	6.4	Smear Intermediate between Rectangle & Triangle	271
6.8	6.4	Wedge Smear	271
7.1	7.2	Continuum at Log T = 3.2 & Log R = -8.0	291
7.2	7.2	" " " 3.3 " "	292
7.3	7.2	" " " 3.4 " "	293
7.4	7.2	" " " 3.5 " "	294
7.5	7.2	" " " 3.6 " "	295
7.6	7.2	" " " 3.7 " "	296
7.7	7.2	" " " 3.8 " "	297
7.8	7.3	TiO 0-0 Band of A-X System	323
7.9	7.3	" " " " " "	324
7.10	7.3	CO Second Overtone System	328
7.11	7.3	" " " "	329
7.12	7.4	Bins 1631 to 1635 in a Linear Plot	349
7.13	7.4	" " " " " " Logarithmic Plot	350
7.14	7.4	Bins 1684 to 1688 in a Linear Plot	351

7.15	7.4	"	"	"	"	"	"	"	"	Logarithmic Plot	352	
7.16	7.4	Log RMO	Plot of	001-000	Band of	H ₂ O	for	u=1	to	4	353	
7.17	7.4	"	"	"	"	"	"	"	"	2.8 to 3.2	354	
7.18	7.5	Log PMO	Plot of	CO	without	Isotopes	for	u=1	to	4	362	
7.19	7.5	"	"	"	"	"	with	"	"	1 to 4	363	
7.20	7.5	Log RMO	"	"	"	without	"	"	"	1 to 4	364	
7.21	7.5	"	"	"	"	"	with	"	"	1 to 4	365	
7.22	7.5	"	"	"	"	"	without	"	"	1 to 2	366	
7.23	7.5	"	"	"	"	"	with	"	"	1 to 2	367	
7.24	7.5	"	"	"	"	"	without	"	"	2 to 3	368	
7.25	7.5	"	"	"	"	"	with	"	"	2 to 3	369	
7.26	7.5	"	"	"	"	"	without	"	"	3 to 4	370	
7.27	7.5	"	"	"	"	"	with	"	"	3 to 4	371	
7.28	7.5	"	"	"	"	"	without	"	"	2.8 to 3.2	372	
7.29	7.5	"	"	"	"	"	with	"	"	2.8 to 3.2	373	
7.30	7.5	Log RMO	TiO	C-X	without	Isotopes	for	u=0	to	20	379	
7.31	7.5	"	"	"	"	with	"	"	"	0 to 20	380	
7.32	7.5	"	"	"	"	without	"	"	"	8 to 9	381	
7.33	7.5	"	"	"	"	with	"	"	"	8 to 9	382	
7.34	7.5	Some Profiles	of	TiO	0-0	Band of	C-X	without	Isotopes		383	
7.35	7.5	"	"	"	"	"	"	"	with	"	384	
7.36	7.5	Log RMO	TiO	C-X	&	c-a	without	Isotopes	for	u=0	to 20	385
7.37	7.5	"	"	"	"	"	with	"	"	0 to 20	386	
7.38	7.5	Log RMO	H ₂ O	Log T =	3.5,	Log R =	-8,	u=0	to	20	391	
7.39	7.5	"	"	"	"	3.4,	"	"	"	0 to 20	392	
7.40	7.5	"	"	"	"	3.3,	"	"	"	0 to 20	393	
7.41	7.5	"	"	"	"	3.5,	"	"	"	1.5 to 2.0	394	
7.42	7.5	Log RMO	CO ₂	Log T =	3.4,	Log R =	-8,	u=0	to	20	397	

7.43	7.5	Log RMO Diatomics Log T = 3.6, Log R = -8, u=0 to 17	399
7.44	7.6	Abundance of Molecules at Different Temperatures	403
7.45	7.6	Comparison Plot of Continuum at Log T = 3.2 & Log R = -8	404

<u>Figure</u>	<u>Subject</u>	
A.1	General Triatomic Molecule with Coordinate System	429
A.2	Moments of Inertia of C_{2v} Molecule	429
G.1	Energy Level Diagram of Asymmetric Top Molecule	501

1 INTRODUCTION

1.1 Introduction to Stellar Opacities

With the advent of modern high speed computers, it is now possible to perform detailed numerical integrations of the equations of stellar structure, enabling one to construct a large number of stellar models. Given a specified mass and chemical composition, one can determine the internal distribution of temperature, density and pressure, as well as the observable quantities of luminosity and effective temperature, leading to such important calculations as stellar evolution, pulsation etc. However, discrepancies between theory and observation are due to our approximations and lack of understanding of the input physics, such as nuclear reaction rates, equation of state and the opacity of the stellar material to radiation. It is the radiative opacity of stellar material which is the subject of this work.

There are three basic modes of energy transport in stars, radiation, conduction and convection, where respectively energy is carried by photons, individual particles and large aggregates of particles, such that the total energy flux at a radial distance r is given by:

$$F(r) = F_{\text{rad}}(r) + F_{\text{cond}}(r) + F_{\text{conv}}(r) \quad (1.1.1)$$

where in each case the radial flow of energy is opposite to the temperature gradient. The radiative flux is given by:

$$F_{\text{rad}}(r) = -\frac{4acT^3}{3\rho\kappa_r} \frac{dT}{dr} = -K_r \frac{dT}{dr} \quad (1.1.2)$$

where ρ is the density, κ_r the radiative opacity and K_r the "radiative conductivity"; a similar expression can also be written for the conductive flux. The total conductivity is:

$$K = K_r + K_c \quad (1.1.3)$$

and the total opacity is:

$$\frac{1}{\kappa} = \frac{1}{\kappa_r} + \frac{1}{\kappa_c} \quad (1.1.4)$$

where K_c is the thermal conductivity and κ_c the "conductive opacity".

Normally in stars, radiation and convection are the main forms of energy transport, with radiation in preference to convection if the logarithmic derivative of temperature with respect to pressure is subadiabatic, and convection in preference to radiation if the temperature gradient is superadiabatic. Conduction is normally unimportant except at high densities, particularly when electrons become degenerate. However, because the energy ultimately escapes into free space by radiation at the photosphere, whichever mechanisms of energy transport operate in the stellar interior, there will always be a region where the transport of radiation is important.

The opacity in equation (1.1.2), which from now on in this work is understood to be just the radiative opacity, is the absorption per unit mass, or mass absorption coefficient, which in the cgs units generally used is in cm^2 per gm. However, it is often convenient to work with the absorption per unit volume, or volume absorption coefficient, which is in cm^2 per cm^3 or cm^{-1} . Given the volume absorption coefficient, the mass absorption coefficient can simply be found by dividing by the density in gm per cm^3 . The opacity here is at a particular temperature and density, i.e. at some radial distance in the star, but it is a mean value, as the opacity is generally dependent on the frequency of the radiation. The mean which is used is the Rosseland mean (see chapter 3 and for example Cox and Giuli (1)), which is a weighted harmonic mean opacity; another mean which we also discuss is the Planck mean, which is a weighted arithmetic mean opacity. It should be noted that the Rosseland mean opacities that we calculate would be of limited use when the medium is optically thin, so the diffusion approximation does not hold, and where convection is important. Although one of these conditions is often fulfilled for the cases we are considering, the monochromatic opacities which we calculate in order to obtain the Rosseland mean opacities, are important for radiative transfer calculations.

Over the vast range of temperatures and densities between the centre and photosphere of a star, many processes can contribute to the opacity, with many calculations having been done on this, see for example Cox and Stewart (2).

1.2 Summary of this Work

In this work, we consider opacities at various densities and temperatures below about 6000°K , which for photospheres corresponds to stars of spectral type of the Sun and later. At these temperatures, the formation of molecules is important, and in this thesis we consider how we determine molecular abundances then how we attempt to compute their opacities. This work at the University of St. Andrews is part of a larger project by Dr. Carson to compute opacities over a greater range of conditions, for example Carson and Alexander (3) are working on temperatures from about 6000°K upwards where molecules can be neglected.

In this thesis, we discuss in chapter 2 how we obtain the abundances of free atoms, ions and molecules, by the iteration of the simultaneous equations of atomic ionization and molecular dissociation, having first to compute the various equilibrium constants, given the initial abundances of the chemical elements. We handle diatomic and triatomic molecules in quite a general way, and allow for all possible isotopic variations by specifying the isotopic abundances, when relevant, of the various elements. So far as is known, no other work has been done in such detail. These calculations are performed over a range of temperatures and densities, but with fixed abundances of the elements and their isotopes obtained from Cameron (4) from the Sun and meteorites, which should be characteristic of the primitive solar nebula, and we consider to be a

typical population I mixture. In principle, we could very easily consider different mixtures, but this possibility is not explored here.

Having obtained the converged abundances for a specified temperature and density, in chapter 3 we discuss how we compute contributions from the various continuous sources of opacity: electron scattering, Rayleigh scattering of atoms and some molecules, free-free and bound-free absorption of some negative atomic and molecular ions and some neutral atoms and molecules, and finally the pressure induced opacity of molecular hydrogen and the opacity due to quasi-molecular hydrogen. With these calculations, we establish the continuum as a foundation onto which we put the bound-bound absorption due to molecular bands.

In chapters 4 and 5, we discuss the theory which we use to compute the bands of diatomic and triatomic molecules respectively. Unfortunately, though the vibrational and rotational constants are often well known for diatomic molecules, the dipole moments or oscillator strengths that we need for computing the absolute band strengths, hence the strengths of individual spectral lines, are often only known approximately or not at all. Though we have to make some approximations in computing the line positions and strengths, in many cases the ultimate accuracy is limited by the input data. It is hoped that at worst we can obtain the gross properties of bands or band systems. For triatomic molecules, the band spectra are much more complex with many millions of lines being present, and at least we have to use very approximate techniques to calculate these bands.

Although we do individual line-by-line calculations, we would be optimistic in hoping for anything much better than obtaining the approximate properties of bands.

Once individual lines have been produced using the theory in the previous two chapters, in chapter 6, on which this work hinges, we discuss how we actually handle these lines in order to compute the opacity. Because generally there are a very large number of lines to handle, and they are very narrow, i.e. millions of lines could be placed over the spectral regions that we deal with without overlapping, we consider various techniques all based on splitting the spectrum into a large number of bins, in which we lose information on individual lines, but retain summed quantities such as line strengths. Though the spectrum is split into many bins, of the order of a few tens of thousands, it is manageable and we can sum over all bins to obtain a total Rosseland and Planck mean opacity. In stellar atmosphere calculations, the opacity is required at many frequency points, rather than just the total mean, and we have the option of storing the generated spectra on some medium such as disk or magnetic tape.

In chapter 7 we put all the theory discussed previously into practice, and display and discuss the results of some numerical calculations. We consider not just final opacities at various temperatures and densities, but also some abundances and examples of some of the intermediate calculations, as well as some tests and checks. In addition, some tables of the adiabatic exponents and some other thermodynamic quantities are also given. Finally in this

thesis, some additional discussions and tables not included in the main body of this work, are found in the appendices following the last chapter, together with the listing and documentation of the computer programs in the Molecular Stellar Opacity Program Volume, with further examples of results.

We only consider spectral lines produced by molecules, though of course there will also be atomic lines which we neglect. However, particularly at the lower temperatures that we consider, the effect of including atomic lines would be expected to be completely negligible, as many of the atoms are combined into molecules, the spectrum can be very heavily blanketed by molecular bands, many of which will be in the infrared part of the spectrum where most of the energy lies, and where relatively few atomic lines are found. Many bands of molecules such as TiO, ZrO, YO and VO are observed in M-type stars, where even if a molecule has a relatively low abundance, if it absorbs in places in the spectrum where there is little other absorption, then its effect is all-important. In carbon stars, one would also observe bands due to molecules such as C₂ and CN. On the other hand in early-type stars, molecules can be completely neglected from both the statistical mechanics calculations and as sources of opacity, the bound-bound absorption being due only to atoms and ions, which then have to be considered in opacity calculations.

Finally, note that we try to keep the notation as consistent as possible. This is particularly important in chapter 2 where we have to define unambiguously such items as different sorts of fractional abundances of various species and different indices. On the printer

used in producing this thesis, because a lower case "L" looks very much like the number "1", to prevent confusion we generally use the letter "h" when considering indices, thus the indices representing the isotopes in a triatomic molecules in chapter 2 are h, m and n, however, for the vibronic quantum number in chapter 5, we instead use the handwritten "ℓ".

1.3 Brief Literature Survey

Before we discuss in detail the methods used in this work, we give here a brief survey of other work on molecular opacities. For a general review on opacities, refer in particular to Carson (5) and also to Hack (6) for opacities and many other aspects of late-type stars. Some examples of earlier work can be found by referring to Yamashita (7) and Cox (8).

Tsuji (9) considers the vibration-rotation and pure rotation bands of CO, OH and H₂O in cool stellar atmospheres, these being normally the most abundant molecules in such atmospheres that produce bands in the infrared where most of the flux is. These bands are overlaid by a continuum due to a number of processes which are discussed in chapter 3, and we adopt some of his data, in particular the bound-free and free-free absorption coefficients of the negative hydrogen ion, which is an important continuous source of opacity in late-type stars.

Given several overlapping bands, Tsuji computes molecular absorption on the basis of the Just-Overlapping Approximation (JOA). Here it is assumed that because there are so many lines in a region of the spectrum, they are all overlapping with the windows between the lines filled in, so that just part of the spectrum can be represented by a pseudo-continuum. Unfortunately as is stated, although the JOA can be used for H₂O at high enough temperatures and turbulent

velocities, because of the very large number of lines it produces, it cannot be used for CO and OH, nor at lower temperatures, for H₂O, as there will be windows between the lines through which flux can pass. In this case the generalization of the JOA to the Partial Overlapping Approximation (POA) is discussed, where the spectral region in question is split up into a number of meshes, where in each the smeared absorption is redistributed so as to leave some continuum, yet retain some overlap. Unfortunately, this method depends on a smearing parameter which is difficult to determine, and we know from our own work that the Rosseland mean can depend very critically on the number and sizes of windows between lines in bands. Tsuji also gives some useful spectra and other plots for several temperatures and pressures.

In later papers by Tsuji (10) and (11), the above work is taken further by allowing for the fact that the bands will not in general be completely smeared out. This is done by adopting Elsasser band models, see Vardya (12) and Golden (13), where an ideal Elsasser band consists of an infinite number of regularly spaced identical spectral lines, and can be treated analytically. Tsuji also considers in some detail the abundances of a large number of molecules in stellar atmospheres in his paper (14).

Auman (15) computes the opacity of H₂O for several temperatures and turbulent velocities by a line-by-line calculation, and gives extensive tabulations of such opacities. This work is subsequently applied to models of late-type stars, see Auman and Bodenheimer (16).

An important technique for calculating opacities is by the so called Opacity Distribution Function (ODF). With this method, the spectrum is split up into a large number of pickets or bins, where in each the details of the variation of the opacity across the bin is lost, but the information about how the opacity is distributed is retained, i.e. how much opacity there is covering a given fraction of the bin. We have in effect re-arranged the absorption so that it changes monotonically across the bin, either smoothly or in the form of a histogram. This method is discussed by Strom and Kurucz (17), who apply it to a model atmosphere of the F5IV star Procyon (α CMi), where virtually all spectral lines would be atomic in origin, and also by Mihalas (18). Kunde (19) uses ODFs for computing CO opacities in stellar atmospheres, and Querci et al. in such papers as (20), (21) and (22) apply ODFs for cool carbon rich stellar atmospheres. Also refer to for example Carbon (23) and Mould (24), the latter giving tabulations of model atmospheres of M-type dwarfs, where of course the densities are much higher than for red giants. Finally, Gustafsson et al. (25) considers ODFs over a grid of atmospheres, with extensive tables given in Bell et al. (26).

Another method of calculating opacities is by opacity sampling, see chapters 6 and 7. In this method, the opacity is computed in detail at a number of grid points across the spectrum, see for example Sneden, Johnson and Krupp (27), and Johnson and Krupp (28), rather than having so many grid points that individual lines are profiled. (27) and (28) use at most a few thousand grid points across the spectrum to calculate model stellar atmospheres with molecular bands,

this being a statistical method as the separation of the grid points is very much larger than the widths of individual profiles, so most spectral lines are missed altogether. However, in our application of opacity sampling to calculate Rosseland mean opacities, we use a very much finer grid, so that in general individual spectral lines will be at least approximately represented, by having one or two grid points across the profile. If we apply a coarser grid so that undersampling results, the contribution to the Rosseland mean from those parts of the spectrum that are either pure continuum or are very heavily congested by lines giving rise to a pseudo-continuum, are likely to be fairly accurate, but the contribution from those regions of partial congestion is likely to be more uncertain.

Finally, most of the basic theory on molecules is obtained from Herzberg (29) and (30) and Kovács (31), the physical constants and atomic ionization potentials from Allen (32), atomic energy levels from Moore (33), and molecular data is obtained from many sources including Herzberg (30) and (34), Rosen (35) and Mizushima (36). These and other sources are quoted when required.

2 DETERMINATION OF EQUILIBRIUM ABUNDANCES

2.1 Introduction

In order to determine the total opacity of a stellar atmosphere, the individual contributions each opacity source makes over the spectrum has to be known. Clearly, the contribution each species makes to the opacity depends on its abundance; and it is this which is considered in this chapter.

The equilibrium abundances of atomic and molecular species, together with the populations of their excited electronic states are calculated on the basis of the condition of local thermodynamic equilibrium (LTE) being satisfied. Because the equations governing the equilibrium abundances are all coupled, it is necessary to include in these calculations those atomic and molecular species, which although they may not necessarily contribute significantly to the total opacity themselves, may nevertheless affect those species which do. Unfortunately, it is often not possible to know whether the inclusion of a particular molecule will significantly affect the abundances of those important molecules, until after the calculation itself is performed. Then, after that, it is only known at those particular conditions of temperature, density and specified mixtures chosen. A similar problem arises when the opacity of a species is determined; it may not be known whether it can be neglected until after it has been calculated.

As the molecular opacities of late-type stars are considered, the temperature range chosen is from about 1000°K to 6000°K , and densities between 10^{-14} and 10^{-2} gm cm^{-3} . Above 6000°K , molecule formation becomes negligible, and already at 1000°K , one is well to the right of the Hayashi forbidden zone in the H-R diagram where no stable stars are expected to exist with such photospheric temperatures, in addition to which, opacities are dominated by solid particles that are not considered in this work. However, at 1000°K , because of strong negative ion formation, the iterative process tends to converge very slowly, particularly at the earlier stages, though eventually sufficient convergence is reached, giving confidence in the method at higher temperatures. The density range includes the region in which red giants lie, where pressure independent partition functions and lines not dominated by pressure broadening could be assumed, though we do have to handle atomic and ionic partition functions correctly (see section 2.2).

Coding in FORTRAN is written by which diatomic and triatomic molecules could be treated in quite a general way. Molecules are not considered in this work that have more than three atoms, as to treat them in quite a general way would be enormously complex, though they could be easily included on an individual basis.

Furthermore, isotopically substituted molecules are included, as they may be present in significant abundances, to affect both the equilibrium abundances and in particular the opacity. The latter being due to the fact that an abundant isotopically substituted

molecule having a shifted spectrum with respect to its parent molecule (i.e. the molecule which normally has the most abundant isotopes) may fill up windows in a part of the spectrum, thus radically altering the opacity in that region; also the fine structure may be different, depending on the identities of the nuclei. Unfortunately, as the molecular partition functions depend on the rotational and vibrational energy levels, which are shifted when isotopes are substituted, it is necessary to calculate the dissociation equilibrium constants for each isotopic molecule in turn, then to perform the iteration on each of them. Thus isotopes rather than elements are considered in the dissociation equilibria, and isotopic molecules are treated in quite a general way. This is particularly complex for triatomic molecules, as there can be up to five different point groups, and the symmetry of a molecule can change completely when one isotope is substituted.

Initially, the atomic abundances both bound and free are specified either by mass or by number, either in absolute form, or for the metals (elements other than hydrogen and helium), relative to the total metal abundance. In addition, one can specify for each element the fractional abundance by number of each isotope that makes up that element. Molecular abundances, however, are not specified, instead, with the necessary data, molecules are allowed to form in the course of iteration.

The iterative process for determining the abundances of free atoms and molecules is subdivided into two equilibrium calculations. First, with the molecular abundances set to zero, iterations are performed to determine equilibrium between atoms, their respective

ions and electrons, where negative ion formation is allowed for in the coding. Then, with the relative abundances of each element in different stages of ionization held constant, iterations are performed to find equilibrium between free atoms and molecules, yielding abundances of diatomic and triatomic molecules, and the fractional abundance of each element that is free. Once these quantities have been calculated, the equilibrium between atoms and their respective ions is redetermined with the molecular abundances held constant. The molecules are then considered again, and the whole process is repeated.

The sequence of ionization equilibrium followed by dissociation equilibrium iterations is considered as a grand iteration, and particularly at low temperatures where molecules and negative ions are present in great abundance, many such iterations may have to be executed until final convergence is reached. In the first grand iteration, the convergence criterion for both the ionization and dissociation iterations is quite loose, however, with the next few grand iterations, the criterion is progressively made more stringent until the maximum stringency required is reached, then with this criterion, iterations are continued until final convergence is attained.

2.2 Determination of Atomic and Ionic Partition Functions and Equilibrium Constants

Before we can proceed with the equilibrium calculations, we have to find the equilibrium constants of the atoms, ions and molecules, which in turn require the partition functions. The determination of these quantities for atoms and ions is explained in this section; the discussion for the molecules is deferred until later.

The partition function of any species is given quite generally by:

$$Q = \sum_i g_i e^{-E_i/kT} \quad (2.2.1)$$

where g_i and E_i are the statistical weight and energy respectively of the i^{th} level. However, the sum in (2.2.1) if taken to the ionization limit is divergent, and we need a cut-off based on physical arguments.

The most convenient way of dealing with this, is to evaluate (2.2.1) with explicit values of g_i and E_i from published sources up to some appropriate limit. A convenient value is in the region of $20,000\text{cm}^{-1}$ above the ground state where the Boltzmann factor is less than 0.01 at 6000°K , then continue the summation assuming the levels are hydrogen-like until the final cut-off is reached.

If N is the total number of particles per cm^3 , then:

$$r = \left(\frac{3}{4\pi N} \right)^{1/3} \quad (2.2.2)$$

where r is the mean distance from an atom or ion to the nearest neighbour. Now if we take a valence electron (electron from the outermost shell) to a sufficient distance from the rest of the atom, we can assume the energy levels are hydrogen-like and the orbital radius is given by:

$$r_n = a_0 \frac{n^2}{Z_\infty} \quad (2.2.3)$$

where a_0 is the first Bohr radius, n is the principal quantum number and Z_∞ is the effective nuclear charge as experienced by the electron at a large distance, such that $Z_\infty = 1$ for neutral atoms, $Z_\infty = 2$ for singly ionized atoms etc. From (2.2.2) and (2.2.3), we can write:

$$n_u = \text{int} \left(\frac{3 Z_\infty^3}{4\pi N a_0^3} \right)^{1/6} \quad (2.2.4)$$

where the int function takes the integer part and n_u is the largest value n can take as the nearest neighbour prevents further levels from existing.

Let E_n be the energy in ergs of the n^{th} hydrogen-like level, then:

$$E_n = E_\infty - \frac{Rhc Z_e^2 (n)}{n^2} \quad (2.2.5)$$

where $Z_e(n)$ is the effective nuclear charge as experienced by the electron at an energy well above its ground state, R is the Rydberg constant and E_∞ is the ionization potential in ergs, such that:

$$E_\infty = h c s_0 I \quad (2.2.6)$$

where I is the ionization potential in eV and s_0 is the conversion factor of 8065.46cm^{-1} for 1eV; and when $n \rightarrow \infty$, $E_n \rightarrow E_\infty$.

Except for the special cases of H, He^+ , Li^{++} etc., (2.2.5) is invalid for small values of n where the levels are no longer hydrogen-like or are completely filled, but as stated above, the lower levels are handled explicitly. For H and H-like ions only, $E_1 = 0$ in (2.2.5) has meaning.

In (2.2.5) the effective nuclear charge would vary with n , such that as $n \rightarrow \infty$, $Z_e(n) \rightarrow Z_\infty$. Thus let $n = n_1$ be the lowest value of n that we can assume a level is hydrogen-like, with the corresponding energy E_{n_1} being specified, then inserting these into (2.2.5) and solving for $Z_e(n)$, we obtain the effective nuclear charge Z_1 for the level n_1 . We can then make up a simple formula that gives these limiting values of Z :

$$Z_e(n) = Z_\infty - \frac{n_1^2}{n^2} (Z_\infty - Z_1) \quad (2.2.7)$$

which can then be put into (2.2.5) for $n \gg n_1$ with which we can calculate E_n .

Having obtained E_n this way for each value of n in the range, the total partition function Q is given by:

$$Q = Q' + \sum_{n=n_l}^{n_u} 2n^2 g_c e^{-E_n/kT} \quad (2.2.8)$$

where Q' is that part of the partition function computed from (2.2.1) using explicit values, $2n^2$ is the statistical weight of the hydrogen-like n^{th} level and g_c is the core statistical weight due to all the other electrons, see the appendices.

When $n = n_u$, (2.2.5) gives a new ionization potential which will be slightly less than the unperturbed value, it is this new value that we should really insert into the formulae below.

Technically N in (2.2.4) should be the total number of particles per cm^3 including electrons and molecules, but this would require an extra level of iteration. However, because of the relatively weak dependence n_u has on N due to the sixth root, we can take N to be the total number of atoms per cm^3 which is a known and fixed quantity, see the next section, regardless of their ionization or association into molecules. Over the temperature range of interest, the total number of particles is unlikely to vary by much more than a factor of two on either side of N , due to the presence of free electrons at higher temperatures and association into molecules at lower temperatures. Also, because the cut-off occurs at large values of r_n for realistic densities, it is reasonable to use the effective nuclear charge at large distances Z_∞ in (2.2.4).

In practice it is found that for most atoms and ions under the conditions of interest, the sum in (2.2.8) contributes negligibly to the partition function as computed from the lower explicit values. However, for atoms like Na and K with low ionization potentials, at higher temperatures the upper levels do become important and the sum in (2.2.8) is significant.

This method cannot be applied to negative ions as there are only a finite number of states, and in principle we can only evaluate (2.2.1) for those states, in practice usually only the ground state, hence the partition function is just the statistical weight of that state, and of course for completely ionized atoms the partition functions are just unity.

The explicit values of g_i and E_i are taken from Charlotte E. Moore (33), giving tables of energy levels of atoms and ions, and Q is computed from (2.2.1) and (2.2.8) rather than taking the tabulated values of Allen (32) and interpolating.

In conditions of thermal equilibrium, the degree of ionization is given by Saha's equation:

$$\frac{N^{h+1} N_e}{N^h} = \frac{2 Q_{h+1}}{Q_h} \frac{(2 \pi m_e k T)^{3/2}}{h^3} e^{-\chi_{h,h+1}/kT} \quad (2.2.9)$$

or more conveniently for computation in log form as:

$$\log \left(\frac{N^{h+1} N_e}{N^h} \right) = -\chi_{h,h+1} \theta - \frac{3}{2} \log \theta + 20.9366 + \log \left(\frac{2 Q_{h+1}}{Q_h} \right) \quad (2.2.10)$$

Where: N_e is the number density of electrons,

N^h is the number density of the h^{th} ion of a given element,

$\chi_{h,h+1}$ is the ionization potential of the h^{th} ion in eV,

Q_h is the partition function of the h^{th} ion,

and $\theta = 5039.935/T$.

So $h = 0$ for neutral atoms, $h > 0$ for positive ions and $h < 0$ for negative ions. In fact, only $h = -1$ is allowed for negative ions, as no stable bound ions of a larger negative charge exist in the gaseous phase, and for many elements like the inert gases, no bound negative ions exist at all. Where possible confusion may occur with other indices, like labelling of different elements, h is used as a superscript.

The left hand side of (2.2.9) is the equilibrium constant, and is defined as:

$$K_{h,h+1} = \frac{N^{h+1} N_e}{N^h} \quad (2.2.11)$$

In this work, intermediate calculations involving abundances, are wherever possible, handled in the log rather than in magnitude, to avoid problems with machine overflow or underflow.

2.3 Iterative Process for Determining Equilibrium Abundances of Atoms and Ions

It is initially assumed that all the atoms are free with no molecules present, and the early part of the iterations treat the mixture as if it consisted purely of atoms with their associated ions.

Before iterations can commence, a trial value for the electron number density is required. The total number density of all atoms, irrespective of their ionization states, is given by:

$$N = \sum_i N_{(i)} = \frac{\rho N_A}{\sum_i A_i m_i} \quad (2.3.1)$$

where ρ and N_A are the mass density and Avogadro's number respectively, and A_i , $N_{(i)}$ and m_i are the fractional abundance by number, the total number density and the atomic mass in atomic mass units (amu) of atom i respectively. In the analysis, the index i is used to label different atoms, but does not in general correspond to their atomic numbers. It is easy for the computer code to handle elements in any order and the input data having elements of very low abundances omitted. Indeed, using this scheme, deuterium can be handled as if it were quite a separate element, rather than as an isotope of hydrogen.

Clearly:

$$N_e \leq \sum_i Z_i N_{(i)} = N \bar{Z} \quad (2.3.2)$$

where Z_i is the atomic number of element i , \bar{Z} is the average nuclear charge per atom and N_e is the number density of free electrons, which for total charge neutrality, cannot exceed the sum of all the nuclear charges.

It is found empirically that a good initial trial value is given by:

$$\log(N_{e \text{ TRIAL}}) = \log(N \bar{Z}) + \min\left\{\frac{3}{2}(\log T - 5)^3, 0\right\} \quad (2.3.3)$$

where the function \min returns the minimum of the two arguments. As logarithms are handled, a physically realistic initial trial value of $N_e > 0$ is chosen. Also, the formula assumes that the system is completely ionized above about 10^5 K, which although being far beyond the range of interest in this application, does allow generality. The choice of a trial value of N_e is not too critical, but a poor initial value will increase the number of iterations before final convergence is reached.

For each ion, we can calculate the ionization equilibrium constant, thus from equations (2.2.10) and (2.2.11) we have:

$$\begin{aligned} \log K_{h,h+1} = & -\chi_{h,h+1} \theta - \frac{3}{2} \log \theta + 20.9366 \\ & + \log\left(\frac{2 q_{h+1}}{q_h}\right) \end{aligned} \quad (2.3.4)$$

Let R_i^h be the relative abundance of the h^{th} ion of element i with respect to the most negative ion of that element, where the most negative ion has a charge of -1 if a stable negative ion exists, otherwise a charge of zero. At high enough temperatures, outside the range of interest here, neutral atoms may be practically absent, and the minimum value h can take will in practice be positive.

Then given N_e and $K_{h,h+1}$ from above, and setting $\log R^k = 0$, where k here is the smallest value h can take as above, the expression:

$$\log R_i^{h+1} = \log R_i^h + \log K_{h,h+1,(i)} - \log N_e \quad (2.3.5)$$

can be evaluated successively for each ion belonging to each element, where $K_{h,h+1,(i)}$ is the equilibrium constant of ion h belonging to element i .

Once all the values of $\log R_i^h$ have been found for element i , $\log R_{\text{max},i}$ can be obtained, and is just the maximum fraction R in the list of ions belonging to a given element, i.e. the most abundant ion.

Then for each element i :

$$\log R_i'^h = \log R_i^h - \log R_{\text{max},i} \quad (2.3.6)$$

is evaluated, and expresses the relative abundance of each ion h of element i with respect to the most abundant ion of that element.

Writing:

$$\bar{\Phi}_i = \sum_h R_i^h \quad (2.3.7)$$

then after summing these relative abundances, we can calculate the fractional abundances of each ion of element i:

$$S_i^h = \frac{R_i^h}{\bar{\Phi}_i} \quad (2.3.8)$$

where by definition: $\sum_h S_i^h = 1$. Then the average number of electrons donated (+) or accepted (-) by atom i is:

$$x_i = \sum_h h S_i^h \quad (2.3.9)$$

Hence the number of electrons per cm^3 donated or accepted on average by atoms of element i is:

$$X_i = N_i x_i \quad (2.3.10)$$

where N_i is the number density of free atoms of element i in all stages of ionization, and is quite distinct from the previously defined $N_{(i)}$, the total number of atoms per cm^3 in any state, combined in molecules or free. As already stated, as molecular abundances are initially set to zero, $N_i = N_{(i)}$ initially. It is extremely useful at the end of all the iterations, when all the abundances have been converged, to know x_i and X_i for each element, as it is easily seen which elements are important net sources or sinks of electrons.

The total number density of free electrons present in the mixture is given by:

$$N_e = \sum_i X_i + M_e = \sum_i \sum_h h N_i S_i^h + \sum_s \sum_t t M_s^t \quad (2.3.11)$$

where M_e is the number density of electrons contributed by charged molecules, derived from the last term where M_s^t is the actual abundance of molecule of type s with charge t . Initially, as the molecular abundances are set to zero, M_e is also set to zero. Subsequently, when molecules are treated, it is found that in practice $M_e \ll N_e$, as abundances of charged molecules appear to be generally very small. As will be discussed later, unlike atomic ions, molecular ions are treated as quite separate molecules.

To make the process of convergence as efficient as possible, rather than simply taking the geometric mean of the output value of N_e from (2.3.11) and the previous input value in (2.3.5), and putting this back into (2.3.5) as our new input value, the new input value is found from the geometric mean of the smallest value so far found that is larger, and the largest value so far found that is smaller than the expected solution, which must lie between these two values. Using these bounds, reduces the amount of "wander" in N_e in the iterations. However, at low temperatures where negative ion formation is important, it is frequently found that $N_e(\text{out}) < 0$. Invariably this means that $N_e(\text{in})$ has been considerably overestimated, and if no previous positive output was obtained in earlier iterations covering the ions to act as a guide, then a new trial value is found simply by

reducing the previous input value, typically by a factor of 10. This is done in subsequent iterations until $N_e(\text{out}) > 0$, after which convergence is relatively rapid. At temperatures near the upper limit of the region of interest, this difficulty is not encountered, and convergence is quite rapid.

Iterations are terminated when either a suitable accuracy has been reached, or failing that, after a maximum specified number of iterations with positive outputs has been attained, negative outputs not being counted. This technique allows computer time to be used more efficiently, as we do not attempt to converge the abundances of the ions to the required accuracy in a given grand iteration, if the convergence process is very slow, as the abundances of the ions tend to converge to different values in the next grand iteration, due to the altered molecular abundances.

Thus, in the program, if we define a quantity $\Delta \log N_e$, such that:

$$\Delta \log N_e = |\log N_e(\text{out}) - \log N_e(\text{in})| \quad (2.3.12)$$

Then the iterations are terminated if:

$$\Delta \log N_e \leq \epsilon \quad (2.3.13)$$

where ϵ is the convergence criterion, typically 10^{-4} or less, except for the first few grand iterations when it is larger. In (2.3.12), if $N_e(\text{out}) < 0$, then some large negative value for the log is assumed so that (2.3.13) is not valid.

As the electronic structure of an atom is to a very high approximation independent of the isotopic form of the atom, the isotopic abundances making up a given element are ignored in these ionization calculations. Thus if deuterium is present, hydrogen in its various ionic forms contains the same fractions of deuterium.

2.4 Introduction to Diatomic Molecules

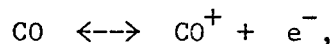
Whereas the case of the atomic ionization equilibrium is quite straightforward, the partition functions are simple to calculate and independent of isotopes, and only one quantity, i.e. the number of free electrons, is the "handle" in the iterative process, the case of molecular dissociation equilibrium is rather more difficult to deal with. For molecules, the partition functions are often strongly dependent on the isotopes substituted, so the equilibrium constants have to be individually determined, also the quantities iterated are the fraction of atoms of each element free in the mixture, defined as:

$$F_i = \frac{N_i}{N_{(i)}} \quad (2.4.1)$$

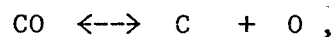
where for each element i , as previously defined, $N_{(i)}$ is the total number of atoms present per cm^3 , and N_i are those atoms that are free, regardless of their states of ionization, or the fractions in various isotopes. Clearly, it follows that $N_{(i)} - N_i$ are those atoms combined in molecules. The aim is to iterate until the fractions for each element have converged. This is rather more convenient than handling the actual number of atoms that are free, as $0 \leq F_i \leq 1$.

Unlike atoms, molecular ions are dealt with quite separately, thus CO and CO^+ are regarded as quite separate molecules, all the properties being quite different, apart of course from their mass and constituent atoms. Thus, although we could consider the molecular

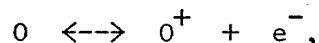
ionization equilibrium, as with the atoms in the previous section, as:



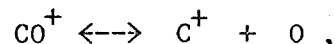
it is far more convenient to consider the dissociation equilibria:



together with the atomic ionization equilibrium:



which are all linked together automatically. Equally, one could instead consider the dissociation equilibrium:



with the associated atomic ionization, but whichever path is specified, the same results must be reached.

There are two types of diatomic molecules, homonuclear, point group $D_{\infty h}$ i.e. $\text{C}^{12}\text{C}^{12}$ and heteronuclear, point group $C_{\infty v}$ i.e. $\text{C}^{12}\text{O}^{16}$ or $\text{C}^{12}\text{C}^{13}$. As isotopes are considered, due account must be made of the isotopic variations, thus if the two isotopes C^{12} and C^{13} are specified to be present in the mixture, we must allow for the three forms of the molecule C_2 to be present, of which two will be homonuclear and one heteronuclear. As the vibrational and rotational

constants are slightly different as between these forms, their partition functions will be different and the band spectrum of one form will be shifted relative to another form. In addition, however, there will be differences between the homonuclear and heteronuclear forms. Apart from a constant factor, the J^{th} rotational level of a molecule has a statistical weight of $2J+1$, but if the molecule is homonuclear, there will be an additional factor for even values of J , and a different factor for odd values, dependent on the spins of the nuclei; hence giving alternating intensities in the fine structure of a band. If the three isotopes O^{16} , O^{17} and O^{18} are also present, clearly there will be six forms of CO present, though all will of course be heteronuclear, and we do not have to worry about the spins of the nuclei.

When the molecular data is read by the program, the dissociation products are checked against the list of atoms previously read in. If any of the dissociation products cannot be matched with the list of atoms, then the molecule is ignored. As molecular ions have charged dissociation products, the matching must take ions into account. Likewise, for any of the excited electronic states of the molecule considered, if there is insufficient data, then those states will be ignored, with the whole molecule being ignored if the ground state is not furnished with sufficient data.

The molecular constants read in as data for a particular molecule, refer to only one isotopic form of that molecule, though several isotopic forms may be present, and that form so referred to is defined as being the parent molecule, briefly mentioned in section

2.1. As explained later, the constants for the isotopically substituted forms have to be calculated, which can be quite an involved process for some triatomic molecules. The parent molecule would normally be the most abundant isotopic form present in a mixture, unless abnormal isotopic abundances are specified, as the data available refers usually to the most abundant isotopes of the elements concerned making up the molecule.

Finally, the object of calculating the partition functions of diatomic molecules is to determine the equilibrium constants, which are then used for calculating the molecular equilibria by iteration. The equilibrium constant for dissociation is defined as:

$$K_{ij} = \frac{N_i N_j}{N_{ij}} \quad (2.4.2)$$

which is the ratio of the product of the abundances of the free atoms i and j to the combined molecule ij , and is the Guldberg and Waage's law of mass action. In the limit of complete association, $K_{ij} = 0$ and complete dissociation $K_{ij} \rightarrow \infty$. In the units we are working in, K_{ij} is in cm^{-3} , and is analogous to the ionization equilibrium constant defined in (2.2.1). The determination of the equilibrium constants is discussed in section 2.7.

2.5 Determination of Rotational Partition Functions of Diatomic Molecules

The total internal partition function of any molecule can be approximated as:

$$Q_I = Q_R Q_V Q_E Q_S \quad (2.5.1)$$

Where: Q_R is the rotational partition function,

Q_V " vibrational " ,

Q_E " electronic " ,

Q_S " symmetry " ,

and $Q_S = 1/\sigma$ where σ is the symmetry number.

$\sigma = 1$ for non-symmetric i.e. heteronuclear diatomic molecules, and $\sigma = 2$ for symmetric i.e. homonuclear diatomic molecules. (2.5.1) is normally a good approximation, as the separation of the electronic states is large compared to the vibrational levels, which is in turn large compared to the rotational levels. It is the rotational levels of diatomic molecules that are considered in this section.

The rotational term values in cm^{-1} are expressed as:

$$F(J) = B_v J(J+1) - D_v J^2(J+1)^2 + \dots \quad (2.5.2)$$

where J is the rotational quantum number and takes the integer values 0,1,2,3...(cases are discussed later where depending on the electronic

state, there are restrictions on this, and J can also take half integer values, Herzberg (29)). Also:

$$B_v = B_e - \alpha_e (v + \frac{1}{2}), \quad D_v = D_e + \beta_e (v + \frac{1}{2}) \quad (2.5.3)$$

where B_e and D_e are the rigid and first order non-rigid rotational constants at the equilibrium separation of the atoms respectively, B_v and D_v the corresponding constants corrected for vibrational interaction, and α_e and β_e are the corresponding correction terms. There will be in general higher order terms in the above three expressions, however, due to their very small value, and the fact that they are usually not available in the literature, they are neglected; and v is the vibrational quantum number.

The rigid rotational constant B_e is defined as:

$$B_e = \frac{h}{8\pi^2 c I_e} \quad (2.5.4)$$

where I_e is the moment of inertia at equilibrium separation in cgs, and h and c have their usual meanings. Finally, all the rotational constants above are in units of cm^{-1} .

The expressions (2.5.2) and (2.5.3) are required for calculating the rotational energy levels, hence the rotational fine structure of a molecular band, and are discussed again in the section dealing with molecular band spectra. However, in order to find the partition function, it is not necessary to sum laboriously over the levels generated by (2.5.2) and (2.5.3), but use a far more efficient

asymptotic expansion of Q_R , see Kassel (37).

Let $b = Bhc/kT$ and $d = Dhc/kT$, where b and d are dimensionless, and the corrections due to vibration are neglected. Then the rotational partition function is:

$$Q_R = \sum_{I=0}^{\infty} (2J+1) e^{-bJ(J+1) + dJ^2(J+1)^2} \quad (2.5.5)$$

where $J = f(I)$, $I = 0, 1, 2, 3, \dots$ and $f(I)$ can have one of four forms, see below. This is the general expression for the rotational partition function of a non-rigid diatomic, or linear polyatomic molecule. As can be seen, particularly at fairly high temperatures, many levels in (2.5.5) may have to be summed, but it can be replaced by the four asymptotic expansions:

$$J=I, \quad Q_{R1} = \frac{1}{b} + \frac{1}{3} + \frac{b}{15} + \frac{2d}{b^3} \left(1 + \frac{6d}{b^2}\right) + \dots \quad (2.5.6)$$

$$J=I+\frac{1}{2}, \quad Q_{R2} = \frac{1}{b} + \frac{1}{12} - \frac{13b}{480} + \frac{2d}{b^3} \left(1 + \frac{6d}{b^2}\right) + \dots \quad (2.5.7)$$

$$J=2I+\frac{1}{2}, \quad Q_{R(e)} = \frac{1}{2b} + \frac{7}{24} + \frac{167b}{960} + \frac{d}{b^3} \left(1 + \frac{6d}{b^2}\right) + \dots \quad (2.5.8)$$

$$J=2I+\frac{3}{2}, \quad Q_{R(o)} = \frac{1}{2b} - \frac{5}{24} - \frac{193b}{960} + \frac{d}{b^3} \left(1 + \frac{6d}{b^2}\right) + \dots \quad (2.5.9)$$

$$Q_{R3} = s_1 Q_{R(e)} + s_2 Q_{R(o)} \quad (2.5.10)$$

Where: $Q_R(e)$ is the sum over levels with $(J-1/2)$ even,

$Q_R(o)$ is the sum over levels with $(J-1/2)$ odd,

and s_1 and s_2 the respective statistical weights due to

nuclear spin.

Q_{R1} is evaluated from (2.5.6) for odd multiplicities, i.e. the molecule has an even number of electrons, and any Λ , the electronic orbital angular momentum, for either homonuclear or heteronuclear molecules, with J taking integer values. Most of the diatomic molecules fall into this category, as it must include all homonuclear molecules, except those that are charged, as there are an even number of electrons. Such examples include CO, C_2 , NH, H_2 etc. Moreover, most of these molecules have a Σ , i.e. $\Lambda = 0$ ground state, making the calculation of the band spectra relatively straightforward.

Q_{R2} is evaluated from (2.5.7) for even multiplicities, i.e. an odd number of electrons, and any Λ for heteronuclear molecules, but is restricted to values of $\Lambda > 0$ for homonuclear molecules, with J taking half integer values. As there are an odd number of electrons, any homonuclear molecules considered must have an odd charge, hence neutral homonuclears are excluded. Also, the above mentioned restriction is due to the alternation of the statistical weights of the rotational levels when there are two identical nuclei, however, when $\Lambda > 0$, there are very close pairs of levels of opposite symmetry and the effects of the statistical weights cancel out, so (2.5.7) can be applied. Such examples include, CaH, CH, CN, OH etc., and O_2^+ is a valid example of a charged homonuclear molecule.

Q_{R3} is evaluated by summing separately alternate levels from (2.5.8) and (2.5.9) and combining them together in (2.5.10), taking account of nuclear spin. Q_{R3} covers those molecules that are not dealt with in the previous two cases, and is relevant for even multiplicities with $\Lambda = 0$ for homonuclear molecules. Such molecules with even multiplicities must have odd positive or negative charges, and have a Σ ground state, e.g. H_2^+ and O_2^+ . As $Q_{R2} = Q_R(e) + Q_R(o)$ and $s_1 + s_2 = 1$, then since, except for large b , $Q_R(e) \approx Q_R(o)$ and hence $Q_{R3} \approx Q_{R2}$, we can calculate Q_{R2} directly from (2.5.7). Because of the above restrictions, the molecule in question would have very low abundances and the increased complexity in the program for handling Q_{R3} , it was decided to omit the method of Q_{R3} from the program, and apply Q_{R2} where relevant. The Q_{R3} method is thus included in this discussion for completeness.

It is found that even for the worst possible case, i.e. H_2 at $1000^\circ K$, with $b < 0.1$, all higher order terms that are omitted from (2.5.6) to (2.5.9) are negligible. Also, if non-rigidity is neglected, and for reasonably small values of b , Q_{R1} , Q_{R2} and Q_{R3} reduce to approximately $1/b$, or kT/Bhc , the standard approximation for the rotational partition function.

If B_e is not known, it can be calculated from (2.5.4), where:

$$\bar{I}_e = \frac{\mu r_e^2}{N_A} \quad (2.5.11)$$

where r_e is the equilibrium internuclear separation in cm, μ the

reduced mass in amu and N_A Avogadro's number, hence:

$$B_e = \frac{N_A h}{8\pi^2 c \mu r_e^2} \quad (2.5.12)$$

Also, if D_e is not known, it can be found from:

$$D_e = \frac{4 B_e^3}{\omega_e^2} \quad (2.5.13)$$

where ω_e is the harmonic vibrational constant of the molecule, see next section.

The rotational statistical weight obtained by the above method is strictly correct only for Σ states, as for states with $\Lambda > 0$ there are missing levels that have to be corrected for, in addition for multiplet states there can be a very large separation of levels that differ in Σ , the projection of the electron spin on the internuclear axis, but have the same total angular momentum apart from spin, i.e. Hund's case (a) for strong spin coupling.

For singlet states with $\Lambda > 0$, we evaluate (2.5.6) which includes the contribution from the non-existent levels $J = 0 \dots \Lambda - 1$ which must be removed by evaluating the sum of (2.5.5) only up to $\Lambda - 1$ then subtracting this from (2.5.6). The zero point of energy must now be moved up to the first level that exists, i.e. $J = \Lambda$ which is accomplished by dividing by the Boltzmann factor for this level. We thus calculate:

$$Q = \left[Q_{R1} - \sum_{J=0}^{\Lambda-1} (2J+1) e^{-\epsilon J(J+1) + d J^2 (J+1)^2} \right] \times e^{\epsilon \Lambda(\Lambda+1) - d \Lambda^2 (\Lambda+1)^2} \quad (2.5.14)$$

For multiplet states we have the additional complication of electron spin to consider. In Hund's case (b) for weak spin coupling, the splitting of levels due to spin that have the same total angular momentum apart from spin is small, and the $2S+1$ ladders in the energy level diagram, with S being the electron spin, can be treated as a single ladder with each level having an additional $2S+1$ statistical weight factor. In practice this factor is put into the electronic statistical weight and (2.5.14) is evaluated in exactly the same way as for the singlets, except that the quantum number N , the total angular momentum quantum number apart from spin, is used in place of J with N always taking integer values hence (2.5.6) is used. Hund's case (b) is always applicable to Σ states.

For Hund's case (a) where the spin splitting is large, we have $2S+1$ separate ladders to consider with different Boltzmann factors so the $2S+1$ cannot be factorized out as before.

From Kovács (31) a good approximation to the term values for Hund's case (a) is given by:

$$F(J) = A\Lambda\Sigma + B[J(J+1) - \Omega^2 + S(S+1) - \Sigma^2] \quad (2.5.15)$$

where A is the spin-orbit coupling constant such that the larger $|A|$ is the better is (2.5.15) as an approximation to case (a), with strict case (b) occurring when $A = 0$ and (2.5.15) is in that case invalid. $\Sigma = S \dots -S$, $\Omega = |\Lambda + \Sigma|$ and there are $2S+1$ ladders given by $|\Lambda+S| \dots |\Lambda-S|$ where $J = \Omega, \Omega+1 \dots$, hence putting $J = 0$ into (2.5.15)

gives us the origin for each ladder even if that level does not exist. The rotational partition function is then found by first obtaining the relative partition function for each ladder from its origin using (2.5.6) or (2.5.7) depending on J being integer or half integer respectively, and subtracting off the contribution to the series from any non-existent levels for $J < \Omega$ like above for case (b). Putting $J = \Omega$ into (2.5.15) gives us the lowest level that actually exists for each ladder, hence the lowest energy level of all is found by taking the minimum of (2.5.15) over all values of Σ . Using this minimum as our new zero point in energy, the Boltzmann factor for each ladder relative to this point is applied and weighted functions are added together giving the final rotational partition function.

Because of spin uncoupling for large enough values of J , case (b) is eventually approached, accordingly, even for non-zero values of A , the case (b) partition function may be a better approximation if those levels most heavily populated are better represented by case (b). If the relative population of each level is given by:

$$p = (2N + 1) e^{-bN(N+1)} \quad (2.5.16)$$

neglecting non-rigidity, the most populated level is given by $N_{\max} = \text{int}(N_* + 0.5)$ where:

$$N_* = \sqrt{\frac{1}{2b}} - \frac{1}{2} \quad (2.5.17)$$

and where N_{\max} is the nearest integer to N_* . Also with $Y = A/B$, if $|Y| \gg N(N+1)$ case (a) is a good approximation (in which case N loses

its meaning as a quantum number though we can still use it notionally), and if $|Y| \ll N(N+1)$ case (b) is a good approximation. Thus, inserting this criterion in (2.5.17):

$$\text{use case (a) if } |Y| > \frac{1}{2b} - \frac{1}{4} \tag{2.5.18}$$

$$\text{use case (b) if } |Y| < \frac{1}{2b} - \frac{1}{4}$$

where either case will obviously be better the further from the changeover we are.

If Y_* is $|Y|$ at the changeover in (2.5.18), and if $A_* = Y_* B$, we can write:

$$A_* = \frac{kT}{2hc} - \frac{B}{4} \tag{2.5.19}$$

such that interestingly A_* is almost independent of B and dependent only on the temperature, as $kT/2hc \gg B/4$ for the temperatures of interest.

However, in the temperature range of interest, it is indeed found that in practice the case (b) approximation is the better one on the basis of the criterion above, even for relatively large values of $|Y|$, due to the smallness of b . Only for some unusual molecules like SnH , which we are unlikely to consider, would $|Y|$ be large enough for case (a) to be a better approximation for some of the temperatures we need consider.

Neglecting non-rigidity and other higher order terms, Kovács (31) gives an expression for the Hund's case (b) approximation:

$$F(N) = B[N(N+1) - \Lambda^2] + A\Lambda^2 \frac{J(J+1) - N(N+1) - S(S+1)}{2N(N+1)} \quad (2.5.20)$$

which differs from (2.5.15) in that here $|Y| \ll N(N+1)$ and case (b) is a good approximation, with the second term representing the deviation from pure case (b) if $A \neq 0$. Unfortunately, the correction term cannot be integrated analytically, in addition to which at small values of N it is no longer valid, as we are in the case (a) regime where (2.5.15) is a better approximation. However, except in unusual cases, the maximum populated levels occur at large enough values of N to be well into the case (b) regime and where the correction term is negligible, and accordingly we do not consider it.

Finally, it must be remembered that (2.5.15) and (2.5.20) as well as more detailed expressions given by Kovács in the case (a) and (b) limits are only approximations. In section 4.2 where we discuss how the rotational lines in the spectra of diatomic molecules are computed, explicit formulae for general coupling cases between (a) and (b) are used for doublets and triplets. Unfortunately, no formulae exist for general multiplicities with general coupling.

2.6 Determination of Vibrational Partition Functions of Diatomic Molecules

The vibrational term values in cm^{-1} are expressed as:

$$G(v) = \omega_e \left(v + \frac{1}{2}\right) - \omega_e x_e \left(v + \frac{1}{2}\right)^2 + \omega_e y_e \left(v + \frac{1}{2}\right)^3 + \dots \quad (2.6.1)$$

where v is the vibrational quantum number that takes integer values $v = 0, 1, 2, \dots$ unlike J , there are no complications with missing lower levels or half integer values. Also ω_e is the harmonic oscillator constant and $\omega_e x_e, \omega_e y_e \dots$ are terms in the anharmonicity with higher order terms being neglected.

As with the rotational constants, for convenience we convert the above constants into dimensionless form, hence $W_e = hc\omega_e/kT$, $W_e X_e = hc\omega_e x_e/kT$ and $W_e Y_e = hc\omega_e y_e/kT$. Then the vibrational partition function, after allowing for the zero point energy, is:

$$Q_v = \sum_{v=0}^{\infty} \exp\left[-W_e v + W_e X_e v(v+1) - W_e Y_e v\left(v^2 + \frac{3v}{2} + \frac{3}{4}\right)\right] \quad (2.6.2)$$

In common with finding the rotational partition function, an efficient way of obtaining Q_v is to replace the sum in (2.6.2) by a series using the method of Kassel (38). Relative to the $v = 0$ level, the term values can be expressed as a power series in v whose coefficients in units of kT/hc are given by:

$$W_0 = W_e - W_e X_e + \frac{3}{4} W_e Y_e$$

$$W_0 X_0 = W_e X_e - \frac{3}{2} W_e Y_e \quad (2.6.3)$$

$$W_0 Y_0 = W_e Y_e$$

Also let:

$$Z = e^{-W_0} \quad (2.6.4)$$

Then an analytic approximation to the partition function of the anharmonic oscillator is:

$$\begin{aligned} Q_r = & \frac{1}{(1-Z)} + W_0 X_0 Z \frac{(1+Z)}{(1-Z)^3} + (W_0 X_0)^2 Z \frac{(1+11Z+11Z^2+Z^3)}{2(1-Z)^5} \\ & + (W_0 X_0)^3 Z \frac{(1+57Z+302Z^2+302Z^3+57Z^4+Z^5)}{6(1-Z)^7} \\ & - W_0 Y_0 Z \frac{(1+4Z+Z^2)}{(1-Z)^4} \\ & - (W_0 X_0)(W_0 Y_0) Z \frac{(1+26Z+66Z^2+26Z^3+Z^4)}{(1-Z)^6} \end{aligned} \quad (2.6.5)$$

where higher order terms in $W_0 X_0$, $W_0 Y_0$ and cross terms are neglected.

2.7 Determination of the Electronic and Total Partition Functions and Equilibrium Constants of Diatomic Molecules

The electronic statistical weight of the i^{th} electronic level neglecting spin splitting, by Tatum (39) is:

$$g_{e_i} = (2 - \delta_{0, \Lambda_i})(2S_i + 1) \quad (2.7.1)$$

where $2S_i + 1$ is the spin multiplicity and δ_{0, Λ_i} the Kronecker delta, such that $\delta_{0, \Lambda_i} = 1$ when $\Lambda_i = 0$ and $\delta_{0, \Lambda_i} = 0$ when $\Lambda_i \neq 0$.

If the first excited electronic state in the molecule is very high with a negligible population, and the substates of the ground state, if there are any, are very close together with very similar rotational and vibrational constants, as occurs in Hund's case (b), then indeed the electronic partition function $Q_E = g_{e_1}$, and if Q_R and Q_V are known, Q_I is immediately found from (2.5.1); this situation is realized for many molecules.

As already explained in section 2.5, if the spin splitting of the electronic state is large, the spin multiplicity is imbedded in the rotational partition function and the definition in (2.7.1) is incorrect. However, for convenience we can retain the $(2 - \delta_{0, \Lambda_i})$ factor in (2.7.1) as the definition of g_{e_i} . Further, if this is the ground state and excited electronic states are neglected, we can still regard this as the electronic partition function. For any degree of

spin coupling, the same vibrational and rotational constants are assumed to apply in the different members of a multiplet, as in practice this would introduce at worst small errors.

However, if the excited electronic states are sufficiently populated to alter the total partition function, then in general the rotational and vibrational constants in these states will be different and we must compute individually the partition functions of each electronic state weighted with the appropriate Boltzmann factor and summed. Thus the total partition function is:

$$Q_1 = Q_S \sum_i g_{e_i} Q_{R_i} Q_{V_i} e^{-T_{0_i} hc/kT} \quad (2.7.2)$$

where Q_{R_i} and Q_{V_i} are the rotational and vibrational partition functions respectively for the i^{th} electronic state, and T_{0_i} is the energy of that state in cm^{-1} after allowing for the zero point energy.

By direct analogy to Saha's equation of ionization equilibrium of atoms, the dissociation equilibrium of diatomic molecules can be written as:

$$K_{ij} = \frac{N_i N_j}{N_{ij}} = (2\pi\mu_{ij}kT/h^2)^{3/2} e^{-D_0^0/kT} \frac{Q_i Q_j}{Q_{ij}} \quad (2.7.3)$$

where K_{ij} is the equilibrium constant as defined in section 2.4, or in log form we can write:

$$\log\left(\frac{N_i N_j}{N_{ij}}\right) = 20.2735 + \frac{3}{2} \log \mu_{ij} + \frac{3}{2} \log T - \theta D_0^0 + \log\left(\frac{Q_i Q_j}{Q_{ij}}\right) \quad (2.7.4)$$

where $N_i, N_j, N_{ij}, Q_i, Q_j$ and Q_{ij} are the number densities and partition functions of the atoms and molecules, and in (2.7.4) μ_{ij} is the reduced mass in amu defined as:

$$\mu_{ij} = \frac{m_i m_j}{m_i + m_j} \quad (2.7.5)$$

$\theta = 5039.935/T$ and D_0^0 is the dissociation energy in eV of the lowest electronic state taken from the lowest vibrational level, with the zero superscript being used to distinguish this from the non-rigidity constant. Hence the equilibrium constants are known, and can be used to calculate the abundances of diatomic molecules.

2.8 Isotopic Shifts of Rotational and Vibrational Constants of Diatomic Molecules

When isotopes are substituted in a molecule, the force constants remain the same between the constituent atoms but the masses are changed, with the result that both the rotational and vibrational constants, hence their energy levels, are changed. Also, the symmetry can change, as already mentioned, and the statistical weights of the rotational levels depend on the spins of the nuclei if the molecule is homonuclear.

From Herzberg (29), let:

$$\rho = \sqrt{\frac{\mu}{\mu^I}} \quad (2.8.1)$$

where μ and μ^I are the reduced masses of the original and the isotopically substituted molecule respectively. Then for the various rotational and vibrational constants:

$$\begin{aligned} \omega_e^I &= \rho \omega_e, \quad \omega_e^I x_e^I = \rho^2 \omega_e x_e, \quad \omega_e^I y_e^I = \rho^3 \omega_e y_e \\ B_e^I &= \rho^2 B_e, \quad D_e^I = \rho^4 D_e, \quad \alpha_e^I = \rho^3 \alpha_e, \quad \beta_e^I = \rho^5 \beta_e \end{aligned} \quad (2.8.2)$$

with α_e and β_e not being needed until the spectrum is computed, but the other constants are used to obtain the isotopic partition functions.

Although the electronic potential wells are not affected by isotopic substitution, as the dissociation potential used in the previous section is measured from the lowest vibrational level, which is shifted, this must be allowed for; likewise this must be done for the electronic energy of any excited states being considered. Thus we make use of (4.3.7) and (4.3.9) for correcting the electronic energy of an excited state and the dissociation potential respectively, where by convention, the single and double primes refer to an upper and lower state respectively, with the latter in this case being the ground electronic state.

Hence for the original molecule, if $D_e^{0''}$ and T_e' are given they are converted to $D_0^{0''}$ and T_0' respectively for use in the determination of the partition function and equilibrium constant. Then for isotopically substituted molecules, (4.3.9) and if necessary (4.3.7) are used with $\frac{I}{e}$ etc. to obtain $D_0^{0''I}$ and $T_0'^I$. If however, $D_0^{0''}$, T_0'' and T_0' are given for the original molecule, we must obtain the constants from the equilibrium positions first using (4.3.7) and (4.3.9) before proceeding as mentioned.

Finally, when dealing with a molecule that has two atoms of the same charge, we have the additional complication of having to distinguish between those molecules with identical nuclei for which $Q_S = 1/2$, and those with different nuclei for which $Q_S = 1$. Of course, only the latter can occur for the isotopic forms if the two nuclei have different charges. As mentioned in section 2.5, for homonuclear molecules, there is in addition an alternation of the statistical

weights of the rotational levels due to the nuclear spin, however, this has a negligible effect on the rotational partition function, but is important when computing the band spectra, and is accordingly discussed in that section. This is because at the temperatures of interest, there is hardly any difference numerically between summing the even and odd levels separately, then adding the sums together with the appropriate weights, and summing all the levels in one.

2.9 Introduction to Triatomic Molecules

The treatment of triatomic molecules is analogous to that of diatomic molecules, but there is much greater complexity, as the molecules can have up to five different point groups and the arrangement of the atoms has to be specified. Also, the isotopic shifts are often non-trivial to evaluate. The following table lists the possible point groups that have to be considered for diatomic and triatomic molecules.

Table (2.1) of Molecular Point Groups

<u>Type of Molecule</u>	<u>Point Group</u>	<u>σ</u>	<u>Examples</u>
Linear Symmetric	$D_{\infty h}$	2	H_2 , CO_2
Linear Non-Symmetric	$C_{\infty v}$	1	OH, HCN
Bent Symmetric	C_{2v}	2	H_2O
Bent Non-symmetric	C_s	1	HNO
Equilateral Triangle	D_{3h}	6	H_3^+

As with diatomic molecules, for the symmetry type to be valid if two atoms have the same charges, they must be identical isotopes, thus $^{16}O^{12}C^{16}O$ belongs to $D_{\infty h}$, but as soon as the molecule is unsymmetrically isotopically substituted e.g. $^{16}O^{12}C^{17}O$, then it belongs to $C_{\infty v}$. Likewise C_{2v} will go over to C_s if H_2O is substituted to give HOD. However, any single substitution in a D_{3h} molecule will make it go over to C_{2v} , and an additional substitution to give three

different isotopes will put the molecule into the C_s point group, see the discussion on H_3^+ in section 5.4.

In the more detailed table below are shown the numbers and symmetries of isotopically substituted diatomic and triatomic molecules, where the substituted molecules include the initial molecules that have the highest possible symmetry. Let x , y and z be the number of isotopes belonging to elements X, Y and Z respectively, N be the total number of different isotopic molecules and M be the number belonging to some particular point group. When the point groups are given in pairs, they refer to a non-linear and linear case respectively.

Table (2.2) of Possible Isotopic Substitutions

<u>A</u>	<u>B</u>	<u>C</u>	<u>N</u>	<u>D</u>	<u>M</u>
X_2	$D_{\infty h}$	C_2	$x(x+1)/2$	$\left\{ \begin{array}{l} D_{\infty h} \\ C_{\infty v} \end{array} \right.$	$\begin{array}{l} x \\ x(x-1)/2 \end{array}$
XY	$C_{\infty v}$	CO	xy	$C_{\infty v}$	xy
X_3	D_{3h}	H_3^+	$x(x+1)(x+2)/6$	$\left\{ \begin{array}{l} D_{3h} \\ C_{2v} \\ C_s \end{array} \right.$	$\begin{array}{l} x \\ x(x-1) \\ x(x-1)(x-2)/6 \end{array}$
X_3	$C_{2v}, D_{\infty h}$	O_3, C_3	$x^2(x+1)/2$	$\left\{ \begin{array}{l} C_{2v}, D_{\infty h} \\ C_s, C_{\infty v} \end{array} \right.$	$\begin{array}{l} x^2 \\ x^2(x-1)/2 \end{array}$
XYX	$C_{2v}, D_{\infty h}$	H_2O, CO_2	$xy(x+1)/2$	$\left\{ \begin{array}{l} C_{2v}, D_{\infty h} \\ C_s, C_{\infty v} \end{array} \right.$	$\begin{array}{l} xy \\ xy(x-1)/2 \end{array}$
XXY	$C_s, C_{\infty v}$	S_2O, N_2O	x^2y	$C_s, C_{\infty v}$	x^2y
XYZ	$C_s, C_{\infty v}$	HCO, HCN	xyz	$C_s, C_{\infty v}$	xyz

Where column A gives the molecule type, B the highest symmetry point group, C examples, D the possible point groups of the isotopic variants and N and M have the meanings as stated above.

Any charged triatomic molecules are considered as quite separate, as is the case with diatomic molecules, and triatomic molecules can split up in a number of ways of which only one need be specified. Thus considering the complete dissociation of HCN, we need only consider the equilibrium:



provided we have already specified for diatomic molecules the equilibrium:



so the system is complete.

Thus when treating the triatomic molecules, the dissociation products must match the species already in the list of atoms and diatomic molecules to give a self contained system.

In many cases when isotopic substitution is considered, it is necessary to know the central atom in order to identify the force constants with the appropriate bonds, and to distinguish say HCN from HNC which are regarded as quite separate molecules.

In keeping with the treatment of diatomic molecules, excited states are also considered, and insufficient data in any state will lead to that state being rejected, the whole molecule being rejected if the ground state is insufficiently specified.

As with the diatomic molecules, the object of determining the partition functions of triatomic molecules is to obtain the equilibrium constants which are needed in computing the molecular abundances by iteration. The equilibrium constant for complete dissociation of a triatomic molecule is defined as:

$$K_{ijk} = \frac{N_i N_j N_k}{N_{ijk}} \quad (2.9.1)$$

which is the ratio of the products of the abundances of the free atoms i , j and k to the combined molecule ijk . Again, as for diatomic molecules, in the limit of complete association, $K_{ijk} = 0$ and complete dissociation $K_{ijk} \rightarrow \infty$, with the units we are working in being in cm^{-6} . Because the equilibrium constants for diatomic and particularly triatomic molecules can have values ranging over many orders of magnitude, care has to be exercised in programming to avoid excessively large or small floating point numbers. The determination of the equilibrium constants is discussed in section 2.12.

2.10 Determination of Rotational Partition Functions of Triatomic Molecules

If the molecule is linear, the rotational partition function is calculated in the same way as for diatomic molecules in section 2.5, neglecting the coupling between rotation and vibration and in addition vibronic motion. If there is also electronic orbital angular momentum or spin, this interacts with the vibronic motion in a complex manner considered beyond the scope of this work, see Herzberg (34), and accordingly we just assume Hund's case (b) as treated in section 2.5. In most cases this does not arise, as for most linear molecules of interest, the ground vibrational level is a $^1\Sigma$ state.

For non-linear molecules, an approximation to the rotational partition function by Herzberg (30) is:

$$Q_R = \sqrt{\frac{\pi}{ABC} \left(\frac{kT}{hc}\right)^3} \quad (2.10.1)$$

where:

$$A = \frac{h}{8\pi^2 c I_A}, \quad B = \frac{h}{8\pi^2 c I_B}, \quad C = \frac{h}{8\pi^2 c I_C} \quad (2.10.2)$$

such that I_A , I_B and I_C are the principal moments of inertia. By convention: $I_A \leq I_B \leq I_C$, hence $A \geq B \geq C$. As the three atoms define a plane, the identities:

$$I_A + I_B = I_C \quad \text{or} \quad 1/A + 1/B = 1/C \quad (2.10.3)$$

are always valid.

For non-linear molecules, there appears to be no simple way of incorporating non-rigidity into the calculation of the rotational partition function, which is calculated simply on the basis of a rigid molecule. In fact, the constants for non-rigidity are generally not readily available for such molecules.

If A, B and C are not known, they can be calculated from molecular geometry, see section 2.13. In fact, it is convenient to do this anyway as such calculations are necessary when isotopic versions are considered.

2.11 Determination of Vibrational Partition Functions of Triatomic Molecules

As with section 2.6 in the case of diatomic molecules, we can find an analytic expression that gives the vibrational partition functions for triatomic molecules, taking into account some of the anharmonic terms.

A triatomic molecule will have three different modes of vibration, of which one is doubly degenerate if the molecule is linear. The vibrational term values in cm^{-1} with first order anharmonicity, are given by the expression:

$$\begin{aligned}
 G(v_1, v_2, v_3) = & \omega_1(v_1 + \frac{1}{2}) + \omega_2(v_2 + \frac{d}{2}) + \omega_3(v_3 + \frac{1}{2}) \\
 & + x_{11}(v_1 + \frac{1}{2})^2 + x_{22}(v_2 + \frac{d}{2})^2 + g_{22}l_2^2 + x_{33}(v_3 + \frac{1}{2})^2 \\
 & + x_{12}(v_1 + \frac{1}{2})(v_2 + \frac{d}{2}) + x_{13}(v_1 + \frac{1}{2})(v_3 + \frac{1}{2}) + x_{23}(v_2 + \frac{d}{2})(v_3 + \frac{1}{2})
 \end{aligned} \tag{2.11.1}$$

Where: v_i are the vibrational quantum numbers,

ω_i are the harmonic constants,

x_{ij} are the lowest anharmonic constants,

l_2 and g_{22} the vibronic quantum number and associated

coupling constant which are only defined for linear molecules,

see section 5.2.

In order to obtain a reasonable analytic expression, the cross terms involving x_{12} , x_{13} and x_{23} together with higher order terms are neglected. Numerical tests show this approximation to be acceptable. Also, because of the relative smallness of the g_{22} term when defined, this can be neglected, leaving for linear molecules a vibrational statistical weight factor g_{v_2} of v_2+1 . Thus:

$$\begin{aligned} d = 1, & \quad g_{v_2} = 1 \text{ for non-linear molecules,} \\ d = 2, & \quad g_{v_2} = v_2 + 1 \text{ for linear molecules,} \end{aligned}$$

where d is the degeneracy of the v_2 mode appearing in (2.11.1).

As in section 2.6, the term values can be expressed relative to the lowest vibrational level, giving:

$$\begin{aligned} W_1 &= (\omega_1 + x_{11}) \frac{hc}{RT} \\ W_2 &= (\omega_2 + dx_{22}) \frac{hc}{RT} \\ W_3 &= (\omega_3 + x_{33}) \frac{hc}{RT} \\ X_{ii} &= x_{ii} \frac{hc}{RT}, \quad i = 1, 2, 3 \end{aligned} \tag{2.11.2}$$

Then the vibrational partition function is given by:

$$Q_v = \sum_{v_1=0}^{\infty} \sum_{v_2=0}^{\infty} \sum_{v_3=0}^{\infty} g_{v_2} \exp \left[-W_1 v_1 - W_2 v_2 - W_3 v_3 - X_{11} v_1^2 - X_{22} v_2^2 - X_{33} v_3^2 \right] \tag{2.11.3}$$

which is to be replaced by an analytic approximation, hence putting:

$$Z_i = e^{-W_i} \tag{2.11.4}$$

the same treatment can be applied as before. Because we have neglected the cross terms, the vibrational partition function can be written as:

$$Q_v = Q_{v_1} Q_{v_2} Q_{v_3} \quad (2.11.5)$$

The complete analytic approximation to the vibrational partition function of a triatomic molecule is given by:

$$\begin{aligned} Q_v = & \prod_{i=1}^3 \left[\frac{1}{(1-z_i)} - X_{ii} z_i \frac{(1+z_i)}{(1-z_i)^3} \right. \\ & + X_{ii}^2 z_i \frac{(1+11z_i+11z_i^2+z_i^3)}{2(1-z_i)^5} \\ & \left. - X_{ii}^3 z_i \frac{(1+57z_i+302z_i^2+302z_i^3+57z_i^4+z_i^5)}{6(1-z_i)^7} \right. \\ & + (d-1)\delta_{i,2} \left\{ \frac{z_2}{(1-z_2)^2} - X_{22} z_2 \frac{(1+4z_2+z_2^2)}{(1-z_2)^4} \right. \\ & \left. \left. + X_{22}^2 z_2 \frac{(1+26z_2+66z_2^2+26z_2^3+z_2^4)}{2(1-z_2)^6} \right\} \right] \quad (2.11.6) \end{aligned}$$

where $(d-1)\delta_{i,2} = 1$ when $i = 2$ and the molecule is linear, otherwise $(d-1)\delta_{i,2} = 0$ and the last set of terms is not evaluated.

For the special case of a molecule with a D_{3h} point group, there are only two modes of vibration, v_1 and v_2 with v_2 being doubly degenerate, thus all terms involving v_3 are dropped and (2.11.6) is evaluated as for a linear molecule with $(d-1)\delta_{i,2} = 1$ but $i = 1$ or 2 only. Thus the above expression can be used for all triatomic molecules.

2.12 Determination of Total Partition Functions and Equilibrium

Constants of Triatomic Molecules

The total partition function for a triatomic molecule can be computed from the general formula (2.7.2) in exactly the same way as in the case of diatomic molecules. If the molecule is non-linear, (2.7.1) has no meaning but the electronic statistical weight can be obtained from the electronic species of the state considered.

The dissociation equilibrium equation of a triatomic molecule splitting up into an atom and diatomic molecule can be very easily obtained from (2.7.4) by replacing one of the atoms by a diatomic molecule.

Thus for $ijk \leftrightarrow ij + k$:

$$\log \left(\frac{N_{ij} N_k}{N_{ijk}} \right) = 20.2735 + \frac{3}{2} \log \mu_{ijk} + \frac{3}{2} \log T \quad (2.12.1)$$

$$- \theta D_{ij;k} + \log \left(\frac{Q_{ij} Q_k}{Q_{ijk}} \right)$$

where $D_{ij;k}$ is the dissociation potential from the lowest vibrational level of the triatomic molecule ijk into atom k and diatomic molecule ij , and:

$$\mu_{ijk} = \frac{(m_i + m_j) m_k}{m_i + m_j + m_k} \quad (2.12.2)$$

the reduced mass of the molecule for the specific dissociation in

amu. The associated equilibrium constant is:

$$K_{ij;k} = \frac{N_{ij} N_k}{N_{ijk}} \quad (2.12.3)$$

However, it is the total dissociation equilibrium which is required, i.e. $ijk \leftrightarrow i + j + k$. Provided that the dissociation equilibrium $ij \leftrightarrow i + j$ has already been dealt with under the diatomic molecules, then with the partial dissociation $ijk \leftrightarrow ij + k$, the complete dissociation follows:

$$\log \left(\frac{N_i N_j N_k}{N_{ijk}} \right) = 40.5470 + 3 \log \mu_{ijk} + 3 \log T \quad (2.12.4)$$

$$- \theta D_{ijk} + \log \left(\frac{Q_i Q_j Q_k}{Q_{ijk}} \right)$$

where D_{ijk} is the total dissociation potential of the molecule, such that:

$$D_{ijk} = D_{ij} + D_{ij;k} \quad (2.12.5)$$

where D_{ij} is D_o^0 from (2.7.4), and μ_{ijk} in amu can be thought of as another reduced mass, such that:

$$\mu_{ijk}^2 = \mu_{ij} \mu_{ij;k} = \frac{m_i m_j m_k}{m_i + m_j + m_k} \quad (2.12.6)$$

Finally, as we actually deal with the dissociation in two steps, given K_{ij} and $K_{ij;k}$ as computed from (2.7.4) and (2.12.1) respectively, the complete dissociation equilibrium constant K_{ijk} , as defined in section 2.9, is given by:

$$K_{ijk} = K_{ij} K_{ijjk} = \frac{N_i N_j N_k}{N_{ijk}} \quad (2.12.7)$$

which is used in the iteration calculations.

2.13 Rotational Isotopic Shifts of Triatomic Molecules

If a molecule is isotopically substituted, then new rotational constants used to find the rotational partition function can be computed from the geometry of the molecule, rather than actually calculating the shifts in the constants, as is the case for diatomic molecules. There are usually small discrepancies between the rotational constants listed in the literature and those constants obtained from geometrical data in the same source, and are presumably due to effects of non-rigidity etc. and insufficiently accurate molecular data.

Let a triatomic molecule consist of the atoms with masses m_1 , m_2 and m_3 , with m_2 being the middle atom at which is located the bond angle α , such that for linear molecules $\alpha = 180^\circ$. Let s_{12} and s_{23} be the bond lengths joining the respective atoms, and the third side of the triangle s_{13} opposite m_2 being in some special cases also a bond; see figure (2.1), where the other quantities are the force constants, as discussed in the next section.

If the masses are given in grams and length in centimetres, then the rotational constants in cm^{-1} can be computed from the formulae:

$$C = \frac{h(m_1 + m_2 + m_3)}{8\pi^2 c [m_2(m_1 s_{12}^2 + m_3 s_{23}^2) + m_1 m_3 (s_{12}^2 + s_{23}^2 - s_{12} s_{23} \cos \alpha)]} \quad (2.13.1)$$

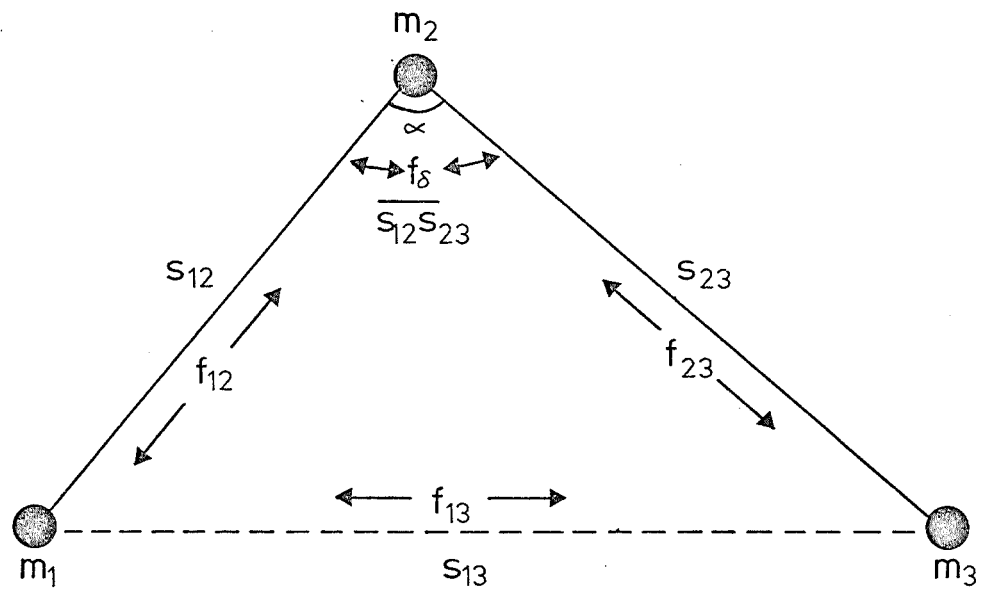


Fig. 2.1

or if s_{13} is given instead:

$$C = \frac{h(m_1 + m_2 + m_3)}{8\pi^2 c [m_1 m_2 s_{12}^2 + m_1 m_3 s_{13}^2 + m_2 m_3 s_{23}^2]} \quad (2.13.2)$$

$$A, B = \frac{1 \pm \sqrt{1 - 2kC^2}}{kC} \quad (2.13.3)$$

with the larger root being A, and where:

$$k = \frac{128\pi^4 c^2}{h^2} \cdot \frac{m_1 m_2 m_3 s_{12}^2 s_{23}^2 \sin^2 \alpha}{(m_1 + m_2 + m_3)} \quad (2.13.4)$$

which satisfy (2.10.3). If the masses are in amu and lengths in Å then (2.13.1) and (2.13.2) must be multiplied by $10^{16}/N_A$ and (2.13.4) by $10^{-32}/N_A$.

Thus given any isotopic masses, values of A, B and C can be obtained and substituted into (2.10.1) to obtain the rotational partition function if the molecule is non-linear.

If the bond angle is opened up so that in the limit the molecule becomes linear, then as $\alpha \rightarrow 180^\circ$, $k \rightarrow 0$ from (2.13.4) and it can be shown that $A \rightarrow \infty$, and $B \rightarrow C$ from (2.13.3) giving the simple rotator, whose partition function is discussed in section 2.5. If the non-rigidity constant D is known for the original molecule, then by analogy with the isotopic shifts in (2.8.2), we can write the isotopically shifted constant:

$$D^I = D \left(\frac{B^I}{B} \right)^2 \quad (2.13.5)$$

For a linear or bent triatomic molecule whose end atoms have the same charge, we have the same situation as discussed with diatomic molecules, needing to consider the statistical weights of the rotational levels due to nuclear spin only for the calculation of the spectrum, and using the appropriate value of Q_S . This also applies when all three nuclei are identical and equivalent i.e. D_{3h} point group.

The mathematics for deriving the expressions for the principal moments of inertia, hence the rotational constants in this section, is given in the appendices.

2.14 Vibrational Isotopic Shifts of Triatomic Molecules

The determination of isotopic shifts of triatomic molecules is a rather complex affair compared to the case of diatomic molecules, particularly in the most general case of a non-linear non-symmetric molecule i.e. point group C_s .

Using the same scheme as the previous section for designating the atoms and bonds, we include the force constants such that f_{12} and f_{23} are the stretching constants for the bonds s_{12} and s_{23} respectively and $f_s/s_{12}s_{23}$ is the bending constant at m_2 ; in some cases the coupling constant f_{13} between the atoms m_1 and m_3 is also used (see figure (2.1)). All force constants are in dyne cm^{-1} , ω is a vibrational frequency in cm^{-1} and ω^I is an isotopically shifted frequency.

The assumption of valence forces is used, and for symmetric molecules the coupling constant f_{13} is also employed as this allows for a more general force field (see Herzberg (30)). For non-symmetric molecules, f_{13} cannot be included in the equations as there would be too many unknowns with the method used.

It is assumed that isotopic substitution does not alter the molecular force constants, thus having solved for the force constants using the initial frequencies and atomic masses, we replace these masses by isotopes and using the force constants to obtain the

isotopically shifted vibrational frequencies. It is further assumed, without loss of generality, that if the two end atoms of the initial molecule belong to the same element, they will also be of the same isotopic form i.e. $O^{16}C^{12}O^{16}$ hence the molecule is symmetric. Thus isotopic substitution will cause a lowering or at best no change in symmetry. The somewhat artificial case of beginning with a molecule like $O^{18}C^{12}O^{16}$ would be considered only as a means of checking, but we do allow for this possibility.

As the treatment in determining isotopic shifts depends strongly on the symmetry of the initial and substituted molecules, it has to be divided up into five subsections A, B and C being for cases where as a result of substitution there is no lowering of symmetry, and D and E where the symmetry is lowered. The special case of the D_{3h} point group is considered as a subclass of C_{2v} and is accordingly handled as a symmetric bent molecule with all force constants and bond lengths equal. However, it is convenient here to depart from what is stated at the end of section 2.11 and consider the v_2 mode to be split into two vibrations such that $\omega_2 = \omega_3$. Then if the isotopic substitution lowers the symmetry to C_{2v} or C_s , the degeneracy is removed, $\omega_2 \neq \omega_3$, and in calculating the vibrational partition function, equation (2.11.6) is used for the general non-linear molecule. When $\omega_2 = \omega_3$, it follows that $x_{12} = x_{13}$ and $x_{22} = x_{23} = x_{33}$. Hirschfelder (40) discusses the vibrational frequencies and force constants of H_3^+ .

2.14A Symmetric Linear to Symmetric Linear or Symmetric Bent to Symmetric Bent

<u>Point Groups</u>	<u>Examples</u>
$D_{\infty h} \rightarrow D_{\infty h}$	$O^{16}C^{12}O^{16} \rightarrow O^{18}C^{12}O^{18}$
$C_{2v} \rightarrow C_{2v}$	$H_2O^{16} \rightarrow D_2O^{16}$
$D_{3h} \rightarrow D_{3h}$	$H_3^+ \rightarrow D_3^+$
$D_{3h} \rightarrow C_{2v}$	$H_3^+ \rightarrow H_2D^+$

Then $m_1 = m_3$, $s_{12} = s_{23}$, $f_{12} = f_{23}$ and as the following equations are general in α , for linear molecules we solve with $\alpha = 180^\circ$.

(i) Determination of the Force Constants

$$g_a = \frac{2\pi^2 c^2 m_1 m_2}{m_1(1+\cos\alpha) + m_2} \left[\omega_1^2 + \omega_2^2 + \sqrt{(\omega_1^2 - \omega_2^2)^2 - \frac{4\omega_1^2 \omega_2^2 m_1^2 \sin^2 \alpha}{m_2(2m_1 + m_2)}} \right] \quad (2.14.1)$$

$$g_t = \frac{4\pi^2 c^2 \omega_3^2 m_1 m_2}{m_1(1-\cos\alpha) + m_2} \quad (2.14.2)$$

$$g_s = \frac{8\pi^4 c^4 \omega_1^2 \omega_2^2 m_1^2 m_2}{g_a(2m_1 + m_2)} \quad (2.14.3)$$

Then:

$$f_{12} = \frac{g_a + g_t}{2}, \quad f_{13} = \frac{g_a - g_t}{2}, \quad f_s/s_{12}^2 = g_s \quad (2.14.4)$$

Equation (2.14.1) is in fact ambiguous, as there exists a negative root giving a second pair of values (g_a, g_b). However, it is found that the smallest $|g_a - g_b|$ is obtained by taking the positive root shown, also in practice $g_a > g_b$; the values so obtained agree with Herzberg (30).

Another difficulty may occasionally arise when the argument of the square root in (2.14.1) is negative, indicating that in that case the theory is insufficient as the force constants must be real quantities. In such cases there is no alternative but to set the quantity under the square root to zero and solve, since the negativity must be due to small inaccuracies in a quantity which is very small in any case.

(ii) Determination of the Isotopic Frequencies

Having obtained g_a , g_b and g_s from above, it is then possible to find the shift in vibrational frequencies when one or more atoms are substituted by isotopes, such that the molecule remains symmetric.

$$\omega_{1,2}^I = \frac{1}{2\pi c} \sqrt{\frac{1}{2m_1^{(i)}m_2^{(j)}} \left[G \pm \sqrt{G^2 - 8g_a g_s (2m_1^{(i)} + m_2^{(j)})m_2^{(j)}} \right]} \quad (2.14.5)$$

$$\omega_3^I = \frac{1}{2\pi c} \sqrt{\frac{g_b}{m_1^{(i)}m_2^{(j)}} \left[m_1^{(i)}(1 - \cos\alpha) + m_2^{(j)} \right]} \quad (2.14.6)$$

Where:

$$G = \left[m_1^{(i)}(1 + \cos\alpha) + m_2^{(j)} \right] g_a + 2 \left[m_1^{(i)}(1 - \cos\alpha) + m_2^{(j)} \right] g_s \quad (2.14.7)$$

where the two roots of (2.14.5) give ω_1^I and ω_2^I and the superscripts (i) and (j) denote isotopically substituted atoms.

The constant g_b can always be eliminated between (2.14.2) and (2.14.6), and if in addition $g_a = g_b$, i.e. $f_{13} = 0$, we can completely eliminate the force constants and express the shifts in frequencies as a function of atomic masses and the bond angle. Hence:

$$\left(\frac{\omega_1^I \omega_2^I}{\omega_1 \omega_2}\right)^2 = \frac{m_1^2 m_2}{m_1^{(i)2} m_2^{(j)}} \left[\frac{2 m_1^{(i)} + m_2^{(j)}}{2 m_1 + m_2} \right] \quad (2.14.8)$$

$$\left(\frac{\omega_3^I}{\omega_3}\right)^2 = \frac{m_1 m_2}{m_1^{(i)} m_2^{(j)}} \left[\frac{m_1^{(i)} (1 - \cos \alpha) + m_2^{(j)}}{m_1 (1 - \cos \alpha) + m_2} \right] \quad (2.14.9)$$

However, these last two equations are not used, as the individual values of ω_1^I and ω_2^I cannot be obtained, and the force constants are needed for non-symmetric substitutions of bent molecules (see subsection E); however, it could be a good check to determine them.

A useful check to see that the equations of part (ii) are the inverse of part (i), is to put the original masses into equations (2.14.5-7). If the square root in (2.14.1) has had to be dropped, as mentioned above, there will no longer of course be perfect agreement with the original frequencies, the amount of disagreement indicating the goodness of the approximation.

Finally, note that at no place do the bond lengths enter into the calculation.

2.14B Non-Symmetric Linear to Non-Symmetric Linear

<u>Point Group</u>	<u>Examples</u>
$C_{\infty v} \rightarrow C_{\infty v}$	$HC^{12}_N^{14} \rightarrow DC^{12}_N^{14}$
$C_{\infty v} \rightarrow C_{\infty v}$	$N_2^{14}O^{16} \rightarrow N^{14}_N^{15}O^{16}$

Then $m_1 \neq m_3$, $s_{12} \neq s_{23}$, $f_{12} \neq f_{23}$ and $\alpha = 180^\circ$.

(i) Determination of the Force Constants

$$f_{12} = \frac{2\pi^2 c^2 m_1 m_3}{(m_1 + m_2)} \left[\omega_1^2 + \omega_3^2 \pm \sqrt{(\omega_1^2 - \omega_3^2)^2 - \frac{4\omega_1^2 \omega_3^2 m_1 m_3}{m_2 (m_1 + m_2 + m_3)}} \right] \quad (2.14.10)$$

$$f_{23} = \frac{16\pi^4 c^4 \omega_1^2 \omega_3^2 m_1 m_2 m_3}{f_{12} (m_1 + m_2 + m_3)} \quad (2.14.11)$$

$$\frac{f_s}{s_{12}s_{23}} = \frac{4\pi^2 c^2 \omega_2^2 s_{12} s_{23}}{s_{12}^2/m_3 + s_{23}^2/m_1 + (s_{12} + s_{23})^2/m_2} \quad (2.14.12)$$

The two-fold ambiguity of equation (2.14.10) leading to two possible values of the pair (f_{12}, f_{23}) is analogous to equation (2.14.1), only in this case the two signs have been left as there appears to be no particular preference to one sign. This is no doubt due to both f_{12} and f_{23} being similar quantities, i.e. both stretching constants, unlike g_a and g_s , and often not being of dissimilar magnitude. However, it is still found that the root taken is the one

that gives the smaller $|f_{12} - f_{23}|$, in agreement with Herzberg (30).

As with (2.14.1) only more likely, is the possibility of a complex solution of (2.14.10), which indeed happens for N_2O . The explanation is clearly that $f_{12} \approx f_{23}$ as the two bonds are similar, so the argument of the square root should be close to zero, however, because the valence bond theory is an approximation, the argument can go slightly negative, giving the above problem. As with the previous subsection, the only alternative is to set the square root term to zero.

(ii) Determination of the Isotopic Frequencies

From the force constants obtained above, the new vibrational frequencies can be found when one or more atoms are isotopically substituted.

$$\omega_2^I = \frac{1}{2\pi c} \sqrt{\frac{f_3}{S_{12}^2 S_{23}^2} \left[\frac{S_{12}^2}{m_3^{(k)}} + \frac{S_{23}^2}{m_1^{(i)}} + \frac{(S_{12} + S_{23})^2}{m_2^{(j)}} \right]} \quad (2.14.13)$$

$$\omega_{1,3}^I = \frac{1}{2\sqrt{2}\pi c} \sqrt{F \pm \sqrt{F^2 - 4f_{12}f_{23} \frac{(m_1^{(i)} + m_2^{(j)} + m_3^{(k)})}{m_1^{(i)} m_2^{(j)} m_3^{(k)}}}} \quad (2.14.14)$$

Where:

$$F = f_{12} \left(\frac{1}{m_1^{(i)}} + \frac{1}{m_2^{(j)}} \right) + f_{23} \left(\frac{1}{m_2^{(j)}} + \frac{1}{m_3^{(k)}} \right) \quad (2.14.15)$$

where the roots of (2.14.14) give ω_1^I and ω_3^I .

The constant $f_{ij}/s_{12}s_{23}$ can be eliminated at once between (2.14.12) and (2.14.13) giving:

$$\left(\frac{\omega_3^I}{\omega_3}\right)^2 = \frac{S_{23}^2/m_i^{(i)} + S_{12}^2/m_3^{(k)} + (S_{12} + S_{23})^2/m_2^{(j)}}{S_{23}^2/m_i + S_{12}^2/m_3 + (S_{12} + S_{23})^2/m_2} \quad (2.14.16)$$

As before, a useful check is to put the original masses into equations (2.14.13-15), and again for a case like N_2O where a real solution has to be "patched up", disagreement between the calculated and original frequencies give an idea of the approximation.

2.14C Non-Symmetric Bent to Non-Symmetric Bent

<u>Point Group</u>	<u>Examples</u>
$C_s \rightarrow C_s$	$HC^{12}O^{16} \rightarrow DC^{12}O^{16}$
$C_s \rightarrow C_s$	$HN^{14}O^{16} \rightarrow DN^{14}O^{16}$

Then $m_1 \neq m_3$, $s_{12} \neq s_{23}$, $f_{12} \neq f_{23}$ and $\alpha < 180^\circ$. This is for the case where triatomic molecules have the lowest possible symmetry, thus the most general method has to be adopted.

Unlike the other cases discussed, it is unfortunately not possible to separate out the force constants and express them in terms of the known molecular properties. Instead, a set of three simultaneous equations has to be solved by iteration, starting with

trial values of the force constants. Having obtained a converged solution for the force constants, it is possible to do the reverse and calculate the isotopic vibrational frequencies. As the method for the latter is essentially the same, with the equations of a similar structure, it is relatively easy to use the same coding for both tasks. We use here the method from Lechner (41).

(i) Determination of the Force Constants

Let:

$$\frac{1}{\mu_{12}} = \frac{1}{m_1} + \frac{1}{m_2}, \quad \frac{1}{\mu_{23}} = \frac{1}{m_2} + \frac{1}{m_3}, \quad (2.14.17)$$

$$\frac{1}{\mu_0} = \frac{1}{\mu_{12} S_{12}^2} - \frac{2 \cos \alpha}{m_2 S_{12} S_{23}} + \frac{1}{\mu_{23} S_{23}^2}.$$

$$b_1 = 1 - \frac{\mu_{12} \mu_{23} \cos^2 \alpha}{m_2^2}, \quad b_2 = 1 - \frac{\mu_{12} \mu_0 \sin^2 \alpha}{m_2^2 S_{23}^2}, \quad (2.14.18)$$

$$b_3 = 1 - \frac{\mu_{23} \mu_0 \sin^2 \alpha}{m_2^2 S_{12}^2}, \quad c_0 = 1 - \frac{\mu_{12} \mu_{23}}{m_2^2}.$$

and also let the scaled force constants be:

$$F_1 = \frac{f_{12}}{4\pi^2 c^2 \mu_{12}}, \quad F_2 = \frac{f_{23}}{4\pi^2 c^2 \mu_{23}}, \quad F_3 = \frac{f_s}{4\pi^2 c^2 \mu_0} \quad (2.14.19)$$

Then the general equations relating the force constants to the vibrational frequencies are:

$$\begin{aligned} F_1 + F_2 + F_3 &= P \\ b_1 F_1 F_2 + b_2 F_1 F_3 + b_3 F_2 F_3 &= Q \quad (2.14.20) \\ c_0 F_1 F_2 F_3 &= R \end{aligned}$$

where:

$$\begin{aligned}
 P &= \omega_1^2 + \omega_2^2 + \omega_3^2 \\
 Q &= \omega_1^2 \omega_2^2 + \omega_1^2 \omega_3^2 + \omega_2^2 \omega_3^2 \\
 R &= \omega_1^2 \omega_2^2 \omega_3^2
 \end{aligned}
 \tag{2.14.21}$$

Clearly, equations (2.14.21) for the squares of the frequencies have a similar structure to equations (2.14.20) for the force constants.

Given ω_1 , ω_2 and ω_3 , P , Q and R are immediately found from (2.14.21), also given trial values of the force constants F_1' , F_2' and F_3' , P' , Q' and R' can be found from (2.14.20), then the differences, $\Delta P = P - P'$ etc. have to be made as small as possible. The trial values can be obtained from sources like Herzberg (30), or estimated from bonds of similar properties.

Equations (2.14.20) can be written in differential form:

$$\begin{aligned}
 \Delta F_1 + \Delta F_2 + \Delta F_3 &= \Delta P \\
 \Delta F_1 (b_1 F_2 + b_2 F_3) + \Delta F_2 (b_1 F_1 + b_3 F_3) + \Delta F_3 (b_2 F_1 + b_3 F_2) &= \Delta Q \\
 c_0 (F_2 F_3 \Delta F_1 + F_1 F_3 \Delta F_2 + F_1 F_2 \Delta F_3) &= \Delta R
 \end{aligned}
 \tag{2.14.22}$$

Then by writing:

$$\begin{bmatrix} 1 & 1 & 1 \\ D_{21} & D_{22} & D_{23} \\ D_{31} & D_{32} & D_{33} \end{bmatrix} \begin{bmatrix} \Delta F_1 \\ \Delta F_2 \\ \Delta F_3 \end{bmatrix} = \begin{bmatrix} \Delta P \\ \Delta Q \\ \Delta R \end{bmatrix}
 \tag{2.14.23}$$

where:

$$\begin{aligned}
 D_{21} &= b_1 F_2 + b_2 F_3, & D_{31} &= c_0 F_2 F_3, \\
 D_{22} &= b_1 F_1 + b_3 F_3, & D_{32} &= c_0 F_1 F_3, \\
 D_{23} &= b_2 F_1 + b_3 F_2, & D_{33} &= c_0 F_1 F_2,
 \end{aligned}
 \tag{2.14.24}$$

and the determinant D is given by:

$$\begin{aligned}
 D &= D_{22} D_{33} - D_{23} D_{32} + D_{23} D_{31} - D_{21} D_{33} \\
 &+ D_{21} D_{32} - D_{22} D_{31}
 \end{aligned}
 \tag{2.14.25}$$

Then (2.14.23) can be inverted directly giving:

$$\begin{aligned}
 \Delta F_1 &= [\Delta P(D_{22} D_{33} - D_{23} D_{32}) + \Delta Q(D_{22} - D_{33}) + \Delta R(D_{23} - D_{22})] / D \\
 \Delta F_2 &= [\Delta P(D_{23} D_{31} - D_{21} D_{33}) + \Delta Q(D_{33} - D_{31}) + \Delta R(D_{21} - D_{23})] / D \\
 \Delta F_3 &= [\Delta P(D_{21} D_{32} - D_{22} D_{31}) + \Delta Q(D_{31} - D_{32}) + \Delta R(D_{22} - D_{21})] / D
 \end{aligned}
 \tag{2.14.26}$$

Hence new trial values $F_i'' = F_i' + \Delta F_i$ are obtained, leading to P'' , Q'' and R'' from (2.14.20), and the whole process is repeated until convergence is reached. On convergence, F_1 , F_2 and F_3 are obtained, from which the force constants f_{12} , f_{23} and f_8 can be found from (2.14.19).

Convergence is assumed to have been reached when:

$$\frac{|\Delta F_1|}{F_1} + \frac{|\Delta F_2|}{F_2} + \frac{|\Delta F_3|}{F_3} < \xi \quad (2.14.27)$$

where typically, $\xi = 3 \times 10^{-6}$, i.e. the average change in the force constants from one iteration to the next is less than one part in a million.

(ii) Determination of the Isotopic Frequencies

Having obtained the force constants above, the isotopic vibrational frequencies can be obtained by inverting the whole problem. μ_{12}^I , μ_{23}^I and μ_0^I are found from $m_1^{(i)}$, $m_2^{(j)}$ and $m_3^{(k)}$ using equations (2.14.17), hence b_1^I , b_2^I , b_3^I and c_0^I are found from (2.14.18). Equations (2.14.19) can be used to write:

$$F_1^I = \frac{\mu_{12}}{\mu_{12}^I} F_1, \quad F_2^I = \frac{\mu_{23}}{\mu_{23}^I} F_2, \quad F_3^I = \frac{\mu_0}{\mu_0^I} F_3 \quad (2.14.28)$$

expressing the isotopic scaled force constants in terms of the scaled force constants of the initial molecule.

Equations (2.14.20) and (2.14.21) are used again, only with superscripts I to indicate isotopic shifts, and the whole problem is dealt with as before only in reverse.

Given F_1^I , F_2^I and F_3^I , P^I , Q^I and R^I can immediately be found from (2.14.20), and trial values ω_1^{-I} , ω_2^{-I} and ω_3^{-I} can be inserted into (2.14.21) to give P^{-I} , Q^{-I} and R^{-I} , whereby the differences $\Delta P^I = P^I - P^{-I}$ etc. are obtained. Obviously we can simply use the frequencies of the initial molecule as trial values for the isotopic molecule.

Equations (2.14.21) can be written in differential form, leading to a form like (2.14.22), only with F_i and ΔF_i replaced by $(\omega_i^I)^2$ and $\Delta(\omega_i^I)^2$ respectively, and putting $b_1 = b_2 = b_3 = c_0 = 1$; then it can be written as (2.14.23) and solved for $\Delta(\omega_i^I)^2$.

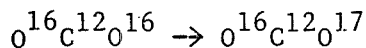
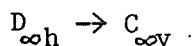
Hence new trial values for the next iteration are $(\omega_i^{II})^2 = (\omega_i^{-I})^2 + \Delta(\omega_i^I)^2$, with the same convergence criterion being applied as before. Thus on convergence, ω_1^I , ω_2^I and ω_3^I are obtained. As before, the method can be checked by inserting the original masses into part (ii).

The method described above for the point group C_s can certainly be applied for at least some of the cases described earlier, but is unnecessarily general as the much simpler formulae already discussed can be used.

2.14D Symmetric Linear to Non-Symmetric Linear

Point Groups

Example



Then after substitution, $m_1 \neq m_3$, $s_{12} = s_{23}$, $f_{12} = f_{23}$ and $\alpha = 180^\circ$.

(i) Determination of the Force Constants

As the initial molecule is linear and symmetric, this has already been discussed in A(i), with $\alpha = 180^\circ$. However, f_{13} has to be ignored as it cannot be used in cases of non-symmetric substitution.

(ii) Determination of the Isotopic Frequencies

The method used in B(ii) is applied, where (2.14.13) and (2.14.14) become:

$$\omega_2^I = \frac{1}{2\pi c} \sqrt{\frac{f_3}{S_{12}^2} \left[\frac{1}{m_3^{(k)}} + \frac{1}{m_1^{(i)}} + \frac{4}{m_2^{(j)}} \right]} \quad (2.14.29)$$

$$\omega_{1,3}^E = \frac{1}{2\sqrt{2}\pi c} \sqrt{F \pm \sqrt{F^2 - 4f_{12}^2 \frac{(m_1^{(i)} + m_2^{(j)} + m_3^{(k)})}{m_1^{(i)} m_2^{(j)} m_3^{(k)}}}} \quad (2.14.30)$$

Where:

$$F = f_{12} \left(\frac{1}{m_1^{(i)}} + \frac{2}{m_2^{(j)}} + \frac{1}{m_3^{(k)}} \right) \quad (2.14.31)$$

2.14E Symmetric Bent to Non-Symmetric Bent

<u>Point Groups</u>	<u>Examples</u>
$C_{2v} \rightarrow C_s$	$H_2O \rightarrow HOD$
$D_{3h} \rightarrow C_s$	$H_3^+ \rightarrow HDT^+$

Then after substitution, $m_1 \neq m_3$, $s_{12} = s_{23}$, $f_{12} = f_{23}$ and $\alpha < 180^\circ$.

(i) Determination of the Force Constants

As with the previous subsection, this has already been discussed in A(i), only with $\alpha < 180^\circ$ in this case, and as before, f_{13} has to be ignored.

(ii) Determination of the Isotopic Frequencies

With the force constants, C(ii) is used to find the isotopic frequencies for the non-symmetrically substituted molecule.

If the isotopic frequencies calculated in subsections D and E for non-symmetric substitution of the initially symmetric molecules are used as starting values, together with the isotopic masses, and if we solve for the force constants and substitute back our original masses, we would not expect to recover exactly our original frequencies, as the force constant f_{13} is not determined, because we are starting with the non-symmetric cases. This is the artificial case mentioned

earlier.

The methods described in the above subsections can be summarised in the following table, where the first entry of each pair represents part (i) of the subsection indicated, to determine the force constants; the second entry indicating part (ii) of the subsection shown, to find the isotopic frequencies. Quantities in parentheses indicate the unlikely applications of the methods.

Table (2.3) of Methods for Obtaining Isotopic Frequencies

		Substituted Molecule				
		D_{3h}	$D_{\infty h}$	$C_{\infty v}$	C_{2v}	C_s
Initial Molecule	D_{3h}	A,A	-	-	A,A	A,C
	$D_{\infty h}$	-	A,A	A,B	-	-
	$C_{\infty v}$	-	(B,A)	B,B	-	-
	C_{2v}	(A,A)	-	-	A,A	A,C
	C_s	(C,A)	-	-	(C,A)	C,C

As Herzberg (30) gives data on D_2O and HOD as well as H_2O , some of the methods above could be tested, in addition to the checks already mentioned. It is found that there is some disagreement in frequencies, particularly as these substitutions involve large mass changes, but it is considered that these are acceptable, particularly as deuterium has such a low abundance in stellar atmospheres. Disagreements for isotopes of other atoms are likely to be much smaller.

Regardless of the type of molecule being considered, we can use a simple approximation given by Herzberg (30) to calculate the isotopic shift of the anharmonic constants:

$$\alpha_{ij}^I = \frac{\alpha_{ij} \omega_i^I \omega_j^I}{\omega_i \omega_j} \quad (2.14.32)$$

Herzberg (30) and Lechner (41), from which our expressions are derived, use the observed fundamental frequencies ν_i in place of the harmonic constants ω_i , the classical vibrational frequencies for infinitesimal amplitudes that we use. Given ν_i , we should strictly speaking convert to ω_i using the following expressions, if the anharmonic constants are known:

$$\begin{aligned} \nu_1 &= \omega_1 + 2\alpha_{11} + \frac{d}{2}\alpha_{12} + \frac{1}{2}\alpha_{13} \\ \nu_2 &= \omega_2 + (1+d)\alpha_{22} + \frac{1}{2}\alpha_{12} + \frac{1}{2}\alpha_{23} \\ \nu_3 &= \omega_3 + 2\alpha_{33} + \frac{1}{2}\alpha_{13} + \frac{d}{2}\alpha_{23} \end{aligned} \quad (2.14.33)$$

where d is the degeneracy of the ν_2 vibrational mode.

After computing the isotopic shifts of the vibrational constants, we have to convert the dissociation potential and the energies of any excited electronic states being considered, in the same way as is done for diatomic molecules. Thus defining $D_e^{0''}$, $D_0^{0''}$, T_e^r and T_0^r in the same way as section 4.3, where the dissociation may be complete or only partial, we can write:

$$\begin{aligned} D_e^{0''} - D_0^{0''} &= \frac{1}{2}(\nu_1'' + d''\omega_2'' + \nu_3'') + \frac{1}{4}(\alpha_{11}'' + d^2''\alpha_{22}'' \\ &+ \alpha_{33}'' + d''\alpha_{12}'' + \alpha_{13}'' + d''\alpha_{23}'') \end{aligned} \quad (2.14.34)$$

and:

$$\begin{aligned} T_e' - T_o' &= \frac{1}{2} (\omega_1'' + d'' \omega_2'' + \omega_3'' - \omega_1' - d' \omega_2' - \omega_3') \\ &+ \frac{1}{4} (\chi_{11}'' + d'' \chi_{22}'' + \chi_{33}'' + d'' \chi_{12}'' + \chi_{13}'' + d'' \chi_{23}'' \\ &\quad - \chi_{11}' - d' \chi_{22}' - \chi_{33}' - d' \chi_{12}' - \chi_{13}' - d' \chi_{23}') \end{aligned} \quad (2.14.35)$$

where we distinguish between d' and d'' as the molecule may be linear in one electronic state but non-linear in the other.

2.15 Molecular and Grand Iteration Scheme for Determining Equilibrium Abundances

As already mentioned in section 2.3, approximate initial atomic ionization equilibrium abundances are found in the absence of molecule formation, and these now have to be used for starting values for the molecular dissociation equilibrium calculations together with the diatomic and triatomic dissociation equilibrium constants discussed above.

For performing the dissociation equilibrium iterations, in addition to the requirements already mentioned, it is necessary to give some initial trial values for F_i , the fraction of atoms of element i free, as defined in (2.4.1) for each element. Of course, the initial state $F_i = 1$ for all i , as is the case with the first set of atomic ionization iterations, can be used. Indeed, for temperatures above typically 3000°K , although molecule formation may still be fairly important from the point of view of opacity, the gas is predominantly monatomic, hence the initial trial values $F_i = 1$ can conveniently be applied. However, at lower temperatures where molecules dominate the mixture, convergence in the earlier stages of iteration can be speeded up by calculating some approximate trial values of F_i ; at least to obtain upper limits.

At low temperatures, it may appear to be better to assume complete molecular association before we execute the atomic ionization iterations for the first time. However, even at the lowest temperature of 1000°K that we are likely to consider, which is already unrealistically low, there are usually still plenty of free atoms, besides which we have to break into the cycles of ionization and dissociation iterations at some point. It is convenient always to start with the ionization iterations, initially neglecting any molecular association, then do the molecular dissociation iterations using appropriate starting values.

Neglecting the formation of triatomic and charged molecules, and considering at any one time a particular diatomic molecule and its constituent atoms in equilibrium and in isolation from other species, we can then write for a heteroelement molecule, (where we use the terms heteroelement and homoelement with reference to atomic numbers only, isotopes not being considered), with $i \neq j$:

$$N_{(i)} = N_i + N_{ij} \tag{2.15.1}$$

$$N_{(j)} = N_j + N_{ij}$$

Where the symbols have their meanings as described in earlier sections, i.e. N_i and N_j are the number of free atoms of type i and j respectively, N_{ij} the number of diatomic molecules consisting of i and j , and $N_{(i)}$ and $N_{(j)}$ are the total number of atoms of type i and j respectively, free and combined; only here they do not include other molecules.

Using the definitions for F_i and K_{ij} , (2.4.1) and (2.4.2) respectively, (2.15.1) becomes:

$$F_i + \frac{F_i F_j N_{(ij)}}{K_{ij}} = 1 \quad (2.15.2)$$

$$F_j + \frac{F_i F_j N_{(ij)}}{K_{ij}} = 1$$

which on being combined and solving for F_i becomes:

$$F_i = \frac{-(K_{ij} + N_{(ij)}) + \sqrt{(K_{ij} + N_{(ij)})^2 + 4N_{(ij)}K_{ij}}}{2N_{(ij)}} \quad (2.15.3)$$

and likewise for F_j if the indices are interchanged.

For a homoelement molecule $i = j$, and we write in place of (2.15.1):

$$N_{(ii)} = N_i + 2N_{ii} \quad (2.15.4)$$

Hence using (2.4.1) and (2.7.6) again:

$$F_i + \frac{2F_i^2 N_{(ii)}}{K_{ii}} = 1 \quad (2.15.5)$$

which becomes:

$$F_i = \frac{-K_{ii} + \sqrt{K_{ii}^2 + 8N_{(ii)}K_{ii}}}{4N_{(ii)}} \quad (2.15.6)$$

Equations (2.15.3) and (2.15.6) can be combined together and expressed neatly as:

$$F_i = \frac{1}{2a_{ij}X_i} \left[\sqrt{(1-X_i+X_j)^2 + 4a_{ij}X_i} - (1-X_i+X_j) \right] \quad (2.15.7)$$

$$a_{ij} = 1 \quad \text{if } i \neq j$$

where: (2.15.8)

$$a_{ij} = 2 \quad \text{if } i = j$$

$$X_i = \frac{N_{(i)}}{K_{ij}} \quad \text{and} \quad X_j = \frac{N_{(j)}}{K_{ij}} \quad (2.15.9)$$

Equation (2.15.7) can be evaluated to find a value of F_i for a particular molecule considered. If $i \neq j$, F_j can of course be found by interchanging the indices.

Unfortunately, (2.15.7) is not always suitable for handling numerically, owing to the very large range the variables can take, it is found that machine overflow can occur at an intermediate step in the evaluation, or loss of significance. Let:

$$x = 1 - X_i + X_j \quad \text{and} \quad y = 4a_{ij}X_i \quad (2.15.10)$$

Also let V and L be the overflow and loss of significance criterion respectively, such that V is a large real number within the range of the machine and $L = 30$ say. Then (2.15.7) can be re-written in four possible ways, subject to the specified restrictions:

$$F_i = \frac{2}{y} \left[\sqrt{x^2 + y} - x \right] \quad (2.15.11)$$

for $-\sqrt{v} < x < \min(L/y, \sqrt{v})$

$$F_i = \frac{2|x|}{y} \left[\sqrt{1 + \frac{y}{x^2}} - 1 \right] \quad (2.15.12)$$

for $\sqrt{v} < x < L/y$

$$F_i = \frac{2|x|}{y} \left[\sqrt{1 + \frac{y}{x^2}} + 1 \right] \quad (2.15.13)$$

for $x < -\sqrt{v}$

$$F_i = \frac{1}{x} - \frac{y}{4x^3} + \frac{y^2}{8x^5} - \frac{5y^3}{64x^7} + \dots \quad (2.15.14)$$

for $x > L/y$

Thus for each molecule in turn, the fractions of constituent atoms which are free are calculated on the assumption that the molecule is in equilibrium with its constituent atoms in isolation from other molecules, and the minimum is then taken of the values of F_i so calculated and the previous minimum of F_i obtained from molecules already considered. For heteroelement molecules, the other fraction F_j is identically treated.

After all molecules have been considered, approximate trial values for the fraction of atoms free for each element are thus obtained. Naturally, the fraction of atoms free of those elements that have no molecules associated with them in the specified mixture,

always remain unity.

With the starting values of F_i so obtained, together with other necessary data already mentioned, it is now possible to consider the equilibrium dissociation of both diatomic and triatomic molecules.

For element i to be in equilibrium with diatomic molecules ij and triatomic molecules ijk , where for any particular element the index i is fixed, but j and k represent other elements which i can combine with, we can write:

$$N_{(i)} = N_i + \sum_j a_{ij} N_{ij} + \sum_j \sum_k a_{ijk} N_{ijk} \quad (2.15.15)$$

where a_{ij} are as before and:

$$\begin{aligned} a_{ijk} &= 1 \quad \text{if } i \neq j \text{ and } i \neq k \\ a_{ijk} &= 2 \quad \text{if } i = j \text{ or } i = k \text{ but } j \neq k \\ a_{ijk} &= 3 \quad \text{if } i = j = k \end{aligned} \quad (2.15.16)$$

Using the definitions for F_i , K_{ij} and K_{ijk} and simplifying:

$$1 = F_i \left[1 + \sum_j \left(\frac{a_{ij} F_j N_{(j)}}{K_{ij}} \right) + \sum_j \sum_k \left(\frac{a_{ijk} F_j F_k N_{(j)} N_{(k)}}{K_{ijk}} \right) \right] \quad (2.15.17)$$

which can be written as:

$$1 = F_i \Psi_i \quad \text{or} \quad F_i = \frac{1}{\Psi_i} \quad (2.15.18)$$

where Ψ_i is the expression in the square brackets of (2.15.17).

Hence, with the initial term of Ψ_i as 1 and trial values of F_i for all i , for each molecule ij or ijk considered in turn, Ψ_i is incremented by the terms in (2.15.17) $a_{ij} F_j^{N(j)} / K_{ij}$ or $a_{ijk} F_j^{N(j)} F_k^{N(k)} / K_{ijk}$ respectively. When the summation is completed after all molecules have been considered, (2.15.18) gives new values of F_i from the computed Ψ_i . For those elements that do not form specified molecules, the terms in (2.15.17) beyond the first never occur, hence $\Psi_i = 1$ always, thus $F_i = 1$. Furthermore, since all the terms in the sum beyond the first are > 0 , it follows that $F_i \leq 1$ for all i .

With the output values of F_i so obtained, we can form the geometric mean of those with the input values of F_i to give new values that can be used as input for the next iteration, as this is rather more satisfactory than simply using the output values as new input.

So far in our discussion in this section, we have omitted to consider the presence of atomic and molecular ions, and the formation of isotopic molecules. It is now our job to consider in a much more general way molecular equilibrium dissociation with ions and isotopes taken into account. The equations already considered have to be generalized, and considerable care has to be used with the definitions and particularly the indices.

Let i , j and k index the elements as before, h , m and n be the charges of the respective atoms and p , q and r index the isotopes belonging respectively to each element.

As before, i , j and k are merely indices that do not necessarily correspond to the atomic numbers. The indices p , q and r index isotopes in such a way that a particular isotope p , is an isotope of element i and no other, and likewise for q and r . Thus these indices can be used without explicitly naming the element and remain unambiguous. In other words, we can consider a common list of isotopes of all elements arranged such that those belonging to each element are grouped together. Then if for example element i has three isotopes with the first being tenth in the list of isotopes, then p can only take the values 10 to 12, if j happens to be the next element in the sequence, then $r = 13$ to whatever its upper limit is, and so on. Thus it follows that if $p = q$ then $i = j$, but the converse is not necessarily true, and $i \neq j$ means $p \neq q$ for all isotopes of i and j .

The indices h , m and n are the actual charges of the specified dissociated atoms that make up the molecule. Thus $h = 1$ indicates that the atom of element i (or more correctly, to be consistent any isotope of element i) has a single positive charge, $h = 0$ indicates a neutral atom, and likewise for m and n . Unlike the isotopic indices, $h = m$ says nothing about the equality or otherwise of i and j . Actually, for computational convenience, these indices in the coding are not charges but indices of ions in a common list, as is done above for isotopes, but it is much easier to treat them directly as charges,

as we can define quantities like $h+m+n$.

In order to proceed further, it is necessary to state carefully the following additional definitions:

$N_{(p)}$ --- The total number of isotopes of type p belonging to element i in the mixture that are free or combined.

N_p --- The number of isotopes of type p that are free.

N_{pq}^{h+m} and N_{pqr}^{h+m+n} --- The abundances of molecules consisting of isotopes p and q , and p , q and r , with charges $h+m$ and $h+m+n$ respectively.

K_{pq}^{hm} and K_{pqr}^{hmn} --- The equilibrium constants of molecules dissociating completely into isotopes with charges indicated.

And also define:

$$F_p = \frac{N_p}{N_{(p)}} \quad (2.15.19)$$

The fraction of atoms of isotope p that are free, i.e. the isotope analogy of the atomic fractions F_i .

$$f_p = \frac{N_p}{N_i} \quad (2.15.20)$$

Of those atoms of element i that are free, f_p is the fraction of isotope p .

$$f_p = \frac{N_{(p)}}{N_{(i)}} \quad (2.15.21)$$

The fraction of all atoms of element i in the mixture, free and combined, that consist of isotope p , and is constant.

The definitions of the equilibrium constants in (2.4.2) and (2.9.1) can be generalized to include isotopes and ions, and are determined from Saha's equation by substituting in the appropriate isotopic quantities. Thus for diatomic molecules:

$$K_{pq}^{hm} = S_i^h S_j^m \frac{N_p N_q}{N_{pq}^{h+m}} \quad (2.15.22)$$

and for triatomic molecules:

$$K_{pqr}^{hmn} = S_i^h S_j^m S_k^n \frac{N_p N_q N_r}{N_{pqr}^{h+m+n}} \quad (2.15.23)$$

where S_i^h etc. as defined in (2.3.8) is the fraction of N_i that is in the h^{th} stage of ionization. Thus $S_i^h N_p$ is the number of free atoms of isotope p in the h^{th} stage of ionization. As:

$$N_p = f_p F_i N_{(i)} \quad (2.15.24)$$

etc., and (2.15.22) and (2.15.23) can be re-written as:

$$K_{pq}^{hm} = S_i^h S_j^m F_i F_j / f_p f_q \frac{N_{(i)} N_{(j)}}{N_{pq}^{h+m}} \quad (2.15.25)$$

and

$$K_{pqr}^{hmn} = S_i^h S_j^m S_k^n F_i F_j F_k f_p f_q f_r \frac{N_{(i)} N_{(j)} N_{(k)}}{N_{pqr}^{h+m+n}} \quad (2.15.26)$$

The indices i, j and k in equation (2.15.15) can be replaced by p, q and r respectively, so that isotopes rather than just elements are indexed, thus (2.15.15) is generalized and becomes:

$$N_{(p)} = N_p + \sum_t \sum_q a_{pq} N_{pq}^{h+m} + \sum_t \sum_q \sum_r a_{pqr} N_{pqr}^{h+m+n} \quad (2.15.27)$$

where a_{pr} and a_{pqr} have the same meanings, apart from the indices, as equation (2.15.15) and we also sum over molecular ions, such that $t = h+m$ or $t = h+m+n$ for diatomic and triatomic molecules respectively, with $t = 0$ for neutral molecules, $t = 1$ for singly ionized positive molecules, etc.

As with (2.15.15), we wish to replace quantities by number by quantities by fraction, apart from the total number of atoms for each element, to make the problem suitable for computation. If the definitions (2.15.21) and (2.15.24-26) are substituted into (2.15.27), then after simplification, (2.15.27) becomes:

$$1 = \frac{f_p F_i}{F_p} \left[1 + \sum_t S_i^h \sum_q a_{pq} S_j^m F_j f_q \frac{N_{(j)}}{K_{pq}^{hm}} \right. \\ \left. + \sum_t S_i^h \sum_q \sum_r a_{pqr} S_j^m S_k^n F_j F_k f_q f_r \frac{N_{(j)} N_{(k)}}{K_{pqr}^{hmn}} \right] \quad (2.15.28)$$

which can be written as:

$$1 = \frac{f_p F_i}{F_p} \Psi_p \quad (2.15.29)$$

where Ψ_p is the expression in the brackets of (2.15.28).

Hence, as before when neglecting isotopes and ion formation, after having set the initial term of Ψ_p as 1 for all isotopes, then the summations in (2.15.28) are evaluated for all isotopic molecules yielding values of Ψ_p . Although $F_p = 1/\Psi_p$, it is more convenient to find output values of f_p and F_i , however, these cannot be found directly from (2.15.29).

From the definitions of F_i , F_p and J_p , the fractions F_i can be found from the expression:

$$F_i = \sum_p \frac{J_p}{\Psi_p} \quad (2.15.30)$$

where the summation is over only those isotopes belonging to element i . Once (2.15.30) has been evaluated for element i , the fractions f_p can be obtained from the expression similarly derived from the above mentioned definitions:

$$f_p = \frac{J_p}{F_i \Psi_p} \quad (2.15.31)$$

After evaluating (2.15.30) and (2.15.31) for isotopes of all elements, we have the output values of F_i and f_p from (2.15.28). As mentioned earlier, the new input values of F_i for the next iteration are obtained from the geometric means of the previous input and output values calculated above. The calculated values of f_p , however, are put directly in as new input values, without taking geometric means, as they are not expected to change very much, and are not the "handle"

of the iterative process.

On the very first entry into the molecular dissociation iterations, in addition to initializing the values of F_i to some trial values as discussed at the beginning of this section, the values of f_p are set equal to \bar{f}_p for all isotopes.

As expected, it is found that $f_p \approx \bar{f}_p$ in general, exact equality being the case, except at initialization, only when a particular element i forms no molecules, in which case $N_i = N_{(i)}$ and $N_p = N_{(p)}$ etc., or when only one isotope of a particular element i is present in the mixture, in which case $f_p = \bar{f}_p = 1$ and both (2.15.30) and (2.15.31) reduce down to (2.15.18).

After performing each iteration, it is necessary to test for convergence. As mentioned much earlier when dealing with ionization, a test is performed on each iteration on the change in the one quantity N_e , the number of free electrons present. However, for molecular dissociation, it is necessary to incorporate in a test in some way, the changes of all the fractions F_i for all N elements.

One such method that could be chosen is to define a quantity S_F , such that:

$$S_F = \frac{1}{N} \sum_{i=1}^N \left| 1 - \frac{F_i(\text{new})}{F_i(\text{old})} \right| \quad (2.15.32)$$

where $F_i(\text{new})$ is the geometric mean of the previous input and output values of the iteration just performed, and $F_i(\text{old})$ is the input

value. As convergence is approached, $S_F \rightarrow 0$, hence the test for convergence would be:

$$S_F \leq \epsilon \quad (2.15.33)$$

where ϵ is, as before, the convergence criterion, typically 10^{-4} or smaller, except for the first few grand iterations when it is larger. With single precision programming used here, however, there is no point having ϵ less than 10^{-6} .

Unfortunately, it is found in practice that this simple test for convergence is not suitable, because although S_F might converge fairly rapidly, some of the individual ratios $F_i(\text{new})/F_i(\text{old})$ may converge much more slowly. This is found to be particularly troublesome in the case of carbon and oxygen, where the predominant molecule formed is carbon monoxide, which is tightly bonded. Here it often noticed that the convergence of the fractions of the atoms is slow, and if there are a large number of fractions of other atoms that have converged, then the above test is insensitive. This may often be the case if all but a few of the fractions have converged.

A much better method is to define a quantity F_{\max} , such that:

$$\Delta F_{\max} = \max \left(\left| 1 - \frac{F_i(\text{new})}{F_i(\text{old})} \right| \right) \quad (2.15.34)$$

over all i . Then with the test:

$$\Delta F_{\text{min}} \leq \epsilon \quad (2.15.35)$$

each individual fraction has to converge to the required degree before (2.15.35) is satisfied, hence completing the dissociation iteration loop in that particular grand iteration. It is nevertheless convenient still to find S_F as a monitor to the progress of the iterations.

As is stated right at the beginning of this chapter, like the ionization iteration loop, the iteration criterion for molecular dissociation is quite loose in the first grand iteration, but becomes progressively more stringent for each grand iteration, until the maximum specified stringency, as said typically 10^{-4} or less, is reached. If after a specified number of iterations, (2.15.35) is not satisfied, then like the ionization iterations, the dissociation iterations belonging to that particular grand iteration, are terminated.

Having left the dissociation iteration loop by whichever method, it is necessary to complete the current grand iteration by computing the number of free electrons contributed by ionized molecules, (including if necessary any electrons absorbed by negative molecular ions), hence completing all the equations in the iterative process.

Re-writing the part of the expression (2.3.11) that is relevant to molecular ions:

$$M_e = \sum_s \sum_t \epsilon M_s^t \quad (2.15.36)$$

where M_e is the number of electrons contributed by charged molecules, and M_s^t the actual abundance of a diatomic or triatomic molecule of type s with charge t . Then (2.15.36) can be expressed as:

$$M_e = \sum_i \sum_j \sum_t (h+m) N_{ij}^{h+m} + \sum_i \sum_j \sum_k \sum_t (h+m+n) N_{ijk}^{h+m+n} \quad (2.15.37)$$

where N_{ij}^{h+m} and N_{ijk}^{h+m+n} are the abundances of diatomic and triatomic molecules for the indicated elements, with charges $t = h+m$ and $t = h+m+n$, where we sum over t .

Making the substitution (2.15.46) and (2.15.47), see below, gives:

$$M_e = \sum_i \sum_j \sum_t (h+m) S_i^h S_j^m F_i F_j \frac{N_{(i)} N_{(j)}}{\bar{K}_{ij}^{hm}} + \sum_i \sum_j \sum_k \sum_t (h+m+n) S_i^h S_j^m S_k^n F_i F_j F_k \frac{N_{(i)} N_{(j)} N_{(k)}}{\bar{K}_{ijk}^{hmn}} \quad (2.15.38)$$

where \bar{K}_{ij}^{hm} and \bar{K}_{ijk}^{hmn} are the mean dissociation constants of the molecules with the indicated elements, averaged over all isotopes belonging to those elements, that split up into atoms with the appropriate charges.

Having obtained M_e from (2.15.38), it is added to the number of electrons obtained from the last execution of the ionization iteration loop, giving the total number of free electrons N_e . It is then possible to begin a new grand iteration, starting again with the ionization iterations, and using the value of N_e incorporating M_e .

The whole process of performing ionization iterations followed by dissociation iterations that constitute a grand iteration, is performed until total convergence is reached, or failing that, until a specified maximum number of allowed grand iterations is attained. As expected, at low temperatures there are a large number of iterations due to abundant molecule and negative ion formation, but at progressively higher temperatures, convergence becomes rapid.

To test for overall convergence of the grand iterations, it is convenient to do the test:

$$\Delta \log N_e + \Delta F_{\min} \leq \epsilon \quad (2.15.39)$$

where $\Delta \log N_e$ and ΔF_{\max} are defined respectively in (2.3.12) and (2.15.34), and ϵ , the convergence criterion, has our usual value of typically 10^{-4} or less.

In the way the equations in the iterative process are arranged, it is not necessary to know directly the abundances of the various molecules, the fractions of them in various isotopic forms, or except for calculating M_e , the mean equilibrium constants. However, as the whole object of performing these calculations is to determine the molecular abundances, which are then used as inputs to the process of determining the opacity, it is necessary to find them together with the other quantities mentioned, at the completion of all iterations.

Taking the definition for the K_{ij} and K_{ijk} from (2.7.6) and (2.12.7) respectively, and allowing for the formation of ions, these equations can be re-written as:

$$\bar{K}_{ij}^{hm} = S_i^h S_j^m \frac{N_i N_j}{N_{ij}^{h+m}} \quad (2.15.40)$$

and

$$\bar{K}_{ijk}^{hmn} = S_i^h S_j^m S_k^n \frac{N_i N_j N_k}{N_{ijk}^{h+m+n}} \quad (2.15.41)$$

Where now several isotopic variants of a molecule ij or ijk exist, so we now consider these equilibrium constants to be some kind of mean of the actual equilibrium constants for the individual isotopic variants, as distinct from the definitions (2.4.2) and (2.9.1) where each element is assumed to have only one isotope, and K_{ij} and K_{ijk} are found directly from Guldberg and Waage's equation.

Using the fact that:

$$\sum_p \sum_q N_{pq}^{h+m} = N_{ij}^{h+m} \quad (2.15.42)$$

and

$$\sum_p \sum_q \sum_r N_{pqr}^{h+m+n} = N_{ijk}^{h+m+n} \quad (2.15.43)$$

together with the definitions (2.15.20), (2.15.22) and (2.15.23), it is easy to show that:

$$\bar{K}_{ij}^{hm} = \frac{1}{\sum_p \sum_q \left(\frac{f_p f_q}{K_{pq}^{hm}} \right)} \quad (2.15.44)$$

and

$$\bar{K}_{ijk}^{hmn} = \frac{1}{\sum_p \sum_q \sum_r \left(\frac{f_p f_q f_r}{K_{pqr}^{hmn}} \right)} \quad (2.15.45)$$

where the fractions S_i^h etc. cancel.

Thus (2.15.44) and (2.15.45) are evaluated whenever it is required to determine M_e , and the molecular abundances at the end of the iterations; in addition, the mean equilibrium constants are a useful check. It is immediately obvious that if elements i and j have one specified isotope each, then there will be only one molecule of the type ij , hence \bar{K}_{ij}^{hm} is just K_{pq}^{hm} from (2.15.44), and likewise for (2.15.45).

It is worth noting that whereas the equilibrium constants K_{pq}^{hm} and K_{pqr}^{hmn} are determined at the very beginning and remain fixed, the mean equilibrium constants \bar{K}_{ij}^{hm} and \bar{K}_{ijk}^{hmn} are not known accurately until convergence is reached, as they depend on the isotopic fractions f_p etc.

Once the mean equilibrium constants are known, then the molecular abundances can be found directly from:

$$N_{ij}^{h1m} = S_i^h S_j^m F_i F_j \frac{N(i) N(j)}{\bar{K}_{ij}^{hm}} \quad (2.15.46)$$

and

$$N_{ijk}^{h+m+n} = S_i^h S_j^m S_k^n F_i F_j F_k \frac{N_{(i)} N_{(j)} N_{(k)}}{\bar{K}_{ijk}^{hmn}} \quad (2.15.47)$$

where the abundances so determined are the sums of the abundances of the individual isotopic molecules making up ij and ijk.

Rather than determining the abundances N_{pq}^{h+m} and N_{pqr}^{h+m+n} of isotopic molecules directly, it is far more convenient, as is the case with isotopes, to determine the fractional abundances. Thus let g_{pq}^{hm} be the fraction of the molecules ij with charge h+m that consist of the isotopic form pq, and likewise for g_{pqr}^{hmn} , then:

$$g_{pq}^{hm} = \frac{N_{pq}^{hm}}{N_{ij}^{h+m}} \quad (2.15.48)$$

and

$$g_{pqr}^{hmn} = \frac{N_{pqr}^{hmn}}{N_{ijk}^{h+m+n}} \quad (2.15.49)$$

Where by definition:

$$\sum_p \sum_q g_{pq}^{hm} = 1 \quad (2.15.50)$$

and

$$\sum_p \sum_q \sum_r g_{pqr}^{hmn} = 1 \quad (2.15.51)$$

Then, these fractions can be determined from:

$$g_{pq}^{hm} = f_p f_q \frac{K_{ij}^{-hm}}{K_{pq}^{hm}} \quad (2.15.52)$$

and

$$g_{pqr}^{hmn} = f_p f_q f_r \frac{K_{ijk}^{-hmn}}{K_{pqr}^{hmn}} \quad (2.15.53)$$

This discussion should be completed by briefly considering several extra quantities that are useful to determine, together with important checks.

The total number of particles per cm^3 is obtained by adding to the number of free electrons, the sum of all free atoms in any stage of ionization, together with the sum of all diatomic and triatomic molecules, thus:

$$N_T = N_e + \sum_i N_i + \sum_s \sum_t M_s^t \quad (2.15.54)$$

which in full is:

$$N_T = \sum_i \sum_h h S_i^h N_i + \sum_i \sum_j \sum_t (h+m) N_{ij}^{h+m} \quad (2.15.55)$$

$$+ \sum_i \sum_j \sum_k \sum_t (h+m+n) N_{ijk}^{h+m+n} + \sum_i N_i + \sum_i \sum_j \sum_t N_{ij}^{h+m}$$

$$+ \sum_i \sum_j \sum_k \sum_t N_{ijk}^{h+m+n}$$

As the number of atoms of element i combined in diatomic molecules is $\sum_j \sum_t a_{ij} N_{ij}^{h+m}$ and in triatomic molecules is $\sum_j \sum_k \sum_t a_{ijk} N_{ijk}^{h+m+n}$, we can easily check to see how well each element has converged from the expression:

$$R_i = \frac{1}{N_{(i)}} \left[N_{(i)} - N_i - \sum_j \sum_t a_{ij} N_{ij}^{h+m} - \sum_j \sum_k \sum_t a_{ijk} N_{ijk}^{h+m+n} \right] \quad (2.15.56)$$

where R_i is the residual abundance of element i , that is free and combined in molecules, expressed as a fraction that does not agree with the total number of atoms of element i . If convergence has occurred properly, then:

$$|R_i| \leq \epsilon \quad (2.15.57)$$

The whole iterative process discussed in this chapter can be repeated for a variety of temperatures, densities and chemical compositions, enabling one to determine molecular abundances under many different conditions. Also, if any of the above number densities are multiplied by kT , we obtain a pressure in dynes per cm^2 .

2.16 The Inclusion of Molecules with more than Three Atoms and Solid Particles

A detailed treatment of the properties of molecules with more than three atoms and of solid particles, is considered to be well beyond the scope of this work. However, in order to help to put this work into perspective, a very brief discussion is given.

All computations in this work neglect the possible formation of solid particles and tetra-atomic and more complex molecules, as this should be a good approximation, except at the very lowest temperatures. However, at such low photospheric temperatures, where by our calculations diatomic and triatomic molecules are very abundant, one could reasonably expect more complex molecules like NH_3 and CH_4 to form, and even solid particles like graphite and silicate to condense out when the partial pressure of the appropriate species in the gas phase rises above the saturated vapour pressure of the solid particles.

To calculate ab initio the partition functions and equilibrium constants of these more complex molecules, in the same general way as is done for diatomic and triatomic molecules, would be very complicated, particularly if the isotopic variations are to be included in the same way. The only solution would be to include molecules on an individual basis, whose equilibrium constants are already known at the relevant temperatures, or can be found from

simple empirical formulae.

Neglecting the presence of isotopes and ions, (2.15.15) generalizes to:

$$N_{(i)} = N_i + \sum_j a_{ij} N_{ij} + \sum_j \sum_k a_{ijk} N_{ijk} + \sum_j \sum_k \sum_l a_{ijkl} N_{ijkl} + \dots \quad (2.16.1)$$

Hence (2.15.17) can be written as:

$$1 = F_i \left[1 + \sum_j \left(\frac{a_{ij} F_j N_{(j)}}{K_{ij}} \right) + \sum_j \sum_k \left(\frac{a_{ijk} F_j F_k N_{(j)} N_{(k)}}{K_{ijk}} \right) + \sum_j \sum_k \sum_l \left(\frac{a_{ijkl} F_j F_k F_l N_{(j)} N_{(k)} N_{(l)}}{K_{ijkl}} \right) + \dots \right] \quad (2.16.2)$$

where i, j, k, l, \dots are the indices of the atoms, and $a_{ijkl\dots}$ gives the number of atoms in a molecule belonging to type i .

Then (2.16.2) can be iterated in the same way as before, yielding abundances which could be used in any opacity calculations. Of course, (2.16.2) could be generalized to include isotopic variants.

If solid particles are to be allowed to form in the mixture, then we can say qualitatively, that the right hand side of (2.16.1) must include terms for the conservation of atoms that do not contribute any pressure in the gas when condensation occurs. The net result of condensation is to reduce the overall pressure and density of the gas phase, and alter the molecular equilibria. The formation of solid particles would affect the opacity both directly, and indirectly by changing the abundances of the species in the gas phase important for

opacity, and would be an exceedingly complex problem to handle.

3 DETERMINATION OF SCATTERING AND CONTINUOUS OPACITY

3.1 Introduction

Having obtained the atomic and molecular abundances from the methods in the previous chapter, these abundances are then used to calculate the opacities, which is the whole object of this work.

We can split up the types of opacity into two components, a background continuous opacity due to electron scattering, Rayleigh scattering, free-free and bound-free absorption, and discrete opacity due to bound-bound absorption. In this chapter, we consider the various forms of continuous opacity, deferring to the following chapters the much more extensive discussion of the determination of bound-bound absorption.

It is convenient to express frequency in a dimensionless form when determining the opacity, thus let u be the reduced frequency, such that:

$$u = \frac{h\nu}{kT} \tag{3.1.1}$$

We can write the total opacity corrected for stimulated emission, see Carson (42) and (43):

$$K'(u) = K_a(u)(1 - e^{-u}) + K_s(u) \tag{3.1.2}$$

where $\kappa_a(u)$ and $\kappa_s(u)$ are respectively the absorption and scattering opacity, and $(1-e^{-u})$ is the stimulated emission factor. The main aim is to obtain the Rosseland mean opacity (RMO) $\bar{\kappa}$, which is given by:

$$\frac{1}{\bar{\kappa}} = \frac{15}{4\pi^4} \int_0^{\infty} \frac{u^4 e^u du}{\kappa'(u) (e^u - 1)^2} \quad (3.1.3)$$

where the Rosseland weighting function:

$$W'(u) = \frac{15}{4\pi^4} \frac{u^4 e^u}{(e^u - 1)^2} \quad (3.1.4)$$

normalizes to unity, and has its maximum at $u = 3.830016\dots$, hence giving the greatest weight to $\kappa'(u)$ at that value.

However, it is more convenient and computationally more efficient to factorize out the stimulated emission factor from (3.1.2), and incorporate it into the weighting function. Writing:

$$\kappa(u) = \kappa'(u) (1 - e^{-u})^{-1} \quad (3.1.5)$$

(3.1.2) can be re-written as:

$$\kappa(u) = \kappa_a(u) + \kappa_s(u) (1 - e^{-u})^{-1} \quad (3.1.6)$$

Hence the RMO is now given by:

$$\frac{1}{\bar{\kappa}} = \frac{15}{4\pi^4} \int_0^{\infty} \frac{u^4 e^{2u} du}{\kappa(u) (e^u - 1)^3} \quad (3.1.7)$$

where the weighting function:

$$W(u) = \frac{15}{4\pi^4} \frac{u^4 e^{2u}}{(e^u - 1)^3} \quad (3.1.8)$$

no longer normalizes to unity, but to the value 1.055313..., and now has its maximum at the value $u = 3.724...$

Because the RMO is an harmonic mean, it is not directly additive, thus the RMO of all opacity sources together is not the sum of the individual RMOs of each opacity source on its own. Thus the integration in (3.1.7) cannot be performed until all the absorption has been accounted for.

As useful additional information, we can also find the Planck mean opacity (PMO), which is given by:

$$\bar{\kappa} = \frac{15}{\pi^4} \int_0^{\infty} \frac{\kappa'(u) u^3 du}{(e^u - 1)} \quad (3.1.9)$$

where the Planck weighting function:

$$B'(u) = \frac{15}{\pi^4} \frac{u^3}{(e^u - 1)} \quad (3.1.10)$$

has its maximum at $u = 2.821439...$, which is also the same value as the Planck function itself, which in dimensionless frequency units is given by:

$$B(u, T) = \frac{2k^3 T^3}{h^2 c^2} \frac{u^3}{(e^u - 1)} \quad (3.1.11)$$

As before, it is more convenient to incorporate the stimulated emission factor in the weighting function, and accordingly the PMO can be written as:

$$\bar{K} = \frac{15}{\pi^4} \int_0^{\infty} \frac{\kappa(u) u^3 du}{e^u} \quad (3.1.12)$$

where the new weighting function:

$$B(u) = \frac{15}{\pi^4} \frac{u^3}{e^u} \quad (3.1.13)$$

has its maximum at $u = 3$ exactly.

Because the PMO is a straight mean, it is directly additive, thus the PMO of all opacity sources together is also the sum of the individual PMOs of each opacity source on its own.

Although we ultimately want the RMO and PMO as mass absorption, i.e. cm^2 per gm, it is much more convenient to determine the volume absorption opacity $\mu(u)$ in cm^{-1} , i.e. cm^2 per cm^3 , as abundances are expressed by number. Thus the total volume absorption at frequency u is given by:

$$\mu(u) = \sum_i N_i \sigma_i(u) \quad (3.1.14)$$

where N_i and $\sigma_i(u)$ are respectively the abundance by number per cm^3 and cross-section in cm^2 for species i . To convert to the mass absorption coefficient $\kappa(u)$, we divide by the density, thus:

$$K(u) = \mu(u)/\rho \quad (3.1.15)$$

where ρ is the density in gm per cm³. We can accordingly replace $K(u)$ by $\mu(u)$ in (3.1.7) and (3.1.12), and take ρ outside the integrals.

In order to determine the RMO for the continuum, it is necessary to determine the opacity at a large number of grid points by adding on each newly calculated spectrum on top of the previous ones, effectively evaluating (3.1.14) for a large number of values of u , then integrating (3.1.7) numerically between $u = 0$ and some appropriately large upper value, say $u = 20$, as $W(20) = 1.27 \times 10^{-5}$ which is small compared to $W(3.724) = 1.92 \times 10^{-1}$ the maximum value.

It is simplest to make the grid points equally spaced, defining an interval δu , then after evaluating the integrand of (3.1.7) at each value of u , integrate using Simpson's rule. Because the continuum is generally changing slowly, the grid does not have to be too fine, but fine enough to allow for sudden changes in the continuum at absorption edges. No more than a few thousand grid points would be adequate.

As there would in general be many species, each producing a spectrum by several different processes, we can build up the total spectrum by considering each process in turn, and within each process deal in turn with each species that contributes to that process. In fact, we can put in a vector for containing $\mu(u)$ the electron scattering, then accumulate the Rayleigh scattering for the various species and also any continuous absorption processes where the

stimulated emission has already been taken into account. Into another vector for $\mu(u)$, we can accumulate the absorption from those processes for which stimulated emission has not been included, then after applying (3.1.5) and (3.1.6) as appropriate, we can integrate (3.1.7).

3.2 Electron and Rayleigh Scattering

We consider electron scattering first, which for conditions of interest here is quite straightforward, see Carson (42) and (43).

As at the frequencies of interest here, the photon energies are highly "non-relativistic" i.e. $h\nu/m_e c^2 \ll 1$, we simply have coherent Thomson scattering which is frequency independent. Thus:

$$\sigma_s(u) = \sigma_T = \frac{8\pi r_e^2}{3} \quad (3.2.1)$$

where $\sigma_T = 6.65246 \times 10^{-25} \text{ cm}^2$ is the Thomson electron cross-section, and $r_e = e^2/m_e c^2 = 2.81794 \times 10^{-13}$ is the classical electron radius.

If electron scattering is the only source of opacity, then:

$$K'(u) = N_e \frac{\sigma(u)}{\rho} \quad (3.2.2)$$

where N_e is the number density of electrons. It is at once seen that on integrating (3.1.3) for the RMO, or (3.1.9) for the PMO, $\bar{K} = K(u)$ for any u .

In practice, it is found that at very low temperatures like 1000°K , as expected, electron scattering is totally negligible as there are very few free electrons. Even at temperatures in the upper end of our range of interest, other processes still dominate, hence in

our context, this particularly simple RMO is never realised on its own.

The other source of scattering opacity considered here is Rayleigh scattering.

If $\sigma_R(\lambda)$ is the Rayleigh scattering cross-section in cm^2 per particle, then from Tarafdar and Vardya (44), we can write:

$$\sigma_R(\lambda) = \frac{128\pi^5 a_0^6 \alpha^2}{3\lambda^4} \left[1 + \frac{A_1}{\lambda^2} + \frac{A_2}{\lambda^4} + \dots \right] \quad (3.2.3)$$

where α is the polarizability in units of a_0 (the first Bohr radius), λ is the wavelength in cm, and the coefficients $A_1, A_2 \dots$ are corrections to the λ^{-4} law. In many cases, these correction terms are not available, so we have to assume the simple λ^{-4} law, and assume that we are considering frequencies less than the characteristic transition frequency of that species, which would in practice be nearly always the case.

Re-writing (3.2.3) as:

$$\sigma_R(\lambda) = \frac{1}{\lambda^4} \left[B_0 + \frac{B_1}{\lambda^2} + \frac{B_2}{\lambda^4} + \dots \right] \quad (3.2.4)$$

where:

$$B_0 = A_0 = \frac{128\pi^5 a_0^6 \alpha^2}{3}, \quad B_1 = B_0 A_1, \quad B_2 = B_0 A_2, \dots \quad (3.2.5)$$

we can at once express the total Rayleigh scattering at any wavelength

due to many species by putting in sums in (3.2.4), hence giving:

$$\mu_R(\lambda) = \frac{1}{\lambda^4} \left[\sum_i B_{0i} N_i + \frac{1}{\lambda^2} \sum_i B_{1i} N_i + \frac{1}{\lambda^4} \sum_i B_{2i} N_i + \dots \right] \quad (3.2.6)$$

in units of cm^{-1} ; where N_i is the number density of species i , and B_{0i} etc. are the coefficients for each species. Thus we obtain at once the whole contribution to the opacity of Rayleigh scattering, without having to compute individual spectra.

Putting (3.2.6) into dimensionless frequency units gives:

$$\begin{aligned} \mu_R(\lambda) = u^4 \left(\frac{kT}{hc} \right)^4 & \left[\sum_i B_{0i} N_i + u^2 \left(\frac{kT}{hc} \right)^2 \sum_i B_{1i} N_i \right. \\ & \left. + u^4 \left(\frac{kT}{hc} \right)^4 \sum_i B_{2i} N_i + \dots \right] \end{aligned} \quad (3.2.7)$$

and neglecting the higher order terms, we can put this straight into (3.1.3), yielding for the RMO:

$$\frac{1}{K} = \frac{15}{4\pi^4} \left(\frac{hc}{kT} \right)^4 \frac{\rho}{\sum_i B_{0i} N_i} \int_0^\infty \frac{e^{-u} du}{(e^u - 1)^2} \quad (3.2.8)$$

which is clearly divergent when the lower limit is zero, see Vardya (45), implying that the RMO is zero even though the opacity is finite everywhere (at zero frequency it vanishes, but so also does the flux). The RMO will however be usually non-zero when account is taken of the other forms of opacity, of which in practice there will always be, and which do not vanish at zero frequency; in fact, free-free opacity becomes infinite. Indeed, as stated earlier, as electron scattering, no matter how small it may be, is included when Rayleigh

scattering is calculated, we never allow the opacity to vanish anywhere. However, if the lower bound in (3.2.8) is a , with $a > 0$, (3.2.8) can be integrated analytically, yielding:

$$\bar{\kappa}_a = \frac{4\pi^4}{15} \left(\frac{kT}{hc}\right)^4 \sum_i \frac{B_{0i} N_i}{\rho} (e^a - 1) \quad (3.2.9)$$

in $\text{cm}^2 \text{gm}^{-1}$, to which could be added the contribution between $u = 0$ and $u = a$ where other forms of opacity will be important. In practice, other forms of opacity cannot be neglected elsewhere in the spectrum for our purposes.

If (3.2.7) is substituted into (3.1.9) with the higher order terms to obtain the PMO, we can write:

$$\bar{\kappa} = \frac{15}{\pi^4} \left(\frac{kT}{hc}\right)^4 \frac{1}{\rho} \left[\sum_i B_{0i} N_i \int_0^\infty \frac{u^7 du}{(e^u - 1)} + \left(\frac{kT}{hc}\right)^2 \sum_i B_{1i} N_i \int_0^\infty \frac{u^9 du}{(e^u - 1)} + \left(\frac{kT}{hc}\right)^4 \sum_i B_{2i} N_i \int_0^\infty \frac{u^{11} du}{(e^u - 1)} + \dots \right] \quad (3.2.10)$$

where these integrals can be evaluated analytically from:

$$\int_0^\infty \frac{x^{2n-1} dx}{e^x - 1} = |B_{2n}| \frac{(2\pi)^{2n}}{4n} \quad (3.2.11)$$

see Abramowitz and Stegun (46), where B_{2n} is a Bernoulli number. Hence we obtain the result:

$$\bar{\kappa} = \frac{15\pi^4}{\rho} \left(\frac{kT}{hc}\right)^4 \left[\frac{8}{15} \sum_i B_{0i} N_i + \frac{64\pi^2}{33} \left(\frac{kT}{hc}\right)^2 \sum_i B_{1i} N_i + \frac{88448}{1365} \pi^4 \left(\frac{kT}{hc}\right)^4 \sum_i B_{2i} N_i + \dots \right] \quad (3.2.12)$$

which, unlike the RMO, gives a non-zero result even though the lower bound is zero. Taking the first term, and writing the PMO in terms of α for an individual absorber, we can write:

$$\bar{R} = \frac{1024\pi^9}{3} \left(\frac{kT}{hc}\right)^4 a_0^6 \alpha^2 \quad (3.2.13)$$

in cm^2 per absorber.

Unfortunately, the polarizabilities of most elements are not well known except for hydrogen and helium, the first row in the periodic table, and the remaining inert gases and group I elements. As in the first period for Li to Ne, $\log \alpha$ is approximately proportional to Z with α decreasing from Li to Ne, this result can be used to interpolate for the other elements in the periodic table lying between their respective alkali and inert gas, if the polarizabilities are otherwise unavailable.

In addition to neutral atoms, the polarizabilities of negative and positive ions could be obtained from a simple empirical formula given by Tarafdar and Vardya (47), if they are otherwise unavailable:

$$\alpha = \alpha_{0h} I^{-(3+h)} \quad (3.2.14)$$

where α_{0h} is 8.1×10^1 , 2.4×10^4 and 4.7×10^6 with $h = -1$, 0 and 1 respectively for negative ions, neutral atoms and positive ions, with α_{0h} being in units of a_0 and I being the ionization/detachment energy in eV.

The Rayleigh scattering coefficients of molecules, except in a few cases like H_2 , are little known or no experimental values are available at all. However, Tarafdar and Vardya (47) gives formulae by which polarizabilities of diatomic molecules could approximately be computed, and gives a very simple semi-empirical relationship for polyatomic molecules:

$$\alpha = \frac{2}{3} \sum_i \alpha_i \quad (3.2.15)$$

where α_i is the polarizability of atom i , with the summation being over all atoms in the molecule; clearly, this could also be used to estimate α for diatomic molecules if no other source of data is available.

The Rayleigh scattering coefficients for H and Ne are obtained from Dalgarno and Kingston (48), who give expressions of the form:

$$n^2 - 1 = C_0 \left[1 + \frac{C_1}{\lambda^2} + \frac{C_2}{\lambda^4} + \dots \right] \quad (3.2.16)$$

where n is the refractive index at atmospheric pressure and C_0, C_1, C_2 etc. are coefficients. These coefficients must be converted into the forms suitable for our use by:

$$A_0 = \frac{8\pi^3}{3} \frac{C_0^2}{N_L^2}, \quad A_1 = 2C_1, \quad A_2 = C_1^2 + 2C_2, \dots \quad (3.2.17)$$

where N_L is the Loschmidt number.

The coefficients for He, C, N and O are given directly by Tarafdar and Vardya (44), (length formalism used). For all the remaining elements we have only the coefficient A_0 obtained from the polarizabilities given by Carson (3) using the interpolation method described earlier, though (48) could be used for the other inert gases, but their abundances are much lower. Also, the Rayleigh scattering by ions is neglected, and accordingly no use is made of (3.2.14) or of Dalgarno (49) who lists polarizabilities of specific atoms and ions.

For the diatomic molecules, the coefficients for H_2 are obtained from Dalgarno and Williams (50), and for C_2 , N_2 and O_2 from Carson (3), the polarizabilities for OH, CO and SiO are obtained from Tarafdar and Vardya (47). Of the triatomic molecules, the calculated value of the polarizability of H_2O is used from (47) given by (3.2.15), and this formula is also used to obtain the polarizability of CO_2 . As the molecules considered here are amongst the most abundant, it is not considered worthwhile to include data for other molecules.

All the Rayleigh coefficients used in this section are tabulated in the appendices.

3.3 Free-Free and Bound-Free Sources of Opacity

Free-free and bound-free absorption are particularly important sources of continuous opacity, with free-free absorption being smoothly varying over the whole spectrum due to electronic transitions between two continuous electronic states, and bound-free absorption for atoms has a sharp cut-off in frequency, i.e. an absorption edge, below which no absorption occurs due to the minimum energy needed to remove a bound electron to infinity. However, unlike other quantities that are computed for atoms and molecules in a general way in this work, here we have to handle the various species responsible for the free-free and bound-free opacity on an individual basis, as we have to interpolate from tables and evaluate empirical formulae supplied by different authors for the various species considered.

In the temperature regime of interest, a very important source of free-free and bound-free absorption is due to H^- . The photodetachment energy of the H^- ion is 0.7551 eV corresponding to $\lambda = 16,419\text{\AA}$, at wavelengths longer than this there is no H_{bf}^- absorption, but we still have H_{ff}^- absorption, due to an electron moving in the field of a neutral H-atom. Tsuji (9) gives both tables and analytic formulae for H^- absorption, however, by comparing both, an error was found in his formula 6, or (3.3.4) here, such that the coefficient of θ^2 in the expression for $G(\theta)$ should read 2.8914×10^{-2} , and the next term in $G(\theta)$ should have θ^3 , not θ^2 again, these corrections are noted in Tsuji (11). In this work, the absorption is in fact obtained by linear

interpolation of the tables, the values being in logs. As the units are in cm^4 per dyne, on multiplying by the electron pressure in dynes per cm^2 and the density of neutral H in particles per cm^3 , gives us the volume absorption opacity in cm^2 per cm^3 or cm^{-1} . One would expect that H^- as a source of opacity will be strongly dependent on the abundances of Na and K, as they are major sources of electrons at low temperatures due to their low ionization potentials, even though these elements have relatively low abundances.

The formulae given by Tsuji for H^- as an alternative to interpolating from the tables are given here, where $\theta = 5040/T$ and λ is in microns (μ). For the range $\theta = 0.6$ to 6.0 ($T = 840^\circ\text{K}$ to 8400°K) and $\lambda = 1.6$ to 100 for H_{ff}^- :

$$K_{\text{ff}}(\lambda, \theta) = [A(\theta)\lambda^{-1} + B(\theta) + C(\theta)\lambda + D(\theta)\lambda^2 + E(\theta)\lambda^3 + F(\theta)\lambda^4] \times 10^{-26} \text{ cm}^4 \text{ dyne}^{-1} \quad (3.3.1)$$

where:

$$\begin{aligned} A(\theta) &= 2.8613 \times 10^{-3} - 1.7104 \times 10^{-2} \theta + 1.9241 \times 10^{-2} \theta^2 \\ &\quad - 3.8625 \times 10^{-3} \theta^3 + 2.0673 \times 10^{-4} \theta^4 \\ B(\theta) &= -5.2107 \times 10^{-3} + 7.2695 \times 10^{-2} \theta - 9.4204 \times 10^{-2} \theta^2 \\ &\quad + 2.0739 \times 10^{-2} \theta^3 - 1.1541 \times 10^{-3} \theta^4 \\ C(\theta) &= 7.5533 \times 10^{-4} - 4.1764 \times 10^{-3} \theta + 1.0863 \times 10^{-2} \theta^2 \\ &\quad + 1.4533 \times 10^{-3} \theta^3 - 1.1748 \times 10^{-4} \theta^4 \\ D(\theta) &= -4.1964 \times 10^{-2} + 6.6949 \times 10^{-1} \theta - 1.0139 \times 10^{-1} \theta^2 \\ &\quad + 1.3046 \times 10^{-2} \theta^3 - 6.8082 \times 10^{-4} \theta^4 \\ E(\theta) &= -3.7419 \times 10^{-7} - 6.3651 \times 10^{-7} \theta + 6.0644 \times 10^{-6} \theta^2 \end{aligned} \quad (3.3.2)$$

$$\begin{aligned}
 & - 2.5328 \times 10^{-6} \theta^3 + 1.1071 \times 10^{-7} \theta^4 \\
 F(\theta) = & 3.5121 \times 10^{-9} - 1.6028 \times 10^{-9} \theta - 2.5083 \times 10^{-8} \theta^2 \\
 & + 1.2852 \times 10^{-8} \theta^3 - 6.3522 \times 10^{-10} \theta^4
 \end{aligned}$$

which is formula 5 by Tsuji. For wavelengths in the range $\lambda = 0$ to 1.65μ , it is better to use formula 6 by Tsuji for H_{ff}^- :

$$\begin{aligned}
 K_{ff}(\lambda, \theta) = & [G(\theta)\lambda + H(\theta)\lambda^2 + I(\theta)\lambda^3 + J(\theta)\lambda^4 \\
 & + K(\theta)\lambda^5] \times 10^{-26} \text{ cm}^4 \text{ dyne}^{-1}
 \end{aligned} \tag{3.3.3}$$

where:

$$\begin{aligned}
 G(\theta) = & - 4.9072 \times 10^{-2} + 1.2953 \times 10^{-1} \theta - 2.8914 \times 10^{-2} \theta^2 \\
 & + 7.8357 \times 10^{-3} \theta^3 - 6.1838 \times 10^{-4} \theta^4 \\
 H(\theta) = & 2.4013 \times 10^{-1} - 1.3996 \times 10^{-1} \theta + 3.7506 \times 10^{-1} \theta^2 \\
 & - 7.7846 \times 10^{-2} \theta^3 + 6.0802 \times 10^{-3} \theta^4 \\
 I(\theta) = & - 2.9875 \times 10^{-1} + 1.0503 \theta - 8.1111 \times 10^{-1} \theta^2 \\
 & + 1.8419 \times 10^{-1} \theta^3 - 1.4761 \times 10^{-2} \theta^4 \\
 J(\theta) = & 9.6893 \times 10^{-2} - 4.6764 \times 10^{-1} \theta + 4.3440 \times 10^{-1} \theta^2 \\
 & - 1.0808 \times 10^{-1} \theta^3 + 9.1163 \times 10^{-3} \theta^4 \\
 K(\theta) = & - 6.7575 \times 10^{-3} + 6.9126 \times 10^{-2} \theta - 7.7600 \times 10^{-2} \theta^2 \\
 & + 2.0616 \times 10^{-2} \theta^3 - 1.8098 \times 10^{-3} \theta^4
 \end{aligned} \tag{3.3.4}$$

in the same temperature range as before, and with the corrections as stated earlier.

For H_{bf}^- , we could use Tsuji's formula 7:

$$\begin{aligned} \kappa_{bf}(\lambda, \theta) = & 0.4158 \times 10^{-26} \theta^{5/2} e^{1.726\theta} [2.0275\lambda + 15.6235\lambda^2 \\ & - 20.4140\lambda^3 + 8.1524\lambda^4 - 2.2916\lambda^5 + 0.6639\lambda^6] \\ & \times (1 - e^{-2.8541\theta/\lambda})^4 \text{ cm}^4 \text{ dyne}^{-1} \end{aligned} \quad (3.3.5)$$

with the stimulated emission factor incorporated. (3.3.5) can be used at any temperature, but with $\lambda < 1.6419\mu$.

At higher temperatures, another important source of opacity is H_{bf} and H_{ff} , i.e. the absorption due to the ionization of neutral hydrogen, and an electron moving in the field of a proton respectively. We evaluate formula 10 of Tsuji (9) but omit the stimulated emission factor, which is included at the end of all calculations associated with this section, as discussed in section 3.1. On multiplying by the abundance of H in cm^{-3} , we again obtain the required volume absorption.

Tsuji's formula 10 which we do use, but without the stimulated emission factor is given here for H_{bf+ff} :

$$\begin{aligned} \kappa_{bf+ff}(\lambda, \theta) = & 1.045 \times 10^{-14} \lambda^3 \sum_{n=n_0}^{n_*-1} n^{-3} \exp[-31.30364(1-n^{-2})\theta] \\ & + (60.60729)^{-1} \exp[-31.30364(1-n_*^{-2})\theta] \text{ cm}^2 \end{aligned} \quad (3.3.6)$$

with λ and θ as for (3.3.1-5), $n_* = 7$ and n_0 is the lowest quantum state which contributes to the absorption at λ . As stated by Tsuji,

the bound-free and free-free Gaunt factors are assumed to be unity, as $n_* = 7$, so for states with $n > n_*$, the sum is approximated by an integral, and the partition function of H is taken as the statistical weight of the ground state i.e. 2. n_0 can be found from the expression:

$$n_0 = \text{int}(\sqrt{10^{-4}R\lambda} + 1) \quad (3.3.7)$$

which rounds up to the nearest integer by including 1 in the bracket, and where R is the Rydberg constant.

As helium is the next most abundant element, we must include it as a source of continuous opacity, there being no bound-free absorption of He^- as no stable negative ion of any importance exists. The absorption is obtained by interpolating the log of the absorption of He_{ff}^- as tabulated by Somerville (51). John and Morgan (52) gives tables for Cl_{ff}^- absorption for both the velocity and length formalisms, the former being used in this work, and for C_{ff}^- we use the tabulation given by Myerscough and McDowell (53). The free-free absorption due to Ne^- , Ar^- , Kr^- , Xe^- , Li^- , Na^- , Cs^- , Hg^- , N^- and O^- are obtained from tables by John (54), though some have negligible abundances even if included in the mixture.

The bound-free absorption for C^- , O^- , F^- , Si^- , S^- , Cl^- , Br^- and I^- are obtained from Robinson and Geltman (55), where the energies are given relative to the photodetachment energy of the negative ion, below which no absorption occurs. All interpolation/extrapolation of tables of cross-sections at energies above the absorption threshold

are performed in the number, rather than the log, as done elsewhere.

For the molecules, we obtain the free-free absorption for the species N_2^- , O_2^- , CO^- , CO_2^- and H_2O^- from tables also by John (54), though H_2^- is also given, Somerville (56) gives a more detailed table which we use; Tsuji (9) also gives an analytic approximation for H_2^- . Because of its large abundance at low temperatures, H_{2ff}^- can be an important source of opacity. The bound-free absorption for OH and CH are obtained from Tarafdar and Das (57), where the transitions are from bound ground states to repulsive excited states, and there is no absorption threshold. For OH we simply interpolate the log of the tabulated values as usual, but for CH we must first make up a new table by combining the three tables for the separate upper states by adding together the corresponding tabulated, or when necessary, interpolated values, then proceed as before.

The tables that we use from the various sources for obtaining the continuous opacity in this section, cover the regions of the $T-\lambda$ plane that is of the greatest interest to us reasonably well, so any extrapolation is likely to be at temperatures or wavelengths where the species in question will not be important. Of course, extrapolating too far beyond the range of the tables is dangerous, however, the alternative is to cut off at the limit of the tables, or extrapolate then cut off at some arbitrary value of T or λ , which could produce spurious effects if the species in question is still important. It was decided that extrapolation without cut off is the lesser of the two evils. Unfortunately, one can never know how important various species are in different parts of the spectrum, until after they have

all been computed.

Fortunately, (51), (52), (54) and (56) give simple expressions which enable us to compute the absorption at lower energies than those tabulated. Re-writing expression 2 of (54) for dimensionless energy:

$$K_u(T) = 10^9 \left(\frac{hc}{kT} \right)^3 \frac{1}{u^3} K_{10}(T) \quad (3.3.8)$$

in $\text{cm}^4 \text{dyne}^{-1}$, where $K_{10}(T)$ is the absorption at 10 microns. For the other references, if $K_0(T)$ is the tabulated value of the scaled absorption, being the first entries in the tables, then:

$$K_u(T) = \left(\frac{hc R_\infty}{kT} \right)^2 \frac{1}{u^2} K_0(T) \quad (3.3.9)$$

in $\text{cm}^4 \text{dyne}^{-1}$, where R_∞ is the Rydberg constant for infinite mass in cm^{-1} . We can also apply the same treatment to C_{ff}^- from (53), who does not give the scaled absorption, by calculating the scaled absorption, then applying (3.3.9).

All the tables for the cross-sections used in this work are given in the appendices.

3.4 Other Sources of Continuous Opacity

Although of apparently negligible importance in our context, for the sake of completeness, the contribution due to quasi-molecular hydrogen is also included by interpolating from tables given by Solomon (58). In this case the absorption is free-bound, i.e. from H_2 in a repulsive state to H_2 in an excited bound state. The units given are in cm^3 per dyne, so on multiplying by the square of the pressure of H, we obtain the correct volume absorption in cm^{-1} . The tables are given in the appendices.

Of possibly more significance, is the pressure-induced opacity of H_2 due to H_2-H_2 and H_2-He collisions, where Linsky (59) gives expressions which we use to compute the opacity. The absorption consists of three components which are added together: translational, rotation-translational and vibration-rotation-translational; these consist of highly broadened overlapping bands which for our purposes can simply be regarded as other sources of continuous opacity and added to the continuum already computed.

The expressions given by Linsky are least square fits over specified temperature and spectral ranges, with stimulated emission included. Considering first the translational opacity, let $k_{\bar{\nu},T}$ be the translational opacity dependent on the wavenumber $\bar{\nu}$ in cm^{-1} and the temperature, then for H_2-H_2 induced opacity:

$$\begin{aligned}
 k_{\bar{\nu},T} &= a\bar{\nu}^2 e^{-\bar{\nu}/b} && \text{for } \bar{\nu} < \bar{\nu}_c \\
 k_{\bar{\nu},T} &= ce^{-\bar{\nu}/d} && \text{for } \bar{\nu} \geq \bar{\nu}_c
 \end{aligned}
 \tag{3.4.1}$$

where for $600^\circ \leq T \leq 3000^\circ\text{K}$:

$$\begin{aligned}
 \log (1/a) &= 7.02391 + 1.3380 \log T \\
 b &= 91.67 + 0.1033T \\
 c &= [15.57906 - 2.06152 \log T - 0.477352(\log T)^2] \times 10^{-7} \\
 \log d &= 2.31317 + 3.8856 \times 10^{-4} T \\
 \bar{\nu}_c &= 274.3 + 0.2762T
 \end{aligned}
 \tag{3.4.2}$$

which are expressions 1 and 2 by Linsky.

For the rotation-translational opacity of $\text{H}_2\text{-H}_2$, Linsky's 11 and 12 are respectively (3.4.3) and (3.4.4):

$$\begin{aligned}
 k_{\bar{\nu},RT} &= ae^{-(\bar{\nu}-\bar{\nu}')^2/b} && \text{for } \bar{\nu} < 1.5\bar{\nu}' \\
 k_{\bar{\nu},RT} &= ce^{-d\bar{\nu}} && \text{for } \bar{\nu} > 1.5\bar{\nu}'
 \end{aligned}
 \tag{3.4.3}$$

where for $600^\circ \leq T \leq 4000^\circ\text{K}$:

$$\begin{aligned}
 a &= 4.2432 \times 10^{-6} - 2.8854 \times 10^{-7} \ln T \\
 b &= 1.2171 \times 10^5 + 258.28T \\
 c &= 2.5830 \times 10^{-4} - 4.3429 \times 10^{-8} T \\
 d &= 1.1332 \times 10^{-2} - 1.1943 \times 10^{-3} \ln T \\
 \bar{\nu}' &= -2973.3 + 600.73 \ln T
 \end{aligned}
 \tag{3.4.4}$$

For the vibration-rotation-translational opacity of H_2-H_2 , we write down Linsky's expressions 18 and 19:

$$k_{\bar{\nu},VRT} = \frac{a' \delta \bar{\nu} e^{-(\bar{\nu} - \bar{\nu}_0)/0.6952T}}{(\bar{\nu} - \bar{\nu}_0)^2 + \delta^2} \quad \text{for } \bar{\nu} < \bar{\nu}_0 = 4161.1 \text{ cm}^{-1}$$

$$k_{\bar{\nu},VRT} = \frac{a' \delta \bar{\nu}}{(\bar{\nu} - \bar{\nu}_0)^2 + \delta^2} \quad \text{for } \bar{\nu}_0 \leq \bar{\nu} \leq \bar{\nu}_0 + 3\delta/2 \quad (3.4.5)$$

$$k_{\bar{\nu},VRT} = a' \bar{\nu} e^{-(\bar{\nu} - \bar{\nu}_0)/b} \quad \text{for } \bar{\nu} > \bar{\nu}_0 + 3\delta/2$$

where for $600^\circ \leq T \leq 3000^\circ K$:

$$\delta^2 = 1.2750 \times 10^5 + 437.50T$$

$$\log a' = -7.0659 + 0.2825 \log T \quad (3.4.6)$$

$$1/a = 1.6288 \times 10^8 + 1.4904 \times 10^5 T$$

$$\log b = 0.9376 + 0.5668 \log T$$

However, Linsky gives all absorption in units of $\text{cm}^{-1} \text{amagat}^{-2}$ with the pressure assumed to be in amagat, where 1 amagat is the volume of 1 mole of an ideal gas at 1 atmosphere at $0^\circ C = 22.4136 \times 10^3 \text{ cm}^3$; but we require the absorption to be in cm^{-1} or $\text{cm}^2 \text{gm}^{-1}$ given the abundances of H_2 and He in cm^{-3} . Using the constants from Allen (32):

$$P(\text{amagat}) = 273.150P(\text{atm})/T \quad (3.4.7)$$

$$= 273.15P(\text{dyne cm}^{-2})/(1.013250 \times 10^6 T)$$

where $0^{\circ}\text{C} = 273.150^{\circ}\text{K}$ and $1 \text{ atmosphere} = 1.013250 \times 10^6 \text{ dyne cm}^{-2}$.

Because helium is also present, we have to include the absorption due to H_2 -He induced opacity; for translational opacity we can combine H_2 - H_2 and H_2 -He from expression 21 of Linsky:

$$\kappa_{\bar{\nu},T} = \kappa_{\bar{\nu},T}(\text{H}_2\text{-H}_2) P_{\text{H}_2} (P_{\text{H}_2} + 1.78 P_{\text{He}}) \text{ cm}^{-1} \quad (3.4.8)$$

where $\kappa_{\bar{\nu},T}$ is the total volume translational opacity in cm^{-1} due to H_2 - H_2 and H_2 -He collisions, $\kappa_{\bar{\nu},T}(\text{H}_2\text{-H}_2)$ is the opacity for H_2 - H_2 in $\text{cm}^{-1} \text{ amagat}^{-2}$ computed from (3.4.1) and (3.4.2) and P_{H_2} and P_{He} are the partial pressures of the gases in amagat. As we have the abundances of H_2 and He in cm^{-3} , using (3.4.7) we can convert (3.4.8) to:

$$\kappa_{\bar{\nu},T} = q \kappa_{\bar{\nu},T}(\text{H}_2\text{-H}_2) N_{\text{H}_2} (N_{\text{H}_2} + 1.78 N_{\text{He}}) \text{ cm}^{-1} \quad (3.4.9)$$

where:

$$q = [273.15k / (1.01325 \times 10^6)]^2 = 1.38523 \times 10^{-39} = 1/N_L^2 \text{ cm}^6 \quad (3.4.10)$$

where k and N_L are Boltzmann's constant and Loschmidt's number respectively, and N_{H_2} and N_{He} are the abundances of the gases in cm^{-3} .

The combined H_2-H_2 and H_2-He induced rotation-translational opacity can similarly be obtained from Linsky's expression 22, which in the form we require is:

$$K_{\bar{\nu},RT} = qk_{\bar{\nu},RT}(H_2-H_2)N_{H_2}(N_{H_2} + 0.10N_{He}) \text{ cm}^{-1} \quad (3.4.11)$$

where $k_{\bar{\nu},RT}(H_2-H_2)$ is the opacity for H_2-H_2 in $\text{cm}^{-1}\text{amagat}^{-2}$ computed from (3.4.3) and (3.4.4).

For the vibration-rotation-translational opacity of H_2-H_2 alone, we can simply write:

$$K_{\bar{\nu},VRT}(H_2-H_2) = qk_{\bar{\nu},VRT}(H_2-H_2)N_{H_2}^2 \text{ cm}^{-1} \quad (3.4.12)$$

with $k_{\bar{\nu},VRT}$ calculated from (3.4.5) and (3.4.6).

The vibration-rotation-translational opacity of H_2-He is computed separately using the expression (3.4.5) but with different coefficients:

$$\begin{aligned} \delta^2 &= -4.033 \times 10^4 + 263.93T \\ \log a' &= -7.7245 + 0.4246 \log T \\ 1/a &= 1.125 \times 10^9 + 1.5866 \times 10^4 T + 24.267 T^2 \\ \log b &= 1.2044 + 0.4956 \log T \end{aligned} \quad (3.4.13)$$

giving $k_{\bar{\nu},VRT}(H_2-He)$ in $\text{cm}^{-1}\text{amagat}^{-2}$. The required opacity is thus obtained from:

$$\kappa_{\bar{\nu}, \text{VRT}}^{(\text{H}_2\text{-He})} = q \kappa_{\bar{\nu}, \text{VRT}}^{(\text{H}_2\text{-He})} N_{\text{H}_2} N_{\text{He}} \text{ cm}^{-1} \quad (3.4.14)$$

The total mass absorption coefficient in $\text{cm}^2 \text{gm}^{-1}$ due to all processes, working in dimensionless energy units, is simply obtained by adding (3.4.9), (3.4.11), (3.4.12) and (3.4.14) and dividing by the density:

$$\kappa(u) = [\kappa_{\text{T}} + \kappa_{\text{RT}} + \kappa_{\text{VRT}}^{(\text{H}_2\text{-H}_2)} + \kappa_{\text{VRT}}^{(\text{H}_2\text{-He})}] / \rho \quad (3.4.15)$$

with stimulated emission included.

Other sources of continuous absorption or diffuse molecular spectra like pre-dissociation or pre-ionization are not considered.

4 COMPUTING THE BAND SPECTRA OF DIATOMIC MOLECULES

4.1 Introduction

So far we have only considered how the continuous opacity is obtained. It is the purpose of this chapter and the next to discuss the theory by which molecular bands are computed, then in chapter 6 we discuss how the corresponding bound-bound opacity is calculated. In this chapter, it is convenient to refer consistently to "states" in an electronic context, i.e. electronic states, hence also singlet states, Σ states etc., but to refer to "levels" in a vibrational or rotational context, i.e. vibrational levels etc.

As far as this work is concerned, there are two types of bands that have to be considered, vibration-rotation (VR) and electronic-vibration-rotation (EVR). In the first case, transitions involve different vibrational and rotational levels within the same electronic state, usually the ground state, whereas in the other case, the transitions involve in addition a change in the electronic state, where again for our purposes, the initial state is normally the ground electronic state; one notable exception being C_2 where there are several low lying electronic states giving rise to many bands. There is in addition a third type of band, pure rotation, which involves a change in rotational energy only. However, although they have the simplest structure of all three types, the bands are not considered as they normally occur in the far infrared where a very small proportion

of the flux occurs, the Rosseland and Planck weighting functions are small, and the background continuum due to free-free transitions, as discussed in the previous chapter, tends to infinity as the wavelength tends to infinity, making the contribution due to lines relatively less important still.

As the VR bands can be considered a subset of the more general EVR bands, the same coding is used to handle the rotational fine structure of both types. In this work, it is convenient to discuss first the properties of the EVR bands in general, mentioning restrictions and differences for VR bands where relevant.

For EVR bands, the following general selection rules for electric dipole radiation have to be observed, see Herzberg (29): $\Delta J = 0$ or ± 1 , except that $J = 0 \nrightarrow J = 0$, $\Delta \Lambda = 0$ or ± 1 , $\Delta \Omega = 0$ or ± 1 if Ω is defined, see sections 2.5 and 4.2, $\Delta S = 0$ i.e. no change in multiplicity; we also have the selection rules of parity for transitions between individual rotational levels, such that $+ \leftrightarrow -$ but $+ \nleftrightarrow +$ and $- \nleftrightarrow -$, where $+$ or $-$ means respectively the total eigenfunction does not or does change sign with reflection. In addition, for the overall selection rules of the electronic states, we have: $\Sigma^+ \leftrightarrow \Sigma^+$, $\Sigma^- \leftrightarrow \Sigma^-$, $\Pi \leftrightarrow \Sigma^+$, and $\Lambda' \leftrightarrow \Lambda''$ for any other values of Λ subject to the above selection rules. Here " \leftrightarrow " means these transitions are allowed, but " \nleftrightarrow " means these transitions are forbidden. If in addition the molecule has two identical nuclei, e.g. $C^{12}C^{12}$ (but not $C^{12}C^{13}$), the additional selection rules for transitions between individual rotational levels are $s \leftrightarrow s$ and $a \leftrightarrow a$ but $s \nleftrightarrow a$, where s or a means respectively the total

eigenfunction is symmetric and does not change sign with respect to the exchange of nuclei, or is antisymmetric and does change sign with respect to this exchange. This leads to the overall selection rules for electronic states, such that $g \leftrightarrow u$ but $g \leftrightarrow g$ and $u \leftrightarrow u$, e.g. $\Sigma_g^+ \leftrightarrow \Sigma_u^+$ applies, and the rotational levels have alternating statistical weights (see section 4.2). For cases where some of these rules do not apply, e.g. electric quadrupole radiation, the transitions are usually very weak and hence are ignored. This also applies for cases where $\Delta S \neq 0$ for electric dipole radiation, so intercombination bands are also ignored.

Also, for transitions to be considered, the following points must be observed:

- (i). the molecule is sufficiently abundant,
- (ii). the initial electronic state must be sufficiently populated, i.e. the ground state or low lying excited state,
- (iii). the rotational and vibrational constants are known or assumed for both electronic states,
- (iv). the electronic transition moment or band oscillator strength is known or assumed,
- (v). the transition is in the spectral region of interest, i.e. precluding transitions in the far ultraviolet.

For VR bands, as always the same rule for J applies, as the same electronic state applies to both upper and lower levels, the conditions $\Delta \Lambda = 0$, $\Delta S = 0$ and if $\Lambda = 0$ $\Sigma^+ \leftrightarrow \Sigma^+$ or $\Sigma^- \leftrightarrow \Sigma^-$ are of course automatically satisfied. If the molecule has nuclei of the

same charge, e.g. $C^{12}C^{12}$ or $C^{12}C^{13}$, there is no net dipole moment so no transitions occur. (Actually this is not strictly true for the latter molecule. The molecule HD is known to have a very small dipole moment, see for example Mizushima (36), so it would be reasonable to assume that all diatomic molecules consisting of atoms with like charges but unlike isotopes would have very small dipole moments. However, for our purposes, such effects are completely negligible).

As before, for transitions to be considered, the following additional conditions must be satisfied:

- (i). the molecule is sufficiently abundant,
- (ii). the electronic state must be sufficiently populated, in practice the ground state,
- (iii). the rotational and vibrational constants for that state are known or assumed,
- (iv). the dipole moment expansion is known or assumed,
- (v). the atoms have different charges.

If these conditions are met, there will automatically be some VR bands in the spectral region of interest, notably in the near infrared, as there is no change in electronic energy.

As a result of the above restrictions, some molecules will be inactive in the spectral region of interest. The best example is H_2 , although it is usually by far the most abundant molecule, as the nuclei have the same charge there is no electric dipole VR spectrum in the near infrared (or pure rotation in the far infrared), the first

excited electronic state is at such a high energy that the resonance band system lies well into the ultraviolet where the flux is unimportant, and closer lying excited electronic states that would give rise to transitions at longer wavelengths are negligibly populated. However, as discussed in the previous chapter, because H_2 can be so abundant, other processes are considered.

The types of electronic states dealt with are restricted to multiplicities between one and three, as this covers the overwhelming majority. Moreover, Kovács (31) gives general formulae for Hönl-London factors and term values only up to triplets, which are complicated enough, and even specific Hönl-London factors for higher multiplicities become very complicated, see the next section.

4.2 Rotational Fine Structure of Bands

In this section we explain how the detailed rotational fine structure of VR and EVR bands is computed for diatomic molecules. For both diatomic and triatomic molecules, we need to compute individual lines that make up a band, as this is required by our methods of determining opacity in chapter 6. The relative line positions are calculated from appropriate term formulae and relative line strengths from Hönl-London factors, then from this we can subsequently obtain absolute line positions and strengths in the spectrum.

The formulae used to determine term values and intensities are based on coupling cases intermediate between Hund's cases (a) and (b), see Herzberg (29) and Kovács (31). Where for case (a), the electron spin is strongly coupled to the internuclear axis, but for case (b) it is very weakly coupled, or not at all, as is the case with Σ states. By using general intensity formulae, selection rules that are specific to the limiting cases are automatically taken into account. Although a few examples of other coupling cases exist, most states conform to either cases (a) or (b) or intermediate; accordingly, this is used as an approximation to all states considered. Likewise, any perturbations between energy levels are neglected throughout this work, where perturbations are caused by two or more levels at nearly the same energy, such that these levels are displaced from their unperturbed positions and the wave functions of each of the perturbed levels are now a linear combination of all wave functions of these

levels if unperturbed, see Herzberg (29). However, for most purposes, these approximations are good, and computed bands should agree reasonably well with observation. Even in poor cases, particularly if the spectroscopic constants are not well determined, it is hoped that the gross features of the spectrum are reproduced, hence accounting approximately for all the absorption even if the details are incorrect.

The three multiplicities considered are handled in detail in the following subsections, where under singlets, some aspects common to all multiplicities are considered.

4.2A Singlets

Most electronic states of interest belonging to molecules with an even number of electrons, including of course all neutral homonuclear molecules, are singlet states where Hund's cases (a) and (b) are the same, and are the simplest to handle.

The rotational term values in cm^{-1} are given by, (see also section 2.5):

$$F(J) = B_v \left[J(J+1) - \Lambda^2 \right] - D_v \left[J(J+1) - \Lambda^2 \right]^2 + \dots \quad (4.2.1)$$

where $J = \Lambda, \Lambda+1, \Lambda+2, \dots$ and B_v and D_v are the rigid and non-rigid rotational constants respectively, given in cm^{-1} , and are dependent on the vibrational levels by:

$$B_v = B_e - \alpha_e(v + \frac{1}{2}) + \dots, \quad D_v = D_e + \beta_e(v + \frac{1}{2}) + \dots \quad (4.2.2)$$

where B_e and D_e are the rotational constants at equilibrium separation, α_e and β_e are the coupling constants between vibration and rotation, and v is the vibrational quantum number with $v = 0, 1, 2, \dots$, and higher order terms in these expressions are neglected as they are generally very small.

As stated earlier,

$$B_e = \frac{h}{8\pi^2 c I_e} \quad (4.2.3)$$

where I_e is the equilibrium moment of inertia in cgs units, or we can write:

$$B_e = \frac{h}{8\pi^2 c \mu r_e^2} \quad (4.2.4)$$

where the reduced mass μ is:

$$\mu = \frac{m_1 m_2}{m_1 + m_2} \quad (4.2.5)$$

and r_e the equilibrium separation of the nuclei.

If the constants D_e , α_e and β_e are not available in the literature, as is often the case, they can be found from the following relations:

$$D_e = \frac{4B_e^3}{\omega_e^2} \quad (4.2.6)$$

$$\alpha_e = \frac{6}{\omega_e} \left[\sqrt{\omega_e x_e B_e^3} - B_e^2 \right] \quad (4.2.7)$$

$$\beta_e = D_e \left[\frac{8\omega_e x_e}{\omega_e} - \frac{5\alpha_e}{B_e} - \frac{\alpha_e^2 \omega_e}{24B_e^3} \right] \quad (4.2.8)$$

where at least B_e , and the harmonic and anharmonic constants ω_e and $\omega_e x_e$ respectively must be known, and where a Morse potential function is assumed, from which these expressions are derived. The Morse potential function, see Herzberg (29), is defined as:

$$V(r) = D_e^0 \left[1 - e^{-\alpha(r-r_e)} \right]^2 \quad (4.2.9)$$

where D_e^0 is the dissociation potential measured from the bottom of the potential well, r_e is the equilibrium separation of the nuclei as stated above, and α is a constant. We can assume that the Morse potential is a reasonably good approximation to the actual potential function; the minimum $V(r) = 0$ occurs when $r = r_e$ and $V(r) \rightarrow D_e^0$ as $r \rightarrow \infty$. However, $V(r)$ does not approach infinity at $r = 0$ by (4.2.9) as it would do for a correct potential, but this region is of little importance. Because the Morse function is an approximation, (4.2.6-8) are approximate relations.

In some cases, B_0 and D_0 are given, expressed for the ground vibrational level, (4.2.2) is then used in reverse to obtain B_e and D_e provided α_e and β_e are known, hence:

$$B_e = B_0 + \frac{\alpha_e}{2}, \quad D_e = D_0 - \frac{\beta_e}{2} \quad (4.2.10)$$

then B_v and D_v are found in the usual way.

In some electronic states where the spectroscopic constants are poorly known, only B_0 may be given, together with some vibrational constants. Unfortunately, B_e cannot then be obtained directly from (4.2.7) and (4.2.10), without resort to some form of iteration. However, as these equations are only approximations and $\alpha_e \ll B_e$, it is not considered worthwhile to solve for B_e , so we just put $B_e = B_0$, solve for α_e from (4.2.7), hence also D_e , then apply (4.2.2) as required.

The Hönl-London factors by Kovács (31) for $\Delta\Lambda = 0$ are:

$$P(J) = (J+\Lambda)(J-\Lambda)/J$$

$$Q(J) = \Lambda^2(2J+1)/J(J+1) \quad (4.2.11)$$

$$R(J) = (J+\Lambda+1)(J-\Lambda+1)/(J+1)$$

and for $\Delta\Lambda = \pm 1$ are:

$$\underline{\Delta\Lambda = +1} \quad \underline{\Delta\Lambda = -1}$$

$$P(J) = R(J-1) = (J-\Lambda-1)(J-\Lambda)/2J$$

$$Q(J) = Q(J) = (J-\Lambda)(J+\Lambda+1)(2J+1)/2J(J+1) \quad (4.2.12)$$

$$R(J) = P(J+1) = (J+\Lambda+1)(J+\Lambda+2)/2(J+1)$$

where the Hönl-London factors give the relative line strengths in a given band due only to rotation, neglecting the frequency and Boltzmann factors, and assuming the rotational wave functions can be separated completely from the vibrational and electronic wave functions according to Born and Oppenheimer (60). The Hönl-London factor appears in (4.4.1), the expression for the total line strength.

In (4.2.11) and (4.2.12), P, Q and R refer to the branches according to whether $\Delta J = -1, 0$ or $+1$ respectively, there being no Q-branch in (4.2.11) if $\Lambda = 0$, and all Hönl-London factors given are expressed in terms of the initial level, which for absorption is the lower level J'' . In (4.2.12), when $\Delta\Lambda = -1$, if we require $R(J)$, replace J by $J+1$ on the right hand side of the corresponding expression, for $Q(J)$ no change is needed, and for $P(J)$, replace J by $J-1$. These are normalized such that:

$$\sum_{J'} S_{J'J''} = 2J'' + 1 \quad (4.2.13)$$

where $S_{J'J''}$ is $P(J)$, $Q(J)$ or $R(J)$ depending if $J' = J''-1, J''$ or $J''+1$

respectively and Λ for the two levels is kept constant. Hence equations (4.2.12) differ from those for $\Delta\Lambda = \pm 1$ on page 208 of Herzberg (29), which are normalized such that:

$$\sum_{\Lambda'} \sum_{J'} S_{J', J''} = 2J'' + 1 \quad (4.2.14)$$

which are half those of (4.2.12)

If $\Lambda > 0$ for any multiplicity, all levels are split into two, i.e. Λ -doubled, however, because of selection rules, we will not get splitting of lines unless both participating electronic states have $\Lambda > 0$. As the theory of Λ -doubling is considered beyond the scope of this work, when required, we split a computed line into two components separated by 1cm^{-1} , a typical value for Λ -doubling, and the sum of the strengths of the two lines taken to be twice that of the original line, with each component equal in strength to the original line if the nuclei are not identical. In the conditions of interest, a separation of 1cm^{-1} is much greater than the line's Doppler width, so the components are assumed not to overlap.

For all multiplicities, if we have an EVR band from a molecule with identical isotopes, then in addition to the Hönl-London factor and Boltzmann factor due to the population of the levels, there is an alternation of the intensities of the spectral lines due to the nuclear spins. If I is the nuclear spin quantum number and N the total molecular angular momentum quantum number apart from electron spin (for singlets $J=N$), then g_I is the nuclear spin statistical weight factor which must multiply the Hönl-London factor, and g_I is

calculated according to the method below. We adopt the conventional notation for transitions between molecular electronic states, where for example $\Pi \leftarrow \Sigma$ means absorption from a lower Σ state to an upper Π state, then $\Pi \rightarrow \Sigma$ is emission from the upper Π state to the lower Σ state. Though we deal only with absorption in this work, this method below is exactly the same for emission, but the initial and final states are interchanged.

$$\underline{\Sigma \leftarrow \Sigma} \text{ and } \underline{\Pi \leftarrow \Sigma}$$

$$u_1 = +1 \text{ for } \Sigma_g^+ \text{ or } \Sigma_u^-,$$

$$u_1 = -1 \text{ for } \Sigma_u^+ \text{ or } \Sigma_g^-,$$

$$u_2 = +1 \text{ for I-integral,}$$

$$u_2 = -1 \text{ for I-1/2-integral,}$$

$$u_3 = +1 \text{ for N-even,}$$

$$u_3 = -1 \text{ for N-odd.}$$

If $U = u_1 u_2 u_3$, then:

$$g_I = \frac{2I + U + 1}{2(2I + 1)} \quad (4.2.15)$$

i.e. $g_I = (I+1)/(2I+1)$ for $U = +1$ and $g_I = I/(2I+1)$ for $U = -1$, if $I = 0$, as is the case for $C^{12}C^{12}$, alternate lines are missing. U and g_I are here expressed in terms of the initial state.

$$\underline{\Sigma \leftarrow \Pi}$$

We do the same analysis as above, only U and g_I are now expressed in

terms of the final state.

$$\Lambda^+ > 0 \leftarrow \Lambda^- > 0$$

Each line is split into two components with intensities in the ratio of the statistical weight factors $2(I+1)/(2I+1)$ and $2I/(2I+1)$, which add up to 2 taking account of Λ -doubling. If $I = 0$, only one line will occur, and for singlet states the spectrum may mimic $\Pi \leftrightarrow \Sigma$ transitions for a heteronuclear molecule.

4.2B Doublets

A doublet is the lowest possible multiplicity of an electronic state of a molecule with an odd number of electrons, and is accordingly a very common species.

The general rotational term values for the two spin components are given approximately by:

$$F_{J-\frac{1}{2}}(J) = F_1(J) = B_v \left[(J + \frac{1}{2})^2 - \Lambda^2 - \frac{1}{2} \sqrt{4(J + \frac{1}{2})^2 + Y(Y-4)\Lambda^2} \right] - D_v \left[(J - \frac{1}{2})(J + \frac{1}{2}) - \Lambda^2 \right]^2 \quad (4.2.16)$$

$$F_{J+\frac{1}{2}}(J) = F_2(J) = B_v \left[(J + \frac{1}{2})^2 - \Lambda^2 + \frac{1}{2} \sqrt{4(J + \frac{1}{2})^2 + Y(Y-4)\Lambda^2} \right] - D_v \left[(J + \frac{1}{2})(J + \frac{3}{2}) - \Lambda^2 \right]^2$$

where $Y = A/B_v$, with A being the spin-orbit coupling constant, such that when $Y = 0$, we have Hund's case (b), with $Y \rightarrow +\infty$ we approach regular Hund's case (a), and when $Y \rightarrow -\infty$ we approach inverted Hund's

case (a).

However, in (4.2.16) obtained from Kovács (31), we are neglecting spin-rotation coupling due to the single unpaired electron, and Λ -doubling, as both these quantities are small, involve fairly complex terms and the constants are frequently unavailable; Λ -doubling is in fact handled crudely as stated in 4.2A. In addition, the centrifugal or non-rigidity terms are taken to be in the case (b) limit, i.e. with $Y = 0$, rather than the more general form as given by Kovács (31) page 62 equation 10, (where there is a misprint, as the very last term should be preceded by a positive sign). Except for strict case (b), the centrifugal terms given in (4.2.16) are expected to be a poor approximation when J is small; however, as these terms are very small compared to the rigid terms in such cases, their errors are unimportant. By the time J becomes large enough for the centrifugal terms to contribute significantly to the total rotational term values, spin uncoupling occurs and case (b) is a good approximation. This was checked numerically by experimenting with realistic values. Note that the expressions for the centrifugal terms given by Herzberg (29) page 232 are incorrect, the corrected form being given in (4.2.16) in the case (b) limit as stated.

For states, $Y = 0$ so we have strict case (b), and (4.2.16) reduces to:

$$F_{J-1/2}(N) = F_1(N) = B_v N(N+1) - D_v N^2(N+1)^2 + \frac{1}{2} \gamma N \quad (4.2.17)$$

$$F_{J+1/2}(N) = F_2(N) = B_v N(N+1) - D_v N^2(N+1)^2 - \frac{1}{2} \gamma(N+1)$$

where the spin-rotational coupling constant γ is included for this special case, as it is often known for Σ states, and N is the angular momentum quantum number apart from spin.

Quite generally, in (4.2.16), $F_2(J) > F_1(J)$ for any value of γ and Λ , also for the series F_1 , $N = J-1/2$ and for F_2 , $N = J+1/2$, even in the case (a) limit when N is no longer defined as a meaningful quantum number, with the rule $N = \Lambda, \Lambda+1, \Lambda+2 \dots$ still applying.

Considerable care has to be taken in the correct assignment of levels, in order to ensure that the correct formulae are selected when the Hönl-London factors are computed. For Σ states, $J = 1/2, 3/2, 5/2 \dots$, each level of J is split into components F_1 and F_2 , such that $F_2(J) \approx F_1(J+1)$ associated with a given value of N as stated above. Thus except when $N = 0$ where there is only a single level of $J = 1/2$ belonging to the F_1 series, each value of N splits into two J -components as given by (4.2.17), such that the splitting is $\gamma(N+1/2)$.

When $\Lambda > 0$, we can define a new quantity Ω , such that $\Omega = |\Lambda + \Sigma|$, so $\Omega = \Lambda \pm 1/2$ giving two series of levels with $J = \Omega, \Omega+1/2, \Omega+3/2 \dots$ where in the case (a) limit, Ω is the total electronic angular momentum quantum number. As with N , Ω is used as a convenient index even when it is not a good quantum number. There is only one level for which $J = \Lambda - 1/2$, and particular care must be taken to index it correctly. The assignments are as follows:

$Y > 2$ $F_1(J)$ belongs to the series with $\Omega = \Lambda - 1/2$ for all J ,
 $F_2(J)$ belongs to the series with $\Omega = \Lambda + 1/2$ for all J ,

$0 < Y < 2$ same as above, except the single level $J = \Lambda - 1/2$ now
 belongs to F_2 , i.e. $F_1(\Lambda - 1/2)$ is renamed $F_2(\Lambda - 1/2)$,

$Y < 0$ $F_1(J)$ belongs to the series with $\Omega = \Lambda + 1/2$ for all J ,
 $F_2(J)$ belongs to the series with $\Omega = \Lambda - 1/2$ for all J .

Thus, when Y changes sign, with the exception of the level $J = \Lambda - 1/2$,
 for a level specified by a given Ω , $F_1(J)$ is renamed $F_2(J)$ and $F_2(J)$
 is renamed $F_1(J)$, see also Mulliken (61).

The rotational constants B_e and D_e and the vibration-rotation
 coupling constants α_e and β_e are defined in the same way as for
 singlets, except that when A is large, we can write:

$$B_{\#} = B_e \left(1 \pm \frac{B_e}{A\Lambda} \dots \right) \quad (4.2.18)$$

as given by Herzberg (29) page 233, such that for some electronic
 states, B_{eff} is given for the two Ω ladders, in which case B_e is
 recovered by simply taking the mean.

The Hönl-London factors for doublets for any intermediate
 coupling cases are obtained from Kovács (31), see the appendices.
 There are in general twelve branches for $S_{J'J''}^{\Sigma\Sigma} = X_{n'n}(J)$, where X is
 P, Q or R and n is an index 1 or 2 according to the series. In fact
 the 24 equations given, allowing for $\Delta\Lambda = 0, \pm 1$, can be compressed into

6 different equations.

In addition to the general selection rules, it is only necessary to ensure that transitions occur between levels that actually exist, as the selection rules specific to the Hund's limiting cases are automatically taken care of by the Hönl-London factors. However, these formulae often break down when a transition involves a level with $J = \Lambda - 1/2$ for $\Lambda > 0$, but it is often found in this case that if such a level is assumed to have strict case (a) "character", quite regardless of Y , the value computed is consistent with the sum rule. Accordingly, the following additional rules are employed:

${}^2\Sigma \leftarrow {}^2\Sigma$: There is no problem as the general formulae can be applied, but the Hönl-London factors for 6 of the 12 possible branches are zero, i.e. forbidden transitions.

${}^2\Pi \leftarrow {}^2\Sigma$: $Q_{11}(1/2) = Q_{12}(1/2) = 2/3$ and $P_{11}(3/2) = P_{12}(3/2) = 1/3$, as $J' = 1/2$ in these cases, otherwise the general formulae are applied when levels exist.

${}^2\Sigma \leftarrow {}^2\Pi$: $Q_{11}(1/2) = Q_{21}(1/2) = 2/3$ and $R_{11}(1/2) = R_{21}(1/2) = 1/3$, as $J'' = 1/2$ in these cases, otherwise the general formulae are applied as above.

$\Lambda' \leftarrow \Lambda''$: With $\min(\Lambda', \Lambda'') > 0$, then if either $J'' = \Lambda'' - 1/2$ or $J' = \Lambda' - 1/2$ or both, strict case (a) is applied by using (4.2.11) or (4.2.12) as appropriate, with Ω inserted instead of Λ , and the other transitions involving these levels being

forbidden. As the case (a) selection rule $\Delta\Sigma = 0$ is applied, transitions beginning or ending on a $J = \Lambda - 1/2$ level can only be "vertical" in the energy level diagram.

The above rules are consistent with Schadee (62) after allowing for his different normalization. Kovács's normalization is adopted throughout this work, such that the sum of all transitions for any level, neglecting any Λ -doubling but including spin splitting, is $2J+1$. Thus for doublets, except for $J = \Lambda - 1/2$ for $\Lambda > 0$, the sum of all branches for a given J is $2(2J+1)$, with $2J+1$ being the sum from the odd level, if it exists.

From the discussion earlier, if $Y < 0$ the indices that refer to the state in question are changed such that $1 \rightarrow 2$ and $2 \rightarrow 1$ with the complication that this switchover occurs for $Y < 2$ with $J = \Lambda - 1/2$. That negative value of Y is substituted into the appropriate formulae of Kovács, yielding both the term values and Hönl-London factors. It must also be pointed out that the smaller of Λ' and Λ'' is substituted into his 12 expressions for the branches when $\Lambda' \neq \Lambda''$, but the respective values of Λ for the appropriate states are substituted in his equations 6 on page 61, as well as for the term values.

For identical nuclei, the statistical weight factors follow exactly those rules for the singlets, except that $N = J - 1/2$ for F_1 and $N = J + 1/2$ for F_2 regardless of whether N is a well defined quantum number. However, this is of somewhat academic interest, as only charged homonuclear molecules fulfil this condition, and the equilibrium abundances of charged molecules are usually negligible.

4.2C Triplets

Triplet electronic states can only belong to molecules with an even number of electrons, many such states are highly excited and are of no importance here. However, there are a number of molecules which can be of great importance that have a ground or low lying triplet states like C_2 , O_2 and TiO . Unfortunately, the general expressions for the term values and Hönl-London factors are considerably more complicated than the doublets.

The general rotational term values for the three spin components are given approximately by:

$$\begin{aligned}
 F_{J_{11}}(J) &= F_1(J) = B_v \left[J(J+1) - \Lambda^2 + \frac{2}{3} - \sqrt{Z_1} - 2Z_2 \right] - D_v \left[(J-1)J - \Lambda^2 \right]^2 \\
 F_{J_2}(J) &= F_2(J) = B_v \left[J(J+1) - \Lambda^2 + \frac{2}{3} + 4Z_2 \right] - D_v \left[J(J+1) - \Lambda^2 \right]^2 \quad (4.2.19) \\
 F_{J_{11}}(J) &= F_3(J) = B_v \left[J(J+1) - \Lambda^2 + \frac{2}{3} + \sqrt{Z_1} - 2Z_2 \right] - D_v \left[(J+1)(J+2) - \Lambda^2 \right]^2
 \end{aligned}$$

where $Z_1 = \Lambda^2 \gamma(\gamma-4) + \frac{4}{3} + 4J(J+1)$ (4.2.20)

and $Z_2 = \frac{1}{3Z_1} \left[\Lambda^2 \gamma(\gamma-1) - \frac{4}{9} - 2J(J+1) \right]$

where $-\Lambda^2 + 2/3$ in (4.2.19) from Kovács (31) page 69 has been omitted by Herzberg (29) page 235, which is inconsistent with the latter's treatment of doublets. As before, Herzberg also gives the incorrect expressions for the centrifugal correction terms, which are corrected here for the case (b) limit. As with the doublets, it is assumed that

by the time J becomes large enough for the centrifugal terms to contribute appreciably to the term values, case (b) is a good approximation, as the general expressions for the centrifugal terms are extremely complex.

In the above, $F_1(J)$ is invalid when $J = \Lambda - 1$ and $0 < Y < 4$, in which case by Budó (63), Z_2 is re-written as

$$Z_2 = \frac{1}{3Z_1} \left[\Lambda^2 (Y-3)(Y-4) - \frac{Y}{9} - 2J(J+1) \right] \quad (4.2.21)$$

and $J = \Lambda$ is put into Z_1 , Z_2 and F_1 .

As with the doublets, the general spin-rotation coupling and Λ -doubling are neglected, as well as the additional spin-spin coupling due to the two unpaired electrons. However as before, for Σ states we can include these coupling terms as they are simpler, the constants often being available.

Accordingly, from Herzberg (29), where we include the centrifugal terms:

$$\begin{aligned} F_{2,1}(N) = F_1(N) &= B_v(N^2 + 3N + 3) - D_v N^2(N+1)^2 - \lambda \\ &\quad - \sqrt{(2N+3)^2 B_v^2 + \lambda^2} - 2\lambda B_v + \gamma(N+1) \\ F_3(N) = F_2(N) &= B_v N(N+1) - D_v N^2(N+1)^2 \\ F_{3,1}(N) = F_3(N) &= B_v(N^2 - N + 1) - D_v N^2(N+1)^2 - \lambda \\ &\quad + \sqrt{(2N-1)^2 B_v^2 + \lambda^2} - 2\lambda B_v - \gamma N \end{aligned} \quad (4.2.22)$$

where γ and λ are the spin-rotation and spin-spin coupling constants respectively, and ξ in Kovács (31) is $2\lambda/3$ in Herzberg (29) or Mizushima (36), the latter giving extensive tabulations of γ for $^2\Sigma$ states and γ and λ for $^3\Sigma$ states. For $F_3(N=1)$ with $J = 0$, the sign in front of the square root must be inverted.

Quite generally, $F_3(J) > F_2(J) > F_1(J)$, and for the series F_1 , $N = J-1$, for F_2 , $N = J$ and for F_3 , $N = J+1$ for any coupling case even if N is not a good quantum number. If $\Lambda > 0$, like the doublets, we can define $\Omega = |\Lambda + \Sigma|$, so $\Omega = \Lambda - 1, \Lambda$ and $\Lambda + 1$. Also care must be taken in the assignment of the levels such that:

$Y > 0$ $F_1(J)$ belongs to the series with $\Omega = \Lambda - 1$,
 $F_2(J)$ belongs to the series with $\Omega = \Lambda$,
 $F_3(J)$ belongs to the series with $\Omega = \Lambda + 1$.

When $Y < 0$, F_1 and F_3 are interchanged. This rule is applied to all values of J even when $|Y|$ is small, as the lowest levels behave in a very complicated way, see for example Challacombe and Almy (64). When A is large and B_{eff} is given for the three levels separately, the middle one can be used as B_e .

As with the doublets, the Hönl-London factors for triplets are found from Kovács (31), see the appendices, with 27 branches in general in the form $S_{J-J''}^{\Sigma-\Sigma''} = X_{n-n''}(J'')$ where n is an index 1, 2 or 3. There are 54 equations for $\Delta\Lambda = 0, \pm 1$ which cannot unfortunately be compressed to 6 like the doublets.

Considerably greater problems were encountered, when attempts were made to determine the Hönl-London factors for the lowest levels, than the doublets. It was decided to treat the $J = \Lambda - 1$ and $J = \Lambda$ levels belonging to the $\Omega = \Lambda - 1$ ladder as strict case (a) regardless of Y when $\Lambda > 0$. Accordingly, the following rules are employed:

${}^3\Sigma \leftarrow {}^3\Sigma$: There is no problem as the general formulae can be applied, but the Hönl-London factors for 15 of the 27 possible branches are zero.

${}^3\Pi \leftarrow {}^3\Sigma$: $Q_{13}(0) = R_{13}(0) = 0$, $Q_{11}(1) = P_{12}(1) = 1/2$, $P_{11}(1) = 1/3$, $Q_{12}(1) = 3/4$, $P_{13}(1) = 1/6$, $Q_{13}(1) = 1/4$, $P_{11}(2) = 9/20$, $P_{12}(2) = 3/4$, $P_{13}(2) = 3/10$, with all other transitions being obtained from the general formulae when the relevant levels exist.

${}^3\Sigma \leftarrow {}^3\Pi$: $R_{11}(0) = 1/3$, $R_{21}(0) = 1/2$, $R_{31}(0) = 1/6$, $Q_{31}(0) = 0$, $Q_{11}(1) = 1/2$, $R_{11}(1) = 9/20$, $Q_{21}(1) = R_{21}(1) = 3/4$, $Q_{31}(1) = 1/4$, $R_{31}(1) = 3/10$, $P_{31}(1) = 0$, otherwise as before, apply the general formulae.

$\Lambda' \leftarrow \Lambda''$: With $\min(\Lambda', \Lambda'') > 0$, if $\Omega = \Lambda - 1$ and $J = \Omega$ or $\Omega + 1$ for the upper or lower states or both, then apply strict case (a) with (4.2.11) or (4.2.12) as appropriate, using Ω in place of Λ and "diagonal" transitions involving these levels are forbidden, i.e. $\Delta\Sigma = 0$.

As with the doublets, these rules are consistent with Schadee (62) after correcting his normalization. When $J > \lambda$, the sum of all branches is $3(2J+1)$ from a given J , but is not true for the lowest values of J which are not tripled. Thus for Σ states, there is only one level for $J = 0$, however, the sum rule of $2J+1$ from a given level should always apply.

Unlike the doublets, where the sum rule is always recovered when the transitions from the lowest levels are "patched up", for the triplets this is only approximately the case using the above prescription, as for some small values of Y for some transitions, the sum rule does break down for the lowest levels. At worst, this would only affect the first few lines in a complex band, with typically many hundreds or thousands of lines, and would thus be expected to have a negligible effect. In view of this, it was unfortunately not considered worth while pursuing this matter further.

It is also found that for the most intermediate case when $J(J+1) \approx |Y|$ with $Y \neq 0$, the sum rule is out by a few percent, but as this affects only a limited range of values of J for a given value of Y , it is again considered that the treatment is sufficient. Far greater uncertainties would be due to the input data, particularly oscillator strengths or transition moments, and in practice one would only expect in many cases at best to reproduce the gross properties of bands.

When $Y < 0$, the indices that refer to the state in question are changed such that $1 \rightarrow 3$, $2 \rightarrow 2$ and $3 \rightarrow 1$. Great care must be used with Kovács's formulae, Y is substituted with a negative value in all the relevant expressions, but in addition Λ must be replaced by $-\Lambda$ in equation 10 page 70 only. This is in addition to the same rule as for the doublets concerning the values of Λ to be inserted into the appropriate expressions.

The following misprints were noted in Kovács's formulae: page 132, $Q_{31}(J)$ in the last term, for $-8\Lambda(J-1)(J-\Lambda+1)\dots$ read $-8\Lambda(J-\Lambda)(J-\Lambda+1)\dots$ and page 133, $R_{32}(J)$ in the second term, for $\dots u_3^-(J+1)\dots$ read $\dots u_3^+(J+1)\dots$

For identical nuclei, the statistical weights follow the same rules as before, only now $N = J-1$ for F_1 , $N = J$ for F_2 and $N = J+1$ for F_3 .

Tatum (39) gives some very useful energy level diagrams for singlet, doublet and triplet electronic states for Hund's cases (a) and (b), together with some of the possible rotational transitions. Also, note that although we neglect transitions between different multiplicities, as stated in section 4.1 because they are very weak, a good example of such transitions observed both in absorption and emission in the ultraviolet are the Cameron bands of CO, $a^3\Pi \leftrightarrow X^1\Sigma^+$, i.e. transitions between the lowest excited electronic state which is a triplet, and the ground electronic state. Kovács (31) and (65) give Hönl-London factors for transitions involving different

multiplicities, also when $|\Delta J| > 1$ which we also neglect. Finally, although we consider states to be strictly Hund's case (b), Tatum and Watson (66) gives Hönl-London factors for ${}^3\Sigma \leftrightarrow {}^3\Sigma$ transitions when spin-spin and spin-orbit interactions do cause these states to approach case (a).

Having discussed the multiplicities in detail, we now make some general points about bands, neglecting the effects of centrifugal stretching and spin splitting.

When $B_{v'} > B_{v''}$, a band head forms on the P-branch at a longer wavelength than the band origin, such that:

$$\bar{\nu} = \bar{\nu}_0 - \frac{(B_{v'} + B_{v''})^2}{4(B_{v'} - B_{v''})} \quad (4.2.23)$$

when:

$$N \simeq \frac{1}{2} + \frac{B_{v'}}{(B_{v'} - B_{v''})} \quad (4.2.24)$$

so the band appears shaded towards the blue, and where $\bar{\nu}_0$ is the position of the band origin in wavenumber. When $B_{v'} < B_{v''}$, a band head forms on the R-branch at a shorter wavelength than the band origin, such that:

$$\bar{\nu} = \bar{\nu}_0 + 2B_{v'} - \frac{(3B_{v'} - B_{v''})^2}{4(B_{v'} - B_{v''})} \quad (4.2.25)$$

when:

$$N \approx -\frac{1}{2} - \frac{B_{v'}}{(B_{v'} - B_{v''})} \quad (4.2.26)$$

so the band appears shaded towards the red. The latter is always the state of affairs for VR bands, as $B_{v'}$ is always smaller than $B_{v''}$, except possibly in some very rare cases.

If the relative population of the energy levels is given by (see also section 2.5):

$$P = (2N+1)e^{-BN(N+1)hc/kT} \quad (4.2.27)$$

then:

$$P_{max} = \sqrt{\frac{2kT}{Bhc}} e^{\left(\frac{Bhc}{4kT} - \frac{1}{2}\right)} \quad (4.2.28)$$

when:

$$N \approx \sqrt{\frac{kT}{2Bhc}} - \frac{1}{2} \quad (4.2.29)$$

which corresponds approximately to the maxima in the P and R branches.

Finally, because higher order terms in the centrifugal stretching are neglected, for sufficiently large N, the levels will turn over in our approximation and become meaningless. This occurs when:

$$BN(N+1) \approx DN^2(N+1)^2 \quad (4.2.30)$$

i.e. when:

$$N \simeq \sqrt{\frac{1}{4} + \frac{B}{D}} - \frac{1}{2} \quad (4.2.31)$$

As N is of course always an integer in these expressions given here, we must round to the nearest integer. So in ascending the rotational energy level ladder, if N or J reaches the value in (4.2.31), the computation of the band is stopped, likewise if the top of the potential well is reached. In practice one would normally expect the band to be cut off long before these safeguards, due to the diminishing Boltzmann factor.

4.3 Vibrational Energy Levels and Matrix Elements

The vibrational term values measured from the bottom of the potential well, see section 2.6, is again:

$$G(v) = \omega_e(v + \frac{1}{2}) - \omega_e x_e(v + \frac{1}{2})^2 + \omega_e y_e(v + \frac{1}{2})^3 + \dots \quad (4.3.1)$$

where ω_e is the harmonic constant, $\omega_e x_e$, $\omega_e y_e \dots$ are anharmonic constants, and $v = 0, 1, 2, \dots$ is the vibrational quantum number.

As the zero point for calculating the vibrational partition function is the lowest vibrational level of the ground electronic state, the Boltzmann factor for this level, neglecting the effect of rotation, must be unity, hence we must refer all other vibrational levels to this. The zero-point energy of the $v = 0$ levels is:

$$G(0) = \frac{1}{2} \omega_e - \frac{1}{4} \omega_e x_e + \frac{1}{8} \omega_e y_e + \dots \quad (4.3.2)$$

hence:

$$G_o(v) = G(v) - G(0) \quad (4.3.3)$$

Frequently the vibrational constants ω_o , $\omega_o x_o$ and $\omega_o y_o$, which refer to the $v = 0$ level, are given such that:

$$G_o(v) = \omega_o v - \omega_o x_o v^2 + \omega_o y_o v^3 + \dots \quad (4.3.4)$$

It is, however, convenient always to work with the same quantities and convert these with the following relations, which are the inverse of those given in section 2.6, terms higher than $\omega_0 y_0$ being omitted:

$$\begin{aligned}\omega_e &= \omega_0 + \omega_0 x_0 + \frac{3}{4} \omega_0 y_0 \\ \omega_e x_e &= \omega_0 x_0 + \frac{3}{2} \omega_0 y_0 \\ \omega_e y_e &= \omega_0 y_0\end{aligned}\tag{4.3.5}$$

When the electronic state in question is an excited state, great care must be exercised in correctly calculating the term values consistently. If T_e and T_0 are electronic energies of an electronic state measured respectively to the bottom of the potential well and the lowest vibrational level, then for the ground electronic state, by definition:

$$T_0'' = 0 \quad \text{or} \quad T_e'' = 0\tag{4.3.6}$$

which respectively define the zero-point energy in whichever system we are working in. For an excited electronic state, T_e' is the energy of the bottom of the potential well of the excited state above the bottom of the potential well of the ground state, and T_0' is similarly measured with respect to the lowest vibrational levels. It follows that:

$$\begin{aligned}T_0' - T_e' &= \frac{1}{2} (\omega_e' - \omega_e'') - \frac{1}{4} (\omega_e' x_e' - \omega_e'' x_e'') \\ &+ \frac{1}{8} (\omega_e' y_e' - \omega_e'' y_e'') + \dots\end{aligned}\tag{4.3.7}$$

which is useful if we consistently want to work with T_e when T_0 is given. Except for the ground state, by definition, T_0 is subject to isotopic shift, unlike T_e which is constant.

If $H(v)$ is the term value for the vibrational level in an excited electronic state, then neglecting rotation and spin etc., we can write:

$$H(v) = G'(v) + T_e' - G''(0) = G'_0(v) + T_0' \quad (4.3.8)$$

which ensures that the Boltzmann factor is correctly set.

Finally, if D_e^0 and D_0^0 are respectively the dissociation potentials, distinct from D_e and D_0 the non-rigid rotational constants, measured from the bottom of the potential well and the $v = 0$ level, we can write:

$$D_e^0 - D_0^0 = G(0) = \frac{1}{2} \omega_e - \frac{1}{4} \omega_e x_e + \frac{1}{8} \omega_e y_e + \dots \quad (4.3.9)$$

where again, D_e^0 is constant but D_0^0 is subject to isotopic shift. If either of these two constants is not available, it can be found from the Morse approximation, thus:

$$D_e^0 = \frac{\omega_e^2}{4\omega_e x_e}, \quad D_0^0 = \frac{\omega_0^2}{4\omega_0 x_0} \quad (4.3.10)$$

which will in general not agree with the empirical value, if available. The Morse potential approximation, see later, allows only for the constants ω_e and $\omega_e x_e$ in the expansion for the vibrational

term values; in practice there are higher order terms of which only $\omega_e y_e$ is usually known. In rare cases $\omega_e z_e$ is also given, however, it is so small in such cases, that it is neglected in calculating the vibrational term values.

As in ascending the rotational ladder for a band, so in ascending the vibrational ladder for a band system, if the Boltzmann factor does not cut off the band system, we stop on reaching the top of the potential well, or when the levels turn over and become meaningless, or indeed when the maximum specified number of levels has been reached. The turnover is not found from a simple quadratic equation, as is done with the rotational levels, due to the presence of the cubic $\omega_e y_e$ term. Instead a test is done for each vibrational level in turn, to see if it has turned over.

We now come to the considerably more difficult problem of calculating the vibrational matrix elements. Originally, it was decided to find the overlap integral $\int \psi_V - \psi_V dr$, the square of which is known as the Franck-Condon factor, by calculating the harmonic overlap integral from Manneback (67), then applying Hutchisson II (68) to determine the anharmonic overlap integrals. Harmonic overlap integrals evaluated from recurrence relations by (67) were found to agree with the more cumbersome method by Hutchisson I (69) after correcting some errors in the latter. In (68), the Morse function is only expanded to three terms in the exponential, then perturbation analysis is used to obtain the anharmonic wave functions and overlap integrals. Unfortunately, a large number of errors were also found in this paper. Bates (70) gives formulae and also tables for determining

harmonic overlap integrals together with anharmonic corrections.

Most fortunately indeed, a recent method by Doktorov et al. (71) was found subsequently to be far superior to the Manneback-Hutchisson method mentioned above. The Schrödinger equation is solved explicitly with the Morse potential, rather than a truncated series, the computer code is far more efficient and there are a number of other important advantages discussed below. Accordingly, the Manneback-Hutchisson method was abandoned in favour of Doktorov's, except that the harmonic overlap integrals by Manneback, together with work from other references could be used as a check.

In addition to EVR bands, Doktorov's method is adapted here for calculating the vibrational transition moments of VR bands, hence tying together two separate branches of spectroscopy, and replacing the many long and complex formulae published in several papers by Bouanich e.g. (72), if the Morse potential is accepted as a good enough approximation.

These analytic techniques are adopted, as detailed numerical integration of wave functions of general Rydberg-Klein-Rees potential functions are considered beyond the scope of this work. For the same reason, it is assumed that the rotational contribution to the matrix elements can be factorized out as the Hönl-London factors, hence they are the rotationless vibrational matrix elements that are determined. This is expected to be a reasonably good approximation except for large J , by which time other uncertainties increase.

Doktorov's equations are taken and recast in a form found suitable for numerical work, as explained below. The Morse potential is again:

$$V(r) = D_e^0 \left[1 - e^{-\alpha(r-r_e)} \right]^2 \quad (4.3.12)$$

where D_e^0 is, as before, the dissociation potential in cm^{-1} , r_e the equilibrium internuclear separation and α a constant. To avoid excessively large or small numbers, it is convenient to express r_e in Ångströms, and hence adjust α accordingly. We can write the following relations:

$$\alpha'' = 10^{-8} \left(\frac{2\pi^2 c \mu}{D_e^{0''} h} \right)^{1/2} \omega_e'' \text{Å}^{-1}, \quad \alpha' = 10^{-8} \left(\frac{2\pi^2 c \mu}{D_e^{0'} h} \right)^{1/2} \omega_e' \text{Å}^{-1} \quad (4.3.13)$$

$$s'' = \frac{2D_e^{0''}}{\omega_e''} - \frac{1}{2}, \quad s' = \frac{2D_e^{0'}}{\omega_e'} - \frac{1}{2} \quad (4.3.14)$$

$$\alpha = \frac{\alpha' + \alpha''}{2} \quad (4.3.15)$$

and:

$$\mu_0 = \frac{2s' + 1}{2s'' + 1} e^{\alpha(r_e' - r_e'')} \quad (4.3.16)$$

where μ is the reduced mass in grams and s is the number of vibrational energy levels, such that the vibrational quantum numbers are restricted to the ranges $0 \leq v'' \leq s''$ and $0 \leq v' \leq s'$. s will lie very roughly between say 20 and 100, and will not in general be an integer by (4.3.14), though of course actually there can only be an integral number of vibrational levels. However, to make the treatment easier and more realistic, s is rounded to the nearest integer, as this is considered a minor approximation, in view of the fact that the Morse potential function is itself only an approximation. Indeed for safety, we restrict $v \leq s-1$. We also have the additional approximation of the α -averaging method, where we have to use the mean value of α from (4.3.15) for both of the electronic states, this being a compromise as Doktorov's equations can only be written in closed form when $\alpha' = \alpha''$. Fraser (73) uses this approximation in calculating the overlap integrals with Morse potentials using earlier methods, see for example Fraser and Jarman (74) and Jarman and Fraser (75). Clearly the further apart the two values of α are, the poorer is the approximation, at worst we can at least hope to obtain trends of the band strengths. (It is noted that there is an error in Doktorov's expression for the energy levels, as his D_e , the dissociation potential, in the anharmonic term must not be squared).

With the above information, we can now calculate the required vibrational matrix elements, defining:

$$T_{v'v''}^{(N)} = \langle v' | r^N | v'' \rangle = \int \Psi_{v'} r^N \Psi_{v''} dr \quad (4.3.17)$$

giving the normal overlap integrals when $N = 0$. In order to find each

required value of $T_{\nu-\nu}^{(N)}$, we must obtain $T_{00}^{(0)}$, $T_{00}^{(1)}$, $T_{00}^{(2)}$... etc., then use recurrence relations. Because of the limitation of the available molecular data, the highest value of N used is 4. Re-writing Doktorov's expressions for $T_{00}^{(N)}$ in a form suitable for numerical evaluation:

$$T_{00}^{(N)} = \left(\frac{-1}{\alpha}\right)^N \left[\frac{(t-1)(t-2) \dots (t-q)}{(2r-1)(2r-2) \dots (2r-q)} \right] \quad (4.3.18)$$

where:

$$X\left(\frac{2}{1+\mu_0}\right)^t \mu_0^{s'} X^{(N)}(t)$$

$$q = |s'' - s'|, \quad r = \max(s', s''), \quad t = s' + s'' \quad (4.3.19)$$

and $X^{(N)}(t)$ are the following functions whose complexity increases rapidly with N :

$$X^{(0)}(t) = 1 \quad (4.3.20)$$

$$X^{(1)}(t) = \ln a + \Psi(t) \quad (4.3.21)$$

$$X^{(2)}(t) = \ln^2 a + 2\Psi(t)\ln a + \Psi^{(1)}(t) + \{\Psi(t)\}^2 \quad (4.3.22)$$

$$X^{(3)}(t) = \ln^3 a + 3\Psi(t)\ln^2 a + 3[\Psi^{(1)}(t) + \{\Psi(t)\}^2]\ln a + \Psi^{(2)}(t) + 3\Psi(t)\Psi^{(1)}(t) + \{\Psi(t)\}^3 \quad (4.3.23)$$

$$X^{(4)}(t) = \ln^4 a + 4\Psi(t)\ln^3 a + 6[\Psi^{(1)}(t) + \{\Psi(t)\}^2]\ln^2 a + 4[\Psi^{(2)}(t) + 3\Psi(t)\Psi^{(1)}(t) + \{\Psi(t)\}^3]\ln a + \Psi^{(3)}(t) + 4\Psi(t)\Psi^{(2)}(t) + 3\{\Psi^{(1)}(t)\}^2 + 6\{\Psi(t)\}^2\Psi^{(1)}(t) + \{\Psi(t)\}^4 \quad (4.3.24)$$

where:

$$a = \frac{2e^{-\alpha\tau_0^n}}{(2s^n+1)(1+\mu_0)} \quad (4.3.25)$$

$$\psi(t) = \frac{d}{dt} \ln \Gamma(t) \quad \text{and} \quad \psi^{(n)}(t) = \frac{d^n}{dt^n} \psi(t) \quad (4.3.26)$$

Numerical values of $\psi^{(N)}(t)$, not to be confused with the symbols for wave functions in (4.3.17), are found by evaluating the asymptotic expansions as given by Abramowitz and Stegun (46), which are rapidly convergent even for fairly small arguments. The expansions used are:

$$\psi(t) = \ln t - \frac{1}{2t} - \frac{1}{12t^2} + \frac{1}{120t^4} - \frac{1}{252t^6} + \frac{1}{240t^8} - \frac{1}{132t^{10}} \dots \quad (4.3.27)$$

$$\psi^{(1)}(t) = \frac{1}{t} + \frac{1}{2t^2} + \frac{1}{6t^3} - \frac{1}{30t^5} + \frac{1}{42t^7} - \frac{1}{30t^9} \dots \quad (4.3.28)$$

$$\psi^{(2)}(t) = -\frac{1}{t^2} - \frac{1}{t^3} - \frac{1}{2t^4} + \frac{1}{6t^6} - \frac{1}{6t^8} + \frac{3}{10t^{10}} - \frac{5}{6t^{12}} \dots \quad (4.3.29)$$

$$\psi^{(3)}(t) = \frac{2}{t^3} + \frac{3}{t^4} + \frac{2}{t^5} - \frac{1}{t^7} + \frac{4}{3t^9} - \frac{3}{t^{11}} + \frac{10}{t^{13}} \dots \quad (4.3.30)$$

Direct summation of the recurrence relations given by Abramowitz and Stegun (46) agree well with (4.3.27-30) even for an unrealistically small value of $t = 5$, however, for large values of t , the direct summation becomes useless due to loss of significance.

With the required values of $T_{00}^{(N)}$, the recurrence relations given by Doktorov can be used to generate $T_{v'v''}^{(N)}$ in a three dimensional array, which has to be in double precision to limit the accumulation of round-off errors. For the v'' progression, i.e. $v'' \rightarrow v''+1$:

$$\begin{aligned}
 T_{v'v''}^{(N)} &= \left[\frac{2S'' - 2v'' + 1}{S' + S'' - v' - v''} \right] \left[\frac{S'' - v''}{v''(2S'' - v'' + 1)} \right]^{1/2} \left\{ - \left[\frac{S' - S'' - v' + v'' - 2}{2S'' - 2v'' + 3} \right] \right. \\
 &\times \left[\frac{(v'' - 1)(2S'' - v'' + 2)}{S'' - v'' + 2} \right]^{1/2} T_{v', v'' - 2}^{(N)} + 2\mu_0 \left[\frac{v'(S' - v')(2S' - v' + 1)}{S' - v' + 1} \right]^{1/2} \\
 &\times \frac{(S'' - v'' + 1)^{1/2} T_{v' - 1, v'' - 1}^{(N)}}{(2S' - v' + 1)} + (S'' - v'' + 1)^{1/2} \left[\frac{(2S'' + 1)(2S' - 2v' - 1)}{4(S'' - v'' + 1)^2 - 1} \right. \\
 &\left. - \mu_0 \frac{(2S' + 1)}{(2S'' - 2v'' + 1)} \right] T_{v', v'' - 1}^{(N)} + \frac{N}{\alpha} \left(\frac{1}{(2S'' - 2v'' + 3)} \left[\frac{(v'' - 1)(2S'' - v'' + 2)}{S'' - v'' + 2} \right]^{1/2} T_{v', v'' - 2}^{(N-1)} \right. \\
 &\left. + \frac{1}{(2S'' - 2v'' + 1)} \left[\frac{v''(2S'' - v'' + 1)}{S'' - v''} \right]^{1/2} T_{v', v''}^{(N-1)} \right. \\
 &\left. - \frac{2(S'' - v'' + 1)^{1/2}(2S' + 1)}{4(S'' - v'' + 1)^2 - 1} T_{v', v'' - 1}^{(N-1)} \right) \left. \right\} \quad (4.3.31)
 \end{aligned}$$

For the v' progression, interchange single and double primes and replace μ_0 by $1/\mu_0$. Coefficients of array elements that are impossible, e.g. $N-1 = -1$ or $v'-1 = -1$ are zero, and care is taken in the computer code to avoid accessing such non-existent elements.

Having computed $T_{00}^{(0)}$, $T_{00}^{(1)}$... we set $v'' = 1$ and compute $T_{01}^{(0)}$, $T_{01}^{(1)}$... then increment v'' by 1 and compute $T_{02}^{(0)}$, $T_{02}^{(1)}$... etc. until either a specified upper limit of v'' is reached, or the Boltzmann factor is used as a criterion; failing that, v'' is ultimately stopped when either the top of the potential well is reached or the levels turn over, as stated earlier. Having computed all the required values

in the Nv'' -plane, we set $v'' = 0$ and $v' = 1$ then compute $T_{10}^{(0)}$, $T_{10}^{(1)}$... and increment v'' as before. This process is repeated for each value of v' until the maximum allowed value is reached, this being from similar tests to v'' except for no Boltzmann factor. For computing efficiency, the order of increasing rate of change of the indices is chosen to be v' , v'' and N .

In developing the coding, a large number of tests were performed to check for errors and consistency. Quite generally, $T_{v'v''}^{(0)}$ satisfies the normalization:

$$\sum_{v''=0}^{\infty} [T_{v'v''}^{(0)}]^2 = \sum_{v'=0}^{\infty} [T_{v'v''}^{(0)}]^2 = 1 \quad (4.3.32)$$

for any v' and v'' respectively for any Morse potential in the two states. As $D_e^{0'} \rightarrow \infty$ and $D_e^{0''} \rightarrow \infty$, the two potential wells approach the harmonic limit, $T_{v'v''}^{(0)}$ approach the values computed by Manneback (67) and $T_{v'v''}^{(1)}$ approach those by Manneback and Rahman (76), after errors were corrected in (76).

We also introduce here the concept of the r -centroid, as defined by Fraser (73), see also for example Nicholls and Jarman (77) and Nicholls (78), where the r -centroid is defined as:

$$\bar{r}_{v'v''} = \frac{\langle v' | r | v'' \rangle}{\langle v' | v'' \rangle} \quad (4.3.33)$$

and can be considered as the characteristic internuclear separation for the electronic-vibration transition, but need not necessarily be close to the average of the internuclear separations of the two

electronic states. In computing the r-centroid for transitions by some appropriate method, e.g. an earlier method for Morse potentials by Nicholls and Jarman (77), we allow to first order at least the electronic transition moment to vary with vibrational transitions, see the next section. However, in computing higher order matrix elements, r-centroids are only an approximation, as generally:

$$\left[\bar{r}_{v'v''} \right]^N \neq \frac{\langle v' | r^N | v'' \rangle}{\langle v' | v'' \rangle} \quad (4.3.34)$$

but the matrix elements of all orders can be computed directly by Doktorov's method, so we do not have to compute r-centroids as such.

However, if we set $\omega_e = \omega_e' = \omega_e''$ but $r_e' \neq r_e''$, a very simple quick check to Doktorov's method is to compute r-centroids by Schamps (79) for two harmonic states with equal frequencies:

$$\bar{r}_{v'v''} = \frac{1}{2} (r_e' + r_e'') - \frac{10^{16} N_A h}{4\pi^2 c \mu \omega_e} \left(\frac{v' - v''}{r_e' - r_e''} \right) \quad (4.3.35)$$

where $\bar{r}_{v'v''}$, r_e' and r_e'' are the r-centroid and the internuclear separation in the two states respectively, all in Ångströms, ω_e is the vibrational frequency of the two states in cm^{-1} , μ is the reduced mass in amu and N_A is Avogadro's number. Then the ratios $T_{v'v''}^{(1)}/T_{v'v''}^{(0)}$ agree with $\bar{r}_{v'v''}$ by Schamps, if Doktorov's method is applied with very large values of $D_e^{0'}$ and $D_e^{0''}$ to approach the harmonic limit, and we do not consider matrix elements where $|T_{v'v''}^{(0)}|$ are very small as residual anharmonicity and numerical round-off errors become important.

Although the formula (4.3.35) can only be strictly applied for equal frequency harmonic oscillators, it is a very quick and easy approximate check for more general cases if ω_e is taken as the mean of the harmonic frequencies of the two electronic states, as often these are not too different and anharmonic effects are generally small for the lowest vibrational levels.

When applying these cross checks to Doktorov's method in the harmonic limit, they are invalid well away from the Condon parabola, (in the $v'v''$ -plane with $N = 0$, the matrix elements with the largest magnitude usually follow a parabolic curve), where $|T_{v'v''}^{(0)}| \ll 1$ due to the residual anharmonicity affecting the wave functions. Also, there is unfortunately no easy way of checking general $T_{v'v''}^{(N)}$ with $N > 1$, but there is confidence in them, as a result of applying Doktorov's method to VR bands, discussed later.

Finally, if $a_0, a_1 \dots$ are coefficients, then:

$$R_{v'v''} = a_0 T_{v'v''}^{(0)} + a_1 T_{v'v''}^{(1)} + a_2 T_{v'v''}^{(2)} + \dots \quad (4.3.36)$$

where $R_{v'v''}$ is the electronic transition moment. If $R_{v'v''}$ is in Debyes, where $1D = 10^{-18}$ esu-cgs, then a_i is in units of $D \text{ \AA}^{-i}$, when $T_{v'v''}^{(N)}$ are computed in \AA . It is most convenient to work consistently in \AA and Debyes.

In the discussion so far, Doktorov's method is applied, as originally intended, to transitions between two different electronic states giving rise to EVR bands, however, Doktorov's method can be used with some modifications to transitions within the same electronic state, giving rise to VR bands.

For VR bands, $T_{v'v''}^{(N)}$ is computed in exactly the same way as before, except that as both electronic states are the same state, we have identical constants, and hence no α -averaging approximation. However, the matrix elements obtained are $\langle v' | r^N | v'' \rangle$, but the elements required are $\langle v' | x^N | v'' \rangle$ where $x = r - r_e$. Expanding $T_{v'v''}^{(N)}$:

$$T_{v'v''}^{(N)} = \langle v' | (\gamma_e + x)^N | v'' \rangle = \gamma_e^N \langle v' | v'' \rangle + N \gamma_e^{N-1} \langle v' | x | v'' \rangle \quad (4.3.37)$$

$$+ \frac{N(N-1)}{2!} \gamma_e^{N-2} \langle v' | x^2 | v'' \rangle + \dots + \langle v' | x^N | v'' \rangle$$

and defining:

$$S_{v'v''}^{(N)} = \langle v' | x^N | v'' \rangle = \int \psi_{v'} x^N \psi_{v''} dx \quad (4.3.38)$$

then rearranging (4.3.37) for each value of N, we can write:

$$S_{v'v''}^{(0)} = T_{v'v''}^{(0)} \quad (4.3.39)$$

$$S_{v'v''}^{(1)} = T_{v'v''}^{(1)} - \gamma_e S_{v'v''}^{(0)} \quad (4.3.40)$$

$$S_{v'v''}^{(2)} = T_{v'v''}^{(2)} - \gamma_e^2 S_{v'v''}^{(0)} - 2\gamma_e S_{v'v''}^{(1)} \quad (4.3.41)$$

$$S_{v'v''}^{(3)} = T_{v'v''}^{(3)} - r_e^3 S_{v'v''}^{(0)} - 3r_e^2 S_{v'v''}^{(1)} - 3r_e S_{v'v''}^{(2)} \quad (4.3.42)$$

$$S_{v'v''}^{(4)} = T_{v'v''}^{(4)} - r_e^4 S_{v'v''}^{(0)} - 4r_e^3 S_{v'v''}^{(1)} - 6r_e^2 S_{v'v''}^{(2)} - 4r_e S_{v'v''}^{(3)} \quad (4.3.43)$$

where (4.3.39-43) are evaluated in this order for given v' and v'' and $T_{v'v''}^{(0)} = \delta_{v'v''}$, i.e. $T_{v'v''}^{(0)} = 1$ if $v' = v''$ otherwise $T_{v'v''}^{(0)} = 0$.

It is indeed found that on calculating the matrix elements $T_{v'v''}^{(N)}$ by Doktorov, then finding $S_{v'v''}^{(N)}$ from (4.3.39-43) with large D_e^0 , the harmonic oscillator result is approached. For the harmonic oscillator, the dimensionless length variable:

$$\xi = \frac{x}{\beta} \quad (4.3.44)$$

where $x = r - r_e$ as already defined, and where:

$$\beta = \left(\frac{h}{4\pi^2 \mu c \omega_e} \right)^{1/2} \quad (4.3.45)$$

by Hutchisson (68) after an error was corrected. From the expressions in (68), derived from the recurrence relations of the Hermite polynomials, we can write down the matrix elements for the harmonic oscillator, agreeing with those given by Shaffer and Krohn (80), given here for those elements up to fourth order that are non-zero:

$$\langle v' | v'' \rangle = 1 \quad \text{for } \Delta v = 0 \quad (4.3.46)$$

$$\langle v' | x | v'' \rangle = -\beta(v+1)^{1/2} / 2^{1/2} \quad \text{for } \Delta v = 1 \quad (4.3.47)$$

$$\langle v' | x^2 | v'' \rangle = \begin{cases} \beta^2 (2v+1)/2 & \text{for } \Delta v = 0 \\ \beta^2 [(v+1)(v+2)]^{1/2}/2 & \text{for } \Delta v = 2 \end{cases} \quad (4.3.48)$$

$$\langle v' | x^3 | v'' \rangle = \begin{cases} -3\beta^3 (v+1)^{3/2}/2 & \text{for } \Delta v = 1 \\ -\beta^3 [(v+1)(v+2)(v+3)]^{1/2}/2^{3/2} & \text{for } \Delta v = 3 \end{cases} \quad (4.3.49)$$

$$\langle v' | x^4 | v'' \rangle = \begin{cases} 3\beta^4 (2v^2+2v+1)/4 & \text{for } \Delta v = 0 \\ \beta^4 (2v+3)[(v+1)(v+2)]^{1/2}/2 & \text{for } \Delta v = 2 \\ \beta^4 [(v+1)(v+2)(v+3)(v+4)]^{1/2}/4 & \text{for } \Delta v = 4 \end{cases} \quad (4.3.50)$$

where v is the initial state, to express these in terms of the final state, we replace v by $v-\Delta v$ in all these expressions.

Each matrix element above has an arbitrary sign, however, it is found that in applying Doktorov's method for computing the matrix elements $\langle v' | x^N | v'' \rangle$ with large D_e^0 to approach the harmonic limit, alternate off-diagonal elements alternate in sign, thus if we adopt $\langle v' | v'' \rangle = +1$ for $\Delta v = 0$ in (4.3.46), the signs for all other matrix elements in (4.3.47-50) follow, and are given by $(-1)^{\Delta v}$. Thus in keeping to this sign convention, the values of $S_{v'v''}^{(N)}$ obtained from (4.3.39-43) by Doktorov's method in approaching the harmonic limit, agree well with (4.3.46-50), hence this is another good check on Doktorov's method. Elements that are zero in the harmonic case, have

by Doktorov, values of small magnitude. Exactly as expected, as D_e^0 is reduced and the potential becomes more anharmonic, the agreement with the harmonic case becomes poorer, in particular, elements that are zero in the harmonic limit become larger in magnitude, except the elements $S_{v'v''}^{(0)}$, which are always given by $\delta_{v'v''}$.

Finally, we can write the dipole moment expansion in terms of x , the same x as previously defined, as:

$$M(x) = M_0 + M_1 x + M_2 x^2 + \dots \quad (4.3.51)$$

where the most convenient units are $D\text{\AA}^{-1}$ as before. Similar to (4.3.36), we can write the transition moment as a linear combination of the matrix elements:

$$R_{v'v''} = M_0 S_{v'v''}^{(0)} + M_1 S_{v'v''}^{(1)} + M_2 S_{v'v''}^{(2)} + \dots \quad (4.3.52)$$

M_0 is the permanent dipole moment of the molecule, but unless we are dealing with pure rotational bands when $\Delta v = 0$, the first term of (4.3.52) is of no interest as $S_{v'v''}^{(0)} = 0$ when $\Delta v \neq 0$.

$S_{v'v''}^{(N)}$ and $R_{v'v''}$ are all symmetric matrices about the main diagonal, unlike transitions between different electronic states. It is however, a convenient check to calculate the full matrices, although only half of each is used. Although the signs of $R_{v'v''}$ in (4.3.36) and (4.3.52) are of no interest, as $R_{v'v''}^2$ are used in computing the band strengths, the relative signs of the individual terms in the two expressions are of course important.

4.4 Determination of Absolute Line Strengths

The Hönl-London factors in section 4.2 can be used to obtain the relative rotational strengths within a given band, and the squares of the vibrational transition moments in section 4.3 can be used to obtain the relative band strengths within a given band system. Here, all the factors are put together to obtain the required absolute line strengths, ensuring in particular that the various statistical weight factors are correctly accounted for.

Quite generally for the strength of an individual line:

$$S = \frac{8\pi^3 \bar{\nu}}{3h} R_{v'v''}^2 S_{J'J''}^{\Sigma'\Sigma''} \frac{e^{-F(n'', v'', \Sigma'', J'') hc/kT}}{Q} \quad (4.4.1)$$

in units of $\text{cm}^2/\text{sec}/\text{molecule}$, for VR or EVR bands. Then $\bar{\nu}$ is the wavenumber of the line in cm^{-1} , $R_{v'v''}$ is the transition moment between the two vibrational levels in esu-cgs, $S_{J'J''}^{\Sigma'\Sigma''}$ is the Hönl-London factor, $F(n'', v'', \Sigma'', J'')$ is the term value in cm^{-1} for the initial state, where n'' represents the electronic state, and Q is the total partition function. From section 4.2, the electron spin statistical weight of $2S+1$ is included in the normalization of the Hönl-London factors, and the factor of two for Λ -doubling, when relevant, is accounted for by splitting the line into two components, as discussed in section 4.2, whose strengths are equal to the original line, neglecting any complication of nuclear spin, and it is one of these components that is given here. If the nuclei are identical, we have

the additional nuclear spin statistical weight of g_I which is only relevant for EVR bands.

Dropping the Boltzmann factor and partition function, we can write the total band strength as:

$$S_{v'v''} = \frac{8\pi^3 \bar{\nu}_{v'v''}}{3h} R^2_{v'v''} (2S''+1) (2 - \delta_{0,\lambda'+\lambda''}) \quad (4.4.2)$$

in units of $\text{cm}^2/\text{sec}/\text{absorber}$, where $\bar{\nu}_{v'v''}$ is the wavenumber of the band origin in cm^{-1} .

Note that for the last term in (4.4.2), the factor of two for Λ -doubling is applied if $\Lambda > 0$ for at least one of the electronic states, and is quite distinct from the electronic statistical weight factor in (2.7.1), which is included in the total partition function, see Whiting and Nicholls (81) and Schadee (82). However, for the transitions $\bar{\Pi} \leftrightarrow \Sigma$, even though the rotational levels of the $\bar{\Pi}$ state are Λ -doubled, the spectral lines will not be Λ -doubled due to the selection rules of the parity of the rotational levels, i.e. $+\leftrightarrow -$, see section 4.1. This is because each rotational level of the $\bar{\Pi}$ electronic state is split into a pair of sublevels of opposite parity, in addition to any spin splitting, with only one transition of each P, Q and R-type between any pair and the appropriate levels in the Σ state, see the diagrams in Herzberg (29).

For VR bands, $R_{v'-v''}^2$ is obtained directly from (4.3.52), but for EVR bands, the total transition moment can be factorized into two parts:

$$R_{v',v''}^2 = q_{v',v''} R_e^2(r) \quad (4.4.3)$$

where $q_{v',v''}$ is the Franck-Condon factor, and is the vibrational part of the transition moment, defined as:

$$q_{v',v''} = \langle v' | v'' \rangle^2 = [T_{v',v''}^{(0)}]^2 \quad (4.4.4)$$

which is a number between 0 and 1 and can be calculated by Doktorov's method. $R_e^2(r)$ is the electronic part of the transition moment, which will in general depend on the r-centroid for the transition, so we cannot in general completely separate out the vibrational and electronic parts of the transition moment.

$R_e^2(r)$ is often given in the literature in forms like:

$$R_e^2(r) = (a_0 + a_1 r + a_2 r^2 + \dots)^2 \quad (4.4.5)$$

or:

$$R_e^2(r) = a e^{-br} \quad (4.4.6)$$

where to first order at least, r is the r-centroid and $a_0, a_1 \dots$ and a and b are coefficients. For higher orders, if we generalize the

r-centroid concept to the $r^{(N)}$ -centroid defined as:

$$\bar{r}_{v'v''}^{(N)} = \frac{\langle v' | r^N | v'' \rangle}{\langle v' | v'' \rangle} = \frac{T_{v'v''}^{(N)}}{T_{v'v''}^{(0)}} \quad (4.4.7)$$

as opposed to (4.3.35), and divide both sides of (4.4.5) by $q_{v'v''}$, we end up with the square of (4.3.36), hence Doktorov's method can be applied directly. The same can be done for (4.4.6) after expanding the exponential, though Doktorov does give a method, which we do not use, that enables the exponential form to be treated directly.

In some cases in the literature, instead of $R_e^2(r)$ being given, we have a band oscillator strength $f_{v'v''}$ or an electronic oscillator strength $f_{el}(\bar{\nu}_{v'v''})$, such that:

$$f_{el}(\bar{\nu}_{v'v''}) = \frac{f_{v'v''}}{q_{v'v''}} \quad (4.4.8)$$

If one of these is given for the 0-0 band, we can write:

$$S_{v'v''} = \frac{11e^2}{m_e c} f_{00} \frac{\bar{\nu}_{v'v''}}{\bar{\nu}_{00}} \frac{q_{v'v''}}{q_{00}} (2S''+1)(2-S_{0,1,1,1,1''}) \quad (4.4.9)$$

in units of $\text{cm}^2/\text{sec}/\text{absorber}$, assuming that $R_e^2(r)$ is constant over the whole band system in the absence of further information. Also, we can relate the band oscillator strength and transition moment by the expression:

$$f_{v'v''} = \frac{8\pi^2 m_e c \bar{\nu}_{v'v''}}{3 h e^2} R_{v'v''}^2 \quad (4.4.10)$$

where m_e is the mass of the electron.

For EVR bands, if two electronic states are close together, it may happen that a vibrational level in the upper electronic state is actually at a lower energy than a particular level in the lower electronic state, giving rise to a reversed band and detected by a negative value of $\bar{\nu}$. In this case, the absolute value of $\bar{\nu}$ is taken, and the Boltzmann factor is applied to the level in the upper electronic state.

5 COMPUTING THE BAND SPECTRA OF TRIATOMIC MOLECULES

5.1 Introduction

Whereas the VR and EVR band spectra of diatomic molecules are calculated ab initio from dipole moments, rotational and vibrational constants etc., this is not followed through to triatomic molecules because of the very much greater complexity in their spectra, particularly non-linear molecules like H₂O. Thus instead of calculating vibrational band strengths from a dipole moment expansion, band strengths are calculated in sequences of fixed Δv_1 , Δv_2 and Δv_3 , as mentioned by Auman (15), with the strength of the first member of the sequence being known. An important additional simplification is to assume that all transitions occur within the ground electronic state, and that electronic transitions can be neglected. The lowest of the excited electronic states of H₂O and CO₂, usually the two most abundant triatomic molecules, are at high energies, so any electronic transitions occur at short wavelengths where there is little flux and the effect on the overall opacity is small. Molecules that do have electronic transitions at longer wavelengths, like NO₂, have lower abundances, so again the effect on the opacity is expected to be small. In view of this, together with the fact that the general theory of triatomic overlap integrals becomes extremely complex, it is considered beyond the scope of this work to deal with triatomic EVR bands. However, for restricted cases, overlap integrals could be calculated by Doktorov et al. (71) and (83).

For diatomic molecules, it is assumed that to a good approximation, the dipole moment expansion is independent of isotopic substitution; and for atoms of equal charge, remains zero even if the nuclei are not identical. This is unfortunately not generally true, particularly with a change in symmetry, for triatomic molecules. Thus for normal CO_2 , being symmetric there is no net dipole moment, so vibrational transitions involving changes in ν_1 , the classical symmetric stretch with the carbon atom remaining stationary, are inactive in the infrared. If we now isotopically substitute one oxygen atom, giving say $\text{O}^{16}\text{C}^{12}\text{O}^{18}$, on the face of it we would appear to have a situation similar to $\text{C}^{12}\text{C}^{13}$, as discussed in the previous chapter, and the dipole moment would remain zero. For the non-vibrating molecule, to a good approximation this would indeed be expected to be the case, however, the carbon atom is no longer at the centre of gravity so moves in the classical symmetric vibration, which is now no longer strictly symmetric; thus quantum mechanically, there is a vibrational transition moment associated with a change in ν_1 , hence ν_1 is active in the infrared. Selection rules connected with the bending mode ν_2 and the antisymmetric stretch ν_3 are also affected, as described in the next section.

The situation for a bent molecule is more complicated. In theory we could apply the method of Secroun et al. (84), if the coefficients of the dipole moment expansion are known for a bent XY_2 molecule like water, where the permanent dipole moment lies along the symmetry axis, which is also the intermediate moment of inertia axis for water, and the transition dipole moment associated with vibrational transitions

will be either perpendicular or parallel to this axis, depending on the change of the vibrational quantum number, discussed later. However, Secroun's method is not applicable to non-symmetric molecules like HOD, as the vibrational transition moment will be at some general angle to the bisector of the HOD angle (no longer an axis of symmetry), which will now also be different from the intermediate moment of inertia. In addition, the permanent dipole moment of the non-vibrating molecule will not in general be aligned with any of the principal moments of inertia.

Additional to VR bands of water vapour, pure rotational bands are also considered, unlike diatomic and linear triatomic molecules, due to the large number of lines at sufficiently short wavelengths in the infrared where the weighting function, for the temperatures of interest, is large enough for these bands possibly to have a significant effect on the total RMO. Most molecules have their pure rotational bands in the far infrared, where the weighting function and the radiative flux are small enough for the bands to be expected to have a negligible effect on the RMO.

Because three atoms can only be collinear or coplanar, there are restrictions on the ranges of the rotational constants A, B and C, where by definition for general polyatomic molecules $A \gg B \gg C$:

(i). A = B = C Spherical Top Molecule: This cannot occur with triatomic molecules, so is of no interest here. The best example is CH_4 , point group T_d .

(ii). A = B > C Oblate Symmetric Top Molecule: This will occur with three identical atoms arranged in an equilateral triangle, point group D_{3h} , or special cases of C_{2v} or C_s where a symmetric top occurs accidentally. H_3^+ is one of the few examples known.

(iii). A > B = C Prolate Symmetric Top Molecule: This cannot occur for any planar molecules, but linear molecules like CO_2 and HCN, point groups $D_{\infty h}$ and $C_{\infty v}$ respectively, can be regarded as special cases of a prolate symmetric top. However, it is convenient to treat linear molecules quite separately.

(iv). A > B > C Asymmetric Top Molecule: This will occur for all molecules in general of point group C_{2v} e.g. H_2O and H_2S , and C_s e.g. HCO radical.

Although (ii) is only realized in a few cases, and (iii) is impossible, discounting linear molecules, they are useful approximations to (iv) under suitable conditions when considering selection rules, line strengths and energy levels.

Because of the approximations that have to be made in computing the bands of triatomic molecules, it is likely that individual lines and even whole bands will correspond very poorly to those in the observed spectra. However, due to the large number of overlapping bands that are characteristic of triatomic molecules at the

temperatures of interest, details of individual bands are lost, and it is hoped that at least the gross properties of the spectra are reproduced. Only with the lower temperatures in a planetary atmosphere, where the lowest vibrational levels are significantly populated, would it be feasible to carry out an accurate line by line calculation for each band.

5.2 Vibration-Rotation Spectra of Linear Molecules

Although the work here deals with linear triatomic molecules in general, in practice it would mostly be applied to CO_2 and its isotopic variants, as CO_2 is normally expected to be the most abundant linear triatomic molecule in stellar atmospheres, and more data is available on it than other linear molecules.

For a given transition $v \rightarrow v+\Delta v$ of the harmonic oscillator, from section 4.3, it is seen that the matrix element $\langle v | x^n | v+\Delta v \rangle$ is zero except for $n = \Delta v, \Delta v+2, \Delta v+4, \dots$, where the matrix element with $n = \Delta v$ contributes most to the total transition moment. Neglecting the effects of the higher order matrix elements, the transition moment is:

$$R_{v, v+\Delta v} = \langle v | x^{\Delta v} | v + \Delta v \rangle = M_{\Delta v} \beta^{\Delta v} \left[\frac{(v+\Delta v)!}{2^{\Delta v} v!} \right]^{1/2} \quad (5.2.1)$$

where $M_{\Delta v}$ is a coefficient in the dipole moment expansion defined in (4.3.51) and β is defined in (4.3.45).

If $R_{0, \Delta v}^2$ is obtained from observation, then $R_{v, v+\Delta v}^2$ can be found easily from:

$$\frac{R_{v, v+\Delta v}^2}{R_{0, \Delta v}^2} = \frac{\langle v | x^{\Delta v} | v + \Delta v \rangle^2}{\langle 0 | x^{\Delta v} | \Delta v \rangle^2} = \frac{(v + \Delta v)!}{v! \Delta v!} \quad (5.2.2)$$

neglecting anharmonicity and higher order matrix elements. Thus, for

general polyatomic molecules with non-degenerate vibrations, the total transition moment can be approximated to a product of the transition moments of the individual vibrations:

$$\left[\frac{R(v_1, v_2, v_3, \dots; v_1 + \Delta v_1, v_2 + \Delta v_2, v_3 + \Delta v_3, \dots)}{R(0, 0, 0, \dots; \Delta v_1, \Delta v_2, \Delta v_3, \dots)} \right]^2 = \prod_i \frac{(v_i + \Delta v_i)!}{v_i! \Delta v_i!} \quad (5.2.3)$$

where for triatomic molecules, $i = 1, 2$ and 3 , giving the formula quoted by Auman (15).

Thus given the first member of a progression of bands with constant Δv_1 , Δv_2 and Δv_3 , we can calculate the other bands in the progression using (5.2.3). Although the anharmonicity is neglected in obtaining the approximate band strengths, it is of course included in the calculation of the energy levels, see section 2.11.

As we can write:

$$\begin{aligned} R^2(v_1, v_2, v_3; v_1 + \Delta v_1, v_2 + \Delta v_2, v_3 + \Delta v_3) \\ = R^2(v_1, v_2 + \Delta v_2, v_3; v_1 + \Delta v_1, v_2, v_3 + \Delta v_3) \end{aligned} \quad (5.2.4)$$

and likewise for any other vibrational quantum number, then given a progression of sum bands with say $\Delta v_1 = 0$, $\Delta v_2 = 1$ and $\Delta v_3 = 1$, we can immediately obtain the difference bands $\Delta v_1 = 0$, $\Delta v_2 = -1$ and $\Delta v_3 = 1$, provided this transition still corresponds to an increase in energy, which is normally the case here as $\omega_2 < \omega_3$ for triatomic molecules in general.

For linear molecules, we have the additional complication that the v_2 mode of vibration is doubly degenerate, giving rise to angular momentum about the internuclear axis specified by ℓ , the vibronic quantum number, such that $\ell = v_2, v_2-2, v_2-4 \dots 1$ or 0 . For CO_2 , and any other linear molecules we are likely to consider, the ground electronic state has no electron spin or orbital angular momentum, so we do not have to consider any coupling between ℓ, Λ and S , which is described in Herzberg (34).

We can consider ℓ to occupy the same rôle as Λ for diatomic molecules, giving rise to the same Hönl-London factors, selection rules and restrictions on J . By Herzberg (30), $\Delta\ell = 0$ and $\Delta\ell = \pm 1$ give rise to parallel and perpendicular bands respectively, and are analogous to the corresponding transitions in Λ for diatomic molecules, except that for them perpendicular bands must involve an electronic transition. It can thus be seen that if $|\Delta v_2|$ is even then $\Delta\ell = 0$ and $|\Delta v_2|$ odd then $\Delta\ell = \pm 1$, see Dennison (85), hence a given band with specified $v_1' v_2' v_3' \leftarrow v_1'' v_2'' v_3''$ consists in fact of several bands $v_1' v_2' \ell' v_3' \leftarrow v_1'' v_2'' \ell'' v_3''$ with ℓ' and ℓ'' taking allowed values, and with the number of bands increasing with v_2' and v_2'' .

Because of the degeneracy of the v_2 bending vibration, the product in (5.2.3) is incorrect for $i = 2$, and has to be replaced by the square of the radial matrix element (RME) of the isotropic plane harmonic oscillator, with the expressions for $i = 1$ and $i = 3$ being retained. With $\Delta v_2 = 0$, there is no problem as $\Delta\ell = 0$ and the square of the RME $\langle v_2'' \ell'' | v_2' \ell' \rangle$ is unity for each substate of ℓ , where for

$\ell = 0$ there is one substate and for $\ell > 0$ the levels are ℓ -doubled, exactly the same as Λ -doubled for diatomic molecules, with two substates. Thus:

$$\sum_{\ell''} \langle v_2'' \ell'' | v_2'' \ell'' \rangle^2 = v_2'' + 1 \quad (5.2.5)$$

which is also the degeneracy if the splitting in ℓ is neglected, and is the total strength that would be put into (5.2.3) if we wished to consider this as one transition and neglected the splitting.

However, in keeping with our treatment for diatomic molecules, each line is computed separately with any degeneracy being "resolved" except for the fundamental $2J+1$ rotational degeneracy. Thus each band with different ℓ is computed separately, and for those levels with $\ell > 0$, ℓ -doubling of the lines is treated in exactly the same way as Λ -doubling for diatomic molecules by using the same coding. Not every rotational line consists of v_2+1 components, however. This is true for the P, Q and R-branches for v_2 odd and P and R-branches for v_2 even, but there are only v_2 components in the Q-branch for v_2 even, as there is no Q-branch with $\ell = 0 \rightarrow 0$. Moreover, there are fewer components in all cases if $J < v_2$ as J cannot be smaller than ℓ .

When $\Delta v_2 = \pm 1$, then $\Delta \ell = \pm 1$ or ∓ 1 subject to allowed values of ℓ . The RMEs in these cases can be obtained from the rather cumbersome formulae quoted by Penner (86) page 155 obtained from Schrödinger (87). If the definition of the binomial coefficient is extended to include negative values, as is the case in Schrödinger's formula, then it is found that the formula agrees with the far simpler expressions

given by Shaffer and Krohn (80) which are used here. From Shaffer and Krohn, we can write the expressions:

Δv_2	Δl	$\frac{\langle v_2' l' r v_2'' l'' \rangle^2}{}$	
1	1	$\frac{1}{2} (v_2'' + l'' + 2)$	
1	-1	$\frac{1}{2} (v_2'' - l'' + 2)$	(5.2.6)
-1	1	$\frac{1}{2} (v_2'' - l'')$	
-1	-1	$\frac{1}{2} (v_2'' + l'')$	

It can be shown that:

$$\sum_{l''} \sum_{l'} \langle v_2' l' | r | v_2'' l'' \rangle^2 = \frac{1}{2} (v_2 + 1)(v_2 + 2) \quad (5.2.7)$$

which is the sum over all v_2+1 possible bands, where the other vibrational quantum numbers are kept constant and v_2 is the smaller of v_2' and v_2'' .

When $|\Delta v_2| > 1$, we use further formulae given by (80) for $\Delta l = 0$ or ± 1 depending on Δv_2 . However, Shaffer also gives RMEs of transitions for $|\Delta l| > 1$ due to higher order effects of Coriolis interactions, McClatchey et al. (88), that contradict the simple selection rules of l . Unfortunately, there are no general Hönl-London factors for $|\Delta l| > 1$ available, though one could in principle "fudge" intensities in the P, Q and R-branches by simply putting $(2J+1)/3$ into each. However, this complication does not arise for most of the strong bands, and in view of this and the additional complexity, all transitions for which $|\Delta l| > 1$ are neglected.

In order to compute the band strengths in a progression, we need to obtain the strength of the first member of the progression and put it into a convenient form. McClatchey et al. (88) gives extensive tabulations of band strengths of several molecules including CO₂ and H₂O as S_v^o(296), the band absorption coefficient in cm⁻¹/(molecule cm⁻²) at 296°K. S_v^o(296) contains several factors that are convenient to multiply out to obtain the "reduced" band strength (S_v/ν̄_o) using:

$$\left(\frac{S_v}{\bar{\nu}_o}\right) = \frac{S_v^o(T) Q_v(T) c}{F \bar{\nu}_o e^{-G_v hc/kT} (1 - e^{-hc\bar{\nu}_o/kT})} \quad (5.2.8)$$

in cm³ per sec per absorber. Where S_v^o(T) is the band absorption coefficient in cm⁻¹/(molecule cm⁻²) at T°K, Q_v(T) is the vibrational partition function at T°K, F is the fraction of molecules in the isotopic form being considered, G_v is the term value in cm⁻¹ of the lower vibrational level, where G_v = 0 for the first member of a progression, and ν̄_o is the band origin in cm⁻¹; all other symbols have their usual meanings. In practice, the stimulated emission factor which is taken out in (5.2.8) makes little difference, and when computing individual line strengths, is included in the weighting function.

The line strengths are calculated from:

$$S = \left(\frac{S_o}{\bar{\nu}_o}\right) \frac{\bar{\nu} R_v^2 S_{j'j''} e^{-[G_v + F_v(j'')] hc/kT}}{Q(T)} \quad (5.2.9)$$

in cm² per sec per isotopic molecule. Where (S_o/ν̄_o) is the reduced band strength of the first member of the progression, R_v² is the square of the relative vibrational transition matrix element, obtained from

(5.2.3) but modified for the vibronic quantum number, $S_{J'J''}$ is the Hönl-London factor, $\bar{\nu}$ is the spectral line's wavenumber in cm^{-1} , $Q(T)$ is the total partition function at $T^\circ\text{K}$ and $G_v + F_v(J'')$ is the total term value of the lower rotational energy level in cm^{-1} . If (5.2.9) is multiplied by the number of molecules of the required isotopic form per cm^3 , we obtain an absorption coefficient in $\text{cm}^2/\text{sec}/\text{cm}^3$ or $(\text{cm sec})^{-1}$, which are the actual units handled.

An additional problem, particularly for CO_2 , is due to the accidental degeneracy of the different vibrational levels, giving rise to Fermi resonances that cause a perturbation of the energy levels when permitted by selection rules, see Herzberg (30) and (34). The effect for two levels is to cause them to "repel" each other so they no longer agree with (2.11.1), and a mixing of the vibrational eigenfunctions so that the strengths of the corresponding bands are redistributed. This becomes even more complicated when more levels are involved, and accordingly this problem is considered beyond the scope of this work, but we must discuss it here qualitatively.

For CO_2 , $\omega_1 \approx 2\omega_2$ and there is a Fermi resonance between the states 10^0_0 and 02^0_0 which causes them no longer to agree with the simple formula, however, 02^2_0 is not affected, causing an anomalously large splitting between $\ell = 0$ and $\ell = 2$. As we are neglecting the shifts on the perturbed levels, this strengthens our argument earlier of treating independently bands that differ only in ℓ' and ℓ'' , as any overlapping of lines is likely to be accidental.

Because of the mixing of the eigenfunctions of the levels in a Fermi polyad, each level assumes some of the properties of the other levels, in addition to being shifted, and some of the vibrational quantum numbers lose their proper meanings and cannot unambiguously designate the members of the polyad. Thus, if one of these levels is in a band at the beginning of some progression, we have a problem as to how to label this band and follow the quantum numbers through the progression. Thus suppose 02^0_0 is at a slightly higher energy than 10^0_0 if no perturbation takes place, which according to McClatchey et al. is the case for CO_2 , the Fermi resonance causes the two states to be moved apart and mixed so that v_1 and v_2 are no longer good quantum numbers. However, for convenience, we can continue to label the upper state as 02^0_0 with notional quantum numbers.

More generally, let $km^{\ell}nr$ designate the level of a polyad from McClatchey et al., where $k = v_{1\max}$, $m = v_{2\min}$, $n = v_3$ and $r = 1, 2, 3, \dots$ the rank in order of decreasing energy with v_3 and ℓ remaining constant. Then as (v_1, v_2, v_3) , (v_1-1, v_2+2, v_3) , $(v_1-2, v_2+4, v_3) \dots$ have all approximately the same energy, we can write in order of decreasing energy:

$$\left. \begin{array}{l} k, m, n, 1 \\ k, m, n, 2 \\ k, m, n, 3 \\ \text{---} \\ k, m, n, k+1 \end{array} \right\} \left\{ \begin{array}{l} 0, m+2k, n \\ 1, m+2k-2, n \\ 2, m+2k-4, n \\ \text{---} \\ k, m, n \end{array} \right.$$

where on the right, the notional quantum numbers we use for labelling bands, are associated with the ranks in a Fermi polyad with $k+1$ members on the left. Because of anharmonicity which is only approximated in (2.11.1), the order may in many cases be reversed or even rearranged differently according to the simple formula, so in practice our notional designation is somewhat arbitrary. When CO_2 is isotopically substituted, the orders in a polyad may also be rearranged. For different triatomic molecules, including non-linear ones, other such relationships between ν_1 , ν_2 and ν_3 can occur in Fermi resonances. Even though the first band of a progression may be perturbed, for continuity with the other members of the progression, we put in (5.2.9) the unperturbed vibrational energy, though $\bar{\nu}_0$ is the actual observed wavenumber of the band origin.

For molecules with a $D_{\infty h}$ point group like CO_2 , ν_1 cannot change without an accompanying permitted change in ν_2 and ν_3 , and ν_2 and ν_3 can only change according to when $|\Delta\nu_2 + \Delta\nu_3|$ is odd. When the molecule is isotopically substituted so that it is no longer symmetric, or for molecules like HCN which can never be symmetric, these selection rules do not apply and many more transitions can occur. However, because of the way we generate the transitions, we do not have to consider these

selection rules.

The rotational energy levels are calculated in exactly the same way as for the diatomic molecules, except that now B and D depend on the three vibrational quantum numbers, and ℓ is used in place of Λ , see Herzberg (30). Thus:

$$B_{[v]} = B_e - \alpha_1(v_1 + \frac{1}{2}) - \alpha_2(v_2 + 1) - \alpha_3(v_3 + \frac{1}{2}) \quad (5.2.10)$$

where each of α_i contains several terms including Coriolis interaction factors which we do not consider separately.

McClatchey et al. (88) gives vibration-rotation intensity factors for several bands of CO_2 , with which we should obtain the correct line intensities on multiplying by the Hönl-London factors etc., also in a series of papers mostly by Valero and Suarez, see for example Valero et al. (89), these factors are given in greater detail together with band strengths and transition moments for a few specific bands. However, because these factors are not available for higher members in a progression, and because we would not expect these factors to alter the gross appearance of the spectrum due to the many overlapping bands, we assume that we can factorize out the rotational line strengths as simple Hönl-London factors in the same way as for diatomic molecules. Thus the rotational fine structure is computed exactly as before using the same coding. Also, when the two end nuclei are identical, the effect of nuclear spin on the statistical weights of the rotational levels, hence line strengths, is identical with that in diatomic molecules, so the same procedure is used. For

normal CO_2 , as the two oxygen atoms have zero nuclear spin, alternate rotational lines are missing.

In computing a given progression of Δv_1 , Δv_2 and Δv_3 , bands are computed by varying v_1'' , v_2'' and v_3'' and allowed values of ℓ'' and ℓ' in nested loops, climbing up the ladders of vibrational levels and cutting off at dissociation, turnover or when bands become too weak. This is repeated for any possible difference bands by taking negative values of Δv_1 , Δv_2 or Δv_3 .

5.3 Vibration-Rotation and Pure Rotation Spectra of Non-Linear Molecules

We consider here in general non-linear triatomic molecules whose three principal moments of inertia are different, and are thus asymmetric tops with point groups C_{2v} and C_s . As with the previous section, in practice our discussion deals with one specific molecule, in this case H_2O , which is normally expected to be the most abundant by far of all triatomic molecules, in view of its stability and the abundances of hydrogen and oxygen.

For bent molecules, there is no problem with any vibronic quantum numbers as all three modes of vibration are non-degenerate, hence (5.2.3) can be used with $i = 1, 2$ and 3 to obtain the intensities in the progressions. Although the vibrational transitions are easier to deal with in these molecules, this is more than outweighed by the very complicated rotational fine structure of bands that must be computed by making appropriate approximations. Accordingly, we deal below entirely with the rotational fine structure of vibration-rotation and pure rotation bands.

For the oblate or prolate symmetric top molecule, each value of J has $J+1$ sublevels specified by the quantum number K which takes values $K = 0, 1, 2, \dots, J$, such that all sublevels with $K > 0$ are doubly degenerate making $2J+1$ sublevels in all. If the molecule is now made into an asymmetric top, this degeneracy is removed and each value of J

has $2J+1$ different energy sublevels in addition to the ever present $2J+1$ statistical weight. Except for a few special cases, the general evaluation of the rotational term values for each of the $2J+1$ sublevels of J is very involved, see Herzberg (30), Wang (90) and King et al. (91), and likewise for the rotational line strengths, see Cross et al. (92) and Wacker and Pratto (93) who both give tabulations of line strengths. Because of this complexity and the expense in computer time of having to process millions of spectral lines, we have to resort to approximate means of calculation.

The $2J+1$ degree secular determinant whose roots give the required sublevel energies, breaks down into several algebraic equations whose degrees increase with J ; for the smaller values of J , these equations are linear or quadratic and can be solved explicitly. Derived from Herzberg (30), these solutions are given below, where $F(J_{\zeta})$ is the rotational term value in cm^{-1} of the ζ sublevel of J with $\zeta = -J, -J+1, \dots, J-1, J$ in order of increasing energy; ζ being an index not a quantum number.

$$F(0_0) = 0 \tag{5.3.1}$$

$$\begin{aligned} F(1_{-1}) &= B + C \\ F(1_0) &= A + C \\ F(1_{+1}) &= A + B \end{aligned} \tag{5.3.2}$$

$$\begin{aligned} F(2_{-2}) &= 2A + 2B + 2C - (2A-B-C)(1+3b^2)^{1/2} \\ F(2_{-1}) &= A + B + 4C \\ F(2_0) &= A + 4B + C \end{aligned} \tag{5.3.3}$$

$$\begin{aligned}
 F(2_{+1}) &= 4A + B + C \\
 F(2_{+2}) &= 2A + 2B + 2C + (2A-B-C)(1+3b^2)^{1/2} \\
 \\
 F(3_{-3}) &= 2A + 5B + 5C - (2A-B-C)(1+15b^2)^{1/2} \\
 F(3_{-2}) &= 5A + 2B + 5C - (2A-B-C)(4-6b+6b^2)^{1/2} \\
 F(3_{-1}) &= 5A + 5B + 2C - (2A-B-C)(4+6b+6b^2)^{1/2} \\
 F(3_0) &= 4A + 4B + 4C \tag{5.3.4} \\
 F(3_{+1}) &= 2A + 5B + 5C + (2A-B-C)(1+15b^2)^{1/2} \\
 F(3_{+2}) &= 5A + 2B + 5C + (2A-B-C)(4-6b+6b^2)^{1/2} \\
 F(3_{+3}) &= 5A + 5B + 2C + (2A-B-C)(4+6b+6b^2)^{1/2}
 \end{aligned}$$

$$\begin{aligned}
 F(4_{-4}) &= 4A + 4B + 32C - 7(A-B)b^*(1+b^{*2}/4)/3 - F(4_{-3}) \\
 F(4_{-3}) &= 5A + 5B + 10C - (2A-B-C)(4-10b+22b^2)^{1/2} \\
 F(4_{-2}) &= 5A + 10B + 5C - (2A-B-C)(4+10b+22b^2)^{1/2} \\
 F(4_{-1}) &= 10A + 5B + 5C - (2A-B-C)(9+7b^2)^{1/2} \\
 F(4_0) &= 20A + 20B + 20C - F(4_{-4}) - F(4_{+4}) \tag{5.3.5} \\
 F(4_{+1}) &= 5A + 5B + 10C + (2A-B-C)(4-10b+22b^2)^{1/2} \\
 F(4_{+2}) &= 5A + 10B + 5C + (2A-B-C)(4+10b+22b^2)^{1/2} \\
 F(4_{+3}) &= 10A + 5B + 5C + (2A-B-C)(9+7b^2)^{1/2} \\
 F(4_{+4}) &= 32A + 4B + 4C - 7(B-C)b(1+b^2/4)/3 - F(4_{+3})
 \end{aligned}$$

$$\text{where: } b = (C-B)/(2A-B-C) \quad \text{and} \quad b^* = (B-A)/(2C-A-B) \tag{5.3.6}$$

All but $F(4_{-4})$, $F(4_0)$ and $F(4_{+4})$ are exact; however, although the latter three can only be obtained exactly by numerically solving a cubic equation, they can be obtained to a good approximation given $F(4_{-3})$ and $F(4_{+3})$. The approximate means of the $F(4_{-4}), F(4_{-3})$ pair and the $F(4_{+4}), F(4_{+3})$ pair are obtained from Mecke's (94) equations,

from which we obtain $F(4_{-4})$ and $F(4_{+4})$, hence $F(4_0)$ follows from Mecke's sum rule.

For $J = 5$, only the sublevels for which $\tau = \pm 2$ can be solved explicitly, and for $J \gg 6$ no further analytic solutions exist, as all the algebraic equations from the determinant are cubic or higher in degree. Consequently, in order to calculate the sublevels for $J \gg 5$, we need to resort to approximate means.

In common with other workers, in order to calculate the approximate energy levels and line strengths, we have to associate each sublevel τ to the K quantum number of either the corresponding prolate or oblate symmetric top as the situation demands. Thus let K_a and K_c be the corresponding prolate and oblate notional quantum numbers respectively, with the angular momentum taken accordingly about the A and B-axes. The correspondence between τ , n , K_a and K_c is indicated here for $J = 5$:

Table (5.1) of Rotational Sublevels of Asymmetric Top with $J = 5$

τ	-5	-4	-3	-2	-1	0	+1	+2	+3	+4	+5
n	0	1	2	3	4	5	6	7	8	9	10
K_a	0	1	1	2	2	3	3	4	4	5	5
K_c	5	5	4	4	3	3	2	2	1	1	0

where n is an additional index such that $n = 0, 1, 2, \dots, 2J$ with:

$$n = \tau + J \tag{5.3.7}$$

and more generally:

$$K_a \text{ is the nearest integer } \gg (J+\tau)/2 \quad (5.3.8)$$

$$K_c \text{ is the nearest integer } \gg (J-\tau)/2$$

$$K_a + K_c = \begin{cases} J, & \text{when } J+K_a+K_c \text{ is even} \\ J+1, & \text{when } J+K_a+K_c \text{ is odd} \end{cases} \quad (5.3.9)$$

$$K_a - K_c = \tau$$

Even though at best only either K_a or K_c can be a good quantum number, the symmetry properties of both are preserved rigorously, such that we have + for K even and - for K odd, hence the selection rules, see Herzberg (30) and further in this section.

Except for the smallest values of J , whose sublevels we can compute exactly anyway, it is seen than in an energy level diagram for an asymmetric top with given J , the sublevels in the upper part of the diagram tend to pair up such that we have $(\tau=J, J-1)$, $(\tau=J-2, J-3)$... and likewise in the lower part of the diagram giving $(\tau=-J, -J+1)$, $(\tau=-J+2, -J+3)$... with a small odd number of unpaired sublevels near the middle. We can approximate the upper pairs by prolate sublevels with K_a being a good quantum number, and the lower pairs being oblate sublevels with K_c being a good quantum number, with a simple interpolation for the odd sublevels in the middle that are not satisfactorily represented by either the prolate or oblate approximations, by using the method of Badger and Zumwalt (95).

If we write:

$$F_B(J) = BJ(J+1) \quad (5.3.10)$$

then for sublevels with $F(J_\tau) > F_B(J)$ can be approximated by the prolate symmetric top:

$$F(J, K_a) = BJ(J+1) \left[1 - \frac{\rho(5-3\kappa)(1+\kappa)}{8(3-\kappa)} \right] + BK_a^2 \rho \frac{(17-14\kappa+\kappa^2)}{8(3-\kappa)} \quad (5.3.11)$$

where $F(J, K_a)$ is the mean term value of the pair of sublevels:

$$\tau = 2K_a - J, 2K_a - J - 1 \quad (5.3.12)$$

For sublevels with $F(J_\tau) < F_B(J)$, we can use the approximation for the oblate symmetric top:

$$F(J, K_c) = BJ(J+1) \left[1 + \frac{\rho(5+3\kappa)(1+\kappa)}{8(3+\kappa)} \right] - BK_c^2 \rho \frac{(17+14\kappa+\kappa^2)}{8(3+\kappa)} \quad (5.3.13)$$

where $F(J, K_c)$ is the mean term value of the pair of sublevels:

$$\tau = J - 2K_c, J - 2K_c + 1 \quad (5.3.14)$$

and where:

$$\rho = (A-C)/B \quad \text{and} \quad \kappa = (2B-A-C)/(A-C) \quad (5.3.15)$$

with κ being the asymmetry parameter, such that for the prolate

symmetric top $\kappa = -1$, the most asymmetric top $\kappa = 0$ and the oblate symmetric top $\kappa = 1$.

Thus in computing these sublevels, we start from say the top with $K_a = J$ and compute pairs of sublevels downwards with decreasing K_a until we leave the valid prolate region, then repeat from the bottom upwards with $K_c = J$, calculating the oblate pairs of sublevels with decreasing K_c until we leave the valid oblate region. There are then an odd number of sublevels left over in the intermediate region, which for simplicity are put equally spaced between the lowest and highest oblate pairs of sublevels.

Most sublevels are fairly well represented by prolate or oblate pairs with a small intermediate region, and as J increases, this pairing improves for sublevels well away from the intermediate region. Also, if we consider a smooth transition from a prolate to an oblate symmetric top, the number of prolate pairs decreases as the number of oblate pairs increases, with the intermediate region moving up across the diagram, and with any individual sublevels changing rapidly from having prolate to oblate character as the intermediate region passes through. For the most asymmetric top, the intermediate region is at the centre at $F(J_0)$, with all the sublevels above being a mirror image of those below.

In computing the energy levels by the method of Badger and Zumwalt (95), of the $2J+1$ sublevels for a given value of J , there will be at least one odd sublevel leaving at most J pairs. As the splitting within the pairs of sublevels cannot be computed by any

convenient method, it follows that on neglecting this splitting, artificial degeneracy is introduced, and in many cases there will be pairs of spectral lines that overlap exactly, which may cause systematic errors in computing the opacity. As with Λ -doubling, we must resolve this splitting artificially.

For a given value of J , let $F^+(J)$ be the highest pair of sublevels $F(J_J)$ and $F(J_{J-1})$, given by the prolate approximation, and $F^-(J)$ be the lowest pair of sublevels $F(J_{-J})$ and $F(J_{-J+1})$, given by the oblate approximation, all in cm^{-1} . Then if we let there be J pairs, even if the actual number of pairs by the above method is less, then the average spacing between any pair is given by:

$$\frac{F^+(J) - F^-(J)}{J} \quad (5.3.16)$$

In the actual pairs produced by Badger and Zumwalt's method, we want to split the sublevels by an amount that is small compared to (5.3.16) but large enough to separate most spectral lines for realistic Doppler widths. However, if we apply the same splitting to all pairs computed, there can still be many transitions that cause spectral lines to overlap artificially. Thus we want the splitting to vary in a simple way that corresponds qualitatively to the actual case, i.e. least splitting for the highest and lowest pairs of sublevels, with the splitting increasing until we reach the intermediate region where neither the prolate nor oblate approximations are valid. The simplest expression that we use is:

$$\Delta F = \frac{k[F^+(J) - F^-(J)]}{JK} \quad (5.3.17)$$

where ΔF is half the required splitting, K is K_a or K_c depending on whether we are in the prolate or oblate region respectively, and k is a constant. Thus in computing the term values of a pair from (5.3.11) or (5.3.13), ΔF is the amount the upper member must be shifted up and the lower member shifted down. It is found that $k = 0.01$ is an optimum value for H_2O , as the splitting of the pairs is generally less than about 1cm^{-1} .

Having obtained at least approximately the energy levels of the asymmetric top, we have to find the selection rules, hence calculate the approximate line strengths. The selection rules for J are as always $\Delta J = 0, \pm 1$ with $J = 0 \rightarrow J = 0$, but the selection rules for τ , which is not a quantum number, depend on the symmetry of the sublevels and the type of band considered, as discussed below. See also Herzberg (30) for more details.

As stated earlier, the symmetry of a sublevel can be obtained from the notional quantum numbers of the corresponding prolate and oblate symmetric tops. The rotational eigenfunction may either remain unchanged or change sign with respect to rotation about the A-axis, the axis of least moment of inertia, with behaviour + or - respectively. The eigenfunction may also either remain unchanged or change sign with respect to rotation about the B-axis, the axis of intermediate moment of inertia, and likewise for the C-axis, the axis of greatest moment of inertia. Because rotation about any two axes in succession is equivalent to rotation about the third, we need consider only two, by convention the C and A-axes in that order. If the

eigenfunction has a "+" character for the C-axis, K_c is even, otherwise K_c is odd, and likewise for K_a with the A-axis. Thus a sublevel with K_c even and K_a odd has a symmetry of $+-$. Thus, A-type bands occur when the permanent dipole moment in pure rotation or the vibrational transitional moment in vibration-rotation is aligned along the A-axis, with only the transitions between the sublevels with the symmetries $++ \leftrightarrow -+$ and $+- \leftrightarrow --$ allowed. B-type bands occur when the dipole moment or vibrational transition moment, as above, is aligned along the B-axis, with only the transitions $++ \leftrightarrow --$ and $+- \leftrightarrow -+$ being allowed. Finally, C-type bands occur when the dipole moment or vibrational transition moment is aligned along the C-axis, with only the transitions $++ \leftrightarrow +-$ and $-+ \leftrightarrow --$ being allowed.

For polyatomic molecules in general, the dipole moment or vibrational transition moment need not necessarily be aligned along one of the principal moments of inertia, and can thus have non-zero components along any two or all three axes, giving in relation to these components two or three types of bands superimposed on one another. However, for triatomic molecules, C-type bands cannot occur as the dipole moment or vibrational transition moment must be in the plane defined by the three atoms containing the A and B-axes. For triatomic molecules with the C_{2v} point group like H_2O , we will have either pure A or B-type bands, but for the C_s point group, the dipole moment or vibrational transition moment will in general have components along both A and B-axes giving both types of bands superimposed like HOD. By superimposed bands, we mean here bands due to the same vibrational and rotational energy levels but different sublevels from the selection rules above, whereas overlapping bands

are different bands due to different vibrational and rotational energy levels whose frequencies just happen to occur in about the same part of the spectrum.

Cross et al. (92) expresses the above mentioned selection rules in the form of a table for the three types of bands, however, we can express this table in the compressed form of table (5.2).

Table (5.2) of Rotational Selection Rules of Asymmetric Top

		0	1	2	3	4	5	J_1					
		0	1	2	3	4	5	6	7	8	9	10	n_1
0	0	W	Y	Z	X	W	Y	Z	X	W	Y	Z	
	1	Y	W	X	Z	Y	W	X	Z	Y	W	X	
1	2	Z	X	W	Y	Z	X	W	Y	Z	X	W	
	3	X	Z	Y	W	X	Z	Y	W	X	Z	Y	
2	4	W	Y	Z	X	W	Y	Z	X	W	Y	Z	
	5	Y	W	X	Z	Y	W	X	Z	Y	W	X	
3	6	Z	X	W	Y	Z	X	W	Y	Z	X	W	
	7	X	Z	Y	W	X	Z	Y	W	X	Z	Y	
4	8	W	Y	Z	X	W	Y	Z	X	W	Y	Z	
	9	Y	W	X	Z	Y	W	X	Z	Y	W	X	
5	10	Z	X	W	Y	Z	X	W	Y	Z	X	W	

$J_2 \quad n_2$

Where for:

P/R-Branches, $J_2 = J_1 + 1$ with $J_1 =$ smaller of J'', J' ,

$J_2 =$ larger of J'', J' ,

Q-Branches, $J_2 = J_1$ and for the sake of argument taking J_1 as the initial level.

Then $n_1 = 0, 1, 2, \dots, 2J_1$, $n_2 = 0, 1, 2, \dots, 2J_2$ and from the definition (5.3.7), $\tau_1 = n_1 - J_1$ and $\tau_2 = n_2 - J_2$.

For a given value of J_1 and J_2 , all possible transitions of sublevels are bounded in columns by $n_1 = 2J_1$ and rows by $n_2 = 2J_2$, and the allowed transitions for the three types of bands are indicated as follows:

W	A-Type Band, P/R-Branches
X	A-Type Band, Q-Branch
Y	$\left\{ \begin{array}{l} \text{B-Type Band, P/R-Branches} \\ \text{C-Type Band, Q-Branch} \end{array} \right.$
Z	$\left\{ \begin{array}{l} \text{B-Type Band, Q-Branch} \\ \text{C-Type Band, P/R-Branches} \end{array} \right.$

It can be seen that the whole table is a repetition of a basic 4X4 matrix.

It can be shown that for one of the three types of bands with J being the initial level, there are for P, Q and R-branches respectively J^2 , $J(J+1)$ and $(J+1)^2$ possible transitions, giving a total of $3J^2 + 3J + 1$ for all three branches for a given value of J , which on summing this over the many initial values of J in a typical band, will give many tens or hundreds of thousands of possible spectral lines. However, most of these lines are very weak and even their

approximate strengths cannot be obtained by our method. Because of the selection rules for the symmetric top, $\Delta K = 0, \pm 1$, those transitions for which either K_a or K_c or both satisfy these rules, give rise to the strong branches whose intensities we can find, at least approximately, and are within a few elements on either side of the main diagonal in the above table.

As stated by Hinkle and Barnes (96), the most important branches are those for which both $|\Delta K_a|$ and $|\Delta K_c|$ are ≤ 1 , followed by the "semiforbidden" branches for which one of these is > 1 , with finally the weak "forbidden" branches where both are > 1 that are the branches that are neglected.

Accordingly, we can write the subbranches that can be handled using the notation of Cross et al.(92), where for example $P_{2,1}^-$ means $\Delta J = -1, \Delta K_a = -2$ and $\Delta K_c = 1$, see table (5.3).

Table (5.3) of Subbranches Considered of Asymmetric Top

<u>A-Type Bands</u>			<u>B-Type Bands</u>		
<u>Subbranch</u>	<u>Δn</u>	<u>$\Delta \tau$</u>	<u>Subbranch</u>	<u>Δn</u>	<u>$\Delta \tau$</u>
$P_{2,1}^-$	-4	-3	$P_{3,1}^-$	-5	-4 o
$P_{0,1}^-$	0	1	$P_{1,1}^-$	-3	-2 e
			$P_{1,1}^-$	-1	0 o
$Q_{2,1}^-$	-3	-3 o	$P_{1,1}^-$	1	2 e
$Q_{0,1}^-$	-1	-1 e	$P_{1,3}^-$	3	4 o
$Q_{0,1}^-$	1	1 o			
$Q_{2,1}^-$	3	3 e	$Q_{1,1}^-$	-2	-2
			$Q_{1,1}^-$	2	2
$R_{0,1}^-$	0	-1			
$R_{2,1}^-$	4	3	$R_{1,3}^-$	-3	-4 e
			$R_{1,1}^-$	-1	-2 o
			$R_{1,1}^-$	1	0 e
			$R_{1,1}^-$	3	2 o
			$R_{3,1}^-$	5	4 e

Where e or o means that the transition is only possible if the initial value of n is even or odd respectively, otherwise the transition is always possible provided both initial and final states exist; this additional notation is in fact the same as that of Cross et al. (92).

For small values of J for which Badger and Zumwalt's (95) method is invalid as the sublevels do not pair up properly, but are obtained from (5.3.1-5), we have to find the relative intensities by interpolating from tables; those by Wacker and Pratto (93) are very extensive, and it is considered sufficient to use the earlier ones of Cross et al. (92).

Accordingly, we determine the mean of the asymmetry parameters κ'' and κ' from (5.3.15) for the two vibrational levels, then use linear interpolation to obtain an approximate relative rotational line strength for the transition considered. The tabulated intensities are the squares of the direction-cosine matrix elements, normalized such that the sum of all (say) upward transitions from a given τ sublevel is $2J+1$. In the process of interpolation, and as any "forbidden" branches are ignored, the sum rule will not in general be preserved, so we have to renormalize the line strengths after having calculated all possible transitions (maximum of seven) from a given sublevel. This renormalization process ensures that all the line strengths are accounted for, even if the strengths are not absolutely correctly distributed.

The number of subbranches we need actually consider is very much reduced by the fact that all P-subbranches are considered as reversed R-subbranches, and half the Q-subbranches are reverses of the other half. Additionally, for B-type bands, many subbranches are inverses of other subbranches, obtained by changing the sign of κ . Thus for A-type bands, we need actually only handle $Q_{0,\bar{1}}$, $Q_{2,\bar{1}}$, $R_{0,1}$ and $R_{2,\bar{1}}$,

and for B-type bands, $Q_{1,\bar{1}}$, $R_{1,1}$, $R_{1,\bar{1}}$ and $R_{3,\bar{1}}$.

For safety, the above method is used up to when the smaller of J' and J'' is ≤ 5 , even though the pairing is fairly good by then. For larger values of J , the rotational line strengths are calculated according to three possible situations:

(i). If $F(J''_{\tau''})$ and $F(J'_{\tau'})$ are well represented by the prolate symmetric top, the relative intensity is calculated from the appropriate Hönl-London factor (4.2.11) or (4.2.12) with K_a in place of Λ . If $|\Delta K_a| > 1$ the transition has zero intensity.

(ii). If $F(J''_{\tau''})$ and $F(J'_{\tau'})$ are well represented by the oblate symmetric top, the same procedure is used as above but with K_c .

(iii). For any other possibility, such as one sublevel having good oblate character with the other having prolate character, or a transition involving one of the intermediate sublevels, the relative strength is calculated from the mean of (i) and (ii).

Unless the asymmetry parameter K is very much different in the two states, because most sublevels are well paired for reasonably large values of J , and $|\Delta\tau| \leq 4$ for our purposes, most transitions will fit into cases (i) or (ii) which are reasonably fair approximations. Unfortunately, case (iii) is a very crude

approximation, as the intensities vary as a very complicated and often non-monotonic function of K , thus the intensities so calculated are as likely to be gross overestimates as underestimates. Accordingly, within the framework of our level of sophistication, the treatment for case (iii) transitions is not much better than a guess.

As before, all possible transitions that we are considering, are calculated first from a given γ sublevel so that the strengths are renormalized such that their sum is $2J+1$. Within the approximations made, we account for all the intensity in the band, though we have neglected the weak "forbidden" branches. Although individual line positions and strengths are approximate, hopefully the gross properties of VR bands of asymmetric top molecules can be reproduced.

The total VR band strengths are computed in exactly the same way as for CO_2 in the previous section, using the data from McClatchey et al. (88), except that the Hönl-London factor $S_{J'J''}$ in (5.2.9) is replaced by $S_{J'J''}^{\tau\tau''}$, the approximate rotational matrix element squared computed by one of the above methods, and $F_V(J'')$ is replaced by $F_V(J''\tau'')$. Also, there is no vibronic quantum number, so the relative vibrational matrix element squared is obtained from (5.2.3) with $i = 1, 2$ and 3 , and the data given by (88) does not have the complication of Fermi resonances included, though of course there still will be Fermi resonances.

For pure rotational bands, exactly the same method is used as described, except that the vibrational quantum numbers are the same in the two levels, hence the line positions are due only to the differences in the rotational term values of the two levels, the rotational constants and asymmetry parameters are the same, and only half the lines are produced, as the other half are in emission. However, (5.2.9) is replaced by:

$$S = \frac{8\pi^3 \bar{\nu}}{3h} \mu_0^2 \sum_{J'J''} S_{J'J''}^{\tau'\tau''} \frac{e^{-[G_v + F_v(J''\tau'')]hc/kT}}{Q(T)} \quad (5.3.18)$$

in units of $\text{cm}^2/\text{sec}/\text{isotopic molecule}$, where μ_0 is the permanent dipole moment of the ground vibrational level. Strictly speaking, μ is dependent on the vibrational quantum numbers, such that (5.3.18) is incorrect for excited vibrational levels. However, the dependence of μ on the vibrational quantum numbers could not be found in the literature, but μ would be expected to change relatively slowly with vibrations, making this error relatively small. Indeed, as the strongest bands come from the lower vibrational levels due to the Boltzmann factor, the overall effect on the spectra should be small. By Ludwig et al. (97), μ_0 for H_2O is 1.87 Debye.

For any molecule of point group C_{2v} , because of the identical nuclei, there will be an additional factor to the statistical weight due to nuclear spin. Using a similar notation as for the diatomic molecules, we can set out the following rules:

$u_1 = +1$ for symmetric electronic states,

$u_1 = -1$ for antisymmetric electronic states,

$u_2 = +1$ for I-integral,

$u_2 = -1$ for I-1/2-integral,

$u_3 = +1$ for v_3 even (A_1 -state),

$u_3 = -1$ for v_3 odd (B_1 -state),

$u_4 = +1$ for K_a or τ even as appropriate,

$u_4 = -1$ for K_a or τ odd as appropriate.

Then as for diatomic molecules, if $U = u_1 u_2 u_3 u_4$, we can put U into (4.2.15) to obtain the nuclear spin statistical weight factor g_I , which is included in the formula for calculating the line strength. For the ground electronic state of H_2O , $u_1 = +1$, $u_2 = -1$, and the product $u_3 u_4 = \pm 1$ determines whether the rotational sublevel in question has an overall symmetry of species A or B respectively. When the C_2 axis (axis of symmetry) coincides with the A-axis, K_a determines the sign of u_4 , in the more usual situation, as for H_2O , the C_2 axis coincides with the B-axis, with τ determining the sign of u_4 , see the appendices.

Because there are many more lines to compute in the bands of asymmetric top molecules than linear molecules, considerably more computer time has to be used to calculate individual bands, and this becomes prohibitive when a large number of bands has to be handled.

Accordingly, rather than calculating each band individually, we calculate the frequencies of the band origins and the total band strengths, including the Boltzmann factor, in a given progression, then sort the bands into the order of decreasing band strength. When each rotational line is computed for the first, and because of the Boltzmann factor, the strongest band in a progression, images of this line shifted and weaker due to the higher members, are immediately obtained without having to recalculate and renormalize each line.

The rotational constants A, B and C used in this section which are dependent on the vibrational quantum numbers, should be given as $A_{[v]}$, $B_{[v]}$ and $C_{[v]}$, obtained from:

$$\begin{aligned} A_{[v]} &= A_e - \alpha_1^A (v_1 + \frac{1}{2}) - \alpha_2^A (v_2 + \frac{1}{2}) - \alpha_3^A (v_3 + \frac{1}{2}) \\ B_{[v]} &= B_e - \alpha_1^B (v_1 + \frac{1}{2}) - \alpha_2^B (v_2 + \frac{1}{2}) - \alpha_3^B (v_3 + \frac{1}{2}) \\ C_{[v]} &= C_e - \alpha_1^C (v_1 + \frac{1}{2}) - \alpha_2^C (v_2 + \frac{1}{2}) - \alpha_3^C (v_3 + \frac{1}{2}) \end{aligned} \quad (5.3.19)$$

see Herzberg (30), where α_1^A etc. are coupling constants and A_e etc. are the rotational constants at equilibrium, as with the diatomic molecules. Thus rather than using the appropriate values of $A_{[v]}$ etc. for both vibrational levels in a given band, computed from (5.3.19), we use those constants applicable to the first member of a progression; so in the progression beginning with the band 001 ← 000, the rotational constants for this band are used throughout the progression. As the turnovers in the bands are due to the differences in the constants between the two vibrational levels, and as these differences do not change much in general in a progression, this would seem a reasonable approximation. Thus, with

this method, all higher members of a progression are just images of the first member, but shifted in frequency and intensity, and the method is very much more efficient in computer time, and more than offsets the approximation of having to assume the same set of rotational constants for all bands in a given progression.

The general theory on the asymmetric top molecule can also be found in Dennison (98). As with CO_2 , detailed work has been carried out on a number of specific bands of H_2O , this time mostly by Toth, Flaud and Camy-Peyret, see for example Camy-Peyret et al. (99) and Toth et al. (100); because we have to handle so many bands, their detailed calculations are considered to be beyond the scope of this work. One can also refer to Luh and Lie (101) for theoretical matrix elements and Ludwig et al. (97) for pure rotational spectra.

In the appendices are reproduced the relevant parts of the tables that we use from Cross et al. (92) of the relative rotational line strengths of asymmetric top molecules, and also an energy level diagram from Herzberg (30).

5.4 Equilateral Triangle Molecules

As mentioned in sections 2.10 and 5.1, we must consider briefly in principle triatomic molecules with an equilateral triangular structure, i.e. point group D_{3h} , the theory of which is covered in detail in Herzberg (30).

As H_3^+ and its isotopic forms are amongst the few examples of this type of molecule known so far; for which there is apparently insufficient spectroscopic data for computing a spectrum, together with expected low abundances in most cases, it is considered beyond the scope of this work to attempt a detailed treatment. For very recent (1980) work on H_3^+ and D_3^+ , see Oka (102), Shy et al. (103) and Carney and Porter (104).

The v_1 symmetric "breathing" vibrational mode of H_3^+ is inactive in the infrared due to symmetry, hence all VR bands are due to transitions involving the doubly degenerate v_2 vibrational mode. As H_3^+ is a symmetric top, for fixed J , $k = -J, -J+1 \dots J-1, J$ with $2J$ levels paired in energy for each $K = |k|$ with $k \neq 0$, which for an oblate top are ordered in decreasing energy for increasing K , see section 5.3. Because of the degeneracy of the v_2 mode, there is an additional vibronic quantum number l , with which there is associated angular momentum in the same way as for linear triatomic molecules. The l used by Oka (102) includes sign, i.e. $l = -v_2, -v_2+2 \dots v_2-2, v_2$, such that $|l|$ gives the quantum number in the same form we use for linear

triatomic molecules, and levels that differ only in the sign of ℓ are paired. The form of the equation for the unperturbed vibrational term values is exactly the same as for linear triatomic molecules, except for the absence of terms involving v_3 .

In addition to the selection rules on K and ℓ as discussed in earlier sections, by Oka (102) we have the rule $\Delta(k-\ell) = 0$, and a further complication for H_3^+ are the ℓ -resonance dyads such that the two levels (J, k, ℓ) and $(J, k \pm 2, \ell \pm 2)$ have the same $k-\ell$ and are completely mixed. Due to identical nuclei, the rotational fine structure will be affected by nuclear spin, as is the case for any D_{3h} molecule.

If we consider H_2D^+ which is of the lower symmetry C_{2v} , or in principle HDT^+ which has the lowest symmetry C_s , clearly we have an asymmetric top with the degeneracy in the v_2 vibrational mode removed, giving us three different vibrational modes. The spectrum of H_2D^+ will thus be more complicated, all three vibrational modes will be active in the infrared, and like H_2O there will be A-type and B-type bands. HDT^+ would give an even more complicated spectrum as the transition moment for any vibrational transition would not in general be aligned along any principal moment of inertia, giving superimposed AB-type bands.

Though H_3^+ is stable in an equilateral triangular configuration, neutral H_3 is apparently not so in its ground state if stable, see Hirschfelder (40), with a linear configuration having a lower energy, so any stable equilateral triangular state that exists, would be an

excited state.

Finally, although H_3^+ may not be an important opacity source in the T - ρ domain of our interest, it appears to be important in the chemistry of the early stages of collapse of interstellar clouds, see for example the very recent paper (1981) by Adams and Smith (105).

6 METHODS OF COMPUTING OPACITIES DUE TO MANY LINES

6.1 Introduction

In the previous two chapters, the discussion is based on how molecular lines are computed without saying anything about how these lines affect the opacity. It is the purpose of this chapter to discuss the various methods that can be used to compute opacities when large numbers of spectral lines are present. Accordingly, this is the most important chapter in this thesis.

Three separate methods are discussed: the Independent Line Method (ILM); the Line Smear Method (LSM); and the Opacity Sampling Method (OSM) with a fine grid. Each has its own advantages and disadvantages in terms of computer time, memory and accuracy, but all are based on splitting the spectrum up into a large number of bins into which individual lines fall, whose frequencies, strengths and widths are computed.

In principle, the RMO with molecular lines can be obtained by having a very fine grid on which first the continuum, then all the spectral lines are computed. However, because typical line widths are very narrow, e.g. the Doppler width of CO at 2000°K is $6.05 \times 10^{-6} u$, where again $u = h\nu/kT$ our dimensionless frequency unit, several million grid points would be required to cover the spectrum. Until recently, computing resources were quite inadequate even to consider

this method, however, with the acquisition of a VAX 11/780 computer by the University of St. Andrews in 1980, a restricted form of this method in the shape of the OSM can be used, due to the large virtual memory of the computer; the OSM being discussed later.

In computing the opacity by the various methods, the spectrum is divided up in four different ways which have to be compatible. We have a uniform coarse grid from $u = 0$ to say $u = 20$ of a few thousand grid points with which the continuum, as discussed in chapter 3, is computed. The spectrum is also divided into regions, with each region being of width $\Delta u = 1$, so we have region 1 with $u = 0$ to 1, region 2 with $u = 1$ to 2 etc., there being 20 such regions, and there must be an exact number of coarse grid intervals in each region, with coarse grid points at $u = 0, 1, 2$ etc. as well as intermediate places. The idea of having these different regions is to enable us to specify different bin sizes and fine grid intervals depending on the line widths in different parts of the spectrum, and blank out if necessary parts of the spectrum where we may wish to ignore lines and only leave the continuum. These regions also act as giant bins, with which we can have opacities in sections of the spectrum.

When bins are specified in a region, the number of bins must be equal to or an exact multiple of the number of coarse grid intervals, so that each coarse grid point is on the boundary between two bins, making the interpolation of the continuum in the bins much easier. If a fine grid is also specified for the OSM, then the number of fine grid intervals must be an even multiple of the number of bins in a region, so that we can apply Simpson's rule of integration for a fine

grid in each bin. In this case, there must be a fine grid point at each bin boundary and at least one in the middle.

Thus if we have say 2001 coarse grid points across the whole spectrum, then we can consider how a particular region can be set up. In a specified region, say 2 with $u = 1$ to 2 inclusive, there will be 101 coarse grid points including ones at $u = 1$ and 2. Then we can have say 1000 bins, which is an exact multiple of 100, the number of coarse grid intervals, and 10,001 fine grid points, giving 10,000 fine grid intervals which is an even multiple of the number of bins, so that for each bin we have 10 fine grid intervals with a fine grid point at each end and shared by neighbouring bins, and 9 across the bin.

Throughout this chapter for all methods of determining the RMO, the line profiles are assumed to be purely Gaussian with widths dependent only on thermal broadening, turbulent velocity and line position, given by the expression:

$$\Delta u_G = \frac{2u}{c} \sqrt{\left(\frac{2N_A kT}{m} + 10^{10} \xi^2\right) \ln 2} \quad (6.1.1)$$

where m is the molecular weight in amu and ξ is the turbulent velocity in km/sec. However, because the Lorentzian profile is easily handled analytically in the ILM, it is included in the next section for the sake of completeness.

6.2 The Independent Line Method

The very narrowness of a spectral line that makes it such a problem to compute the contribution it makes to the RMO using a grid, is a positive asset using the ILM in uncongested parts of the spectrum.

Let $\bar{\kappa}_c^{pq}$ and $\bar{\kappa}_l^{pq}$ be the RMOs in the bin $u = p$ to $u = q$ of the continuum alone, and the continuum plus a single spectral line respectively, then the definitions are:

$$\frac{1}{\bar{\kappa}_c^{pq}} = \int_p^q \frac{W(u) du}{\kappa_c(u)} \quad (6.2.1)$$

$$\frac{1}{\bar{\kappa}_l^{pq}} = \int_p^q \frac{W(u) du}{\kappa_l(u) + \kappa_c(u)} \quad (6.2.2)$$

Where $W(u)$, $\kappa_c(u)$ and $\kappa_l(u)$ are the weighting function, continuous opacity and line opacity respectively, with u_0 being the line centre located within the bin.

Using the above definition, we can write:

$$\frac{1}{\bar{\kappa}_l^{pq}} = \frac{1}{\bar{\kappa}_c^{pq}} + \int_p^q \frac{W(u) du}{\kappa_l(u) + \kappa_c(u)} - \int_p^q \frac{W(u) du}{\kappa_c(u)} \quad (6.2.3)$$

As the line is narrow, it is reasonable to assume that $W(u)$ and $\kappa_c(u)$ are constant over the profile, hence they can be replaced by $W(u_0)$ and $\kappa_c(u_0)$ respectively. Hence (6.2.3) can be re-written as:

$$\frac{1}{\bar{K}_l^{\rho q}} = \frac{1}{\bar{K}_c^{\rho q}} - \frac{W(u_0)}{K_c(u_0)} \int_p^q \frac{K_l(u) du}{K_l(u) + K_c(u)} \quad (6.2.4)$$

If the bin $u = p$ to $u = q$ is wide compared to a line width, and the line is located comfortably within the bin so that its wings are also included, then the integral in (6.2.4) can be taken over the limits $u = 0$ to $u = \infty$, hence we can define:

$$X = \frac{W(u_0)}{K_c(u_0)} \int_0^{\infty} \frac{K_l(u) du}{K_l(u) + K_c(u)} \quad (6.2.5)$$

so that (6.2.4) can conveniently be written as:

$$\frac{1}{\bar{K}_l^{\rho q}} = \frac{1}{\bar{K}_c^{\rho q}} - X \quad (6.2.6)$$

where X can be regarded as effectively a measure of the amount of flux in the bin removed by the spectral line. This definition can be applied even if the line is near the edge of the bin so that one of its wings spills over into a neighbouring bin; it just means we take all the contribution in one bin. The definition (6.2.5) can be integrated analytically for a pure Lorentzian profile and an analytic expression exists for a pure Gaussian profile. Unfortunately, no convenient approximation is known to exist for a general Voigt profile. It is this analytic treatment that enables the lines to be handled by the ILM.

The Lorentzian profile in dimensionless frequency units is:

$$F(u) = \frac{\Delta u_L / 2\pi}{(u-u_0)^2 + (\Delta u_L / 2)^2} \quad (6.2.7)$$

where Δu_L is the Lorentzian full width at half maximum, and $F(u)$ is the profile normalized such that:

$$\int_0^\infty F(u) du = 1 \quad (6.2.8)$$

Also let:

$$K_L(u) = \frac{hs}{kT} F(u) \quad (6.2.9)$$

where the factor h/kT has to be included as we are working in dimensionless frequency units, such that if $K_c(u)$ and $K_l(u)$ are mass absorption coefficients in cm^2/gm , s is the line strength in $\text{cm}^2/\text{sec}/\text{gm}$.

After substituting (6.2.7) and (6.2.9) into (6.2.5) and simplifying, we get:

$$X = \frac{hs}{kT} \frac{\Delta u_L}{2\pi} \frac{W(u_0)}{K_c(u_0)} \int_0^\infty \frac{du}{K_c(u_0) [(u-u_0)^2 + (\Delta u_L / 2)^2] + \frac{hs}{kT} \frac{\Delta u_L}{2\pi}} \quad (6.2.10)$$

Using the fact that:

$$\int_{-\infty}^\infty \frac{dx}{ax^2 + b} = \frac{\pi}{\sqrt{ab}} \quad (6.2.11)$$

(6.2.10) can be integrated to give:

$$X = \frac{hs}{kT} W(u_0) \sqrt{\frac{\pi \Delta u_L}{K_c^3(u_0) [\pi K_c(u_0) \Delta u_L + \frac{2hs}{kT}]}} \quad (6.2.12)$$

If a_L is defined as the ratio of the absorption in the centre of the Lorentzian profile alone, to the absorption of the continuum alone, then:

$$a_L = \frac{K_l(u_0)}{K_c(u_0)} = \frac{2hs}{\pi kT} \frac{1}{K_c(u_0) \Delta u_L} \quad (6.2.13)$$

Then (6.2.12) simplifies to:

$$X = \frac{\pi W(u_0) \Delta u_L}{2K_c(u_0)} \cdot \frac{a_L}{\sqrt{a_L + 1}} \quad (6.2.14)$$

Hence, it is immediately seen that in the weak line limit $a_L \ll 1$, $X \propto a_L$ and in the strong line limit $a_L \gg 1$, $X \propto \sqrt{a_L}$ where the line becomes saturated, and increasing the line strength further, causes a correspondingly smaller increase in the RMO. Although the integral in (6.2.10) can be evaluated between the finite limits p and q , to correct for the effects of the wings if the bin is not wide enough, a rather cumbersome expression involving arctangents is obtained, but is generally of little practical use.

In the rest of this discussion, we deal with the Gaussian profile, given by:

$$F(u) = \frac{1}{\sqrt{2\pi} \sigma} e^{-\frac{(u-u_0)^2}{2\sigma^2}} \quad (6.2.15)$$

or
$$F(u) = 2 \sqrt{\frac{\ln 2}{\pi}} \cdot \frac{1}{\Delta u_G} e^{-4(u-u_0)^2 \ln 2 / \Delta u_G^2} \quad (6.2.16)$$

where
$$\Delta u_G = 2 \sqrt{2 \ln 2} \sigma \quad (6.2.17)$$

and $F(u)$ is normalized to unity as before. Although (6.2.16) is more cumbersome, it is found more convenient to work with Δu_G than σ .

On substituting (6.2.9) and (6.2.16) into (6.2.5), we obtain:

$$X = \frac{W(u_0)}{K_c(u_0)} \int_0^\infty \frac{du}{1 + \frac{1}{2} \sqrt{\frac{\pi}{\ln 2}} \frac{kT}{h\nu} K_c(u_0) \Delta u_G e^{4(u-u_0)^2 \ln 2 / \Delta u_G^2}} \quad (6.2.18)$$

If a_G is defined as the ratio of the absorption in the centre of the Gaussian profile alone, to the absorption of the continuum alone, then:

$$a_G = \frac{K_l(u_0)}{K_c(u_0)} = 2 \sqrt{\frac{\ln 2}{\pi}} \cdot \frac{h\nu}{kT} \frac{1}{K_c(u_0) \Delta u_G} \quad (6.2.19)$$

If we also make the substitutions

$$x = \frac{2 \sqrt{\ln 2} (u-u_0)}{\Delta u_G} \text{ and } dx = \frac{2 \sqrt{\ln 2} du}{\Delta u_G} \quad (6.2.20)$$

together with (6.2.19) into (6.2.18), we obtain:

$$X = \frac{\Delta u_G}{2 \sqrt{\ln 2}} \cdot \frac{W(u_0)}{K_c(u_0)} \cdot a_G \int_{-\infty}^{\infty} \frac{dx}{a_G + e^{x^2}} \quad (6.2.21)$$

Unfortunately, there exists no simple analytic solution to the integral in (6.2.21). However, using the fact that:

$$F_R(y) = \int_0^{\infty} \frac{t^k dt}{e^{t-y} + 1} \quad (6.2.22)$$

is the complete Fermi-Dirac integral of order k , and can be expressed as functions involving rational Chebyshev Polynomials depending on k and the range of y , see Cody and Thacher (106), and also making the substitutions:

$$x^2 = t \quad \text{and} \quad dx = \frac{1}{2} t^{-1/2} dt \quad (6.2.23)$$

it can be shown that:

$$\int_0^{\infty} \frac{dx}{a_c + e^{x^2}} = \frac{1}{2a_c} \int_0^{\infty} \frac{t^{-1/2} dt}{e^{(t-\ln a_c)} + 1} = \frac{F_{-1/2}(\ln a_c)}{2a_c} \quad (6.2.24)$$

which on substituting into (6.2.21) gives:

$$X = \frac{W(u_0) \Delta u_c}{2\sqrt{\ln 2} \kappa_c(u_0)} F_{-1/2}(\ln a_c) \quad (6.2.25)$$

after allowing for a factor of two, as we are integrating over half the range, and the integrand in (6.2.21) is an even function.

As a quick check, an approximate value for (6.2.25) can be found from the expression:

$$X = \frac{W(u_0) \Delta u_c}{\sqrt{\ln 2} \kappa_c(u_0)} \cdot \frac{a_c \sqrt{\ln(a_c + 2)}}{(a_c + 1)} A(a_c) \quad (6.2.26)$$

where the function $A(a_G)$ is a correction that does not differ much from unity, and is given by the integral:

$$A(a_G) = \int_0^{\infty} \frac{(a_G + 1) dy}{a_G + (a_G + 2)y^2} \quad (6.2.27)$$

such that $A(0) = \frac{1}{2} \sqrt{\pi/\ln 2} = 1.0645$ which is a maximum, $A(2.6) = 1$, $A(21.7) = 0.9802$ which is a minimum, and thereafter as $a_G \rightarrow \infty$, $A(a_G) \rightarrow 1$. As $A(a_G)$ has its maximum deviation from unity in the limit of vanishing line strength, it follows that this simple analytic approximation is for all practical purposes rarely less accurate than 2%.

From (6.2.26), it is easy to see how X varies with line strength, in the weak line limit $a_G \ll 1$, $X \propto a_G$ as is the case with the Lorentzian profile, but in the strong line limit with $a_G \gg 1$, $X \propto \sqrt{\ln a_G}$, i.e. the line becomes effectively more completely saturated than in the Lorentzian case, and any further increase in strength results in a very small increase in the opacity. This is due to the fact that the absorption in the wings drops off much more rapidly than in the Lorentzian case.

The ILM discussed so far is exact, provided that: (i) there is no more than one line in a bin, (ii) the weighting function and continuum are assumed to be constant over the profile, and (iii) edge effects are neglected, so a line centre that is just inside a bin is assumed to contribute all its opacity to that bin and none to the neighbouring bin.

Unless lines are very broad or lie close to an absorption edge, (ii) is a very good approximation, and provided bins are wide compared to line widths, (iii) is also a good approximation. The problem in the practical application of the ILM is that (i) is often not valid, and great care must be taken in the use of the ILM.

Suppose there are n lines in the bin, each producing its own contribution X_i , then (6.2.6) can be written as:

$$\frac{1}{K_i^{pv}} = \frac{1}{K_c^{pv}} - \sum_{i=1}^n X_i \quad (6.2.28)$$

where $\bar{\kappa}_1^{pq}$ is the RMO for n lines and continuum, provided the lines do not overlap, and:

$$X_i = \frac{W(u_i) \Delta u_i F_{-1/2}(\ln a_i)}{2\sqrt{\ln 2} \kappa_c(u_i)} \quad (6.2.29)$$

$$\text{where } a_i = 2 \sqrt{\frac{\ln 2}{\pi}} \cdot \frac{h\nu_i}{kT} \cdot \frac{1}{\kappa_c(u_i) \Delta u_i} \quad (6.2.30)$$

As soon as there is any overlap between lines, the ILM no longer gives the correct opacity, as the contribution to the RMO of the overlapping lines is less than if the lines are separate, which is discussed more fully in the case of only two lines in the next section. Thus for $n > 1$, the ILM gives at best an upper bound to the opacity. If, however, $\sum_i \Delta u_i \ll w$ where w is the bin width, there is a good chance the lines do not overlap and the ILM gives the correct opacity if any information about the line positions is retained.

However, it is assumed that no information about individual lines is retained, so after each line is put in the bin with its own value of X subtracted from the right hand side of (6.2.28), all information about its strength, width and frequency is lost, so nothing can be said about any overlap. Thus as the number of lines in a bin increases, the likelihood of overlap increases so the value of the RMO given by the ILM becomes more likely to be simply an upper bound.

In very congested parts of the spectrum, where the number of lines in a bin can be large, the right hand side of (6.2.28) can easily be negative, which means that the ILM has broken down completely as there is a great deal of overlap, and we are trying to remove more flux from the bin than there actually is. In this case, all we can say is that the upper bound to the RMO is infinity.

The ILM can be used to obtain a lower bound to the opacity when $n > 1$, by lumping all the lines together in the centre of the bin to obtain a single line whose strength is the sum of the strengths of all the individual lines, and whose width is the minimum of all the line widths. Thus the contribution given by the total overlap is expressed as:

$$X_o = \frac{W(u_o) \Delta u_o}{2\sqrt{\ln 2} \kappa_c(u_o)} \cdot F_{-1/2}(\ln b) \quad (6.2.31)$$

where

$$b = 2\sqrt{\frac{\ln 2}{\pi}} \cdot \frac{h}{kT} \cdot \sum_{i=1}^n S_i \cdot \frac{1}{\kappa_c(u_o) \Delta u_o} \quad (6.2.32)$$

and where $W(u_o)$ and $\kappa_c(u_o)$ are the weighting function and continuum

respectively at the bin centre, and Δu_0 is the minimum of all profile widths.

For the sum in (6.2.28), writing X_s to mean the contribution of the lines if they are assumed to be separate, it can be seen that for $n > 1$:

$$X_0 \leq X \leq X_s \quad (6.2.33)$$

where X is obtained by profiling the lines, then integrating numerically to obtain the actual value.

If the spectrum is divided into m bins, then by the ILM we can write:

$$\frac{1}{\bar{K}_{max}} = \sum_{j=1}^m \left[\max \left\{ \left(\frac{1}{K_{c_j}} - X_{s_j} \right), 0 \right\} \right] \quad (6.2.34)$$

and:

$$\frac{1}{\bar{K}_{min}} = \sum_{j=1}^m \left[\frac{1}{K_{c_j}} - X_{o_j} \right] \quad (6.2.35)$$

where the maximum function in (6.2.34) ensures zero is returned in breakdown cases. Because in practice there will always be parts of the spectrum where there is not heavy congestion, (6.2.34) will always give a finite value for \bar{K}_{max} . For those bins with no lines, of course:

$$X_{o_j} = X_{s_j} = 0 \quad (6.2.36)$$

and for those with one line:

$$X_{0j} = X_{s_j} > 0 \quad (6.2.37)$$

If the whole spectrum has lines that are well separated, then by choosing bin sizes appropriately, the ILM can give good results. In practice, however, at places like band heads, there may be heavy congestion even if the the spectrum is otherwise uncluttered.

It is also possible to treat the whole spectrum as one giant bin, so that in (6.2.28) $p = 0$ and $q = \infty$, a finite value for the RMO will be obtained, avoiding the summation in (6.2.34). Unfortunately this suffers from loss of significance in a computer, all information about the variation of the opacity over the spectrum is lost, and no account is taken when lines are so congested that the ILM breaks down in those parts of the spectrum. It can nevertheless be done as a simple check against the bin method.

In applying the ILM on a computer, five arrays are needed to store five separate quantities associated with each bin, they are: (i) the total number of lines in that bin, (ii) the right hand side of (6.2.28), which is initialized with the reciprocal of the RMO of the continuum, then for every line, the contribution X_i is subtracted off, (iii) the sum of the line strengths used in computing X_0 at the end, and also for obtaining an opacity by the LSM, discussed in section 6.4, (iv) the minimum of all line widths used in finding X_0 and (v) the sum of all line widths, only used for the LSM.

We can also use the sum of the line strengths in (iii) to calculate the PMO in each bin. Then:

$$\bar{\kappa}_l^{pq} = B(u_0) \left[\omega \kappa_c(u_0) + \frac{h}{kT} \sum_{i=1}^n S_i \right] \quad (6.2.38)$$

where $\bar{\kappa}_l^{pq}$ is the PMO of the continuum and n lines in the bin p to q of width $w = q-p$ and u_0 is the frequency of the bin centre, and we assume the continuum and Planck weighting function do not change over the bin. The total PMO for the whole spectrum is simply obtained by summing (6.2.38) over all bins. This is clearly much more efficient than computing the contribution to the PMO for every line individually when the lines are computed.

As discussed in section 6.1, we can vary the bin sizes over the spectrum taking the best compromise, so that bins are wide compared to the Gaussian widths of the lines, but not too wide, using (6.1.1) with a typical value of m as a guide.

Finally for interest, we can derive expressions for the equivalent infinite opacity rectangle (EIOR) and the equivalent equal area rectangle (EEAR) of a profile. The first is a rectangle of infinite opacity but whose contribution to the RMO is the same as the profile, where to be meaningful, the bin width must of course be wider than both. Because the rectangle has an infinite area, the PMO due to it is infinite, hence also for the whole spectrum, and is thus meaningless. However, this rectangle can be regarded in a sense as the "equivalent width" of the profile. The EEAR is that rectangle

whose contribution to the RMO is not only the same as the profile, but whose area is also the same, thus the PMO is also the same as that of the profile.

Let Δu_∞ be the full width of the EIOR, then re-writing (6.2.3):

$$\frac{1}{\bar{k}_L} = \frac{1}{\bar{k}_c} + \int_{u_0 - \Delta u_\infty/2}^{u_0 + \Delta u_\infty/2} \frac{W(u) du}{k_L(u) + k_c(u)} - \int_{u_0 - \Delta u_\infty/2}^{u_0 + \Delta u_\infty/2} \frac{W(u) du}{k_c(u)} \quad (6.2.39)$$

where again u_0 is the dimensionless frequency at the bin centre, and we assume that $W(u)$ and $k_c(u)$ are constants over the bin. As:

$$k_L(u) = \infty \quad \text{when } |u - u_0| \leq \frac{\Delta u_\infty}{2}$$

and: (6.2.40)

$$k_L(u) = 0 \quad \text{when } |u - u_0| > \frac{\Delta u_\infty}{2}$$

it can at once be seen that:

$$\frac{1}{\bar{k}_L} = \frac{1}{\bar{k}_c} - \frac{W(u_0) \Delta u_\infty}{k_c(u_0)} \quad (6.2.41)$$

therefore from (6.2.6), we can see that:

$$\Delta u_\infty = \frac{k_c(u_0)}{W(u_0)} X \quad (6.2.42)$$

So for the Lorentzian profile, from (6.2.14) we can write:

$$\Delta u_\infty = \frac{\pi}{2} \Delta u_L \cdot \frac{a_L}{\sqrt{a_L + 1}} \quad (6.2.43)$$

and for the Gaussian profile, from (6.2.25) we can write:

$$\Delta u_{\infty} = \frac{\Delta a_c}{2\sqrt{\ln 2}} F_{-1/2}(\ln a_c) \quad (6.2.44)$$

with a_L and a_G being defined in (6.2.13) and (6.2.19) respectively. If the sum of the EIORS over several profiles in a bin equals or exceeds the bin width, then this indicates that the ILM has broken down for that bin.

If we now define Δu_r as being the full width of the EEAR, and replace Δu_{∞} by Δu_r in (6.2.39), then we can write:

$$\kappa_l(u) = d \quad \text{when} \quad |u - u_0| \leq \frac{\Delta u_r}{2}$$

and: (6.2.45)

$$\kappa_l(u) = 0 \quad \text{when} \quad |u - u_0| > \frac{\Delta u_r}{2}$$

where d is the height of the rectangle above the continuum. For area to be conserved:

$$\Delta u_r d = \frac{hs}{kT} \quad (6.2.46)$$

where s is the strength, see (6.2.9). On integration:

$$\frac{1}{\kappa_l} = \frac{1}{\kappa_c} - W(u_0) \Delta u_r \left[\frac{1}{d + \kappa_c(u_0)} - \frac{1}{\kappa_c(u_0)} \right] \quad (6.2.47)$$

then on substituting for d , and as before from (6.2.6) after some algebra, we obtain the result:

$$\Delta u_r = \frac{\frac{hs}{kT} \kappa_c(u_0) X}{\frac{hs}{kT} W(u_0) - \kappa_c^2(u_0) X} \quad (6.2.48)$$

Then for the Lorentzian profile, using (6.2.14) again, we obtain:

$$\Delta u_r = \frac{\frac{hs}{kT}}{\frac{2}{\pi} \frac{hs}{kT} \frac{\sqrt{a_L+1}}{\Delta u_L a_L} - \kappa_c(u_o)} \quad (6.2.49)$$

and for the Gaussian profile, using (6.2.25) again, we obtain:

$$\Delta u_r = \frac{\frac{hs}{kT}}{2\sqrt{\ln 2} \frac{hs}{kT} \frac{1}{\Delta u_c F_{-1/2}(\ln a_c)} - \kappa_c(u_o)} \quad (6.2.50)$$

Note that the weighting function drops out of (6.2.43), (6.2.44), (6.2.49) and (6.2.50), and the continuum also out of the first two.

6.3 The Partial Overlap of Two Gaussian Profiles

An analytic approximation is discussed below that enables the contribution to the RMO in a bin to be computed from two Gaussian profiles that have any degree of overlap, and represents an improvement to the ILM.

In conducting numerical experiments by integrating overlapping Gaussian profiles, the remarkable result is found that as two strong profiles which are completely overlapping are separated, the contribution they make to the bin increases linearly over a large part of the range. This can be explained by the fact that the integrand in (6.2.18) for strong lines, has the form approaching that of a rectangle, with a flat top centred at u_0 and very steep sides, and represents, in a sense, a measure of the flux removed at each frequency point. With two partially overlapping profiles, the integrand is not additive, as in the region of overlap, the height is hardly altered and we effectively have a rectangle of greater width. As the two profiles are separated, the width hence area of the effective rectangle increases linearly until the profiles no longer overlap, giving two separate rectangles.

In (6.2.18), substituting for a_c , and finding $u-u_0$ that gives half the value at the maximum when $u = u_0$, we can show that

$$\epsilon = \Delta u_c \sqrt{\frac{\ln(a_c + 2)}{\ln 2}} \quad (6.3.1)$$

where t is the full width to half maximum of the integrand, which is effectively the width of the rectangle in the strong line limit. Thus if two profiles with Δu_1 , a_1 and Δu_2 , a_2 are centred respectively at u_1 and u_2 , and if:

$$|u_1 - u_2| > \frac{t_1 + t_2}{2} \quad (6.3.2)$$

then the profiles do not overlap. Then defining:

$$Y = \frac{\kappa_e(u_0)}{W(u_0)} X = \frac{\Delta u}{2\sqrt{\ln 2}} F_{-1/2}(\ln a) \quad (6.3.3)$$

it can be seen from (6.2.26) that in the strong line limit, $Y/t \approx 1$ for a single profile.

From the above, we can obtain simple approximate relationships that enable us to calculate the contribution from two overlapping profiles. Let Y_0 be the contribution from the two profiles that are completely overlapping, Y_s be the sum of the contributions for two separate profiles and Y_p be the contribution from two partially overlapping profiles. Then for the separations v_1 and v_2 with $v_1 < v_2$:

$$v_1 = Y_0 - Y_s/2 \quad (6.3.4)$$

$$v_2 = Y_s/2$$

Then for:

$$\begin{aligned} v < v_1, & \quad Y_p = Y_o \\ v_1 < v < v_2, & \quad Y_p = v - v_1 + Y_o \\ v > v_2, & \quad Y_p = Y_s \end{aligned} \tag{6.3.5}$$

so that:

$$\frac{dY_p}{dv} = \begin{cases} 0 & \text{for } v < v_1 \\ 1 & \text{for } v_1 < v < v_2 \end{cases} \tag{6.3.6}$$

which holds well in the strong line limit if Y_p is obtained by direct numerical integration, with a long linear portion in the range $v_1 < v < v_2$, with a rapid change to a horizontal slope in the vicinity of $v = v_1$ and $v = v_2$. Because $Y_o > Y_s/2$, v_1 will always be non-zero.

Because the integrand in (6.2.18) is not well represented by a rectangle for weak lines, the approximate rules given above are poor, but can still be applied as the contributions are much smaller.

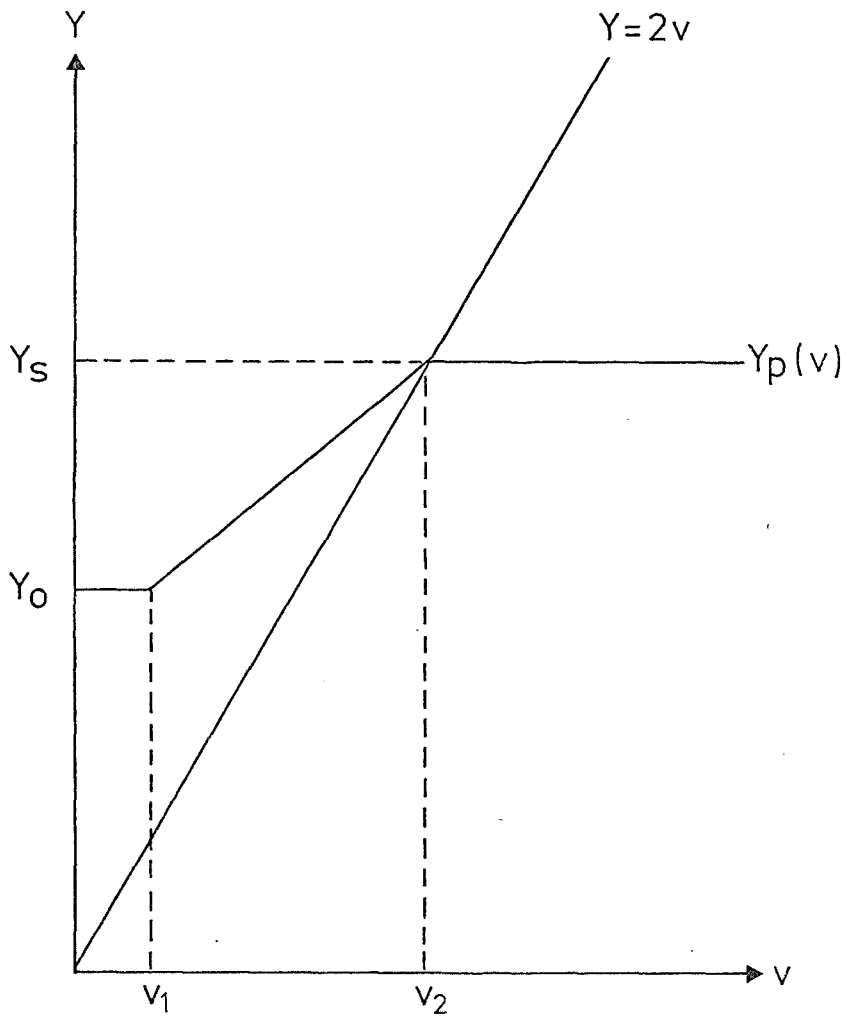


Fig. 6.1

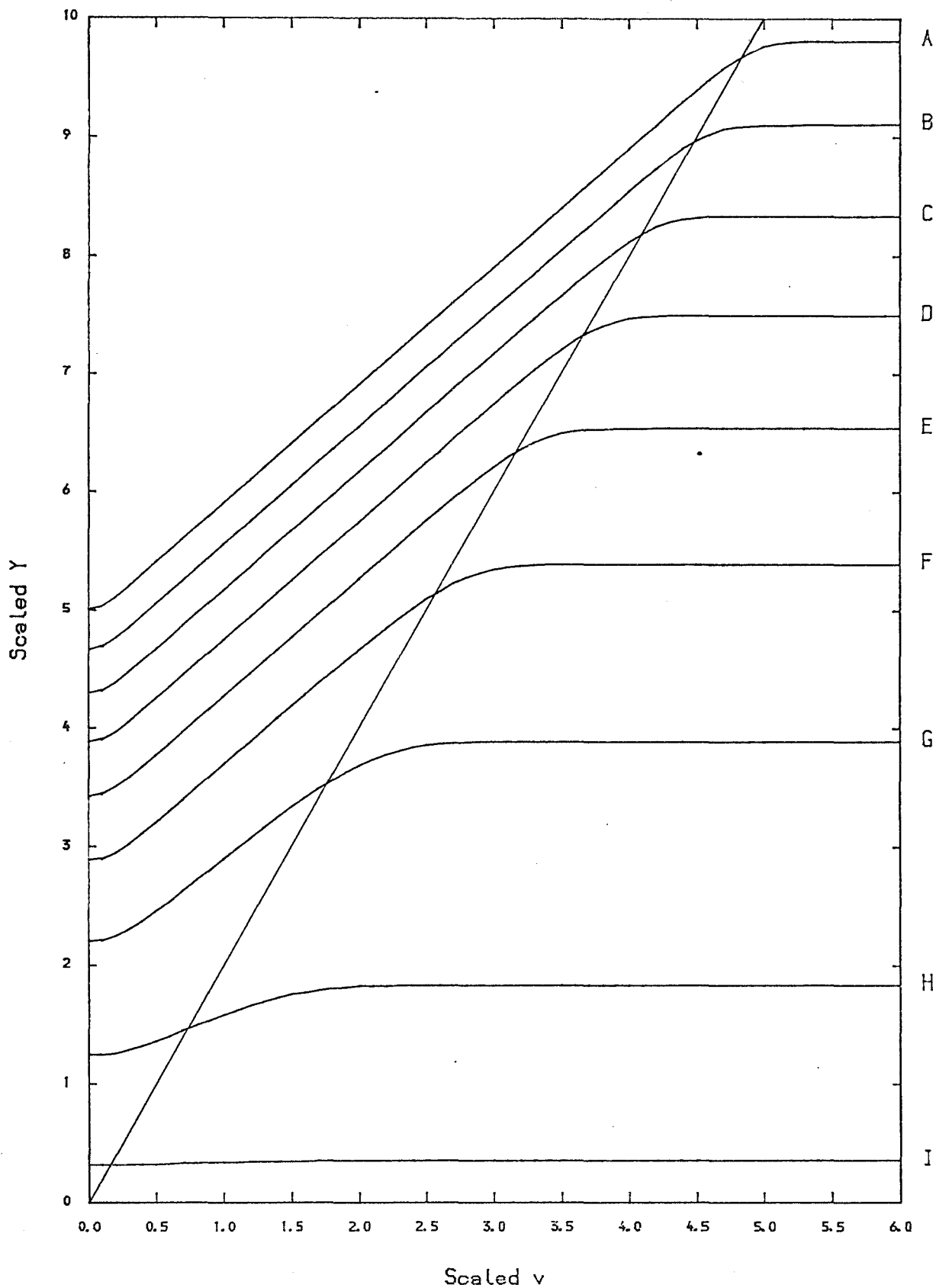


Fig. 6.2

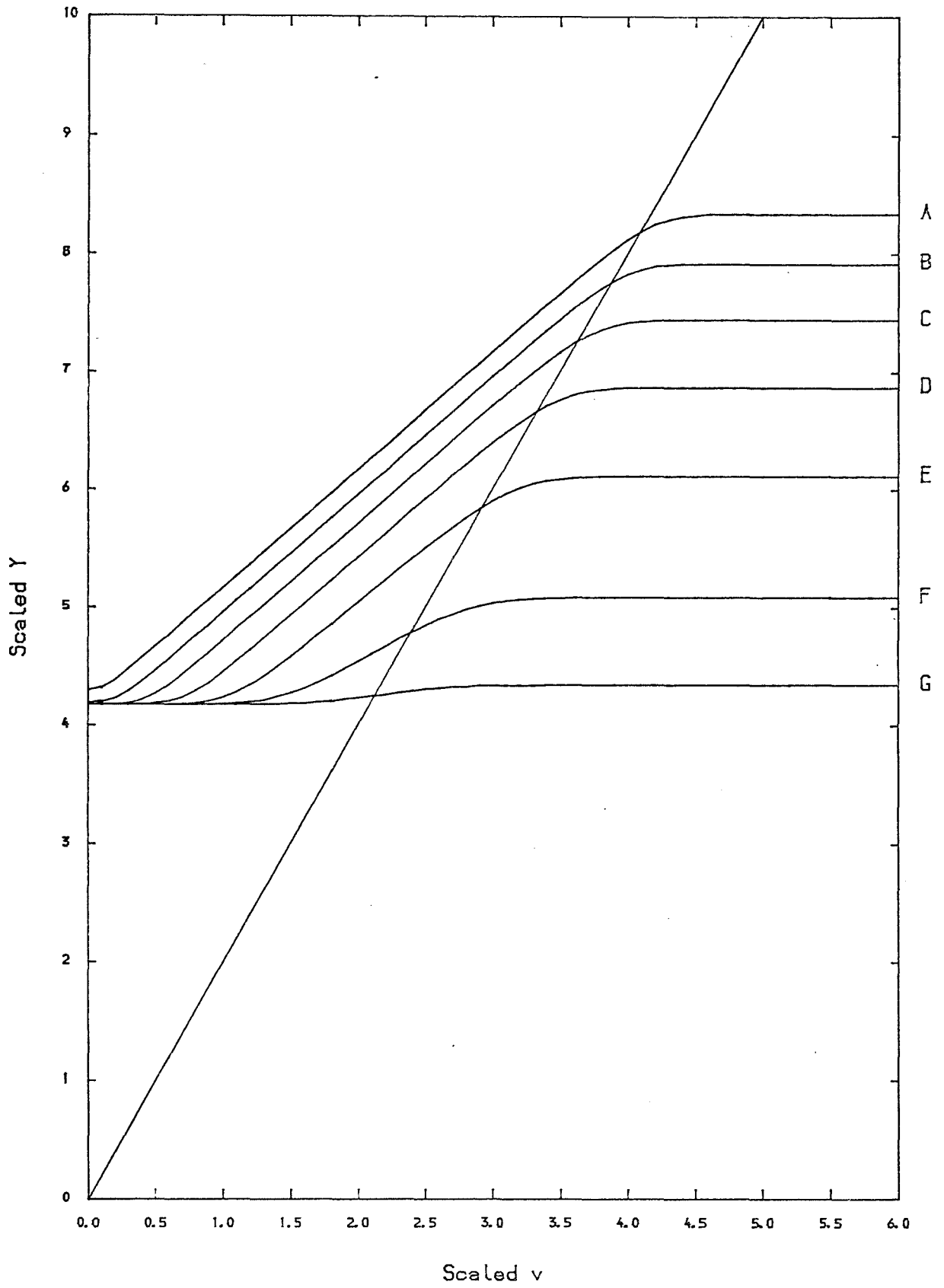


Fig. 6.3

Figure (6.1) represents the idealized behaviour of the function $Y_p(v)$ such that it increases linearly from $v = v_1$ to $v = v_2$, where v_2 is on the line $Y = 2v$, otherwise $Y_p(v)$ is constant. Figures (6.2) and (6.3) represent the actual behaviour of $Y_p(v)$ for a number of profiles of different strengths in reduced units. In all cases, the bin width, the height of the continuum and the weighting function are taken as unity, hence the area under the continuum is also unity. All profile widths are taken as $1/20$ of the bin width, and it is convenient to scale v and Y by dividing by this factor, so that the abscissae is in terms of the width of one of the profiles, the maximum separation of the profiles being here six times the width of one profile.

In figure (6.2), curves A to I show the behaviour of the function for the case where both profiles are of equal strength for $s_1 = s_2 = 10^6, 10^5 \dots 10^{-2}$ respectively, where s_i is the area under profile i . It can be clearly seen that for strong lines, the behaviour of $Y_p(v)$ is very close to the idealized case, with curvature over only a small portion of the function in the vicinity of v_1 and v_2 , with v_1 being very close to the Y -axis in this figure. For curves G, H and I, with $s_1 = s_2 = 1, 10^{-1}$ and 10^{-2} respectively, the curves level out progressively further to the right of the line $Y = 2v$ and our approximation becomes progressively worse, but as the contributions become smaller and the differences between total overlap and non-overlap also become less, the errors remain small; the extreme case here being for curve I. So we can still apply the approximate method as stated above.

Figure (6.3) shows the effect of keeping one profile constant and progressively weakening the other. Curves A to G represent the case for $s_1 = 10^4$ and $s_2 = 10^4, 10^3 \dots 10^{-2}$ respectively. Again it is seen that for the lowest curves, the deviation from the idealized case is largest, but the errors will still be small as the differences between the total overlap and non-overlap cases are small, though the total contribution may be large, this being due to the dominant profile. In this family of curves, it is seen that as the differences in s_1 and s_2 increase, the distance of v_1 from the Y-axis increases, and the smaller is the effect of the weaker profile on the total overlap, this not being perceptible here for curves C to G. Other families of curves produced in a similar way with $s_1 \gg s_2$ will be similar but shifted, except that if both profiles are weak, the effect of the weaker of the two on the total contribution for total overlap will be greater, this causing a larger spread on the left hand side.

Though Y_s can always be obtained from the two separate profiles, Y_o can only be found directly if both profiles have the same width, in which case:

$$Y_o = \frac{\Delta u_1}{2\sqrt{\ln 2}} \cdot F_{-1/2} [\ln(a_1 + a_2)] \quad (6.3.7)$$

otherwise Y_o has to be found by an approximation.

If the two profiles have different widths, Δu_1 and Δu_2 , then let $\Delta u_2 \leq \Delta u_1$, let a_i be defined from (6.2.30) with $i = 1$ or 2 , but also define a_2' for the narrower profile that is broadened to the same width as profile 1, such that:

$$a_2' = 2 \sqrt{\frac{\ln 2}{\pi}} \cdot \frac{h s_2}{h T} \cdot \frac{1}{\kappa_c \Delta u_1} \quad (6.3.8)$$

so that $a_2' \leq a_2$ and strictly speaking κ_c in (6.2.30) and (6.3.8) is taken at the mid point between the two profiles. Then Y_a is the total overlap with broadened line 2:

$$Y_a = \frac{\Delta u_1}{2\sqrt{\ln 2}} \cdot F_{-1/2} \left[\ln(a_1 + a_2') \right] \quad (6.3.9)$$

Y_0 is restricted to the range $Y_1 < Y_0 \leq Y_a$, where Y_1 is obtained from (6.3.3) for line 1, such that for $\Delta u_2 \rightarrow 0$, $Y_0 \rightarrow Y_1$, line 2 becomes a δ function and causes no absorption and $\Delta u_2 = \Delta u_1$, $Y_0 = Y_a$, line 2 has the same width as line 1.

Now if we let:

$$x = \frac{\Delta u_2}{\Delta u_1} \quad (6.3.10)$$

and:

$$y = \frac{Y_0 - Y_1}{Y_a - Y_1} \quad (6.3.11)$$

such that both x and y can lie between 0 and 1 only, then for any line

strengths $y = f(x)$, such that by definition $y = 0$ when $x = 0$ and $y = 1$ when $x = 1$.

If Δu_2 is varied from 0 to Δu_1 and Y_0 is obtained by direct numerical integration over the profiles, then x and y from (6.3.10) and (6.3.11) respectively are obtained, and on plotting for given strengths, it is seen that the curve is approximately of the form:

$$y = x^p \quad \text{with} \quad p > 0 \quad (6.3.12)$$

where p should be a constant, given by:

$$p = \frac{\log y}{\log x} \quad (6.3.13)$$

for any point on the curve. In practice, it is found that p does vary over the curve, so the most representative value taken is that where the line $y + x = 1$ intersects the curve, the line being the principal diagonal in the unit square for the range covered by x and y .

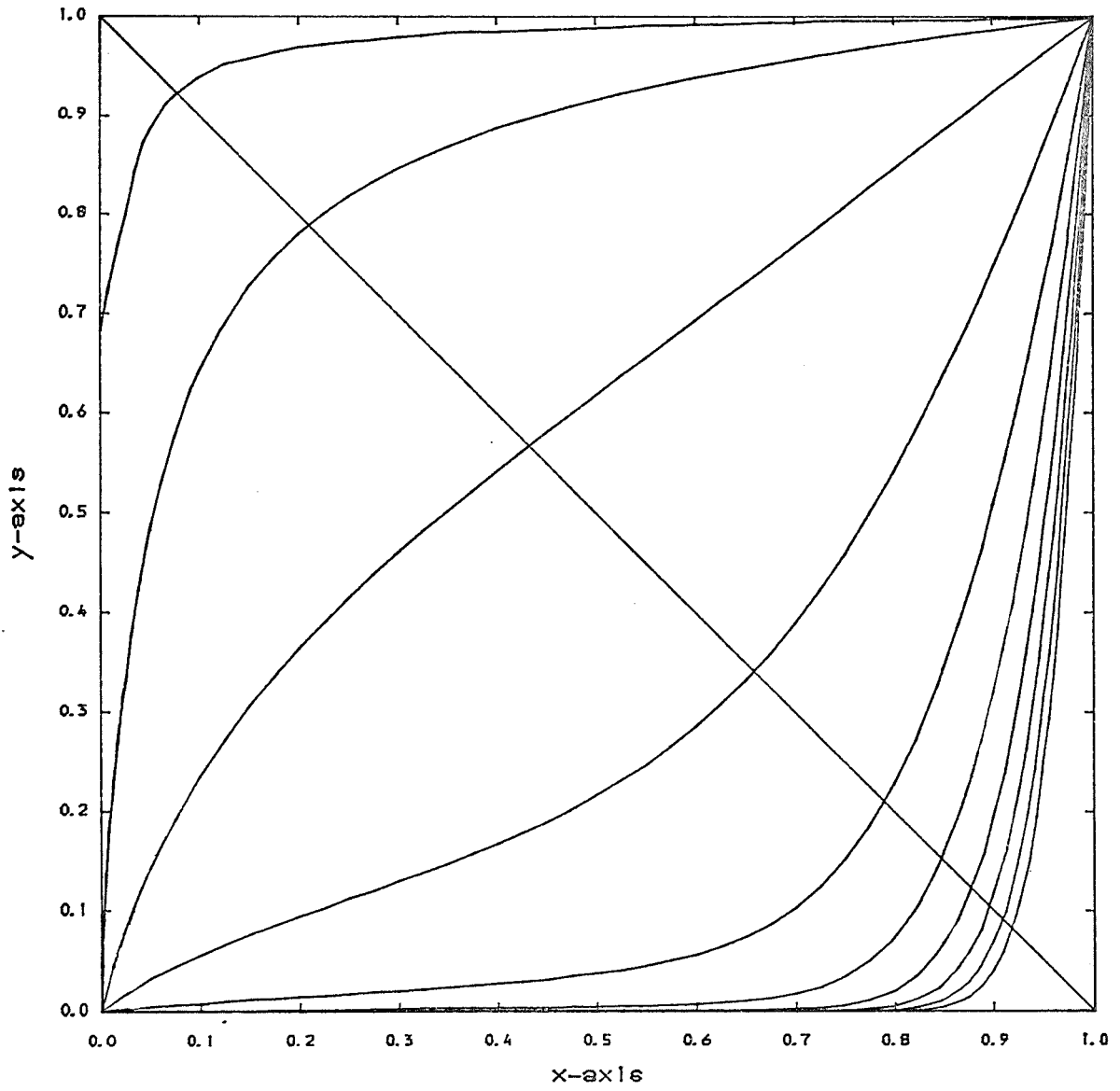


Fig. 6.4

Figure (6.4) illustrates this very well for 10 curves with the strengths in the same dimensionless units as for figures (6.2) and (6.3), with $s_1 = s_2 = 10^{-3}, 10^{-2} \dots 10^6$, intersecting the main diagonal progressively from upper left to lower right. Most other families of curves produced by profiles of different strengths are found to behave in a similar way. If the contribution produced by two profiles of different widths and strengths is plotted as a function of their separation, a curve similar to one of those in figures (6.2) and (6.3) results. Moreover, if a family of curves is produced by keeping both profiles of fixed and equal strengths, but with various values of Δu_2 , with $\Delta u_2 \leq \Delta u_1$, the family is very similar to that in figure (6.3).

We can tabulate p for the various values of the relative line strengths r_1 and r_2' , such that:

$$r_1 = \frac{h s_1}{kT} \cdot \frac{1}{k_c \Delta u_1} \quad (6.3.14)$$

and:

$$r_2' = \frac{h s_2}{kT} \cdot \frac{1}{k_c \Delta u_1} \quad (6.3.15)$$

where r_2' is the relative strength of the second line if broadened to that of the first line.

Table (6.1) of Overlap Parameters for Different Relative Line Strengths

Log r_1	Log r_2											
	-2	-1	0	1	2	3	4	5	6	7	8	9
-2	0.032	0.14	0.46	0.78	0.89	0.93	0.95	0.96	0.97	0.97	0.98	0.98
-1	0.046	0.15	0.48	0.81	0.93	0.96	0.98	0.99	0.99	1.00	1.00	1.00
0	0.30	0.37	0.68	1.08	1.22	1.23	1.22	1.21	1.19	1.18	1.17	1.16
1	2.14	2.22	2.30	2.57	2.64	2.41	2.17	2.00	1.87	1.78	1.70	1.64
2	6.18	6.92	7.06	6.97	6.60	5.45	4.31	3.55	3.07	2.74	2.51	2.34
3	-	13.09	12.22	12.53	12.52	11.36	8.67	6.41	5.03	4.19	3.64	3.26
4	-	-	17.12	18.05	18.23	17.78	15.99	11.92	8.57	6.57	5.34	4.55
5	-	-	-	20.21	20.92	23.23	22.79	20.49	15.19	10.81	8.16	6.54
6	-	-	-	-	27.23	25.19	27.98	27.66	24.92	18.55	13.12	9.79
7	-	-	-	-	-	44.30	31.12	32.51	32.40	29.29	21.75	15.36
8	-	-	-	-	-	-	-	39.92	38.22	37.25	33.56	25.26
9	-	-	-	-	-	-	-	-	43.73	41.39	41.85	37.98

The rows of this table are labelled by $\log r_1$ and the columns by $\log r_2$. Note that values of p below the main diagonal are very approximate.

Thus given parameters for the two lines, we can calculate r_1 and r_2 from the formulae above, obtain p from the table by interpolation; given p , y is found from (6.3.12) from which Y_0 is obtained from (6.3.11), then Y_p can be found as already described.

If $r_2' \ll r_1$, this corresponds to a weak narrow line overlapping with a strong broader line, with the result that there is practically no difference between Y_1 , the strong line on its own, and Y_a the overlap of the two lines with line 2 being broadened to line 1. In this case, the value of p is essentially meaningless, as in (6.3.11) we are interpolating between two values which are practically the same.

In computing X for the case of two lines in a bin, the strength, width and frequency of the first line are retained until the second line falls into the bin, then X can be computed. If the bin never has more than one line, then after all spectral lines have been generated, X is computed at the end.

If the bin has more than two lines, then for every additional line, its own value of X is computed and subtracted off the right hand side of (6.2.28) as before, where X_1 and X_2 are already covered by the two line case. For bins with many lines, the effect of the two line treatment is at best to lower the value of the RMO for the ILM, giving a slightly better upper bound to the opacity. Unfortunately, there is no easy way of handling the overlap of three or more lines.

So to summarize, there are five possibilities that can occur with the ILM:

- (i). 0 lines, empty bin with continuum on its own,
- (ii). 1 line, ILM gives an exact value,

- (iii). 2 lines, ILM gives an exact value if there is no overlap, or a good approximate value if there is overlap,
- (iv). 3 or more lines with a positive value in (6.2.28), ILM gives an upper bound to the opacity, but the more congestion there is in the bin, the further the true opacity is to be from this bound,
- (v). 3 or more lines with a zero or negative value in (6.2.28), ILM breaks down completely, and other methods must be used to obtain even an estimate of the opacity.

The case of breakdown for only one or two lines in a bin indicates that the bin is simply too small.

6.4 The Line Smear Method

If we do not wish to apply the ILM, or in cases where it is unreliable or breaks down completely, the LSM discussed below enables us to at least obtain an approximate estimate of the RMO in a bin. At the end of the computation of all spectral lines, because the individual information about lines in a bin is lost, all we have to work on is the number of lines, the sum of their widths, the sum of their strengths and the upper and lower bounds of the opacity given by the ILM if applied.

Let us consider the case of extreme congestion, i.e. there are so many lines in a bin that we can replace the continuum by a level pseudo-continuum due to the effects of all the profiles combined together, see figure (6.5). Let W and C be constant over the bin, and represent the average weighting function and continuum respectively, w the bin width and S the sum of all line strengths, given by:

$$S = \frac{h}{kT} \sum_{i=1}^n s_i \quad (6.4.1)$$

so that S and C have the same units. Also let \bar{K} be understood to represent the RMO of that bin on its own here.

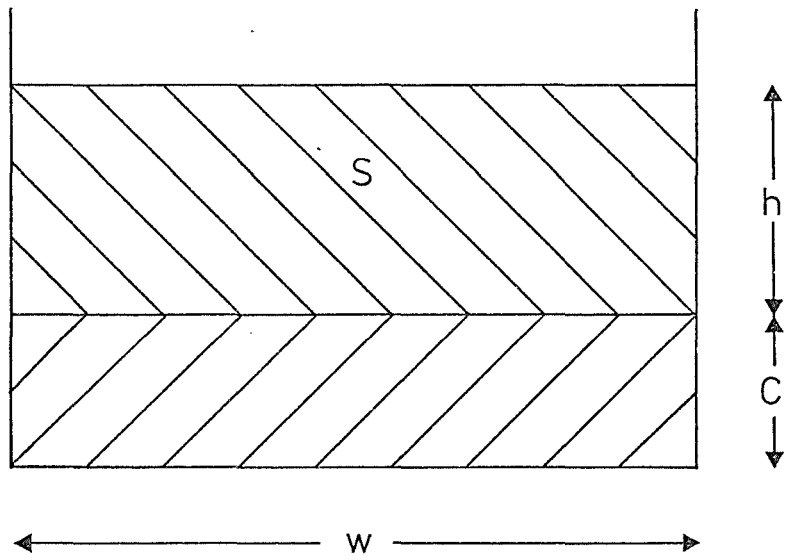


Fig. 6.5

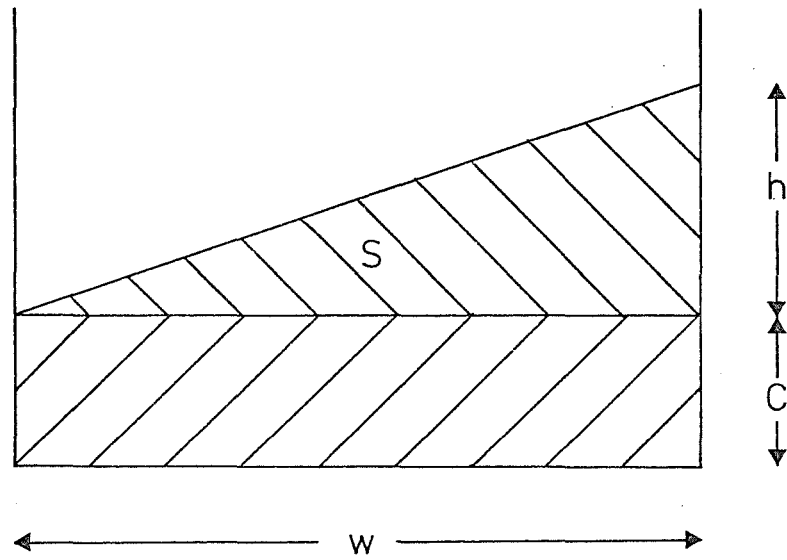


Fig. 6.6

If the height of the new pseudo-continuum above the true continuum is h , then its total height is clearly $h+C$, and it is easily seen that the RMO over the bin is given by:

$$\frac{1}{\bar{k}} = \frac{\omega W}{C+h} \quad (6.4.2)$$

If we conserve area, so as $h = S/w$, we can write:

$$\frac{1}{\bar{k}} = \frac{\omega^2 W}{\omega C + S} \quad (6.4.3)$$

which is an absolute upper bound to the RMO in a bin, and corresponds to completely smearing all the lines, this bound being otherwise unobtainable in breakdown cases of the ILM. However, when the ILM gives a positive value in (6.2.28), generally it gives a better upper bound than (6.4.3)

If the congestion is less extreme, then although there will still be a lot of absorption, there will also be windows in the bin through which radiation can pass. The crudest way of representing this is to put the absorption in the form of a triangle of height h sitting on top of the continuum, so that at one extreme end there is no absorption corresponding to the windows, and at the other there is absorption by an amount h , see figure (6.6). This can be regarded as a very crude Opacity Distribution Function (ODF).

Let u_0 be the frequency of the bin centre and $K_1(u)$ be the distribution of smeared absorption, such that $K_1(u_0 - w/2) = 0$ and $K_1(u_0 + w/2) = h$, then:

$$K_1(u) = \frac{h}{w} (u - u_0 + w/2) \quad (6.4.4)$$

Again conserving area, as $h = 2S/w$, we can write:

$$K_1(u) = \frac{2S}{w^2} (u - u_0 + w/2) \quad (6.4.5)$$

then the RMO is obtained from:

$$\frac{1}{R} = \int_{u_0 - w/2}^{u_0 + w/2} \frac{w du}{\frac{2S}{w^2} (u - u_0 + w/2) + C} \quad (6.4.6)$$

which on integration gives:

$$\frac{1}{R} = \frac{w^2 w}{2S} \ln \left(\frac{2S}{wC} + 1 \right) \quad (6.4.7)$$

If S is zero in this or (6.4.3), then we get:

$$\frac{1}{R} = \frac{wW}{C} \quad (6.4.8)$$

which is just the continuum on its own.

If the RMO from (6.4.3) is $\bar{\kappa}_r$ for rectangular smear, $\bar{\kappa}_t$ from (6.4.7) is the triangular smear and $\bar{\kappa}_c$ from (6.4.8) is the continuum alone, then we can show that for $S > 0$:

$$\bar{\kappa}_c < \bar{\kappa}_t < \bar{\kappa}_r \quad (6.4.9)$$

which we would intuitively expect to be the case.

From Abramowitz and Stegun (46):

$$\ln x = 2 \left[\left(\frac{x-1}{x+1} \right) + \frac{1}{3} \left(\frac{x-1}{x+1} \right)^3 + \frac{1}{5} \left(\frac{x-1}{x+1} \right)^5 + \dots \right] \quad (6.4.10)$$

which is valid for $x > 0$. Then substituting:

$$x = \frac{2S}{\omega C} + 1 \quad (6.4.11)$$

into only the first term in (6.4.10) and neglecting higher order terms, then (6.4.7) becomes:

$$\frac{1}{\bar{\kappa}_t} = \frac{\omega^2 W}{S} \left[\frac{2S}{\omega C} \cdot \frac{1}{2S/\omega C + 2} + \dots \right] \quad (6.4.12)$$

which gives:

$$\frac{1}{\bar{\kappa}_t} = \frac{\omega^2 W}{\omega C + S} + \dots \quad (6.4.13)$$

which gives the result in (6.4.3) if the higher order terms are dropped. Including these terms causes $1/\bar{\kappa}_t > 1/\bar{\kappa}_r$, therefore

$\bar{\kappa}_r > \bar{\kappa}_t$. If we put $S = 0$ to obtain $\bar{\kappa}_c$, it is seen that $\bar{\kappa}_c < \bar{\kappa}_t < \bar{\kappa}_r$.

In addition to considering the two forms of smearing discussed so far, we could also distribute the line strengths in the form of the part of some giant profile, which is more like an ODF. However, unlike an ODF, we have no information about the distribution of the opacity across the bin, but only the sum of the line strengths and widths, so nothing more useful could be extracted from this concept than what is discussed below.

Suppose we wish to consider a degree of smearing intermediate between the triangular smear and complete rectangular smear. Let us split the sum of the total line strength S into components S_1 and S_2 , then:

$$S = S_1 + S_2, \quad S_1 = \rho S, \quad S_2 = (1-\rho)S \quad (6.4.14)$$

where $0 \leq \rho < 1$ is a smearing parameter, S_1 is a rectangle on top of the continuum of height h_1 and S_2 is a triangle on top of S_1 with height h_2 , see figure (6.7). Then as $h_1 = S_1/w$, if we replace C by $C+S_1/w$ in (6.4.7), we get:

$$\frac{1}{\bar{\kappa}} = \frac{\omega^2 w}{2S_2} \ln \left(\frac{2S_2}{\omega C + S_1} + 1 \right) \quad (6.4.15)$$

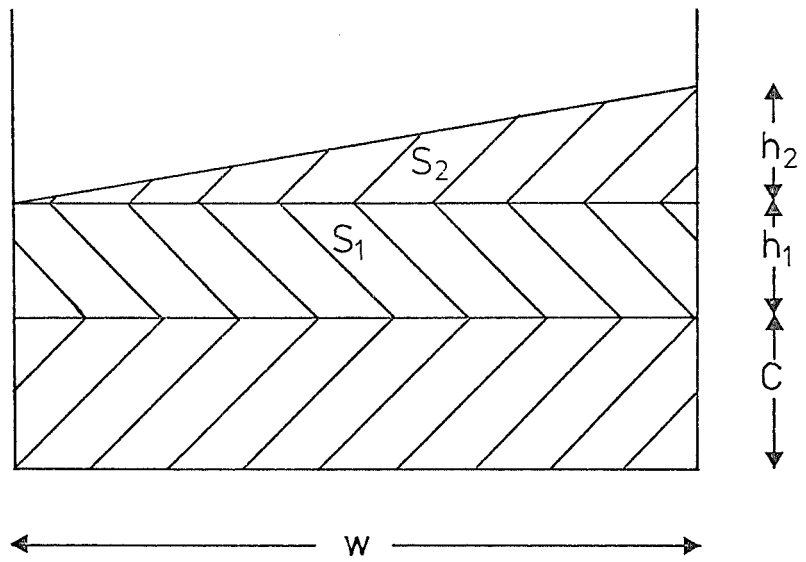


Fig. 6.7

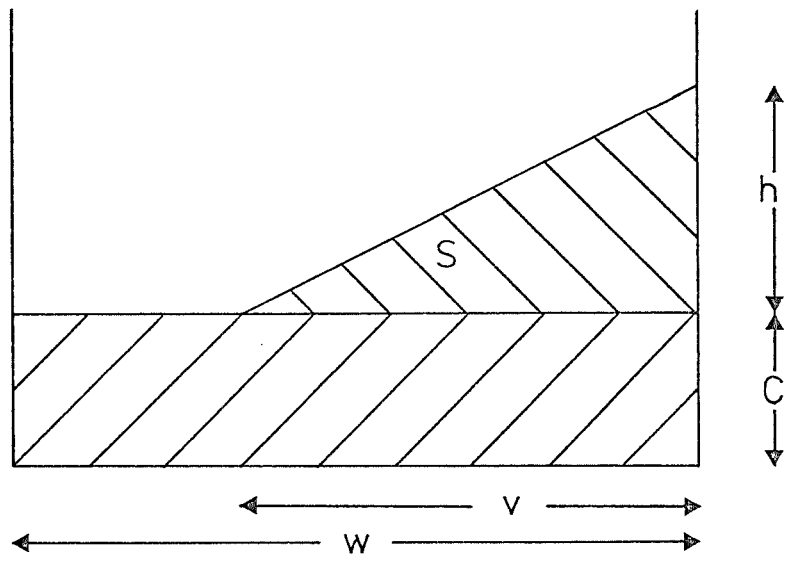


Fig. 6.8

then using (6.4.14) we can write:

$$\frac{1}{k} = \frac{\omega^2 W}{2(1-p)S} \ln \left(\frac{\omega C - pS + 2S}{\omega C + pS} \right) \quad (6.4.16)$$

where if $p = 0$ we have (6.4.7), the least amount of smearing, and as $p \rightarrow 1$ we approach (6.4.3) the greatest amount of smearing.

If we want to deal with smearing that is less than the triangular smear given by $p = 0$, then we can consider a triangular wedge of area S with width v , with $w-v$ being just continuum, see figure (6.8). This would correspond to a relatively uncongested bin with quite a lot of continuum. Replacing w by v in (6.4.7) to correspond to integration over just that part of the bin with the wedge, then adding the contribution of the remainder of the bin containing just continuum, we get:

$$\frac{1}{k} = \frac{\omega^2 W}{2S} \ln \left(\frac{2S}{vC} + 1 \right) + \frac{(\omega-v)W}{C} \quad (6.4.17)$$

Letting:

$$v = (p+1)\omega \quad (6.4.18)$$

where $p+1$ is the fraction of the bin covered by the wedge, with $-1 < p \leq 0$, we can substitute this into (6.4.17) giving:

$$\frac{1}{k} = \frac{\omega W}{2CS} \left\{ (p+1)^2 \omega C \ln \left[\frac{2S}{(p+1)\omega C} + 1 \right] - 2pS \right\} \quad (6.4.19)$$

As $p \rightarrow 0$ from the negative side, the last portion of the continuum on its own vanishes and the opacity increases rapidly, hence by choosing $p+1$ as the fraction rather than another variable like q say, we avoid the problem of loss of significance, and hence continuity between the two smearing methods.

Thus given a specified sum of line strengths S in a bin, so that the area S is fixed, and taking equations (6.4.19) and (6.4.16) together, we can vary the smearing hence opacity in a bin, such that in the range $-1 < p \leq 0$ we apply (6.4.19) to obtain smearing from a triangular wedge increasing from the limit of a δ function with no opacity, to a triangle across the bin. Then increasing p further so that it is in the range $0 \leq p < 1$, we apply (6.4.16) with S partitioned between a triangle and rectangle, with the opacity continuing to increase as the smearing approaches that of just a rectangle. However, the most difficult part of this work is to find some way of pinning down the smearing parameter with the limited amount of information available, as we know nothing about the distribution of line strengths or how the lines overlap. We want to correlate p in some way with the sum of the line widths, which is a measure of the congestion.

Originally it was thought that we could relate p in a simple way to the sum of the line widths expressed as a fraction of the bin width, however, very extensive numerical experiments indicated that no simple relationship exists. In these experiments, a bin is created into which a specified number of lines are placed, whose widths are a

specified fraction of the bin width but line positions within the bin and strengths are chosen by random numbers, to simulate actual cases where many possibilities of line strengths and overlaps can occur.

Working in dimensionless scaled units, let the weighting function, continuum and bin width all be unity, x be the relative frequency of the centre of a profile, chosen by a random number such that $0 \leq x \leq 1$, and y be another random number in the same range, such that:

$$s = a e^{-by} \tag{6.4.20}$$

where s is the line strength and a and b are constants. The expression (6.4.20) is chosen to simulate actual cases where lines come from different levels where there will be the effect of the Boltzmann factor.

In (6.4.20), a and b are chosen so that when $y = 0$, $s = a$ is the strongest possible line, and $s = a \exp(-b)$ is the weakest possible line when $y = 1$. To simulate realistic cases, line strengths are chosen to range from about $0.01\Delta x$ to $10^8\Delta x$, where Δx is the line width as a fraction of bin width, and the lower limit corresponds to the typical cut-off when generating actual lines.

In handling these artificial bins, we have a grid fine enough to profile the generated lines correctly, so that the opacity in the bin can be obtained by direct numerical integration of the grid once all the required lines have been produced. These bins are wrap-around, so

that with a line near one edge of the bin, the part of the profile that would otherwise be lost is put in at the other edge, which would simulate the actual case of parts of profiles that would spill over into neighbouring bins.

If n is the number of lines in a bin, then with the four fixed parameters n , a , b and Δx , we can produce many bins then find the value of p , which if inserted into (6.4.16) or (6.4.19) as appropriate, fits best. Naturally, those bins that have by chance more overlap than average would be expected to have a smaller opacity than given by p , and vice versa for those with less overlap than average. Hence p is determined by some sort of an average bin. The most efficient way is to find the average opacity and total strength for many bins, then given $\bar{\kappa}$ and S , solve for p in (6.4.16) and (6.4.19) by iteration. This can be done for various values of the four parameters, in particular n , to see what correlation can be obtained.

It is indeed found that no simple correlation exists, accordingly we take the simplest empirical rule that gives the best fit by assuming that p depends only on the sum of the line widths. Hence, for $p < 0$:

$$p = e^{-kl} - e^{kq} \quad (6.4.21)$$

and for $p \geq 0$:

$$p = 1 - e^{-m(q-l)} \quad (6.4.22)$$

where
$$q = \frac{1}{w} \sum_{i=1}^n \Delta \alpha_i \quad (6.4.23)$$

and k , l and m are constants. It is found that the best fit is given by having the approximate values $k = 2.5$, $l = 5.0$ and $m = 0.012$. Hence for $q < 5$, p is obtained from (6.4.21) which together with S is substituted into (6.4.19) to give smearing over part of the bin, and for $q \geq 5$, p is found from (6.4.22) which on putting into (6.4.16) will give us smearing over the whole bin.

If the opacity in many bins is computed by direct integration of a grid and by this empirical smearing method, it is found that when p is well away from zero, i.e. under-congestion or over-congestion, the agreement is often not too bad, but in cases when p is close to zero, i.e. complete triangular smear, the smearing technique can produce an opacity out by often more than an order of magnitude either way.

However, if the opacity by this LSM is computed in tandem with the ILM, then if a value is obtained that is outside the bounds given by the ILM, the appropriate bound is chosen as the opacity in that bin. For cases of one or two lines in a bin, only the ILM should be used.

6.5 The Opacity Sampling Method

Ideally we require a grid that is fine enough so that each spectral line on being profiled can be represented properly. However, as already stated in section 6.1, this could not be done in practice for the whole spectrum with realistic line widths, due to the limitation of the available computer memory. So we have to compromise by using a fine grid that is fine enough to represent each line, bearing in mind computer memory and execution time on the one hand, yet not too coarse so that our accuracy is low and lines can be missed. We thus aim if possible to have about one fine grid point per Doppler width, so that on average about three grid points will cover a profile. This is quite distinct from say Johnson and Krupp (28), who use a very much coarser grid for the calculation of model stellar atmospheres, the finest grid being used having a spacing of 12.5cm^{-1} , which corresponds to 4.5×10^{-3} in the dimensionless frequency units used by us at their $T_{\text{eff}} = 4000^{\circ}\text{K}$, and is large compared to the Doppler width of say CO at $u = 1$, which is 8.6×10^{-6} at that temperature.

Thus if a spectral line is given by:

$$K_{\nu}(u) = 2 \sqrt{\frac{\ln 2}{\pi}} \cdot \frac{h s}{k T} \cdot \frac{1}{\Delta u_G} e^{-4(u-u_0)^2 \ln 2 / \Delta u_G^2} \quad (6.5.1)$$

in $\text{cm}^2 \text{gm}^{-1}$ and with the strength s in $\text{cm}^2 \text{sec}^{-1} \text{gm}^{-1}$ with stimulated emission not being included, we find the grid point closest to the line centre at u_0 , then evaluate (6.5.1) for each value of u computed

from the grid in one direction, until the ratio $\kappa_1(u)/\kappa_c(u)$ is less than some specified value, say 0.01, then repeat this in the other direction for the other side of the profile, so the whole profile is represented. $\kappa_1(u)$ is accumulated in an array for the fine grid points in exactly the same way as the continuum $\kappa_c(u)$ is accumulated earlier, with the fine grid initialized with the continuum obtained by interpolation from the coarse grid. The above test for cutting off a profile is done with respect to the background continuum, rather than what has already been accumulated in the fine grid, so as to make this test independent of the order that lines are computed.

Having computed all lines, a spectrum with many hundreds of thousands, or computer memory permitting, millions of data points is obtained, and the RMO could be found directly by integrating across the whole spectrum using (3.1.7) with an appropriate upper limit, as can be done with the coarse grid for the continuum. However, the spectrum in this form is rather unwieldy and inconvenient to store on some medium like magnetic tape for future use, and is not directly comparable to the spectrum produced by the ILM and LSM. So instead, by an appropriate choice of bin sizes and fine grid intervals, as discussed in section 6.1, we can integrate (6.2.1) with $\kappa(u)$ for all sources of opacity using Simpson's rule over the bin. The spectrum is then in a form directly comparable to the ILM and LSM, as we now have it in the form of $1/\bar{\kappa}_i$ for each bin i .

If the OSM is computed in tandem with the ILM, then for bins that have one or two lines, the ILM gives a better result because the OSM is only approximate. However, if there are more lines, and particularly for congested bins, the OSM is much more reliable, and we never have the problem of infinite or negative opacity that can occur with the ILM. Having obtained the reciprocal opacity for each bin, by whichever method, the total RMO is found simply from:

$$\frac{1}{R} = \sum_{i=1}^n \frac{1}{R_i} \quad (6.5.2)$$

for n bins.

In deciding the separation of the fine grid points, we can use (6.1.1) with a typical molecule like CO, then neglecting turbulent velocity, at 1000°K, $\Delta u/u = 4.28 \times 10^{-6}$ and at 6000°K, $\Delta u/u = 1.05 \times 10^{-5}$, which covers the temperature range of greatest interest to us. If we do not have enough computer memory to put a fine grid all the way from $u = 0$ to 20, as is the case with this work, we can stop at $u = 15$ where the weighting function is already quite small, leaving just the continuum at higher energies. Even so, if we are still short of memory, we can still compromise by not having the grid quite as fine as one grid point per Doppler width near the limits of the range covered where the weighting function is small, so errors are less important. In practice, because $\Delta u \rightarrow 0$ as $u \rightarrow 0$, we are compelled to under-sample in our first region of $u = 0$ to 1, so we can choose a sampling interval to match at $u = 0.5$ or $u = 1$. If turbulent velocity is included, then we can of course use a coarser grid, or have better

sampling.

Although we obtain the final RMO $\bar{\kappa}$ for the whole spectrum as mass absorption in $\text{cm}^2 \text{gm}^{-1}$, it is in fact much more convenient to work in volume absorption $\mu(u)$ in cm^{-1} for individual species, be they sources of continuous opacity or profiled lines; in the latter case a line strength s is in $\text{cm}^{-1} \text{sec}^{-1}$. Thus all equations in chapter 3 and 6 involving $\kappa(u)$ in $\text{cm}^2 \text{gm}^{-1}$ that are used numerically in this work, are in fact used with $\mu(u)$, where the two are related by (3.1.15). Also, it is more convenient when computing $1/\bar{\kappa}_i$ for each bin by whichever method, to omit the constant $15/4\pi^4$. Thus in evaluating the sum (6.5.2) over all bins to obtain the required RMO in $\text{cm}^2 \text{gm}^{-1}$, we apply a constant factor of $15\rho/4\pi^4$ to the right hand side, and this factor must actually be applied to the computed values of every bin to obtain the correct RMO in each bin.

So far in this thesis we have discussed all the required theory, it is the purpose of the next chapter to discuss the results and tests performed using the theory. The programming methods employed in obtaining our results are rather involved, and any discussion beyond mentioning brief points where relevant, is considered beyond the scope of this thesis.

7 PRESENTATION AND DISCUSSION OF RESULTS

7.1 Introduction

In this final chapter, all the theory discussed in the previous chapters is put into practice, and the results of calculations based on this theory are considered. A 10X13 grid of continuous opacities in the T - ρ plane is computed, with the results in the next section. Subsequently, some examples of opacities for a few grid points with the contribution of diatomic and triatomic molecular bands calculated in detail, are considered, together with examples of some intermediate calculations necessary in determining opacities, and some tests.

All calculations presented here have been performed on a VAX 11/780 computer acquired by the University of St. Andrews in the first half of 1980. As the VAX is fast and interactive, code could rapidly be developed and tested. Prior to this, while working in St. Andrews, use was made of an IBM 360/44, which could only be effectively used in batch mode. However, while working in Dublin, development was performed on the IBMs 370/148 and 158 at the Central Data Processing Services of the Irish government, which, although they could only be used in batch mode, were powerful machines. In addition, use was made at Dunsink Observatory of a Data General Nova minicomputer, which could be used interactively for testing small sections of code, and an Apple II microcomputer for graphics.

The opacities are calculated using the two computer programs MIXOP and TRIATOM. The latest versions of these are listed in the program volume of this thesis, together with some documentation and examples of actual output. An attempt has been made to adhere as much as possible to the conventions of standard FORTRAN IV, this being a subset of FORTRAN 77 used by the VAX, in order to make the programs as compatible as possible with compilers on other machines. However, we have had to depart from FORTRAN IV for such features as file manipulation, this being discussed more fully in the program volume.

The MIXOP program calculates the abundances and continuous opacities using the theory discussed in chapters 2 and 3. This program can generate files that are subsequently used by TRIATOM which calculates spectral lines for diatomic and triatomic molecules, based on the theory discussed in chapters 4 and 5 respectively, and the opacities due to these lines by chapter 6. We consider first the results of applying MIXOP.

7.2 Abundances and Continuous Opacities

In this section, the results of calculating the abundances and continuous opacities due to various species over a range of temperatures and densities are considered.

The following sources of data were used as the input for the statistical mechanics calculations: abundances of elements and isotopes from Cameron (4), atomic masses and spins of nuclei from the American Institute of Physics Handbook (107), atomic ionization potentials and electron affinities from Allen (32), atomic energy levels from Moore (33), most diatomic molecular rotational and vibrational constants from Rosen (35) and Mizushima (36), except for TiO from Phillips (108) and ClO from Cooper (109), and triatomic molecular data from Herzberg (30) and (34). With (30) also used as a source of the trial values for the force constants of the bonds of the two non-linear non-symmetric molecules considered, i.e. HCO and HNO. The sources of the data for continuous opacities are given in chapter 3, with the data given in the appendices. Finally, some sections of the coding in the MIXOP program were obtained from Carson (3), together with the subroutine for computing Fermi-Dirac integrals used by the ILM in the program TRIATOM.

In the mixture, we have the 22 most abundant elements: H, He, C, N, O, F, Ne, Na, Mg, Al, Si, P, S, Cl, Ar, K, Ca, Ti, Cr, Mn, Fe and Ni, of which we allow for the formation of the stable negative ions of H, C, O, F, Na, Al, Si, P, S and Cl, and two positive ions of all elements from He onwards. In the molecular equilibrium calculations, we allow for the formation of the 36 diatomic molecules: H_2 , C_2 , N_2 , O_2 , OH, NH, CH, CN, CO, NO, SO, CaH, MgH, AlH, SiH, SiN, AlO, SiO, NaCl, MgCl, KCl, CaCl, Na_2 , NaH, SH, MgO, HCl, HF, ClO, TiO, H_2^+ , CH^+ , CO^+ , N_2^+ , O_2^+ and OH^+ , and the 9 triatomic molecules: H_2O , HCN, HCO, HNO, N_2O , CO_2 , NO_2 , O_3 and SO_2 , together with their isotopic variations, there being 202 and 119 possible variations of diatomic and triatomic molecules respectively, due to the presence of 60 different isotopes. Though this list appears formidable, there would be plenty of scope for including many more atoms and molecules. However, the object of this work is to devise a method to compute opacities and illustrate it with a number of examples.

Many of the molecules in this list are chosen because their abundances are likely to be very high at low temperatures, such as obviously H_2 as its constituent atoms are very abundant, or CO as it is tightly bound, or because they are likely to be important sources of opacity even for relatively low abundances, like TiO. Also, in order to calculate the contribution to the opacity due to bands, discussed later in this chapter, we have to know the oscillator strengths or dipole moments, which are not always readily available, and some of these molecules are chosen because such quantities are known. However, some of these molecules tend to have low abundances

for any set of conditions, such as the molecular ions, and would be of essentially no importance in the statistical mechanics or opacity calculations, but at least illustrate that the computer program can handle abundances over a very great range of values.

The abundances of some molecules are very sensitive to the initial abundances of the elements, the most spectacular example of this being C_2 . As CO is the most tightly bound of all diatomic molecules, and as the elements C and O tend to have comparable abundances, most of the C and O is bound up in CO at lower temperatures, with the surplus of either C or O combining with other elements as well as itself. In our mixture, as O is more abundant than C by a factor of 1.8, oxygen containing compounds predominate by far over carbon containing compounds, with C_2 in particular tending to have a negligible abundance. In carbon stars, C is in surplus, the reverse is true, and in particular C_2 is abundant and an important source of opacity, as it has a large number of bands across the spectrum. Thus one can see qualitatively, that the opacity can be very sensitive to the initial abundances of the elements. Because all the equations governing molecular dissociation are coupled, in many cases it is impossible to say even qualitatively whether a particular species will be abundant or not at a particular temperature and density, before actually performing the calculations, this problem having been stated at the beginning of chapter 2. In reality, one should allow for the formation of many more molecules, but it is believed that the sample here is representative.

The RMOs and PMOs due to the continuum, together with the abundances of the various species were calculated over 128 grid points in the T - ρ plane in a 10×13 matrix, with the iteration convergence criterion $\xi = 10^{-6}$. Because the densities are considered in log form, it was decided also to handle the temperatures in the log. The densities chosen are $\log \rho = -14$ to -2 in steps of 1 and temperatures of $\log T = 3.0$ to 3.9 in steps of 0.1, thus covering the range $T = 1000^\circ\text{K}$ to 7943°K . The grid points with $\log \rho = -2$ and -3 for $\log T = 3.0$ are not computed because of problems with floating point numbers exceeding the machine's range, and it is not considered worthwhile to handle specially these highly unlikely cases. This grid thus embraces very well, with a substantial overkill, the domain in the H-R diagram for late-type stars. Table (7.1) gives the RMO and PMO in that order in the log to four figures of accuracy for each grid point, by integrating the spectrum computed with 4001 data points, the first point being the dummy point at zero energy. All the opacities are in $\text{cm}^2 \text{gm}^{-1}$, and $\log \rho$ is written as log R.

It is seen that generally the opacities increase with increasing temperature or density, but not necessarily monotonically in any orthogonal direction in the table. It would, however, require the computation of many hundreds, if not thousands, of grid points to investigate the detailed behaviour of the opacities with temperature and density.

Table (7.1) of Log RMO and Log PMO for Continuum

	T	1000	1259	1585	1995	2512
	Log T	3.0	3.1	3.2	3.3	3.4
Log R						
-14		-7.5588	-6.2429	-5.2485	-4.5990	-3.7880
		-6.4344	-5.9364	-5.1839	-4.5777	-3.7975
-13		-7.7640	-6.4774	-5.5177	-4.7351	-4.0474
		-6.4356	-5.9920	-5.3732	-4.6874	-4.0440
-12		-7.9016	-6.7287	-5.7731	-4.8909	-4.2942
		-6.4360	-6.0203	-5.5030	-4.7957	-4.2543
-11		-7.6665	-6.9406	-5.9472	-5.0183	-4.4140
		-6.4353	-6.0304	-5.5608	-4.8580	-4.3236
-10		-7.1920	-6.9024	-6.0980	-5.1980	-4.3981
		-6.4270	-6.0301	-5.5920	-4.8986	-4.1499
-9		-6.7696	-6.5590	-6.1168	-5.3362	-4.2628
		-6.3504	-5.9946	-5.5924	-4.8883	-3.6953
-8		-6.2885	-6.0497	-5.7300	-5.1409	-3.9712
		-5.9315	-5.7365	-5.4552	-4.7638	-3.2818
-7		-5.5153	-5.2696	-5.0651	-4.5988	-3.5754
		-5.0758	-5.0008	-4.9044	-4.4275	-3.0079
-6		-4.6066	-4.4825	-4.4612	-4.0148	-3.0545
		-4.0932	-4.0390	-4.0011	-3.7966	-2.7514
-5		-3.7514	-3.8323	-3.9537	-3.4230	-2.4335
		-3.0950	-3.0430	-3.0133	-2.9048	-2.2792
-4		-3.0036	-3.1284	-2.6911	-2.1198	-1.2273
		-2.0940	-2.0185	-1.7948	-1.5407	-0.9664
-3		--	-2.5290	-2.0904	-1.3455	-0.4539
		--	-1.0350	-0.9219	-0.5728	-0.0196
-2		--	-1.9319	-1.5238	-0.8906	-0.1577
		--	-0.0413	0.0099	0.1667	0.5223

Table (7.1) Continued

	T	3162	3981	5012	6310	7943
	Log T	3.5	3.6	3.7	3.8	3.9
Log R						
-14		-3.4375	-2.4662	-0.7264	0.3991	0.4862
		-3.4460	-2.4749	-0.7271	0.3988	0.4864
-13		-3.4507	-2.8683	-1.2104	0.1431	0.4855
		-3.4588	-2.8794	-1.2126	0.1417	0.4871
-12		-3.5043	-3.1819	-1.6894	-0.2527	0.4773
		-3.5109	-3.1843	-1.6949	-0.2561	0.4928
-11		-3.6095	-3.3212	-2.1401	-0.6805	0.4140
		-3.6098	-3.3125	-2.1498	-0.6800	0.5146
-10		-3.6430	-3.2137	-2.4687	-1.0487	0.2754
		-3.5826	-3.2074	-2.4767	-1.0176	0.5422
-9		-3.4735	-2.7840	-2.4079	-1.1585	0.1970
		-3.1831	-2.7048	-2.3925	-1.0966	0.5731
-8		-2.9626	-2.1414	-1.8805	-0.8938	0.3045
		-2.5344	-1.9853	-1.8270	-0.8414	0.6380
-7		-2.3350	-1.4741	-1.0890	-0.4620	0.5694
		-1.9025	-1.3041	-1.0173	-0.3907	0.7946
-6		-1.8278	-0.8564	-0.2871	0.0709	0.9239
		-1.4602	-0.6894	-0.2121	0.1650	1.0971
-5		-1.3201	-0.3171	0.4291	0.7288	1.3728
		-1.0768	-0.1693	0.5039	0.8280	1.5468
-4		-0.3301	0.4605	1.2333	1.5178	1.9473
		-0.1730	0.5739	1.3142	1.6225	2.1282
-3		0.4017	1.0879	1.7938	2.2125	2.6751
		0.5935	1.1913	1.8864	2.3360	2.8673
-2		0.6296	1.2838	1.8290	2.4748	3.2579
		1.0052	1.4812	1.9740	2.6365	3.4846

It is interesting to see what the continuum looks like at some grid points, and accordingly we show in figures (7.1-7) the continuum for $\log \rho = -8$ at $\log T = 3.2$ to 3.8 without stimulated emission. Note that the scale in opacity is doubled for the last three figures to illustrate the features better. A number of interesting features can be pointed out, where in all cases the opacity increases to infinity at $u = 0$ due to free-free absorption. At $\log T = 3.2$, the continuum is dominated by Rayleigh scattering at high frequencies and free-free absorption at very low frequencies, the minimum in between is filled by pressure-induced H_2-H_2 and H_2-He opacity causing the marked behaviour between about $u = 0.5$ and $u = 6$. At $\log T = 3.3$ the pressure-induced opacity has become less important, and at $\log T = 3.4$ it no longer shows up on the plot; the H_{bf}^- absorption threshold at about $u = 3.3$ being obvious. At $\log T = 3.5$, a very small bump at $u \approx 13$ is visible, and can be identified with Cl_{bf}^- . Although Cl has a relatively small abundance, it has the largest electron affinity of all elements, so is a very efficient sink of electrons, and it is not surprising that the effect of the negative ion can just be seen. However at $\log T = 3.6$, this has vanished, but at $\log T = 3.7$, in addition to the absorption threshold of H_{bf}^- , an absorption edge of neutral H_{bf} is clearly visible; this is in fact the Balmer jump. Finally, at $\log T = 3.8$, this jump has become much more pronounced, and has been joined by the Paschen jump to the left, and left of the H_{bf}^- edge is a very weak "glitch", which is attributed to the Brackett jump.

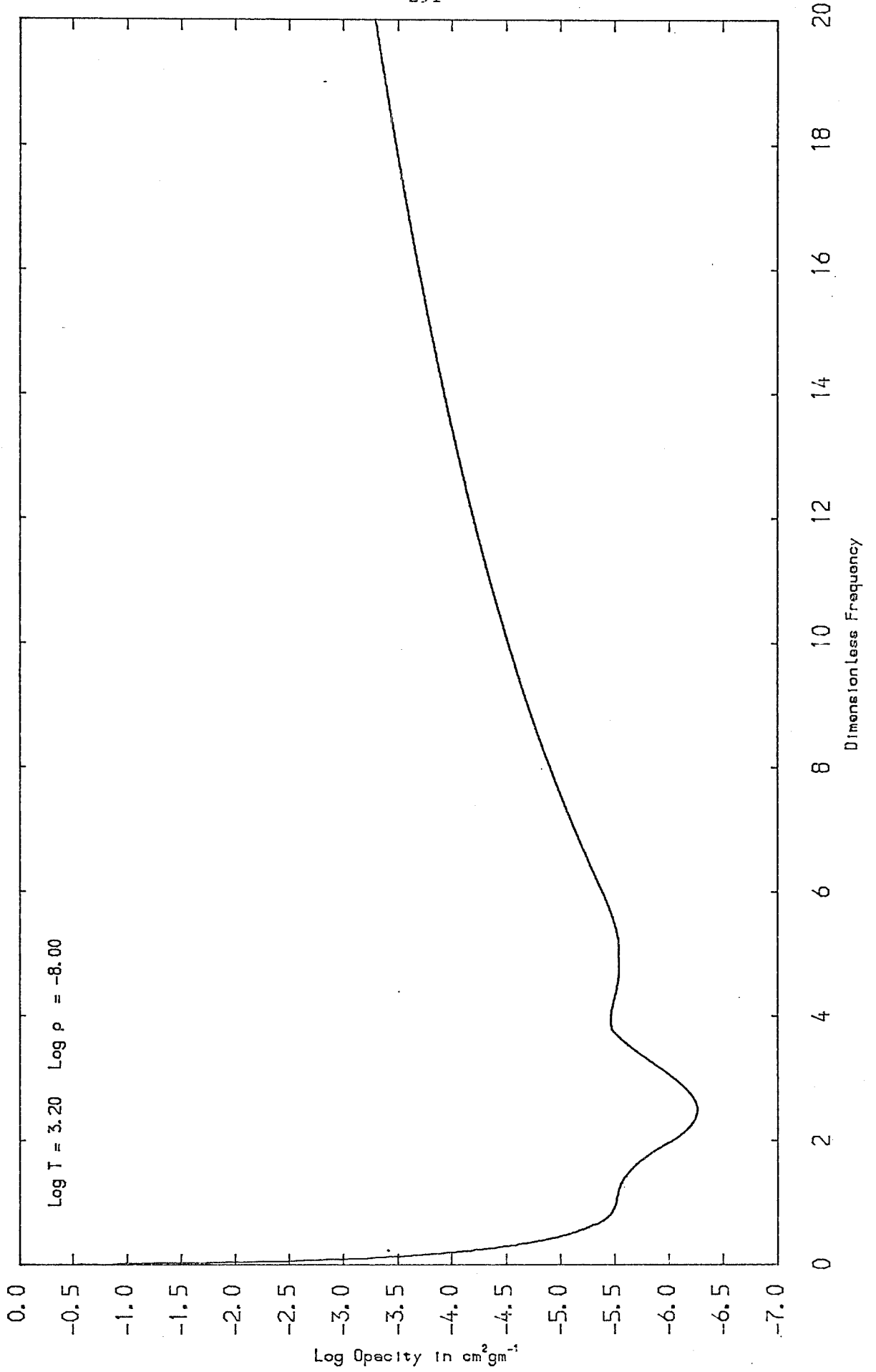


Fig. 7.1

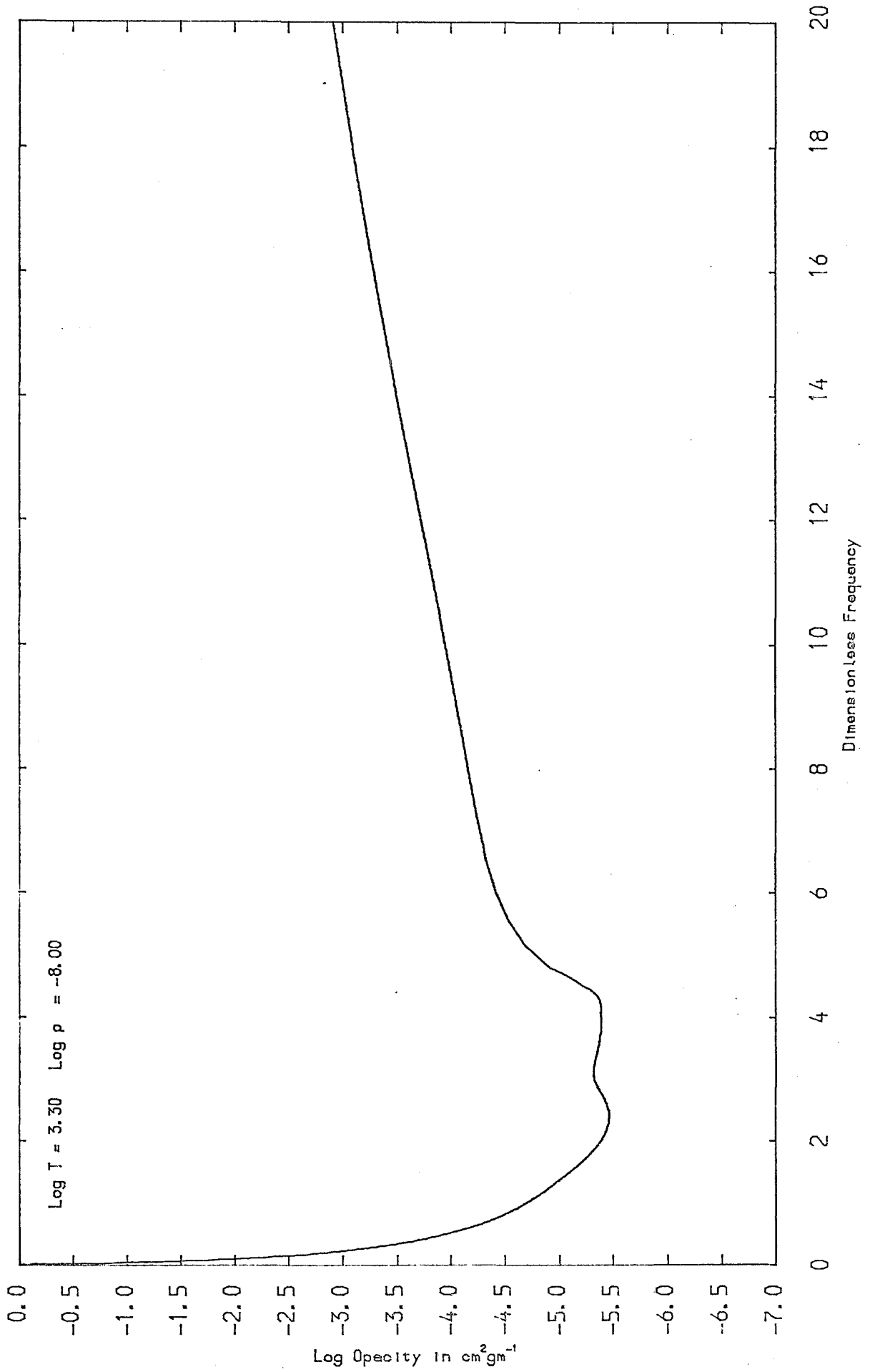


Fig. 7.2

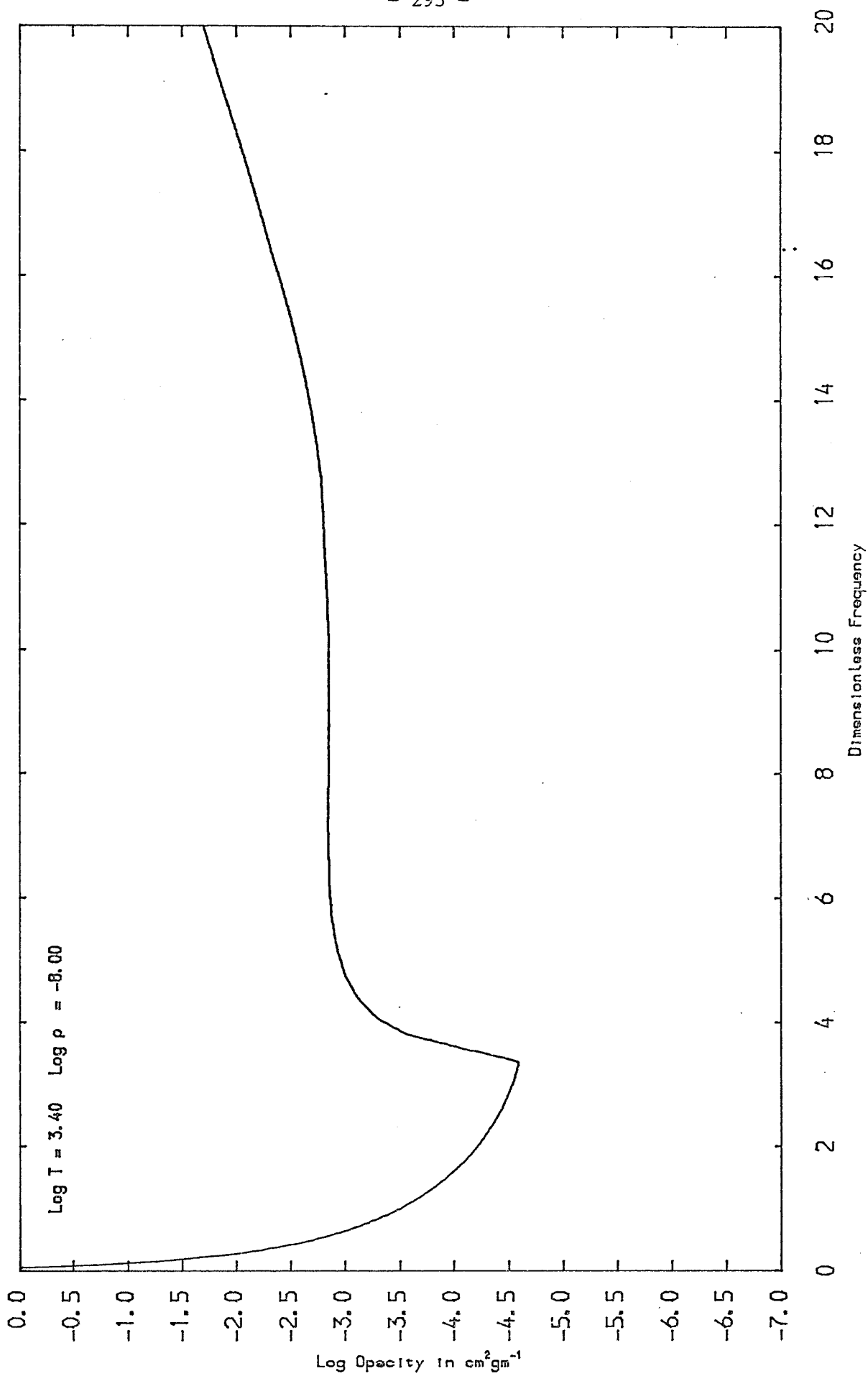


Fig. 7.3

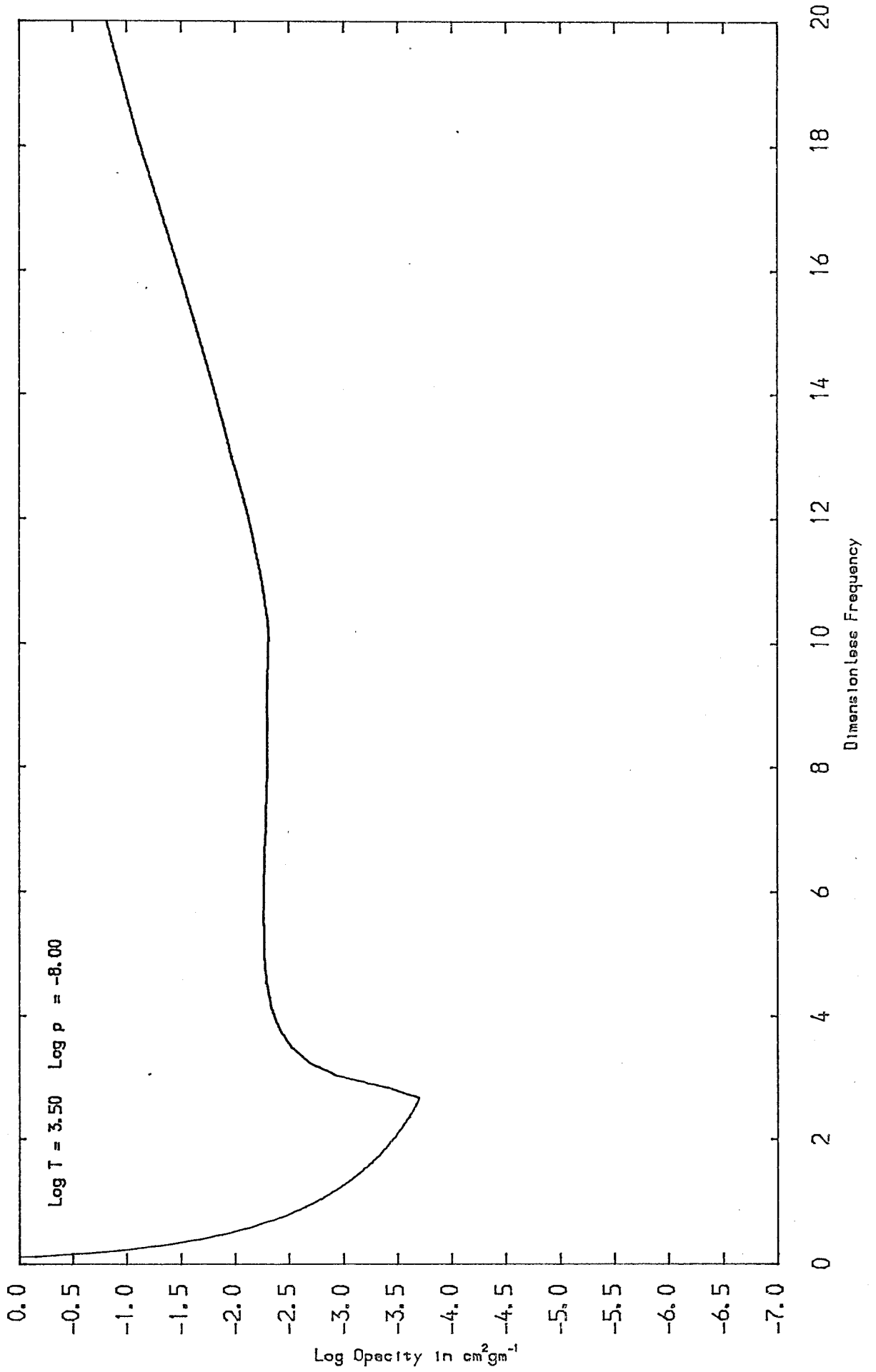


Fig. 7.4

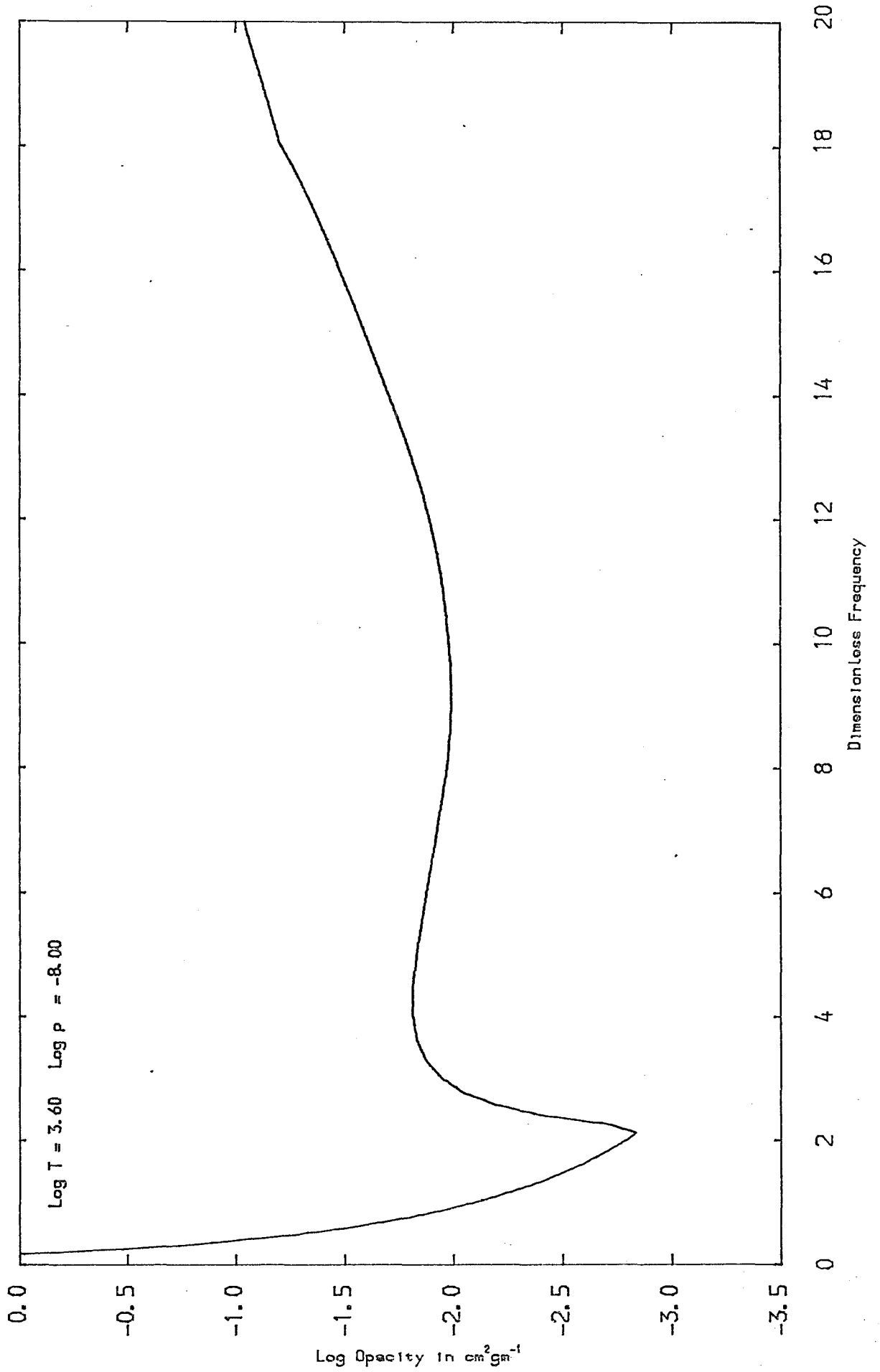


Fig. 7,5

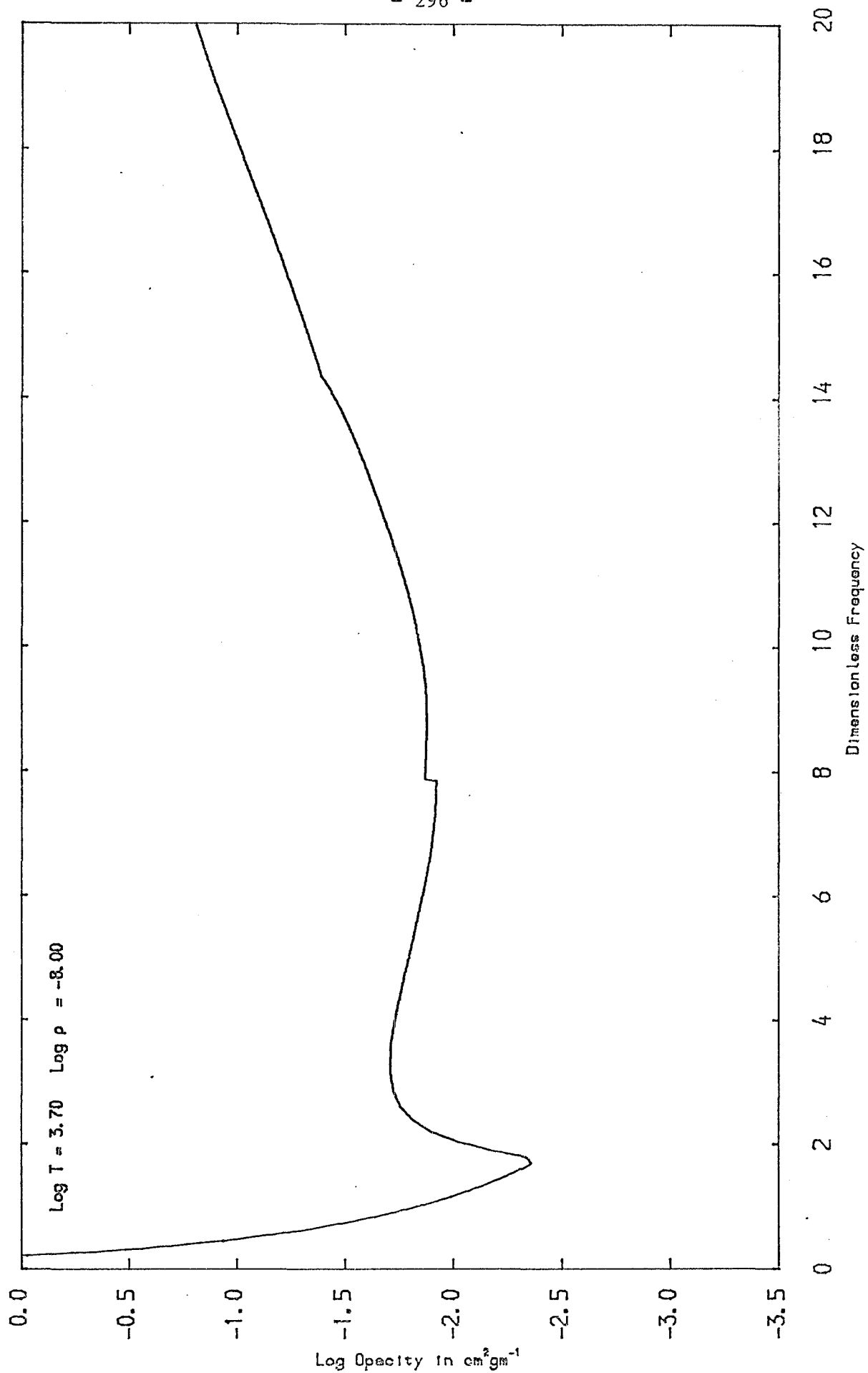


Fig. 7.6

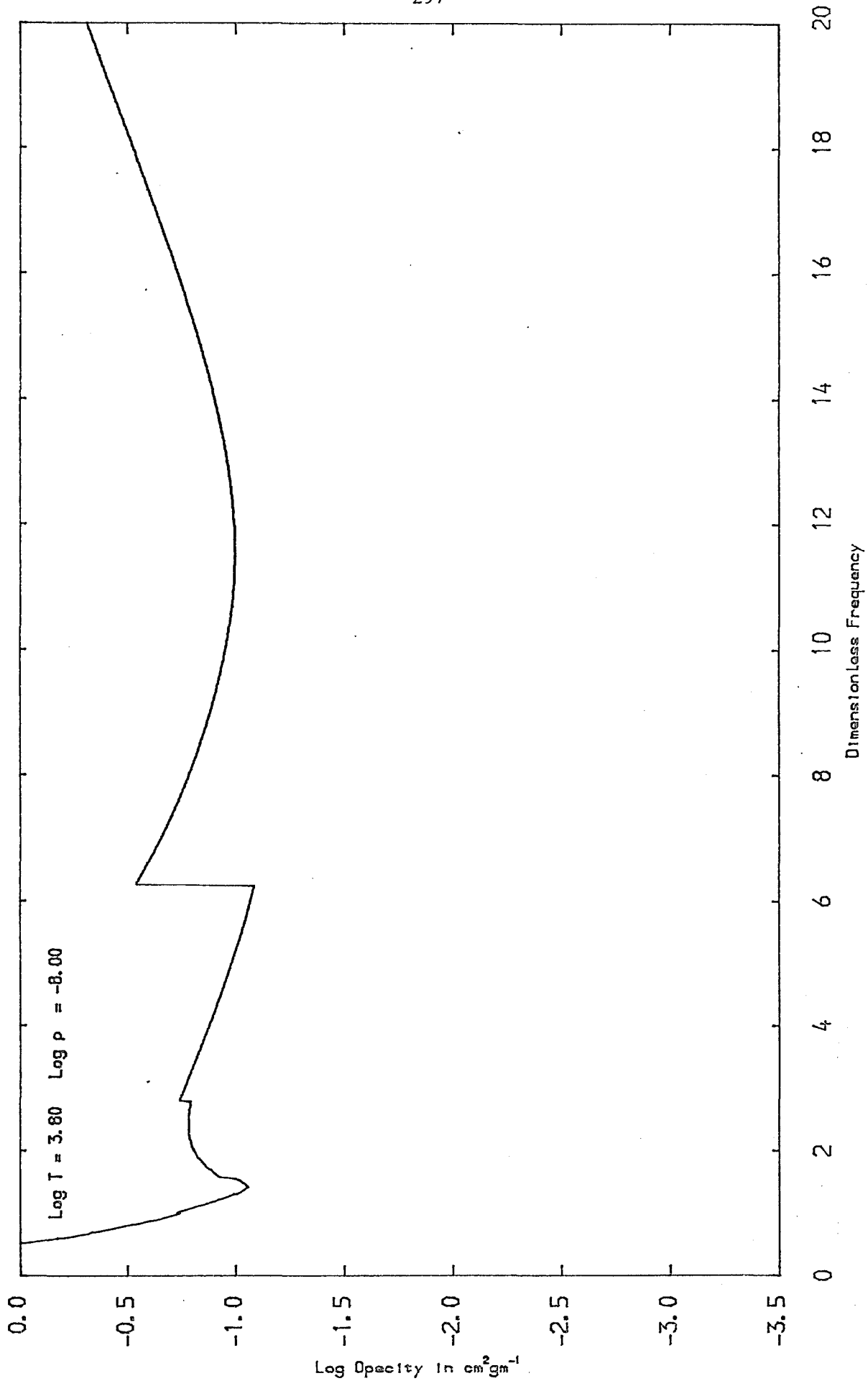


Fig. 7.7

The noticeable bump at $u \approx 18$ for $\log T = 3.6$, and visible again for $\log T = 3.7$, but shifted, corresponds to a wavelength of 2000\AA and turns out to be due to OH_{bf} as given by Tarafdar and Das (57), the cross-section being tabulated at rather coarse intervals. Although OH is a relatively abundant species at these grid points, and is an important source of opacity, it is expected that such a feature will have a very small effect on the total PMO and RMO, particularly as it occurs where the weighting functions are very small. However, in investigating OH_{bf} further, it was found that anomalies can occur when extrapolating the table to very long wavelengths. So it was decided to let the cross-section fall off beyond the table according to a power law as determined approximately by the tabulated points at the limits of 1000 and 5000\AA . This was also applied to CH_{bf} from the limits 1200 and 3000\AA . Refer to chapter 3 and the appendices.

Thus if $\kappa_{\lambda}(T)$ is the cross-section per particle at a wavelength for a particular temperature, then we can write:

$$\kappa_{\lambda}(T) = \left(\frac{\lambda}{\lambda_0}\right)^{n(T)} \kappa_0(T) \quad (7.2.1)$$

where λ_0 is the wavelength at the last tabulated point, $\kappa_0(T)$ is the interpolated or extrapolated cross-section for that temperature at λ_0 and $n(T)$ is an exponent dependent on temperature, obtained from the empirical formula:

$$n(T) = -k \left(\frac{T}{4000}\right)^m \quad (7.2.2)$$

where for OH_{bf} $\lambda_0 = 5000\text{\AA}$, $k = 3.14$ and $m = -1.33$, and for CH_{bf} $\lambda_0 = 3000\text{\AA}$, $k = 9.56$ and $m = -0.54$, which give a good fit. In dimensionless frequency units, if λ_0 is in Angströms, we can write in place of (7.2.1):

$$K_u(T) = \left(\frac{10^8 hc}{\lambda_0 kT} \right)^{n(T)} \cdot \frac{1}{u^{n(T)}} \cdot K_o(T) \quad (7.2.3)$$

It is not considered feasible in this thesis to give extensive tabulations of the abundances of all the various species for all grid points computed. However, for the seven grid points discussed in detail above, tables (7.2-8) give the abundances in cm^{-3} for the various species, being a restricted version of the output produced by the program. Some examples of more detailed tables of abundances are found in the program volume. In the tables, ENN is the number density of free electrons, and the columns headed ANF, FAF, AM2 and AM3 are the abundances of the free atoms, the fraction of atoms free, the abundances of the diatomic molecules and triatomic molecules respectively.

It is immediately seen that with increasing temperature, of those atomic species combined into molecules, their fractions free approach unity with the abundances of all the molecules decreasing due to dissociation, exactly as expected. At the lowest temperature, the four most abundant molecules in order of decreasing abundance are H_2 , CO, N_2 , and SiO, the abundances of the last three being high due to their large dissociation potentials. Although as the temperature is increased the abundances of all individual molecules eventually fall,

because CO is very stable, it does not appreciably dissociate until at quite high temperatures, whilst the abundances of, for example, CH and CN actually increase considerably to a maximum before decreasing. This behaviour is presumably due to the fact that as CO dissociates even slightly, because it is so abundant, a considerable amount of carbon, which is in short supply, is released and is free to combine with other atoms. This illustrates very well indeed how difficult it is to predict abundances before performing the calculations of statistical mechanics.

Because H^- is such an important source of opacity, it is interesting to consider it briefly. In table (7.9) for the grid points with $\log T = 3.2, 3.5$ and 3.8 with $\log \rho = -8$, H^-_{fr} is the fractional abundance of H^- as a fraction of all free H atoms, H^-_{ab} is the absolute abundance of the ion in cm^{-3} , and ENI is the number of electrons contributed (+) or absorbed (-) in cm^{-3} due to the tabulated element. It is seen that at $\log T = 3.2$, H^- has a very low abundance, with most of the electrons responsible for its formation coming from Na and K, due to their low ionization potentials, with H being a strong sink of electrons. At $\log T = 3.5$, the abundance of H^- is considerably higher, with H being a large sink of electrons and many other elements now contributing electrons. Finally at the last grid point, from being the largest sink of electrons, H now becomes the largest source, this is due to a significant fraction of protons forming, yet H^- is higher still, i.e. many of the electrons needed to form H^- come from H itself.

Table (7.2) of Abundances

Log T = 3.20 Log R = -8.00 ENN = 4.06350E+07

ANF		FAF		AM2		AM3	
H	4.81098E+12	1.04593E-03	H2	2.29615E+15	H2O	1.25742E+12	
He	3.19665E+14	1.00000E+00	C2	2.84850E-11	HCN	7.31695E+05	
C	1.44024E-03	8.43823E-16	N2	2.70486E+11	HCO	4.48163E+05	
N	5.26609E+02	9.73449E-10	O2	3.27750E+01	HNO	1.59186E-01	
O	1.48390E+05	4.77159E-08	OH	1.61334E+08	N2O	3.28365E-04	
F	3.69813E+01	1.04355E-07	NH	6.09529E+03	CO2	4.31538E+08	
Ne	4.97576E+11	1.00000E+00	CH	2.66803E-03	NO2	6.82174E-07	
Na	8.67390E+09	9.99452E-01	CN	1.02344E+00	O3	8.85927E-16	
Mg	1.51862E+11	9.89535E-01	CO	1.70637E+12	SO2	3.86927E+01	
Al	1.21134E+10	9.85247E-01	NO	2.80069E+04			
Si	6.70740E+05	4.63716E-06	SO	6.64134E+05			
P	1.38859E+09	1.00000E+00	CaH	9.99027E+04			
S	2.17614E+06	3.00896E-05	MgH	1.60599E+09			
Cl	1.37220E+06	1.66433E-03	AlH	1.75261E+08			
Ar	1.69523E+10	1.00000E+00	SiH	1.29676E+05			
K	6.04843E+08	9.95618E-01	SiN	3.20437E-02			
Ca	1.04262E+10	9.99743E-01	AlO	6.12554E+06			
Ti	1.22033E+05	3.04027E-04	SiO	1.44644E+11			
Cr	1.83699E+09	1.00000E+00	NaCl	1.38868E+06			
Mn	1.34519E+09	1.00000E+00	MgCl	3.48611E+04			
Fe	1.20055E+11	1.00000E+00	KCl	2.66182E+06			
Ni	6.94292E+09	1.00000E+00	CaCl	2.58553E+06			
			Na2	2.69890E-01			
			NaH	3.36689E+06			
			SH	7.23192E+10			
			MgO	4.90133E+03			
			HCl	8.16432E+08			
			HF	3.54379E+08			
			ClO	1.49010E-04			
			TiO	4.01266E+08			
			H2+	8.03421E-21			
			CH+	4.91579E-25			
			CO+	2.63763E-27			
			N2+	1.58311E-25			
			O2+	1.41410E-24			
			OH+	3.59162E-23			

Table (7.3) of Abundances

Log T = 3.30 Log R = -8.00 ENN = 7.58397E+08

ANF		FAF		AM2		AM3	
H	1.43765E+14	3.12552E-02	H2	2.22668E+15	H2O	1.24538E+12	
He	3.19665E+14	1.00000E+00	C2	2.64770E-07	HCN	6.02438E+05	
C	1.36253E+01	7.98295E-12	N2	2.70483E+11	HCO	2.19682E+06	
N	8.33677E+05	1.54107E-06	O2	5.73242E+04	HNO	3.66151E+01	
O	2.95449E+08	9.50038E-05	OH	1.20416E+10	N2O	7.22951E-02	
F	9.30670E+03	2.62620E-05	NH	9.42726E+05	CO2	3.13596E+08	
Ne	4.97576E+11	1.00000E+00	CH	3.86734E+00	NO2	2.67833E-03	
Na	8.67490E+09	9.99567E-01	CN	1.17510E+02	O3	8.41013E-10	
Mg	1.52338E+11	9.92636E-01	CO	1.70648E+12	SO2	5.81905E+02	
Al	1.22219E+10	9.94074E-01	NO	4.83166E+06			
Si	5.28357E+07	3.65280E-04	SO	2.84832E+07			
P	1.38859E+09	1.00000E+00	CaH	3.20970E+05			
S	9.87040E+07	1.36478E-03	MgH	1.12999E+09			
Cl	3.78313E+07	4.58853E-02	AlH	6.64825E+07			
Ar	1.69523E+10	1.00000E+00	SiH	2.94826E+06			
K	6.07488E+08	9.99973E-01	SiN	4.54235E+00			
Ca	1.04284E+10	9.99955E-01	AlO	6.37276E+06			
Ti	2.48026E+06	6.17921E-03	SiO	1.44589E+11			
Cr	1.83699E+09	1.00000E+00	NaCl	6.37633E+04			
Mn	1.34519E+09	1.00000E+00	MgCl	7.82266E+03			
Fe	1.20055E+11	1.00000E+00	KCl	1.63511E+04			
Ni	6.94292E+09	1.00000E+00	CaCl	1.46477E+05			
			Na2	9.70672E-02			
			NaH	3.69594E+06			
			SH	7.21949E+10			
			MgO	5.60671E+04			
			HCl	7.86409E+08			
			HF	3.54370E+08			
			ClO	1.35301E-01			
			TiO	3.98908E+08			
			H2+	7.55134E-12			
			CH+	4.62337E-16			
			CO+	9.75202E-18			
			N2+	1.78215E-16			
			O2+	1.56734E-14			
			OH+	1.56199E-13			

Table (7.4) of Abundances

Log T = 3.40 Log R = -8.00 ENN = 7.62530E+09

ANF		FAF		AM2		AM3	
H	1.73078E+15	3.76281E-01	H2	1.43344E+15	H2O	8.41897E+11	
He	3.19665E+14	1.00000E+00	C2	3.88781E-04	HCN	4.80824E+05	
C	1.97263E+04	1.15574E-08	N2	2.70178E+11	HCO	6.80897E+06	
N	2.87739E+08	5.31893E-04	O2	2.12131E+07	HNO	2.36259E+03	
O	1.20769E+11	3.88341E-02	OH	2.95750E+11	N2O	5.90707E+00	
F	9.24133E+05	2.60775E-03	NH	4.21283E+07	CO2	2.74047E+08	
Ne	4.97576E+11	1.00000E+00	CH	1.03658E+03	NO2	2.03024E+00	
Na	8.67754E+09	9.99871E-01	CN	5.23698E+03	O3	4.90311E-05	
Mg	1.52755E+11	9.95357E-01	CO	1.70652E+12	SO2	6.26007E+03	
Al	1.22632E+10	9.97432E-01	NO	2.85958E+08			
Si	1.68525E+09	1.16510E-02	SO	7.24947E+08			
P	1.38859E+09	1.00000E+00	CaH	6.16812E+05			
S	2.38954E+09	3.30403E-02	MgH	7.12233E+08			
Cl	3.78802E+08	4.59446E-01	AlH	2.50948E+07			
Ar	1.69523E+10	1.00000E+00	SiH	2.88176E+07			
K	6.07505E+08	1.00000E+00	SiN	2.33087E+02			
Ca	1.04283E+10	9.99940E-01	AlO	6.47947E+06			
Ti	2.61877E+07	6.52428E-02	SiO	1.42931E+11			
Cr	1.83699E+09	1.00000E+00	NaCl	1.36296E+03			
Mn	1.34519E+09	1.00000E+00	MgCl	1.74673E+03			
Fe	1.20055E+11	1.00000E+00	KCl	3.37067E+01			
Ni	6.94292E+09	1.00000E+00	CaCl	1.00015E+04			
			Na2	5.17061E-03			
			NaH	1.12234E+06			
			SH	6.92076E+10			
			MgO	4.08054E+05			
			HCl	4.45660E+08			
			HF	3.53455E+08			
			ClO	2.16555E+01			
			TiO	3.75201E+08			
			H2+	7.45611E-05			
			CH+	5.58662E-09			
			CO+	4.23737E-10			
			N2+	3.05845E-09			
			O2+	1.59178E-06			
			OH+	6.20808E-06			

Table (7.5) of Abundances

Log T = 3.50 Log R = -8.00 ENN = 3.35211E+10

	ANF	FAF	AM2	AM3
H	4.35106E+15	9.45946E-01	H2 1.24237E+14	H2O 6.93065E+09
He	3.19665E+14	1.00000E+00	C2 1.70228E+01	HCN 1.81066E+06
C	7.30509E+07	4.27998E-05	N2 2.55630E+11	HCO 6.34065E+06
N	2.87944E+10	5.32271E-02	O2 1.77737E+07	HNO 2.06046E+03
O	1.23393E+12	3.96781E-01	OH 1.14300E+11	N2O 1.83797E+01
F	7.90625E+07	2.23101E-01	NH 2.95352E+08	CO2 2.45219E+07
Ne	4.97576E+11	1.00000E+00	CH 3.56515E+05	NO2 3.14110E+00
Na	8.67865E+09	9.99998E-01	CN 1.23999E+06	O3 2.16697E-04
Mg	1.53296E+11	9.98879E-01	CO 1.70670E+12	SO2 4.51612E+02
Al	1.22927E+10	9.99834E-01	NO 6.19806E+08	
Si	9.83737E+10	6.80106E-01	SO 1.21354E+09	
P	1.38859E+09	1.00000E+00	CaH 3.96499E+04	
S	3.97617E+10	5.49787E-01	MgH 1.71777E+08	
Cl	7.90850E+08	9.59216E-01	AlH 1.79337E+06	
Ar	1.69523E+10	1.00000E+00	SiH 2.32237E+08	
K	6.07505E+08	1.00000E+00	SiN 1.93971E+04	
Ca	1.04288E+10	9.99996E-01	AlO 2.50796E+05	
Ti	3.64716E+08	9.08635E-01	SiO 4.60387E+10	
Cr	1.83699E+09	1.00000E+00	NaCl 1.86379E+00	
Mn	1.34519E+09	1.00000E+00	MgCl 1.76519E+02	
Fe	1.20055E+11	1.00000E+00	KCl 4.67125E-02	
Ni	6.94292E+09	1.00000E+00	CaCl 4.32789E+01	
			Na2 3.82118E-06	
			NaH 1.32438E+04	
			SH 3.13468E+10	
			MgO 1.75402E+05	
			HCl 3.36249E+07	
			HF 2.75316E+08	
			ClO 3.60722E+01	
			TiO 3.66729E+07	
			H2+ 5.14350E+00	
			CH+ 1.45609E-02	
			CO+ 7.55379E-04	
			N2+ 2.55688E-03	
			O2+ 4.21559E-02	
			OH+ 3.15180E-01	

Table (7.6) of Abundances

Log T = 3.60 Log R = -8.00 ENN = 2.25574E+11

ANF		FAF		AM2		AM3	
H	4.59033E+15	9.97963E-01	H2	4.68073E+12	H2O	8.78000E+06	
He	3.19665E+14	1.00000E+00	C2	1.49138E+06	HCN	5.37686E+06	
C	2.09719E+11	1.22872E-01	N2	4.16657E+10	HCO	2.91524E+06	
N	4.57066E+11	8.44898E-01	O2	6.76401E+05	HNO	8.66986E+01	
O	1.60695E+12	5.16727E-01	OH	5.70574E+09	N2O	1.83314E+00	
F	3.39774E+08	9.58788E-01	NH	2.95019E+08	CO2	7.53704E+05	
Ne	4.97576E+11	1.00000E+00	CH	8.02061E+07	NO2	8.49735E-02	
Na	8.67866E+09	1.00000E+00	CN	1.75906E+08	O3	6.81415E-06	
Mg	1.53459E+11	9.99940E-01	CO	1.49682E+12	SO2	4.99146E-01	
Al	1.22947E+10	9.99998E-01	NO	9.83578E+07			
Si	1.44419E+11	9.98443E-01	SO	8.02274E+07			
P	1.38859E+09	1.00000E+00	CaH	7.70785E+02			
S	7.06021E+10	9.76218E-01	MgH	9.19881E+06			
Cl	8.23178E+08	9.98427E-01	AlH	2.00390E+04			
Ar	1.69523E+10	1.00000E+00	SiH	3.12959E+07			
K	6.07505E+08	1.00000E+00	SiN	1.34030E+04			
Ca	1.04289E+10	1.00000E+00	AlO	6.93841E+02			
Ti	4.01373E+08	9.99961E-01	SiO	1.93854E+08			
Cr	1.83699E+09	1.00000E+00	NaCl	8.59027E-03			
Mn	1.34519E+09	1.00000E+00	MgCl	5.36009E+00			
Fe	1.20055E+11	1.00000E+00	KCl	2.88078E-04			
Ni	6.94292E+09	1.00000E+00	CaCl	1.10760E-01			
			Na2	2.86401E-08			
			NaH	2.98687E+02			
			SH	1.63977E+09			
			MgO	6.12927E+03			
			HCl	1.29695E+06			
			HF	1.46046E+07			
			ClO	6.62707E+00			
			TiO	1.57927E+04			
			H2+	4.98008E+03			
			CH+	2.03633E+03			
			CO+	3.16380E+01			
			N2+	1.20611E+01			
			O2+	3.06980E+00			
			OH+	9.52063E+01			

Table (7.7) of Abundances

Log T = 3.70 Log R = -8.00 ENN = 6.07987E+11

	ANF	FAF	AM2	AM3
H	4.59904E+15	9.99857E-01	H2 3.28467E+11	H2O 6.89872E+04
He	3.19665E+14	1.00000E+00	C2 2.57844E+06	HCN 2.73907E+04
C	1.67660E+12	9.82304E-01	N2 1.72642E+08	HCO 3.70355E+04
N	5.40566E+11	9.99249E-01	O2 1.26433E+05	HNO 1.53502E+00
O	3.07894E+12	9.90059E-01	OH 8.04222E+08	N2O 9.14373E-03
F	3.53924E+08	9.98716E-01	NH 3.82313E+07	CO2 1.90553E+03
Ne	4.97576E+11	1.00000E+00	CH 8.24998E+07	NO2 1.72718E-03
Na	8.67866E+09	1.00000E+00	CN 1.81672E+07	O3 1.82191E-06
Mg	1.53468E+11	1.00000E+00	CO 3.00973E+10	SO2 3.68272E-03
Al	1.22948E+10	1.00000E+00	NO 4.73471E+06	
Si	1.44644E+11	9.99994E-01	SO 9.95804E+06	
P	1.38859E+09	1.00000E+00	CaH 1.72372E+01	
S	7.22174E+10	9.98552E-01	MgH 6.47681E+04	
Cl	8.24382E+08	9.99887E-01	AlH 2.14899E+02	
Ar	1.69523E+10	1.00000E+00	SiH 4.95356E+05	
K	6.07505E+08	1.00000E+00	SiN 1.05260E+02	
Ca	1.04289E+10	1.00000E+00	AlO 3.93054E+00	
Ti	4.01388E+08	1.00000E+00	SiO 3.13260E+05	
Cr	1.83699E+09	1.00000E+00	NaCl 6.57678E-05	
Mn	1.34519E+09	1.00000E+00	MgCl 2.38067E-02	
Fe	1.20055E+11	1.00000E+00	KCl 2.81178E-06	
Ni	6.94292E+09	1.00000E+00	CaCl 4.81378E-04	
			Na2 1.98691E-10	
			NaH 8.10146E+00	
			SH 9.47427E+07	
			MgO 4.95934E+01	
			HCl 9.33138E+04	
			HF 4.55093E+05	
			ClO 2.67244E+00	
			TiO 1.49881E+01	
			H2+ 2.06114E+06	
			CH+ 6.24386E+05	
			CO+ 6.00118E+03	
			N2+ 3.39219E+02	
			O2+ 4.12513E+02	
			OH+ 2.46767E+04	

Table (7.8) of Abundances

Log T = 3.80 Log R = -8.00 ENN = 9.28295E+12

	ANF	FAF		AM2		AM3
H	4.59961E+15	9.99982E-01	H2	4.10317E+10	H2O	9.61026E+02
He	3.19665E+14	1.00000E+00	C2	1.15694E+05	HCN	7.20718E+01
C	1.70665E+12	9.99909E-01	N2	1.68355E+06	HCO	1.30836E+02
N	5.40962E+11	9.99980E-01	O2	1.25374E+04	HNO	3.56449E-02
O	3.10961E+12	9.99921E-01	OH	1.04160E+08	N2O	7.29061E-05
F	3.54350E+08	9.99919E-01	NH	6.74059E+06	CO2	1.15742E+00
Ne	4.97576E+11	1.00000E+00	CH	1.45813E+07	NO2	2.69137E-05
Na	8.67866E+09	1.00000E+00	CN	4.72006E+05	O3	1.53712E-07
Mg	1.53468E+11	1.00000E+00	CO	1.38715E+08	SO2	1.90408E-05
Al	1.22948E+10	1.00000E+00	NO	2.25273E+05		
Si	1.44645E+11	1.00000E+00	SO	8.23914E+05		
P	1.38859E+09	1.00000E+00	CaH	5.44957E+00		
S	7.23148E+10	9.99900E-01	MgH	6.73436E+03		
Cl	8.24463E+08	9.99986E-01	AlH	3.83915E+01		
Ar	1.69523E+10	1.00000E+00	SiH	3.03334E+04		
K	6.07505E+08	1.00000E+00	SiN	3.16520E+00		
Ca	1.04289E+10	1.00000E+00	AlO	2.50960E-01		
Ti	4.01388E+08	1.00000E+00	SiO	1.85899E+03		
Cr	1.83699E+09	1.00000E+00	NaCl	9.02739E-06		
Mn	1.34519E+09	1.00000E+00	MgCl	1.62894E-03		
Fe	1.20055E+11	1.00000E+00	KCl	4.71838E-07		
Ni	6.94292E+09	1.00000E+00	CaCl	3.83972E-05		
			Na2	1.87787E-10		
			NaH	3.14231E+00		
			SH	6.43556E+06		
			MgO	3.37553E+00		
			HCl	1.16259E+04		
			HF	2.87232E+04		
			ClO	7.89728E-01		
			TiO	2.30235E-01		
			H2+	4.04343E+07		
			CH+	1.56214E+06		
			CO+	6.14085E+03		
			N2+	6.03478E+02		
			O2+	1.15014E+03		
			OH+	1.94992E+05		

Table (7.9) of Sources and Sinks of Electrons

	Log T = 3.2	Log T = 3.5	Log T = 3.8
H ⁻ fr	1.666E-11	3.105E-10	7.661E-09
H ⁻ ab	8.015E+01	1.351E+06	3.524E+07
	ENI	ENI	ENI
H	-8.01569E+01	-1.33842E+06	8.53856E+12
He	0.00000E+00	1.14931E-14	3.96740E+03
C	-7.69260E-13	1.38541E+00	2.51569E+11
N	5.76927E-31	1.17869E-02	7.81864E+08
O	-6.20094E-04	-7.05069E+03	4.96293E+09
F	-9.88856E-02	-1.84780E+02	1.59384E+03
Ne	0.00000E+00	3.18175E-12	4.55510E+03
Na	1.72067E+06	8.58221E+09	8.67731E+09
Mg	1.28637E+00	5.33218E+09	1.53117E+11
Al	1.73809E+03	7.11520E+09	1.22777E+10
Si	-1.48525E-03	1.75830E+08	1.41705E+11
P	-6.30568E-01	1.44804E+03	9.45333E+08
S	-4.66691E+00	1.11269E+04	2.91580E+10
Cl	-1.20247E+04	-3.39993E+03	1.48785E+07
Ar	5.20125E-27	1.81213E-04	6.45913E+06
K	3.89180E+07	6.07137E+08	6.07455E+08
Ca	6.66073E+03	9.48428E+09	1.08077E+10
Ti	4.25266E-04	1.60970E+08	4.01624E+08
Cr	4.19389E+00	4.84168E+08	1.82600E+09
Mn	3.13122E-02	5.94433E+07	1.33526E+09
Fe	1.35685E-01	1.48004E+09	1.19414E+11
Ni	1.08719E-02	4.09378E+07	6.85840E+09

The fraction of a molecular species in a particular isotopic form is not expected to change much over the various grid points, and is of no importance for the continuous opacity, though isotopic variations of molecules can be important when band spectra are considered. However, as an example for CO at $\log T = 3.5$ and $\log \rho = -8$, the fractional abundances of $C^{12}O^{16}$, $C^{12}O^{17}$, $C^{12}O^{18}$, $C^{13}O^{16}$, $C^{13}O^{17}$ and $C^{13}O^{18}$ are respectively 9.865×10^{-1} , 3.700×10^{-4} , 2.018×10^{-3} , 1.107×10^{-2} , 4.153×10^{-6} and 2.265×10^{-5} , given that the fractional abundances of C^{12} and C^{13} are respectively 9.889×10^{-1} and 1.110×10^{-2} and for O^{16} , O^{17} and O^{18} are respectively 9.976×10^{-1} , 3.740×10^{-4} and 2.039×10^{-3} . It can be seen that the figures for the isotopic variants of CO do not agree exactly with the products of the figures for the individual isotopes. This is to be expected, as the isotopic molecules have slightly different dissociation potentials, measured from the lowest vibrational level, and different partition functions. In the mixture, there are also 15 different isotopic versions of TiO and as many as 24 of SO_2 ; and examples of these and many other molecules are found in the program volume.

Before the discussion in this section can be completed, we must consider how accurate and reliable are the results presented here. For the grid point with $\log T = 3.8$ and $\log \rho = -8$, where the continuum has the sharp jumps, see figure (7.7), tests were performed on integrating across the spectrum with 1001, 2001, 4001 and 10001 points. It was found that for the last three cases, the PMO and RMO changed only in the fifth significant digit, with even the first case

giving quite a good agreement. These differences are presumably due to the effect of the absorption edges, which are very pronounced at this temperature. It is thus considered that 4001 coarse grid points were good enough for the integration, and accordingly, all the opacities in table (7.1) were generated with that number of points. At least as far as these integrations are concerned, these opacities are reliable. As a matter of interest, the spectra for the run of temperatures at the extremes of $\log \rho = -14$ and -2 were examined and found to be rather uninteresting, with no appreciable sharp absorption edges.

When the approximate general treatment of higher electronic states of atoms and ions was included in the work in order to obtain better partition functions, see section 2.2 and the appendices, it was important to check this against cases where this treatment was neglected. It was found that the partition functions of the positive ions were unaffected, (this treatment does not apply to the negative ions) and above about 4000°K , only the partition functions of the group I elements Na and K and the transition elements Ti, Cr, Mn, Fe and Ni were affected appreciably. This behaviour of the group I elements is expected because of their low ionization and first excitation potentials, and the transition elements have a very large number of levels due to the partially filled 3d orbitals. When this effect, together with the attendant depression of the ionization potentials, is included in the statistical mechanics, no appreciable changes occur in the abundances of any of the species, including the molecules which have a small abundance at these temperatures. Even the abundance of KCl, which is negligibly small, is not much affected

by the partition function of K increasing by more than a factor of two at 6000°K with this approximate general treatment included. We can thus conclude that errors due to this treatment do not significantly affect the statistical mechanics over the range of interest, however, they will be important at much higher temperatures where many of the highly excited electronic states are appreciably populated.

Probably a greater source of uncertainty are errors in computing the partition functions of molecules, but here again, the errors are likely to be greatest at the higher temperatures where the molecules have low abundances. These errors would be due to neglecting higher order terms in the anharmonicity and non-rigidity, which are usually unavailable, and which may be important for highly excited rotational and vibrational levels, these being significantly populated at higher temperatures.

Whereas the partition functions enter Saha's equation linearly, so errors propagate linearly, the dissociation potential of a molecule enters exponentially, so an uncertainty in the dissociation potential can result in possibly a large uncertainty in the abundance of not only the molecule in question, but of many other molecules, as their equilibria are all coupled. Unfortunately, dissociation potentials are often known only approximately, so they would be expected to be the greatest sources of uncertainty in the statistical mechanics calculations. We consistently take the dissociation potentials from the lowest vibrational level, not the bottom of the potential well, and allow for isotopic shifts, as discussed earlier in this work. The abundances given in tables (7.2-8) for each molecule, are the sums of

the individual isotopic forms computed separately, and would be expected to be better than neglecting isotopes or computing with "average" molecules. Finally, as we have neglected the effects of pressure on dissociation and partition functions, this approximation is liable to cause uncertainties at the higher densities.

Note that the continua calculated for the examples in sections 7.4 and 7.5 do not take account of the pressure-induced H_2-H_2 and H_2-He opacity, which is however included in table (7.1) and the accompanying graphs. If this source of opacity were included, it would have at worst a fairly modest effect on the figures given in these sections, but would not alter the discussion qualitatively in any way. However, the tables of opacities for diatomic and triatomic molecules in section 7.6 do include the pressure-induced opacity. At very low temperatures, pressure-induced opacity can be very important, as is shown when some of the entries in table (7.1) are compared with their values when pressure-induced opacity is neglected. Thus for $\log \rho = -8$ and $\log T = 3.0, 3.1, 3.2, 3.3$ and 3.4 , $\log RMO$ without pressure-induced opacity reduces to $-7.9651, -7.0444, -6.1505, -5.2894$ and -3.9783 respectively, with the corresponding values for $\log PMO$ being $-6.4347, -6.0315, -5.5922, -4.7857$ and -3.2821 . At higher temperatures at this density the effect is negligible.

Within the framework of our computations and data available, it is hoped that the abundances and continuous opacities produced by the MIXOP program are reliable.

7.3 Some Examples of Computing Band Absorption

The purpose of this section is to give a few examples of computing band absorption cross-sections using Franck-Condon factors, Hönl-London factors etc., in order to illustrate some of the theory discussed in this thesis, rather than giving exhaustive tabulations. This, and the remaining sections of chapter 7 are mostly concerned with various aspects of the TRIATOM program.

Table (7.10) below gives a comparison of the Franck-Condon factors $q_{v'v''}$, defined in (4.4.4), by various methods for the Swan system of C_2 , $d^3\Pi_g \leftrightarrow a^3\Pi_u$. Although C_2 is not likely to be important in our mixture, as discussed in the previous section, the Swan system of C_2 is well known and has been used as an example in some of the development work on the coding. For each value of v' and v'' , the first entry is the Franck-Condon factor we have computed for a Morse potential using Doktorov's method (71), the values given by Jain (110) using a Rydberg-Klein-Rees potential (R-K-R) are given second, with for comparison, the Franck-Condon factor for a harmonic potential computed using Manneback's (67) method. Our computed band origins in cm^{-1} are the last entry for each v' and v'' . The following data used in our calculations are obtained from Rosen (35):

$$\begin{aligned}
 a^3\Pi_u: & T_e'' = 714.24, \quad \omega_e'' = 1641.35, \quad \omega_e''x_e'' = 11.67, \\
 d^3\Pi_g: & T_e' = 20022.50, \quad \omega_e' = 1788.22, \quad \omega_e'x_e' = 16.44, \quad \omega_e'y_e' = -0.5067,
 \end{aligned}$$

with the values for $D_e^{0''}$ and $D_e^{0'}$ calculated from (4.3.10).

It can immediately be seen that in many cases Jain's values lie in between the values we have calculated using Doktorov's and Manneback's methods, giving us confidence in these methods. In particular, the agreement for the strong bands is often good, and that for the 0-0 band, the strongest of the system, is excellent. In most cases the agreement for the weaker bands is poor, which is to be expected as the effects of anharmonicity are greatest for them, and will be sensitive to the type of potential function adopted. In many cases the values computed by Doktorov's method for weaker bands overestimate the band strengths relative to Jain's values, but this would be at the expense of some of the stronger bands, in order to satisfy the normalization of the Franck-Condon factors.

The r-centroids in table (7.11) for the Swan bands of C_2 are again obtained from several methods. The first entry for each band is computed using Doktorov's method for calculating the first and zero order matrix elements, $\langle v' | r | v'' \rangle$ and $\langle v' | v'' \rangle$ respectively, from which the r-centroid is obtained from their ratio, as defined in (4.3.33). The second entry is taken from Jain as before, with the values obtained using an R-K-R potential function. For an additional comparison, the values computed using Schamps's (79) formula, see (4.3.35), are also given, where $\omega_e = 1714.79$, the mean of ω_e'' and ω_e' , and $r_e'' = 1.3119 \text{ \AA}$ and $r_e' = 1.2660 \text{ \AA}$ from Rosen. The values tabulated are in Angströms, scaled by 10^4 .

Table (7.10) of Franck-Condon Factors of the Swan System

v''	0	1	2	3	4	5	6	7	8
0	0.732	0.166	0.065	0.023	0.009	0.003	0.001	0.001	
	0.733	0.212	0.043	0.008	0.001				
	0.726	0.242	0.031	0.002	0.000				
	19380	17762	16168	14596	13048	11524	10022	8545	7090
1	0.262	0.381	0.157	0.106	0.050	0.024	0.011	0.005	0.002
	0.240	0.364	0.278	0.092	0.022	0.004			
	0.222	0.336	0.358	0.078	0.006	0.000			
	21134	19516	17921	16350	14802	13277	11776	10298	8844
2	0.003	0.434	0.199	0.098	0.113	0.067	0.040	0.021	0.011
	0.022	0.372	0.168	0.267	0.120	0.037			
	0.044	0.296	0.123	0.389	0.133	0.014			
	22850	21232	19638	18066	16518	14994	13492	12014	10560
3	0.003	0.008	0.542	0.108	0.044	0.099	0.070	0.051	0.032
	0.001	0.056	0.425	0.075	0.225	0.137	0.059		
	0.007	0.099	0.286	0.026	0.367	0.187	0.027	0.001	
	24526	22908	21313	19742	18194	16670	15168	13690	12236
4		0.010	0.011	0.604	0.064	0.011	0.077	0.062	0.055
		0.000	0.001	0.091	0.451	0.027	0.176	0.149	0.070
	0.001	0.022	0.147	0.234	0.000	0.315	0.235	0.043	0.002
	26158	24540	22946	21374	19826	18302	16800	15322	13868
5			0.025	0.012	0.629	0.044	0.000	0.055	0.048
			0.002	0.117	0.471	0.010	0.129	0.157	0.074
		0.004	0.044	0.179	0.169	0.013	0.251	0.274	0.063
	27744	26126	24531	22960	21412	19887	18386	16908	15454

Table (7.11) of r-Centroids of the Swan System

v"	0	1	2	3	4	5	6	7	8
0	12979	12116	12010	11728	11566	11407	11273	11153	11045
	12940	12230	11663						
	12890	12265	11640	11015	10390	9766	9141	8516	7891
1	13644	13211	11974	12020	11696	11552	11391	11262	11143
	13710	13074	12300	11721					
	13514	12890	12230	11640	11015	10390	9766	9141	8516
2	17433	13683	13642	11716	12060	11657	11542	11376	11250
	14690	13847	13251	12378	11773	11297			
	14139	13514	12890	12265	11640	11015	10390	9766	9141
3	12842	17433	13743	14365	11142	12149	11605	11536	11359
		14878	13951	13608	12415	11738	11377		
	14764	14139	13514	12890	12265	11640	11015	10390	9766
4	22054	13012	17555	13823	15428	9256	12321	11526	11541
			15209	14078	14262	12442	11855	11331	
	15389	14764	14139	13514	12890	12265	11640	11015	10390
5	13339	27174	13189	17839	13918	16723	X	12634	11396
				15236	14217		12382	12016	11283
	16013	15389	14764	14139	13514	12890	12265	11640	11015

X = -334217

Again notice that in many cases, the values from Jain lie in between those values we have computed by the two methods, and again the agreement is best for the strongest bands, the ones that matter most. Although Schamps's method is a crude approximation, with the r -centroids constant for any fixed Δv , it is very simple to apply and gives at worst an estimate of the r -centroids; indeed here, the agreement is often better than Doktorov's method, which is remarkable in view of its simplicity. For very weak bands, Doktorov's method is unreliable, as one is taking the ratio of two quantities which are small, and due to the approximations of the method, have a large uncertainty. The spurious value of -33.4217 using Doktorov's method for $v'' = 6$ and $v' = 5$ occurs as $\langle v' | r | v'' \rangle = -3.866 \times 10^{-2}$ and $\langle v' | v'' \rangle = 1.157 \times 10^{-3}$, both being anomalous compared to neighbouring matrix elements: the Franck-Condon factor for this, being the square of the latter figure, is 1.338×10^{-6} . In spite of such problems, as Doktorov's method is used to compute the zero order matrix elements, to be consistent, it is best to use the same method for the higher order elements. Besides, as discussed in chapter 4, in applying Doktorov's method, we are not required to compute the r -centroids as such.

We now consider examples of Hönl-London factors. Table (7.12) lists computed Hönl-London factors for $J'' \leq 3$ for the 0-0 Swan band of C_2 . The constants needed for the two states, all being in cm^{-1} , are:

$$a^3\Pi_u: B_e'' = 1.63246, \alpha_e'' = 0.01661, A'' = -15.25,$$

$$d^3\Pi_g: B_e' = 1.7527, \alpha_e' = 0.01608, A' = -16.48,$$

from which B_0 and Y for $v' = v'' = 0$ are obtained for the two electronic states, see chapter 4.

The first column is the type of branch, where the first digit 1, 2 or 3, indicates a P, Q or R-branch respectively, and the second and third digits indicate the series to which the lower and upper levels of the branch belong respectively, this notation being the reverse of the normal molecular spectroscopic notation where the upper level is given first. The last two indices are the same as those defined in section 4.2C for the triplets. As $Y < 0$ for both states, they are both reversed states, and as $\Lambda' = \Lambda'' = 1$, for the series F_1, F_2 and F_3 , $\Omega = 2, 1$ and 0 respectively for the three ladders, hence also the lowest values of J . The remaining columns are clear, with $\Delta\Omega = \Omega' - \Omega''$ and with $S_{J'J''}^{\Sigma'\Sigma''}$ computed using Kovács's (31) formulae, see the appendices, except where breakdown cases occur, see then section 4.2C. As $\Lambda > 0$ for both states, there is in addition Λ -doubling which we do not consider here, however for $C^{12}C^{12}$, as the spins of the nuclei are zero, one component has zero strength so there is only one line for each transition considered anyway.

Table (7.12) of Hönl-London Factors
of the 0-0 Swan Band

Branch	J''	Ω''	$\Delta\Omega$	$S_{J''}^{\Sigma''\Sigma''}$
332	0.0	0.0	1	0.00000E+00
333	0.0	0.0	0	1.00000E+00
123	1.0	1.0	-1	0.00000E+00
133	1.0	0.0	0	1.00000E+00
222	1.0	1.0	0	1.41202E+00
223	1.0	1.0	-1	0.00000E+00
232	1.0	0.0	1	0.00000E+00
233	1.0	0.0	0	0.00000E+00
321	1.0	1.0	1	4.89192E-02
322	1.0	1.0	0	1.42210E+00
323	1.0	1.0	-1	4.08000E-02
331	1.0	0.0	2	0.00000E+00
332	1.0	0.0	1	0.00000E+00
333	1.0	0.0	0	2.00000E+00
112	2.0	2.0	-1	4.93814E-02
113	2.0	2.0	-2	0.00000E+00
122	2.0	1.0	0	1.42065E+00
123	2.0	1.0	-1	0.00000E+00
132	2.0	0.0	1	4.20051E-02
133	2.0	0.0	0	2.00000E+00
211	2.0	2.0	0	3.20185E+00
212	2.0	2.0	-1	6.78814E-02
213	2.0	2.0	-2	2.72060E-04
221	2.0	1.0	1	6.92617E-02
222	2.0	1.0	0	7.89584E-01
223	2.0	1.0	-1	1.03240E-01
231	2.0	0.0	2	2.94859E-04
232	2.0	0.0	1	1.04174E-01
233	2.0	0.0	0	1.44646E-02
311	2.0	2.0	0	1.67950E+00
312	2.0	2.0	-1	2.52111E-02
313	2.0	2.0	-2	1.42453E-04
321	2.0	1.0	1	2.95956E-02
322	2.0	1.0	0	2.55232E+00
323	2.0	1.0	-1	5.99546E-02
331	2.0	0.0	2	4.35025E-04
332	2.0	0.0	1	5.66260E-03
333	2.0	0.0	0	2.95656E+00

Table (7.12) Continued

Branch	J''	Ω''	$\Delta\Omega$	$-S_{J''}^{\Sigma''}$
111	3.0	2.0	0	1.67866E+00
112	3.0	2.0	-1	3.08006E-02
113	3.0	2.0	-2	4.20000E-04
121	3.0	1.0	1	2.62440E-02
122	3.0	1.0	0	2.54931E+00
123	3.0	1.0	-1	6.47790E-03
131	3.0	0.0	2	1.54327E-04
132	3.0	0.0	1	6.23952E-02
133	3.0	0.0	0	2.95476E+00
211	3.0	2.0	0	2.11581E+00
212	3.0	2.0	-1	9.35136E-02
213	3.0	2.0	-2	3.30923E-04
221	3.0	1.0	1	9.53644E-02
222	3.0	1.0	0	5.56874E-01
223	3.0	1.0	-1	1.07563E-01
231	3.0	0.0	2	3.66389E-04
232	3.0	0.0	1	1.08520E-01
233	3.0	0.0	0	2.40353E-02
311	3.0	2.0	0	3.02479E+00
312	3.0	2.0	-1	4.09808E-02
313	3.0	2.0	-2	1.73950E-04
321	3.0	1.0	1	1.87548E-02
322	3.0	1.0	0	3.62169E+00
323	3.0	1.0	-1	6.32329E-02
331	3.0	0.0	2	4.33808E-04
332	3.0	0.0	1	3.61640E-03
333	3.0	0.0	0	3.96054E+00

Table (7.13) of Comparison Between Computed and Expected Sums of Hönl-London Factors

J''	SUM _t	SUM _c	J''	SUM _t	SUM _c
0	1	1.00000	10	63	63.0392
1	6	5.92384	11	69	69.0317
2	15	15.1725	12	75	75.0258
3	21	21.1458	13	81	81.0212
4	27	27.1362	14	87	87.0175
5	33	33.1168	15	93	93.0146
6	39	39.0958	16	99	99.0123
7	45	45.0769	17	105	105.010
8	51	51.0613	18	111	111.009
9	57	57.0489	19	117	117.008

For $J'' \gg 3$ all 27 branches are possible, 9 for each P, Q and R-branches due to the three ladders in both electronic states. For $J'' < 3$, not only are there fewer branches, due to impossible transitions that would involve non-existent levels with $J < \Omega$, but some transitions have zero strengths due to the selection rules discussed in section 4.2C. As $|Y| \approx 9$ for both states, the Hönl-London factors eventually approach those for Hund's case (b) for $J \gg 3$ for both states.

The values of the computed sums of the strengths from a given J'' are compared to the theoretical values in the table (7.13) for $J'' \leq 19$, on the basis of the adopted normalization, where SUM_t and SUM_c are respectively the theoretical and computed sums.

For the transitions considered here, the computed values agree very well with the sum rule, where for the smallest values of J , the special treatment, as discussed in chapter 4, has to be applied. Notice that the normalization of $3(2J+1)$ applies only for $J > 1$. As discussed generally in chapter 4, for $J = 0$, there is only one level, that belonging to the ladder with $\Omega = 0$, so the normalization is $(2J+1)$, for $J = 1$, there are two levels belonging to the ladders with $\Omega = 0$ and 1, so the normalization is $2(2J+1)$, thereafter there are three levels for each value of J . It is thus technically incorrect to state generally that the sum is always $(2S+1)(2J+1)$. However, when considering an electronic state as a whole, at the temperatures that we are interested in, the effect on the total partition function is

negligible, and the factor of $(2S+1)$ in (2.7.1) is not inconsistent with this discussion. As J increases, the agreement between the calculated and theoretical values improves considerably as we approach the case (b) limit, as Kovács's formulae for triplets agree best with the normalization in one or other of the limiting spin coupling cases.

An example of a triplet system is shown in figures (7.8) and (7.9), and is the 0-0 band of the $A^3\bar{\Phi} \leftarrow X^3\Delta$ system of TiO , known as the γ -system, plotted at $2000^\circ K$. This turns out to be more picturesque than the Swan system above. The constants for the two electronic states are:

$$\begin{aligned} X^3\Delta: \quad T_e'' &= 0.00, & \omega_e'' &= 1009.02, & \omega_e''x_e'' &= 4.498, & \omega_e''y_e'' &= -0.0107, \\ B_e'' &= 0.535412, & D_e'' &= 6.029 \times 10^{-7}, & \alpha_e'' &= 3.011 \times 10^{-3}, & \beta_e'' &= 3.4 \times 10^{-9}, \\ A'' &= 50.61, \end{aligned}$$

$$\begin{aligned} A^3\bar{\Phi}: \quad T_e' &= 14163.32, & \omega_e' &= 867.78, & \omega_e'x_e' &= 3.942, \\ B_e' &= 0.507390, & D_e' &= 6.918 \times 10^{-7}, \\ A' &= 57. \end{aligned}$$

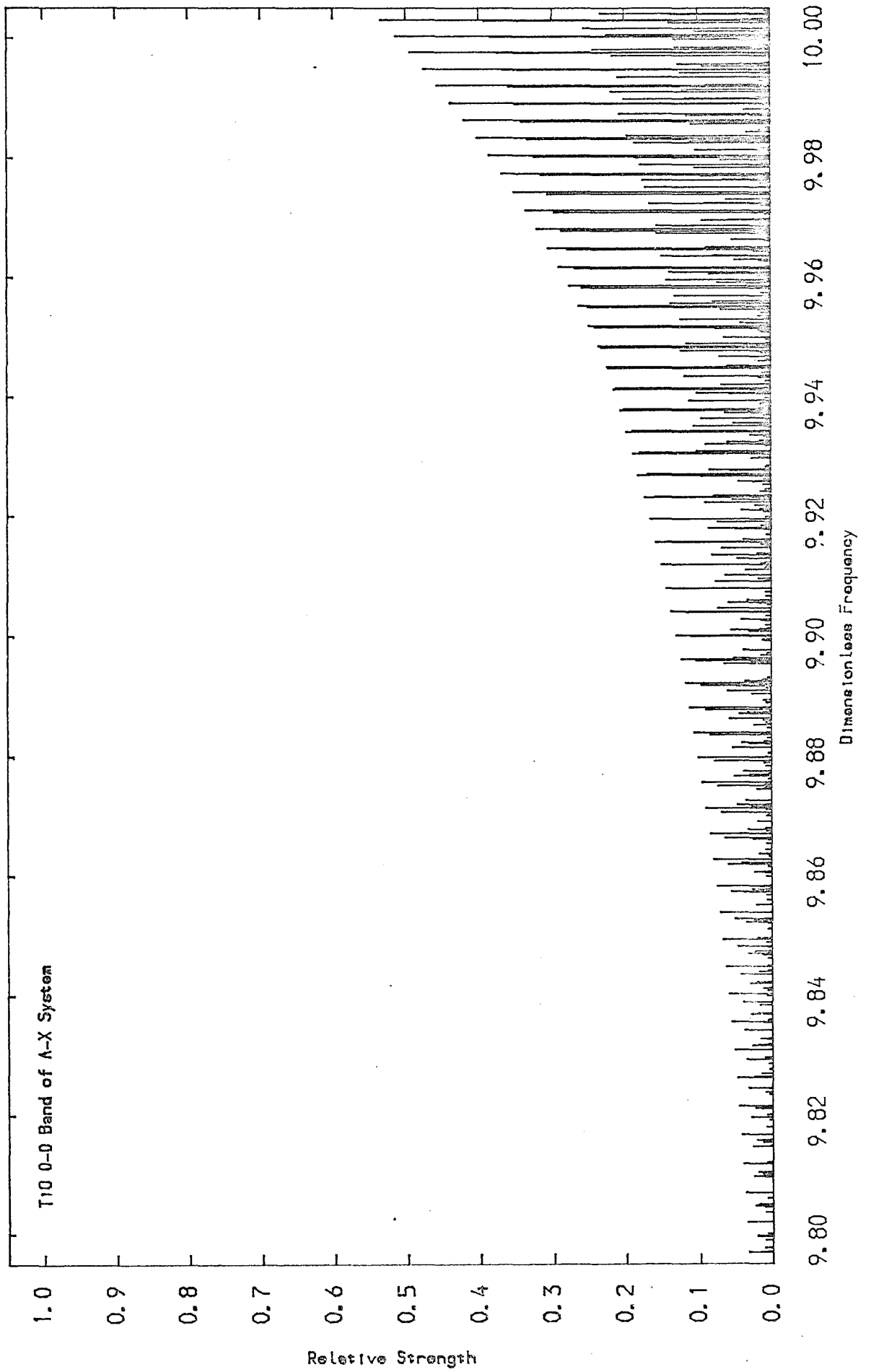


Fig. 7.8

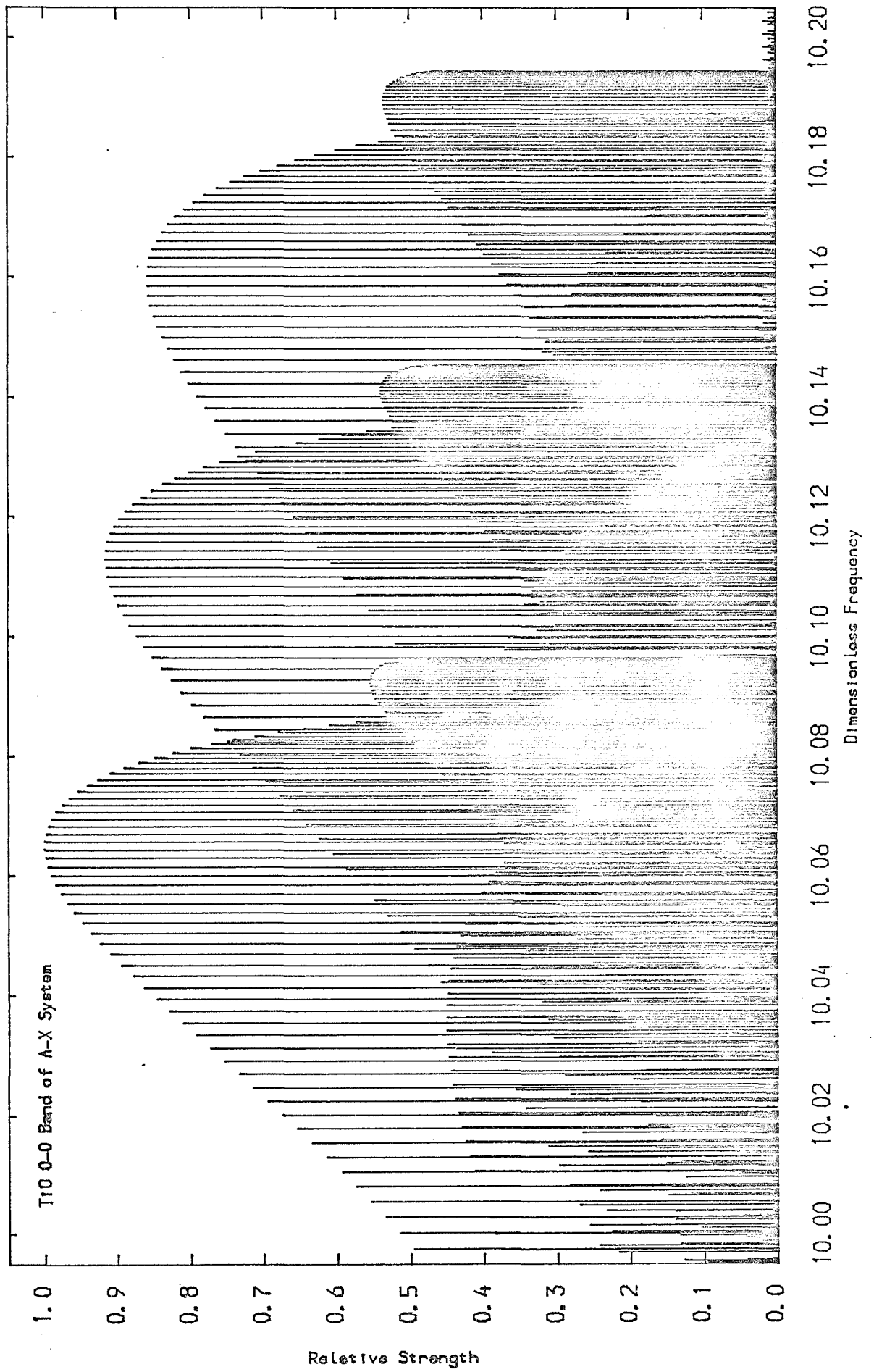


Fig. 7.9

Notice that the structure is very complicated indeed, with many overlapping branches visible; yet this is just one band. It is easy to see from this, that when TiO is abundant, it can be an important source of opacity, as there will be many overlapping bands, each as complex as this one shown. However, it must be pointed out that such detail would never actually be observed in practice in real stellar spectra, after various broadening mechanisms, including instrumental broadening, have taken their toll. Moreover, the spectrum shown is idealized, with the line positions and strengths computed using the theory in chapter 4 with the above constants, with Λ -doubling not shown and various higher order effects, that may in practice also be important, also being neglected. Nevertheless, this should at least give a general impression of the band.

An example of the band strengths in absorption for the vibration-rotation transitions of CO are given in tables (7.14) and (7.15) for values of v' and v'' from 0 to 11. Table (7.14) lists the band strengths in $\text{cm}^2/\text{sec}/\text{absorber}$ computed from (4.4.2) using the constants for the dipole moment expansion:

$$M_0 = -0.1221, M_1 = 3.093, M_2 = -0.199, M_3 = -2.665, M_4 = 0.26,$$

where M_i is in $\text{D}\text{\AA}^{-i}$, obtained from Bouanich (111). On dividing by the total partition function and multiplying by the Boltzmann factor for the v'' vibrational level and by the abundance of CO in cm^{-3} , we obtain table (7.15) for the band strengths in the form of volume absorption,

i.e. $\text{cm}^2/\text{sec}/\text{cm}^3$ or $\text{cm}^{-1}\text{sec}^{-1}$, at $T = 2000^\circ\text{K}$ and $\rho = 10^{-8} \text{ gm cm}^{-3}$ for the standard mixture. Strictly speaking, these band strengths are in fact the strengths of the fictitious $J''=0 \rightarrow J'=0$ transitions with unit Hönl-London factor, as the rotational partition function has not been removed as it is included in the total partition function; on multiplying by the rotational partition function, the true band strengths would be recovered. Note that as stated in chapter 4, M_0 does not enter the calculations, also as no higher terms than M_4 are used, band strengths with $\Delta v > 4$ will not be strictly correct, as contributions due to M_5 , M_6 etc. are neglected, and should in reality be allowed for, however, such bands are usually very weak.

With the band strengths as computed above, the detailed structure of individual bands can be computed, with the line strengths obtained from (4.4.1). Figures (7.10) and (7.11) show at 2000°K , the second overtone system of the vibration-rotation bands of CO, i.e. $\Delta v = 3$. Unlike the example for TiO which is a single very complex band, the figures here show seven overlapping bands, each being very simple, with one P and R-branch each. Because the differences of the rotational constants for each pair of participating vibrational levels are larger than for the fundamental and first overtone systems, the turnovers in the R-branches are more marked, giving a more aesthetically pleasing picture. In order of decreasing frequency and strength, the bands are: 3-0, 4-1, 5-2, 6-3, 7-4, 8-5 and 9-6, the upper level being given first by convention. The constants for the ground electronic state that are used are:

$$X^1\Sigma: D_e^0 = 90543, \quad \omega_e = 2169.82, \quad \omega_e x_e = 13.294, \quad \omega_e y_e = 0.0115, \\ B_e = 1.931271, \quad D_e = 6.1198 \times 10^{-6}, \quad \alpha_e = 1.7513 \times 10^{-2}.$$

Table (7.14) of CO Band Strengths in $\text{cm}^2/\text{sec}/\text{absorber}$

ν'	ν''					
0	1	2	3	4	5	
0	0.000E+00					
1	2.892E-07	0.000E+00				
2	2.017E-09	5.700E-07	0.000E+00			
3	8.487E-12	6.165E-09	8.418E-07	0.000E+00		
4	9.486E-15	3.615E-11	1.256E-08	1.104E-06	0.000E+00	
5	8.328E-16	6.369E-14	9.607E-11	2.132E-08	1.357E-06	0.000E+00
6	1.503E-16	4.170E-15	2.479E-13	2.039E-10	3.255E-08	1.599E-06
7	1.332E-17	9.848E-16	1.190E-14	7.306E-13	3.783E-10	4.636E-08
8	1.024E-18	1.031E-16	3.671E-15	2.516E-14	1.806E-12	6.406E-10
9	7.776E-20	9.081E-18	4.476E-16	1.021E-14	4.322E-14	3.947E-12
10	6.100E-21	7.763E-19	4.467E-17	1.437E-15	2.353E-14	6.278E-14
11	5.036E-22	6.772E-20	4.258E-18	1.609E-16	3.793E-15	4.742E-14
	6	7	8	9	10	11
6	0.000E+00					
7	1.831E-06	0.000E+00				
8	6.285E-08	2.052E-06	0.000E+00			
9	1.016E-09	8.214E-08	2.262E-06	0.000E+00		
10	7.871E-12	1.532E-09	1.043E-07	2.460E-06	0.000E+00	
11	7.789E-14	1.461E-11	2.221E-09	1.295E-07	2.645E-06	0.000E+00

Table (7.15) of CO Band Strengths in $(\text{cm sec})^{-1}$ at 2000°K

ν'	ν''					
0	1	2	3	4	5	
0	0.000E+00					
1	5.283E+02	0.000E+00				
2	3.683E+00	2.228E+02	0.000E+00			
3	1.550E-02	2.410E+00	7.175E+01	0.000E+00		
4	1.733E-05	1.413E-02	1.071E+00	2.092E+01	0.000E+00	
5	1.521E-06	2.489E-05	8.189E-03	4.039E-01	5.824E+00	0.000E+00
6	2.745E-07	1.630E-06	2.113E-05	3.864E-03	1.397E-01	1.585E+00
7	2.433E-08	3.849E-07	1.015E-06	1.384E-05	1.624E-03	4.593E-02
8	1.871E-09	4.028E-08	3.129E-07	4.766E-07	7.751E-06	6.347E-04
9	1.420E-10	3.549E-09	3.816E-08	1.934E-07	1.855E-07	3.911E-06
10	1.114E-11	3.034E-10	3.808E-09	2.722E-08	1.010E-07	6.221E-08
11	9.198E-13	2.647E-11	3.630E-10	3.048E-09	1.628E-08	4.698E-08
	6	7	8	9	10	11
6	0.000E+00					
7	4.269E-01	0.000E+00				
8	1.465E-02	1.147E-01	0.000E+00			
9	2.368E-04	4.589E-03	3.087E-02	0.000E+00		
10	1.835E-06	8.559E-05	1.424E-03	8.353E-03	0.000E+00	
11	1.815E-08	8.165E-07	3.031E-05	4.397E-04	2.277E-03	0.000E+00

Fig. 7.10

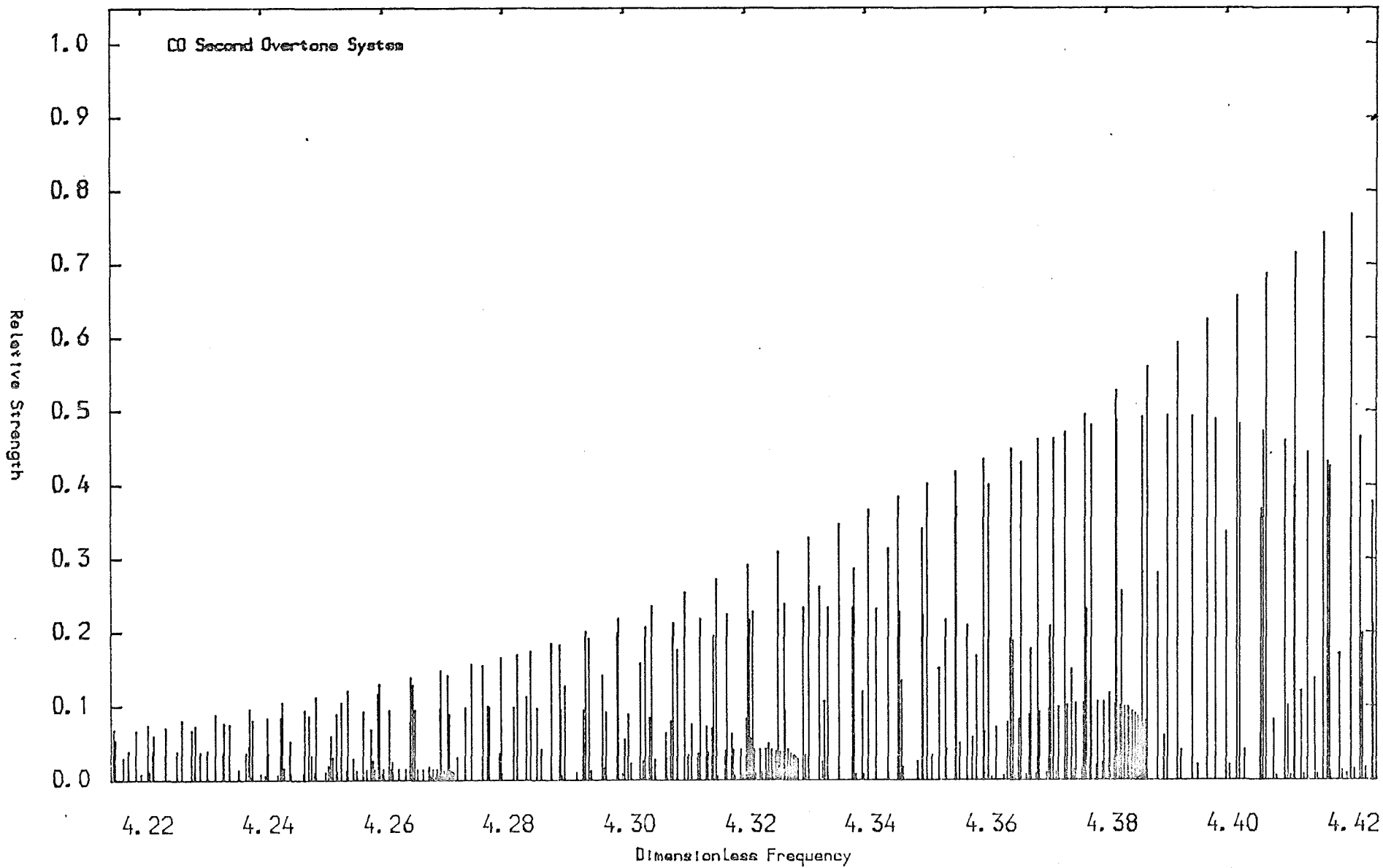
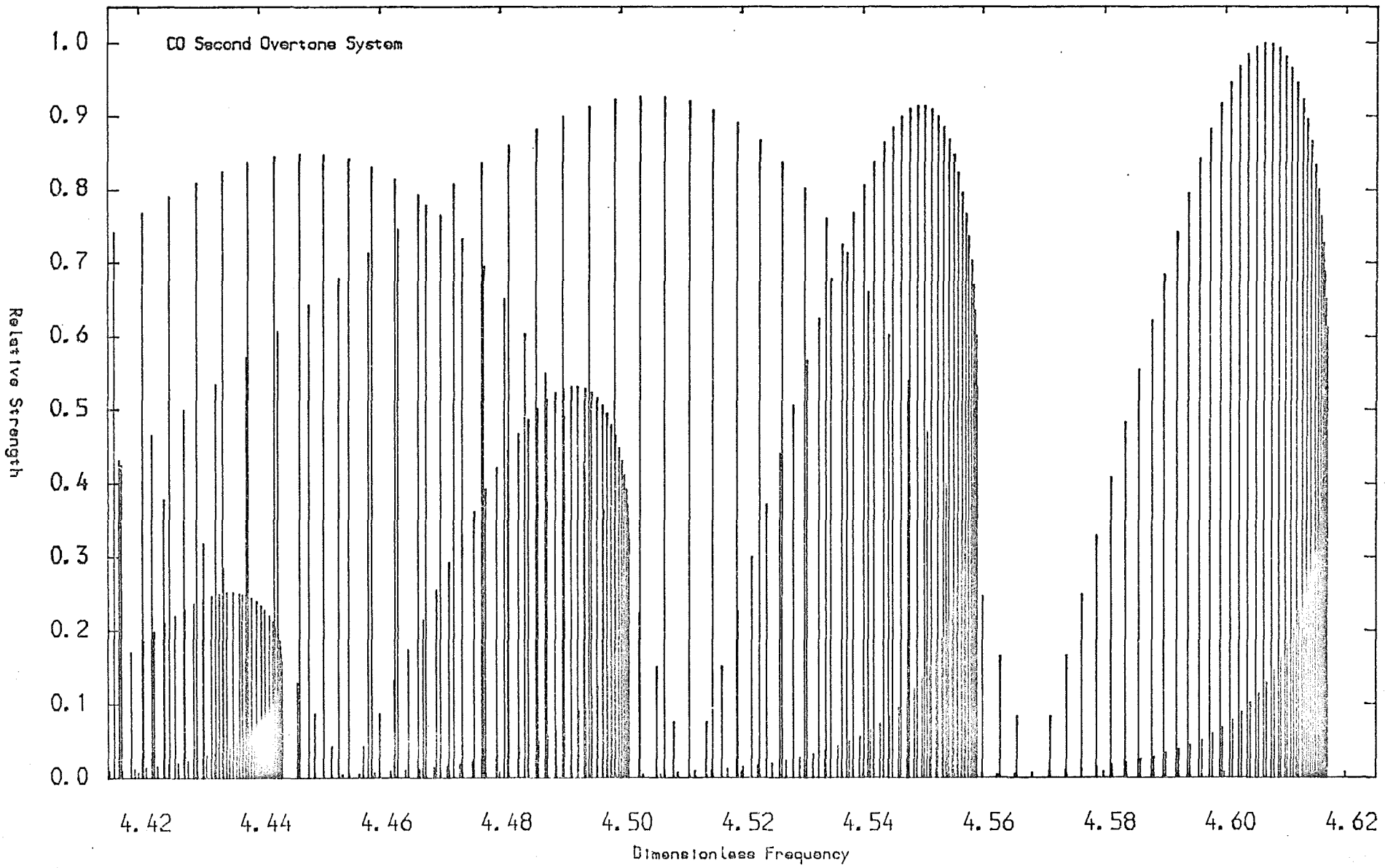


Fig. 7.11



Note that because the constants for CO are well known, and we are dealing with simple singlet bands without the complications of spin coupling etc., various higher order effects that are neglected are unlikely to be very important, and figures (7.10) and (7.11) are likely to represent quite accurately the true spectrum of CO, unlike the case for TiO.

Finally, an example of a part of a band of H₂O is given. Table (7.16) lists the transitions of the 001 ← 000 band of H₂O up to J" = 4, this being an A-type band. From left to right the columns are: J" the initial rotational level, m" the initial sublevel, where m" = n" + 1 = τ" + J" + 1, see (5.3.7), t which is simply the number of the transition, though a maximum of 7 is allowed for, in the cases here t ≤ 6, g_I the nuclear spin statistical weight factor, see the discussion near the end of section 5.3, S the line strength in the form of volume absorption in cm⁻¹ and u the dimensionless frequency of the line.

The strength S is computed from (5.2.9) for the case with the asymmetric top, as discussed in section 5.3. On multiplying by the abundance of the molecule in cm⁻³, an integrated absorption in the form of cm⁻¹sec⁻¹ is obtained, then to be consistent with the units in our handling of lines and continuum in bins, as discussed in chapter 6, an additional factor of h/kT is included, giving the final strength as cm⁻¹, with the factor g_I also included. As stated in chapter 5, the quantities $S_{J'J''}^{\tau'-\tau''}$ are normalized so that the sum from an initial

sublevel over all transitions is $2J+1$, as there are also $2J+1$ sublevels, the sum over all transitions over all sublevels from a given J is $(2J+1)^2$. From each initial sublevel, transitions are considered in turn to the final sublevels of increasing energy, for the P, Q and R-branches in turn. With the aid of table (5.2) of the rotational selection rules, it is possible to identify the upper sublevels involved, hence the subbranches.

The calculations are again performed with the standard mixture, at $T = 2000^\circ\text{K}$ and $\rho = 10^{-8} \text{ gm cm}^{-3}$. The constants for H_2O as obtained from Herzberg (30) are:

$$\begin{aligned} \omega_1 &= 3825.32, \quad \omega_2 = 1653.91, \quad \omega_3 = 3935.59, \\ x_{11} &= -43.89, \quad x_{22} = -19.50, \quad x_{33} = -46.37, \\ x_{12} &= -20.02, \quad x_{13} = -155.06, \quad x_{23} = -19.81, \\ A_e &= 27.210, \quad B_e = 14.596, \quad C_e = 9.507, \\ \alpha_1^A &= 0.747, \quad \alpha_2^A = -3.323, \quad \alpha_3^A = 1.241, \\ \alpha_1^B &= 0.222, \quad \alpha_2^B = -0.167, \quad \alpha_3^B = 0.112, \\ \alpha_1^C &= 0.180, \quad \alpha_2^C = 0.135, \quad \alpha_3^C = 0.129, \end{aligned}$$

together with the reduced band strength $(S_o/\bar{\nu}_o) = 6.398 \times 10^{-11} \text{ cm}^3/\text{sec}/\text{absorber}$, calculated from data from McClatchey et al. (88).

Table (7.16) of Some Transitions of Water 001 ← 000 Band

J''	m''	t	g _I	S _{J'J''} ^{τ''}	S	u
0	1	1	0.250	1.00000E+00	1.08916E-12	2.7186
1	1	1	0.750	1.00000E+00	3.17176E-12	2.6846
1	1	2	0.750	1.95370E+00	6.31177E-12	2.7344
1	1	3	0.750	4.62995E-02	1.52024E-13	2.7792
1	2	1	0.250	1.50000E+00	1.58235E-12	2.7045
1	2	2	0.250	1.50000E+00	1.59777E-12	2.7308
1	3	1	0.750	1.50000E+00	4.71607E-12	2.6970
1	3	2	0.750	1.50000E+00	4.78853E-12	2.7384
2	1	1	0.250	1.95371E+00	1.98565E-12	2.6682
2	1	2	0.250	7.71327E-02	8.06457E-14	2.7448
2	1	3	0.250	2.87323E+00	3.00800E-12	2.7484
2	1	4	0.250	9.59312E-02	1.02323E-13	2.8002
2	2	1	0.750	1.50000E+00	4.54625E-12	2.6702
2	2	2	0.750	8.33303E-01	2.56479E-12	2.7117
2	2	3	0.750	2.65120E+00	8.26026E-12	2.7450
2	2	4	0.750	1.54957E-02	5.00019E-14	2.8429
2	3	1	0.250	1.50003E+00	1.49422E-12	2.6627
2	3	2	0.250	8.33314E-01	8.38304E-13	2.6891
2	3	3	0.250	2.63588E+00	2.71783E-12	2.7562
2	3	4	0.250	3.07841E-02	3.26121E-14	2.8318
2	4	1	0.750	7.71324E-02	2.23233E-13	2.6542
2	4	2	0.750	3.25617E+00	9.58259E-12	2.6989
2	4	3	0.750	1.66670E+00	4.99556E-12	2.7488
2	5	1	0.250	4.64393E-02	4.41899E-14	2.6204
2	5	2	0.250	3.26600E+00	3.19871E-12	2.6971
2	5	3	0.250	1.68756E+00	1.68672E-12	2.7524
3	1	1	0.750	2.87960E+00	8.32077E-12	2.6531
3	1	2	0.750	1.95982E-01	5.86490E-13	2.7476
3	1	3	0.750	3.81393E+00	1.14690E-11	2.7610
3	1	4	0.750	1.10485E-01	3.40096E-13	2.8263
3	2	1	0.250	2.65441E+00	2.54867E-12	2.6551
3	2	2	0.250	6.02634E-01	5.93251E-13	2.7223
3	2	3	0.250	3.71464E+00	3.70544E-12	2.7585
3	2	4	0.250	2.83160E-02	2.93579E-14	2.8671
3	3	1	0.750	2.63583E+00	7.39308E-12	2.6440
3	3	2	0.750	6.01901E-01	1.70951E-12	2.6774
3	3	3	0.750	3.53829E-02	1.04169E-13	2.7753
3	3	4	0.750	3.63985E+00	1.07058E-11	2.7727
3	3	5	0.750	8.70322E-02	2.62732E-13	2.8457
3	4	1	0.250	1.66670E+00	1.52301E-12	2.6466
3	4	2	0.250	1.95548E-01	1.78930E-13	2.6502
3	4	3	0.250	2.13775E+00	1.99431E-12	2.7020
3	4	4	0.250	2.98023E+00	2.84456E-12	2.7645
3	4	5	0.250	1.97721E-02	1.97582E-14	2.8943
3	5	1	0.750	1.68855E+00	4.60376E-12	2.6433
3	5	2	0.750	9.62770E-02	2.58055E-13	2.5986
3	5	3	0.750	2.14547E+00	5.95985E-12	2.6932
3	5	4	0.750	3.04633E+00	8.70942E-12	2.7719

Table (7.16) Continued

J''	m''	t	g _I	$\frac{r''}{S_{J''J''}}$	S	u
3	5	5	0.750	2.33761E-02	6.96822E-14	2.8901
3	6	1	0.250	1.54988E-02	1.28814E-14	2.5509
3	6	2	0.250	3.53902E-02	3.01873E-14	2.6180
3	6	3	0.250	5.18858E+00	4.55361E-12	2.6936
3	6	4	0.250	1.76053E+00	1.58476E-12	2.7628
3	7	1	0.750	3.08628E-02	7.72782E-14	2.5621
3	7	2	0.750	5.20085E+00	1.36897E-11	2.6933
3	7	3	0.750	1.76828E+00	4.77622E-12	2.7638
4	1	1	0.250	3.81675E+00	3.43731E-12	2.6386
4	1	2	0.250	3.05447E-01	2.86996E-13	2.7529
4	1	3	0.250	4.78307E+00	4.52812E-12	2.7737
4	1	4	0.250	9.47288E-02	9.26689E-14	2.8662
4	2	1	0.750	3.71708E+00	1.00321E-11	2.6403
4	2	2	0.750	5.04788E-01	1.41156E-12	2.7356
4	2	3	0.750	4.74215E+00	1.34402E-11	2.7726
4	2	4	0.750	3.59774E-02	1.06412E-13	2.8935
4	3	1	0.250	3.64376E+00	3.14311E-12	2.6261
4	3	2	0.250	5.04383E-01	4.41081E-13	2.6623
4	3	3	0.250	1.27746E-01	1.16270E-13	2.7709
4	3	4	0.250	4.58043E+00	4.21016E-12	2.7983
4	3	5	0.250	1.43685E-01	1.34851E-13	2.8572
4	4	1	0.750	2.98361E+00	7.59436E-12	2.6297
4	4	2	0.750	3.04891E-01	7.80008E-13	2.6431
4	4	3	0.750	1.52253E+00	3.99126E-12	2.7083
4	4	4	0.750	4.14757E+00	1.11645E-11	2.7810
4	4	5	0.750	4.13973E-02	1.16710E-13	2.9126
4	5	1	0.250	3.04314E+00	2.54761E-12	2.6232
4	5	2	0.250	1.10522E-01	9.06987E-14	2.5715
4	5	3	0.250	1.52469E+00	1.30683E-12	2.6857
4	5	4	0.250	1.71309E-02	1.53928E-14	2.8156
4	5	5	0.250	4.24045E+00	3.78782E-12	2.7990
4	5	6	0.250	6.40584E-02	5.93259E-14	2.9020
4	6	1	0.750	1.76079E+00	4.21023E-12	2.6235
4	6	2	0.750	2.82916E-02	6.51231E-14	2.5256
4	6	3	0.750	1.27654E-01	3.04929E-13	2.6209
4	6	4	0.750	3.85452E+00	9.46404E-12	2.6939
4	6	5	0.750	3.20836E+00	8.12556E-12	2.7788
4	6	6	0.750	2.03911E-02	5.47734E-14	2.9472
4	7	1	0.250	1.77199E+00	1.41057E-12	2.6227
4	7	2	0.250	8.74391E-02	6.75979E-14	2.5471
4	7	3	0.250	3.87117E+00	3.16288E-12	2.6919
4	7	4	0.250	3.24820E+00	2.73899E-12	2.7782
4	7	5	0.250	2.11995E-02	1.89590E-14	2.9465
4	8	1	0.750	1.97763E-02	4.14683E-14	2.4903
4	8	2	0.750	1.70909E-02	3.69689E-14	2.5689
4	8	3	0.750	7.14858E+00	1.61745E-11	2.6872
4	8	4	0.750	1.81455E+00	4.23722E-12	2.7733
4	9	1	0.250	2.33310E-02	1.63365E-14	2.4948
4	9	2	0.250	7.15900E+00	5.39919E-12	2.6871
4	9	3	0.250	1.81767E+00	1.41495E-12	2.7735

Because of our approximate treatment for computing the spectrum of H_2O , an example of a detailed line-by-line plot would not be realistic as individual line strengths and positions are approximate, and very weak transitions are neglected. However, because of the average way we handle lines, a smeared representation would be more realistic, and in the next section a plot of the "binned" $001 \leftarrow 000$ band of H_2O is shown.

Finally, as the fine structure of a band of a linear molecule, such as CO_2 , is the same as for a diatomic molecule, we do not consider any examples.

7.4 Some Tests and Timings of Computing Band Opacities with Bins

Before we can compute with confidence band opacities with the TRIATOM program, it is necessary to consider some tests of the various methods discussed in chapter 6.

With the three separate methods: the Independent Line Method (ILM), which includes the treatment of the partial overlap of two Gaussian profiles, the Line Smear Method (LSM) and the Opacity Sampling Method (OSM), together with a total rectangular smear (TRS) and the total overlap of lines in a bin (TOL), the four schemes are considered which combine these methods in different ways, as some of these methods are inapplicable in certain circumstances on their own, as mentioned in chapter 6 and below. The four schemes are summarized as follows:

- (i). LSM,
- (ii). ILM + LSM + (TRS + TOL),
- (iii). OSM,
- (iv). OSM + ILM + (LSM + TRS + TOL),

where the brackets indicate that the methods are held in reserve and are used as a last resort if the other methods are inapplicable. If $1/\bar{\kappa}$ is the reciprocal of the RMO for an individual bin, it is convenient to define a new quantity K , such that $K = 1/\bar{\kappa}$, then the required K is obtained from $K(\text{ILM})$, $K(\text{LSM})$, $K(\text{OSM})$, $K(\text{TRS})$ and $K(\text{TOL})$

according to the method, with the choice depending on the scheme adopted. We now consider in detail, each scheme in turn.

For scheme (i) with $K = K(\text{LSM})$, the LSM on its own is not very useful for obtaining RMOs, due to the uncertainties in smearing lines in bins, as discussed in section 6.4. However, scheme (i) uses the least amount of computer time, because of the smaller amount of processing, and can give at least a rough idea of the RMO, particularly if there are large regions of the spectrum which are continuum alone, where of course none of the methods is applied, and where there is significant absorption, the congestion is so large that the LSM is not so approximate. In addition, scheme (i) can be used to obtain the PMOs more quickly than the other schemes, as the sum of the line strengths are still stored in bins.

Scheme (ii) uses a combination of the ILM and LSM with the TRS and TOL held in reserve in the following way, where n is the number of lines in a bin, see also the end of section 6.3:

- (a). for $n = 1$ or 2 and $K(\text{ILM}) > 0$, then $K = K(\text{ILM})$,
- (b). for $n = 1$ or 2 and $K(\text{ILM}) \leq 0$, then $K = \min[K(\text{ILM}), K(\text{TOL})]$,
- (c). for $n > 2$ and $K(\text{ILM}) > 0$, then $K = \max[K(\text{TRS}), K(\text{ILM})]$,
- (d). for $n > 2$ and $K(\text{ILM}) \leq 0$, then $K = \min[K(\text{LSM}), K(\text{TOL})]$.

Cases (a) and (c) apply when the ILM does not break down, with it nearly always in case (c) giving a value for the upper limit of the opacity that is considerably less than the value for the TRS computed from (6.4.3). The maximum function takes care of the unlikely event

of $0 < K(\text{ILM}) < K(\text{TRS})$ with the ILM giving a larger but finite value of the opacity than the TRS. The breakdown case (b) should never occur with the correct choice of bin size and can be regarded as an "emergency" case. For congested bins, case (d) is very common with the value computed from the LSM far more likely to be chosen than the absolute lower bound to the opacity from the TOL. Because of the necessity of applying the ILM, scheme (ii) is more expensive in computer time than scheme (i); however, it would be expected to give much more reliable RMOs, particularly if there are large regions of the spectrum which have lines, but which are not heavily congested.

Scheme (iii) is just the OSM on its own, so $K = K(\text{OSM})$ unconditionally. This has the disadvantage of requiring large amounts of computer memory for sufficient sampling and is also expensive in computer time, but with sufficient sampling would give an accurate value of the RMO. With the expense of less reliable RMOs, a coarser grid could be used, thus saving memory and processing time. Examples with different grid sizes are discussed below. No matter how fine a grid is chosen, we are obliged to undersample in the limit of very low frequency, as discussed in chapter 6, though with a fine enough grid, the region undersampled will be close to $u = 0$, which has a small weighting function and hence does not introduce much error into the final RMO.

Finally, scheme (iv) is the most comprehensive and requires the greatest amount of computing resources. If $\bar{\Delta}u$ is the average width of the lines in a bin, i.e. $\bar{\Delta}u = (1/n)\sum_i \Delta u_i$, d is the separation of the fine grid intervals and k is some specified control parameter,

typically unity, then the following cases can be considered:

- (a). for $n = 1$ or 2 , $\bar{\Delta}u \gg kd$ and $K(\text{ILM}) > 0$, then $K = K(\text{ILM})$,
- (b). for $n = 1$ or 2 , $\bar{\Delta}u \gg kd$ and $K(\text{ILM}) \leq 0$,
then $K = \min[K(\text{OSM}), K(\text{TOL})]$,
- (c). for $n = 1$ or 2 and $\bar{\Delta}u < kd$, then take cases (a) or (b) of scheme (ii),
- (d). for $n > 2$ and $\bar{\Delta}u \gg kd$,
then $K = \min\{\max[K(\text{ILM}), K(\text{OSM}), K(\text{TRS})], K(\text{TOL})\}$,
- (e). for $n > 2$ and $\bar{\Delta}u < kd$, then take cases (c) or (d) of scheme (ii).

In other words, if the grid is considered to be fine enough, the OSM is essentially used for $n > 2$, with the ILM used for $n = 1$ or 2 , except in breakdown cases, which there should not be. However, if the grid is considered to be too coarse, the OSM is ignored and scheme (ii) is used in place. The purpose of the maximum and minimum functions is to ensure that the required value is within the possible bounds for each bin. In particular for case (d), if the sampling interval is sufficiently small, $K = K(\text{OSM})$ in practice, with $K(\text{OSM})$ lying well within the permitted bounds. However, if we choose to undersample with d large by setting k to a small value, there is no guarantee that $K(\text{OSM})$ will necessarily lie within the permitted bounds. Thus lines in a bin could be completely missed, in which case $K(\text{OSM})$ is just the continuum with $K(\text{TOL})$ likely to be a better value as the TOL is a true lower bound to the opacity, or upper bound to its reciprocal. On the other hand, it could just be that although the bins are relatively uncongested, all the grid points happen to lie near the maximum of the spectral lines, in which case the OSM will

overestimate the opacity, with the ILM likely to be a better value, or at worst if that has broken down, K(TRS) is always available as a last resort.

In order to investigate the various methods above in practice, a number of realistic numerical experiments were performed, with some of the examples discussed here. In all cases the vibration-rotation spectrum of CO and its isotopic variants were computed at 2000°K on top of the continuum produced in the usual way at that temperature and $\rho = 10^{-8} \text{ gm cm}^{-3}$. CO was chosen simply because it is abundant and produces a simple spectrum, requiring less overheads in processor time than molecules which produce more complex spectra. However, by including the isotopic variants, a relatively complex spectrum can be produced cheaply.

The spectrum was computed using 2500 bins in the region $u = 1$ to 2, in order to cover the fundamental bands of CO, with the rest of the spectrum blanked off. The bins selected from this region in table (7.18) are all in the vicinity of $u = 1.65$, as $\Delta u = 6.05 \times 10^{-6} u$ for CO at 2000°K, $\Delta u \approx 10^{-5}$ in this part of the spectrum. Also, as the bin widths are $1/2500 = 4 \times 10^{-4}$, the bins are thus about 40 profiles wide. Table (7.17) lists the various sampling intervals used to compute the contribution in each bin by the OSM. In keeping with the rules discussed in section 6.1, there have to be an even number of sampling intervals per bin. From left to right for six different sampling intervals, table (7.17) lists the total number of sampling intervals in the region $u = 1$ to 2, the number of sampling intervals per bin, the approximate number of sampling intervals per profile width and the

separation between sampling points in the fine grid, i.e. the reciprocal of the total number of sampling intervals in the whole region.

Table (7.17) of Different Sampling Intervals

	<u>Total No.</u>	<u>No. Per Bin</u>	<u>Approx. No. Pr. Width</u>	<u>Sep.</u>
1	10000	4	0.1	10^{-4}
2	20000	8	0.2	5×10^{-5}
3	50000	20	0.5	2×10^{-5}
4	100000	40	1	10^{-5}
5	200000	80	2	5×10^{-6}
6	500000	200	5	2×10^{-6}

For the 10 bins given in table (7.18), each identified by its number, the following 15 entries are given: n the number of lines in the bin, u_0 the value of u at the bin centre, $\bar{\Delta}u$ the average width, $\bar{r} = (1/n) \sum_i r_i$ the average relative strength of lines, r being defined in (6.3.14), then $K(\text{CON})$, $K(\text{LSM})$, $K(\text{TRS})$, $K(\text{TOL})$ and $K(\text{ILM})$, where $K(\text{CON})$ refers to the continuum alone, finally $K(\text{OSM})$ for the six sizes of sampling intervals in the order of table (7.17).

Table (7.18) of Some Tests on a Sample of Bins

	<u>1650</u>	<u>1651</u>	<u>1605</u>	<u>1664</u>	<u>1668</u>
n	0	1	1	2	2
$\frac{u_o}{\Delta u}$	1.6598	1.6602	1.6418	1.6654	1.6670
\bar{r}	0.00000E+00	1.00493E-05	9.93828E-06	1.00816E-05	1.00911E-05
CON	2.04740E+10	2.04887E+10	1.98156E+10	2.06788E+10	2.07374E+10
LSM	2.04740E+10	1.92413E+10	1.86222E+10	1.82304E+10	1.82798E+10
TRS	2.04740E+10	9.04470E+04	1.32199E+04	2.33835E+05	3.28104E+05
TOL	2.04740E+10	1.80242E+10	1.73209E+10	1.82582E+10	1.83352E+10
ILM	2.04740E+10	1.80242E+10	1.73209E+10	1.69848E+10	1.83357E+10
OSM1	1.74926E+10	1.87819E+10	1.98156E+10	1.39869E+10	1.38261E+10
OSM2	1.89833E+10	1.96353E+10	1.65140E+10	1.55604E+10	1.90096E+10
OSM3	1.97265E+10	1.87819E+10	1.72058E+10	1.70290E+10	1.86414E+10
OSM4	1.94494E+10	1.90271E+10	1.74787E+10	1.73252E+10	1.85019E+10
OSM5	1.93997E+10	1.89724E+10	1.73358E+10	1.69370E+10	1.82978E+10
OSM6	1.93950E+10	1.89736E+10	1.73183E+10	1.69896E+10	1.83434E+10

	<u>1608</u>	<u>1628</u>	<u>1625</u>	<u>1632</u>	<u>1634</u>
n	4	5	6	8	15
$\frac{u_o}{\Delta u}$	1.6430	1.6510	1.6498	1.6526	1.6534
\bar{r}	9.85960E-06	9.92536E-06	9.92932E-06	9.97639E-06	9.95133E-06
CON	1.98595E+10	2.01521E+10	2.01083E+10	2.02107E+10	2.02399E+10
LSM	1.55209E+10	1.47780E+10	1.38568E+10	1.22992E+10	7.96234E+09
TRS	1.41564E+04	2.96205E+04	2.60146E+04	4.39681E+06	3.83720E+04
TOL	1.74039E+10	1.77002E+10	1.76543E+10	1.81438E+10	1.77925E+10
ILM	1.35302E+10	1.37724E+10	1.21183E+10	1.02288E+10	0.00000E+00
OSM1	3.33124E+09	1.34336E+10	1.96433E+10	1.96185E+10	5.14582E+09
OSM2	1.49000E+10	1.51252E+10	1.36841E+10	1.27831E+10	9.24099E+09
OSM3	1.32837E+10	1.57200E+10	1.33078E+10	1.40405E+10	9.25021E+09
OSM4	1.36431E+10	1.56237E+10	1.14954E+10	1.38238E+10	8.17420E+09
OSM5	1.35699E+10	1.55080E+10	1.22490E+10	1.36921E+10	8.51596E+09
OSM6	1.35306E+10	1.55155E+10	1.22183E+10	1.37269E+10	8.43988E+09

Note that the K s given in table (7.18) are reciprocal volume absorption in cm, and do not include the constant in the Rosseland weighting function, see the end of section 6.5. The RMO in $\text{cm}^2 \text{gm}^{-1}$ for each bin obtained from any of the methods is found from:

$$\bar{K} = \frac{1}{K} \cdot \frac{4\pi^4}{15\rho} = \frac{2.59758 \times 10^9}{K} \quad (7.4.1)$$

in $\text{cm}^2 \text{gm}^{-1}$, for $\rho = 10^{-8} \text{gm cm}^{-3}$.

The bins selected for table (7.18) are chosen not only to be a representative sample in the runs performed, but also to show a number of interesting features. In all cases, the results converge to some value as the sampling interval becomes smaller for the OSM, indicating that for the finest grid, the results are quite accurate. In our general application of the OSM, we strive to sample at approximately intervals of profile widths, which in practice means about three fine grid points across a profile including its wings, so the values of $K(\text{OSM4})$ are of particular interest here. Although more accurate values are obtained from $K(\text{OSM5})$ and $K(\text{OSM6})$, insufficient memory is available at St. Andrews to cover the whole spectrum with such a fine grid, in addition to being more expensive in processing time, OSM5 and OSM6 can be regarded as oversampling. By saving memory and processing time, we could undersample with OSM3 with the further sacrifice of accuracy, with any lower sampling being of little value.

If we assume $K(\text{OSM6})$ to be the accurate value for each bin, then the percentage errors for $K(\text{OSM4})$ for bins 1650, 1651, 1605, 1664, 1668, 1628, 1625, 1632 and 1634 are approximately 0.3, 0.3, 1, 2, 0.9, 0.8, 0.7, -6, 0.7 and -3 respectively. This shows that even for the worst cases the errors are acceptable, and for most cases the errors are small. It is easy to see that the errors for the lower sampling cases will in general be larger. When the spectrum is taken as a whole, the sampling errors will tend to cancel out. Moreover, where there are large regions of continuum, no sampling errors occur, and where bins are very congested indeed, there being no examples in the cases here, the sampling errors will tend to be small. This is because heavy congestion tends to produce a pseudo-continuum, so even gross undersampling may not be too bad in some cases.

We can briefly consider some of the features shown by these bins. Normally for bins that have only continuum, $K(\text{OSM}) = K(\text{CON})$, however, bin 1650 is chosen although there are no lines in the bin, $K(\text{OSM}) < K(\text{CON})$ which can be explained by the spillover of wings from lines in the neighbouring bins 1649 and 1651. This is easily shown by summing over 1649, 1650 and 1651, where 1649 and 1651 each have only one line. All figures must be multiplied by 10^{10} .

$$K(\text{OSM6}) = 1.96510 + 1.93950 + 1.89736 = 5.80196,$$

$$K(\text{ILM}) = 1.95194 + 2.04740 + 1.80242 = 5.80176,$$

which is very good agreement. As there is unlikely to be any overlap, the ILM is very good, and gives correct values. Except as stated in

chapter 6, all the contribution from any line is put into one bin.

From the above discussion, it is immediately seen why $K(\text{ILM}) < K(\text{OSM6})$ for bin 1651. For bin 1605, $K(\text{ILM}) \approx K(\text{OSM6})$ indicating that the line is well within the bin. Bin 1664 has two lines which are obviously not overlapping to any great extent as it is clear that $K(\text{TOL}) > K(\text{ILM}) \approx K(\text{OSM6})$, however, in bin 1668 the two lines are heavily overlapping, or one is relatively weak and they are partially overlapping (a cut-off is used to prevent any very weak lines from being generated), as $K(\text{TOL}) \approx K(\text{ILM}) \approx K(\text{OSM6})$. (Note that on subsequent detailed examination of the bins, the above statements were confirmed, in particular for bin 1668, the two profiles were almost totally overlapping). With the remaining bins, the congestion is increased until for bin 1634, even though the sum of the profile widths is still much less than the bin width, the ILM breaks down and cannot be used as a guide. This is because the wings of the strong lines beyond the Doppler width can still be an important source of absorption, refer to (6.3.1). Note that when the ILM breaks down, the subsequent lines in that bin are no longer treated for the ILM, to save computer time, and for these bins $K(\text{ILM})$ is set to zero.

From the theory in chapter 6, we know that $K(\text{TOL}) \gg K(\text{OSM}) \gg K(\text{ILM})$, which is seen to be true here, save for those cases where edge effects occur. When there are two or more lines in a bin, one has a quantitative idea about the amount of overlap, by how $K(\text{OSM})$ is related to $K(\text{ILM})$ and $K(\text{TOL})$. Thus for bin 1608 the agreement between $K(\text{OSM6})$ and $K(\text{ILM})$ is very good indeed, indicating no overlap, whereas for bin 1628, $K(\text{OSM6})$ lies comfortably

in between the other two. For some of the undersampling cases, $K(\text{OSM})$ lies outside the permitted range and would clearly be incorrect; the treatment for scheme (iv) handles such cases. For comparison, $K(\text{LSM})$ and $K(\text{TRS})$ are also included; note that in all cases here $K(\text{TRS}) \ll K(\text{OSM})$, though for very heavy congestion this may no longer be the case.

As stated in section 6.3, even for three or more lines in a bin, the partial overlap treatment for the first two lines can give a slightly better upper bound to the opacity. Thus in some earlier tests performed at the time the partial overlap treatment was implemented, in general there was found to be very little difference between bins with and without the partial overlap treatment, with more than one line, which is to be expected as the bins are very wide compared to profile widths for the cases handled. One notable exception was a particular bin with 15 lines, (not bin 1634) where $K(\text{ILM})$ increased from 2.34719×10^9 to 2.76351×10^9 with the partial overlap treatment, and represents an improvement in the upper bound of the RMO in that bin; compare this to $K(\text{TOL}) = 1.55136 \times 10^{10}$ and $K(\text{OSM6}) = 8.02109 \times 10^9$.

Finally, a number of timing runs were performed, where in order to cut overheads, the least amount of output was generated. From left to right in table (7.19) are listed the scheme, the central processor unit (CPU) time in seconds, the number of sampling intervals across the region $u = 1$ to 2, if applicable and $\sum K$, the sums of the contributions over the bins by the various schemes, with all cases having 2500 bins. Note that scheme (iv) cases (c) or (e) were never

invoked. For comparison, ΣK is also given for the continuum alone, the ILM on its own, where for breakdown cases the contribution is zero and the TOL; the last two giving the bounds.

Table (7.19) of CPU Timing Runs and Sums Over Bins

<u>Scheme</u>	<u>CPU Time in sec</u>	<u>No. Smpl. Intv.</u>	<u>ΣK</u>
(i)	35		3.44346E+13
(ii)	41		3.35348E+13
(iii)	37	10000	3.47964E+13
(iii)	39	20000	3.51139E+13
(iii)	46	50000	3.49957E+13
(iii)	52	100000	3.50235E+13
(iii)	60	200000	3.50246E+13
(iii)	86	500000	3.50239E+13
(iii)	97	600000	3.50236E+13
(iv)	47	10000	3.55513E+13
(iv)	60	50000	3.50587E+13
(iv)	111	600000	3.50368E+13
CON			4.11083E+13
ILM			3.33915E+13
TOL			3.96619E+13

In the cases considered here, there is quite a lot of continuum over the range, which "dilutes" the errors. Nevertheless, it is clear that though scheme (ii) is relatively fast, it gives a rather poor result compared to even scheme (iii) with 20,000 sampling intervals

which uses less CPU time. It can be seen that even gross undersampling can give quite a good result as the random errors tend to cancel, as stated earlier, though individual bins could be quite in error. Because of the extra processing time and edge effects when the ILM is applied, there is no advantage in scheme (iv) unless there is a shortage of memory. It must be noted that these times are approximate; because of the properties of the operating system in a multi-user environment, identical runs can produce different CPU times. Moreover, for actual production runs, considerably more complex spectra, like that of H_2O are generated, and will have larger overheads. Thus the timings here act only as a rough guide.

To complete this section, some graphical examples are shown, with all computations performed at $T = 2000^{\circ}K$ and $\rho = 10^{-8} \text{ gm cm}^{-3}$. Figure (7.12) is a plot of part of the fundamental sequence of bands of CO, including any isotopic variants abundant enough to produce a spectrum, covering the bins 1631 to 1635, which includes the last two bins in table (7.18). The bin sizes are $1/2500 = 4 \times 10^{-4}$ and the separation of the sampling points of the fine grid is $1/600,000 = 1.6667 \times 10^{-6}$, corresponding to about 6 fine grid points per profile width, (600,000 grid intervals is about the maximum that can be handled with the VAX in its usual configuration, after taking account of the memory required for other arrays and the program itself). The profiles are drawn using a supplied plotting subroutine that draws smooth curves through a sequence of points. Since the runs for table (7.18) were performed, more molecules were added to the mixture, together with better data, so the opacities in the bins corresponding to those in table (7.18) are slightly different, but no qualitative changes have

occurred, with the opacities in figure (7.12) ranging from $5.51 \times 10^{-6} \text{ cm}^2 \text{ gm}^{-1}$ to $1.18 \times 10^2 \text{ cm}^2 \text{ gm}^{-1}$, these being the actual opacities at the grid points, not the means over the bins.

With this linear plot, the spectrum looks deceptively empty, and it is hard to see how there can be a significant amount of absorption in bin 1634, where the ILM breaks down. However, we know from the theory in chapter 6, that once the relative strength of a profile is large compared to the continuum, say 100, increasing the strength of the profile by even many orders of magnitude will not cause a large increase of the RMO in that bin, with the quantity X, defined in (6.2.5), proportional to the square root of the log of the profile's strength. Thus in showing the strongest profiles correctly, the much weaker ones, which are still strong, are apparently lost. A much more realistic plot is figure (7.13), where the log of the opacities is plotted, and gives a much better representative idea of how much absorption there really is. In particular, it can be seen that bin 1634 is really quite congested, and the 8 profiles visible in that bin could not be fitted in without some overlap, as indeed predicted by the ILM.

Figures (7.14) and (7.15) show respectively a linear and log plot of the absorption in the bins 1684 to 1688 for a band head, with the same bin sizes and fine grid separations as before, and with the absorption ranging from $5.36 \times 10^{-6} \text{ cm}^2 \text{ gm}^{-1}$ to $1.30 \text{ cm}^2 \text{ gm}^{-1}$. Again the log plot gives a more realistic impression of the absorption, particularly at the band head.

Fig. 7.12

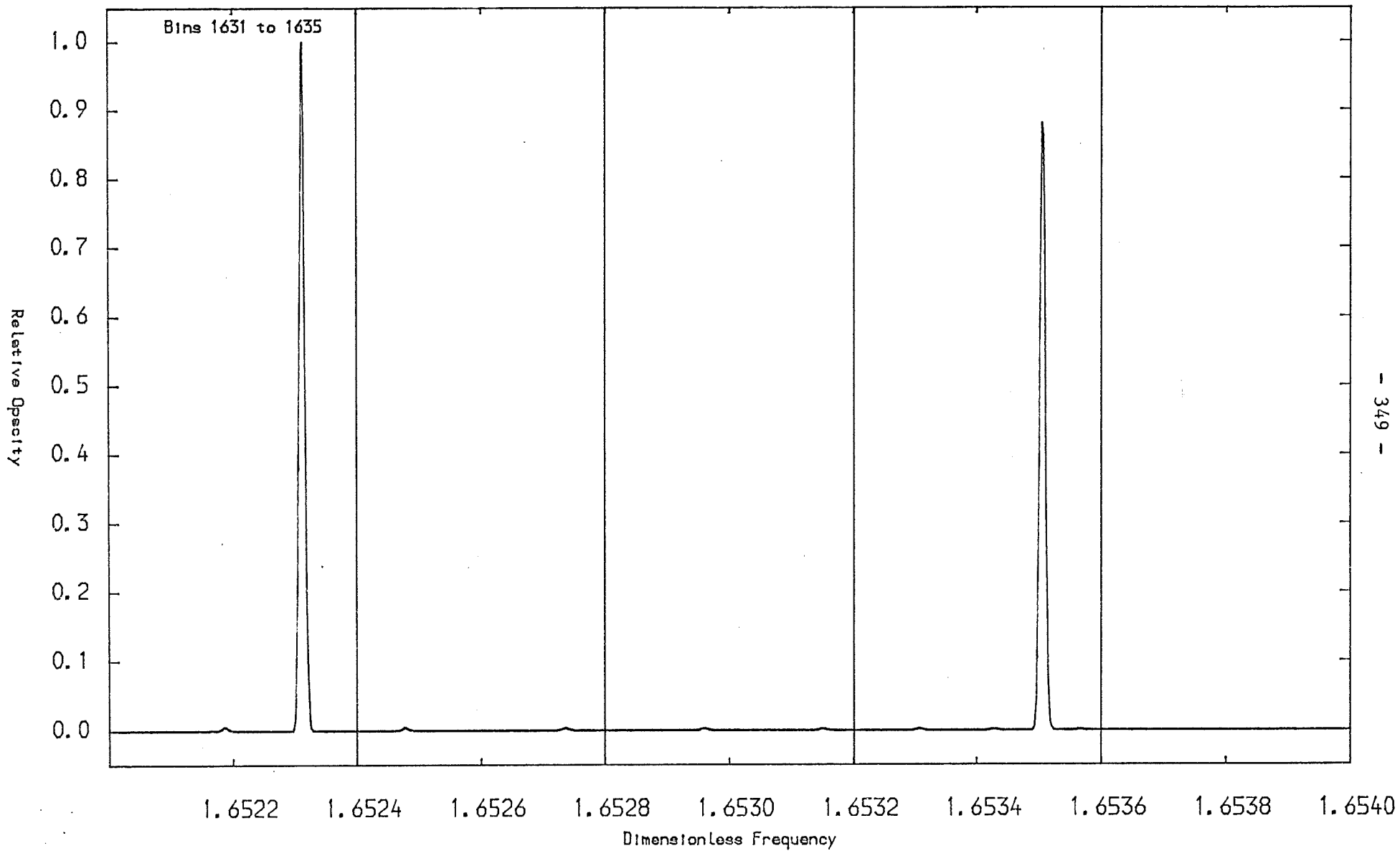


Fig. 7.13

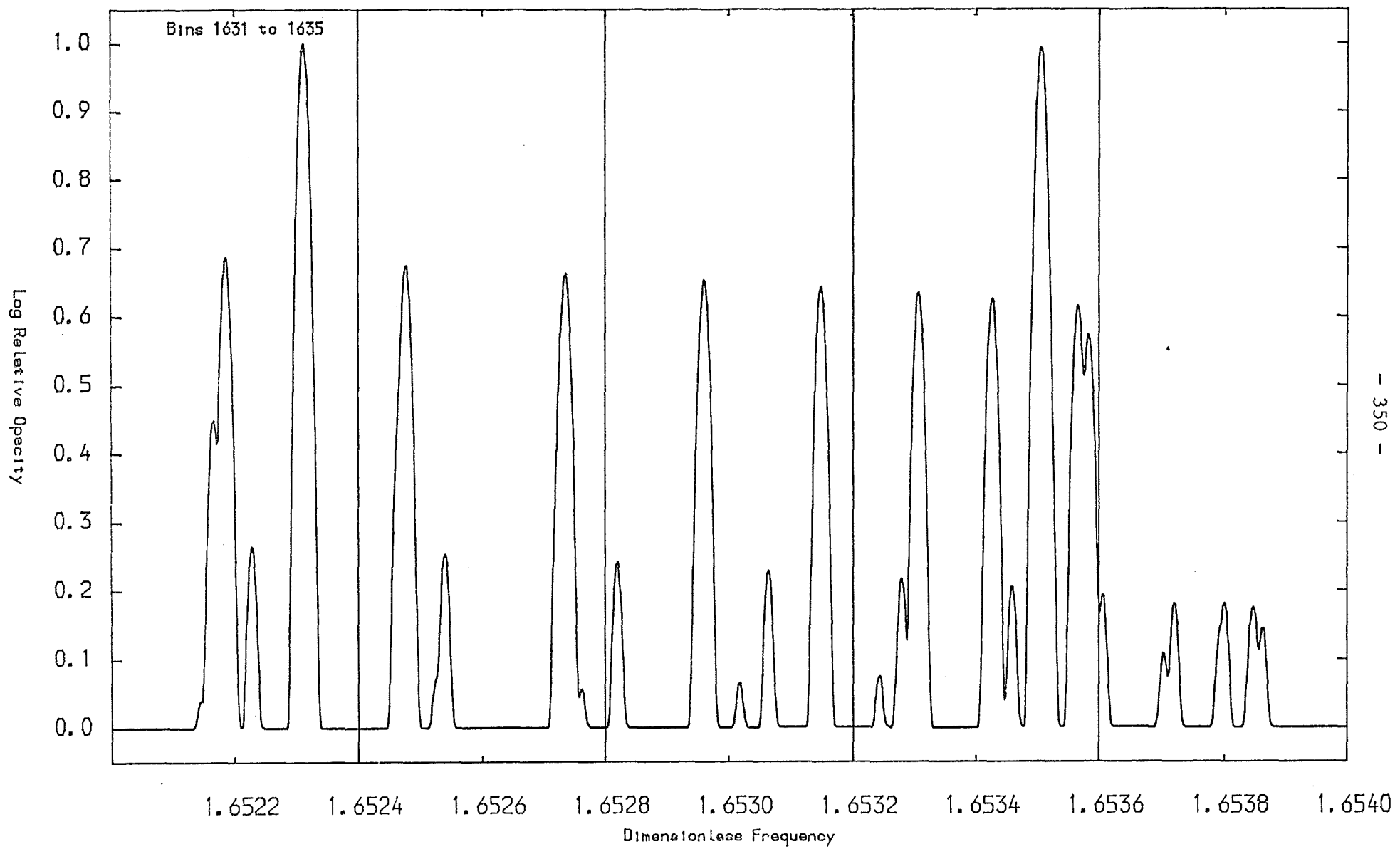


Fig. 7.14

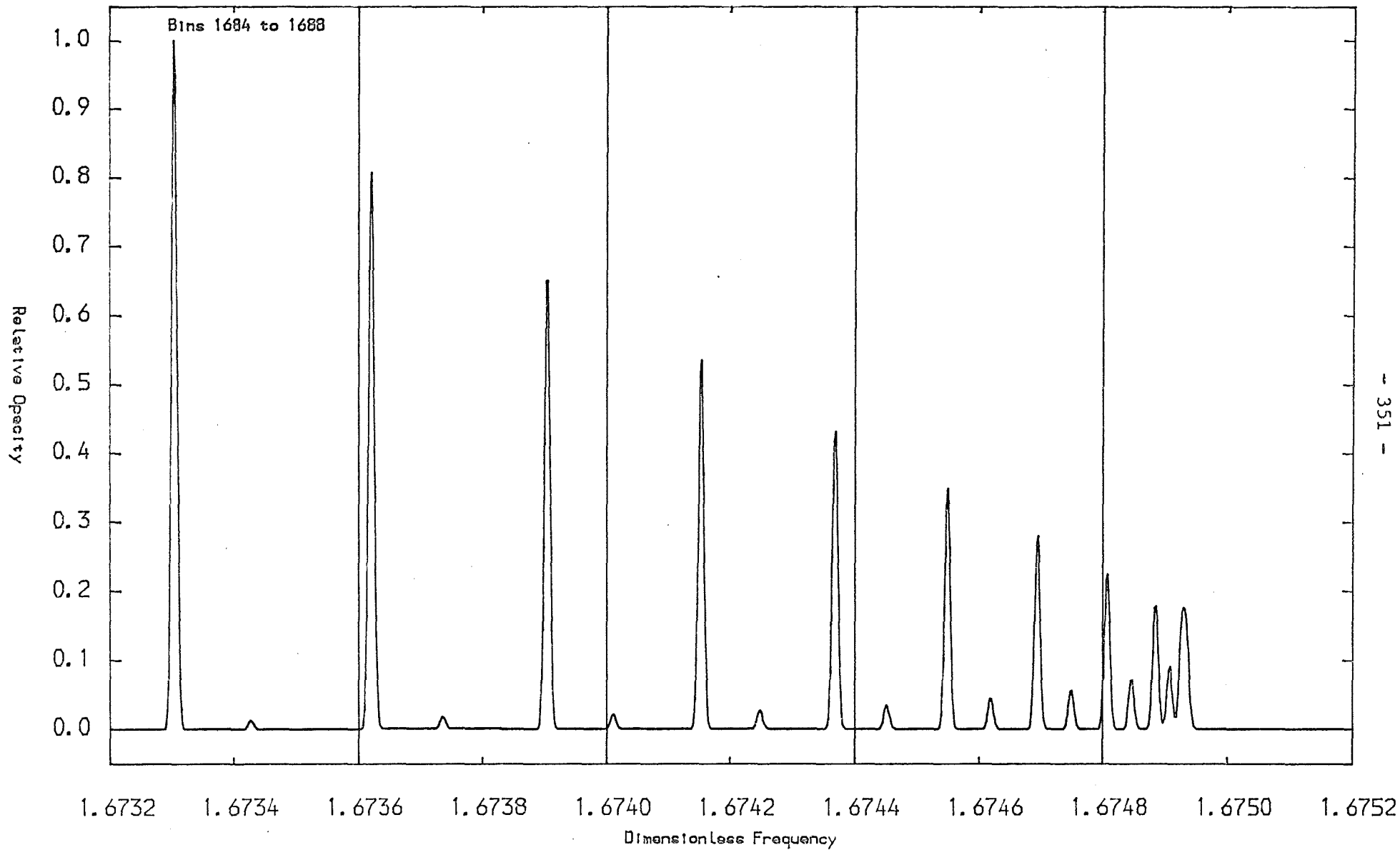


Fig. 7.15

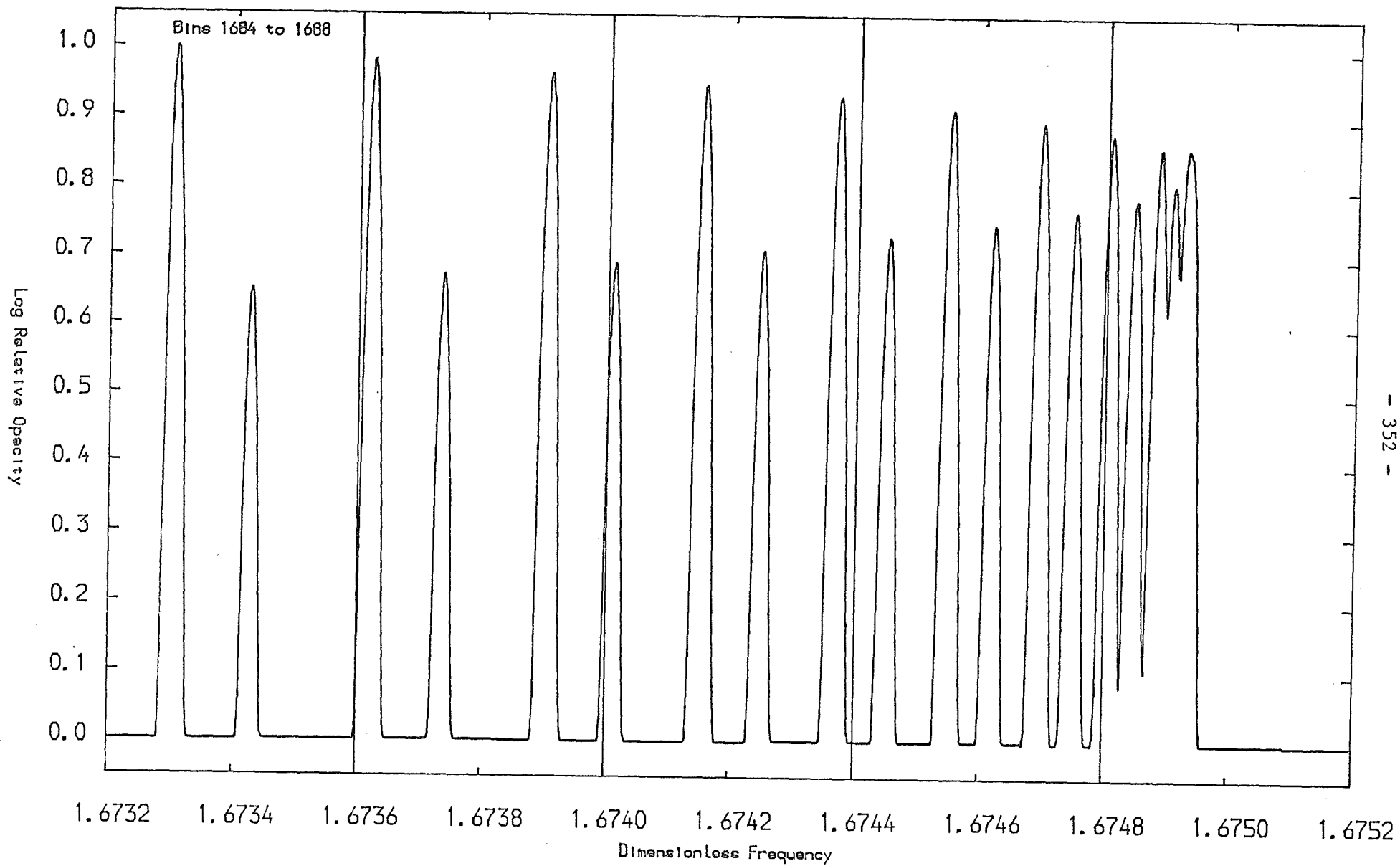


Fig. 7.16

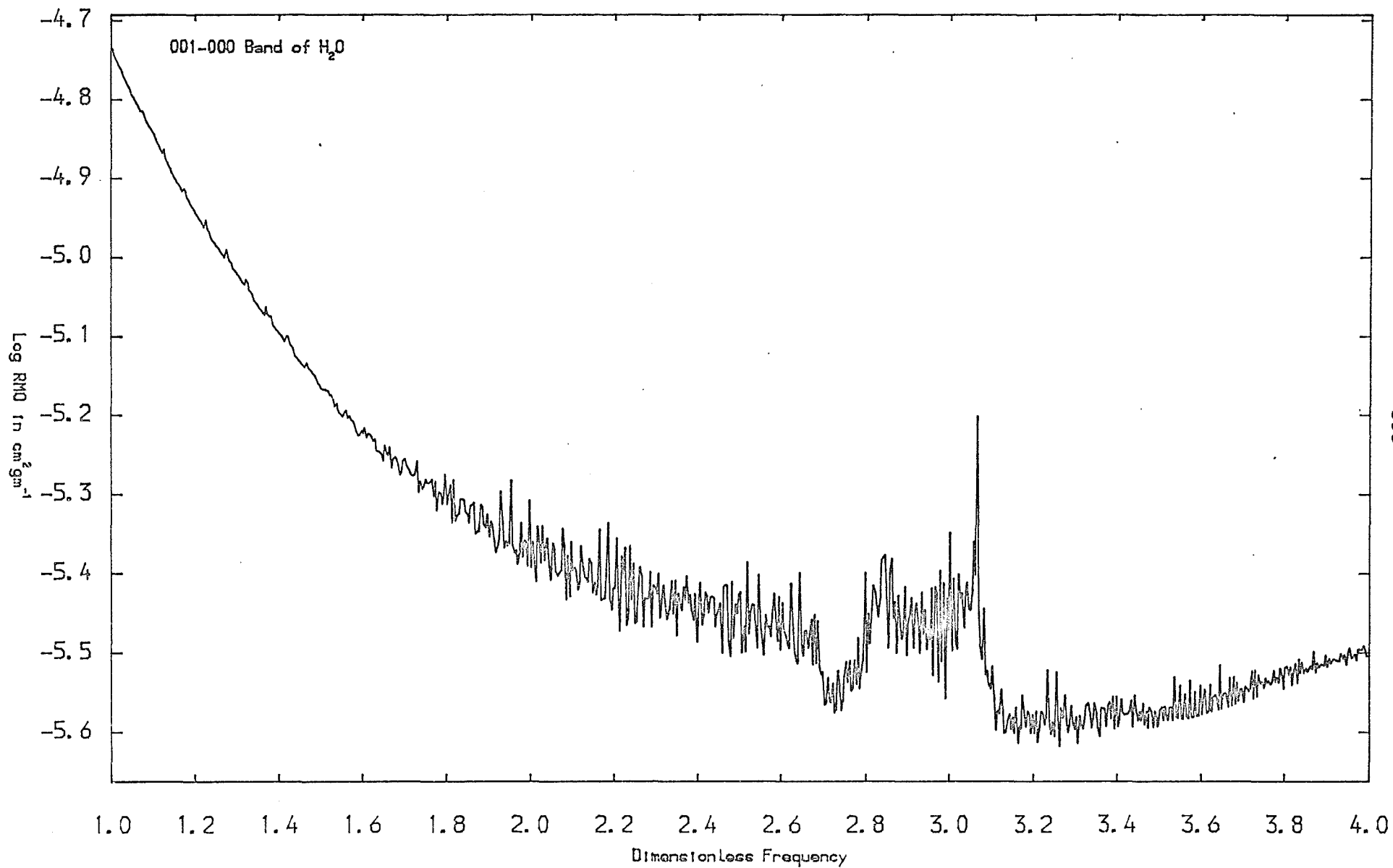
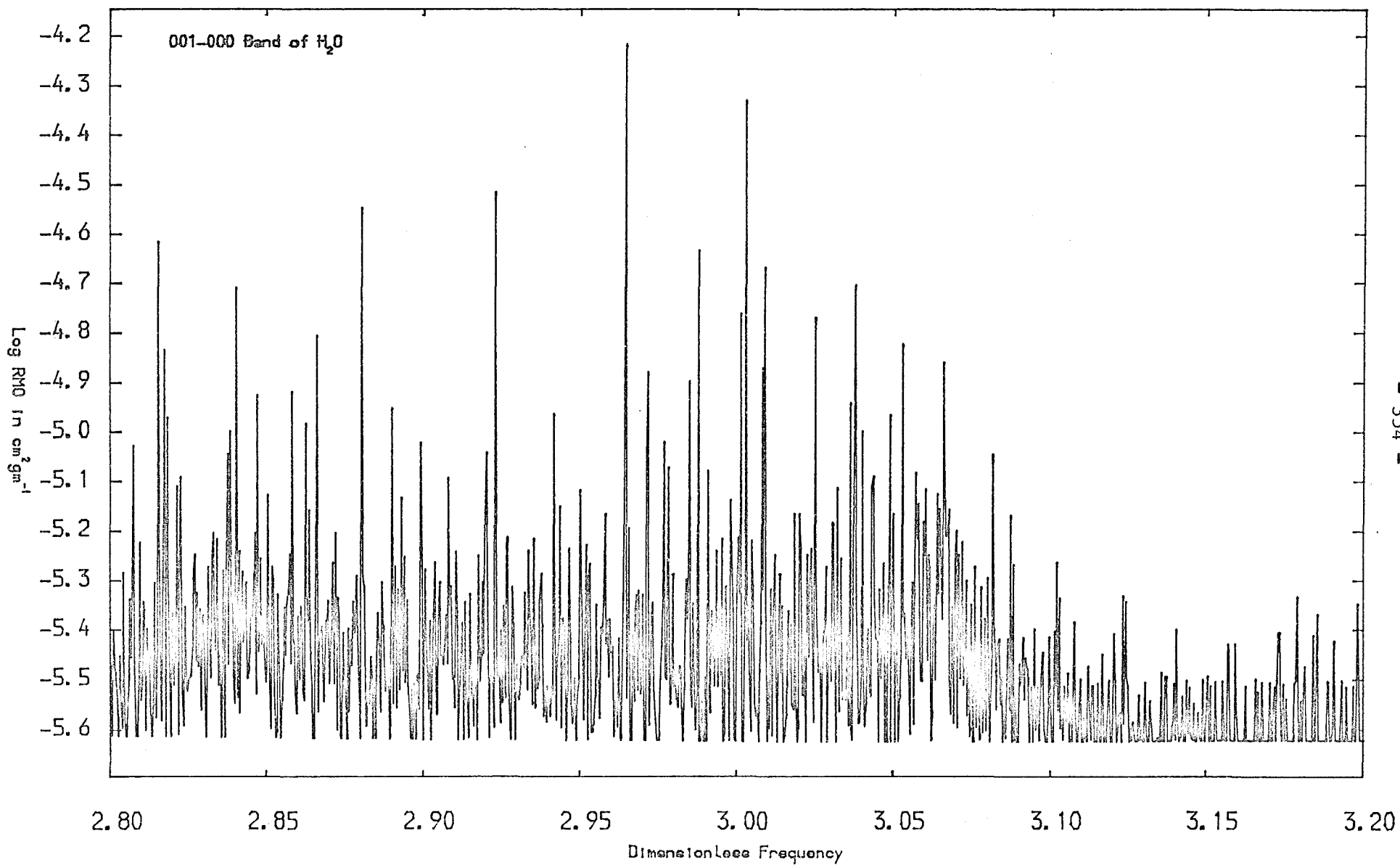


Fig. 7.17



Having plotted examples of spectral lines belonging to bands, and the contents of individual bins, we now show in figure (7.16) a plot of the A-type 001 ← 000 vibration-rotation band of H₂O sitting on top of the continuum, after it has been put into bins. Thus figure (7.16) is a smeared plot, with the individual lines not being shown, and with the connected points plotted at each bin centre.

Rather than plotting simply the RMO for each bin, which contains the weighting function and bin width, it is much better to remove these factors by plotting the average opacities that give those RMOs when integrated over each bin. Thus plots with different bin sizes can be compared.

Thus for bin *i* with width *w_i*, where the weighting function is assumed to be constant, we can write:

$$\frac{1}{\bar{K}_i(\text{RMO})} = \int_{u_i - w/2}^{u_i + w/2} \frac{W(u) du}{K(u)} = \frac{w_i W(u_i)}{\langle K_i(\text{RMO}) \rangle} \quad (7.4.2)$$

thus:

$$\langle K_i(\text{RMO}) \rangle = w_i W(u_i) \bar{K}_i(\text{RMO}) \quad (7.4.3)$$

which is the average over the bin, and is the quantity plotted; it can be regarded as the reduced RMO. Likewise for the PMO, we can write:

$$\bar{K}_i(\text{PMO}) = \int_{u_i - w/2}^{u_i + w/2} B(u) K(u) du = w_i B(u_i) \langle K_i(\text{PMO}) \rangle \quad (7.4.4)$$

thus:

$$\langle K_i(\text{PMO}) \rangle = \frac{\bar{K}_i(\text{PMO})}{\omega_i B(u_i)} \quad (7.4.5)$$

It is immediately seen that we can consider the reduced RMOs and PMOs for lines alone, by simply subtracting the continuum. Thus:

$$\langle K_i(\text{RMO}_i) \rangle = \omega_i W(u_i) \bar{K}_i(\text{RMO}) - K_c(u_i) \quad (7.4.6)$$

and:

$$\langle K_i(\text{PMO}_i) \rangle = \frac{\bar{K}_i(\text{PMO})}{\omega_i B(u_i)} - K_c(u_i) \quad (7.4.7)$$

which can be used for plotting bands without the underlying continuum.

Figure (7.16) is in fact plotted with bin widths of $1/250 = 4 \times 10^{-3}$ and a fine grid separation of $1/200,000 = 5 \times 10^{-6}$, with the OSM on its own. Even though we have to make many approximations in order to compute the spectrum of the asymmetric top molecule, with the detailed individual line positions and strengths being very approximate, it is very gratifying indeed to see that the gross appearance of the band does correspond approximately to theory, with the P, Q and R-branches being clearly visible, though the prominent spike is due to one bin with an exceptional amount of absorption. Finally, figure (7.17) shows in greater detail the Q-branch, which is of course several subbranches superimposed, and with the single prominent spike no longer present. The same fine grid is used, but

the bin sizes are ten times smaller than for the previous figure. For these and all the previous figures, the stimulated emission factor is not included.

In actual production runs, the various tests performed, that are outlined in this section, are used as a guide. However, in order to find an optimum between CPU time and accuracy, together with the constraints of memory, parameters for specifying the cut-offs in abundances, bands, lines etc, have to be found by experience.

7.5 Results of Some Computed Total Opacities with Continuum and Molecular Bands

In this section, we give some examples of total opacities due to molecular bands sitting on the continuum. Thus, these are the results of applying TRIATOM to compute the molecular bands, after having applied MIXOP to obtain the background continuum together with the abundances. Because a considerable amount of effort in this work has been devoted to handling isotopic variants of molecules, we consider this in detail first, and show that indeed in certain circumstances, isotopic variants are important when computing opacities.

We examine in detail first the isotope effect for CO at $\log T = 3.3$ and $\log \rho = -8$. The continuum from $u = 0$ to 20 is computed using 4000 coarse grid intervals for all the species discussed in chapter 3, and the bands of CO are computed using the OSM on its own within the region $u = 1$ to 4, using a fine grid interval of $1/200,000 = 5 \times 10^{-6}$, i.e. 600,000 fine grid intervals in all. This compares favourably with the line widths which increase from 6.0×10^{-6} to 2.4×10^{-5} as u increases over the region. This covers the fundamental and first overtone systems of CO, and just the very tail-end of the second overtone system. In order to have as fine a sampling interval as possible over the region $u = 1$ to 4, the regions $u = 0$ to 1 and $u = 4$ to 20 are ignored in the band calculations, leaving just the continuum. However, in the region $u = 0$ to 1 there is no absorption due to CO anyway, and in the region $u = 4$ to 20, only

the second overtone system is effectively lost, as the higher order overtones are much weaker and occur where the background continuum is strong and the weighting functions are much smaller.

The fine grid over the region studied is put into 7500 bins, all of equal width, i.e. $1/2500 = 4 \times 10^{-4}$, so there are 80 fine grid intervals per bin, and the bins are at least 17 profile widths wide. Note that although the separation of the coarse grid points is 12.5 bin widths, which contradicts the rule stated in section 6.1 that this ratio must be an integer, this restriction only applies when the ILM is used, due to the particular way the bins are handled in the code. The bands are computed for a 20X20 matrix, so in theory there would be a maximum of 19 and 18 bands in the fundamental and first overtone progressions respectively, for each isotopic form, when isotopes are considered. However, a cut-off of 1% for the relative line strength, i.e. the area under the profile on its own compared to the area of a slab of continuum equal to the Gaussian width of the profile, would be expected to cut off most of the higher bands in the progression.

In the examples here, we compare the absorption due to CO when all its isotopes are lumped into $C^{12}O^{16}$ to the absorption due to the separate isotopic variants, hence the total abundance of CO is the same in both cases, and the differences in absorption are due entirely to the isotope effect. Table (7.20) lists the absolute and fractional abundances of the isotopic variants of CO at $\log T = 3.3$ and $\log \rho = -8$, as computed by the MIXOP program with a convergence criterion of $\epsilon = 10^{-6}$. Note that the six figures of accuracy, are given here merely to show the results printed by the computer, as such true precision is of course quite meaningless.

Table (7.20) of the Isotopic Abundances of CO

at Log T = 3.3 and Log ρ = -8

<u>Molecule</u>	<u>Ab. Abundance</u>	<u>Fr. Abundance</u>
$C^{12}O^{16}$	1.68348E+12	9.86522E-01
$C^{12}O^{17}$	6.30445E+08	3.69442E-04
$C^{12}O^{18}$	3.43368E+09	2.01214E-03
$C^{13}O^{16}$	1.88962E+10	1.10732E-02
$C^{13}O^{17}$	7.07641E+06	4.14679E-06
$C^{13}O^{18}$	3.85415E+07	2.25854E-05
All Forms	1.70648E+12	

Table (7.21) to Show the Isotope Effect of CO

	<u>Con. Alone</u>	<u>Without Isp.</u>	<u>With Isp.</u>
ΣK for u = 1 to 2	4.09299E+13	3.85180E+13	3.49299E+13
ΣK for u = 2 to 3	1.54675E+14	1.39142E+14	1.20754E+14
ΣK for u = 3 to 4	1.92847E+14	1.86551E+14	1.82655E+14
PMO	1.63802E-05	1.83269E-01	1.83103E-01
RMO	5.13515E-06	5.39360E-06	5.69989E-06

CO is the second most abundant molecule in the mixture, and is to be compared to H₂ with an abundance of 2.22668×10^{15} for all its isotopic forms, and 2.69439×10^{15} for all particles, with the absolute abundances being as usual in cm⁻³.

Table (7.21) gives the sums of the contributions K in cm over the bins in the spectral regions $u = 1$ to 2, 2 to 3 and 3 to 4, for the continuum alone, and the continuum plus CO without and with isotopic forms respectively. The RMOs in these regions can be obtained by simply applying (7.4.1). The total PMO and RMO in the table are for the whole spectrum including the continuum in the regions not covered by the fine grid, and are in cm² gm⁻¹.

It is clearly seen that the RMO in the region $u = 2$ to 3 increases by about 13%, with the overall RMO increasing by about 6%, whereas the PMO hardly changes at all, as expected. Thus the effect on the RMO is large compared to the fractional abundances of the isotopically substituted species, most being in the form of C¹³O¹⁶. This effect can easily be explained by the filling in of the windows, and even though C¹³O¹⁶ is only about 1% as abundant as C¹²O¹⁶, because CO is such an abundant species, some of the isotopically substituted forms are still abundant, hence the isotope effect is important for CO.

Fig. 7.18

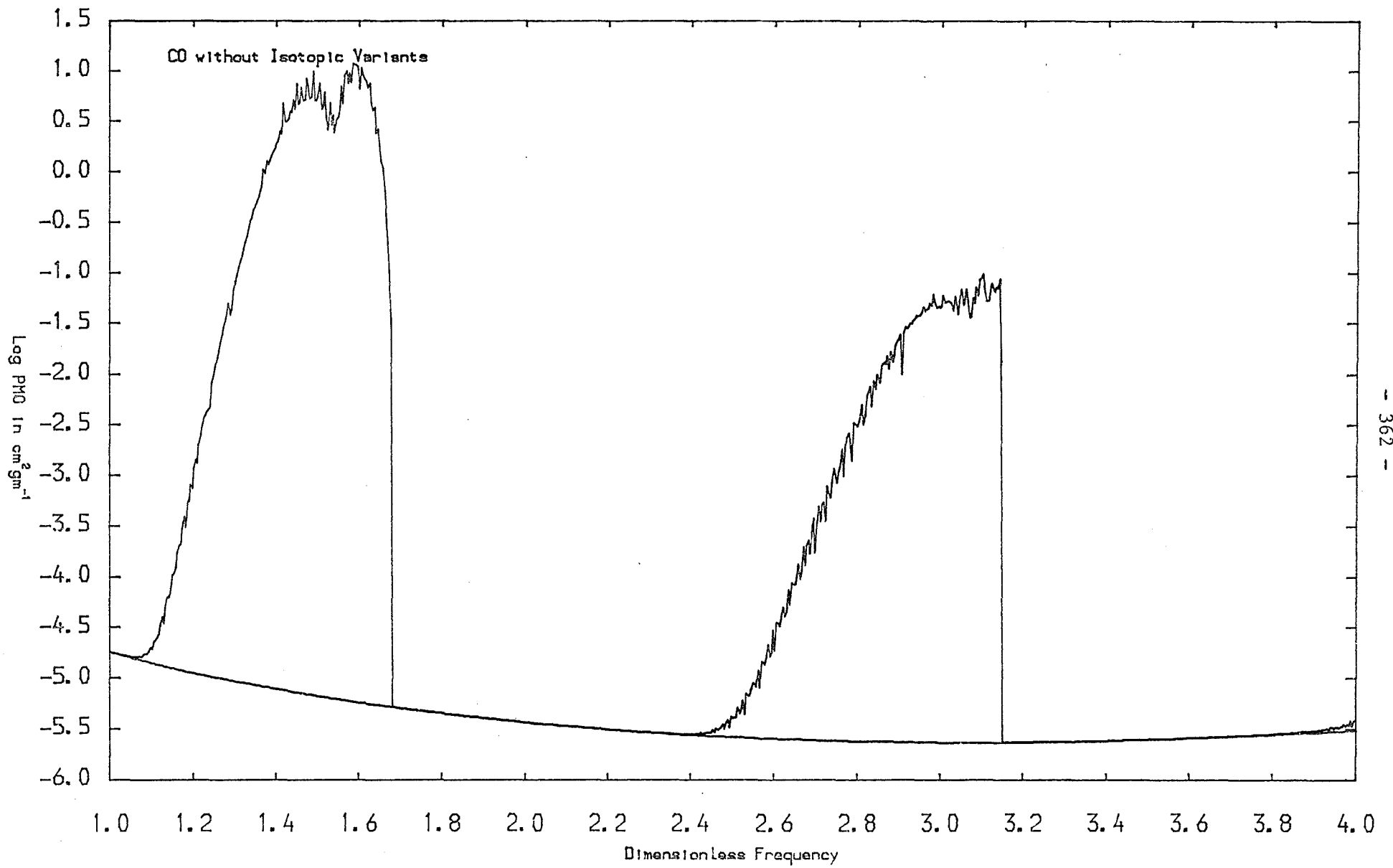


Fig. 7.19

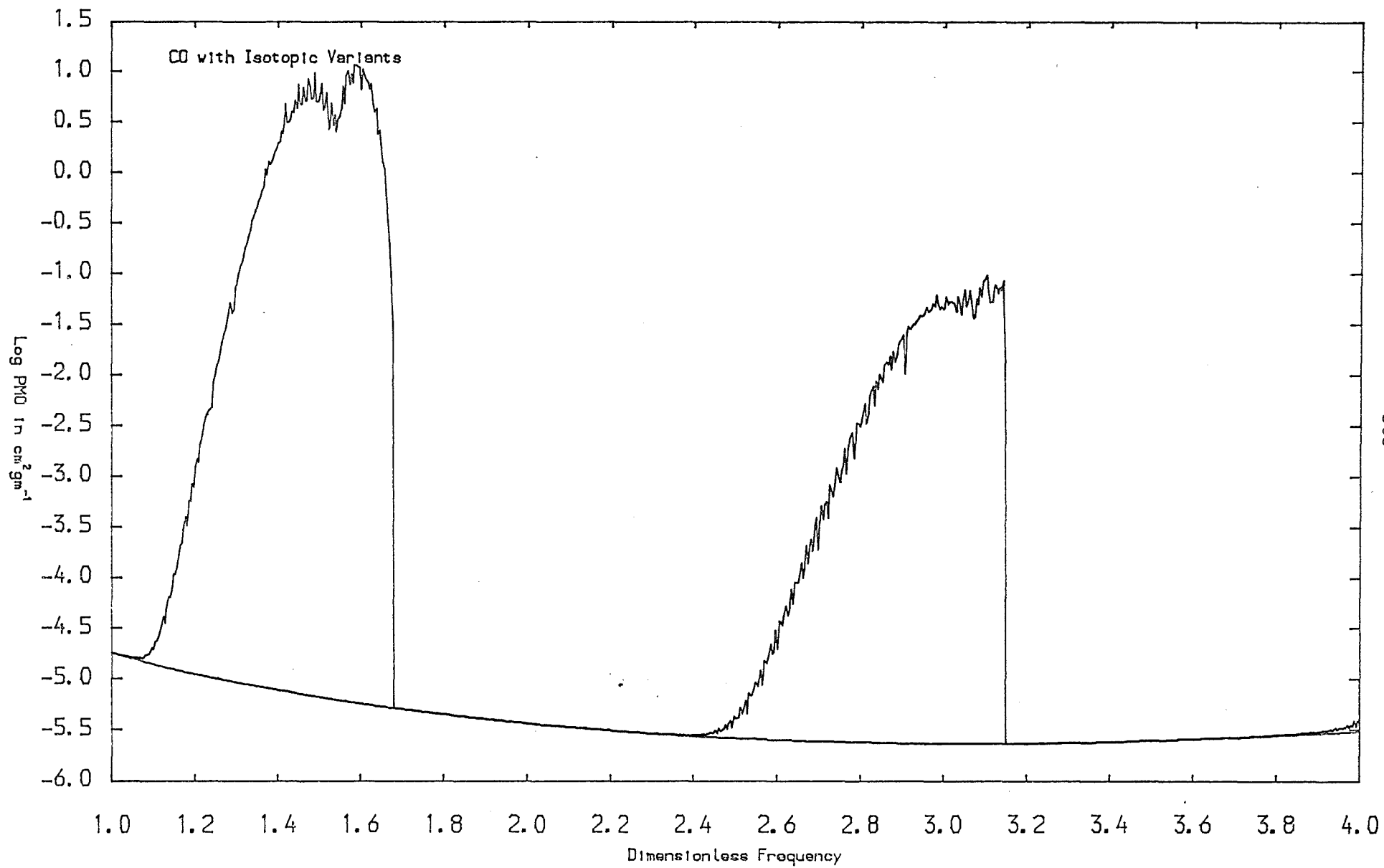


Fig. 7.20

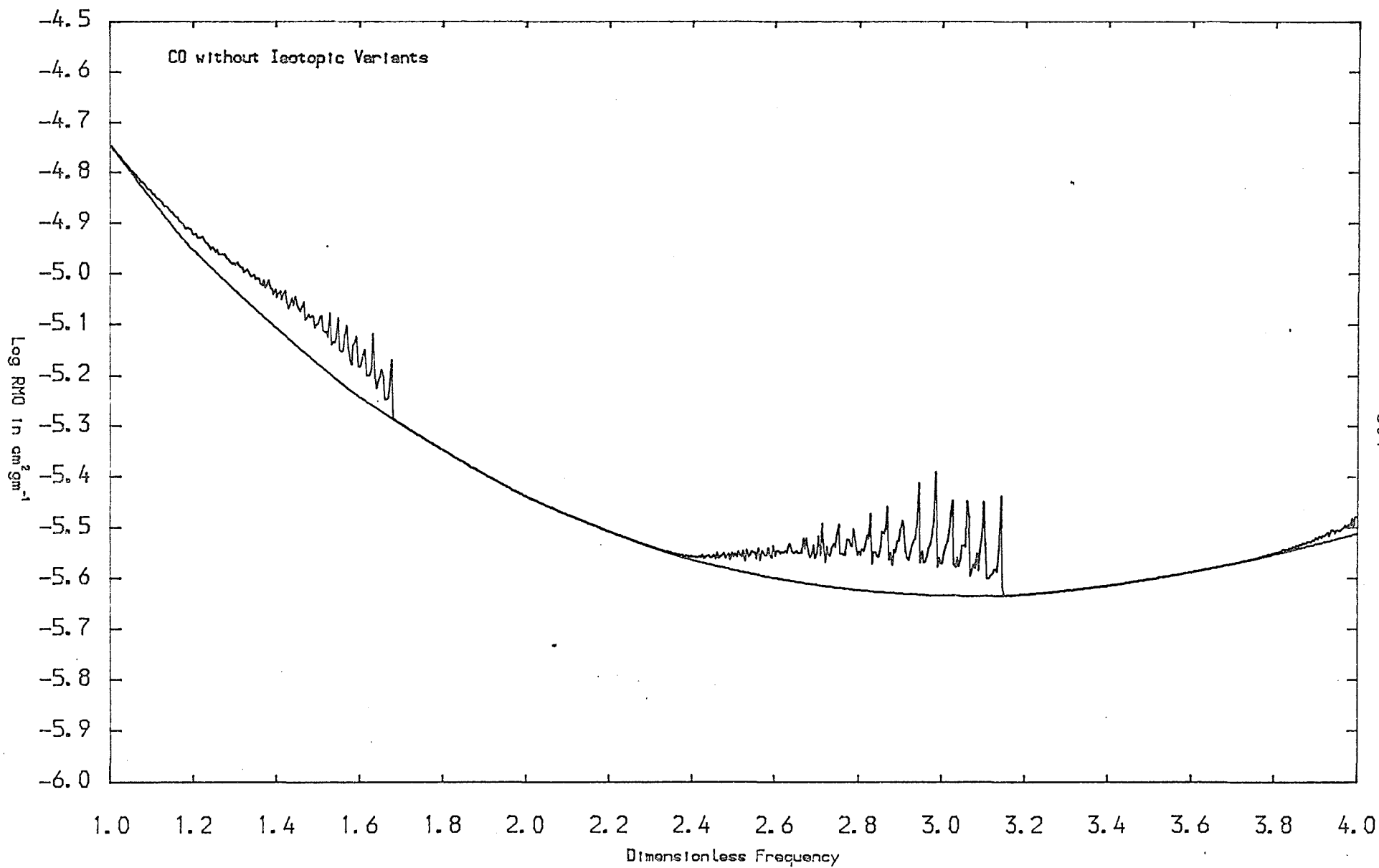


Fig. 7.21

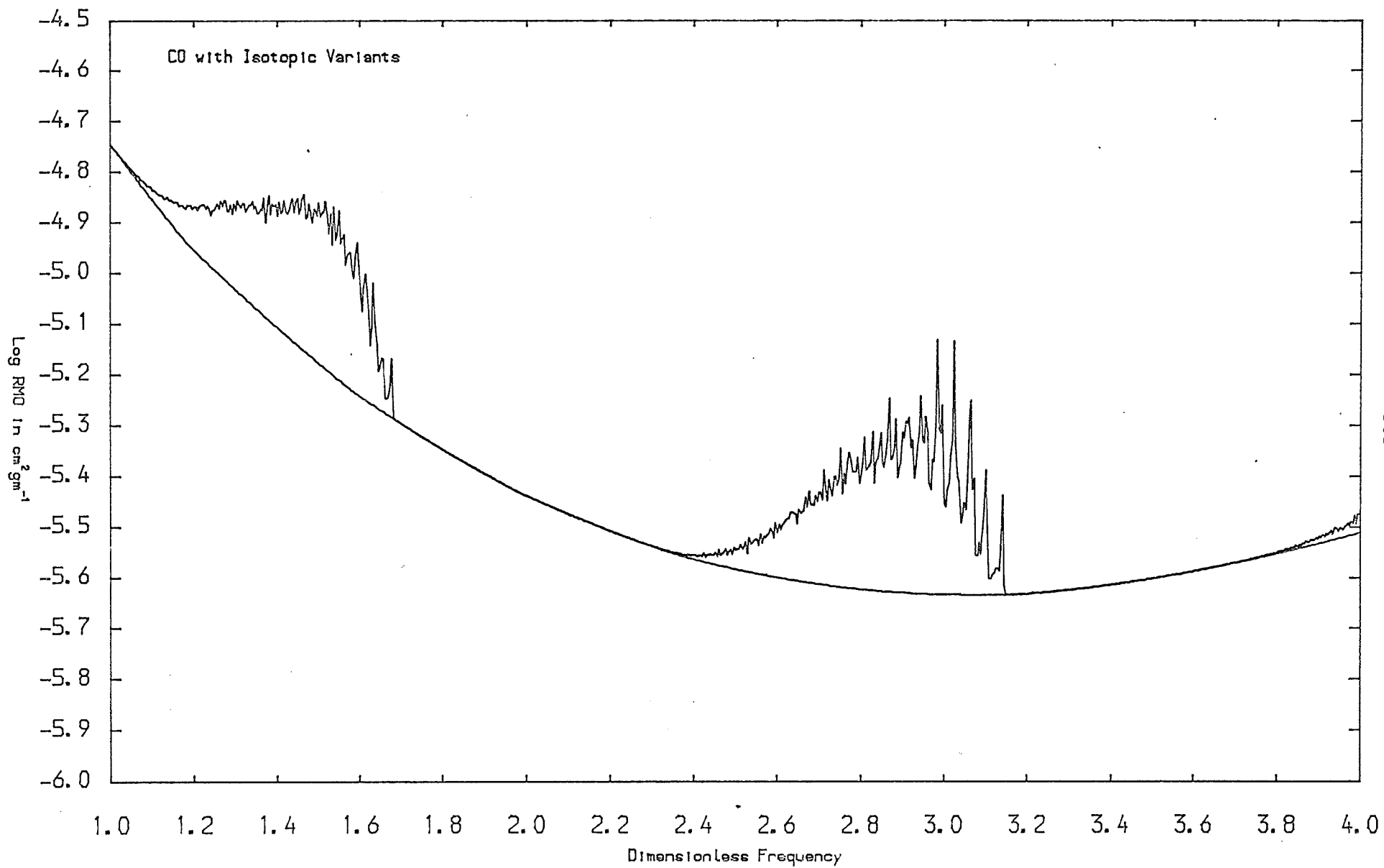


Fig. 7.22

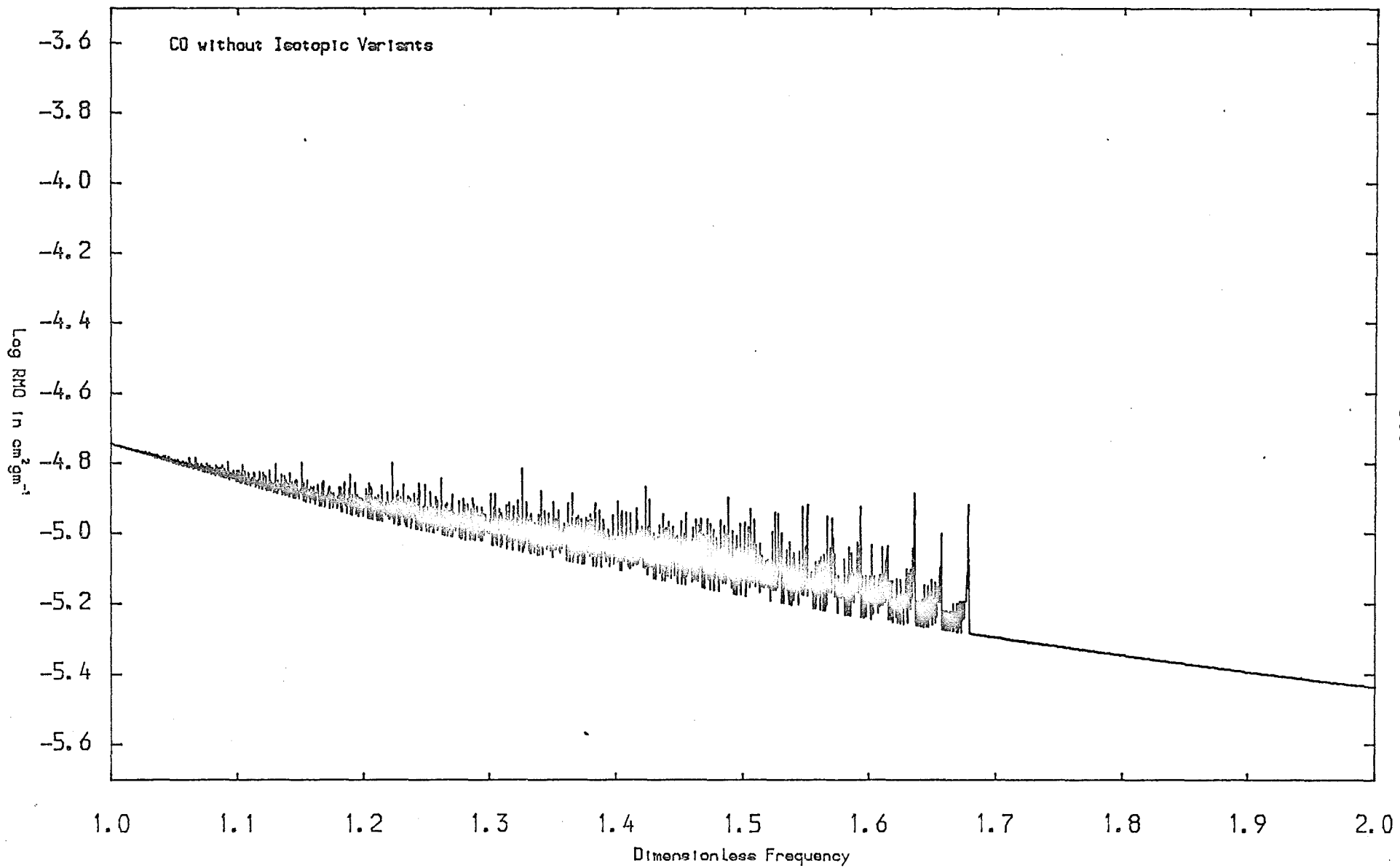


Fig. 7.23

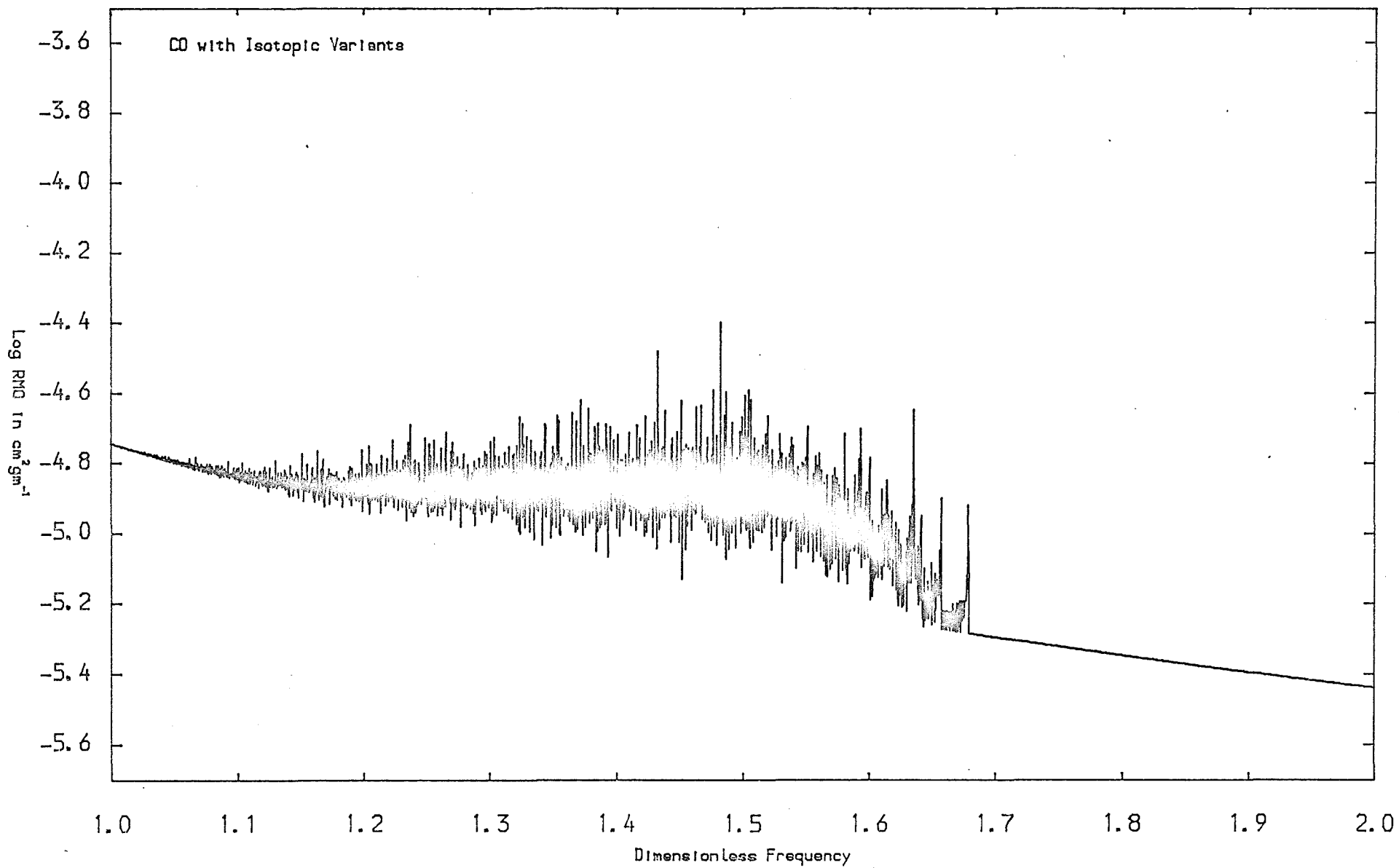


Fig. 7.24

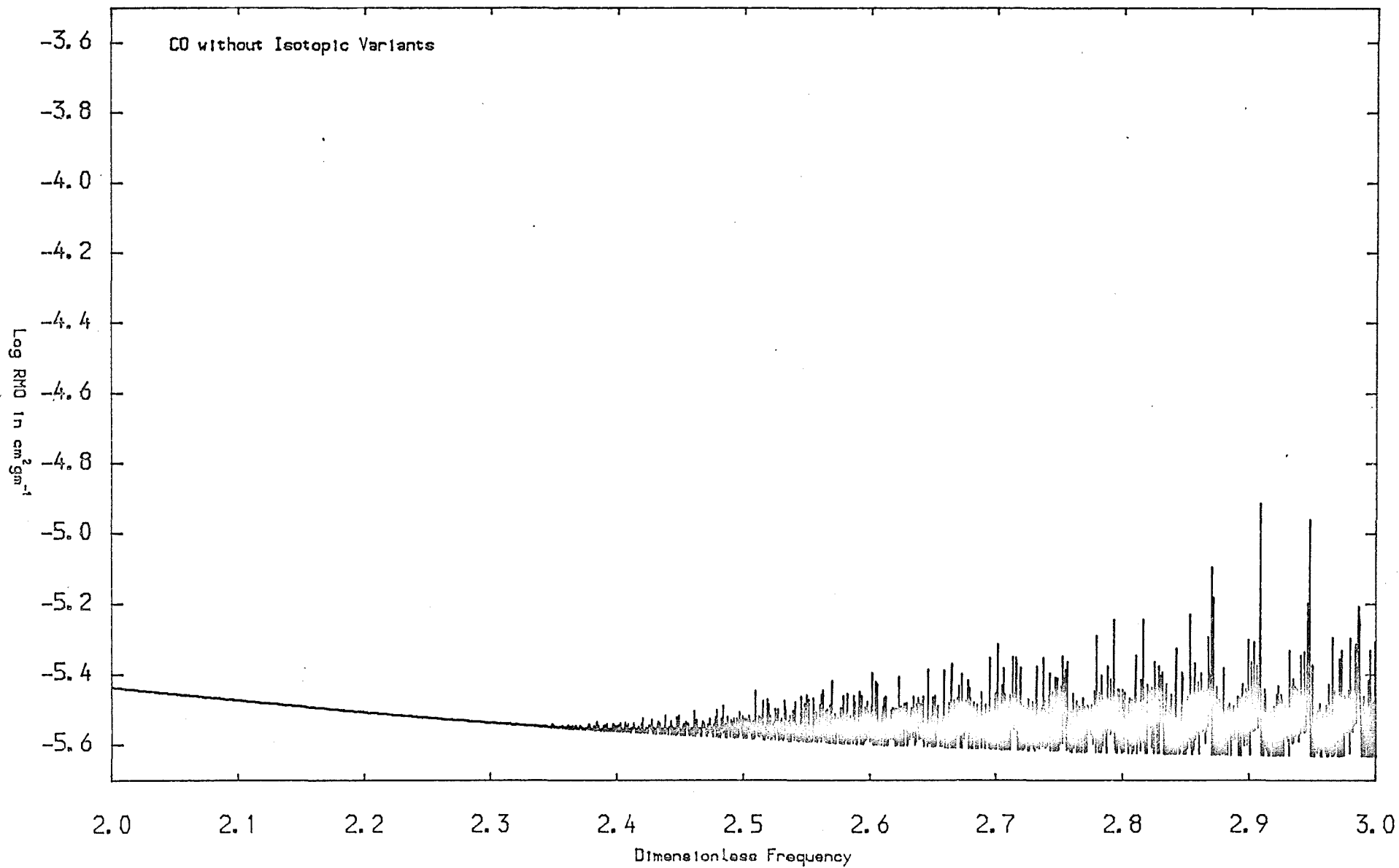


Fig. 7.25

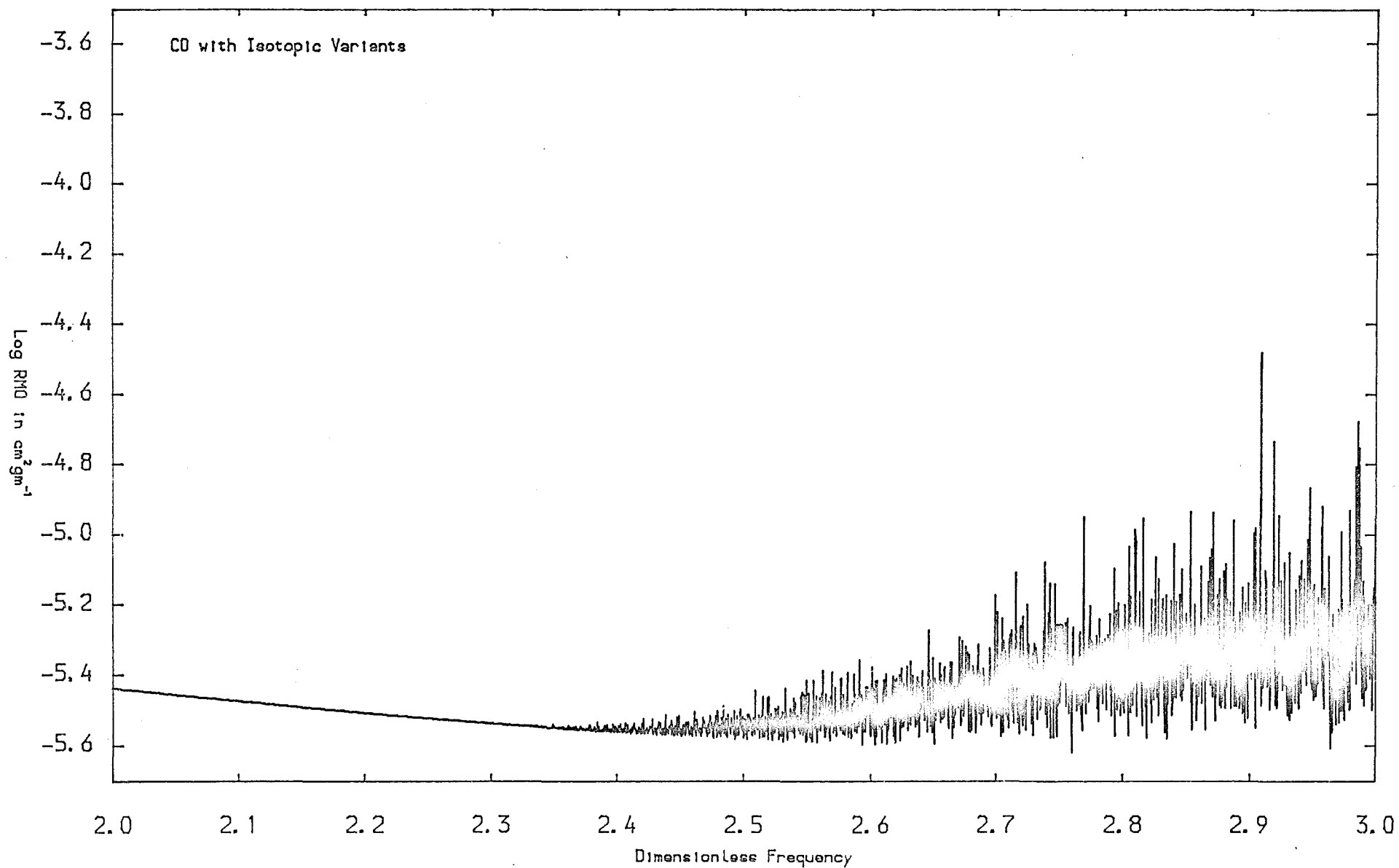


Fig. 7.26

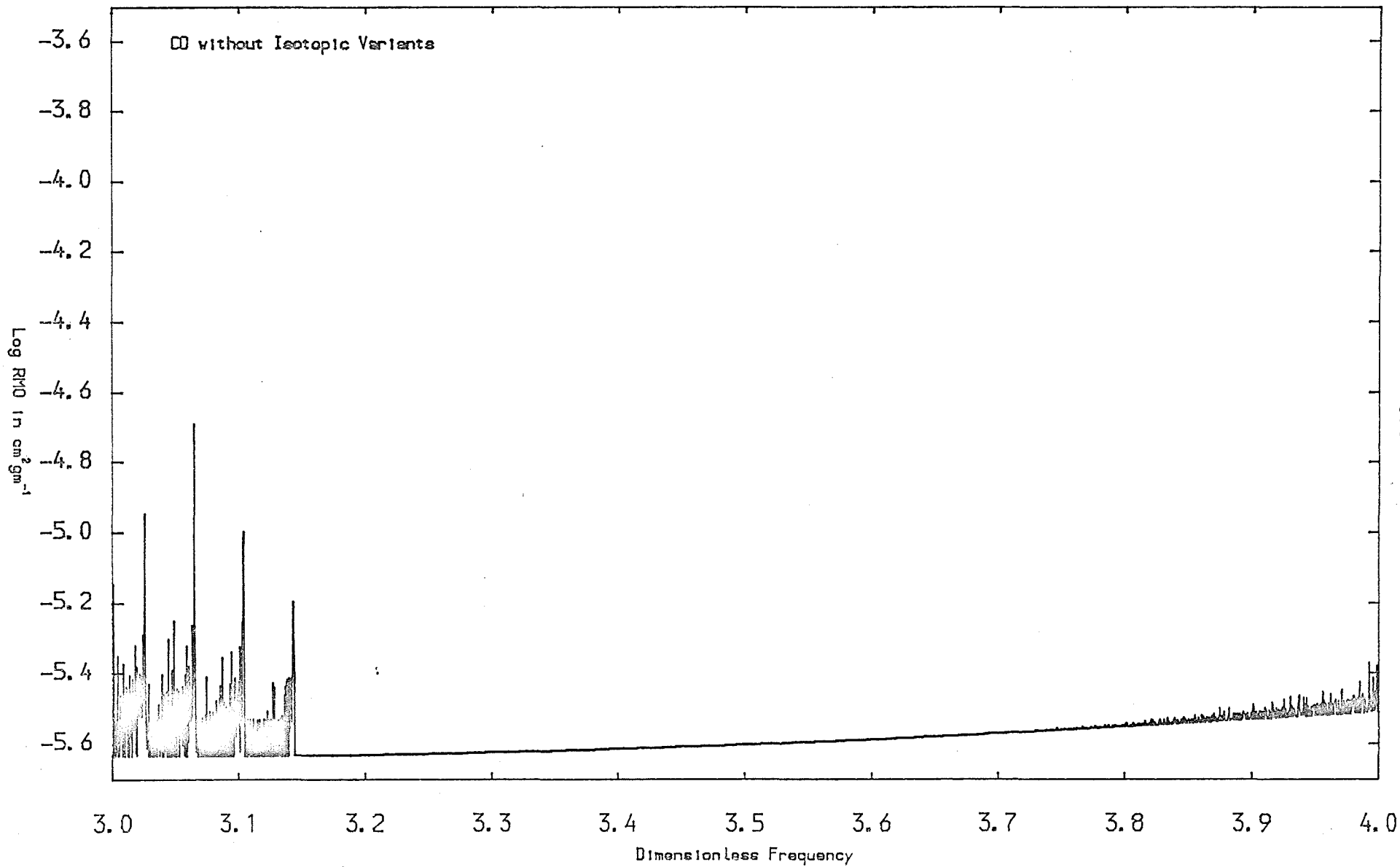


Fig. 7.27

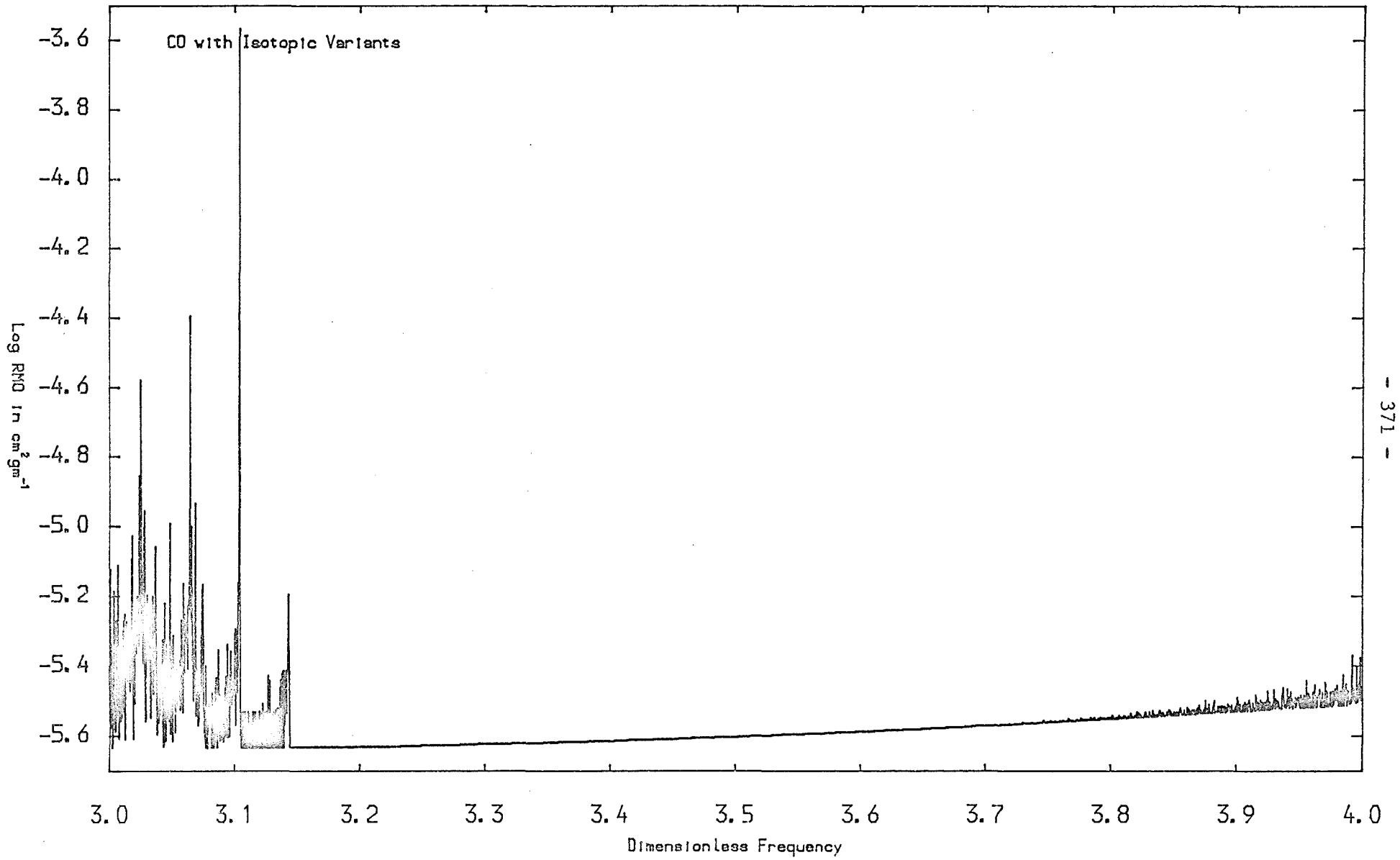


Fig. 7.28

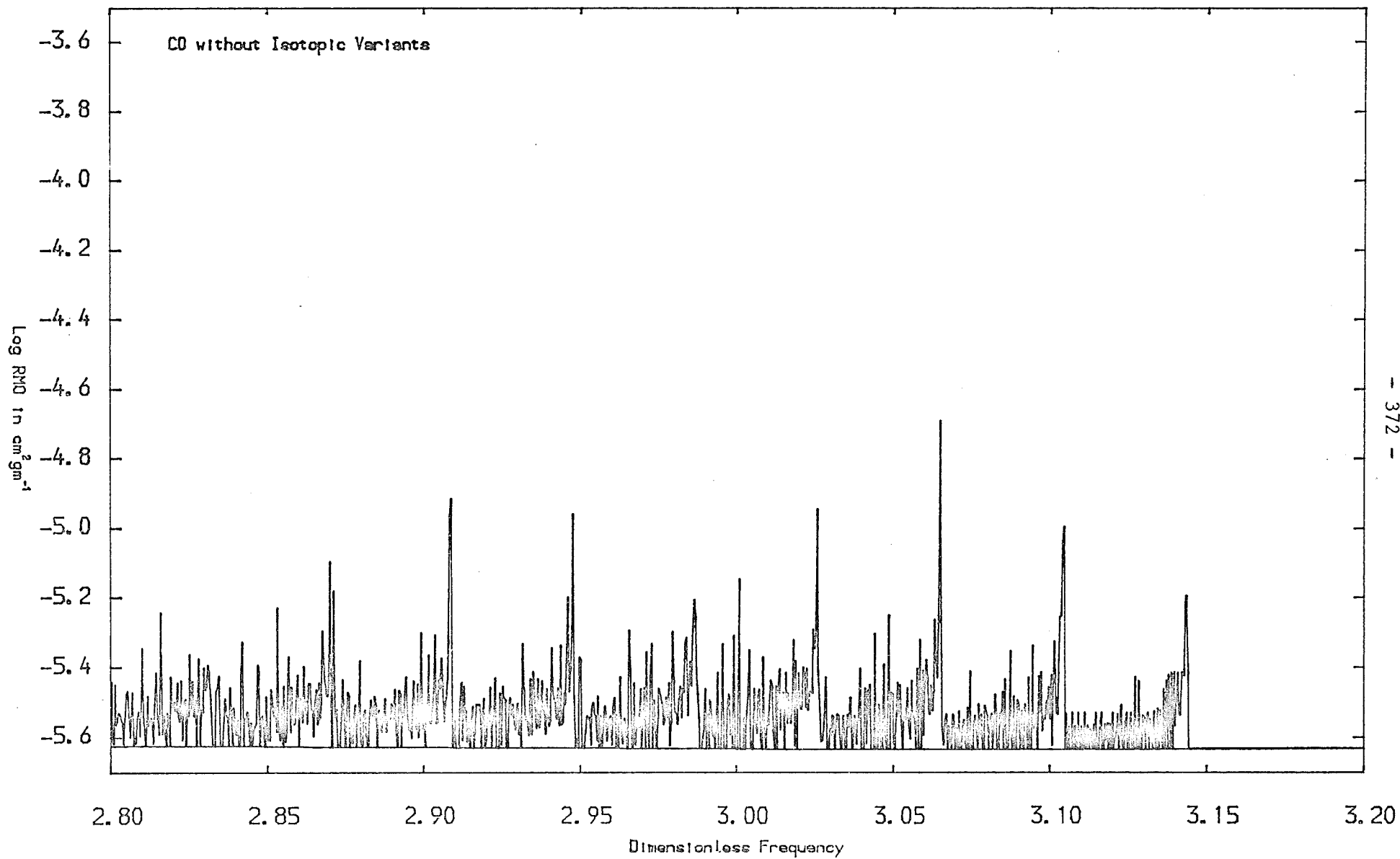
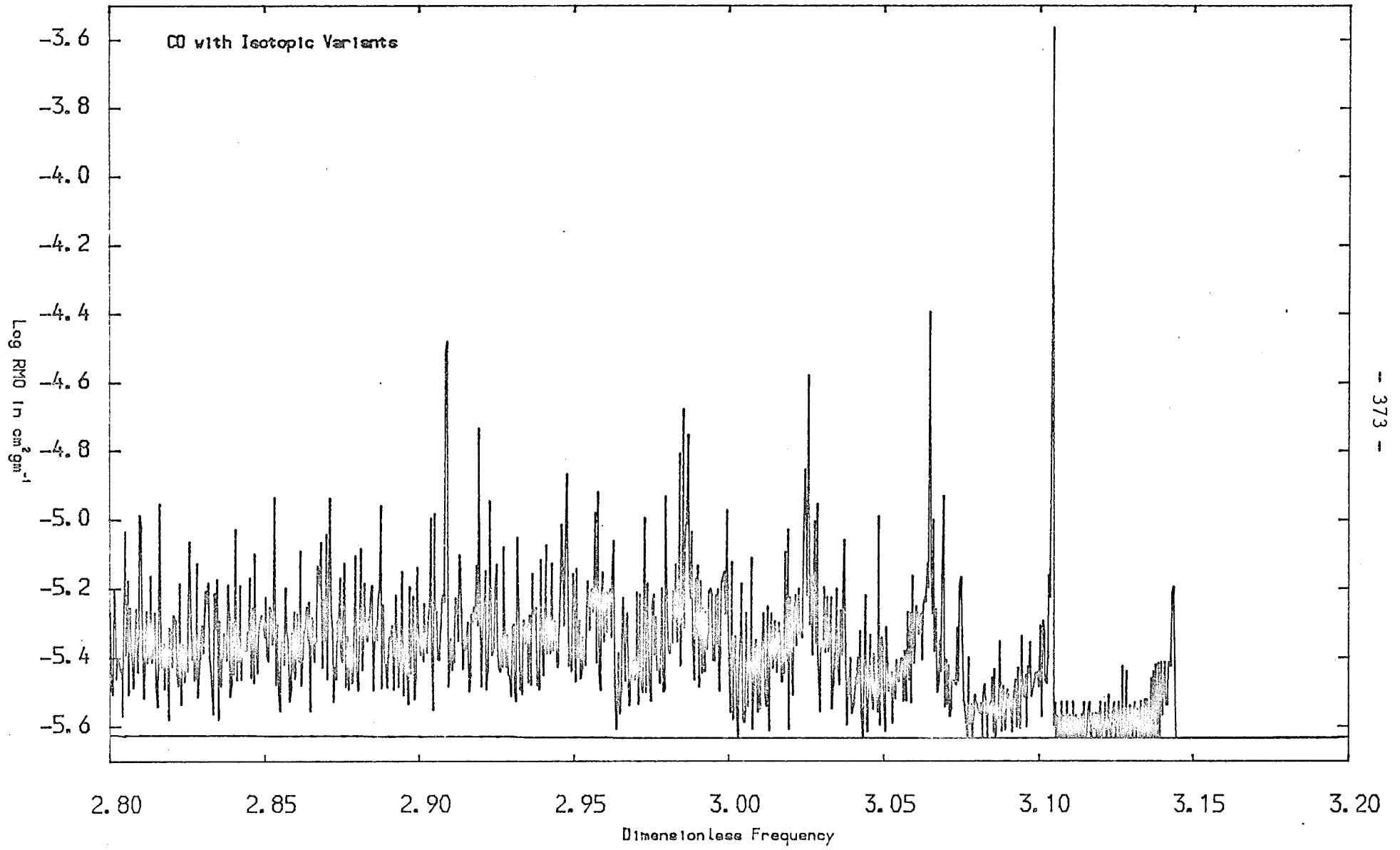


Fig. 7.29



Figures (7.18-29) show up the isotope effect much better, and are arranged in pairs with everything else being equal. The plotted RMOs and PMOs are obtained using the relations (7.4.3) and (7.4.5) respectively. In figures (7.18-21), the smearing has been increased by a factor of ten, by effectively creating new bins with each consisting of ten computed bins. The remaining figures are all plotted as computed, with bin widths of 4×10^{-4} . In all cases the values are plotted at bin centres and are joined to neighbouring bins by straight lines.

For the sake of completeness, the PMO for the two cases is shown in figures (7.18) and (7.19), there being virtually no noticeable difference at this level of smearing. The fundamental and first overtone systems are centred at about $u = 1.4$ and 2.9 respectively, with the tail-end of the second overtone system at the extreme right, and for comparison, the continuum is drawn under the bands. The sharp band head of the first overtone system is quite marked here. However, the pair of figures (7.20) and (7.21) for the RMO show a very marked difference indeed, with the average values lifted considerably above the continuum due to the isotope effect. From these two plots, it is immediately obvious why the total RMOs for the two cases in the table above are substantially different. The remaining plots compare in greater detail this part of the spectrum with the full number of bins as computed, and the last pair of figures (7.28) and (7.29) show a further magnified view of the first overtone system with the underlying continuum again shown. Black areas are caused by

neighbouring bins that are rapidly alternating in strength, and cannot be resolved due to the thickness of the pen.

Because the two stable isotopes of Cl are of comparable abundance, it is worth briefly considering the isotope effect on HCl, the most abundant Cl containing compound in the mixture. The computations were performed at the same temperature and density as before, with the spectrum computed using the same arrangements of grid points and bins. The coefficients M_i in $\text{D}\text{\AA}^{-i}$ for the dipole moment expansion used are:

$$M_0 = 1.0935, M_1 = 0.925, M_2 = 0.163, M_3 = -3.83, M_4 = -9.3,$$

as obtained from Kaiser (112), and the constants for the ground electronic state needed for computing the vibration-rotation spectrum are:

$$\begin{aligned} X^1\Sigma^+ : D_e^0 &= 37222, & \omega_e &= 2990.95, & \omega_e x_e &= 52.819, & \omega_e y_e &= 0.2244, \\ B_e &= 10.593416, & D_e &= 5.31936 \times 10^{-6}, & \alpha_e &= 0.307181, \\ \beta_e &= 7.51 \times 10^{-6}, \end{aligned}$$

as obtained from Rosen (35). The tables giving the abundances and the effect on the opacity are given below. As before, the effect of all isotopic forms lumped into the most abundant species, i.e. HCl^{35} , are compared to the case where they are considered separately.

Table (7.22) of the Isotopic Abundances of HCl
at Log T = 3.3 and Log ρ = -8

<u>Molecule</u>	<u>Ab. Abundance</u>	<u>Fr. Abundance</u>
HCl ³⁵	5.93956E+08	7.55276E-01
HCl ³⁷	1.92441E+08	2.44709E-01
DCl ³⁵	9.74004E+03	1.23855E-05
DCl ³⁷	3.15580E+03	4.01292E-06
All Forms	7.86409E+08	

Table (7.23) to Show the Isotope Effect of HCl

	<u>Con. Alone</u>	<u>Without Isp.</u>	<u>With Isp.</u>
ΣK for u = 1 to 2	4.09299E+13	4.04035E+13	4.00348E+13
ΣK for u = 2 to 3	1.54675E+14	1.53117E+14	1.52203E+14
ΣK for u = 3 to 4	1.92847E+14	1.88870E+14	1.85878E+14
PMO	1.63802E-05	7.13946E-05	7.13793E-05
RMO	5.13515E-06	5.19740E-06	5.24224E-06

It is seen that the isotope effect is much smaller than for CO, which can be explained by the much lower abundances of HCl. However, the differential effect, i.e. the difference between the two cases compared to the continuum on its own, is large and is due entirely to HCl³⁷, the deuterated versions having quite negligible abundances. Because of the different vibrational constants, the region u = 1 to 4 that is studied, covers only the fundamental and part of the first

overtone system. Plots were examined, but because of the much lower abundances, the differences between the two cases do not show up nearly so well as for CO, and are not shown here.

Finally, for demonstrating the isotope effect of individual molecules, we consider the astrophysically important molecule TiO. These runs were done at the higher temperature of $\log T = 3.5$, but at the same density of $\log \rho = -8$. The electronic transitions considered occur at a considerably shorter wavelength than the bands of CO and HCl considered above, hence the weighting functions are much smaller. So this higher temperature increases the weighting functions for the band, but is not so high that the abundance of TiO becomes too small to be important.

As there are five isotopes of Ti and three of O that are in the statistical mechanics calculations, there are fifteen isotopic variants of TiO in the mixture, which is the greatest number of variants for any diatomic molecule considered. However, in order to save CPU time, a cut-off for the abundances of 10^6 cm^{-3} ensures that those molecules containing O^{17} and O^{18} are neglected, as their abundances are very low, leaving the five variants with O^{16} . Three quarters of Ti is in the form of Ti^{48} , with the remainder consisting of isotopes of comparable abundances. Thus in these examples, we compare the opacities with all forms of TiO lumped into $Ti^{48}O^{16}$ with the five variants containing O^{16} , neglecting the other ten. The abundances are given here in table (7.24).

Table (7.24) of the Isotopic Abundances of TiO

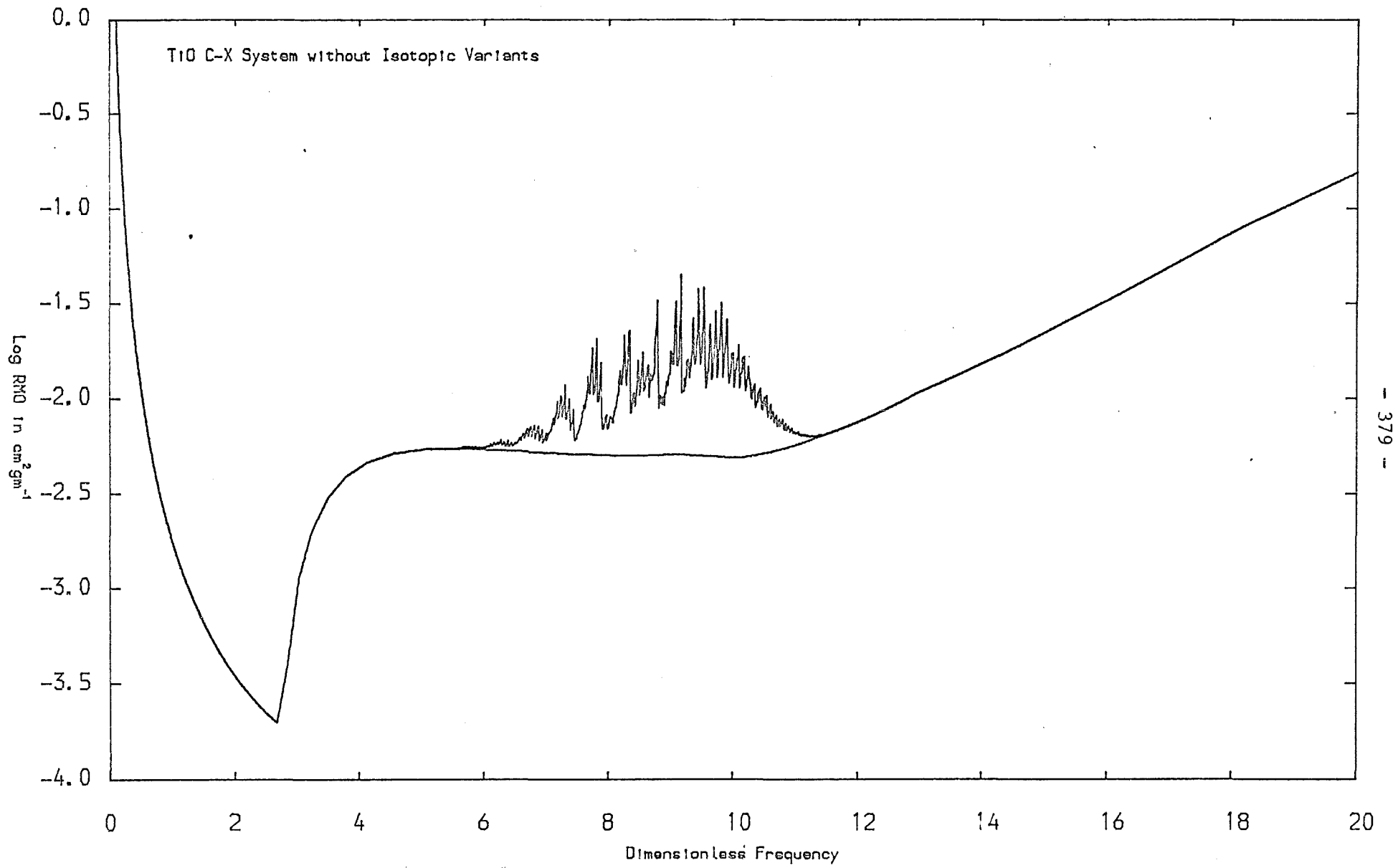
at Log T = 3.5 and Log ρ = -8

<u>Molecule</u>	<u>Ab. Abundance</u>	<u>Fr. Abundance</u>
Ti ⁴⁶ O ¹⁶	2.90090E+06	7.91020E-02
Ti ⁴⁷ O ¹⁶	2.66325E+06	7.26217E-02
Ti ⁴⁸ O ¹⁶	2.70507E+07	7.37621E-01
Ti ⁴⁹ O ¹⁶	2.01590E+06	5.49697E-02
Ti ⁵⁰ O ¹⁶	1.95378E+06	5.32759E-02
Remaining forms	8.84643E+04	2.41225E-03
All Forms	3.66729E+07	

Table (7.25) to Show the Isotope Effect of the TiO α -System

	<u>Con. Alone</u>	<u>Without Isp.</u>	<u>With Isp.</u>
ΣK for u = 5 to 6	6.95670E+10	6.91210E+10	6.93354E+10
ΣK for u = 6 to 7	5.09290E+10	4.49843E+10	4.56555E+10
ΣK for u = 7 to 8	3.45094E+10	2.11746E+10	1.98330E+10
ΣK for u = 8 to 9	2.12651E+10	9.49404E+09	7.25427E+09
ΣK for u = 9 to 10	1.23194E+10	3.64956E+09	2.52078E+09
ΣK for u = 10 to 11	6.61716E+09	3.52894E+09	3.49121E+09
ΣK for u = 11 to 12	2.82051E+09	2.72639E+09	2.75736E+09
PMO	2.92128E-03	4.20785E-03	4.18460E-03
RMO	1.08995E-03	1.11014E-03	1.11196E-03

Fig. 7.30



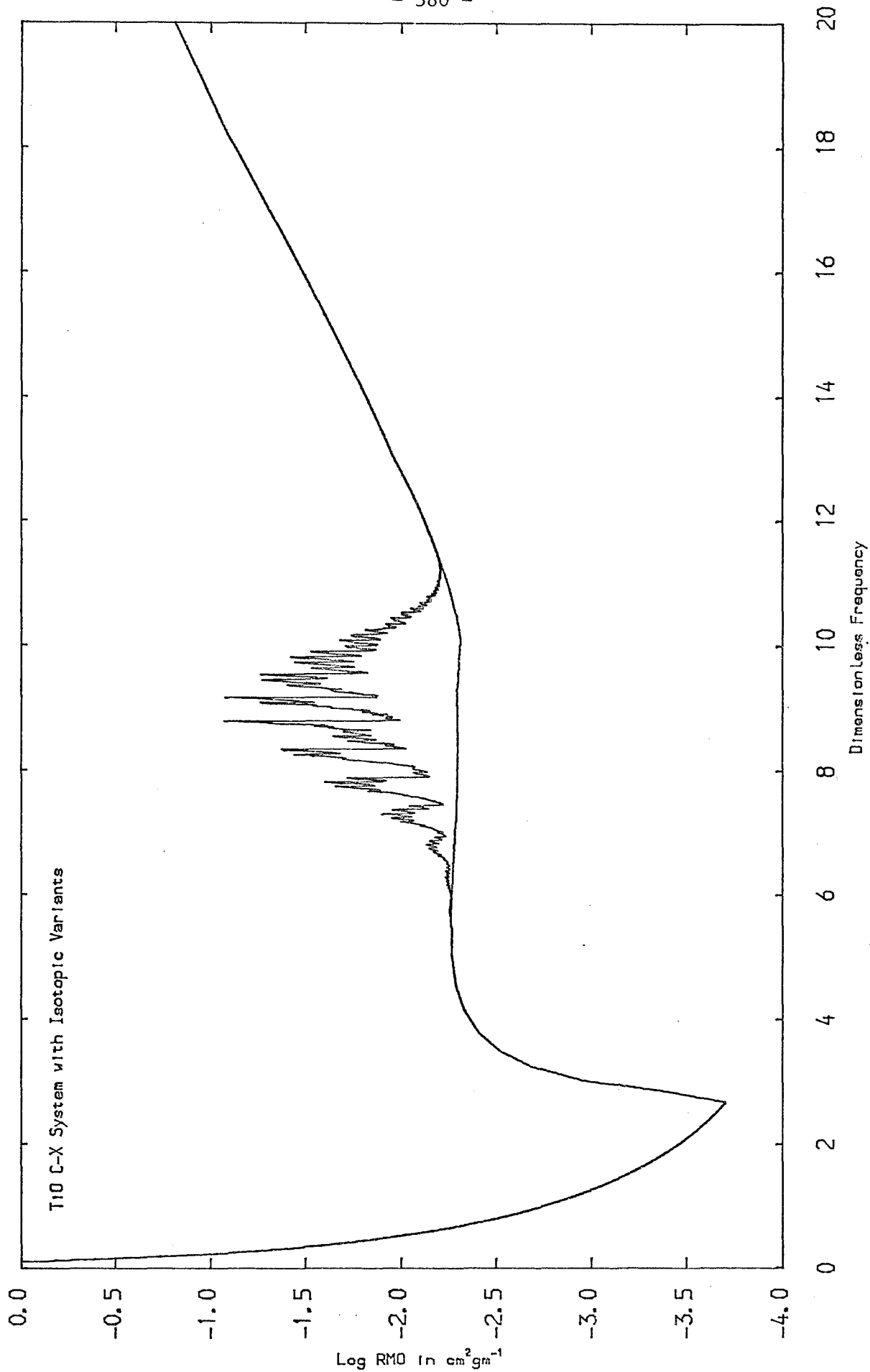


Fig. 7.31

Fig. 7.32

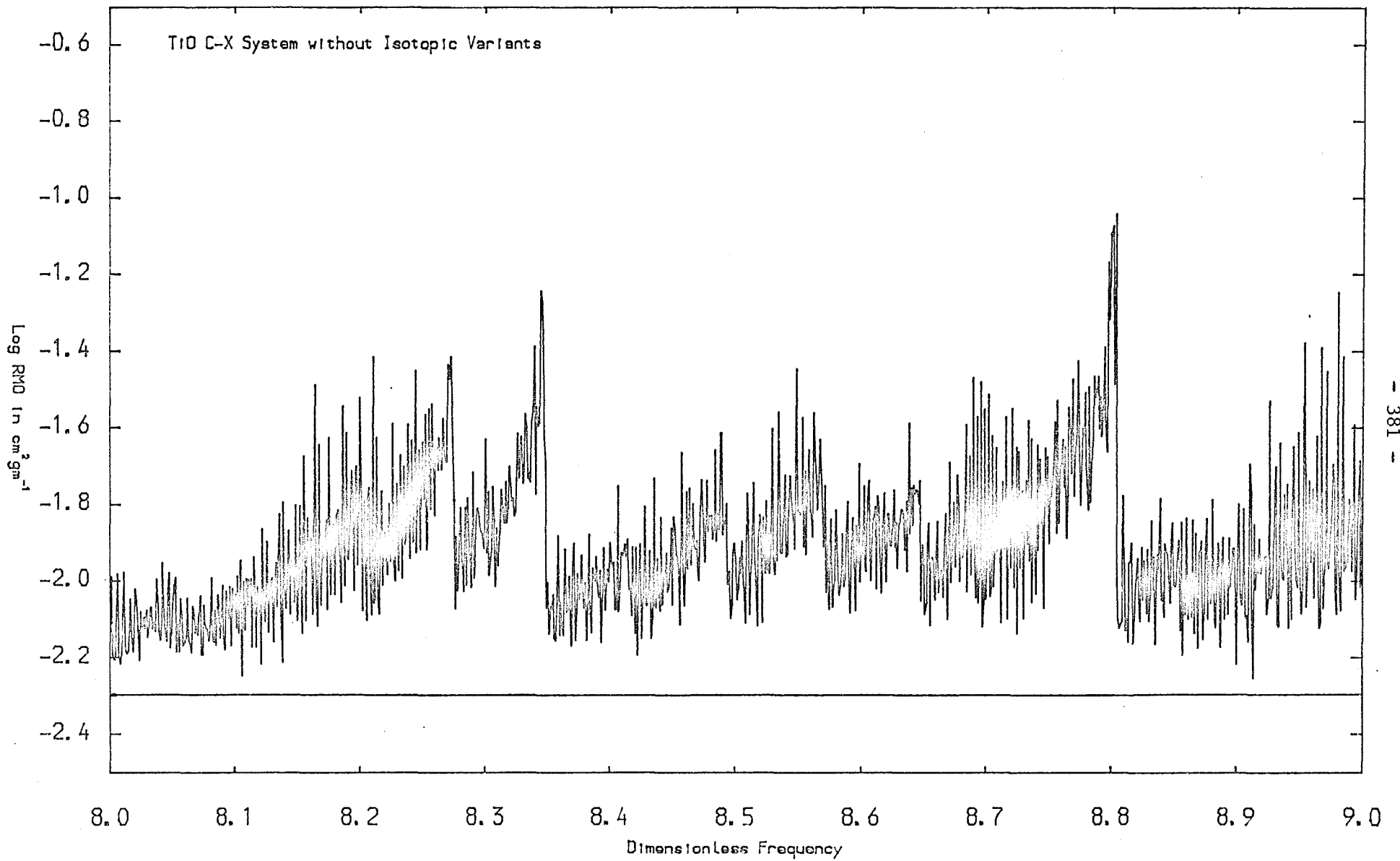


Fig. 7.33

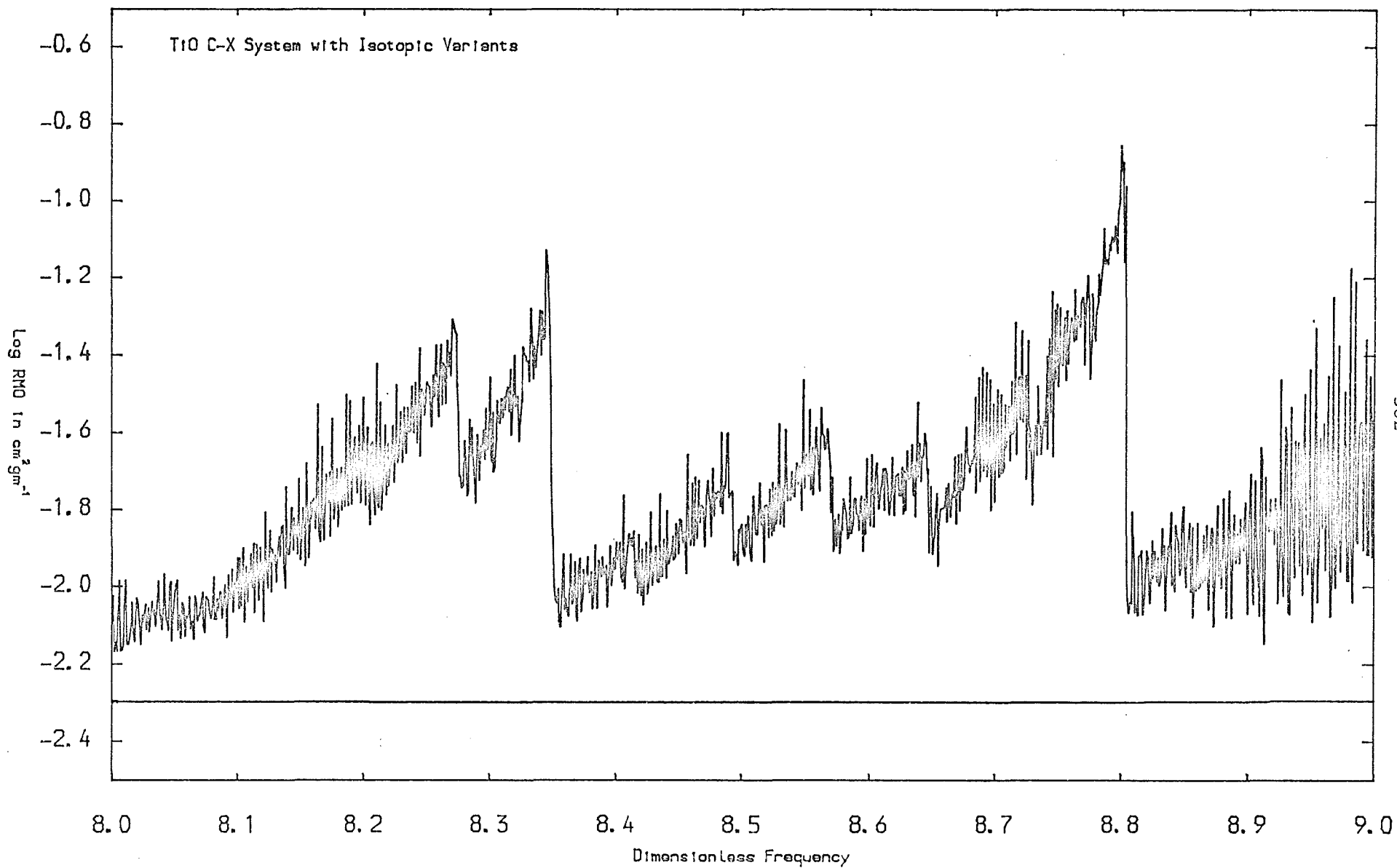


Fig. 7.34

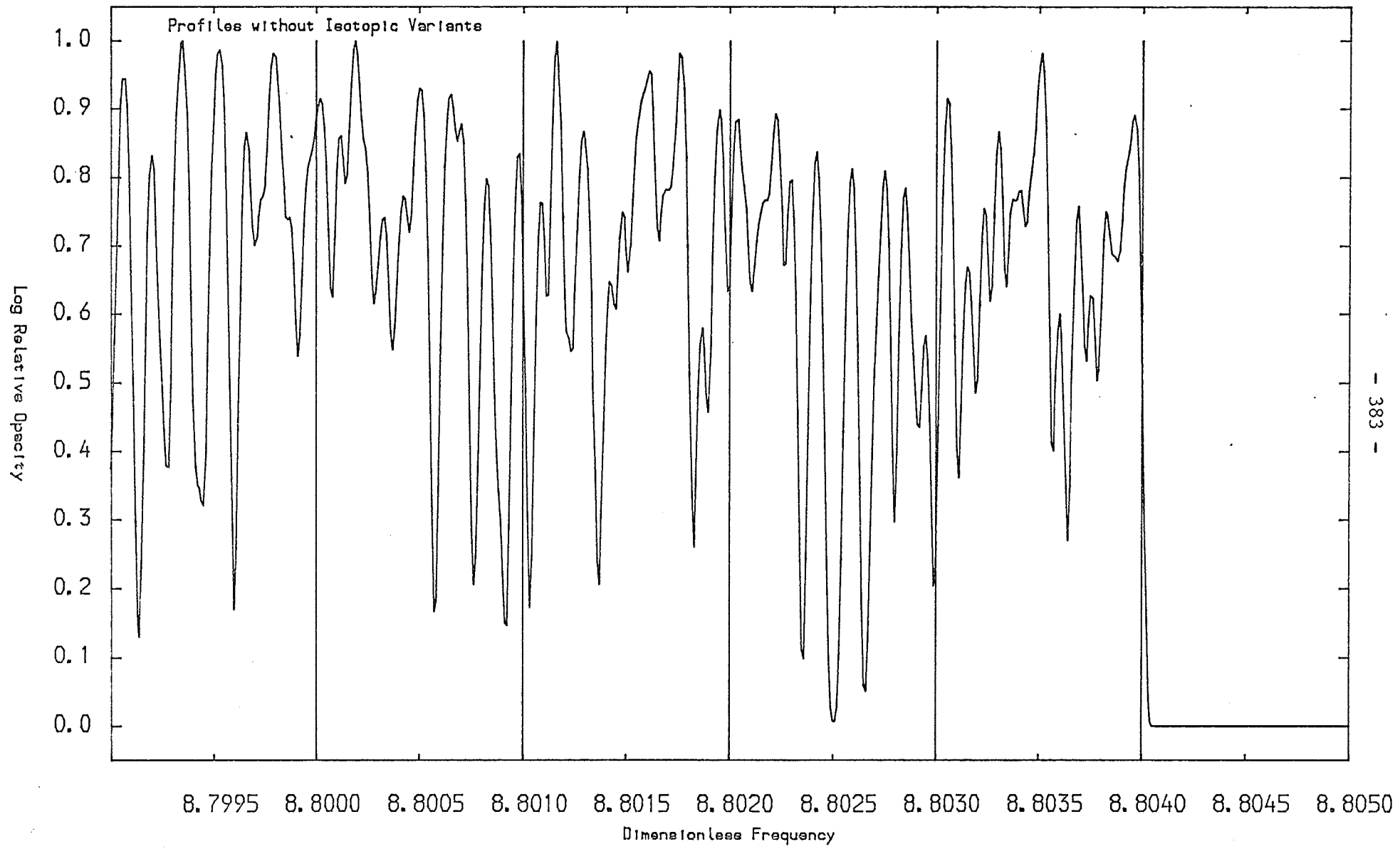


Fig. 7.35

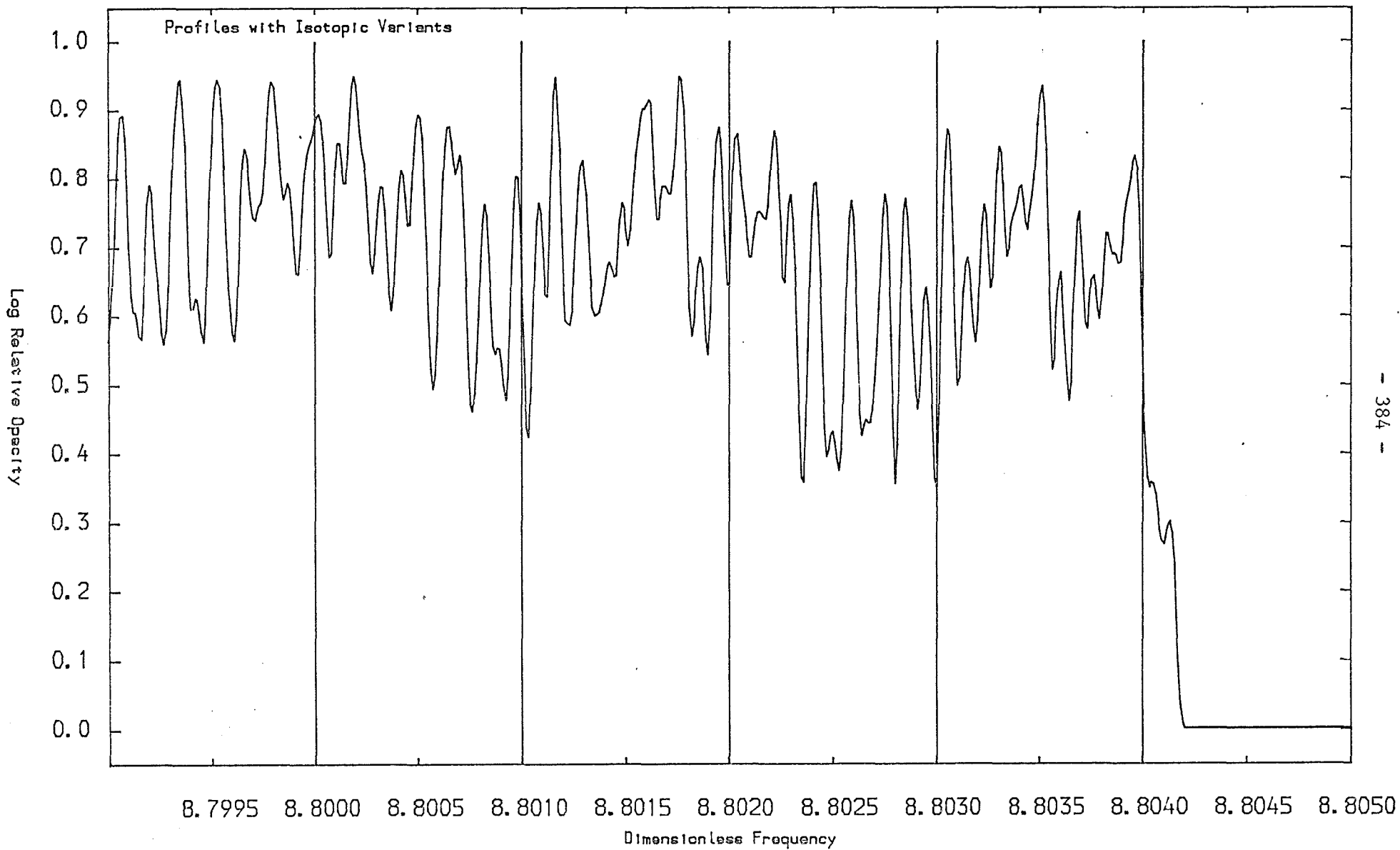
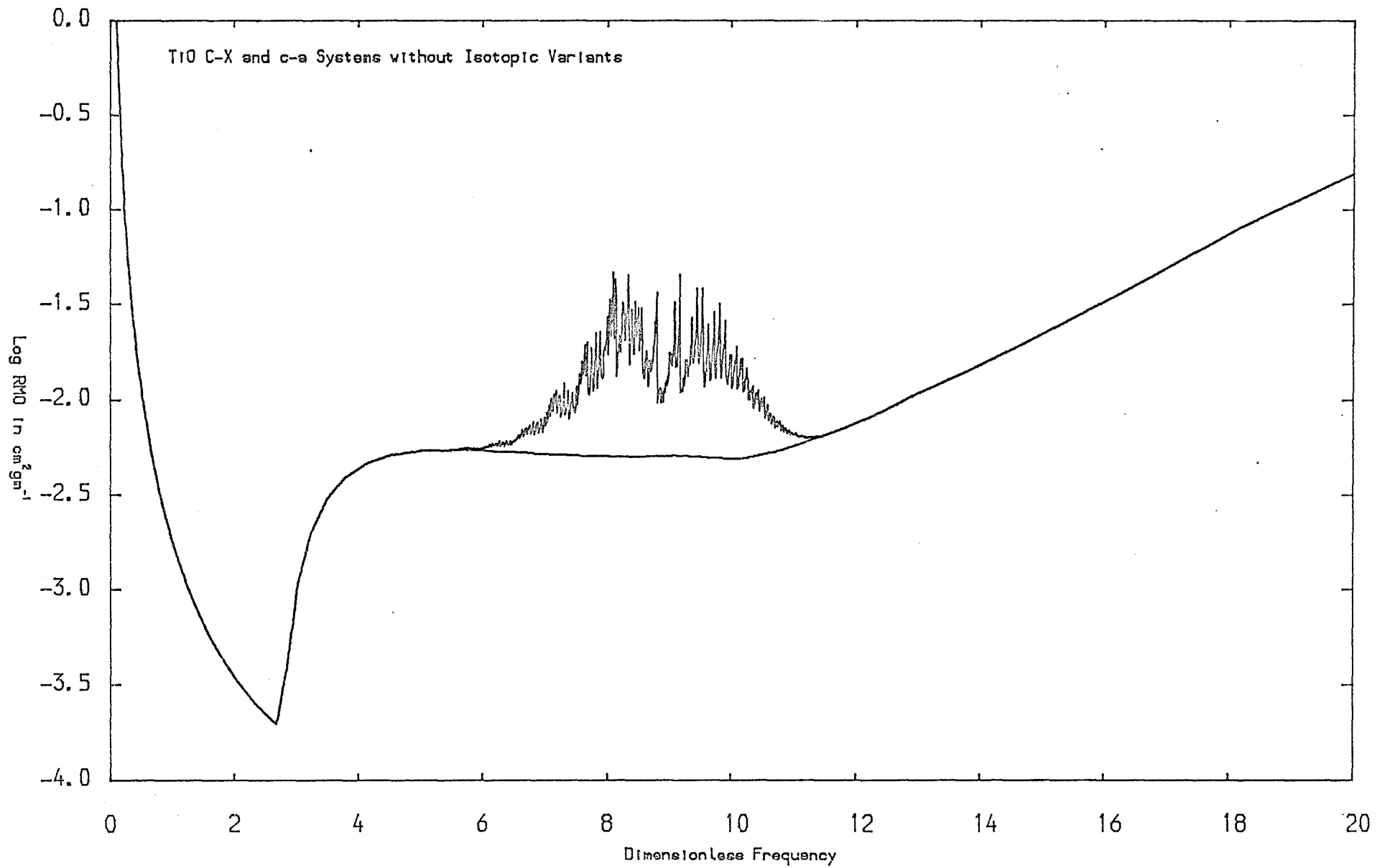


Fig. 7.36



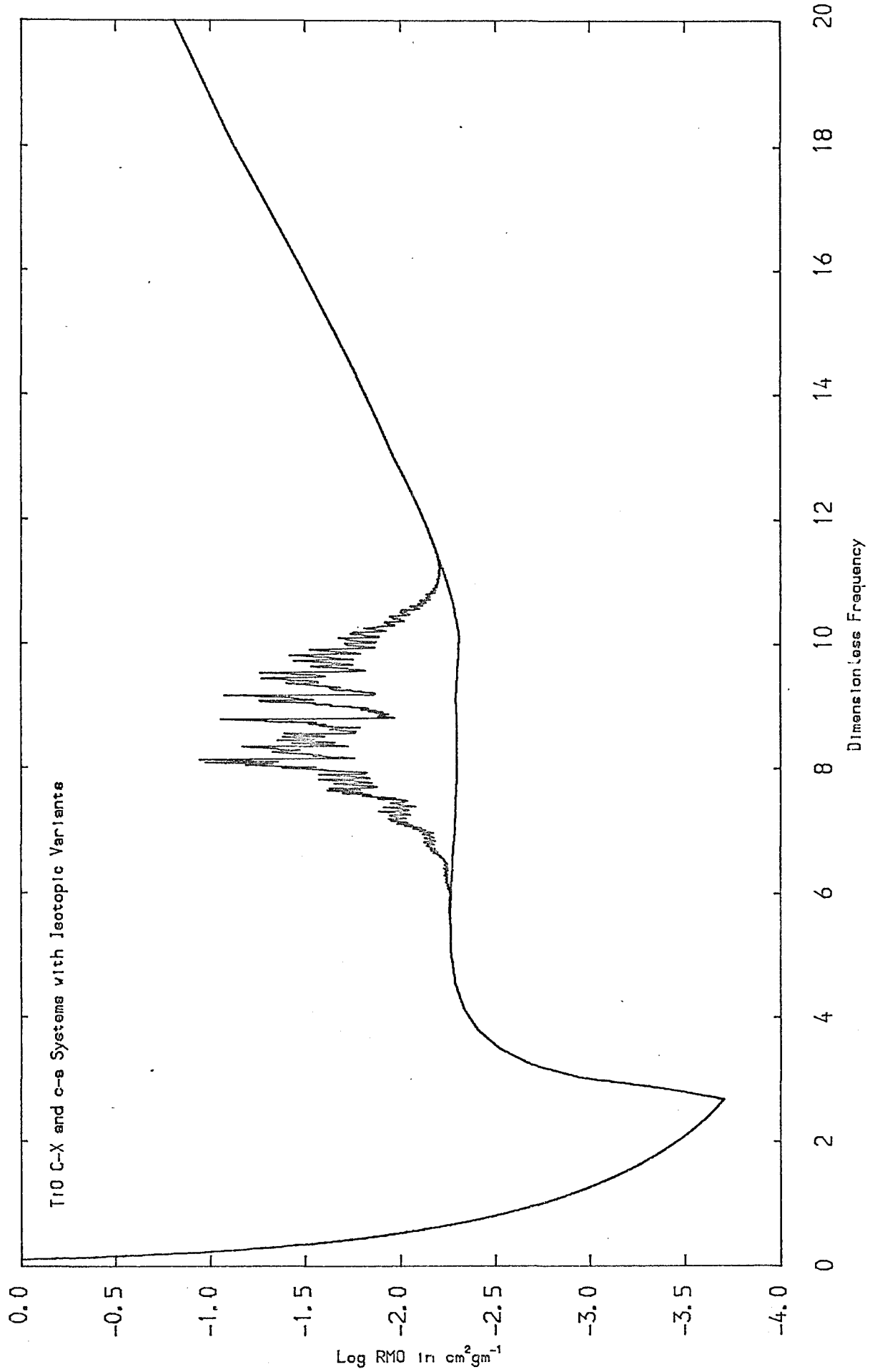


Fig. 7.37

We consider first the $C^3\Delta \leftarrow X^3\Delta$ system, i.e. the α -system, on its own. The constants for the lower state are given in section 7.3, for the upper state, we have:

$$\begin{aligned} C^3\Delta: \quad T'_e &= 19424.86, \quad \omega'_e = 838.26, \quad \omega'_e x'_e = 4.759, \quad \omega'_e y'_e = 0.0488, \\ B'_e &= 0.489888, \quad D'_e = 6.627 \times 10^{-7}, \quad \alpha'_e = 3.062 \times 10^{-3}, \quad \beta'_e = 9.6 \times 10^{-9}, \\ A' &= 48.599, \end{aligned}$$

together with $f_{e1}(\bar{\nu}_{00}) = 0.18$ from Feinberg and Davis (113).

Table (7.25) shows the isotope effect over the part of the spectrum where the bands occur, elsewhere there is just continuum. Note that the regions $u = 5$ to 6 and 6 to 7 each have 1000 bins and 30,000 sampling intervals, the remaining regions except the last each have 1000 bins and 20,000 sampling intervals, with the last region $u = 11$ to 12 having 800 bins and 14,400 sampling intervals.

It is seen that the isotope effect is greatest in the fifth region, where it increases the opacity by 31%. However, the overall effect on the RMO is very small, as the bands occur well away from the maximum of the Rosseland weighting function. Note that the PMO noticeably decreases, which can be explained in part by the fact that we have neglected the isotopic variants with O^{17} and O^{18} , but they are included in the total abundance when not considering isotopes. This probably also partly explains why the RMOs in the regions $u = 5$ to 6 , 6 to 7 and 11 to 12 on the fringes of the band system, actually

decrease when isotopes are allowed for. In these regions, the lines are very weak and differences between overlapping and non-overlapping lines are not great, so in splitting a very weak line into various isotopic components, its very small contribution to the RMO does not increase much, and is likely to decrease if some of the weaker components are neglected. Moreover, because we have a cut-off of 1% for the relative line strength, some lines just above the threshold could be ignored when split into their isotopic components.

Figure (7.30) shows the TiO α -system smeared to an effective bin width of 0.01, and shows very clearly indeed, that although TiO is an important monochromatic absorber, the effect on the RMO in this case is small because of the weighting function and the strong H⁻ continuum. Were these bands to occur in the region $u = 2$ to 4, the effect on the RMO would be large.

Figure (7.31) shows the same again with the isotopic variants allowed for, and figures (7.32) and (7.33) show a part of the band system plotted to the full resolution of bins for the two cases, with the continuum drawn underneath for comparison. Notice that in allowing for isotopes, not only are the fluctuations of the bins reduced, but the peaks actually become higher. This can be explained by comparing figures (7.34) and (7.35) for the two cases, which are plots of the actual profiles in the vicinity of the peak at $u = 8.8$, and is identified as being the head of the 0-0 band. In these two figures, only those profiles belonging to the 0-0 band are plotted, together with the bins as drawn. Notice that in the case where isotopes are allowed for, the fluctuation of the absorption is less,

and although the peaks of the individual profiles are reduced, as we have redistributed one quarter of $\text{Ti}^{48}\text{O}^{16}$ into the other isotopic forms, these other forms fill in the windows very efficiently, hence increasing the opacity in each bin. Note that the continuum is at $5.06 \times 10^{-3} \text{ cm}^2 \text{ gm}^{-1}$ and the top of the highest profile in figure (7.34) has an absorption of $3.64 \times 10^{-1} \text{ cm}^2 \text{ gm}^{-1}$, with figure (7.35) being on the same scale. For the profile widths, $\Delta u = 5.0 \times 10^{-6} u = 4.4 \times 10^{-5}$ at $u = 8.8$.

Finally, figures (7.36) and (7.37) show the plots as for figures (7.30) and (7.31) with the addition of the $c^{1\bar{\Phi}} \leftarrow a^1\Delta$ system, i.e. the β -system, on the basis of the following constants:

$$\begin{aligned} a^1\Delta: \quad T_e'' &= 577.22, \quad \omega_e'' = 1016.30, \quad \omega_e'' x_e'' = 3.93, \quad B_e'' = 0.53620, \\ D_e'' &= 5.94 \times 10^{-7}, \\ c^{1\bar{\Phi}}: \quad T_e' &= 18516.81, \quad \omega_e' = 917.55, \quad \omega_e' x_e' = 4.42, \quad B_e' = 0.52147, \\ D_e' &= 4.57 \times 10^{-7}, \end{aligned}$$

together with the band oscillator strength $f_{00} = 0.249$ from Feinberg and Davis (114). It is seen that the β -system is entirely overlapped by the α -system, and again there is a marked difference between the cases with and without isotopic variants.

We now consider the importance of H_2O as an opacity source in late-type stars. Table (7.26) lists the reduced band strengths for the various progressions together with the band types. As discussed in chapter 5, progressions of difference bands are also generated. Note that the first entry is for the pure rotation bands, the reduced band strengths being obtained from (5.2.9) and (5.3.18), hence:

$$\begin{pmatrix} S_0 \\ \bar{\nu}_0 \end{pmatrix} = \frac{8\pi^3}{3h} \cdot \mu_0^2 \quad (7.5.1)$$

with $\mu_0 = 1.87D = 1.87 \times 10^{-18}$ esu-cgs from Ludwig et al. (97). Being pure rotation, S_0 and $\bar{\nu}_0$ are of course not individually defined quantities.

Table (7.26) of Reduced Band Strengths of Water

Δv_1	Δv_2	Δv_3	$(S_0/\bar{\nu}_0)$	Type
0	0	0	4.36400E-08	B
0	0	1	6.39800E-11	A
0	0	2	2.05320E-14	B
0	1	0	2.00080E-10	B
0	1	1	5.10860E-12	A
0	1	2	4.00800E-15	B
0	2	0	6.27610E-13	B
0	2	1	2.46730E-13	A
0	3	0	1.28830E-15	B
0	3	1	1.29230E-14	A
0	4	1	1.46730E-16	A
1	0	0	2.97560E-12	B
1	0	1	3.09730E-12	A
1	1	0	1.05080E-13	B
1	1	1	1.69980E-13	A
1	2	0	1.56620E-14	B
2	0	0	2.20820E-13	B
2	1	0	1.23510E-15	B

Fig. 7.38

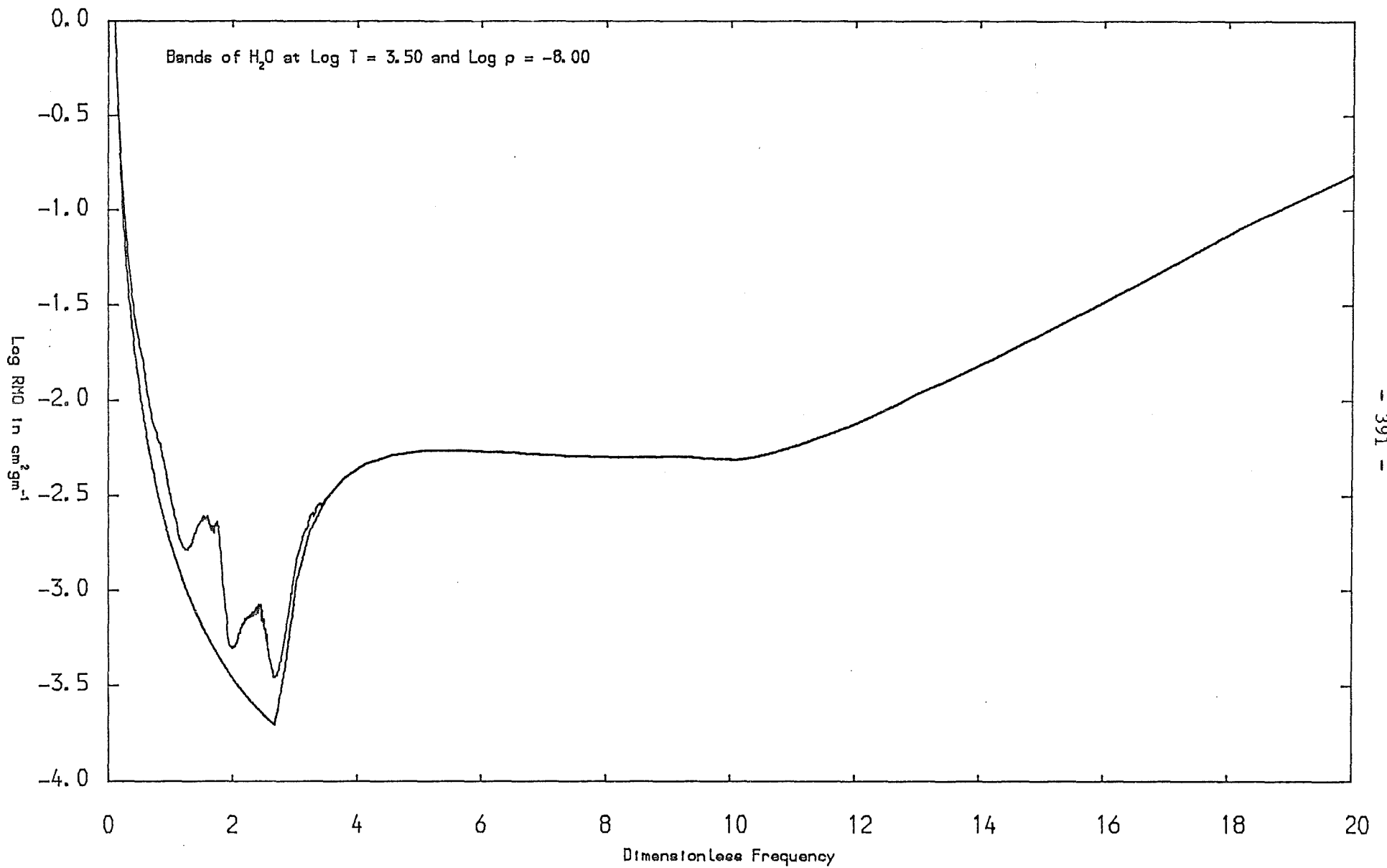
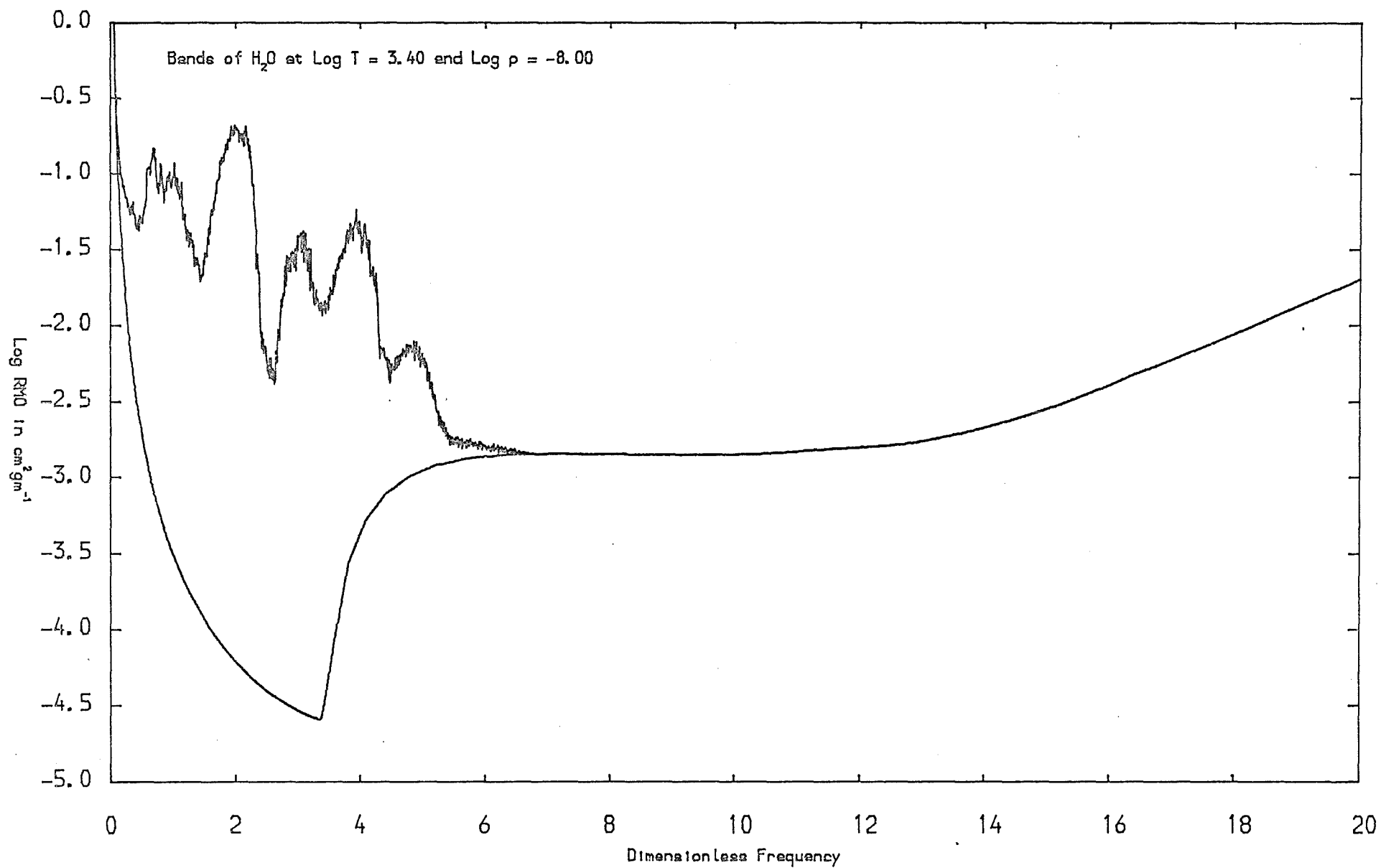


Fig. 7.39



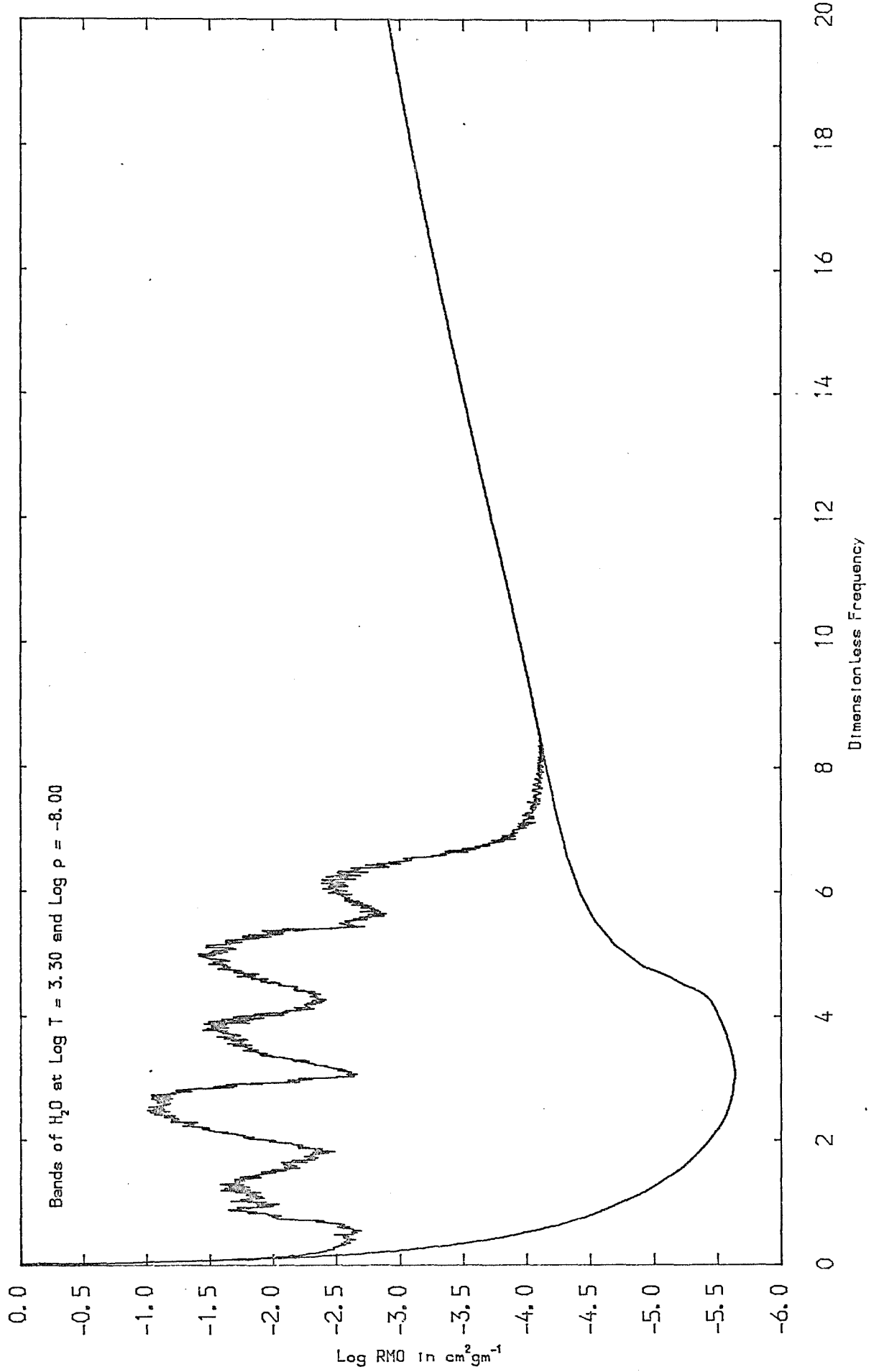


Fig. 7.40

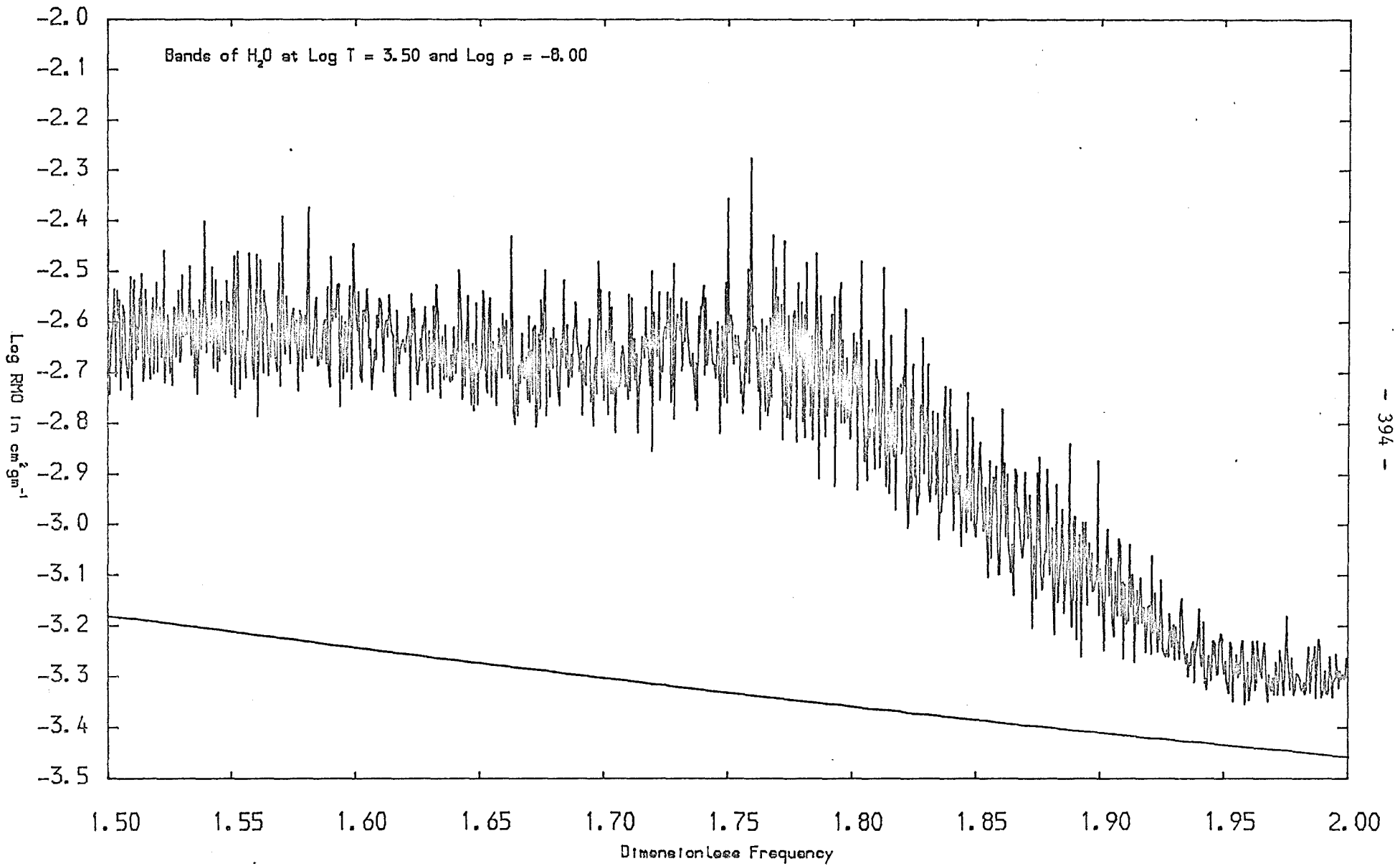


Fig. 7.41

All computations were performed with 2000 bins and 100,000 sampling intervals in each of the regions $u = 0$ to 1 and 1 to 2, 1600 bins and 73,600 sampling intervals in the region $u = 2$ to 3, 1000 bins and 50,000 sampling intervals in each of the regions $u = 3$ to 4 and 4 to 5, 1000 bins and 30,000 sampling intervals in each of the regions $u = 5$ to 6 and 6 to 7, and thereafter to $u = 11$, 1000 bins and 20,000 sampling intervals for each $\Delta u = 1$ region.

From table (7.5) at $\log T = 3.5$ and $\log \rho = -8$, H_2O has an abundance of $6.93065 \times 10^9 \text{ cm}^{-3}$, and is one of the more abundant species. The effect on the total RMO is to increase it from the continuum value of 1.08195×10^{-3} to 1.90432×10^{-3} , in $\text{cm}^2 \text{ gm}^{-1}$, which is an increase of nearly a factor of two. An examination of figure (7.38) clearly shows why this is, with the trough longer in wavelength than the H^- absorption threshold, being partially filled in. With the same density but a drop in temperature to $\log T = 3.4$, the abundance of H_2O has increased to 8.41897×10^{11} (see table (7.4)), and the effect on the RMO being an increase from 1.05120×10^{-4} to 3.39139×10^{-3} , which is a very much larger change than before. Figure (7.39) shows this effect in a spectacular way, with the trough being completely filled in. Finally, at $\log T = 3.3$ with the same density, the abundance has increased to 1.24538×10^{12} (see table (7.3)), and the effect on the RMO is to increase it from 5.13515×10^{-6} to 4.90044×10^{-4} ; though figure (7.40) is not much different from the previous one. In the figures (7.38-40), the smearing has been increased to an effective bin width of 0.01. Figure (7.41) plotted to the full resolution of

bins, shows a part of the absorption of the first case, and it can be seen that even in that case, no bins go down to the continuum, indicating a great deal of absorption. Note that we have lumped all the isotopic forms of H₂O into the most abundant form, however, because there are no windows, isotopic effects are expected to be small.

In dropping down in temperature, the CPU time increases substantially, being approximately 20 minutes, 2 hours and 2 hours 40 minutes respectively for the three cases.

The other triatomic molecule which we discuss in detail in this work is CO₂, and accordingly an example of its spectrum is given in figure (7.42) for log T = 3.4 and log ρ = -8, with the bins and sampling intervals set up in the same way as for the previous examples of H₂O. The reduced band strengths in cm³/sec/absorber calculated from the data given in McClatchey et al. (88) is given here in table (7.27).

Table (7.27) of Reduced Band Strengths of Carbon Dioxide

Δv_1	Δv_2	Δv_3	$(S_o/\bar{\gamma}_o)$
0	0	1	1.36050E-09
0	0	3	7.13960E-15
0	1	0	4.28750E-10
0	1	2	2.49310E-16
1	0	1	1.34460E-11
0	2	1	9.53930E-12

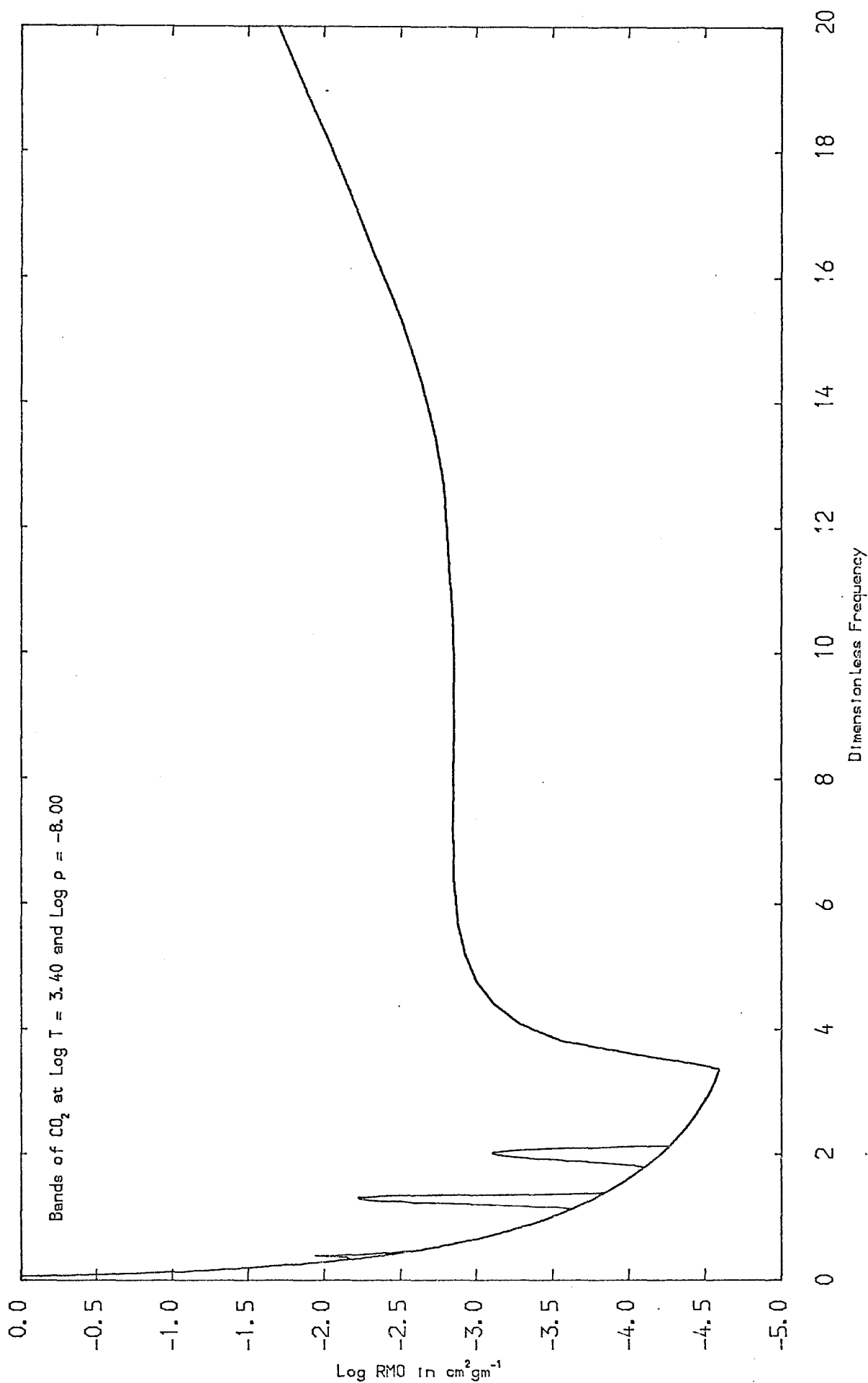


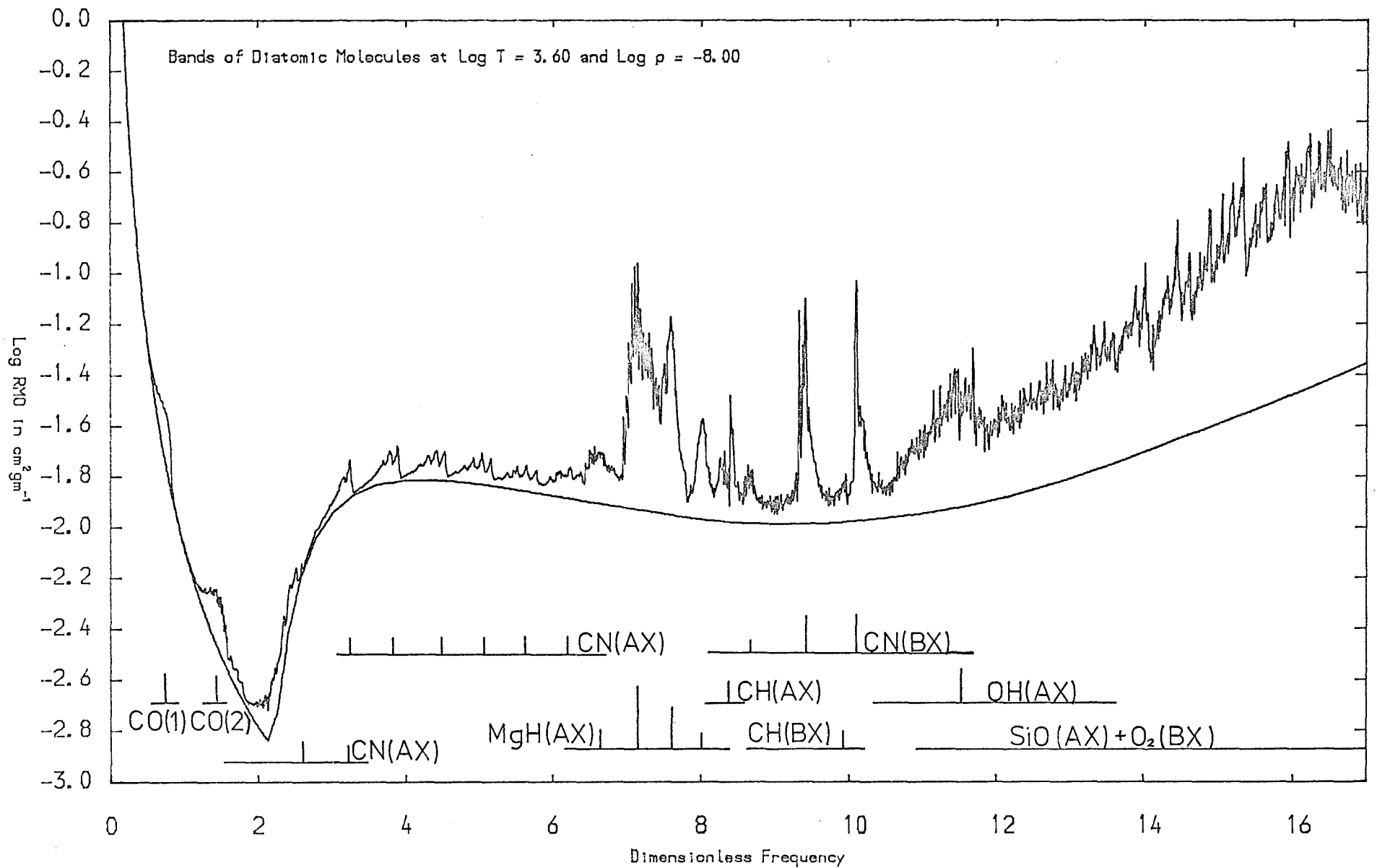
Fig. 7.42

As seen from table (7.4), the abundance of CO_2 is much lower than for H_2O , and this factor combined with the fact that CO_2 absorbs over a more restricted region of the spectrum than H_2O causes the total RMO to increase by a modest amount from $1.05120 \times 10^{-4} \text{ cm}^2 \text{ gm}^{-1}$ to 1.11651×10^{-4} . Note that the total CPU time is about 28 minutes.

Finally in this section, figure (7.43) is an example of a spectrum with many diatomic molecules, including their isotopic variants. The grid point with $\log T = 3.6$ and $\log \rho = -8$ was chosen because a large number of bands due to different molecules show up. Some of the features on this plot are identified by the molecule and its band system in parenthesis; the two states are identified for electronic transitions, with a single number indicating a progression of vibration-rotation bands. A full list of all the band systems of the diatomic molecules that are considered in our calculations is given in the appendices, though in practice the absorption due to many bands may not actually be computed because of molecules having low abundances, or initial excited electronic states having a small population.

Note that the RMO is increased from $7.2217 \times 10^{-3} \text{ cm}^2 \text{ gm}^{-1}$ to 9.17911×10^{-3} with a total CPU time of about 18 minutes. The same sampling and bin configuration is used as for the previous examples of H_2O and CO_2 , with the regions $u = 11$ to 17 having 800 bins and 14400 sampling intervals for each $\Delta u = 1$ region, and the whole spectrum is plotted with an effective bin size of 0.01, i.e. 1700 effective bins across the whole spectrum.

Fig. 7.43



Because of the excessive demands of processor time, it was not considered feasible to carry out any calculations with both diatomic and triatomic molecules together. However, in the next section, tables are given for the opacities of diatomic molecules with continuum covering many grid points in the T - ρ plane, and a few examples of H_2O and continuum, and CO_2 and continuum, considered separately. In all cases the bin and grid configuration is the same as for the example just discussed, and the effect of pressure-induced H_2 - H_2 and H_2 -He opacity is included.

To aid comparison with the work from other sources, the following table gives the conversions from dimensionless frequency $u = h\nu/kT$ to wavelength λ in microns for several temperatures. To convert wavelength to dimensionless frequency, simply substitute λ for u in the first column and read off the values in the other columns as u .

Table (7.28) of Conversions between u and λ in Microns

Log T	3.2	3.3	3.4	3.5	3.6	3.7	3.8
				or u			
1	9.078	7.211	5.728	4.550	3.614	2.871	2.280
2	4.539	3.606	2.864	2.275	1.807	1.435	1.140
3	3.026	2.404	1.909	1.517	1.205	0.957	0.760
u 4	2.270	1.803	1.432	1.137	0.904	0.718	0.570
or 5	1.816	1.442	1.146	0.910	0.723	0.574	0.456
λ 10	0.908	0.721	0.573	0.455	0.361	0.287	0.228
15	0.605	0.481	0.382	0.303	0.241	0.191	0.152
17	0.534	0.424	0.337	0.268	0.213	0.169	0.134
20	0.454	0.361	0.286	0.227	0.181	0.144	0.114
$u\lambda=hc/kT=$	9.078	7.211	5.728	4.550	3.614	2.871	2.280

7.6 Comparisons of Abundances and Opacities and Tables of Thermodynamic Quantities

In this final section of chapter 7, some further results are presented in the form of tables and diagrams, and discussion.

Figure (7.44) is a plot of the log of the abundances of some of the molecules in tables (7.2-8) for the grid points $\log T = 3.2$ to 3.8 with $\log \rho = -8$ in all cases. To prevent too much congestion, the figure is limited to the 15 molecules H_2 , C_2 , N_2 , O_2 , OH, NH, CH, CN, CO, NO, SiO, SH, TiO, H_2O and CO_2 . Though the figure is only approximate, as smooth curves were drawn by eye through the tabulated points, it does give a good representation of how the abundances vary with temperature. Note in particular that as CO has a very high dissociation potential, its abundance stays essentially constant to a high temperature and then falls rapidly. On the other hand many molecules with fairly low dissociation potentials like OH, have low abundances at low temperatures but increase to a maximum at some intermediate temperature before falling again, due to the change in availability of the constituent atoms by the dissociation of some more abundant molecules.

Figure (7.45) is a repeat of the continuous absorption plotted as for figure (7.1) at $\log T = 3.2$ and $\log \rho = -8$ drawn as a solid curve, with for comparison the same without pressure-induced H_2-H_2 and H_2-He opacity drawn as the dash-dotted curve, and that computed by Nordlund

(115) as the dotted curve with the pressure-induced opacity included. It is immediately seen how important the pressure-induced opacity can be at some grid points, as discussed at the end of section 7.2.

Table (7.29) gives the log of the computed RMO and PMO in $\text{cm}^2\text{gm}^{-1}$ for the grid points $\log T = 3.2$ to 3.8 and $\log \rho = -14$ to -2 , for all the diatomic molecules considered in the band calculations, together with their isotopic variants and the continuum. Note that in comparing with table (7.1), the total effect of the diatomic molecules on the RMO is modest at most, though the PMO may be increased by many orders of magnitude. Because of the negligible molecular abundances towards the upper right hand corner of table (7.29), the values there are essentially for the continuum on its own.

Table (7.30) gives the comparisons of the log of the RMO for a number of different cases covering a few grid points. For each grid point the four entries are respectively H_2O and continuum, CO_2 and continuum, the diatomic molecules including their isotopic variants and continuum, and continuum alone. Note that for H_2O and CO_2 , the isotopic variants have been added to the most abundant form for each. It is seen that for some grid points, H_2 has a far greater effect on the RMO than either CO_2 or all the diatomic molecules together. Table (7.31) is arranged in the same way as before for the corresponding PMOs.

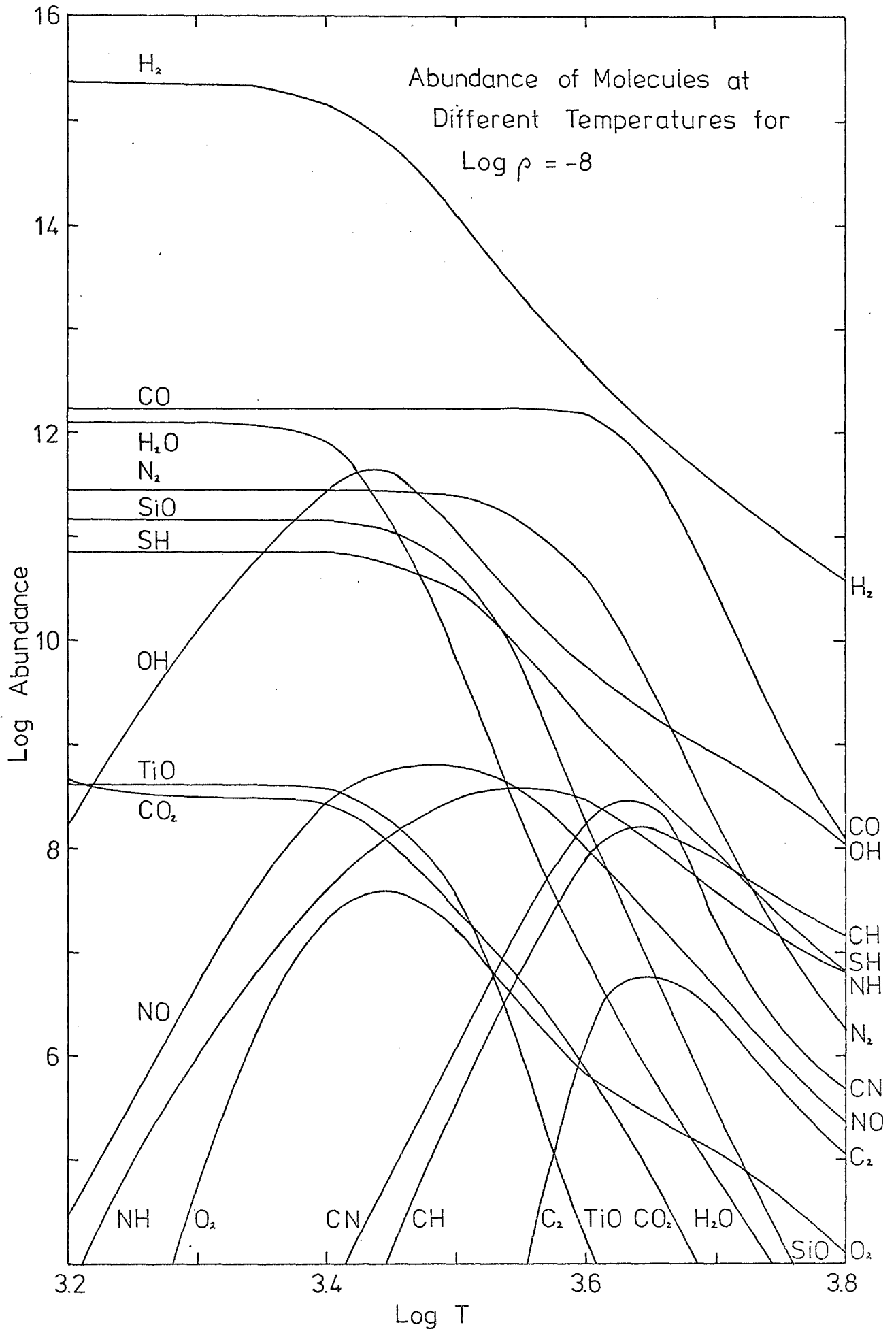


Fig. 7.44

Fig. 7.45

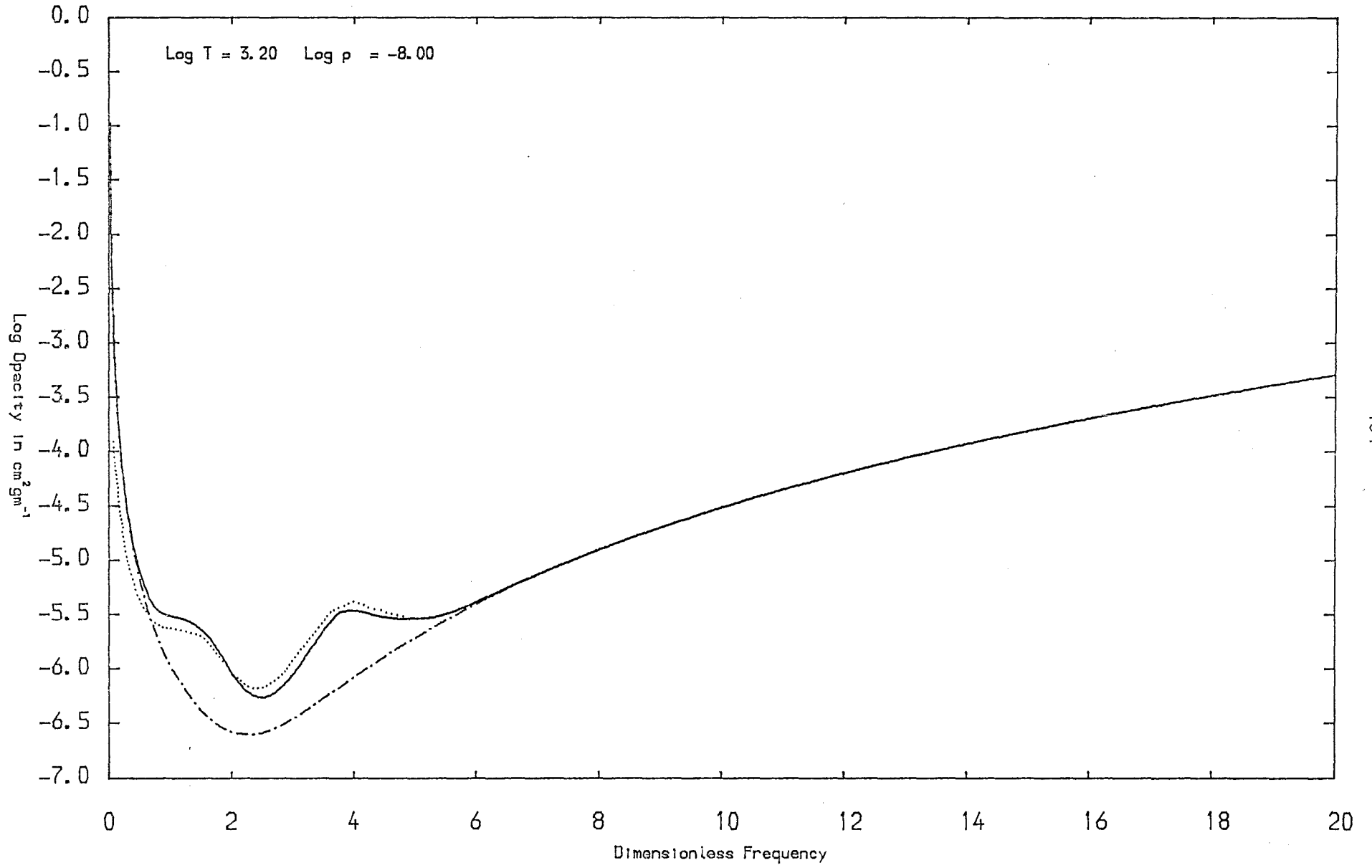


Table (7.29) of Log RMO and Log PMO for Continuum + Diatomic Molecules

T	1585	1995	2512	3162	3981	5012	6310
Log T	3.2	3.3	3.4	3.5	3.6	3.7	3.8
Log R							
-14	-5.1487 -0.5313	-4.5419 -0.7280	-3.7707 -0.9535	-3.4323 -2.4158	-2.4662 -2.4749	-0.7264 -0.7271	0.3991 0.3988
-13	-5.4057 -0.5354	-4.6578 -0.7256	-4.0151 -0.9533	-3.4102 -1.6677	-2.8682 -2.8781	-1.2104 -1.2126	0.1431 0.1417
-12	-5.6467 -0.5368	-4.7840 -0.7199	-4.2461 -0.9526	-3.4313 -1.2963	-3.1783 -3.1508	-1.6894 -1.6949	-0.2527 -0.2561
-11	-5.8100 -0.5372	-4.8872 -0.7120	-4.3339 -0.9466	-3.5201 -1.2003	-3.2962 -2.9855	-2.1400 -2.1497	-0.6804 -0.6800
-10	-5.9504 -0.5373	-5.0544 -0.7182	-4.2742 -0.9244	-3.5506 -1.1863	-3.1412 -2.2735	-2.4672 -2.4744	-1.0487 -1.0176
-9	-5.9727 -0.5373	-5.1888 -0.7171	-4.1179 -0.8743	-3.3718 -1.1567	-2.6676 -1.6309	-2.3747 -2.3375	-1.1573 -1.0960
-8	-5.6329 -0.5373	-5.0250 -0.7027	-3.8521 -0.7711	-2.8722 -0.9372	-2.0372 -1.2594	-1.8314 -1.7415	-0.8887 -0.8384
-7	-5.0161 -0.5371	-4.5248 -0.6582	-3.4914 -0.5418	-2.2624 -0.3726	-1.3985 -0.6559	-1.0273 -0.9099	-0.4461 -0.3823
-6	-4.4407 -0.5366	-3.9574 -0.5471	-2.9958 -0.1863	-1.7728 0.2126	-0.7916 0.2361	-0.2120 -0.0406	0.1096 0.1874
-5	-3.9360 -0.5346	-3.3418 -0.3450	-2.3784 0.2159	-1.2726 0.7113	-0.2506 0.9677	0.5124 0.8621	0.7940 0.8815
-4	-2.6704 -0.5127	-2.0731 -0.0952	-1.1891 0.5833	-0.2884 1.1283	0.5213 1.4882	1.3012 1.6591	1.5828 1.6882
-3	-2.0611 -0.3953	-1.2909 0.1500	-0.4067 0.8695	0.4511 1.4398	1.1500 1.8327	1.8468 2.1180	2.2614 2.3865
-2	-1.4869 0.1021	-0.8097 0.4524	-0.0747 1.0709	0.7120 1.6280	1.3676 2.0351	1.9036 2.3296	2.5183 2.7380

Table (7.30) of Comparison of Log RMO for some Grid Points

Log T	3.3	3.4	3.5
Log R			
	-3.4605	-3.8462	-3.6429
-10	-5.1192	-4.3723	-3.6430
	-5.0554	-4.2742	-3.5506
	-5.1980	-4.3981	-3.6430
	-3.3095	-2.4696	-2.7203
-8	-5.0690	-3.9449	-2.9623
	-5.0250	-3.8521	-2.8722
	-5.1409	-3.9712	-2.9626
	-3.1970	-2.1694	-1.3051
-6	-4.0000	-3.0461	-1.8277
	-3.9574	-2.9958	-1.7728
	-4.0148	-3.0545	-1.8278

Table (7.31) of Comparison of Log PMO for some Grid Points

Log T	3.3	3.4	3.5
Log R			
	0.9710	-2.9801	-3.5825
-10	-3.5192	-4.0882	-3.5826
	-0.7182	-0.9244	-1.1863
	-4.8986	-4.1499	-3.5826
	0.8141	0.5711	-2.4317
-8	-3.5782	-3.1983	-2.5341
	-0.7027	-0.7711	-0.9372
	-4.7638	-3.2818	-2.5344
	-0.4609	-0.6516	-0.9009
-6	-3.3979	-2.7278	-1.4600
	-0.5471	-0.1863	0.2126
	-3.7966	-2.7514	-1.4602

Table (7.32) of Pressure and Internal Energy

	T	1000	1259	1585	1995	2512
	Log T	3.0	3.1	3.2	3.3	3.4
Log R						
-14		2.884E-03 -8.115E+11	6.795E-03 3.790E+11	1.680E-02 4.318E+12	4.132E-02 1.219E+13	1.021E-01 3.037E+13
-13		6.142E-03 -1.492E+12	1.091E-02 -1.347E+12	2.306E-02 -5.679E+11	5.347E-02 1.383E+12	1.175E-01 3.264E+12
-12		3.873E-02 -1.561E+12	5.197E-02 -1.523E+12	7.829E-02 -1.301E+12	1.703E-01 1.803E+11	2.711E-01 5.533E+11
-11		3.646E-01 -1.567E+12	4.623E-01 -1.542E+12	6.061E-01 -1.455E+12	1.155E+00 -4.254E+11	1.804E+00 2.755E+11
-10		3.623E+00 -1.568E+12	4.565E+00 -1.544E+12	5.807E+00 -1.496E+12	8.982E+00 -1.019E+12	1.685E+01 1.878E+11
-9		3.621E+01 -1.568E+12	4.559E+01 -1.545E+12	5.757E+01 -1.509E+12	7.833E+01 -1.314E+12	1.510E+02 -1.632E+11
-8		3.621E+02 -1.568E+12	4.558E+02 -1.545E+12	5.744E+02 -1.513E+12	7.423E+02 -1.422E+12	1.210E+03 -7.912E+11
-7		3.621E+03 -1.568E+12	4.558E+03 -1.545E+12	5.740E+03 -1.514E+12	7.288E+03 -1.457E+12	1.021E+04 -1.187E+12
-6		3.621E+04 -1.568E+12	4.558E+04 -1.545E+12	5.739E+04 -1.514E+12	7.244E+04 -1.469E+12	9.466E+04 -1.343E+12
-5		3.621E+05 -1.568E+12	4.558E+05 -1.545E+12	5.739E+05 -1.514E+12	7.231E+05 -1.472E+12	9.214E+05 -1.396E+12
-4		3.621E+06 -1.568E+12	4.558E+06 -1.545E+12	5.738E+06 -1.514E+12	7.226E+06 -1.473E+12	9.133E+06 -1.413E+12
-3		-- --	4.558E+07 -1.545E+12	5.738E+07 -1.514E+12	7.225E+07 -1.474E+12	9.106E+07 -1.418E+12
-2		-- --	4.557E+08 -1.545E+12	5.738E+08 -1.514E+12	7.223E+08 -1.474E+12	9.097E+08 -1.420E+12

Table (7.32) Continued

T	3162	3981	5012	6310	7943
Log T	3.5	3.6	3.7	3.8	3.9
Log R					
-14	2.543E-01 7.597E+13	6.361E-01 1.904E+14	1.595E+00 4.784E+14	4.004E+00 1.208E+15	1.005E+01 3.023E+15
-13	2.737E-01 7.887E+12	6.605E-01 1.941E+13	1.626E+00 4.845E+13	4.057E+00 1.253E+14	1.014E+01 3.126E+14
-12	4.672E-01 1.077E+12	9.042E-01 2.308E+12	1.934E+00 5.351E+12	4.495E+00 1.447E+13	1.104E+01 4.070E+13
-11	2.402E+00 3.954E+11	3.341E+00 5.968E+11	5.006E+00 1.010E+12	8.523E+00 2.465E+12	1.845E+01 1.025E+13
-10	2.174E+01 3.260E+11	2.771E+01 4.253E+11	3.570E+01 5.660E+11	4.767E+01 9.655E+11	7.699E+01 3.874E+12
-9	2.146E+02 3.101E+11	2.713E+02 4.066E+11	3.425E+02 5.184E+11	4.356E+02 7.205E+11	5.957E+02 1.811E+12
-8	2.096E+03 2.290E+11	2.705E+03 4.005E+11	3.410E+03 5.124E+11	4.303E+03 6.657E+11	5.562E+03 1.133E+12
-7	1.850E+04 -1.783E+11	2.682E+04 3.704E+11	3.406E+04 5.091E+11	4.294E+04 6.503E+11	5.452E+04 9.150E+11
-6	1.479E+05 -7.958E+11	2.519E+05 1.562E+11	3.386E+05 4.870E+11	4.288E+05 6.431E+11	5.417E+05 8.441E+11
-5	1.266E+06 -1.149E+12	2.069E+06 -4.348E+11	3.228E+06 3.227E+11	4.257E+06 6.160E+11	5.399E+06 8.165E+11
-4	1.185E+07 -1.284E+12	1.692E+07 -9.308E+11	2.701E+07 -2.236E+11	4.021E+07 4.234E+11	5.319E+07 7.609E+11
-3	1.158E+08 -1.329E+12	1.527E+08 -1.148E+12	2.184E+08 -7.604E+11	3.324E+08 -1.453E+11	4.849E+08 4.595E+11
-2	1.149E+09 -1.344E+12	1.469E+09 -1.224E+12	1.942E+09 -1.011E+12	2.705E+09 -6.500E+11	3.902E+09 -1.439E+11

Table (7.33) of CP and CV

Log R	T	1000	1259	1585	1995	2512
	Log T	3.0	3.1	3.2	3.3	3.4
-14		3.336E+10	1.232E+11	3.741E+11	9.877E+11	3.854E+12
		3.121E+09	6.531E+09	1.810E+10	2.419E+10	4.813E+10
-13		9.125E+08	2.421E+09	1.332E+10	1.416E+10	4.588E+10
		3.922E+08	8.216E+08	5.431E+09	2.717E+09	4.907E+09
-12		1.778E+08	2.827E+08	2.318E+09	2.547E+09	1.357E+09
		1.185E+08	1.919E+08	1.874E+09	1.886E+09	5.890E+08
-11		1.295E+08	1.514E+08	7.646E+08	4.744E+09	3.215E+08
		9.123E+07	1.104E+08	6.722E+08	3.896E+09	2.104E+08
-10		1.255E+08	1.329E+08	3.290E+08	3.126E+09	7.541E+08
		8.913E+07	9.610E+07	2.794E+08	2.638E+09	6.224E+08
-9		1.251E+08	1.291E+08	1.939E+08	1.267E+09	2.637E+09
		8.887E+07	9.277E+07	1.539E+08	1.108E+09	2.178E+09
-8		1.238E+08	1.281E+08	1.513E+08	5.111E+08	2.597E+09
		8.756E+07	9.183E+07	1.140E+08	4.426E+08	2.119E+09
-7		1.246E+08	1.276E+08	1.385E+08	2.566E+08	1.189E+09
		8.834E+07	9.141E+07	1.020E+08	2.111E+08	1.007E+09
-6		1.250E+08	1.279E+08	1.340E+08	1.751E+08	4.979E+08
		8.874E+07	9.172E+07	9.767E+07	1.360E+08	4.224E+08
-5		1.242E+08	1.280E+08	1.325E+08	1.492E+08	2.567E+08
		8.795E+07	9.183E+07	9.626E+07	1.121E+08	2.091E+08
-4		1.250E+08	1.275E+08	1.321E+08	1.403E+08	1.780E+08
		8.874E+07	9.131E+07	9.585E+07	1.038E+08	1.383E+08
-3		--	1.276E+08	1.321E+08	1.381E+08	1.531E+08
		--	9.141E+07	9.585E+07	1.018E+08	1.158E+08
-2		--	1.274E+08	1.321E+08	1.374E+08	1.454E+08
		--	9.120E+07	9.593E+07	1.012E+08	1.089E+08

Table (7.33) Continued

	T Log T	3162 3.5	3981 3.6	5012 3.7	6310 3.8	7943 3.9
Log R						
-14		1.520E+13 9.593E+10	5.930E+13 1.914E+11	2.275E+14 3.837E+11	5.702E+14 7.670E+11	1.943E+15 1.519E+12
-13		1.661E+11 9.693E+09	6.297E+11 1.924E+10	2.433E+12 3.893E+10	7.773E+12 8.339E+10	2.003E+13 1.524E+11
-12		3.277E+09 1.067E+09	9.337E+09 2.019E+09	3.072E+10 4.136E+09	1.134E+11 1.124E+10	2.498E+11 1.761E+10
-11		3.483E+08 2.010E+08	5.500E+08 2.946E+08	1.126E+09 5.535E+08	4.132E+09 2.142E+09	1.409E+10 6.647E+09
-10		1.935E+08 1.183E+08	2.053E+08 1.238E+08	2.600E+08 1.625E+08	7.787E+08 6.008E+08	4.495E+09 3.454E+09
-9		2.297E+08 1.547E+08	1.805E+08 1.107E+08	1.839E+08 1.128E+08	3.308E+08 2.459E+08	1.637E+09 1.372E+09
-8		6.529E+08 5.232E+08	1.865E+08 1.164E+08	1.736E+08 1.051E+08	2.187E+08 1.466E+08	6.486E+08 5.305E+08
-7		1.890E+09 1.507E+09	2.901E+08 2.055E+08	1.783E+08 1.092E+08	1.859E+08 1.166E+08	3.254E+08 2.426E+08
-6		1.591E+09 1.270E+09	8.969E+08 6.995E+08	2.283E+08 1.509E+08	1.797E+08 1.104E+08	2.215E+08 1.486E+08
-5		7.294E+08 6.021E+08	1.323E+09 1.011E+09	5.476E+08 4.056E+08	2.156E+08 1.387E+08	1.932E+08 1.223E+08
-4		3.417E+08 2.797E+08	7.474E+08 5.900E+08	9.286E+08 6.821E+08	4.485E+08 3.158E+08	2.291E+08 1.475E+08
-3		2.088E+08 1.650E+08	3.610E+08 2.889E+08	5.945E+08 4.504E+08	6.473E+08 4.559E+08	4.205E+08 2.825E+08
-2		1.655E+08 1.269E+08	2.175E+08 1.707E+08	3.126E+08 2.427E+08	4.145E+08 3.045E+08	4.426E+08 3.032E+08

Table (7.34) of Gamma0 and Gammal

T	1000	1259	1585	1995	2512
Log T	3.0	3.1	3.2	3.3	3.4
Log R					
-14	10.6893 1.3421	18.8596 1.2730	20.6696 0.9921	40.8254 1.3398	80.0645 1.3381
-13	2.3269 1.3712	2.9471 1.2337	2.4532 0.6981	5.2106 1.3099	9.3509 1.3595
-12	1.5002 1.4025	1.4734 1.2927	1.2364 0.9475	1.3501 0.9977	2.3030 1.4499
-11	1.4196 1.4099	1.3716 1.3524	1.1375 1.0922	1.2176 1.0613	1.5280 1.4399
-10	1.4085 1.4074	1.3830 1.3810	1.1773 1.1686	1.1848 1.0838	1.2115 1.1831
-9	1.4076 1.4076	1.3914 1.3910	1.2601 1.2579	1.1434 1.1009	1.2107 1.1140
-8	1.4137 1.4145	1.3946 1.3948	1.3279 1.3276	1.1548 1.1395	1.2258 1.1087
-7	1.4100 1.4101	1.3962 1.3963	1.3584 1.3583	1.2159 1.2107	1.1803 1.1207
-6	1.4082 1.4074	1.3946 1.3948	1.3718 1.3720	1.2871 1.2853	1.1788 1.1565
-5	1.4120 1.4121	1.3940 1.3938	1.3764 1.3766	1.3310 1.3303	1.2273 1.2191
-4	1.4081 1.4082	1.3966 1.3967	1.3779 1.3777	1.3518 1.3519	1.2868 1.2845
-3	-- --	1.3963 1.3962	1.3777 1.3776	1.3564 1.3564	1.3220 1.3209
-2	-- --	1.3973 1.3967	1.3772 1.3771	1.3582 1.3578	1.3353 1.3349

Table (7.34) Continued

	T	3162	3981	5012	6310	7943
Log T		3.5	3.6	3.7	3.8	3.9
Log R						
-14		158.4220 1.3367	309.8830 1.3357	592.9410 1.3298	743.3770 1.3280	1279.2900 1.3355
-13		17.1395 1.3477	32.7326 1.3411	62.4966 1.3198	93.2134 1.2489	131.4590 1.3350
-12		3.0709 1.4133	4.6250 1.3848	7.4284 1.3133	10.0838 1.0473	14.1836 1.2318
-11		1.7322 1.5502	1.8668 1.5128	2.0344 1.3866	1.9294 1.0014	2.1191 0.8757
-10		1.6364 1.6175	1.6585 1.6208	1.5999 1.5282	1.2961 1.1773	1.3013 1.0381
-9		1.4848 1.4784	1.6308 1.6267	1.6298 1.6218	1.3450 1.3286	1.1931 1.1298
-8		1.2479 1.2187	1.6020 1.6005	1.6518 1.6510	1.4916 1.4890	1.2227 1.2045
-7		1.2542 1.1444	1.4120 1.3997	1.6331 1.6321	1.5939 1.5932	1.3413 1.3351
-6		1.2526 1.1392	1.2822 1.2114	1.5125 1.5028	1.6278 1.6259	1.4900 1.4876
-5		1.2114 1.1574	1.3091 1.1762	1.3499 1.2902	1.5550 1.5431	1.5806 1.5771
-4		1.2213 1.2010	1.2667 1.1837	1.3615 1.2244	1.4201 1.3477	1.5527 1.5290
-3		1.2656 1.2582	1.2496 1.2162	1.3199 1.2228	1.4198 1.2752	1.4885 1.3796
-2		1.3038 1.3013	1.2744 1.2629	1.2879 1.2473	1.3612 1.2676	1.4596 1.3164

Table (7.35) of Gamma2 and Gamma3

T	1000	1259	1585	1995	2512
Log T	3.0	3.1	3.2	3.3	3.4
Log R					
-14	1.3330 1.3353	1.3297 1.3156	1.3106 1.2352	1.3327 1.3345	1.3327 1.3340
-13	1.3427 1.3499	1.3118 1.2932	1.1776 1.1053	1.3274 1.3231	1.3337 1.3401
-12	1.3865 1.3910	1.3008 1.2989	1.0787 1.0691	1.1216 1.1082	1.3650 1.3877
-11	1.4074 1.4081	1.3480 1.3492	1.0862 1.0867	1.0526 1.0531	1.4010 1.4121
-10	1.4073 1.4073	1.3794 1.3799	1.1494 1.1519	1.0521 1.0537	1.1443 1.1492
-9	1.4075 1.4075	1.3908 1.3908	1.2450 1.2476	1.0678 1.0699	1.0703 1.0731
-8	1.4134 1.4137	1.3944 1.3945	1.3214 1.3229	1.1104 1.1133	1.0655 1.0681
-7	1.4098 1.4099	1.3961 1.3962	1.3562 1.3568	1.1895 1.1929	1.0801 1.0831
-6	1.4082 1.4080	1.3947 1.3947	1.3710 1.3713	1.2742 1.2766	1.1213 1.1251
-5	1.4117 1.4118	1.3942 1.3941	1.3762 1.3763	1.3260 1.3270	1.1951 1.1990
-4	1.4080 1.4081	1.3965 1.3966	1.3778 1.3778	1.3498 1.3504	1.2716 1.2743
-3	-- --	1.3962 1.3962	1.3777 1.3777	1.3559 1.3560	1.3162 1.3173
-2	-- --	1.3972 1.3970	1.3773 1.3773	1.3580 1.3580	1.3335 1.3339

Table (7.35) Continued

	T 3162	3981	5012	6310	7943
Log T	3.5	3.6	3.7	3.8	3.9
Log R					
-14.	1.3327 1.3337	1.3327 1.3334	1.3325 1.3318	1.3323 1.3312	1.3327 1.3334
-13	1.3329 1.3366	1.3328 1.3348	1.3320 1.3289	1.3283 1.3087	1.3326 1.3332
-12	1.3460 1.3633	1.3375 1.3494	1.3297 1.3256	1.3045 1.2445	1.3227 1.3005
-11	1.4727 1.4976	1.4198 1.4473	1.3463 1.3567	1.2109 1.1744	1.1698 1.1271
-10	1.5972 1.6048	1.5901 1.6015	1.4879 1.5011	1.1851 1.1839	1.0859 1.0821
-9	1.4519 1.4602	1.6198 1.6224	1.6126 1.6161	1.3034 1.3093	1.0971 1.1000
-8	1.1678 1.1751	1.5877 1.5924	1.6485 1.6495	1.4725 1.4778	1.1645 1.1702
-7	1.0904 1.0949	1.3540 1.3659	1.6248 1.6276	1.5858 1.5885	1.3024 1.3100
-6	1.0878 1.0920	1.1471 1.1553	1.4656 1.4774	1.6186 1.6214	1.4673 1.4738
-5	1.1113 1.1159	1.1131 1.1195	1.2175 1.2304	1.5048 1.5177	1.5621 1.5675
-4	1.1657 1.1708	1.1276 1.1340	1.1506 1.1603	1.2666 1.2837	1.4816 1.4970
-3	1.2382 1.2420	1.1732 1.1796	1.1607 1.1693	1.1957 1.2088	1.2932 1.3128
-2	1.2927 1.2946	1.2376 1.2425	1.2036 1.2110	1.2073 1.2176	1.2451 1.2592

Table (7.36) of Chi T and Chi R

	T	1000	1259	1585	1995	2512
	Log T	3.0	3.1	3.2	3.3	3.4
	Log R					
-14		3.6287 0.1256	3.8191 0.0675	4.0149 0.0480	3.9076 0.0328	3.9558 0.0167
-13		2.2343 0.5893	2.7798 0.4186	3.9286 0.2846	3.2763 0.2514	3.5692 0.1454
-12		1.1961 0.9349	1.3894 0.8774	2.6221 0.7664	2.3909 0.7390	2.1159 0.6296
-11		1.0211 0.9932	1.0493 0.9861	1.5231 0.9603	3.5733 0.8717	1.2073 0.9424
-10		1.0021 0.9992	1.0067 0.9986	1.1584 0.9926	3.1476 0.9147	1.3844 0.9765
-9		1.0002 1.0000	1.0012 0.9997	1.0490 0.9982	1.9741 0.9629	2.6502 0.9201
-8		1.0005 1.0006	1.0005 1.0002	1.0153 0.9997	1.3480 0.9867	2.9972 0.9045
-7		1.0002 1.0001	1.0002 1.0001	1.0045 0.9999	1.1145 0.9958	2.0597 0.9495
-6		0.9999 0.9995	0.9999 1.0001	1.0015 1.0002	1.0365 0.9986	1.4022 0.9811
-5		1.0004 1.0001	0.9996 0.9999	1.0005 1.0001	1.0114 0.9995	1.1346 0.9933
-4		1.0002 1.0000	1.0001 1.0001	1.0001 0.9998	1.0041 1.0001	1.0437 0.9982
-3		-- --	1.0003 0.9999	0.9999 1.0000	1.0011 1.0000	1.0139 0.9992
-2		-- --	1.0003 0.9995	0.9998 0.9999	1.0003 0.9998	1.0040 0.9997

Table (7.36) Continued

T	3162	3981	5012	6310	7943
Log T	3.5	3.6	3.7	3.8	3.9
Log R					
-14	3.9806 0.0084	3.9931 0.0043	4.0011 0.0022	4.0037 0.0018	4.0029 0.0010
-13	3.7701 0.0786	3.8828 0.0410	3.9481 0.0211	4.0027 0.0134	3.9764 0.0102
-12	2.6236 0.4602	3.1062 0.2994	3.4901 0.1768	3.8589 0.1039	3.8096 0.0868
-11	1.3169 0.8949	1.5704 0.8104	1.9766 0.6816	2.7655 0.5190	3.6382 0.4132
-10	1.0402 0.9884	1.0699 0.9773	1.1434 0.9552	1.4625 0.9083	2.9268 0.7977
-9	1.0490 0.9957	1.0110 0.9975	1.0172 0.9951	1.1018 0.9878	1.8293 0.9469
-8	1.3825 0.9766	1.0152 0.9990	1.0031 0.9995	1.0271 0.9982	1.2893 0.9851
-7	2.4441 0.9125	1.1162 0.9913	1.0082 0.9994	1.0086 0.9996	1.0958 0.9954
-6	2.4974 0.9095	1.7169 0.9447	1.0666 0.9936	1.0091 0.9988	1.0325 0.9984
-5	1.7429 0.9555	2.3241 0.8985	1.4512 0.9558	1.0640 0.9924	1.0208 0.9978
-4	1.2747 0.9834	1.8602 0.9345	2.0284 0.8993	1.4056 0.9490	1.0950 0.9848
-3	1.0909 0.9941	1.3526 0.9733	1.7503 0.9264	1.8064 0.8982	1.4475 0.9268
-2	1.0293 0.9981	1.1216 0.9909	1.3217 0.9684	1.5457 0.9312	1.5995 0.9019

Finally, tables (7.32-36) give some values of computed thermodynamic quantities for the grid points $\log T = 3.0$ to 3.9 and $\log \rho = -14$ to -2 . As mentioned in section 7.2, the grid points for $\log \rho = -2$ and -3 with $\log T = 3.0$ are omitted because of problems with machine overflow and underflow. For each pair of entries in table (7.32), is given the total pressure in dyne cm^{-2} and the total internal energy in erg gm^{-1} respectively, with the contribution due to radiation included. The specific heats c_p and c_v (shown as CP and CV respectively) in $\text{erg gm}^{-1}\text{degree}^{-1}$ are given in the following table, with the remaining tables giving the adiabatic exponents γ , Γ_1 , Γ_2 and Γ_3 , together with χ_T and χ_ρ (shown respectively as Gamma0, Gammal, Gamma2, Gamma3, Chi T and Chi R).

For a given grid point (T, ρ) , the total pressure P and internal energy E are calculated, then in order to obtain the remaining quantities, $P+\delta P$ and $E+\delta E$ have to be calculated from the points $(T, \rho+\delta\rho)$ and $(T+\delta T, \rho)$, where in our calculations $\delta\rho = \rho/1000$ and $\delta T = T/1000$. The expressions for these thermodynamic quantities are given in an appendix. With the zero point for the internal energy defined as neutral unbound atoms, at low temperatures and high densities the total internal energy is negative due to the formation of negative ions and molecules, and large and positive at high temperatures and low densities due to ionization and the contribution of radiation. Also at low densities due to the dominance of radiation, γ tends to become large and Γ_1 , Γ_2 and Γ_3 tend to approach $4/3$. However, note the abnormally small values of Γ_1 for some of the

grid points with $\log T = 3.2$ and 3.3 . This appears to be a real effect, as in many of the columns the smallest values of f_1 are found in the vicinity of where E changes sign, i.e. where many of the molecules are undergoing dissociation.

8 SUMMARY.

As the title of this thesis suggests, we consider in some detail the theory necessary to calculate molecular opacities, and then illustrate this work with some results given in the previous chapter. Because of the restrictions of the computing resources at St. Andrews, it is unfortunately not possible to obtain exhaustive tabulations of opacities, particularly for triatomic molecules.

In the discussion in this final chapter of the thesis, we first summarise very briefly the results presented in chapter 7. In section 7.2, a table is given of the log RMO and log PMO for the continuous absorption alone for a number of grid points in the T - ρ plane, and for a few of these grid points the abundances of the atomic and molecular species are tabulated and the absorption coefficient is plotted against photon energy. A table is also given to show which atoms are important sources or sinks of electrons for three separate grid points. Section 7.3 gives some numerical examples of Hönl-London factors and vibrational matrix elements based on the theory discussed earlier in the thesis, together with plots to illustrate the band structure. In section 7.4, some numerical examples of the LSM, ILM and OSM, as discussed in chapter 6, are given for comparisons, with a number of plots included to illustrate the discussion. The isotope effect of CO, HCl and TiO is discussed in some detail with illustrations in section 7.5, where examples of the results of the computed band spectra of H₂O, CO₂ and of many diatomic molecules

together are also included. Finally in section 7.6, one example is given of the comparison of the continuum obtained from this work and that of the work of Nordlund (115). Some of the abundances tabulated in section 7.2 are also illustrated in a plot in section 7.6. Tables of opacities for many diatomic molecules, and H_2O and CO_2 separately, are given for some of the grid points, and this final section is completed with tables of some thermodynamic quantities for 128 grid points.

With the results given in chapter 7, a number of very important points can be made. We are quite justified in including isotopic molecules in the opacity calculations, as borne out by the detailed examination of the isotope effect of CO and TiO. For CO, even though the next most abundant isotopic variant $C^{13}O^{16}$ is only about 1% as abundant as $C^{12}O^{16}$, because CO is such an abundant molecule, the other isotopic variants are very efficient at filling in the windows and increasing the opacity, particularly in an important part of the spectrum. For TiO, it is clear that isotopes are important, as the dominant isotope Ti^{48} represents about 75% of all Ti, with the four other forms considered making up 25% and being of comparable abundance. Though TiO absorbs well away from the maximum of the Rosseland and Planck weighting functions, it is still clearly an important source of opacity.

Though the theory of the isotopic shifts of the vibrational and rotational constants of triatomic molecules is considered in some detail in this thesis, because of the constraints of CPU time, no attempt is made to compute the spectra of isotopically substituted H_2O

and CO_2 . However, as the bands due to these molecules consist of a very large number of overlapping lines, no appreciable number of windows would be expected to be left, so isotopic effects are not anticipated to be as important as for diatomic molecules, though as discussed, isotopically substituted triatomic molecules are still considered in the statistical mechanics calculations.

More generally, the total effect of all diatomic molecules is to increase the RMO by fairly modest amounts, the effect being greatest at the highest densities. For those grid points at which the opacity was computed with H_2O and CO_2 , it is clear that H_2O can have a very drastic effect indeed on the RMO, and can increase it by several orders of magnitude compared to that for the continuum alone, whereas CO_2 has at most a modest effect due to its much lower abundance, and also to the fact that its bands do not spread so much over the spectrum. We can thus conclude that H_2O is likely to be a very important source of opacity at low temperatures, and could swamp other effects in the total contribution to the RMO. From tables (7.2-9), it is clearly seen that H_2O is a close second in abundance to CO at $\log \rho = -8$ and $\log T \leq 3.4$, but for higher temperatures, H_2O rapidly dissociates and becomes much less important. Thus the opacities computed for diatomic molecules but without triatomic molecules would be reasonably good at higher temperatures, but would be considerably in error at lower temperature. Because of the limited resources, no computations could be done with diatomic and triatomic molecules together, but this would be an obvious step in any later work in computing extensive tables of opacities. We can also make the point here that pressure-induced $\text{H}_2\text{-H}_2$ and $\text{H}_2\text{-He}$ absorption can be a very

important source of continuous opacity for low temperatures and high pressures, though when molecular bands are included in the calculations, in particular those of H_2O , the effect of pressure-induced opacity is likely to be very much less important.

It must be pointed out that all the spectra given in this work are plots of absorption against frequency, for specified temperatures and densities with a fixed abundance of the chemical elements. To convert these into spectra that would be observed, would require using these computed opacities in solving the radiative transfer problem for a stellar atmosphere. Nevertheless, the plots do give an approximate qualitative idea of how the absorption by certain species, when abundant, would appear in the spectra.

In addition to the importance of molecular opacity in the atmospheres of late-type stars, the presence of molecules in a gas can obviously influence the equation of state, and amongst the results given in chapter 7, are tables of the pressure, internal energy and the adiabatic exponents Γ_1 , Γ_2 and Γ_3 . The latter are important respectively for dynamical instability, convective instability and pulsational instability. All red giants have extensive convective envelopes, and many are observed to be pulsating to various degrees or are otherwise irregular. As they exist well to the right of the cepheid pulsational instability strip in the H-R diagram, quite different mechanisms are responsible for their pulsation than in the case of cepheids, and clearly the presence of molecules in their atmospheres plays an important rôle.

Though the conditions in the interstellar medium are quite different from those in stellar atmospheres, in particular the molecules are not in equilibrium and their formation involves complicated reactions with interstellar grains, some of the basic theory discussed in this work is still relevant. Some aspects of this work are even more relevant to the study of planetary atmospheres, in particular when considering the importance of the greenhouse effect of H_2O and CO_2 in the terrestrial atmosphere.

We can now briefly consider what improvements could be made to this work. The simplest and easiest to implement would be to extend the calculation of the opacity to cover more grid points, in particular for triatomic molecules as suggested above, and to sample the spectrum at finer intervals, though these would all require a considerable amount of computer time. Although the most important molecules expected in stellar atmospheres are already included in the mixture we are dealing with, together with some other representative molecules which we have also included, nevertheless, further improvements could be made if more molecules were added.

In computing the spectrum line-by-line, approximations have to be made because of the very large number of lines that have to be processed. Doktorov's method used in this thesis to obtain the vibrational matrix elements is very quick, as analytic expressions are used to obtain the necessary integrals. Those analytic expressions are only possible if a Morse potential function is assumed for the electronic states involved, while the possibly more accurate

Rydberg-Klein-Rees potential functions would require numerical integration. Also, we only consider the rotationless vibrational matrix elements, by assuming that the Hönl-London factors can be simply factorized out, while more accurate band calculations would require this to be taken into account. However, we are also seriously limited by the available data for some molecules. For a simple molecule like CO whose spectroscopic constants are well known, an accurate calculation of the structure of its bands, with the suggested improvements above, would be quite feasible. This is clearly not the case for TiO, as it is such a complex system in comparison, and in addition there is the complication of Λ -doubling, which we deal with in an approximate way, as a detailed treatment would be very involved.

One particularly important limitation on our calculations is the lack of convenient molecular oscillator strengths or electronic transition moments. Unfortunately, many authors give transition moments in different units, sometimes not even specifying their units, using different symbols in their notation and are sometimes ambiguous as to whether the electronic statistical weight factor is included. It would be a great aid to computations involving molecular spectra, if some convenient up-to-date compilation of the known or computed molecular transition moments and oscillator strengths could be made.

As already stated in chapter 5, our treatment of triatomic molecules is very approximate, due to their much greater complexity compared to diatomic molecules, and to the need to save computer time in view of the millions of lines that may have to be calculated. One

obvious improvement for H_2O , would be to calculate each band individually with its own rotational constants that include the effects of the vibration-rotation coupling, rather than using those of the first pair of levels in a progression in the way discussed. This would of course increase the CPU time considerably. Any other improvements would require still more CPU time and considerably more theory. Finally, improved tables of the cross-sections for bound-free and free-free absorption by atoms and molecules would improve the continuous spectrum; note the discussion on OH and CH in section 7.2.

So far we have not considered the effect of turbulent velocity, nor in particular, the effect of different abundances, where there would be plenty of scope for future work. In carbon stars where there is a surplus of carbon over oxygen, the spectra would be heavily blanketed by C_2 and CN, such as in stars like R Coronae Borealis, and it would be interesting to calculate opacities in such cases.

APPENDIX A

Determination of the Principal Moments of Inertia for any Triatomic Molecule

In section 2.13 formulae are given for calculating the rotational constants A, B and C for any triatomic molecule, given the atomic masses and bond lengths. The derivation of these formulae is given here.

Let a triatomic molecule consist of the atoms with the masses m_1 , m_2 and m_3 with the lengths of the corresponding opposite sides s_{23} , s_{13} and s_{12} respectively, as shown in figure (A.1). Let α be the apex angle of the molecule at m_2 , with m_1 and m_3 representing the two end atoms. We also define the rectangular coordinate system with the origin at m_2 , s_{23} being directed along the x-axis and s_{12} being directed in the positive y-direction, as shown. Then if (x_1, y_1) are the coordinates for m_1 , and likewise for m_2 and m_3 :

$$(x_1, y_1) = (s_{12} \cos \alpha, s_{12} \sin \alpha) \tag{A.1}$$

$$(x_2, y_2) = (0, 0)$$

$$(x_3, y_3) = (s_{23}, 0)$$

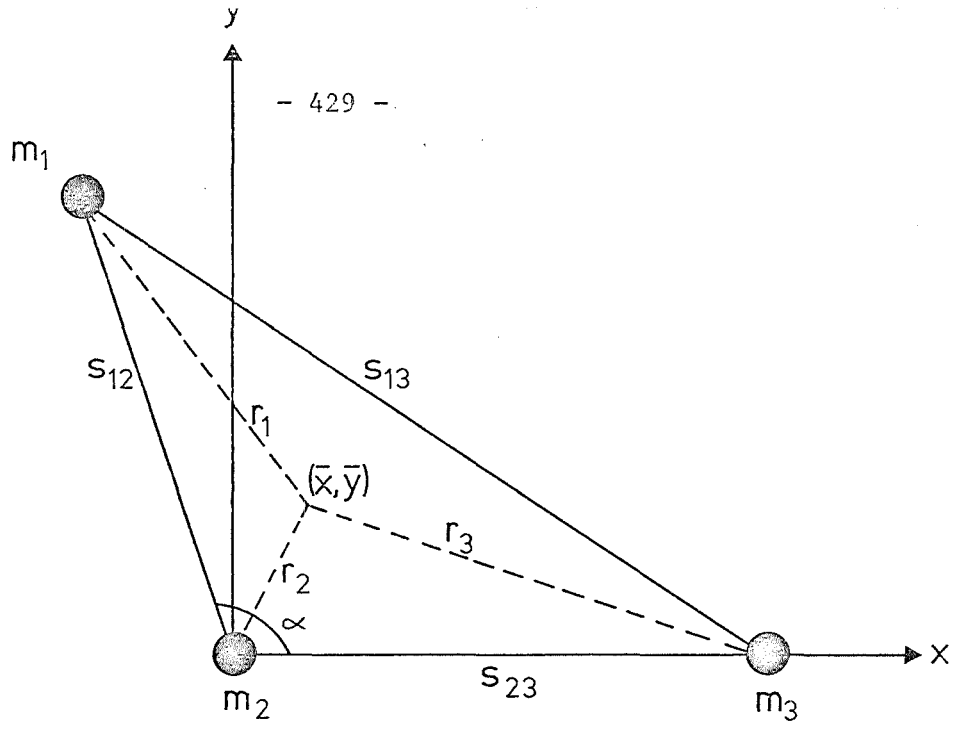


Fig. A.1

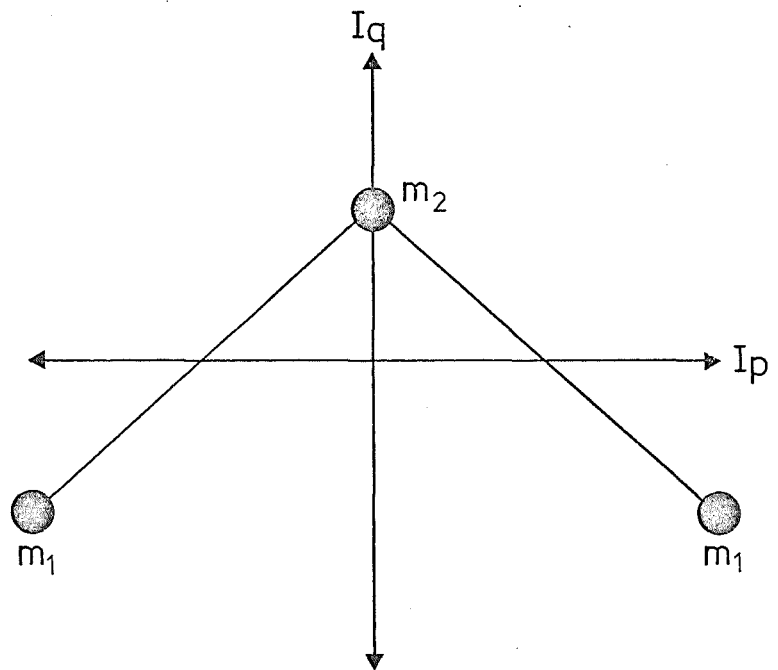


Fig. A.2

If (\bar{x}, \bar{y}) are the coordinates for the centre of mass of the system, then taking moments about this point:

$$\sum_{i=1}^3 m_i (x_i - \bar{x}) = 0, \quad \sum_{i=1}^3 m_i (y_i - \bar{y}) = 0 \quad (\text{A.2})$$

and putting:

$$M = m_1 + m_2 + m_3 \quad (\text{A.3})$$

then:

$$\bar{x} = \frac{1}{M} \sum_{i=1}^3 m_i x_i, \quad \bar{y} = \frac{1}{M} \sum_{i=1}^3 m_i y_i \quad (\text{A.4})$$

then from (A.1):

$$\bar{x} = \frac{m_1 s_{12} \cos \alpha + m_3 s_{23}}{M}, \quad \bar{y} = \frac{m_1 s_{12} \sin \alpha}{M} \quad (\text{A.5})$$

We need to find the three principal moments of inertia of the system, I_A , I_B and I_C , where by convention I_A is the smallest, I_B the intermediate and I_C the largest moment of inertia. As already stated in section 2.10, the three atoms define a plane, so:

$$I_A + I_B = I_C \quad (\text{A.6})$$

where I_C is the moment of inertia about (\bar{x}, \bar{y}) perpendicular to the plane, then:

$$I_c = m_1 r_1^2 + m_2 r_2^2 + m_3 r_3^2 \quad (\text{A.7})$$

where r_i is the distance of atom m_i from the centre of mass, so:

$$r_i^2 = (x_i - \bar{x})^2 + (y_i - \bar{y})^2 \quad (\text{A.8})$$

From (A.1) and (A.5) we can write:

$$r_1^2 = \left(S_{12} \cos \alpha - \frac{m_1 S_{12} \cos \alpha + m_3 S_{23}}{M} \right)^2 + S_{12}^2 \sin^2 \alpha \left(1 - \frac{m_1}{M} \right)^2 \quad (\text{A.9})$$

$$r_2^2 = \frac{(m_1 S_{12} \cos \alpha + m_3 S_{23})^2}{M^2} + \frac{(m_1 S_{12} \sin \alpha)^2}{M^2} \quad (\text{A.10})$$

$$r_3^2 = \left(S_{23} - \frac{m_1 S_{12} \cos \alpha + m_3 S_{23}}{M} \right)^2 + \frac{(m_1 S_{12} \sin \alpha)^2}{M^2} \quad (\text{A.11})$$

Then applying (A.9-11) to (A.7), we obtain:

$$\begin{aligned} I_c &= m_1 \left[\left(S_{12} \cos \alpha - \frac{m_1 S_{12} \cos \alpha + m_3 S_{23}}{M} \right)^2 + S_{12}^2 \sin^2 \alpha \left(1 - \frac{m_1}{M} \right)^2 \right] \\ &+ \frac{m_3}{M^2} \left[(m_1 S_{12} \cos \alpha + m_3 S_{23})^2 + (m_1 S_{12} \sin \alpha)^2 \right] \\ &+ m_3 \left[\left(S_{23} - \frac{m_1 S_{12} \cos \alpha + m_3 S_{23}}{M} \right)^2 + \left(\frac{m_1 S_{12} \sin \alpha}{M} \right)^2 \right] \end{aligned} \quad (\text{A.12})$$

From which it follows that on simplification, we obtain the result:

$$I_c = \frac{1}{M} \left[m_2 (m_1 S_{12}^2 + m_3 S_{23}^2) + m_1 m_3 (S_{12}^2 + S_{23}^2 - 2 S_{12} S_{23} \cos \alpha) \right] \quad (\text{A.13})$$

or as s_{13} is the third side of the triangle, obtained from the cosine formula being the coefficient of $m_1 m_3$:

$$I_c = \frac{1}{M} [m_1 m_2 s_{12}^2 + m_1 m_3 s_{13}^2 + m_2 m_3 s_{23}^2] \quad (\text{A.14})$$

from which (2.13.1) and (2.13.2) are obtained respectively using (2.10.2), for the largest of the principal moments of inertia.

We now need to find I_A and I_B which lie in the plane of the molecule, and which for the most general case of the C_s point group, will not be orientated in any special direction.

Let us define the x' and y' -axes which pass through the centre of mass and parallel to the x and y -axes, such that $x' = x - \bar{x}$ and $y' = y - \bar{y}$. Now by Massey and Kestelman (116), but working only in two dimensions, we first consider the moment of inertia of m_i about some general axis passing through the centre of mass along the direction of the unit vector $\hat{v} = l\hat{i} + m\hat{j}$ with m_i located at (x'_i, y'_i) . The perpendicular distance of the mass m_i from this axis is given by $p_i^2 = r_i^2 - (\hat{v} \cdot \underline{r}_i)^2$, where \underline{r}_i is the radius vector of m_i from the centre of mass. Then the moment of inertia for all the atoms about this axis is given by:

$$\begin{aligned} I &= \sum_{i=1}^3 m_i p_i^2 = \sum_{i=1}^3 m_i [(x_i'^2 + y_i'^2)(l^2 + m^2) - (lx_i' + my_i')^2] \\ &= l^2 \sum_{i=1}^3 m_i y_i'^2 + m^2 \sum_{i=1}^3 m_i x_i'^2 - 2lm \sum_{i=1}^3 m_i x_i' y_i' \quad (\text{A.15}) \\ &= al^2 + bm^2 - 2hlm \end{aligned}$$

Writing the general equation of an ellipse, with the origin of the coordinates at its centre, in the same form:

$$ax'^2 + by'^2 - 2hxy' = 1 \quad (\text{A.16})$$

where the radius vector of a point on this ellipse in the direction \hat{v} from the centre of mass is r , and as $x = rl$ and $y = rm$, then it is seen that $I = 1/r^2$, hence (A.16) is the ellipse that represents the moment of inertia in the plane, and where:

$$a = \sum_{i=1}^3 m_i y_i'^2, \quad b = \sum_{i=1}^3 m_i x_i'^2, \quad h = \sum_{i=1}^3 m_i x_i' y_i' \quad (\text{A.17})$$

with a and b being the moments of inertia about the x' and y' -axes respectively and h being the cross term. Then we need to rotate the coordinate system such that we have no cross term.

If we define a new coordinate system (ξ, η) rotated by ϕ relative to (x', y') , then:

$$\begin{aligned} x' &= \xi \cos \phi - \eta \sin \phi \\ y' &= \xi \sin \phi + \eta \cos \phi \end{aligned} \quad (\text{A.18})$$

then we want to find the value of ϕ such that we can write the equation of the ellipse in the standard form:

$$p\xi^2 + q\eta^2 = 1 \quad (\text{A.19})$$

without a cross term, such that p and q are now the principal moments of inertia in the plane, with:

$$p = \sum_{i=1}^3 m_i \eta_i^2, \quad q = \sum_{i=1}^3 m_i \xi_i^2 \quad (\text{A.20})$$

Now if we apply (A.18) to (A.16), we obtain:

$$\begin{aligned} a(\xi \cos \phi - \eta \sin \phi)^2 + b(\xi \sin \phi + \eta \cos \phi)^2 \\ - 2h(\xi \cos \phi - \eta \sin \phi)(\xi \sin \phi + \eta \cos \phi) = 1 \end{aligned} \quad (\text{A.21})$$

hence:

$$\begin{aligned} a(\xi^2 \cos^2 \phi - 2\xi\eta \cos \phi \sin \phi + \eta^2 \sin^2 \phi) \\ + b(\xi^2 \sin^2 \phi + 2\xi\eta \cos \phi \sin \phi + \eta^2 \cos^2 \phi) \\ - 2h(\xi^2 \cos \phi \sin \phi - \xi\eta \sin^2 \phi + \xi\eta \cos^2 \phi - \eta^2 \cos \phi \sin \phi) = 1 \end{aligned} \quad (\text{A.22})$$

The coefficient of $\xi\eta$ must be zero as we have no cross term, hence:

$$-2a \cos \phi \sin \phi + 2b \cos \phi \sin \phi + 2h \sin^2 \phi - 2h \cos^2 \phi = 0 \quad (\text{A.23})$$

and using the fact that:

$$2 \cos \phi \sin \phi = \sin 2\phi \quad (\text{A.24})$$

$$\cos^2 \phi - \sin^2 \phi = \cos 2\phi$$

then from (A.23) we obtain:

$$\tan 2\phi = \frac{2h}{(b-a)} \quad (\text{A.25})$$

which is the condition that the cross term vanishes.

Re-writing (A.22) without the terms involving $\xi\eta$ when the condition of (A.25) is valid:

$$\begin{aligned} a(\xi^2 \cos^2 \phi + \eta^2 \sin^2 \phi) + b(\xi^2 \sin^2 \phi + \eta^2 \cos^2 \phi) \\ - 2h(\xi^2 \cos \phi \sin \phi - \eta^2 \cos \phi \sin \phi) = 1 \end{aligned} \quad (\text{A.26})$$

on multiplying out, collecting the terms in ξ^2 and η^2 , then using the trigonometric identities:

$$2 \cos^2 \phi = 1 + \cos 2\phi \quad (\text{A.27})$$

$$2 \sin^2 \phi = 1 - \cos 2\phi$$

together with the first in (A.24), we can write:

$$\begin{aligned} \xi^2 \left[\frac{1}{2}(a + a \cos 2\phi + b - b \cos 2\phi) - h \sin 2\phi \right] \\ + \eta^2 \left[\frac{1}{2}(a - a \cos 2\phi + b + b \cos 2\phi) + h \sin 2\phi \right] = 1 \end{aligned} \quad (\text{A.28})$$

which is the equation of the ellipse in the standard form, hence:

$$p = \frac{1}{2} [a + b + (a-b) \cos 2\phi] - h \sin 2\phi \quad (\text{A.29})$$

$$q = \frac{1}{2} [a + b - (a-b) \cos 2\phi] + h \sin 2\phi$$

then I_A will be the smaller of p and q , and I_B the larger.

But:

$$\cos 2\phi = \frac{1}{\sqrt{\tan^2 2\phi + 1}} = \frac{(b-a)^2}{4h^2 + (b-a)^2} \tag{A.30}$$

$$\sin 2\phi = \frac{1}{\sqrt{\cot^2 2\phi + 1}} = \frac{4h^2}{4h^2 + (b-a)^2}$$

using (A.25), then substituting these into (A.29), we obtain:

$$p = \frac{1}{2} \left[a + b + (a-b) \frac{(b-a)^2}{4h^2 + (b-a)^2} \right] - h \frac{4h^2}{4h^2 + (b-a)^2} \tag{A.31}$$

$$q = \frac{1}{2} \left[a + b - (a-b) \frac{(b-a)^2}{4h^2 + (b-a)^2} \right] + h \frac{4h^2}{4h^2 + (b-a)^2}$$

then combining the pair together, we can write:

$$I_{A,B} = \frac{1}{2} \left[a + b \pm \sqrt{4h^2 + (b-a)^2} \right] \tag{A.32}$$

where $I_{A,B}$ means I_A with the negative root and I_B with the positive root, as $I_A \leq I_B$ by definition:

However, it is more convenient to express (A.32) in reciprocal form, hence on re-arranging:

$$I_{A,B}^{-1} = \frac{(a+b) \pm \sqrt{(a+b)^2 - 4(ab-h^2)}}{2(ab-h^2)} \tag{A.33}$$

where I_A^{-1} is now the positive root, and we need only determine the

quantities $(a+b)$ and $(ab-h^2)$. Hence applying the mass and coordinates of the atoms to (A.17):

$$a = m_1 (y_1 - \bar{y})^2 + m_2 \bar{y}^2 + m_3 \bar{y}^2$$

$$b = m_1 (x_1 - \bar{x})^2 + m_2 \bar{x}^2 + m_3 (x_3 - \bar{x})^2 \quad (\text{A.34})$$

$$h = m_1 (x_1 - \bar{x})(y_1 - \bar{y}) + m_2 \bar{x} \bar{y} - m_3 (x_3 - \bar{x}) \bar{y}$$

then:

$$ab - h^2 = \left[m_1 (y_1 - \bar{y})^2 + m_2 \bar{y}^2 + m_3 \bar{y}^2 \right] \left[m_1 (x_1 - \bar{x})^2 + m_2 \bar{x}^2 + m_3 (x_3 - \bar{x})^2 \right] - \left[m_1 (x_1 - \bar{x})(y_1 - \bar{y}) + m_2 \bar{x} \bar{y} - m_3 (x_3 - \bar{x}) \bar{y} \right]^2 \quad (\text{A.35})$$

On multiplying this out and substituting for x_i, y_i, \bar{x} and \bar{y} from (A.1) and (A.5), then (A.35) eventually simplifies right down to:

$$ab - h^2 = \frac{m_1 m_2 m_3 S_{12}^2 S_{23}^2 \sin^2 \alpha}{M} \quad (\text{A.36})$$

Having determined $(ab-h^2)$, and as $(a+b) = I_C$ for a plane with I_C already known earlier, and writing:

$$I_{A,B}^{-1} = \frac{I_C + \sqrt{I_C^2 - 4(ab-h^2)}}{2(ab-h^2)} \quad (\text{A.37})$$

all principal moments of inertia are now known directly in terms of the masses of the atoms, their separations and the apex angle of the molecule.

Finally, in order to obtain the expressions for the rotational constants in section 2.13, I_A , I_B and I_C are replaced by A, B and C respectively using (2.10.2), which gives the definitions of the rotational constants in terms of the moments of inertia. (A.37) can now be re-written as:

$$A, B = \frac{1 \pm \sqrt{1 - \left(\frac{8\pi^2 c}{h}\right)^2 \cdot 4(ab - h^2) C^2}}{\left(\frac{8\pi^2 c}{h}\right)^2 \cdot 2(ab - h^2) C} \quad (\text{A.38})$$

putting:

$$k = \frac{128\pi^2 c^2}{h^2} \cdot (ab - h^2) = \frac{128\pi^2 c^2}{h^2} \cdot \frac{m_1 m_2 m_3 s_{12}^2 s_{23}^2 \sin^2 \alpha}{M} \quad (\text{A.39})$$

and keeping to the convention that $A \gg B \gg C$, (A.38) can be written as (A.40) and (A.41) for A and B respectively, and from (A.13) we can write (A.42) for C:

$$A = \frac{1 + \sqrt{1 - 2kC^2}}{kC} \quad (\text{A.40})$$

$$B = \frac{1 - \sqrt{1 - 2kC^2}}{kC} \quad (\text{A.41})$$

$$C = \frac{hM}{8\pi^2 c \left[m_2 (m_1 s_{12}^2 + m_3 s_{23}^2) + m_1 m_3 (s_{12}^2 + s_{23}^2 - 2s_{12} s_{23} \cos \alpha) \right]} \quad (\text{A.42})$$

and as a check, it is immediately seen from (A.40) and (A.41) that

(2.10.3) is satisfied, i.e. $1/A + 1/B = 1/C$.

As already stated in section 2.13, if the bond angle of the molecule is opened up so that in the limit the molecule is linear, i.e. $\alpha \rightarrow 180^\circ$, then $k \rightarrow 0$ from (A.39), and it is immediately seen that $A \rightarrow \infty$ from (A.40) and $B \rightarrow C$ from (A.41) if we replace $(1-2kC^2)$ by $(1-kC^2)$, the first two terms in the binomial expansion.

Finally, we can consider briefly the special case of a molecule with the C_{2v} point group, where clearly from symmetry, the two principal moments of inertia in the plane must be respectively perpendicular to and parallel to the axis of symmetry. Let I_p and I_q be respectively these moments of inertia, see figure (A.2), then it is easy to show that their ratio is given by:

$$\frac{I_p}{I_q} = \frac{m_2}{\tan^2(\alpha/2) (2m_1 + m_2)} \quad (\text{A.43})$$

and using data from Herzberg (34), we can tabulate this ratio for a few C_{2v} triatomic molecules in their ground electronic states:

Table (A.1) of I_p/I_q for some C_{2v} Molecules

NH ₂	0.55
PH ₂	0.89
H ₂ O	0.52
H ₂ S	0.87
NO ₂	0.05
SO ₂	0.17
O ₃	0.13

where in all cases $I_p < I_q$, hence $I_p = I_A$ and $I_q = I_B$, so the intermediate moment of inertia lies along the symmetry axis. Thus as stated in section 5.3, the sign of u_4 is determined by ζ for all these molecules, so for ζ even, $u_4 = +1$ and for ζ odd $u_4 = -1$. No cases could be found for triatomic molecules for which $I_p > I_q$, i.e. $I_p = I_B$ and $I_q = I_A$, so the smallest moment of inertia lies along the symmetry axis, and the sign of u_4 is determined by whether K_a is even or odd. If $I_p = I_q$, then we have an oblate symmetric top, which is accidental if $m_1 \neq m_2$, but clearly if $m_1 = m_2$ then it is easy to see that $\alpha = 60^\circ$ and we have an equilateral triangle molecule of point group D_{3h} like H_3^+ .

Related to this are the selection rules for the v_3 mode of vibration, where vibrational levels have the species A_1 and B_1 :

$$\underline{I_p < I_q}$$

A-Type Bands $A_1 \leftrightarrow B_1$ for Δv_3 odd,

B-Type Bands $\left\{ \begin{array}{l} A_1 \leftrightarrow A_1 \\ B_1 \leftrightarrow B_1 \end{array} \right\}$ for Δv_3 even,

$$\underline{I_p > I_q}$$

A-Type Bands $\left\{ \begin{array}{l} A_1 \leftrightarrow A_1 \\ B_1 \leftrightarrow B_1 \end{array} \right\}$ for Δv_3 even,

B-Type Bands $A_1 \leftrightarrow B_1$ for Δv_3 odd,

where apparently for triatomic molecules we need consider only the first case.

APPENDIX B

Determination of Vibrational Partition Functions and some other
Vibrational Properties

As stated in section 2.6, we can use the method of Kassel (38) to obtain an analytic expression for the vibrational partition function of a diatomic molecule, and hence using the same method in section 2.11, we can similarly obtain an expression for a triatomic molecule.

Given the vibrational partition function (2.6.2) in terms of the dimensionless vibrational constants, and converting to dimensionless constants in terms of the zero point energy by (2.6.3), we can write:

$$Q_v = \sum_{v=0}^{\infty} e^{-W_0 v + W_0 X_0 v^2 - W_0 Y_0 v^3} \tag{B.1}$$

$$= \sum_{v=0}^{\infty} e^{-W_0 v} e^{W_0 X_0 v^2} e^{-W_0 Y_0 v^3}$$

neglecting terms higher than $W_0 Y_0$, then expanding the exponentials other than the first, we obtain:

$$Q_v = \sum_{v=0}^{\infty} e^{-W_0 v} \left[1 + W_0 X_0 v^2 + \frac{(W_0 X_0)^2 v^4}{2!} + \frac{(W_0 X_0)^3 v^6}{3!} + \dots \right]$$

$$\times \left[1 - W_0 Y_0 v^3 + \frac{(W_0 Y_0)^2 v^6}{2!} - \dots \right] \tag{B.2}$$

then multiplying out the square brackets and neglecting terms $O(v^7)$

and higher:

$$Q_n = \sum_{r=0}^{\infty} e^{-W_0 r} \left[1 + W_0 X_0 r^2 + \frac{(W_0 X_0)^2}{2} r^4 + \frac{(W_0 X_0)^3}{6} r^6 + \dots \right. \\ \left. - W_0 Y_0 r^3 - (W_0 X_0)(W_0 Y_0) r^5 - \dots + \frac{(W_0 Y_0)^2}{2} r^6 + \dots \right] \quad (\text{B.3})$$

Now as in (2.6.4), if we let:

$$Z = e^{-W_0} \quad \text{then} \quad Z^r = e^{-W_0 r} \quad (\text{B.4})$$

then (B.3) can be written as:

$$Q_n = \sum_{r=0}^{\infty} Z^r + W_0 X_0 \sum_{r=0}^{\infty} r^2 Z^r + \frac{(W_0 X_0)^2}{2} \sum_{r=0}^{\infty} r^4 Z^r + \frac{(W_0 X_0)^3}{6} \sum_{r=0}^{\infty} r^6 Z^r \\ - W_0 Y_0 \sum_{r=0}^{\infty} r^3 Z^r - (W_0 X_0)(W_0 Y_0) \sum_{r=0}^{\infty} r^5 Z^r + \frac{(W_0 Y_0)^2}{2} \sum_{r=0}^{\infty} r^6 Z^r \quad (\text{B.5})$$

Given that $Z < 1$ always, it is easy to see that:

$$\sum_{r=0}^{\infty} Z^r = \frac{1}{(1-Z)} \quad (\text{B.6})$$

and by Kassel we can define a function $P_n(Z)$, such that:

$$P_n(Z) = \sum_{r=0}^{\infty} r^n Z^r \quad (\text{B.7})$$

$$\text{as } \frac{d}{dZ} P_n(Z) = \sum_{r=0}^{\infty} r^{n+1} Z^{r-1} = \frac{1}{Z} \sum_{r=0}^{\infty} r^{n+1} Z^r \quad (\text{B.8})$$

it follows that:

$$P_n(z) = z \frac{d}{dz} P_n(z) \quad (\text{B.9})$$

Together with the recurrence relation of (B.9) and the relation of (B.6), we can obtain $P_n(z)$ for any n by successive differentiation:

$$P_0(z) = \frac{1}{(1-z)} \quad (\text{B.10})$$

$$P_1(z) = \frac{z}{(1-z)^2} \quad (\text{B.11})$$

$$P_2(z) = \frac{z(1+z)}{(1-z)^3} \quad (\text{B.12})$$

$$P_3(z) = \frac{z(1+4z+z^2)}{(1-z)^4} \quad (\text{B.13})$$

$$P_4(z) = \frac{z(1+11z+11z^2+z^3)}{(1-z)^5} \quad (\text{B.14})$$

$$P_5(z) = \frac{z(1+26z+66z^2+26z^3+z^4)}{(1-z)^6} \quad (\text{B.15})$$

$$P_6(z) = \frac{z(1+57z+302z^2+302z^3+57z^4+z^5)}{(1-z)^7} \quad (\text{B.16})$$

then applying (B.10-16) to (B.5) we obtain the final result:

$$\begin{aligned}
 Q_n = & \frac{1}{(1-z)} + W_0 X_0 \frac{z(1+z)}{(1-z)^3} + (W_0 X_0)^2 \frac{z(1+11z+11z^2+z^3)}{2(1-z)^5} \\
 & + \left[\frac{(W_0 X_0)^2}{6} + \frac{(W_0 Y_0)^2}{2} \right] \frac{z(1+57z+302z^2+302z^3+57z^4+z^5)}{(1-z)^7} \quad (B.17) \\
 & - W_0 Y_0 \frac{z(1+4z+z^2)}{(1-z)^4} - (W_0 X_0)(W_0 Y_0) \frac{z(1+26z+66z^2+26z^3+z^4)}{(1-z)^6}
 \end{aligned}$$

which is (2.6.5), except that the term for $(W_0 Y_0)^2$ is dropped as it is found to be negligible. By using the same procedure for triatomic molecules, the expression (2.11.6) can similarly be obtained.

For the sake of interest, we can also apply Kassel's method for obtaining an expression for the sum of relative band strengths in a progression for the harmonic oscillator.

With the expressions (4.3.46-50) for the matrix elements, and as stated in section 5.2, if we neglect all transitions other than $n = \Delta v$ for the n^{th} order matrix element, with Δv being positive, so considering only $\langle v | x^n | v+n \rangle$, then the relative strength of a band in a progression $v = n$ as given by (5.2.2) is:

$$\frac{R_{v,v+n}^2}{R_{0,n}^2} = \frac{\langle v | x^n | v+n \rangle^2}{\langle 0 | x^n | n \rangle^2} = \frac{(v+n)!}{v! n!} \quad (B.18)$$

Now if $S_n(z)$ is the sum of all relative band strengths in the n^{th} progression with the Boltzmann factor, it is given by:

$$S_n(z) = \sum_{v=0}^{\infty} e^{-W_0 v} \frac{(v+n)!}{v! n!} = \sum_{v=0}^{\infty} z^v \frac{(v+n)!}{v! n!} \quad (B.19)$$

from which we can write down the expressions for $S_0(z)$, $S_1(z)$, $S_2(z)$

etc. On applying Kassel's method as before by substituting $P_n(Z)$ for the summation in each of $S_n(Z)$, we obtain expressions for each of $S_n(Z)$ which all simplify down to:

$$S_n(Z) = \frac{1}{(1-Z)^{n+1}} \quad (\text{B.20})$$

However, from the binomial expansion from Abramowitz and Stegun (46):

$$(1-x)^{-n-1} = \sum_{m=n}^{\infty} \binom{n}{m} x^{n-m} \quad \text{for } |x| < 1 \quad (\text{B.21})$$

we can see at once that:

$$\frac{1}{(1-Z)^{n+1}} = \sum_{v=n}^{\infty} Z^{v-n} \cdot \frac{v!}{n!(v-n)!} \quad (\text{B.22})$$

and if we start the summation from $v = 0$, we must replace v by $v+n$ under the summation, giving the right hand side of (B.19).

In (B.20), $S_1(Z)$ is the sum of the progression for the first harmonic or fundamental, $S_2(Z)$ for the second harmonic or first overtone etc.; $S_0(Z)$ is the "zeroth harmonic" and represents the sum of strengths in pure rotational bands, assuming the permanent dipole moment does not change with vibrational energy (in reality of course it must, in order to produce vibration-rotation bands), and $S_0(Z)$ is also of course the partition function. No such simple analytic technique could be used for the anharmonic oscillator, because the matrix elements can no longer be written in a simple analytic form. For emission, (B.20) still applies but with n still being positive and v now being the final vibrational level.

We can also for the sake of interest, determine how $S_n(Z)$ behaves if the molecule is isotopically substituted. Let μ and μ^I be respectively the reduced mass of the initial molecule and isotopically substituted molecule, then by (2.8.1) and (2.8.2), i.e. respectively:

$$\rho = \sqrt{\frac{\mu}{\mu^I}} \quad \text{and} \quad \omega_e^I = \rho \omega_e \quad (\text{B.23})$$

and for the harmonic oscillator (4.3.45) and (5.2.1), i.e. respectively:

$$\beta = \left(\frac{h}{4\pi^2 \mu c \omega_e} \right)^{1/2} \quad \text{and} \quad R_{\nu, \nu+\Delta\nu} = M_{\Delta\nu} \beta^{\Delta\nu} \left[\frac{(\nu+\Delta\nu)!}{2^{\Delta\nu} \nu!} \right]^{1/2} \quad (\text{B.24})$$

we can show that:

$$Z^I = Z \sqrt{\frac{\mu}{\mu^I}} \quad (\text{B.25})$$

and:

$$\frac{R_{\nu, \nu+n}^{I^2}}{R_{\nu, \nu+n}^2} = \frac{\langle \nu | z^n | \nu+n \rangle^{I^2}}{\langle \nu | z^n | \nu+n \rangle^2} = \left(\frac{\mu}{\mu^I} \right)^{n/2} \quad (\text{B.26})$$

Each band is shifted in frequency by ν^I/ν , and it is seen from (B.23) that this will give an additional factor to the band strength for absorption neglecting stimulated emission, and emission respectively by:

$$\frac{\nu^I}{\nu} = \sqrt{\frac{\mu}{\mu^I}} \quad \text{and} \quad \frac{\nu^{I^4}}{\nu^4} = \left(\frac{\mu}{\mu^I} \right)^2 \quad (\text{B.27})$$

Hence applying (B.25-27) to (B.20), we obtain for absorption:

$$S_n(Z^I) = \left(\frac{\mu}{\mu^I}\right)^{\frac{n+1}{2}} \cdot \frac{1}{\left(1 - Z^{\sqrt{\mu/\mu^I}}\right)^{n+1}} \quad (\text{B.28})$$

and for emission:

$$S_n(Z^I) = \left(\frac{\mu}{\mu^I}\right)^{\frac{n+4}{2}} \cdot \frac{1}{\left(1 - Z^{\sqrt{\mu/\mu^I}}\right)^{n+1}} \quad (\text{B.29})$$

where again n is positive and in the analysis, v is the final level. Both (B.28) and (B.29) are invalid for $n = 0$, i.e. pure rotation, but we can write the shift of the vibrational partition function simply as:

$$S_0(Z^I) = \frac{1}{\left(1 - Z^{\sqrt{\mu/\mu^I}}\right)} \quad (\text{B.30})$$

As we are dealing with purely vibrational effects, we are of course neglecting the changes of the rotational constants.

One can refer to the more extensive paper by Kassel (117) for the application of the function $P_n(Z)$ and its derivatives on the determination of various molecular thermodynamic functions.

Finally, in the application of Doktorov's method as discussed in section 4.3, we have to assume a Morse potential function, where the terms in $\omega_e y_e$ and beyond are assumed to be zero, and we use ω_e and the dissociation potential D_e^0 , or the first anharmonic term $\omega_e x_e$ if D_e^0 is not available; the two being related by (4.3.10). However, in a few rare cases, notably for the first excited electronic states of the

hydrides of the group I elements, the constant $\omega_e x_e$ is negative, i.e. the first anharmonic term is positive, as this term is normally defined with a negative sign in the expression for the energy levels, causing the potential well to depart grossly from that of a Morse potential. In this case there will be no turnover in the levels if the higher order terms are neglected, and it is easy to see that Doktorov's method cannot be used if D_e^0 is not available.

We could of course assume a nearly harmonic potential with ω_e left unchanged but with a very small value of $\omega_e x_e$ with a correspondingly large value of D_e^0 , then apply Doktorov's method as usual. A possibly better alternative is to fit a Morse potential, provided that ω_e , $\omega_e x_e$ and $\omega_e y_e$ are known.

If the term values are as usual:

$$G(v) = \omega_e (v + \frac{1}{2}) - \omega_e x_e (v + \frac{1}{2})^2 + \omega_e y_e (v + \frac{1}{2})^3 + \dots \quad (\text{B.31})$$

neglecting higher terms, we want to replace the last terms by $x_f x_f$, an effective anharmonic constant. Differentiating and equating to zero for the turnover in levels corresponding to dissociation:

$$\frac{dG(v)}{dv} = \omega_e - 2\omega_e x_e (v + \frac{1}{2}) + 3\omega_e y_e (v + \frac{1}{2})^2 = 0 \quad (\text{B.32})$$

then solving for v, we can write:

$$v = \frac{2\omega_e x_e - 3\omega_e y_e \pm 2\sqrt{\omega_e^2 x_e^2 - 3\omega_e \cdot \omega_e y_e}}{6\omega_e y_e} \quad (\text{B.33})$$

Now letting:

$$G(v) = \omega_e (v + \frac{1}{2}) - \omega_f \alpha_f (v + \frac{1}{2})^2 \quad (\text{B.34})$$

then for dissociation:

$$\frac{dG(v)}{dv} = \omega_e - 2\omega_f \alpha_f v - \omega_f \alpha_f = 0 \quad (\text{B.35})$$

giving:

$$v = \frac{\omega_e}{2\omega_f \alpha_f} - \frac{1}{2} \quad (\text{B.36})$$

then equating (B.33) and (B.36) and simplifying, we obtain the result:

$$\omega_f \alpha_f = \frac{1}{2} \omega_e \alpha_e \pm \sqrt{\omega_e^2 \alpha_e^2 - 3\omega_e \cdot \omega_e \alpha_e} \quad (\text{B.37})$$

where the positive root should be taken.

For example, the $A^1\Sigma$ state of NaH has the constants: $\omega_e = 310.60$, $\omega_e \alpha_e = -5.410$ and $\omega_e \gamma_e = -0.1970$, then applying (B.37), we obtain $\omega_f \alpha_f = 4.589$; then this together with ω_e enables us to apply Doktorov's method as usual.

Note also that in this case the given value of the vibration-rotation coupling constant α_e is also negative, so that B_v increases with v to a maximum before decreasing, due to higher order coupling constants which we neglect, rather than decreasing monotonically which is normally the case. The best way of dealing

with this is to make α'_e and β_e consistent with our assumed Morse potential, and calculate them from (4.2.7) and (4.2.8) respectively, using $\omega_f x_f$.

Although this method is very crude, we hope that in such breakdown cases, we can at least approximately represent the gross properties of the spectra. Though we could also use (B.37) to fit a Morse potential for the usual non-breakdown cases of $\omega_e x_e$ if $\omega_e y_e$ is known, it is thought best not to apply this method in such cases.

APPENDIX C

Data for Determining Sources of Continuous Opacity

Tables of data that are used in chapter 3 for determining the continuous opacity are given here.

For Rayleigh scattering, the coefficient B_0 , and for some elements up to neon and some molecules, B_1 and B_2 are given as defined in (3.2.4) and (3.2.5), the data being obtained from the various sources as stated in section 3.2. Note that many of these coefficients may be outside the range of floating point numbers in the machine used, in which case they have to be scaled.

Table (C.1) of Rayleigh Scattering Coefficients

	Z	B ₀	B ₁	B ₂		
H	1	5.813E-45	2.452E-10	4.801E-20		
He	2	5.616E-46	4.750E-11	1.850E-21		
Li	3	5.223E-42				
Be	4	1.129E-42				
B	5	2.236E-43				
C	6	4.426E-44	2.743E-10	6.960E-20		
N	7	2.275E-44	1.922E-10	3.362E-20		
O	8	7.621E-45	1.008E-10	1.038E-20		
F	9	3.937E-45				
Ne	10	2.041E-45	4.480E-11	2.120E-21		
Na	11	9.520E-42	Se 34	1.526E-43	La 57	2.273E-41
Mg	12	4.277E-42	Br 35	1.107E-43	Ce 58	1.896E-41
Al	13	1.922E-42	Kr 36	8.029E-44	Pr 59	1.582E-41
Si	14	8.635E-43	Rb 37	3.265E-41	Nd 60	1.320E-41
P	15	3.880E-43	Sr 38	2.429E-41	Pm 61	1.102E-41
S	16	1.743E-43	Y 39	1.807E-41	Sm 62	9.191E-42
Cl	17	7.832E-44	Zr 40	1.344E-41	Eu 63	7.669E-42
Ar	18	3.519E-44	Nb 41	9.997E-42	Gd 64	6.399E-42
K	19	1.886E-41	Mo 42	7.436E-42	Tb 65	5.339E-42
Ca	20	1.368E-41	Tc 43	5.532E-42	Dy 66	4.455E-42
Sc	21	9.920E-42	Ru 44	4.115E-42	Ho 67	3.717E-42
Ti	22	7.196E-42	Rh 45	3.061E-42	Er 68	3.101E-42
V	23	5.219E-42	Pd 46	2.277E-42	Tm 69	2.587E-42
Cr	24	3.786E-42	Ag 47	1.694E-42	Yb 70	2.159E-42
Mn	25	2.746E-42	Cd 48	1.260E-42	Lu 71	1.801E-42
Fe	26	1.992E-42	In 49	9.374E-43	Hf 72	1.503E-42
Co	27	1.445E-42	Sn 50	6.973E-43	Ta 73	1.254E-42
Ni	28	1.048E-42	Sb 51	5.187E-43	W 74	1.046E-42
Cu	29	7.601E-43	Te 52	3.859E-43	Re 75	8.731E-43
Zn	30	5.513E-43	I 53	2.870E-43	Os 76	7.284E-43
Ga	31	3.999E-43	Xe 54	2.135E-43	Ir 77	6.078E-43
Ge	32	2.901E-43	Cs 55	3.265E-41	Pt 78	5.071E-43
As	33	2.104E-43	Ba 56	2.724E-41	Au 79	4.231E-43
					Hg 80	3.531E-43
H2		8.140E-45	1.573E-10	1.978E-20		
C2		4.605E-44	2.743E-10	6.960E-20		
N2		3.867E-44	1.540E-10	5.929E-21		
O2		3.247E-44	1.014E-10	2.571E-21		
CO		3.284E-44				
OH		2.011E-44				
SiO		9.107E-44				
H2O		2.570E-44				
CO2		1.147E-43				

The following tables (C.2-23) as used in section 3.3, are for the various sources of continuous absorption in the form of log absorption in cm^4 per dyne, except for OH_{bf} and CH_{bf} which are in cm^2 , with the negative sign omitted in all cases for convenience. Because these tables come from different sources, as stated in section 3.3 and below, the tabulation intervals are different and in different units, which we retain. All rows are tabulated by wavelength or energy and columns by temperature or θ . Where we have the following conversion factors:

$$\lambda(\text{\AA}) = 1/ER_{\infty} = 911.26708/E, \quad \theta = 5039.935/T \quad (\text{C.1})$$

with E being the energy in Rydbergs and R_{∞} the Rydberg constant for infinite mass.

For He_{ff}^- from Somerville (51), $\text{H}_{2\text{ff}}^-$ from Somerville (56), C_{ff}^- from Myerscough and McDowell (53) and Cl_{ff}^- from John and Morgan (52), the first row is used for extrapolation to low energies, performed by taking the number whose log is tabulated here and dividing by E^2 , or applying (3.3.9) if working in dimensionless energy units. For John (54) for wavelengths longer than 10μ , apply his expression:

$$k_{\lambda}(T) = 10^{-3} \lambda^3 k_{10}(T) \quad (\text{C.2})$$

with λ in μ and k_{10} the absorption at 10μ , or use (3.3.8) if working in dimensionless energy units. Note also, as stated in section 3.3,

that the table for CH_{bf} is obtained by combining three tables as given by Tarafdar and Das (57), and that the extrapolation of OH_{bf} and CH_{bf} in tables (C.22) and (C.23) respectively, to longer wavelengths, is performed according to the method discussed in section 7.2. Finally, as stated in section 3.3, we have added the first row to table (C.5) for C_{ff}^- , in order to apply the same extrapolation method as Somerville etc.

Table (C.2) of H_{ff+bf}^- in cm^4/dyne from Tsuji (9)

W/L in Microns	Theta								
	0.6	0.8	1.0	1.2	1.4	1.6	1.8	2.0	2.2
100.0	22.488	22.361	22.268	22.195	22.136	22.086	22.044	22.006	21.973
80.0	22.682	22.555	22.462	22.389	22.330	22.280	22.238	22.200	22.167
60.0	22.931	22.805	22.712	22.639	22.580	22.530	22.487	22.450	22.417
40.0	23.284	23.157	23.064	22.991	22.932	22.882	22.839	22.802	22.769
20.0	23.886	23.759	23.656	23.593	23.534	23.484	23.441	23.404	23.370
16.0	24.079	23.953	23.860	23.787	23.728	23.678	23.635	23.597	23.564
14.0	24.195	24.069	23.976	23.903	23.843	23.794	23.751	23.713	23.680
12.0	24.329	24.203	24.109	24.037	23.977	23.927	23.884	23.847	23.813
10.0	24.487	24.361	24.268	24.195	24.135	24.086	24.043	24.005	23.972
8.0	24.681	24.554	24.461	24.388	24.329	24.279	24.236	24.199	24.165
6.5	24.861	24.735	24.641	24.569	24.509	24.459	24.416	24.379	24.346
6.0	24.931	24.804	24.711	24.638	24.579	24.529	24.486	24.448	24.415
5.5	25.006	24.880	24.786	24.714	24.654	24.604	24.562	24.524	24.491
5.0	25.089	24.962	24.869	24.796	24.737	24.687	24.644	24.607	24.574
4.5	25.180	25.054	24.961	24.888	24.829	24.779	24.736	24.699	24.665
4.0	25.282	25.156	25.063	24.990	24.931	24.881	24.839	24.801	24.768
3.8	25.327	25.200	25.107	25.035	24.976	24.926	24.883	24.846	24.813
3.6	25.374	25.247	25.154	25.082	25.023	24.973	24.930	24.893	24.860
3.4	25.423	25.297	25.204	25.131	25.072	25.023	24.980	24.943	24.910
3.2	25.476	25.349	25.256	25.184	25.125	25.076	25.033	24.996	24.963
3.0	25.531	25.405	25.312	25.240	25.181	25.132	25.090	25.052	25.019
2.8	25.591	25.465	25.372	25.300	25.241	25.192	25.150	25.113	25.079
2.6	25.655	25.529	25.437	25.365	25.306	25.257	25.215	25.177	25.144
2.4	25.725	25.598	25.506	25.434	25.376	25.327	25.284	25.247	25.214
2.2	25.800	25.674	25.582	25.510	25.452	25.403	25.360	25.323	25.290
2.0	25.882	25.756	25.665	25.593	25.535	25.486	25.443	25.406	25.372
1.9	25.926	25.801	25.709	25.638	25.580	25.531	25.488	25.451	25.417
1.8	25.973	25.848	25.756	25.685	25.627	25.578	25.535	25.497	25.463
1.7	26.023	25.897	25.806	25.735	25.677	25.627	25.585	25.547	25.512
1.6	26.056	25.907	25.770	25.625	25.460	25.273	25.067	24.848	24.623
1.5	26.045	25.816	25.574	25.315	25.047	24.779	24.515	24.258	24.009
1.4	26.010	25.709	25.400	25.093	24.794	24.508	24.234	23.971	23.719
1.3	25.968	25.612	25.266	24.937	24.627	24.335	24.058	23.794	23.540
1.2	25.928	25.534	25.167	24.828	24.514	24.219	23.941	23.677	23.423
1.1	25.895	25.477	25.098	24.754	24.438	24.143	23.865	23.600	23.347
1.0	25.873	25.439	25.054	24.708	24.391	24.096	23.818	23.554	23.300
0.9	25.865	25.420	25.033	24.686	24.369	24.074	23.797	23.533	23.279
0.8	25.871	25.421	25.033	24.686	24.370	24.076	23.798	23.534	23.281
0.7	25.895	25.443	25.055	24.709	24.393	24.099	23.822	23.558	23.305
0.6	25.939	25.488	25.100	24.755	24.440	24.146	23.869	23.605	23.352
0.5	26.110	25.560	25.174	24.829	24.514	24.220	23.943	23.679	23.426
0.4	26.118	25.669	25.283	24.939	24.623	24.329	24.052	23.788	23.535
0.3	26.277	25.828	25.442	25.097	24.781	24.487	24.210	23.946	23.693
0.2	26.519	26.068	25.681	25.336	25.020	24.726	24.449	24.185	23.931
0.1	26.936	26.484	26.096	25.750	25.434	25.140	24.862	24.598	24.345

Table (C.2) Continued

W/L in Microns	Theta							
	2.4	2.6	2.8	3.0	3.5	4.0	4.5	5.0
100.0	21.943	21.916	21.892	21.869	21.819	21.776	21.738	21.704
80.0	22.137	22.110	22.086	22.063	22.012	21.969	21.932	21.898
60.0	22.387	22.360	22.335	22.312	22.262	22.219	22.181	22.148
40.0	22.739	22.712	22.687	22.664	22.614	22.571	22.533	22.499
20.0	23.341	23.313	23.288	23.265	23.215	23.171	23.133	23.098
16.0	23.534	23.507	23.482	23.459	23.408	23.364	23.326	23.291
14.0	23.650	23.623	23.598	23.575	23.523	23.480	23.441	23.407
12.0	23.783	23.756	23.731	23.708	23.657	23.613	23.574	23.540
10.0	23.942	23.914	23.889	23.866	23.815	23.771	23.732	23.697
8.0	24.135	24.108	24.083	24.060	24.008	23.964	23.925	23.890
6.5	24.315	24.288	24.263	24.240	24.189	24.144	24.105	24.070
6.0	24.385	24.358	24.333	24.309	24.258	24.214	24.175	24.139
5.5	24.461	24.433	24.408	24.385	24.334	24.289	24.250	24.215
5.0	24.544	24.516	24.491	24.468	24.417	24.372	24.333	24.297
4.5	24.635	24.608	24.583	24.560	24.508	24.464	24.424	24.388
4.0	24.738	24.711	24.686	24.663	24.611	24.566	24.525	24.488
3.8	24.783	24.756	24.731	24.707	24.655	24.610	24.569	24.532
3.6	24.830	24.803	24.778	24.754	24.702	24.657	24.616	24.578
3.4	24.880	24.853	24.827	24.804	24.752	24.706	24.665	24.627
3.2	24.933	24.906	24.880	24.857	24.804	24.758	24.716	24.678
3.0	24.989	24.962	24.936	24.913	24.860	24.813	24.877	24.732
2.8	25.049	25.022	24.996	24.973	24.919	24.872	24.829	24.789
2.6	25.114	25.086	25.061	25.037	24.983	24.935	24.891	24.850
2.4	25.184	25.156	25.130	25.106	25.051	25.002	24.957	24.916
2.2	25.259	25.231	25.205	25.180	25.125	25.075	25.029	24.986
2.0	25.342	25.313	25.287	25.262	25.205	25.153	25.106	25.062
1.9	25.386	25.357	25.330	25.305	25.247	25.195	25.147	25.103
1.8	25.432	25.403	25.376	25.350	25.292	25.239	25.191	25.146
1.7	25.481	25.452	25.424	25.398	25.389	25.285	25.236	25.190
1.6	24.396	24.169	23.945	23.724	23.187	22.668	22.166	21.677
1.5	23.767	23.531	23.301	23.077	22.535	22.015	21.512	21.023
1.4	23.474	23.238	23.007	22.782	22.240	21.720	21.217	20.728
1.3	23.296	23.059	22.828	22.603	22.061	21.541	21.038	20.549
1.2	23.178	22.942	22.711	22.486	21.944	21.424	20.922	20.432
1.1	23.102	22.865	22.635	22.410	21.868	21.348	20.845	20.356
1.0	23.056	22.819	22.589	22.364	21.822	21.302	20.800	20.310
0.9	23.035	22.798	22.568	22.343	21.800	21.281	20.779	20.290
0.8	23.037	22.800	22.570	22.345	21.803	21.283	20.780	20.291
0.7	23.060	22.824	22.593	22.369	21.826	21.307	20.804	20.315
0.6	23.107	22.871	22.640	22.416	21.873	21.354	20.851	20.362
0.5	23.182	22.945	22.715	22.490	21.948	21.428	20.925	20.436
0.4	23.290	23.054	22.823	22.599	22.056	21.537	21.034	20.545
0.3	23.448	23.212	22.981	22.756	22.214	21.695	21.192	20.703
0.2	23.687	23.450	23.220	22.995	22.453	21.933	21.431	20.941
0.1	24.101	23.864	23.634	23.409	22.867	22.347	21.844	21.355

Table (C.3) of He_{ff}^- in cm^4/dyne from Somerville (51)

Energy in Rydbergs	Theta					
	0.2	0.3	0.4	0.5	0.6	0.8
0.000	29.351	29.198	29.105	29.039	27.149	28.907
0.006	24.907	24.754	24.662	24.595	24.542	24.463
0.008	25.156	25.004	24.910	24.845	24.793	24.714
0.010	25.350	25.198	25.106	25.039	24.987	24.907
0.015	25.701	25.550	25.458	25.391	25.339	25.260
0.020	25.951	25.801	25.708	25.642	25.590	25.511
0.025	26.146	25.996	25.903	25.836	25.785	25.706
0.030	26.304	26.152	26.061	25.996	25.943	25.866
0.035	26.438	26.286	26.195	26.129	26.078	26.001
0.040	26.553	26.402	26.312	26.246	26.194	26.119
0.050	26.747	26.597	26.506	26.441	26.390	26.315
0.060	26.907	26.757	26.666	26.600	26.551	26.478
0.070	27.040	26.889	26.801	26.738	26.688	26.614
0.080	27.156	27.007	26.917	26.854	26.807	26.733
0.090	27.258	27.111	27.022	26.959	26.910	26.839
0.100	27.350	27.203	27.115	27.052	27.004	26.932
0.110	27.433	27.286	27.199	27.137	27.089	27.018
0.120	27.509	27.364	27.276	27.214	27.167	27.095
0.130	27.578	27.434	27.347	27.286	27.238	27.167
0.140	27.644	27.499	27.413	27.352	27.305	27.232
0.150	27.703	27.559	27.474	27.413	27.366	27.293
0.160	27.759	27.616	27.532	27.471	27.424	27.350
0.170	27.812	27.670	27.585	27.524	27.478	27.403
0.180	27.863	27.721	27.636	27.575	27.527	27.453
0.190	27.910	27.770	27.684	27.623	27.575	27.500
0.200	27.955	27.815	27.730	27.670	27.622	27.544
0.220	28.039	27.900	27.815	27.754	27.706	27.625
0.240	28.115	27.975	27.893	27.830	27.780	27.699
0.260	28.185	28.048	27.963	27.900	27.851	27.767
0.280	28.250	28.114	28.029	27.967	27.914	27.827
0.300	28.312	28.175	28.089	28.025	27.971	27.883
0.400	28.564	28.428	28.338	28.268	28.210	28.113
0.500	28.759	28.622	28.526	28.451	28.388	28.284
0.600	28.917	28.775	28.676	28.595	28.529	28.420
0.700	29.051	28.903	28.799	28.714	28.646	28.533

Table (C.3) Continued

Energy in 1.0 Rydbergs	Theta					
	1.2	1.6	2.0	2.8	3.6	
0.000	28.848	28.801	28.730	28.676	28.597	28.538
0.006	24.406	24.359	24.287	24.234	24.156	24.099
0.008	24.656	24.609	24.538	24.485	24.407	24.352
0.010	24.851	24.804	24.733	24.680	24.602	24.548
0.015	25.203	25.157	25.087	25.036	24.963	24.910
0.020	25.453	25.409	25.340	25.290	25.218	25.166
0.025	25.650	25.604	25.538	25.488	25.417	25.367
0.030	25.810	25.764	25.699	25.650	25.580	25.530
0.035	25.947	25.903	25.836	25.788	25.719	25.666
0.040	26.063	26.020	25.955	25.907	25.839	25.783
0.050	26.261	26.218	26.155	26.107	26.034	25.975
0.060	26.424	26.381	26.318	26.269	26.192	26.130
0.070	26.561	26.519	26.455	26.404	26.323	26.256
0.080	26.680	26.638	26.573	26.520	26.434	26.365
0.090	26.785	26.742	26.676	26.622	26.532	26.457
0.100	26.879	26.836	26.767	26.710	26.616	26.539
0.110	26.963	26.921	26.851	26.790	26.693	26.613
0.120	27.041	26.996	26.924	26.863	26.759	26.680
0.130	27.112	27.067	26.991	26.928	26.824	26.740
0.140	27.177	27.130	27.052	26.987	26.879	26.796
0.150	27.237	27.189	27.108	27.041	26.932	26.845
0.160	27.292	27.243	27.161	27.092	26.983	26.893
0.170	27.345	27.294	27.210	27.140	27.026	26.939
0.180	27.394	27.342	27.256	27.184	27.069	26.979
0.190	27.439	27.386	27.298	27.225	27.109	27.018
0.200	27.481	27.428	27.339	27.264	27.147	27.055
0.220	27.561	27.506	27.413	27.336	27.216	27.123
0.240	27.633	27.575	27.480	27.402	27.279	27.185
0.260	27.697	27.638	27.541	27.461	27.337	27.241
0.280	27.757	27.697	27.597	27.516	27.389	27.293
0.300	27.812	27.750	27.648	27.565	27.439	27.342
0.400	28.034	27.967	27.860	27.772	27.640	27.541
0.500	28.201	28.131	28.019	27.928	27.793	27.693
0.600	28.334	28.262	28.147	28.057	27.917	27.815
0.700	28.445	28.372	28.254	28.162	28.023	27.921

Table (C.4) of Li_{ff}^- in $cm^4/dyne$ from John (54)

W/L in Microns	Temperature in $^{\circ}K$								
	15000	12500	10000	7500	5000	2500	1000	500	100
10.00	25.432	25.229	25.000	24.699	24.301	23.491	22.602	22.379	22.501
5.00	25.921	25.745	25.509	25.143	24.699	24.041	23.187	23.019	23.141
2.50	26.284	26.102	25.854	25.495	25.060	24.523	23.733	23.575	23.678
1.50	26.538	26.357	26.113	25.745	25.337	24.886	24.113	23.947	24.022
1.00	26.745	26.553	26.319	25.959	25.569	25.187	24.398	24.229	24.292
0.75	26.886	26.699	26.481	26.143	25.770	25.387	24.602	24.432	24.483
0.50	27.097	26.921	26.721	26.398	26.027	25.678	24.886	24.699	24.750

Table (C.5) of C_{ff}^- in $cm^4/dyne$ from Myerscough and McDowell (53)

Eng. in Rydbergs	Temperature in $^{\circ}K$						
	10000	9000	8000	7000	6000	5000	4000
0.000	27.724	27.927	28.098	28.244	28.373	28.486	28.592
0.040	25.796	25.690	25.577	25.449	25.302	25.131	24.928
0.050	25.979	25.873	25.762	25.633	25.485	25.315	25.110
0.060	26.124	26.020	25.910	25.783	25.629	25.462	25.248
0.070	26.220	26.117	26.004	25.876	25.730	25.558	25.350
0.080	26.310	26.213	26.092	25.971	25.824	25.648	25.462
0.090	26.377	26.283	26.167	26.046	25.896	25.721	25.506
0.100	26.432	26.328	26.215	26.086	25.943	25.770	25.565
0.200	26.921	26.824	26.699	26.569	26.432	26.252	26.051
0.300	27.337	27.229	27.113	27.000	26.824	26.658	26.456
0.500	27.699	27.585	27.481	27.347	27.201	27.032	26.824
0.700	28.027	27.921	27.824	27.678	27.538	27.367	27.167
0.900	28.292	28.187	28.071	27.959	27.796	27.620	27.432
1.000	28.444	28.347	28.229	28.097	27.959	27.770	27.569

Table (C.6) of N_{ff}^- in cm^4/dyne from John (54)

W/L in Microns	Temperature in $^{\circ}\text{K}$								
	15000	12500	10000	7500	5000	2500	1000	500	100
10.00	25.084	25.064	25.044	25.023	25.000	24.971	24.939	24.924	24.703
5.00	25.686	25.668	25.646	25.627	25.606	25.582	25.567	25.545	25.212
2.50	26.290	26.271	26.253	26.234	26.218	26.205	26.188	26.123	25.697
1.50	26.738	26.721	26.703	26.688	26.678	26.670	26.620	26.517	26.045
1.00	27.095	27.080	27.065	27.054	27.046	27.030	26.943	26.815	26.318
0.75	27.352	27.338	27.326	27.316	27.310	27.277	27.162	27.022	26.510
0.50	27.719	27.708	27.697	27.688	27.674	27.613	27.463	27.309	26.780

Table (C.7) of O_{ff}^- in cm^4/dyne from John (54)

W/L in Microns	Temperature in $^{\circ}\text{K}$								
	15000	12500	10000	7500	5000	2500	1000	500	100
10.00	25.224	25.206	25.184	25.161	25.130	25.077	25.006	24.963	24.697
5.00	25.827	25.810	25.788	25.764	25.735	25.688	25.635	25.583	25.203
2.50	26.431	26.412	26.393	26.372	26.347	26.311	26.255	26.159	25.688
1.50	26.876	26.860	26.842	26.824	26.804	26.772	26.684	26.551	26.034
1.00	27.234	27.220	27.203	27.189	27.172	27.131	27.003	26.848	26.306
0.75	27.491	27.478	27.463	27.450	27.402	27.377	27.222	27.053	26.498
0.50	27.857	27.845	27.833	27.818	27.796	27.708	27.520	27.336	26.767

Table (C.8) of Ne_{ff}^- in cm^4/dyne from John (54)

W/L in Microns	Temperature in $^{\circ}\text{K}$								
	15000	12500	10000	7500	5000	2500	1000	500	100
10.00	25.530	25.516	25.484	25.442	25.388	25.318	25.271	25.259	25.066
5.00	26.133	26.117	26.088	26.047	25.996	25.932	25.900	25.879	25.577
2.50	26.735	26.721	26.692	26.654	26.607	26.558	26.526	26.460	26.063
1.50	27.181	27.170	27.143	27.109	27.069	27.026	26.963	26.857	26.413
1.00	27.535	27.529	27.504	27.475	27.440	27.393	27.289	27.161	26.688
0.75	27.785	27.785	27.764	27.738	27.703	27.642	27.513	27.370	26.879
0.50	28.131	28.149	28.131	28.108	28.065	27.979	27.815	27.658	27.151

Table (C.9) of Na_{ff}^- in cm^4/dyne from John (54)

W/L in Microns	Temperature in $^{\circ}\text{K}$								
	15000	12500	10000	7500	5000	2500	1000	500	100
10.00	23.975	23.947	23.889	23.783	23.570	23.118	22.624	22.452	22.550
5.00	24.569	24.538	24.481	24.367	24.161	23.721	23.257	23.128	23.219
2.50	25.161	25.125	25.051	24.921	24.721	24.310	23.857	23.719	23.762
1.50	25.585	25.538	25.456	25.319	25.125	24.721	24.260	24.108	24.120
1.00	25.921	25.854	25.770	25.620	25.432	25.051	24.569	24.398	24.394
0.75	26.149	26.081	25.959	25.824	25.658	25.268	24.770	24.602	24.585
0.50	26.469	26.398	26.276	26.131	25.959	25.553	25.046	24.886	24.851

Table (C.10) of Cl_{ff}^- in cm^4/dyne from John and Morgan (52)

Eng. in Rydbergs	Theta					
	0.4	0.6	0.8	1.0	1.2	1.4
0.00	28.226	28.105	28.017	27.947	27.886	27.836
0.02	24.830	24.708	24.618	24.545	24.484	24.429
0.04	25.432	25.308	25.215	25.137	25.071	25.012
0.06	25.783	25.654	25.554	25.471	25.399	25.333
0.08	26.029	25.896	25.788	25.697	25.616	25.544
0.10	26.218	26.075	25.959	25.860	25.770	25.690
0.15	26.545	26.375	26.234	26.113	26.007	25.914
0.20	26.752	26.554	26.390	26.251	26.131	26.026
0.25	26.896	26.670	26.487	26.334	26.206	26.094
0.30	27.000	26.750	26.553	26.394	26.259	26.143

Table (C.10) Continued

Eng. in Rydbergs	Theta				
	1.6	1.8	2.0	2.5	3.0
0.00	27.790	27.750	27.712	27.631	27.559
0.02	24.381	24.337	24.296	24.206	24.127
0.04	24.959	24.910	24.866	24.770	24.684
0.06	25.275	25.221	25.171	25.061	24.967
0.08	25.479	25.418	25.363	25.240	25.134
0.10	25.618	25.553	25.492	25.358	25.244
0.15	25.827	25.752	25.682	25.532	25.408
0.20	25.936	25.851	25.777	25.618	25.487
0.25	25.996	25.910	25.833	25.670	25.536
0.30	26.043	25.955	25.876	25.708	25.573

Table (C.11) of Ar_{ff}^- in $cm^4/dyne$ from John (54)

W/L in Microns	Temperature in °K								
	15000	12500	10000	7500	5000	2500	1000	500	100
10.00	25.102	25.145	25.206	25.298	25.417	25.652	25.559	25.000	23.967
5.00	25.706	25.747	25.807	25.900	26.020	26.228	26.045	25.499	24.444
2.50	26.307	26.352	26.412	26.500	26.627	26.785	26.530	25.983	24.907
1.50	26.752	26.799	26.860	26.951	27.071	27.193	26.876	26.326	25.243
1.00	27.107	27.152	27.218	27.309	27.427	27.517	27.153	26.595	25.510
0.75	27.361	27.407	27.472	27.564	27.676	27.735	27.347	26.785	25.699
0.50	27.724	27.767	27.833	27.921	28.018	28.027	27.614	27.053	25.963

Table (C.12) of Kr_{ff}^- in $cm^4/dyne$ from John (54)

W/L in Microns	Temperature in °K								
	15000	12500	10000	7500	5000	2500	1000	500	100
10.00	24.979	25.052	25.138	25.268	25.453	25.382	24.682	24.203	23.351
5.00	25.582	25.652	25.740	25.863	26.034	25.900	25.203	24.742	23.836
2.50	26.183	26.253	26.338	26.455	26.590	26.389	25.710	25.245	24.301
1.50	26.627	26.692	26.775	26.883	26.983	26.750	26.074	25.599	24.640
1.00	26.983	27.045	27.121	27.215	27.291	27.032	26.354	25.873	24.907
0.75	27.237	27.295	27.366	27.449	27.502	27.228	26.547	26.064	25.095
0.50	27.648	27.652	27.712	27.775	27.790	27.495	26.815	26.333	25.361

Table (C.13) of Xe_{ff}^- in $cm^4/dyne$ from John (54)

W/L in Microns	Temperature in °K								
	15000	12500	10000	7500	5000	2500	1000	500	100
10.00	24.542	24.562	24.629	24.726	24.879	24.845	24.142	23.638	22.692
5.00	25.144	25.165	25.228	25.323	25.465	25.356	24.654	24.167	23.172
2.50	25.747	25.767	25.827	25.917	26.029	25.836	25.154	24.664	23.636
1.50	26.191	26.214	26.267	26.350	26.433	26.194	25.513	25.013	23.975
1.00	26.544	26.570	26.620	26.690	26.747	26.479	25.790	25.286	24.241
0.75	26.796	26.824	26.873	26.932	26.967	26.676	25.983	25.476	24.429
0.50	27.167	27.186	27.232	27.277	27.275	26.947	26.253	25.745	24.695

Table (C.14) of Cs_{ff}^- in $cm^4/dyne$ from John (54)

W/L in Microns	Temperature in °K								
	15000	12500	10000	7500	5000	2500	1000	500	100
10.00	23.578	23.640	23.606	23.527	23.387	22.733	22.168	21.849	20.904
5.00	24.201	24.229	24.208	24.149	23.983	23.301	22.770	22.405	21.380
2.50	24.745	24.796	24.796	24.745	24.569	23.821	23.325	22.925	21.849
1.50	25.149	25.208	25.208	25.187	24.959	24.201	23.697	23.274	22.187
1.00	25.444	25.523	25.538	25.538	25.301	24.495	23.979	23.547	22.454
0.75	25.638	25.745	25.770	25.796	25.538	24.699	24.180	23.738	22.643
0.50	25.886	26.046	26.108	26.102	25.886	25.000	24.456	24.004	22.908

Table (C.15) of Hg_{ff}^- in $cm^4/dyne$ from John (54)

W/L in Microns	Temperature in °K								
	15000	12500	10000	7500	5000	2500	1000	500	100
10.00	24.244	24.143	24.013	23.857	23.708	23.511	23.833	24.470	24.793
5.00	24.854	24.745	24.620	24.456	24.337	24.137	24.417	24.821	25.073
2.50	25.456	25.357	25.229	25.076	24.959	24.796	25.018	25.112	25.114
1.50	25.886	25.824	25.678	25.523	25.456	25.319	25.638	25.767	25.635
1.00	26.260	26.167	26.041	25.886	25.854	25.721	26.113	26.319	26.098
0.75	26.509	26.420	26.292	26.137	26.108	26.000	26.432	26.692	26.385
0.50	26.854	26.770	26.638	26.481	26.469	26.337	26.824	27.186	26.750

Table (C.16) of H_{2ff}^- in cm^4/dyne from Somerville (56)

Eng. in Rydbergs	Theta						
	0.8	1.0	1.2	1.6	2.0	2.8	3.6
0.000	28.767	28.708	28.670	28.623	28.593	28.559	28.538
0.006	24.323	24.264	24.227	24.181	24.152	24.118	24.100
0.008	24.573	24.514	24.478	24.432	24.403	24.371	24.354
0.010	24.767	24.710	24.672	24.627	24.599	24.567	24.551
0.015	25.120	25.063	25.027	24.983	24.959	24.928	24.917
0.020	25.371	25.315	25.281	25.239	25.215	25.189	25.178
0.025	25.565	25.511	25.478	25.438	25.416	25.393	25.383
0.030	25.726	25.674	25.640	25.602	25.582	25.561	25.551
0.040	25.979	25.932	25.900	25.866	25.845	25.827	25.815
0.050	26.179	26.131	26.103	26.071	26.053	26.031	26.015
0.060	26.343	26.297	26.270	26.239	26.220	26.197	26.177
0.080	26.604	26.561	26.535	26.504	26.483	26.451	26.424
0.100	26.807	26.764	26.740	26.708	26.682	26.642	26.609
0.120	26.975	26.932	26.907	26.870	26.842	26.793	26.754
0.140	27.114	27.073	27.045	27.003	26.971	26.921	26.876
0.160	27.235	27.192	27.162	27.117	27.082	27.025	26.979
0.180	27.341	27.297	27.265	27.216	27.178	27.117	27.071
0.220	27.519	27.471	27.435	27.381	27.338	27.272	27.221
0.260	27.664	27.613	27.573	27.514	27.469	27.398	27.344
0.300	27.785	27.730	27.690	27.625	27.577	27.503	27.447

Table (C.17) of N_{2ff}^- in cm^4/dyne from John (54)

W/L in Microns	Temperature in °K								
	15000	12500	10000	7500	5000	2500	1000	500	100
10.00	24.706	24.530	24.452	24.536	24.435	24.455	24.362	24.346	24.269
5.00	25.312	25.156	25.057	25.123	25.044	25.067	24.996	24.975	24.793
2.50	25.910	25.777	25.672	25.697	25.664	25.695	25.633	25.570	25.295
1.50	26.329	26.220	26.161	26.154	26.111	26.144	26.073	25.979	25.654
1.00	26.686	26.567	26.511	26.536	26.467	26.475	26.389	26.277	25.928
0.75	26.967	26.830	26.777	26.815	26.721	26.684	26.580	26.472	26.120
0.50	27.358	27.231	27.181	27.235	27.148	27.051	26.863	26.730	26.377

Table (C.18) of O_{2ff}^- in $cm^4/dyne$ from John (54)

W/L in Microns	Temperature in °K								
	15000	12500	10000	7500	5000	2500	1000	500	100
10.00	25.036	24.996	24.936	24.860	24.770	24.684	24.592	24.517	24.211
5.00	25.638	25.599	25.538	25.462	25.373	25.292	25.214	25.147	24.726
2.50	26.242	26.202	26.144	26.071	25.987	25.914	25.815	25.712	25.208
1.50	26.688	26.650	26.593	26.527	26.453	26.379	26.231	26.094	25.551
1.00	27.045	27.008	26.955	26.896	26.833	26.752	26.554	26.393	25.821
0.75	27.299	27.263	27.213	27.161	27.103	27.010	26.777	26.602	26.015
0.50	27.654	27.620	27.573	27.526	27.470	27.353	27.081	26.889	26.284

Table (C.19) of CO_{ff}^- in $cm^4/dyne$ from John (54)

W/L in Microns	Temperature in °K								
	15000	12500	10000	7500	5000	2500	1000	500	100
10.00	24.602	24.636	24.613	24.368	24.348	24.270	24.235	24.211	23.674
5.00	25.207	25.209	25.205	25.000	24.914	24.866	24.863	24.821	24.157
2.50	25.830	25.812	25.762	25.618	25.541	25.495	25.489	25.397	24.625
1.50	26.291	26.301	26.229	26.042	26.038	25.939	25.914	25.790	24.967
1.00	26.635	26.668	26.627	26.435	26.423	26.321	26.192	26.051	25.232
0.75	26.879	26.921	26.889	26.708	26.717	26.627	26.462	26.281	25.423
0.50	27.225	27.280	27.254	27.071	27.081	26.975	26.793	26.593	25.692

Table (C.20) of $H_2O_{ff}^-$ in $cm^4/dyne$ from John (54)

W/L in Microns	Temperature in °K								
	15000	12500	10000	7500	5000	2500	1000	500	100
10.00	-	-	-	25.416	24.602	23.788	22.904	22.309	21.288
5.00	-	-	-	25.896	25.086	24.276	23.404	22.813	21.702
2.50	-	-	-	26.257	25.495	24.733	23.900	23.298	22.164
1.50	-	-	-	26.524	25.800	25.076	24.258	23.644	22.501
1.00	-	-	-	26.760	26.045	25.330	24.535	23.914	22.768
0.75	-	-	-	26.910	26.210	25.510	24.727	24.107	22.965
0.50	-	-	-	27.130	26.440	25.750	24.985	24.372	23.240

Table (C.21) of $\text{CO}_{2\text{ff}}^-$ in cm^4/dyne from John (54)

W/L in Microns	Temperature in °K								
	15000	12500	10000	7500	5000	2500	1000	500	100
10.00	24.836	24.870	24.821	24.801	24.703	24.302	23.717	23.333	22.454
5.00	25.427	25.466	25.419	25.391	25.281	24.866	24.280	23.889	22.933
2.50	26.020	26.048	26.013	25.963	25.836	25.402	24.821	24.406	23.398
1.50	26.465	26.463	26.440	26.376	26.230	25.793	25.197	24.762	23.735
1.00	26.818	26.807	26.762	26.699	26.533	26.095	25.483	25.039	24.002
0.75	27.076	27.056	26.991	26.921	26.747	26.304	25.680	25.231	24.190
0.50	27.420	27.398	27.337	27.237	27.041	26.587	25.955	25.502	24.456

Table (C.22) of OH_{bf} in cm^2 from Tarafdar and Das (57)

W/L in Microns	Temperature in °K				
	6000	5000	4000	3000	2000
0.50	20.215	20.629	21.269	22.363	24.590
0.45	20.539	20.893	21.442	22.387	24.330
0.40	20.084	20.441	20.991	21.928	23.812
0.35	19.883	20.178	20.640	21.437	23.063
0.30	19.730	19.959	20.316	20.947	22.244
0.25	19.450	19.607	19.860	20.305	21.206
0.20	19.111	19.180	19.298	19.504	19.910
0.15	18.812	18.788	18.767	18.745	18.728
0.10	19.105	19.088	19.076	19.071	19.072

Table (C.23) of CH_{bf} in cm^2 from Tarafdar and Das (57)

W/L in Microns	Temperature in °K				
	6000	5000	4000	3000	2000
0.30	20.623	20.939	21.441	22.298	23.034
0.28	20.547	20.812	21.234	21.963	23.457
0.26	21.599	21.943	22.467	23.335	25.007
0.24	19.870	20.064	20.367	20.886	21.947
0.22	19.780	19.896	20.075	20.376	20.971
0.20	18.394	18.355	18.310	18.263	18.216
0.19	18.493	18.483	18.462	18.437	18.412
0.18	18.599	18.611	18.613	18.611	18.609
0.17	18.845	18.896	18.936	18.967	18.991
0.16	18.815	18.963	19.134	19.286	19.373
0.15	18.754	18.914	19.150	19.503	19.575
0.14	18.480	18.587	18.910	19.074	19.699
0.13	18.025	18.041	18.084	18.180	18.418
0.12	17.750	17.695	17.638	17.575	17.513

For the bound-free absorption of the negative ions tabulated below from Robinson and Geltman (55), the absorption is given in the number in cm^2 with a factor of 10^{-18} omitted from the second entry onwards, against the energy in Rydbergs relative to the photodetachment energy, with the first entry being the photodetachment energy in Rydbergs. Thus the actual energies are the sums of the first entries for each ion and the relative energies as tabulated.

Table (C.24) of Bound-Free Absorption in 10^{-18}cm^2 from Robinson and Geltman (55)

Energy in C Rydbergs	O	F	Si	S	Cl	Br	I
0.09188	0.1077	0.2534	0.1022	0.1521	0.2656	0.2472	0.2248
0.000	0.00	0.00	0.00	0.00	0.00	0.00	0.00
0.005	7.18	4.08	2.93	26.20	6.49	6.98	12.90
0.010	8.82	5.37	4.29	27.40	9.27	10.90	13.80
0.020	10.00	6.42	5.45	25.60	11.20	13.70	13.80
0.030	10.50	6.84	6.16	24.90	11.70	14.30	13.60
0.050	11.40	7.27	6.76	27.10	12.40	14.80	21.50
0.070	12.40	7.63	7.09	32.00	13.40	15.50	22.10
0.090	13.30	7.98	7.35	37.40	14.80	16.60	23.70
0.110	14.10	8.31	7.61	42.20	25.80	18.00	26.10
0.130	14.80	8.61	7.89	46.20	27.60	19.80	29.00
0.150	15.40	14.50	8.19	49.20	29.50	21.60	32.30
0.170	15.90	16.80	8.49	51.40	31.50	23.60	35.60
0.190	16.20	17.00	8.80	53.00	33.70	25.60	38.90
0.210	16.50	17.10	9.11	53.90	35.70	27.70	42.00
0.230	16.70	17.20	9.41	54.40	37.70	29.70	44.90
0.250	16.80	17.30	9.70	54.40	39.50	31.60	47.60
0.300	16.90	17.50	10.40	52.60	46.00	36.30	53.50
0.400	16.60	19.60	11.40	42.80	52.00	44.30	61.50
0.500	16.00	18.90	12.10	30.40	54.40	50.30	64.90
0.600	15.10	18.10	12.60	20.10	53.50	54.00	63.60
0.700	14.10	17.30	12.80	12.80	49.80	54.60	58.20
0.800	13.10	16.40	12.80	7.82	43.60	51.60	50.10
0.900	12.10	15.60	12.80	4.64	35.60	44.90	41.10

Finally as used in section 3.4, the log of the absorption of quasi-molecular hydrogen from Solomon (58) is given here in cubic centimetres per square dyne against wavenumber, again with the negative signs omitted.

Table (C.25) of Quasi-H₂ in cm³/dyne² from Solomon (58)

W/NUM	Theta			
	0.4	0.8	1.2	1.6
16000	20.086	21.770	23.658	25.638
20000	19.602	21.036	22.699	24.444
24000	19.215	20.387	21.824	23.337
30000	18.886	19.638	20.699	21.886
40000	18.444	18.770	19.357	20.000
50000	18.143	18.092	18.310	18.620
60000	18.076	17.638	17.509	17.495
70000	17.796	17.114	16.770	16.509

Note that as stated in chapter 3, all this data here is included in the coding even though some species may have negligible abundances, or we may not consider them at all, like the negative Hg ion for free-free absorption.

APPENDIX D

Adopted Core Statistical Weights of Atoms and Ions

As Stated in section 2.2, when computing partition functions, we must include in an approximate general way the effect of all the excited states up to the ionization potential. The ionization potential is reduced by collisions with the nearest neighbours, thus preventing the sum from being divergent. We can consider that for a single electron at a sufficient distance from the rest of the atom, the atom can be considered to be hydrogen-like, as discussed, but with an effective core statistical weight g_c due to all the other electrons, in addition to the $2n^2$ factor.

For the elements up to Ni, table (D.1) lists the adopted core statistical weights, the principal quantum number n from which the summation in (2.2.8) is started, the term value T in cm^{-1} with which this corresponds to, where $T = hcE_n$, and the adopted configuration or configurations from which g_c is obtained by simply adding up all possible combinations of arranging the electrons in the specified orbitals. The configuration of the core is given in brackets, where from Li onwards, there is an inert gas structure contributing unity to g_c , and the configuration of the remaining electrons but one, if there are any. The lowest adopted configuration of the remaining "hydrogen-like" electron is given outside the brackets. For positive ions, g_c and n are obtained from the atoms in the same isoelectronic

sequences; for negative ions this whole treatment is not relevant.

The term values, given here only for the neutral atoms, are obtained from Moore (33) for the lowest level for which the outermost electron is in the ns orbital, with n as tabulated, except for the transition elements. Because the transition elements have a very much more complicated electronic structure due to the incompletely filled $3d$ orbitals in our case, for Sc to Ni, T is approximately obtained from the mean of the first occurrence of ns and $(n+1)s$ for the outermost electron, or if the term for $(n+1)s$ is not available, the last level tabulated is used. Note that the values for T given in the table, which are used as data for the computer program, are given to an accuracy which is really quite meaningless in most cases, and for the sake of completeness, values of T are given for those elements between H and Ti that are not in the mixture. For the transition elements, two configurations appear to be most common, with g_c obtained from the sum of the two; other configurations being neglected.

The summation over the actual levels is stopped at $20,000\text{cm}^{-1}$, and technically when we deal with all the remaining levels in this average way, we should avoid counting levels twice or missing them altogether. However, over the temperatures that we are concerned with, because individual levels above $20,000\text{cm}^{-1}$ contribute so little to the partition function, though the ensemble may be important, we do not have to worry about this additional complication, which for the transition elements would be difficult to handle. This whole treatment is particularly for the transition elements a gross

simplification to a very complicated situation. However, as is discussed in section 7.2, this treatment makes no difference to the partition function of the ions, and of the neutral atoms, only Na, K and the transition elements are significantly affected over the temperatures within the range of interest. For our cases, the levels that contribute most to the partition function are the lowest and possibly the highest just below the ionization limit due to their very large number, with little contribution in between.

Table (D.1) of Core Statistical Weights

<u>Z</u>	<u>Element</u>	<u>g_c</u>	<u>n</u>	<u>T</u>	<u>Configurations</u>
1	H	1	2	82258.94	2s
2	He	2	2	163061.02	(1s)2s
3	Li	1	3	27206.12	(He)3s
4	Be	2	3	54677.20	(He2s)3s
5	B	1	3	40040.00	(He2s ²)3s
6	C	6	3	60353.00	(He2s ² 2p)3s
7	N	15	3	83319.30	(He2s ² 2p ²)3s
8	O	20	3	75281.25	(He2s ² 2p ³)3s
9	F	15	3	102681.24	(He2s ² 2p ⁴)3s
10	Ne	6	3	134252.52	(He2s ² 2p ⁵)3s
11	Na	1	4	25739.86	(Ne)4s
12	Mg	2	4	42350.19	(Ne3s)4s
13	Al	1	4	25347.69	(Ne3s ²)4s
14	Si	6	4	39760.20	(Ne3s ² 3p)4s
15	P	15	4	56090.59	(Ne3s ² 3p ²)4s

<u>Z</u>	<u>Element</u>	<u>ξ_c</u>	<u>n</u>	<u>T</u>	<u>Configurations</u>
16	S	20	4	53977.52	(Ne3s ² 3p ³)4s
17	Cl	15	4	72484.20	(Ne3s ² 3p ⁴)4s
18	Ar	6	4	93447.22	(Ne3s ² 3p ⁵)4s
19	K	1	5	21026.80	(Ar)5s
20	Ca	2	5	32428.38	(Ar4s)5s
21	Sc	65	5	34451.45	(Ar3d4s & Ar3d ²)5s
22	Ti	210	5	40994.87	(Ar3d ² 4s & Ar3d ³)5s
23	V	250	5	37227.44	(Ar3d ³ 4s & Ar3d ⁴)5s
24	Cr	672	5	41269.56	(Ar3d ⁴ 4s & Ar3d ⁵)5s
25	Mn	714	5	44794.47	(Ar3d ⁵ 4s & Ar3d ⁶)5s
26	Fe	540	5	48924.19	(Ar3d ⁶ 4s & Ar3d ⁷)5s
27	Co	285	5	45491.09	(Ar3d ⁷ 4s & Ar3d ⁸)5s
28	Ni	100	5	47530.88	(Ar3d ⁸ 4s & Ar3d ⁹)5s

APPENDIX E

Hönl-London Factors for Doublets and Triplets

As stated in chapter 4, section 2B, the Hönl-London factors for doublets given by Kovács (31) can be compressed into six different expressions, three for $\Delta\lambda = 0$ and three for $\Delta\lambda = \pm 1$. Given Kovács's equations 6 on page 61:

$$u^{\pm}(j) = \left[\lambda^2 \gamma(\gamma-4) + 4 \left(j + \frac{1}{2} \right)^2 \right]^{1/2} \pm \lambda(\gamma-2) \quad (\text{E.1})$$

$$C^{\pm}(j) = \frac{1}{2} \left\{ u^{\pm}(j)^2 + 4 \left[\left(j + \frac{1}{2} \right)^2 - \lambda^2 \right] \right\}$$

and defining:

$$\begin{aligned} k &= 4(2i-3)(2j-3) \\ m &= 2i-3 \\ n &= 2j-3 \end{aligned} \quad (\text{E.2})$$

where i and j are the series to which the upper and lower levels belong respectively, with each taking the values 1 or 2; then we can compress the expressions given for the doublet strengths. Let the function C^m be C^- or C^+ depending on the sign of m , i.e. for $i = 1$ or 2 respectively, and similarly for C^n , u^m and u^n , then for $\Delta\lambda = 0$

we can write:

$$\begin{aligned}
 P_{ij}(\mathcal{J}) &= \frac{(\mathcal{J}-\Lambda-\frac{1}{2})(\mathcal{J}+\Lambda+\frac{1}{2})}{4\mathcal{J}c'^m(\mathcal{J}-1)c''^n(\mathcal{J})} \left\{ u'^m(\mathcal{J}-1)u''^n(\mathcal{J}) + k(\mathcal{J}-\Lambda+\frac{1}{2})(\mathcal{J}+\Lambda-\frac{1}{2}) \right\}^2 \\
 Q_{ij}(\mathcal{J}) &= \frac{(\mathcal{J}+\frac{1}{2})}{2\mathcal{J}(\mathcal{J}+1)c'^m(\mathcal{J})c''^n(\mathcal{J})} \left\{ (\Lambda+\frac{1}{2})u'^m(\mathcal{J})u''^n(\mathcal{J}) \right. \\
 &\quad \left. + k(\Lambda-\frac{1}{2})(\mathcal{J}-\Lambda+\frac{1}{2})(\mathcal{J}+\Lambda+\frac{1}{2}) \right\}^2 \quad (E.3) \\
 R_{ij}(\mathcal{J}) &= \frac{(\mathcal{J}-\Lambda+\frac{1}{2})(\mathcal{J}+\Lambda+\frac{3}{2})}{4(\mathcal{J}+1)c'^m(\mathcal{J}+1)c''^n(\mathcal{J})} \left\{ u'^m(\mathcal{J}+1)u''^n(\mathcal{J}) + k(\mathcal{J}-\Lambda+\frac{3}{2})(\mathcal{J}+\Lambda+\frac{1}{2}) \right\}^2
 \end{aligned}$$

and for $\Delta\Lambda = \pm 1$, we can write:

$$\underline{\Delta\Lambda = +1} \quad \underline{\Delta\Lambda = -1}$$

$$\begin{aligned}
 P_{ij}(\mathcal{J}) &= R_{ji}(\mathcal{J}-1) = \frac{(\mathcal{J}-\Lambda-\frac{3}{2})(\mathcal{J}-\Lambda-\frac{1}{2})}{8\mathcal{J}c'^m(\mathcal{J}-1)c''^n(\mathcal{J})} \left\{ u'^m(\mathcal{J}-1)u''^n(\mathcal{J}) \right. \\
 &\quad \left. + k(\mathcal{J}-\Lambda+\frac{1}{2})(\mathcal{J}+\Lambda+\frac{1}{2}) \right\}^2 \\
 Q_{ij}(\mathcal{J}) &= Q_{ji}(\mathcal{J}) = \frac{(\mathcal{J}-\Lambda-\frac{1}{2})(\mathcal{J}+\frac{1}{2})(\mathcal{J}+\Lambda+\frac{3}{2})}{4\mathcal{J}(\mathcal{J}+1)c'^m(\mathcal{J})c''^n(\mathcal{J})} \left\{ u'^m(\mathcal{J})u''^n(\mathcal{J}) \right. \\
 &\quad \left. + k(\mathcal{J}-\Lambda+\frac{1}{2})(\mathcal{J}+\Lambda+\frac{1}{2}) \right\}^2 \quad (E.4) \\
 R_{ij}(\mathcal{J}) &= P_{ji}(\mathcal{J}+1) = \frac{(\mathcal{J}+\Lambda+\frac{3}{2})(\mathcal{J}+\Lambda+\frac{5}{2})}{8(\mathcal{J}+1)c'^m(\mathcal{J}+1)c''^n(\mathcal{J})} \left\{ u'^m(\mathcal{J}+1)u''^n(\mathcal{J}) \right. \\
 &\quad \left. + k(\mathcal{J}-\Lambda+\frac{1}{2})(\mathcal{J}+\Lambda+\frac{1}{2}) \right\}^2
 \end{aligned}$$

If either the coupling constants Y' or Y'' for the two electronic states are negative, then in (E.3) or (E.4) as appropriate, the indices on the left hand side are changed, such that $i \rightarrow 3-i$ or $j \rightarrow 3-j$ respectively, according to the convention discussed in section 4.2B. If $\Lambda' \neq \Lambda''$, the appropriate values are inserted into (E.1) for the two electronic states, but the smaller of the two must be used in (E.4). Finally, as discussed in section 4.2B, in a few

cases (E.3) or (E.4) may break down even for valid transitions.

For the Hönl-London factors of triplets, although there are many similarities between the 54 expressions given by Kovács, which are used to advantage in programming, these expressions cannot be compressed as for the doublets, so the full expressions given by Kovács are reproduced here, with the correction as noted in section 4.2C.

Given Kovács's equations 9 and 10 on page 70:

$$a_1^{\pm}(\mathcal{J}) = [\Lambda^2 \gamma(\gamma-4) + 4\mathcal{J}^2]^{\frac{1}{2}} \pm \Lambda(\gamma-2) \tag{E.5}$$

$$a_3^{\pm}(\mathcal{J}) = [\Lambda^2 \gamma(\gamma-4) + 4(\mathcal{J}+1)^2]^{\frac{1}{2}} \pm \Lambda(\gamma-2)$$

and:

$$C_1(\mathcal{J}) = \Lambda^2 \gamma(\gamma-4)(\mathcal{J}-\Lambda+1)(\mathcal{J}+\Lambda) + 2(2\mathcal{J}+1)(\mathcal{J}-\Lambda)\mathcal{J}(\mathcal{J}+\Lambda)$$

$$C_2(\mathcal{J}) = \Lambda^2 \gamma(\gamma-4) + 4\mathcal{J}(\mathcal{J}+1)$$

$$C_3(\mathcal{J}) = \Lambda^2 \gamma(\gamma-4)(\mathcal{J}-\Lambda)(\mathcal{J}+\Lambda+1) + 2(2\mathcal{J}+1)(\mathcal{J}-\Lambda+1) \tag{E.6}$$

$$\times (\mathcal{J}+1)(\mathcal{J}+\Lambda+1)$$

respectively, then the Hönl-London factors are obtained from Kovács's table 3.8 for $\Delta\Lambda = 0$ and 3.10 for $\Delta\Lambda = \pm 1$, which we will refer to here as (E.7) and (E.8) respectively.

Branches	Line strengths
$AA = 0$	${}^3X(\text{int}) - {}^3X(\text{int})$
$P_1(J)$	$\frac{(J-A)(J+A)}{16JC_1^2(J-1)C_1^2(J)} \{ (J-A+1)(J+A-1)u_1^+(J-1)u_1^+(J) + (J-A-1)(J+A+1)u_1^-(J-1)u_1^-(J) + 8(J-A-1)(J-A)(J+A-1)(J+A) \}^2$
$Q_1(J)$	$\frac{2J+1}{16J(J+1)C_1^2(J)C_1^2(J)} \{ (A-1)(J-A+1)(J+A)u_1^+(J)u_1^+(J) + (A+1)(J-A)(J+A+1)u_1^-(J)u_1^-(J) + 8.1(J-A)^2(J+A)^2 \}^2$
$R_1(J)$	$\frac{(J-A+1)(J+A+1)}{16(J+1)C_1^2(J+1)C_1^2(J)} \{ (J-A+2)(J+A)u_1^+(J+1)u_1^+(J) + (J-A)(J+A+2)u_1^-(J+1)u_1^-(J) + 8(J-A)(J-A+1)(J+A)(J+A+1) \}^2$
${}^qP_{21}(J)$	$\frac{(J-A)(J+A)}{2JC_2^2(J-1)C_1^2(J)} \{ (J-A+1)(J+A-1)u_1^+(J) - (J-A-1)(J+A+1)u_1^-(J) - 2.1(J-A)(J+A)(Y''-2) \}^2$
${}^RQ_{21}(J)$	$\frac{2J+1}{2J(J+1)C_2^2(J)C_1^2(J)} \{ (A-1)(J-A+1)(J+A)u_1^+(J) - (A+1)(J-A)(J+A+1)u_1^-(J) - 2.1^2(J-A)(J+A)(Y''-2) \}^2$
${}^S R_{21}(J)$	$\frac{(J-A+1)(J+A+1)}{2(J+1)C_2^2(J+1)C_1^2(J)} \{ (J-A+2)(J+A)u_1^+(J) - (J-A)(J+A+2)u_1^-(J) - 2.1(J-A)(J+A)(Y''-2) \}^2$
${}^R P_{31}(J)$	$\frac{(J-A)(J+A)}{16JC_3^2(J-1)C_1^2(J)} \{ (J-A+1)(J+A-1)u_3^-(J-1)u_1^+(J) + (J-A-1)(J+A+1)u_3^+(J-1)u_1^-(J) - 8(J-A)^2(J+A)^2 \}^2$
${}^S Q_{31}(J)$	$\frac{2J+1}{16J(J+1)C_3^2(J)C_1^2(J)} \{ (A-1)(J-A+1)(J+A)u_3^-(J)u_1^+(J) + (A+1)(J-A)(J+A+1)u_3^+(J)u_1^-(J) - 8.1(J-A)(J-A+1)(J+A)(J+A+1) \}^2$
${}^T R_{31}(J)$	$\frac{(J-A+1)(J+A+1)}{16(J+1)C_3^2(J+1)C_1^2(J)} \{ (J-A+2)(J+A)u_3^-(J+1)u_1^+(J) + (J-A)(J+A+2)u_3^+(J+1)u_1^-(J) - 8(J-A)(J-A+2)(J+A)(J+A+2) \}^2$

(E.7)

${}^o P_{12}(J)$	$\frac{(J-A)(J+A)}{2JC_1^2(J-1)C_2^2(J)} \{ (J-A+1)(J+A-1)u_1^+(J-1) - (J-A-1)(J+A+1)u_1^-(J-1) - 2.1(J-A-1)(J+A-1)(Y''-2) \}^2$
${}^P Q_{12}(J)$	$\frac{2J+1}{2J(J+1)C_1^2(J)C_2^2(J)} \{ (A-1)(J-A+1)(J+A)u_1^+(J) - (A+1)(J-A)(J+A+1)u_1^-(J) - 2.1^2(J-A)(J+A)(Y''-2) \}^2$
${}^q R_{12}(J)$	$\frac{(J-A+1)(J+A+1)}{2(J+1)C_1^2(J+1)C_2^2(J)} \{ (J-A+2)(J+A)u_1^+(J+1) - (J-A)(J+A+2)u_1^-(J+1) - 2.1(J-A+1)(J+A+1)(Y''-2) \}^2$
$P_2(J)$	$\frac{4(J-A)(J+A)}{JC_2^2(J-1)C_2^2(J)} \{ \frac{1}{2} 1^2(Y''-2)(Y''-2) + (J-A-1)(J+A+1) + (J-A+1)(J+A-1) \}^2$
$Q_2(J)$	$\frac{4(2J+1)}{J(J+1)C_2^2(J)C_2^2(J)} \{ \frac{1}{2} 1^2(Y''-2)(Y''-2) + (A+1)(J-A)(J+A+1) + (A-1)(J-A+1)(J+A) \}^2$
$R_2(J)$	$\frac{4(J-A+1)(J+A+1)}{(J+1)C_2^2(J+1)C_2^2(J)} \{ \frac{1}{2} 1^2(Y''-2)(Y''-2) + (J-A)(J+A+2) + (J-A+2)(J+A) \}^2$
${}^q P_{32}(J)$	$\frac{(J-A)(J+A)}{2JC_3^2(J-1)C_2^2(J)} \{ (J-A+1)(J+A-1)u_3^-(J-1) - (J-A-1)(J+A+1)u_3^+(J-1) + 2.1(J-A)(J+A)(Y''-2) \}^2$
${}^R Q_{32}(J)$	$\frac{2J+1}{2J(J+1)C_3^2(J)C_2^2(J)} \{ (A-1)(J-A+1)(J+A)u_3^-(J) - (A+1)(J-A)(J+A+1)u_3^+(J) + 2.1^2(J-A+1)(J+A+1)(Y''-2) \}^2$
${}^S R_{32}(J)$	$\frac{(J-A+1)(J+A+1)}{2(J+1)C_3^2(J+1)C_2^2(J)} \{ (J-A+2)(J+A)u_3^-(J+1) - (J-A)(J+A+2)u_3^+(J+1) + 2.1(J-A+2)(J+A+2)(Y''-2) \}^2$

Branches	Line strengths
$AA = 0$	${}^3X(\text{int}) - {}^3X(\text{int})$
${}^N P_{13}(J)$	$\frac{(J-A)(J+A)}{16JC_1'(J-1)C_3''(J)} \{ (J-A+1)(J+A-1)u_1'+(J)u_3''-(J) + (J-A-1)(J+A+1)u_1''-(J-1)u_3'+(J) - 8(J-A-1)(J-A+1)(J+A-1)(J+A+1) \}^2$
${}^O Q_{12}(J)$	$\frac{2J+1}{16J(J+1)C_1'(J)C_3''(J)} \{ (A-1)(J-A+1)(J+A)u_1'+(J)u_3''-(J) + (A+1)(J-A)(J+A+1)u_1''-(J)u_3'+(J) - 8.1(J-A)(J-A+1)(J+A)(J+A+1) \}^2$
${}^P R_{13}(J)$	$\frac{(J-A+1)(J+A+1)}{16(J+1)C_1'(J+1)C_3''(J)} \{ (J-A+2)(J+A)u_1'+(J+1)u_3''-(J) + (J-A)(J+A+2)u_1''-(J+1)u_3'+(J) - 8(J-A+1)^2(J+A+1)^2 \}^2$
${}^O P_{23}(J)$	$\frac{(J-A)(J+A)}{2JC_2'(J-1)C_3''(J)} \{ (J-A+1)(J+A-1)u_3''-(J) - (J-A-1)(J+A+1)u_3'+(J) + 2.1(J-A+1)(J+A+1)(Y'-2) \}^2$
${}^P Q_{23}(J)$	$\frac{2J+1}{2J(J+1)C_2'(J)C_3''(J)} \{ (A-1)(J-A+1)(J+A)u_3''-(J) - (A+1)(J-A)(J+A+1)u_3'+(J) + 2.1^2(J-A+1)(J+A+1)(Y'-2) \}^2$
${}^Q R_{23}(J)$	$\frac{(J-A+1)(J+A+1)}{2(J+1)C_2'(J+1)C_3''(J)} \{ (J-A+2)(J+A)u_3''-(J) - (J-A)(J+A+2)u_3'+(J) + 2.1(J-A+1)(J+A+1)(Y'-2) \}^2$
${}^P_2(J)$	$\frac{(J-A)(J+A)}{16JC_2'(J-1)C_3''(J)} \{ (J-A+1)(J+A-1)u_3''-(J-1)u_3'+(J) + (J-A-1)(J+A+1)u_3'+(J-1)u_3''+(J) + 8(J-A)(J-A+1)(J+A)(J+A+1) \}^2$
${}^Q_2(J)$	$\frac{2J+1}{16J(J+1)C_2'(J)C_3''(J)} \{ (A-1)(J-A+1)(J+A)u_3''-(J)u_3''-(J) + (A+1)(J-A)(J+A+1)u_3'+(J)u_3'+(J) + 8.1(J-A+1)^2(J+A+1)^2 \}^2$
${}^R_3(J)$	$\frac{(J-A+1)(J+A+1)}{16(J+1)C_2'(J+1)C_3''(J)} \{ (J-A+2)(J+A)u_3''-(J+1)u_3'+(J) + (J-A)(J+A+2)u_3'+(J+1)u_3''+(J) + 8(J-A+1)(J-A+2)(J+A+1)(J+A+2) \}^2$

(E.7) Continued

Branches		Line strengths
$\Delta A = +1$	$\Delta A = -1$	${}^3X(\text{int}) - {}^3Y(\text{int})$
$P_1(J)$	$R_1(J-1)$	$\frac{(J-A-1)(J-A)}{32JC_1'(J-1)C_1''(J)} \{(J-A+1)(J+A)u_1'+(J-1)u_1''+(J-A-2)(J+A+1)u_1'-(J-1) \times u_1''-(J)+8(J-A-2)(J-A)(J+A)^2\}^2$
$Q_1(J)$	$Q_1(J)$	$\frac{(J-A)(J+A+1)(2J+1)}{32J(J+1)C_1'(J)C_1''(J)} \{(J-A+1)(J+A)u_1'+(J)u_1''+(J-A-1)(J+A+2) \times u_1'-(J)u_1''-(J)+8(J-A-1)(J-A)(J+A)(J+A+1)\}^2$
$R_1(J)$	$P_1(J+1)$	$\frac{(J+A+1)(J+A+2)}{32(J+1)C_1'(J+1)C_1''(J)} \{(J-A+1)(J+A)u_1'+(J+1)u_1''+(J-A)(J+A+3)u_1'-(J+1) \times u_1''-(J)+8(J-A)^2(J+A)(J+A+2)\}^2$
${}^Q P_{21}(J)$	${}^Q R_{12}(J-1)$	$\frac{(J-A-1)(J-A)}{4JC_2'(J-1)C_1''(J)} \{(J-A+1)(J+A)u_1'+(J)-(J-A-2)(J+A+1)u_1''-(J)-2(A+1)(J-A)(J+A)(Y''-2)\}^2$
${}^R Q_{21}(J)$	${}^P Q_{12}(J)$	$\frac{(J-A)(J+A+1)(2J+1)}{4J(J+1)C_2'(J)C_1''(J)} \{(J-A+1)(J+A)u_1'+(J)-(J-A-1)(J+A+2)u_1''-(J)-2(A+1)(J-A)(J+A)(Y''-2)\}^2$
${}^S R_{21}(J)$	${}^O P_{12}(J+1)$	$\frac{(J+A+1)(J+A+2)}{4(J+1)C_2'(J+1)C_1''(J)} \{(J-A+1)(J+A)u_1'+(J)-(J-A)(J+A+3)u_1''-(J)-2(A+1)(J-A)(J+A)(Y''-2)\}^2$
${}^R P_{31}(J)$	${}^P R_{13}(J-1)$	$\frac{(J-A-1)(J-A)}{32JC_3'(J-1)C_1''(J)} \{(J-A+1)(J+A)u_3'+(J-1)u_3''+(J-A-2)(J+A+1)u_3'-(J-1) \times u_3''-(J)+8(J-A-1)(J-A)(J+A)(J+A+1)\}^2$
${}^S Q_{31}(J)$	${}^O Q_{13}(J)$	$\frac{(J-A)(J+A+1)(2J+1)}{32J(J+1)C_3'(J)C_1''(J)} \{(J-A+1)(J+A)u_3'+(J)u_3''+(J-A-1)(J+A+2) \times u_3'-(J)u_3''-(J)+8(J-A)^2(J+A)(J+A+2)\}^2$
${}^T R_{31}(J)$	${}^N P_{13}(J+1)$	$\frac{(J+A+1)(J+A+2)}{32(J+1)C_3'(J+1)C_1''(J)} \{(J-A+1)(J+A)u_3'+(J+1)u_3''+(J-A)(J+A+3)u_3'-(J+1) \times u_3''-(J)+8(J-A)(J-A+1)(J+A)(J+A+3)\}^2$

(E.8)

${}^O P_{12}(J)$	${}^S R_{21}(J-1)$	$\frac{(J-A-1)(J-A)}{4JC_1'(J-1)C_2''(J)} \{(J-A+1)(J+A)u_1'+(J-1)u_1''-(J-A-2)(J+A+1)u_1'-(J-1) \times u_1''-(J)+2.1(J-A-2)(J+A)(Y''-2)\}^2$
${}^P Q_{12}(J)$	${}^R Q_{21}(J)$	$\frac{(J-A)(J+A+1)(2J+1)}{4J(J+1)C_1'(J)C_2''(J)} \{(J-A+1)(J+A)u_1'+(J)-(J-A-1)(J+A+2)u_1''-(J)-2.1(J-A-1)(J+A+1)(Y''-2)\}^2$
${}^Q R_{12}(J)$	${}^Q P_{21}(J+1)$	$\frac{(J+A+1)(J+A+2)}{4(J+1)C_1'(J+1)C_2''(J)} \{(J-A+1)(J+A)u_1'+(J+1)u_1''-(J-A)(J+A+3)u_1'-(J+1) \times u_1''-(J)+2.1(J-A)(J+A+2)(Y''-2)\}^2$
$P_2(J)$	$R_2(J-1)$	$\frac{2(J-A-1)(J-A)}{JC_2'(J-1)C_2''(J)} \{1/2.1(A+1)(Y''-2)(Y''-2)+(J-A+1)(J+A)+ (J-A-2)(J+A+1)\}^2$
$Q_2(J)$	$Q_2(J)$	$\frac{2(J-A)(J+A+1)(2J+1)}{J(J+1)C_2'(J)C_2''(J)} \{1/2.1(A+1)(Y''-2)(Y''-2)+(J-A+1)(J+A)+ (J-A-1)(J+A+2)\}^2$
$R_2(J)$	$P_2(J+1)$	$\frac{2(J+A+1)(J+A+2)}{(J+1)C_2'(J+1)C_2''(J)} \{1/2.1(A+1)(Y''-2)(Y''-2)+(J-A+1)(J+A)+ (J-A)(J+A+3)\}^2$
${}^Q P_{32}(J)$	${}^Q R_{23}(J-1)$	$\frac{(J-A-1)(J-A)}{4JC_3'(J-1)C_2''(J)} \{(J-A+1)(J+A)u_3'+(J-1)u_3''-(J-A-2)(J+A+1)u_3'-(J-1) \times u_3''-(J)+2.1(J-A-1)(J+A+1)(Y''-2)\}^2$
${}^R Q_{32}(J)$	${}^P Q_{23}(J)$	$\frac{(J-A)(J+A+1)(2J+1)}{4J(J+1)C_3'(J)C_2''(J)} \{(J-A+1)(J+A)u_3'+(J)-(J-A-1)(J+A+2)u_3''-(J)+2.1(J-A)(J+A+2)(Y''-2)\}^2$
${}^S R_{32}(J)$	${}^O P_{23}(J+1)$	$\frac{(J+A+1)(J+A+2)}{4(J+1)C_3'(J+1)C_2''(J)} \{(J-A+1)(J+A)u_3'+(J+1)u_3''-(J-A)(J+A+3)u_3'-(J+1) \times u_3''-(J)+2.1(J-A+1)(J+A+3)(Y''-2)\}^2$

(E.8) Continued

$(1 - 1 - 1)(1 - 1 - 1)(1 - 1 - 1) \times \frac{(1 - 1 - 1)(1 - 1 - 1)(1 - 1 - 1)}{(1 - 1 - 1)(1 - 1 - 1)(1 - 1 - 1)}$	$(1 - 1 - 1)$	$H_{11}(1)$
$(1 - 1 - 1)(1 - 1 - 1)(1 - 1 - 1) \times \frac{(1 - 1 - 1)(1 - 1 - 1)(1 - 1 - 1)}{(1 - 1 - 1)(1 - 1 - 1)(1 - 1 - 1)}$	$(1 - 1 - 1)$	$\partial_{11}(1)$
$(1 - 1 - 1)(1 - 1 - 1)(1 - 1 - 1) \times \frac{(1 - 1 - 1)(1 - 1 - 1)(1 - 1 - 1)}{(1 - 1 - 1)(1 - 1 - 1)(1 - 1 - 1)}$	$(1 - 1 - 1)$	$H_{12}(1)$
$(1 - 1 - 1)(1 - 1 - 1)(1 - 1 - 1) \times \frac{(1 - 1 - 1)(1 - 1 - 1)(1 - 1 - 1)}{(1 - 1 - 1)(1 - 1 - 1)(1 - 1 - 1)}$	$(1 - 1 - 1)$	$\partial_{12}(1)$
$(1 - 1 - 1)(1 - 1 - 1)(1 - 1 - 1) \times \frac{(1 - 1 - 1)(1 - 1 - 1)(1 - 1 - 1)}{(1 - 1 - 1)(1 - 1 - 1)(1 - 1 - 1)}$	$(1 - 1 - 1)$	$H_{21}(1)$
$(1 - 1 - 1)(1 - 1 - 1)(1 - 1 - 1) \times \frac{(1 - 1 - 1)(1 - 1 - 1)(1 - 1 - 1)}{(1 - 1 - 1)(1 - 1 - 1)(1 - 1 - 1)}$	$(1 - 1 - 1)$	$\partial_{21}(1)$
$(1 - 1 - 1)(1 - 1 - 1)(1 - 1 - 1) \times \frac{(1 - 1 - 1)(1 - 1 - 1)(1 - 1 - 1)}{(1 - 1 - 1)(1 - 1 - 1)(1 - 1 - 1)}$	$(1 - 1 - 1)$	$H_{22}(1)$
$(1 - 1 - 1)(1 - 1 - 1)(1 - 1 - 1) \times \frac{(1 - 1 - 1)(1 - 1 - 1)(1 - 1 - 1)}{(1 - 1 - 1)(1 - 1 - 1)(1 - 1 - 1)}$	$(1 - 1 - 1)$	$\partial_{22}(1)$
$(1 - 1 - 1)(1 - 1 - 1)(1 - 1 - 1) \times \frac{(1 - 1 - 1)(1 - 1 - 1)(1 - 1 - 1)}{(1 - 1 - 1)(1 - 1 - 1)(1 - 1 - 1)}$	$(1 - 1 - 1)$	$H_{31}(1)$
$(1 - 1 - 1)(1 - 1 - 1)(1 - 1 - 1) \times \frac{(1 - 1 - 1)(1 - 1 - 1)(1 - 1 - 1)}{(1 - 1 - 1)(1 - 1 - 1)(1 - 1 - 1)}$	$(1 - 1 - 1)$	$\partial_{31}(1)$
$(1 - 1 - 1)(1 - 1 - 1)(1 - 1 - 1) \times \frac{(1 - 1 - 1)(1 - 1 - 1)(1 - 1 - 1)}{(1 - 1 - 1)(1 - 1 - 1)(1 - 1 - 1)}$	$(1 - 1 - 1)$	$H_{32}(1)$
$(1 - 1 - 1)(1 - 1 - 1)(1 - 1 - 1) \times \frac{(1 - 1 - 1)(1 - 1 - 1)(1 - 1 - 1)}{(1 - 1 - 1)(1 - 1 - 1)(1 - 1 - 1)}$	$(1 - 1 - 1)$	$\partial_{32}(1)$

Line strengths
 $X(m) - X'(m)$

Branches
 $M = +1$
 $M = -1$

It can be seen that for (E.8), the transitions for $\Delta\Lambda = -1$ are denoted in the same way as with (E.4). Note that for (E.7) and (E.8), the superscripts N, O, P, Q, R, S and T, which are often quoted in the literature, refer to the behaviour of the quantum number N, even if it is not a good quantum number, being the total angular momentum apart from spin, such that for a branch with an N superscript $\Delta N = -3$, for an O superscript $\Delta N = -2$ etc., the main symbol referring of course to J. However, if $\Delta J = \Delta N$, the superscript is not written by convention. Another convention is that if the indices are equal, one is often dropped, e.g. $P_1(J)$ is written for $P_{11}(J)$ etc.

As with the doublets, when $\Lambda' = \Lambda''$, the appropriate values are inserted into (E.5) and (E.6) for the two electronic states, but the smaller of the two is inserted into (E.8). However, if $Y < 0$ for one or both electronic states, this negative value is inserted into (E.5), (E.6) and (E.7) or (E.8), and Λ is replaced by $-\Lambda$ in (E.5) and (E.6) for the appropriate electronic state or states, but is left unchanged in (E.7) or (E.8). Also the indices on the left hand side of (E.7) or (E.8) are changed such that $i \rightarrow 4-i$ or $j \rightarrow 4-j$ as appropriate. As with the doublets, some breakdown cases occur even for valid transitions, these are discussed in section 4.2C.

APPENDIX F

The Isotropic Plane Harmonic Oscillator

Some of the matrix elements by Shaffer and Krohn (80) are given here below. In common with the discussion at the beginning of section 5.2, we assume that the matrix elements $\langle v'l' | r^n | v'l \rangle$ that contribute most to the total transition moment, are those for which $n = |\Delta v|$, where the unprimed and primed quantum numbers denote the initial and final states respectively. Other matrix elements, including those for which $|\Delta l| > 1$ are neglected.

If:

$$V = (v + v' + 2)/2 \quad \text{and} \quad L = (l + l')/2 \quad (\text{F.1})$$

then the following can be written:

<u>n</u>	<u>v'</u>	<u>l'</u>	$\frac{\langle v'l' r^n v'l \rangle^2}{}$	
1	<u>v+1</u>	<u>l+1</u>	(V+L)/2	(F.2)
	<u>v+1</u>	<u>l-1</u>	(V-L)/2	

2	<u>v+2</u>	<u>l</u>	(V-L)(V+L)/4	(F.3)
---	------------	----------	--------------	-------

3	<u>v+3</u>	<u>l+1</u>	(V-L)(V+L-1)(V+L+1)/8	(F.4)
	<u>v+3</u>	<u>l-1</u>	(V-L-1)(V-L+1)(V+L)/8	

$$4 \quad v_{\pm 4} \quad \ell \quad (V-L-1)(V-L+1)(V+L-1)(V+L+1)/16 \quad (F.5)$$

$$5 \quad v_{\pm 5} \quad \ell_{\pm 1} \quad (V-L-1)(V-L+1)(V+L-2)(V+L)(V+L+2)/32 \quad (F.6)$$

$$v_{\pm 5} \quad \bar{\ell}_{\pm 1} \quad (V-L-2)(V-L)(V-L+2)(V+L-1)(V+L+1)/32$$

$$6 \quad v_{\pm 6} \quad \ell \quad (V-L-2)(V-L)(V-L+2)(V+L-2)(V+L)(V+L+2)/64 \quad (F.7)$$

$$7 \quad v_{\pm 7} \quad \ell_{\pm 1} \quad (V-L-2)(V-L)(V-L+2)(V+L-3)(V+L-1)(V+L+1) \\ X(V+L+3)/128 \quad (F.8)$$

$$v_{\pm 7} \quad \bar{\ell}_{\pm 1} \quad (V-L-3)(V-L-1)(V-L+1)(V-L+3)(V+L-2)(V+L) \\ X(V+L+2)/128$$

The theory as supplied by Carson (3) of the isotropic plane harmonic oscillator is given in the following pages.

$$\frac{\phi e}{e} \frac{z d}{\phi_{\text{ms}} \phi_{\text{ms}}} + \frac{\phi e}{e} \frac{z d}{\phi_{\text{ms}} \phi_{\text{ms}}} + \frac{d e}{e} \frac{z}{\phi_{\text{ms}}} + \frac{\phi e d e}{e} \frac{z}{\phi_{\text{ms}} \phi_{\text{ms}}} -$$

$$\frac{\phi e}{e} \frac{z d}{\phi_{\text{ms}} \phi_{\text{ms}}} + \frac{\phi e d e}{e} \frac{z}{\phi_{\text{ms}} \phi_{\text{ms}}} - \frac{z d e}{e} \phi_{\text{ms}} =$$

$$\left(\frac{\phi e}{e} \frac{z}{\phi_{\text{ms}}} - \frac{d e}{e} \phi_{\text{ms}} \right) \frac{\phi e}{e} \frac{z}{\phi_{\text{ms}}} - \left(\frac{\phi e}{e} \frac{z}{\phi_{\text{ms}}} - \frac{d e}{e} \phi_{\text{ms}} \right) \frac{d e}{e} \phi_{\text{ms}} =$$

$$\left(\frac{\phi e}{e} \frac{z}{\phi_{\text{ms}}} - \frac{d e}{e} \phi_{\text{ms}} \right) \left(\frac{\phi e}{e} \frac{z}{\phi_{\text{ms}}} - \frac{d e}{e} \phi_{\text{ms}} \right) = \frac{z e}{e}$$

$$z d / e = \frac{h e}{\phi e}, \quad z d / h = \frac{z e}{\phi e}$$

$$\frac{(z e / h + 1)}{z / h} = \frac{h e}{\phi e}, \quad \frac{(z e / h + 1)}{z e / h} = \frac{z e}{\phi e}$$

$$z e \frac{z}{h} - \frac{z}{h} = \phi e \left(\frac{z e}{h} + 1 \right)$$

$$\frac{z e}{h} - \frac{z}{h} = \phi e \phi_{\text{ms}}$$

$$\frac{z}{h} = \phi_{\text{ms}}$$

$$\frac{z}{h} = \frac{h e}{\phi e}, \quad \frac{z}{e} = \frac{z e}{\phi e}$$

$$h_y h_z + z_y z_z = d p d e$$

$$d_y d_z + p_{\text{ms}} d_p = d_y$$

$$d_x = d p_{\text{ms}} \phi - p_{\text{ms}} \phi d_p$$

$$\frac{\phi e}{e} \frac{z}{\phi_{\text{ms}}} + \frac{d e}{e} \phi_{\text{ms}} =$$

$$\frac{\phi e}{e} \frac{z}{e} + \frac{d e}{e} \frac{z}{h} =$$

$$\frac{\phi e h e}{e \phi e} + \frac{d e h e}{e \phi e} = \frac{h e}{e}$$

$$\frac{\phi e}{e} \frac{z}{\phi_{\text{ms}}} - \frac{d e}{e} \phi_{\text{ms}} =$$

$$\frac{\phi e}{e} \frac{z}{h} - \frac{d e}{e} \frac{z}{e} =$$

$$\frac{\phi e z e}{e \phi e} + \frac{d e z e}{e \phi e} = \frac{z e}{e}$$

$$\frac{h e}{e} + \frac{z e}{e} = h_y \Delta_{z,y}$$

$$\phi = p_{\text{ms}} \phi, \quad y = p_{\text{ms}} \phi, \quad x = p_{\text{ms}} \phi$$

$$p^2 = x^2 + y^2$$

Lagrange in Plane Polar Coordinates:

$$\frac{\partial^2}{\partial x^2} = \cos^2 \phi \frac{\partial^2}{\partial \rho^2} - \frac{2 \cos \phi \sin \phi}{\rho} \frac{\partial^2}{\partial \rho \partial \phi} + \frac{2 \cos \phi \sin \phi}{\rho^2} \frac{\partial}{\partial \phi}$$

$$+ \frac{\sin^2 \phi}{\rho} \frac{\partial}{\partial \rho} + \frac{\sin^2 \phi}{\rho^2} \frac{\partial^2}{\partial \phi^2}$$

$$\frac{\partial^2}{\partial y^2} = \left(\sin \phi \frac{\partial}{\partial \rho} + \frac{\cos \phi}{\rho} \frac{\partial}{\partial \phi} \right) \left(\sin \phi \frac{\partial}{\partial \rho} + \frac{\cos \phi}{\rho} \frac{\partial}{\partial \phi} \right)$$

$$= \sin^2 \phi \frac{\partial^2}{\partial \rho^2} + \frac{\sin \phi \cos \phi}{\rho} \frac{\partial^2}{\partial \phi \partial \rho} - \frac{\sin \phi \cos \phi}{\rho^2} \frac{\partial}{\partial \phi}$$

$$+ \frac{\cos \phi \sin \phi}{\rho} \frac{\partial^2}{\partial \rho \partial \phi} + \frac{\cos^2 \phi}{\rho} \frac{\partial}{\partial \rho} + \frac{\cos^2 \phi}{\rho^2} \frac{\partial^2}{\partial \phi^2} - \frac{\cos \phi \sin \phi}{\rho^2} \frac{\partial}{\partial \phi}$$

$$\nabla^2 = \frac{\partial^2}{\partial x^2} + \frac{\partial^2}{\partial y^2} = \frac{\partial^2}{\partial \rho^2} + \frac{1}{\rho} \frac{\partial}{\partial \rho} + \frac{1}{\rho^2} \frac{\partial^2}{\partial \phi^2}$$

$$= \frac{1}{\rho^2} \left[\rho^2 \frac{\partial^2}{\partial \rho^2} + \rho \frac{\partial}{\partial \rho} + \frac{\partial^2}{\partial \phi^2} \right]$$

$$= \frac{1}{\rho} \frac{\partial}{\partial \rho} \left(\rho \frac{\partial}{\partial \rho} \right) + \frac{1}{\rho^2} \frac{\partial^2}{\partial \phi^2}$$

Then for the Isotropic Plane Harmonic Oscillator:

Let $V = \frac{1}{2} k \rho^2 = \frac{1}{2} k (x^2 + y^2)$ and $\nu = \frac{1}{2\pi} \sqrt{\frac{k}{\mu}}$

Given the Schrödinger wave equation: $\nabla_{x,y}^2 \Psi + \frac{8\pi^2 \mu}{h^2} [E - V] \Psi = 0,$

① $\Psi = X(x) Y(y)$

$$\left. \begin{aligned} \left\{ \frac{\partial^2}{\partial x^2} + \frac{8\pi^2 \mu}{h^2} \left[E_x - \frac{1}{2} k x^2 \right] \right\} X(x) = 0 \\ \left\{ \frac{\partial^2}{\partial y^2} + \frac{8\pi^2 \mu}{h^2} \left[E_y - \frac{1}{2} k y^2 \right] \right\} Y(y) = 0 \end{aligned} \right\} \begin{aligned} \text{where } E_x &= (n_x + \frac{1}{2}) h\nu \\ E_y &= (n_y + \frac{1}{2}) h\nu \\ E &= E_x + E_y \\ &= (n_x + n_y + 1) h\nu \\ &= (n + 1) h\nu \end{aligned}$$

$$\left. \begin{aligned} X(x) &= \frac{1}{\sqrt{2^{n_x} n_x!} \sqrt{\pi/\alpha}} e^{-\frac{1}{2} \alpha x^2} H_{n_x}(\sqrt{\alpha} x) \\ Y(y) &= \frac{1}{\sqrt{2^{n_y} n_y!} \sqrt{\pi/\alpha}} e^{-\frac{1}{2} \alpha y^2} H_{n_y}(\sqrt{\alpha} y) \end{aligned} \right\} \text{where } \alpha = \frac{2\pi^2 \mu k}{h^2}$$

② $\Psi = R(\rho) \Phi(\phi)$

$$\left[\frac{\partial^2}{\partial \rho^2} + \frac{1}{\rho} \frac{\partial}{\partial \rho} + \frac{1}{\rho^2} \frac{\partial^2}{\partial \phi^2} \right] R(\rho) \Phi(\phi) + \frac{8\pi^2 \mu}{h^2} \left[E - \frac{1}{2} k \rho^2 \right] R(\rho) \Phi(\phi) = 0$$

$$\Phi(\phi) \left(\frac{\partial^2}{\partial \rho^2} + \frac{1}{\rho} \frac{\partial}{\partial \rho} \right) R(\rho) + R(\rho) \frac{1}{\rho^2} \frac{\partial^2}{\partial \phi^2} \Phi(\phi) + \frac{8\pi^2 \mu}{h^2} \left[E - \frac{1}{2} k \rho^2 \right] R(\rho) \Phi(\phi) = 0$$

$$2\gamma \left(\gamma - 2 \frac{\partial}{\partial t} \cdot \partial \right) \gamma_1 \partial \partial + \frac{\partial^2 \gamma}{\partial t^2} \partial \gamma = \left(\frac{\partial^2 \gamma}{\partial t^2} \gamma_1 \partial \partial \right) \frac{\partial \gamma}{\partial t} \gamma_1 \partial \partial = \frac{\partial^2 \gamma}{\partial t^2}$$

$$\frac{\partial^2 \gamma}{\partial t^2} \gamma_1 \partial \partial = \frac{\partial \gamma}{\partial t} \frac{\partial \gamma}{\partial t} \frac{\partial \gamma}{\partial t} = \frac{\partial \gamma}{\partial t}$$

$$\gamma_1 \partial \partial = \partial \partial = \frac{\partial \gamma}{\partial t}, \quad \frac{\partial \gamma}{\partial t} \frac{\partial \gamma}{\partial t} \frac{\partial \gamma}{\partial t} = \partial \partial$$

$$\partial \partial = \partial \partial$$

$$0 = R'' + \frac{1}{R'} + \left\{ \frac{\gamma^2}{8\pi^2 \mu} \left(E - \frac{1}{2} h \rho^2 \right) - \frac{\rho^2}{\gamma^2} \right\} R = 0$$

$$0 = \left(\frac{\partial^2}{\partial t^2} + \frac{1}{R'} \frac{\partial}{\partial t} \right) R(\rho) + \left\{ \frac{\gamma^2}{8\pi^2 \mu} \left(E - \frac{1}{2} h \rho^2 \right) - \frac{\rho^2}{\gamma^2} \right\} R(\rho) = 0$$

$$0 = \frac{\partial^2}{\partial t^2} R(\rho) + \frac{1}{R'} \frac{\partial}{\partial t} R(\rho) + \left\{ \frac{\gamma^2}{8\pi^2 \mu} \left(E - \frac{1}{2} h \rho^2 \right) - \frac{\rho^2}{\gamma^2} \right\} R(\rho) = 0$$

$$\frac{\partial^2}{\partial t^2} \Phi(\rho) = -\rho^2 \Phi(\rho)$$

$$\frac{\partial^2}{\partial t^2} \Phi(\rho) = -\rho^2 \Phi(\rho) = \frac{\partial^2 \Phi(\rho)}{\partial t^2}$$

$$\frac{\partial^2}{\partial t^2} \Phi(\rho) = \frac{\partial^2 \Phi(\rho)}{\partial t^2}$$

$$0 = \left(\frac{\partial^2}{\partial t^2} + \frac{1}{R'} \frac{\partial}{\partial t} \right) \Phi(\rho) + \left\{ \frac{\gamma^2}{8\pi^2 \mu} \left(E - \frac{1}{2} h \rho^2 \right) - \frac{\rho^2}{\gamma^2} \right\} \Phi(\rho) = 0$$

$$0 = \left[\frac{\partial^2}{\partial t^2} + \frac{1}{R'} \frac{\partial}{\partial t} + \left\{ \frac{\gamma^2}{8\pi^2 \mu} \left(E - \frac{1}{2} h \rho^2 \right) - \frac{\rho^2}{\gamma^2} \right\} \right] \Phi(\rho) = 0$$

$$= 4\tau \frac{d^2}{d\tau^2} + 2 \frac{d}{d\tau}$$

$$\frac{1}{\rho} \frac{d}{d\rho} = \frac{1}{\tau^{1/2}} 2\tau^{1/2} \frac{d}{d\tau} = 2 \frac{d}{d\tau}$$

$$\text{Hence } \frac{d^2}{d\rho^2} + \frac{1}{\rho} \frac{d}{d\rho} = 4 \left(\tau \frac{d^2}{d\tau^2} + \frac{d}{d\tau} \right)$$

$$\text{Thus } 4 \left\{ \tau \frac{d^2}{d\tau^2} R(\tau) + \frac{d}{d\tau} R(\tau) \right\} + \left\{ \frac{8\pi^2 \mu}{h^2} (E - \frac{1}{2}kT) - \frac{l^2}{\tau} \right\} R(\tau) = 0$$

$$\tau R''(\tau) + R'(\tau) + \frac{1}{4} \left[\frac{8\pi^2 \mu}{h^2} (E - \frac{1}{2}kT) - \frac{l^2}{\tau} \right] R(\tau) = 0$$

$$\text{If } \alpha^2 = \frac{4\pi^2 \mu k}{h^2}, \quad \beta = \frac{8\pi^2 \mu E}{h^2}, \quad \nu = \frac{1}{2\pi} \sqrt{\frac{k}{\mu}}$$

$$\text{Let } R(\rho) = \rho^l e^{-\frac{\alpha}{2}\rho^2} P(\rho)$$

$$R'(\rho) = l\rho^{l-1} e^{-\frac{\alpha}{2}\rho^2} P(\rho) - \alpha\rho^{l+1} e^{-\frac{\alpha}{2}\rho^2} P(\rho) + \rho^l e^{-\frac{\alpha}{2}\rho^2} P'(\rho)$$

$$\begin{aligned} R''(\rho) &= l(l-1)\rho^{l-2} e^{-\frac{\alpha}{2}\rho^2} P(\rho) - \alpha l\rho^l e^{-\frac{\alpha}{2}\rho^2} P(\rho) + l\rho^{l-1} e^{-\frac{\alpha}{2}\rho^2} P'(\rho) \\ &\quad - \alpha(l+1)\rho^l e^{-\frac{\alpha}{2}\rho^2} P(\rho) + \alpha^2\rho^{l+2} e^{-\frac{\alpha}{2}\rho^2} P(\rho) - \alpha\rho^{l+1} e^{-\frac{\alpha}{2}\rho^2} P'(\rho) \\ &\quad + l\rho^{l-1} e^{-\frac{\alpha}{2}\rho^2} P'(\rho) - \alpha\rho^{l+1} e^{-\frac{\alpha}{2}\rho^2} P'(\rho) + \rho^l e^{-\frac{\alpha}{2}\rho^2} P''(\rho) \end{aligned}$$

$$0 = R'' + \frac{1}{\rho} R' - \frac{l^2}{\rho^2} R - \alpha^2 R + \beta R$$

$$= \rho^l e^{-\frac{\alpha}{2}\rho^2} P''(\rho) + \rho^l e^{-\frac{\alpha}{2}\rho^2} P'(\rho) \left\{ -2\alpha\rho + \frac{l(2l+1)}{\rho} \right\}$$

$$+ \rho^l e^{-\frac{\alpha}{2}\rho^2} P(\rho) \left\{ \beta - \alpha(2l+1) - \alpha \right\}$$

or $P(x) = L_m^{(1)}(x) = \frac{d^m}{dx^m} L_{m+k}(x)$ (Associated Legendre Polynomial)

$P(x) = L_k^{(1)}(x) = \frac{d}{dx} L_k(x)$

This has a polynomial solution of order $m = k - l \geq 0$ given by:

$$\sigma \frac{d^2}{dx^2} P + \{(l+1) - \sigma\} \frac{dP}{dx} + \left\{ \frac{\beta - 2\alpha(l+1)}{4} \right\} P = 0$$

$$\sigma \cdot \alpha^2 \frac{d^2}{dx^2} P + \{(l+1) - \sigma\} \alpha \frac{dP}{dx} + \left\{ \frac{\beta - 2\alpha(l+1)}{4} \right\} P = 0$$

Put $\sigma = \alpha z$, $z = \frac{x}{\alpha}$, $\frac{d}{dx} = \alpha \frac{d}{dz}$, $\frac{d^2}{dx^2} = \alpha^2 \frac{d^2}{dz^2}$

$$z \frac{d^2 P}{dz^2} + \{(l+1) - \alpha z\} \frac{dP}{dz} + \left\{ \frac{\beta - 2\alpha(l+1)}{4} \right\} P = 0$$

$$4z \frac{d^2 P}{dz^2} + \{2(l+1) + 2 - 4\alpha z\} \frac{dP}{dz} + \{\beta - 2\alpha(l+1)\} P = 0$$

$$\therefore 4z \frac{d^2 P}{dz^2} + \left\{ \frac{2(l+1)}{z} - 2\alpha \sqrt{z} \right\} 2 \frac{dP}{dz} + 2 \frac{dP}{dz} + \{\beta - \alpha(2l+1) - \alpha\} P = 0$$

$$\frac{d^2 P}{dz^2} = 2\sqrt{z} \frac{d}{dz} \left[2\sqrt{z} \frac{dP}{dz} \right] = 4z \frac{d^2 P}{dz^2} + 2 \frac{dP}{dz}$$

Put $z = \rho^2$, $\frac{d}{dz} = \frac{d\rho}{d\rho} \frac{d}{d\rho} = 2\rho \frac{d}{d\rho}$, $\frac{d^2}{dz^2} = 2\sqrt{z} \frac{d}{dz}$

$$P''(\rho) + \left\{ \frac{2(l+1)}{\rho} - 2\alpha\rho \right\} P'(\rho) + \{\beta - \alpha(2l+1) - \alpha\} P(\rho) = 0$$

defined by: $\frac{d^2}{dx^2} L_m^{(l)}(x) + (l+1-x) \frac{d}{dx} L_m^{(l)}(x) + m L_m^{(l)}(x) = 0$

If $\frac{\beta - 2\alpha(l+1)}{4\alpha} = m$ (an integer ≥ 0)

i.e. $\frac{\beta}{2\alpha} = \frac{E}{\hbar^2} = 2m + l + 1 = n + 1 = 2k - l + 1$

where n is the vibrational quantum number. For a given n

then: $l = n - 2m$

$$= n, n-2, n-4, \dots \begin{cases} 0 & n \text{ even} \\ 1 & n \text{ odd} \end{cases}$$

Thus we have:

$$R(\rho) = N_\rho \rho^l e^{-\frac{\alpha}{2}\rho^2} L_m^{(l)}(\alpha\rho^2) = N_\rho e^{-\frac{\alpha}{2}\rho^2} Q_{n,l}(\rho)$$

where $Q_{n,l}(\rho)$ is a polynomial of order

$$n = 2m + l = 2k - l \text{ where } k = m + l$$

and N_ρ is a normalizing constant such that $\int_0^\infty R^2(\rho) \rho d\rho = 1$

Alternatively, using $\sigma = \alpha r = \alpha \rho^2$, i.e. $\rho = (\sigma/\alpha)^{1/2}$

$$R(\rho) = N_\rho e^{-\frac{1}{2}\sigma} \left(\frac{\sigma}{\alpha}\right)^{l/2} L_m^{(l)}(\sigma)$$

Since $\rho d\rho = \frac{d\sigma}{2\alpha}$

$$N_p^{-2} = \frac{1}{2\alpha^{\ell+1}} \int_0^\infty e^{-\alpha\sigma} \sigma^\ell \left[L_m^{(\ell)}(\sigma) \right]^2 d\sigma = \frac{1}{2\alpha^{\ell+1}} S$$

$$\text{where } S = \int_0^\infty e^{-\alpha\sigma} \sigma^\ell \left[L_m^{(\ell)}(\sigma) \right]^2 d\sigma = \frac{[(m+\ell)!]^3}{m!}$$

$$\text{Thus } N_p = \left[2\alpha^{\ell+1} \frac{m!}{[(m+\ell)!]^3} \right]^{1/2}$$

$$\text{and } R(p) = \left[2\alpha \frac{m!}{[(m+\ell)!]^3} \right]^{1/2} e^{-\sigma/2} \sigma^{\ell/2} L_m^{(\ell)}(\sigma)$$

$$\text{Using } L_n(x) = e^x \frac{d^n}{dx^n} (x^n e^{-x})$$

$$= (-1)^n \left[x^n - \frac{n^2}{1!} x^{n-1} + \frac{n^2(n-1)^2}{2!} x^{n-2} - \dots + (-1)^n n! \right]$$

$$L_0(x) = L_0^0(x) = L_0^{(0)}(x) = 1,$$

$$L_1(x) = L_1^0(x) = L_1^{(0)}(x) = -x+1, \quad L_1^1(x) = L_2^1(x) = -1,$$

$$L_2(x) = L_2^0(x) = L_2^{(0)}(x) = x^2 - 4x + 2, \quad L_2^1(x) = L_3^1(x) = 2x - 4, \quad L_2^2(x) = L_4^2(x) = 2,$$

$$\text{then we have for } Q_{n,\ell}(p) = p^\ell L_m^{(\ell)}(\alpha p^2) = p^\ell L_{m+\ell}^\ell(\alpha p^2) = p^\ell L_{\frac{n+\ell}{2}}^\ell(\alpha p^2)$$

$$Q_{0,0}(p) = L_0^0(\alpha p^2) = 1,$$

$$Q_{1,1}(p) = p L_1^1(\alpha p^2) = -p,$$

$$Q_{2,0}(p) = L_1^0(\alpha p^2) = -\alpha p^2 + 1,$$

$$Q_{2,2}(p) = p^2 L_2^2(\alpha p^2) = 2p^3,$$

$$Q_{3,1}(p) = p L_2^1(\alpha p^2) = 2\alpha p^3 - 4p,$$

$$Q_{4,0}(p) = L_2^0(\alpha p^2) = \alpha^2 p^4 - 4\alpha p^2 + 2,$$

$$L_n(x) = e^x \frac{d^n}{dx^n} (x^n e^{-x}) \quad \text{again}$$

$$= (-1)^n \left[x^n - \frac{n^2}{1!} x^{n-1} + \frac{n^2(n-1)^2}{2!} x^{n-2} - \dots + (-1)^n n! \right]$$

$$L_0(x) = 1,$$

$$L_1(x) = -x + 1,$$

$$L_1'(x) = -1,$$

$$L_2(x) = x^2 - 4x + 2,$$

$$L_2'(x) = 2x - 4,$$

$$L_3(x) = -x^3 + 9x^2 - 18x + 6,$$

$$L_3'(x) = -3x^2 + 18x - 18,$$

$$L_4(x) = x^4 - 16x^3 + 72x^2 - 96x + 24, \quad L_4'(x) = 4x^3 - 48x^2 + 144x - 96,$$

$$L_2^3(x) = 2,$$

$$L_3^2(x) = -6x + 18,$$

$$L_3^3(x) = -6,$$

$$L_4^2(x) = 12x^2 - 96x + 144,$$

$$L_4^3(x) = 24x - 96,$$

$$L_4^4(x) = 24,$$

with $x^{l/2} L_k^l(x) = F_{n,l}$ where $n = 2k - l$, then:

$$l=0: x^0 L_0^0(x) = 1 = F_{0,0}(x),$$

$$l=3: x^{3/2} L_3^3(x) = -6x^{3/2} = F_{3,3}(x),$$

$$x^0 L_1^0(x) = -x + 1 = F_{2,0}(x),$$

$$l=4: x^{4/2} L_4^4(x) = 24x = F_{4,4}(x).$$

$$x^0 L_2^0(x) = x^2 - 4x + 2 = F_{4,0}(x),$$

$$l=1: x^{1/2} L_1^1(x) = -x^{1/2} = F_{1,1}(x),$$

$$x^{1/2} L_2^1(x) = 2x^{3/2} - 4x^{1/2} = F_{3,1}(x),$$

$$l=2: x^{2/2} L_2^2(x) = 2x = F_{2,2}(x),$$

$$x^{2/2} L_3^2(x) = -6x^2 + 18x = F_{4,2}(x),$$

APPENDIX G

Line Strengths and Energy Level Diagram of the Asymmetric Top

For transitions with the asymmetric top for which $\min(J', J'') > 5$, the line strengths are obtained approximately from the Hönl-London factors of singlets, as stated in section 5.3. For smaller values of J , the following tables obtained from Cross et al. (92) are used. At the end of this appendix is a reproduction of an energy level diagram from Herzberg (30).

For all tables, columns 1 to 5 list the strength for the asymmetry parameter $K = -1, -0.5, 0, 0.5$ and 1 , followed by the notation of the participating sublevels in the form $J_1, \tau_1 : J_2, \tau_2$, with these subscripts being defined in terms of the initial and final sublevels, as stated in section 5.3. Using the same notation as Cross et al., if a transition takes place in the order $1 \rightarrow 2$ as above, this is defined as the primary transition, then the opposite transition $1 \leftarrow 2$ is then defined as the reverse. For an inverse transition, the order is $1 \rightarrow 2$ but the signs of τ_1, τ_2 and K are all inverted, then an inverse-reverse transition has the order $1 \leftarrow 2$ with inverted signs. All the sublevels in table (5.3) are obtained as follows from tables (G.1-6):

Table (G.1) for A-Type Bands

Primary: $Q_{0,\bar{1}}$, $\Delta\tau = 1$ and $Q_{2,\bar{1}}$, $\Delta\tau = 3$,

Reverse: $Q_{0,1}$, $\Delta\tau = -1$ and $Q_{2,1}$, $\Delta\tau = -3$.

With all primary Q-subbranches ordered in increasing $\min(\tau_1, \tau_2)$ for this and (G.4).

Table (G.2) for A-Type Bands

Primary: $R_{0,1}$, $\Delta\tau = -1$,

Reverse: $P_{0,\bar{1}}$, $\Delta\tau = 1$.

All primary R-subbranches are ordered in increasing τ_1 for this and (G.3), (G.5) and (G.6).

Table (G.3) for A-Type Bands

Primary: $R_{2,\bar{1}}$, $\Delta\tau = 3$,

Reverse: $P_{2,1}$, $\Delta\tau = -3$.

Table (G.4) for B-Type Bands

Primary and Inverse-Reverse: $Q_{1,\bar{1}}$, $\Delta\tau = 2$,

Reverse and Inverse: $Q_{\bar{1},1}$, $\Delta\tau = -2$.

With the primary Q-subbranches listed with $\max(\tau_1, \tau_2) < 2$, for $\max(\tau_1, \tau_2) \geq 1$ take the inverse transition.

Table (G.5) for B-Type Bands

Primary and Inverse: $R_{1,1}$, $\Delta\tau = 0$,

Reverse and Inverse-Reverse: $P_{\bar{1},\bar{1}}$, $\Delta\tau = 0$.

With the primary R-subbranches having $\tau_1 \leq 0$, if $\tau_1 > 0$ take inverse transition.

Table (G.6) for B-Type Bands

Primary: $R_{1,\bar{1}}$, $\Delta\tau = 2$ and $R_{3,\bar{1}}$, $\Delta\tau = 4$,

Reverse: $P_{\bar{1},1}$, $\Delta\tau = -2$ and $P_{\bar{3},1}$, $\Delta\tau = -4$,

Inverse: $R_{\bar{1},1}$, $\Delta\tau = -2$ and $R_{\bar{1},3}$, $\Delta\tau = -4$,

Inverse-Reverse: $P_{1,\bar{1}}$, $\Delta\tau = 2$ and $P_{3,\bar{1}}$, $\Delta\tau = 4$.

With the primary R-subbranches listed with $\Delta\tau > 0$, if $-\Delta\tau$ is required, take the inverse transition.

Table (G.1) for A-Type Bands

-1.0	-0.5	0.0	0.5	1.0		
1.5000	1.5000	1.5000	1.5000	1.5000	1, 0	: 1, 1
0.0000	0.0488	0.2233	0.5110	0.8333	2,-2	: 2, 1
0.8333	0.8333	0.8333	0.8333	0.8333	2,-1	: 2, 0
3.3333	3.2845	3.1100	2.8223	2.5000	2, 1	: 2, 2
0.0000	0.1458	0.4522	0.7055	0.8750	3,-3	: 3, 0
0.5833	0.5944	0.6406	0.7403	0.8750	3,-2	: 3,-1
0.0000	0.0165	0.1328	0.5722	1.4583	3,-1	: 3, 2
2.3333	2.1875	1.8811	1.6278	1.4583	3, 0	: 3, 1
5.2500	5.2155	5.0431	4.5104	3.5000	3, 2	: 3, 3
0.0000	0.2547	0.5617	0.7558	0.9000	4,-4	: 4,-1
0.4500	0.4847	0.6026	0.7587	0.9000	4,-3	: 4,-2
0.0000	0.0638	0.4568	1.1214	1.5750	4,-2	: 4, 1
1.8000	1.5598	1.3196	1.3221	1.5750	4,-1	: 4, 0
0.0000	0.0078	0.0650	0.4363	2.0250	4, 0	: 4, 3
4.0500	3.9363	3.4242	2.6168	2.0250	4, 1	: 4, 2
7.2000	7.1708	7.0244	6.4494	4.5000	4, 3	: 4, 4
0.0000	0.3368	0.6052	0.7775	0.9167	5,-5	: 5,-2
0.3667	0.4374	0.6127	0.7777	0.9167	5,-4	: 5,-3
0.0000	0.1599	0.7983	1.3242	1.6500	5,-3	: 5, 0
1.4667	1.1750	1.1058	1.3464	1.6500	5,-2	: 5,-1
0.0000	0.0274	0.2754	1.2576	2.2000	5,-1	: 5, 2
3.3000	3.0662	2.3397	1.9105	2.2000	5, 0	: 5, 1
0.0000	0.0054	0.0374	0.2359	2.5667	5, 1	: 5, 4
5.8667	5.7742	5.2949	3.9338	2.5667	5, 2	: 5, 3
9.1667	9.1399	9.0073	8.4696	5.5000	5, 4	: 5, 5

Table (G.2) for A-Type Bands

-1.0	-0.5	0.0	0.5	1.0		
1.0000	1.0000	1.0000	1.0000	1.0000	0, 0	: 1,-1
2.0000	1.9707	1.8660	1.6934	1.5000	1,-1	: 2,-2
1.5000	1.5000	1.5000	1.5000	1.5000	1, 0	: 2,-1
1.5000	1.5000	1.5000	1.5000	1.5000	1, 1	: 2, 0
3.0000	2.9029	2.7201	2.5893	2.5000	2,-2	: 3,-3
2.6667	2.6564	2.6243	2.5710	2.5000	2,-1	: 3,-2
2.6667	2.6509	2.5581	2.2500	1.6667	2, 0	: 3,-1
1.6667	1.6667	1.6667	1.6667	1.6667	2, 1	: 3, 0
1.6667	1.6724	1.7345	1.8636	2.0000	2, 2	: 3, 1
4.0000	3.8312	3.6728	3.5773	3.5000	3,-3	: 4,-4
3.7500	3.7210	3.6540	3.5758	3.5000	3,-2	: 4,-3
3.7500	3.6902	3.3801	2.9261	2.6250	3,-1	: 4,-2
3.0000	2.9882	2.9391	2.8258	2.6250	3, 0	: 4,-1
3.0000	3.0230	3.0992	2.9055	1.8750	3, 1	: 4, 0
1.7500	1.7564	1.7796	1.8207	1.8750	3, 2	: 4, 1
1.7500	1.7567	1.8001	2.0331	2.5000	3, 3	: 4, 2
5.0000	4.7897	4.6619	4.5745	4.5000	4,-4	: 5,-5
4.8000	4.7478	4.6583	4.5743	4.5000	4,-3	: 5,-4
4.8000	4.6530	4.1758	3.8400	3.6000	4,-2	: 5,-3
4.2000	4.1637	4.0354	3.8290	3.6000	4,-1	: 5,-2
4.2000	4.2462	4.1441	3.4387	2.8000	4, 0	: 5,-1
3.2000	3.2074	3.2063	3.1148	2.8000	4, 1	: 5, 0
3.2000	3.2109	3.3475	3.4848	2.1000	4, 2	: 5, 1
1.8000	1.8082	1.8449	1.9363	2.1000	4, 3	: 5, 2
1.8000	1.8082	1.8478	2.0650	3.0000	4, 4	: 5, 3
6.0000	5.7727	5.6582	5.5730	5.5000	5,-5	: 6,-6
5.8333	5.7578	5.6576	5.5730	5.5000	5,-4	: 6,-5
5.8333	5.5604	5.0867	4.8106	4.5833	5,-3	: 6,-4
5.3333	5.2600	5.0537	4.8094	4.5833	5,-2	: 6,-3
5.3333	5.3738	4.9227	4.1961	3.7500	5,-1	: 6,-2
4.5000	4.5001	4.4187	4.1486	3.7500	5, 0	: 6,-1
4.5000	4.5219	4.7032	4.1218	3.0000	5, 1	: 6, 0
3.3333	3.3473	3.3934	3.3887	3.0000	5, 2	: 6, 1
3.3333	3.3475	3.4370	3.8686	2.3333	5, 3	: 6, 2
1.8333	1.8422	1.8843	2.0137	2.3333	5, 4	: 6, 3
1.8333	1.8422	1.8847	2.0660	3.5000	5, 5	: 6, 4

Table (G.3) for A-Type Bands

-1.0	-0.5	0.0	0.5	1.0		
0.0000	0.0293	0.1340	0.3066	0.5000	1,-1	: 2, 2
0.0000	0.0776	0.1905	0.2062	0.1667	2,-2	: 3, 1
0.0000	0.0103	0.0423	0.0956	0.1667	2,-1	: 3, 2
0.0000	0.0157	0.1086	0.4167	1.0000	2, 0	: 3, 3
0.0000	0.1061	0.1316	0.1176	0.1250	3,-3	: 4, 0
0.0000	0.0213	0.0643	0.1025	0.1250	3,-2	: 4, 1
0.0000	0.0480	0.2884	0.5114	0.3750	3,-1	: 4, 2
0.0000	0.0118	0.0609	0.1742	0.3750	3, 0	: 4, 3
0.0000	0.0123	0.0800	0.3944	1.5000	3, 1	: 4, 4
0.0000	0.0963	0.0849	0.0882	0.1000	4,-4	: 5,-1
0.0000	0.0300	0.0664	0.0869	0.1000	4,-3	: 5, 0
0.0000	0.1032	0.3516	0.3166	0.3000	4,-2	: 5, 1
0.0000	0.0269	0.1159	0.2317	0.3000	4,-1	: 5, 2
0.0000	0.0310	0.2336	0.7788	0.6000	4, 0	: 5, 3
0.0000	0.0116	0.0657	0.2228	0.6000	4, 1	: 5, 4
0.0000	0.0117	0.0696	0.3386	2.0000	4, 2	: 5, 5
0.0000	0.0723	0.0638	0.0730	0.0833	5,-5	: 6,-2
0.0000	0.0346	0.0601	0.0729	0.0833	5,-4	: 6,-1
0.0000	0.1677	0.2651	0.2272	0.2500	5,-3	: 6, 0
0.0000	0.0440	0.1455	0.2168	0.2500	5,-2	: 6, 1
0.0000	0.0613	0.4448	0.6089	0.5000	5,-1	: 6, 2
0.0000	0.0265	0.1389	0.3522	0.5000	5, 0	: 6, 3
0.0000	0.0268	0.1768	0.8748	0.8333	5, 1	: 6, 4
0.0000	0.0114	0.0661	0.2480	0.8333	5, 2	: 6, 5
0.0000	0.0114	0.0667	0.2976	2.5000	5, 3	: 6, 6

Table (G.4) for B-Type Bands

-1.0	-0.5	0.0	0.5	1.0		
1.5000	1.5000	1.5000	1.5000	1.5000	1,-1	: 1, 1
2.5000	2.1289	1.6667	1.2044	0.8333	2,-2	: 2, 0
0.8333	0.8333	0.8333	0.8333	0.8333	2,-1	: 2, 1
3.5000	2.3196	1.4583	1.0583	0.8750	3,-3	: 3,-1
1.4583	1.3160	1.1667	1.0173	0.8750	3,-2	: 3, 0
1.4583	2.4417	2.8872	2.4417	1.4583	3,-1	: 3, 1
4.5000	2.2157	1.3527	1.0617	0.9000	4,-4	: 4,-2
2.0250	1.6126	1.2886	1.0584	0.9000	4,-3	: 4,-1
2.0250	3.6119	3.1154	2.0622	1.5750	4,-2	: 4, 0
1.5750	1.8280	1.9208	1.8280	1.5750	4,-1	: 4, 1
5.5000	2.0634	1.3413	1.0753	0.9167	5,-5	: 5,-3
2.5667	1.7823	1.3300	1.0751	0.9167	5,-4	: 5,-2
2.5667	4.3650	2.8164	2.0038	1.6500	5,-3	: 5,-1
2.2000	2.4936	2.3333	1.9781	1.6500	5,-2	: 5, 0
2.2000	3.2340	4.4017	3.2340	2.2000	5,-1	: 5, 1

Table (G.5) for B-Type Bands

-1.0	-0.5	0.0	0.5	1.0		
1.0000	1.0000	1.0000	1.0000	1.0000	0, 0	: 1, 0
1.5000	1.5000	1.5000	1.5000	1.5000	1,-1	: 2,-1
2.0000	2.1383	2.2847	2.4086	2.5000	2,-2	: 3,-2
1.6667	1.6667	1.6667	1.6667	1.6667	2, 0	: 3, 0
2.5000	2.9584	3.2533	3.4083	3.5000	3,-3	: 4,-3
1.8750	1.9563	2.1079	2.3549	2.6250	3,-1	: 4,-1
3.0000	3.9100	4.2585	4.4117	4.5000	4,-4	: 5,-4
2.1000	2.3919	2.8748	3.3165	3.6000	4,-2	: 5,-2
2.8000	2.3609	2.2028	2.3609	2.8000	4, 0	: 5, 0
3.5000	4.9126	5.2653	5.4140	5.5000	5,-5	: 6,-5
2.3333	3.0161	3.8409	4.3122	4.5833	5,-3	: 6,-3
3.0000	2.4633	2.6305	3.2338	3.7500	5,-1	: 6,-1

Table (G.6) for B-Type Bands

-1.0	-0.5	0.0	0.5	1.0		
1.5000	1.2774	1.0000	0.7226	0.5000	1, 0	: 2, 2
0.0000	0.0101	0.0486	0.1097	0.1667	2,-2	: 3, 2
1.6667	1.0000	0.5168	0.2792	0.1667	2,-1	: 3, 1
2.5000	2.3874	2.1498	1.6667	1.0000	2, 1	: 3, 3
0.0000	0.0416	0.1091	0.1323	0.1250	3,-3	: 4, 1
1.8750	0.6941	0.2692	0.1537	0.1250	3,-2	: 4, 0
0.0000	0.0032	0.0297	0.1452	0.3750	3,-1	: 4, 3
2.6250	2.2398	1.5000	0.7602	0.3750	3, 0	: 4, 2
3.5000	3.4065	3.2266	2.7406	1.5000	3, 2	: 4, 4
0.0000	0.0855	0.1259	0.1144	0.1000	4,-4	: 5, 0
2.1000	0.4522	0.1666	0.1162	0.1000	4,-3	: 5,-1
0.0000	0.0163	0.1252	0.2753	0.3000	4,-2	: 5, 2
2.8000	1.9900	0.8877	0.4022	0.3000	4,-1	: 5, 1
0.0000	0.0014	0.0140	0.1159	0.6000	4, 0	: 5, 4
3.6000	3.3039	2.6797	1.4796	0.6000	4, 1	: 5, 3
4.5000	4.4115	4.2535	3.8266	2.0000	4, 3	: 5, 5
0.0000	0.1186	0.1174	0.0965	0.0833	5,-5	: 6,-1
2.3333	0.2984	0.1253	0.0966	0.0833	5,-4	: 6,-2
0.0000	0.0514	0.2305	0.2771	0.2500	5,-3	: 6, 1
3.0000	1.6127	0.5238	0.2920	0.2500	5,-2	: 6, 0
0.0000	0.0062	0.0737	0.3538	0.5000	5,-1	: 6, 3
3.7500	3.1792	1.9335	0.7698	0.5000	5, 0	: 6, 2
0.0000	0.0009	0.0077	0.0758	0.8333	5, 1	: 6, 5
4.5833	4.3109	3.7946	2.4389	0.8333	5, 2	: 6, 4
5.5000	5.4140	5.2643	4.8829	2.5000	5, 4	: 6, 6

single level of the asymmetric top is really double on account of the possibility of inversion (*inversion doubling*) and always one component is positive, the other negative. For planar asymmetric top molecules (H_2O , H_2CO , C_2H_4 ...) there is no such doubling. It can be shown (see Chapter IV, section 4a) that for them in a totally symmetric vibrational and electronic state the highest level J_{+J} of each set of a given J is +, the two next highest are --, the two next +, and so on (see the first column of signs in Fig. 19).

The above classification according to the symmetry properties of the total eigenfunctions [*over-all species classification* according to Mulliken (645)] is not as frequently used as a classification according to the *symmetry properties of the rotational eigenfunction* only [see Dennison (279)]. For the sake of brevity let us call the three principal axes about which the moments of inertia are I_A, I_B, I_C respectively the a, b, c axes. The rotational eigenfunction ψ_r is a function of the orientation of this system of axes with respect to a fixed coordinate system. $|\psi_r|^2$ gives the probability of finding the various orientations of the axes. Because of the symmetry of the momental ellipsoid, an orientation that differs from a given one by a rotation through 180° about one of the axes must have the same probability. Therefore ψ_r must remain unchanged or only change sign for such a rotation. We call these rotations $C_2^a, C_2^b,$ and C_2^c (the axes are two-fold axes of symmetry of the momental ellipsoid). Thus the rotational levels of an asymmetric top may be distinguished by their behavior (+ or -) with respect to the three operations, C_2^a, C_2^b, C_2^c . Since one of these operations is equivalent to the other two carried out in succession, it is sufficient to determine the behavior with respect to two of them; usually C_2^c and C_2^a are chosen. There are thus four different types (species) of levels, briefly described by ++, +- , -+, and --, where the first sign refers to the behavior with respect to C_2^c , the second to the behavior with respect to C_2^a .

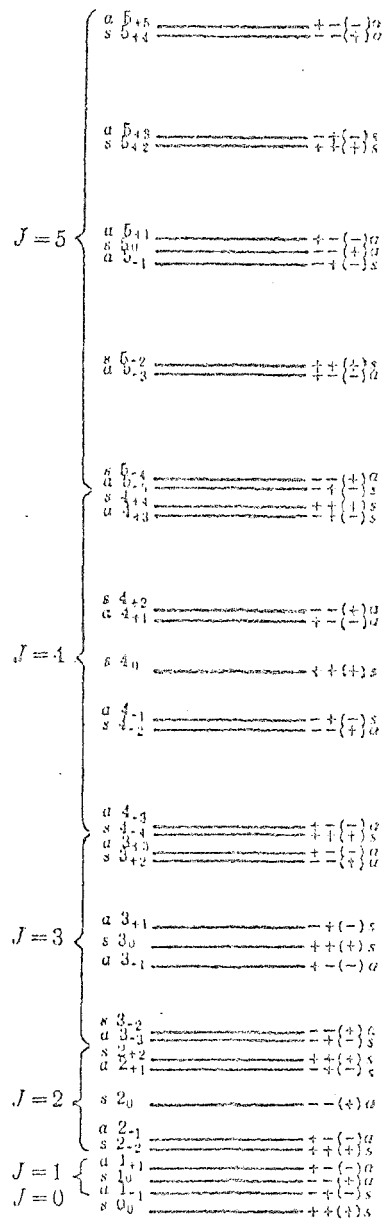


FIG. 19. Symmetry properties of the rotational levels of asymmetric top molecules for $J = 0$ to 5 .—The designation ++, +-, ... applies to any case, the properties s (symmetric) and a (antisymmetric) given at the right refer to the case that the C_2 lies in the a axis (H_2CO , ...) , those at the left to the case that the C_2 lies in the b axis (H_2O , ...). For the sake of clarity the different sets of levels with a given J have been drawn separated. The spacing of the levels within each set corresponds approximately to the most asymmetric case (see p. 48).

APPENDIX H

Sources of Molecular Oscillator Strengths and Transition Moments

The data on various diatomic molecules that are used in obtaining the results in chapter 7, together with the sources, are listed below in table (H.1). This list includes some molecules, which though allowed for in the computations, may not actually contribute to the results, due to their low abundances or due to their bands lying in parts of the spectrum that are beyond the range considered.

Electronic transitions are specified by the two electronic states given, vibration-rotation transitions are indicated by the single electronic state concerned. The column for the transition moment, or oscillator strength, lists the values that are used to obtain the absolute band strengths, and hence the line strengths, in the following way: (1) for electronic transitions, the values are the coefficients for the transition moment in (4.3.36) as a_0 , a_1 , a_2 etc. in $\text{D}\text{\AA}^{0-1}$, for all vibration-rotation bands, the coefficients are M_0 , M_1 , M_2 etc. in (4.3.52) also in $\text{D}\text{\AA}^{0-1}$, (2) the value given is $f_{el}(\bar{\nu}_{00})$, i.e. the electronic oscillator strength of the 0-0 band, (3) the value given is f_{00} , i.e. the band oscillator strength of the 0-0 band. Note that cases (2) and (3) do not apply to vibration-rotation transitions. The final column lists the source of the data.

Though as stated in section 4.4, that $R_e^2(r)$ is often given in the literature as (4.4.5) or (4.4.6), although r is the r -centroid, or more generally the $r^{(N)}$ -centroid, in Ångströms, $R_e^2(r)$ is itself often expressed in a.u., i.e. in units of $(ea_0)^2$, which is an unfortunate combination of units. Before applying Doktorov's method, we must convert the coefficients of the transition moment, as obtained from the various sources, into units of $D\text{Å}^0^{-1}$. Also, in most cases the electronic statistical weight factor of $(2S+1)(2-\delta_{0,A'+A''})$ is included in $R_e^2(r)$, and must be removed before computing the band strengths, as this factor is already accounted for in the normalization of the Hönl-London factors with due regard to Λ -doubling.

Thus for some cases, such as Schadee (118), $R_e^2(r)$ is given in the form:

$$R_e^2(r) = p(q_0 + q_1 r + q_2 r^2 + \dots)^2 \quad (\text{H.1})$$

in a.u. with r in Å. We require the coefficients to be in the form of (4.3.36) with the electronic statistical weight factor divided out. Thus given that $ea_0 = 2.5416 \times 10^{-18}$ esu-cgs, it is easy to show that:

$$a_i = \frac{2.5416 \sqrt{p} q_i}{\sqrt{(2S+1)(2-\delta_{0,A'+A''})}} \quad (\text{H.2})$$

in $D\text{Å}^0^{-1}$. Likewise, if:

$$R_e^2(r) = p e^{-qr} \quad (\text{H.3})$$

then it can be shown that:

$$a_i = \frac{2.5416 \sqrt{P}}{\sqrt{(2S+D)(2-\delta_0, \lambda'+\lambda'')}} \cdot \frac{(-1)^i q^i}{2^i i!} \quad (\text{H.4})$$

in DA^{0-i} .

Table (H.1) of Molecular Oscillator Strengths and Transition Moments

Mol.	Transition	Data Used	Source
C ₂	A ¹ Π _u - X ¹ Σ _g ⁺	(1) 1.078	(119)
C ₂	D ¹ Σ _u ⁺ - X ¹ Σ _g ⁺	(1) 0.9164	(119)
C ₂	b ³ Σ _g ⁻ - a ³ Π _u	(1) 0.8365	(119)
C ₂	d ³ Π _g - a ³ Π _u	(1) 0.1556, -0.7891	(118)
C ₂	e ³ Π _g - a ³ Π _u	(1) 0.7337	(119)
C ₂	C ¹ Π _g - A ¹ Π _u	(1) 1.724	(119)
C ₂	E ¹ Σ _g ⁺ - A ¹ Π _u	(1) 2.702	(119)
N ₂	B ³ Π _g - A ³ Σ _u ⁺	(1) 24.59, -74.27, 112.1; -112.9, 85.23	(118)
N ₂	C ³ Π _u - B ³ Π _g	(1) 1.089, -2.542, 1.204	(120)
O ₂	B ³ Σ _u ⁻ - X ³ Σ _g ⁻	(1) 1.365, -161.1, 47.83	(118)
OH	X ² Π	(1) 1.6777, 0.64306, -1.1091 -1.9508, 1.4176	(121)
OH	A ² Σ ⁺ - X ² Π	(1) 1.124, -0.8432	(122)
CH	A ² Δ - X ² Π	(2) 0.0049	(123)
CH	B ² Σ ⁻ - X ² Π	(2) 0.027	(123)
CH	C ² Σ ⁺ - X ² Π	(2) 0.008	(32)
CN	A ² Π - X ² Σ ⁺	(1) 0.7169, 0.1195	(118)
CN	B ² Σ ⁺ - X ² Σ ⁺	(1) 0.6012, -1.550	(118)
CO	X ¹ Σ ⁺	(1) -0.1221, 3.093, -0.199, -2.665, 0.26	(111)
CO	A ¹ Π - X ¹ Σ ⁺	(1) 1.402	(124)
NO	X ² Π	(1) -0.166, 2.21, -1.50	(125)
NO	A ² Σ ⁺ - X ² Π	(1) 289.3, -750.4, 649.5, -187.4	(118)
NO	B ² Π - X ² Π	(1) 0.2961, -0.4758	(118)
NO	C ² Σ ⁺ - X ² Π	(2) 0.0017	(123)
NO	D ² Σ ⁺ - X ² Π	(2) 0.0137	(123)

<u>Mol.</u>	<u>Transition</u>	<u>Data Used</u>	<u>Source</u>
MgH	$A^2\Pi - X^2\Sigma^+$	(1) 4.689	(124)
AlO	$A^2\Sigma^+ - X^2\Sigma^+$	(1) 1.312	(124)
SiO	$X^1\Sigma^+$	(1) 3.0575, 2.657	(126)
SiO	$A^1\Pi - X^1\Sigma^+$	(1) 1.743	(124)
Na ₂	$B^1\Pi_u - X^1\Sigma_g^+$	(1) 6.15, 0.43	(127)
NaH	$A^1\Sigma^+ - X^1\Sigma^+$	(1) 6.23	(124)
SH	$A^2\Sigma^+ - X^2\Pi$	(1) 0.3139	(124)
MgO	$B^1\Sigma^+ - X^1\Sigma^+$	(1) 8.133	(124)
HCl	$X^1\Sigma^+$	(1) 1.0935, 0.925, 0.163, -3.83, -9.3	(112)
HF	$X^1\Sigma^+$	(1) 1.7982, 1.5220, -0.2335, -1.0958	(128)
ClO	$X^2\Pi$	(1) 1.2036, -1.3269, -1.7895, 3.0550, -1.0576	(129)
ClO	$A^2\Pi - X^2\Pi$	(1) 20.836, -48.512, 48.714, -21.911, 3.5940	(129)
TiO	$C^3\Delta - X^3\Delta$	(2) 0.18	(113)
TiO	$c^1\tilde{Q} - a^1\tilde{A}$	(3) 0.249	(114)
CO ⁺	$A^2\Pi - X^2\Sigma^+$	(1) 30.53, 52.81 -22.59	(118)
CO ⁺	$B^2\Sigma^+ - X^2\Sigma^+$	(2) 0.0166	(118)
N ₂ ⁺	$B^2\Sigma_u^+ - X^2\Sigma_g^+$	(1) 0.789, 1.42, -0.611	(118)

APPENDIX I

Determination of the Internal Energies and Adiabatic Exponents of a Gas of Electrons, Atoms, Ions and Molecules

The total internal energies given in table (7.32) are obtained by summing over the individual species whose energies are obtained by the method discussed here. The zero point in energy corresponds to the state with all atoms free, neutral and in their ground states.

Atoms and Ions

Let $I_{h,h+1}$ be the ionization potential in ergs of the h^{th} ion of some element, where $1\text{eV} = 1.6021927 \times 10^{-12}$ erg by Allen (32). If we also write for generality the electron affinity as I_{-10} , which is by convention positive if the negative ion is stable, then the internal energy E^h for the h^{th} ion, apart from translation and ignoring any energy of excitation, is given by:

$$\begin{aligned} E^{-1} &= -I_{-10} \\ E^0 &= 0 \\ E^1 &= I_{01} \\ E^2 &= I_{01} + I_{12} \\ E^3 &= I_{01} + I_{12} + I_{23} \\ &\dots \\ E^n &= \sum_{h=0}^{n-1} I_{h,h+1} \end{aligned} \tag{I.1}$$

where n is the most positive ion considered, with of course $n \leq Z$. If S^h is the fraction of the uncombined element in question in the h^{th} stage of ionization as given by (2.3.8), then the total average internal energy per atom in all stages of ionization, together with translation, is given by:

$$E = -S^{-1}I_{-10} + \sum_{h=1}^n S^h \sum_{k=0}^{h-1} I_{k,k+1} + 3kT/2 \quad (\text{I.2})$$

$$E = -S^{-1}I_{-10} + \sum_{h=1}^n S^h E^h + 3kT/2$$

where if no stable negative ion exists, the first term is omitted. The contribution due to free electrons must also be added to the gas, this being just $3kT/2$ per electron.

Diatomic Molecules

From Herzberg (29), the following relations can be written per molecule in ergs:

$$\begin{aligned} \text{Rotation:} \quad E_r &= kT \\ \text{Vibration:} \quad E_v &= hc\omega_e / (e^{hc\omega_e/kT} - 1) \\ \text{Electronic:} \quad E_e &= -hcD_0^0 \\ \text{Translation:} \quad E_t &= 3kT/2 \end{aligned} \quad (\text{I.3})$$

where ω_e and D_0^0 are in wavenumber, and the latter is the dissociation potential measured from the lowest vibrational level (see (4.3.9)).

In these calculations, isotope effects are neglected, so the constants

are taken for the most abundant isotope, non-rigidity and anharmonicity are neglected in E_r and E_v respectively, and we only consider the contribution of the ground electronic state to the energy. However, in most cases these approximations will be good. Because E_e is normally by far the largest in magnitude in (I.3), molecules normally contribute negative values of energy to the gas, when the zero point is taken as stated earlier.

Triatomic Molecules

The relations for triatomic molecules given here are obtained from the relations for polyatomic molecules given by Herzberg (30):

$$\begin{aligned}
 \text{Rotation: } E_r &= kT && (\text{Linear Molecules}) \\
 E_r &= 3kT/2 && (\text{Non-Linear Molecules}) \\
 \text{Vibration: } E_v &= hc \sum_{i=1}^3 d_i \omega_i / (e^{hc\omega_i/kT} - 1) && (I.4) \\
 \text{Electronic: } E_e &= -hcD_0^0 \\
 \text{Translation: } E_t &= 3kT/2
 \end{aligned}$$

where d_i is the degeneracy of the i^{th} vibrational mode, such that $d_1 = d_3 = 1$, and $d_2 = 1$ or 2 depending on whether the molecule is non-linear or linear respectively. Also D_0^0 is the energy from the lowest vibrational level for complete dissociation. The same approximations as used for diatomic molecules are applied.

Charged Molecules

Though generally of negligible abundance, for the sake of completeness, we can also consider molecular ions. For generality in (I.3), E_e is replaced by:

$$E_e = -hcD_o^0 + E_i^h + E_j^m \quad (I.5)$$

and likewise for (I.4) with an additional term E_k^n for each of the dissociation products. However, only one of the dissociation products will be in general ionized, so will contribute a non-zero value to (I.5).

The theory, as supplied by Carson (3), for calculating the average energy of a rotator and of an oscillator is given in the following pages. For any additional discussion on the thermodynamic properties of molecules, one can refer to Herzberg (29) and (30).

In order to calculate the adiabatic exponents γ , γ_1 , γ_2 and γ_3 for a given grid point (T, ρ) , the total internal energy E and total pressure P are computed for that grid point, together with $E+\delta E$ and $P+\delta P$ computed from the grid points $(T, \rho+\delta \rho)$ and $(T+\delta T, \rho)$, as discussed in section 7.6 where tables of the adiabatic exponents are given. Note that the contribution of radiation must be included in the total pressure and internal energy, such that for P in dyne cm^{-2} and E in erg gm^{-1} the contribution is $(1/3)aT^4$ and aT^4/ρ respectively.

The theory, also as supplied by Carson (3), for obtaining the adiabatic exponents in terms of the known quantities is given further in this appendix. Cox and Giuli (1) can be referred to for further discussion.

Average Energy of a Rotator

Linear Molecules

$$E_J = b J(J+1) ; \quad b = \frac{h^2}{2I} \quad g_J = 2J+1$$

$$Z_r = \sum_{J=0}^{\infty} (2J+1) e^{-b J(J+1)/kT} = \sum_{J=0}^{\infty} (2J+1) e^{-\beta J(J+1)} ; \quad \beta = \frac{1}{kT}$$

$$\approx \int_0^{\infty} (2J+1) e^{-\beta J(J+1)} dJ = \int_0^{\infty} e^{-\beta x} dx ; \quad x = J(J+1)$$

$$= \left[-\frac{1}{\beta} e^{-\beta x} \right]_0^{\infty} = \frac{1}{\beta}$$

$$\bar{E}_r = \frac{1}{Z_r} \sum_{J=0}^{\infty} (2J+1) b J(J+1) e^{-b J(J+1)/kT}$$

$$= -\frac{1}{Z_r} b \frac{d}{d(b/kT)} \sum_{J=0}^{\infty} (2J+1) e^{-b J(J+1)/kT} = -\frac{kT}{Z} \beta \frac{d}{d\beta} Z_r$$

$$= -kT \beta^2 \frac{d}{d\beta} \left[\frac{1}{\beta} \right] = -kT \beta^2 \cdot \frac{-1}{\beta^2} = kT$$

Thus $\bar{E}_r = kT$

Non-Linear Molecules

$$E_J = bJ(J+1); \quad b = \frac{h^2}{2I} \quad g_J = (2J+1)^2$$

$$Z_r = \sum_{J=0}^{\infty} (2J+1)^2 e^{-bJ(J+1)/kT}$$

$$\approx \int_0^{\infty} (2J+1)^2 e^{-\beta J(J+1)} dJ = \int_0^{\infty} 4(J+\frac{1}{2})^2 e^{-\beta[(J+\frac{1}{2})^2 - \frac{1}{4}]} dJ$$

Let $j = J + \frac{1}{2}$

$$Z_r = \int_{\frac{1}{2}}^{\infty} 4j^2 e^{-\beta(j^2 - \frac{1}{4})} dj = 4e^{\beta/4} \int_{\frac{1}{2}}^{\infty} j^2 e^{-\beta j^2} dj$$

Now $\int_0^{\infty} x^{2n} e^{-\beta x^2} dx = \frac{\Gamma(n+\frac{1}{2})}{2\beta^{n+\frac{1}{2}}}$ $\Gamma(\frac{1}{2}) = \sqrt{\pi}$

$$\int_0^{\infty} j^2 e^{-\beta j^2} dj = \frac{\Gamma(\frac{3}{2})}{2\beta^{3/2}} = \frac{1}{4} \sqrt{\frac{\pi}{\beta^3}}$$

$\Gamma(\frac{3}{2}) = \frac{1}{2}\sqrt{\pi}$

$$Z_r = e^{\beta/4} \sqrt{\frac{\pi}{\beta^3}} \approx \sqrt{\frac{\pi}{\beta^3}} \quad \text{if } \beta \ll 1$$

$$\bar{E}_r = \frac{1}{Z_r} \sum_{J=0}^{\infty} (2J+1)^2 bJ(J+1) e^{-bJ(J+1)/kT}$$

$$= - \frac{kT}{Z_r} \beta \frac{d}{d\beta} Z_r = kT \beta \cdot \sqrt{\frac{\beta^3}{\pi}} \cdot \frac{3}{2} \sqrt{\frac{\pi}{\beta^5}} = \frac{3}{2} kT$$

Thus $\bar{E}_r = \frac{3}{2} kT$

Average Energy per Oscillator

One-dimensional S.H.O.

$$E_v = (v + \frac{1}{2}) h\nu_0 \quad g_v = 1$$

$$Z_v = \sum_{v=0}^{\infty} 1 \cdot e^{-v h\nu_0 / kT} = \sum_{v=0}^{\infty} e^{-v\alpha} = \frac{1}{1 - e^{-\alpha}} \quad ; \quad \alpha = \frac{h\nu_0}{kT}$$

$$\begin{aligned} \bar{E}_v &= \frac{1}{Z_v} \sum_{v=0}^{\infty} v h\nu_0 \cdot 1 \cdot e^{-v h\nu_0 / kT} = \frac{kT}{Z_v} \sum_{v=0}^{\infty} v\alpha \cdot e^{-v\alpha} \\ &= \frac{kT\alpha}{Z_v} \sum_{v=0}^{\infty} v e^{-v\alpha} \end{aligned}$$

$$\text{Now } \sum_{v=0}^{\infty} v e^{-v\alpha} = -\frac{d}{d\alpha} \sum_{v=0}^{\infty} e^{-v\alpha} = -\frac{d}{d\alpha} \left(\frac{1}{1 - e^{-\alpha}} \right) = \frac{e^{-\alpha}}{(1 - e^{-\alpha})^2}$$

$$\bar{E}_v = kT\alpha \frac{e^{-\alpha}}{(1 - e^{-\alpha})^2} \cdot (1 - e^{-\alpha}) = kT\alpha \frac{e^{-\alpha}}{1 - e^{-\alpha}} = kT\alpha \frac{1}{e^{\alpha} - 1}$$

$$\text{Thus } \underline{\bar{E}_v = kT\alpha \frac{1}{e^{\alpha} - 1}}$$

$$T \rightarrow \infty \quad \alpha \rightarrow 0 \quad \bar{E}_v \rightarrow kT$$

$$T \rightarrow 0 \quad \alpha \rightarrow \infty \quad \bar{E}_v \rightarrow kT\alpha e^{-\alpha} \rightarrow 0$$

Two-dimensional S.H.O. (Isotropic Plane Oscillator)

$$E_v = (v+1)h\nu_0 \quad g_v = v+1$$

$$Z_v = \sum_{v=0}^{\infty} (v+1)e^{-v\alpha} = \frac{e^{-\alpha}}{(1-e^{-\alpha})^2} + \frac{1}{1-e^{-\alpha}} = \frac{1}{(1-e^{-\alpha})^2}$$

$$\bar{E}_v = \frac{kT\alpha}{Z_v} \sum_{v=0}^{\infty} (v+1)v\alpha e^{-v\alpha} = \frac{kT\alpha}{Z_v} \sum_{v=0}^{\infty} (v^2+v)\alpha e^{-v\alpha}$$

$$N_{v=0} \sum_{v=0}^{\infty} v^2 e^{-v\alpha} = -\frac{d}{d\alpha} \sum_{v=0}^{\infty} v e^{-v\alpha} = -\frac{d}{d\alpha} \left[\frac{e^{-\alpha}}{(1-e^{-\alpha})^2} \right]$$

$$= - \left[\frac{-2e^{-2\alpha}}{(1-e^{-\alpha})^3} + \frac{-e^{-\alpha}}{(1-e^{-\alpha})^2} \right]$$

$$= \frac{2e^{-2\alpha}}{(1-e^{-\alpha})^3} + \frac{e^{-\alpha}}{(1-e^{-\alpha})^2}$$

$$\bar{E}_v = \frac{kT\alpha}{Z_v} \left[\frac{2e^{-2\alpha}}{(1-e^{-\alpha})^3} + \frac{2e^{-\alpha}}{(1-e^{-\alpha})^2} \right]$$

$$= 2kT\alpha \left[\frac{e^{-2\alpha}}{(1-e^{-\alpha})} + e^{-\alpha} \right] = 2kT\alpha \frac{e^{-\alpha}}{1-e^{-\alpha}} = 2kT\alpha \frac{1}{e^{\alpha}-1}$$

Thus $\bar{E}_v = 2kT\alpha \frac{1}{e^{\alpha}-1}$ [= 2 x \bar{E}_v (1-dimensional)]

Adiabatic Exponents

If $dQ = 0$ $dS = \frac{dQ}{T} = 0$

Define
$$\left. \begin{aligned} \Gamma_1 &= - \left(\frac{\partial \ln P}{\partial \ln V} \right)_S = \left(\frac{\partial \ln P}{\partial \ln \rho} \right)_S \\ \frac{\Gamma_2}{\Gamma_2 - 1} &= \left(\frac{\partial \ln P}{\partial \ln T} \right)_S \\ \Gamma_3 - 1 &= - \left(\frac{\partial \ln T}{\partial \ln V} \right)_S = \left(\frac{\partial \ln T}{\partial \ln \rho} \right)_S \end{aligned} \right\} \text{ Where } V = \frac{1}{\rho}$$

Only two gammas are independent. In general

$$\frac{\Gamma_1}{\Gamma_3 - 1} \equiv \frac{\Gamma_2}{\Gamma_2 - 1}$$

Γ_1 important in dynamical instability of stars, and to a lesser extent in pulsating stars

Γ_2 " " convective instability

Γ_3 " " pulsational instability

Now if $dQ = \left[\left(\frac{\partial E}{\partial \ln \rho} \right)_T - \frac{P}{\rho} \right] \frac{d\rho}{\rho} + \left(\frac{\partial E}{\partial \ln T} \right)_\rho \frac{dT}{T} = 0$

then, using $c_v \equiv \left(\frac{\partial E}{\partial T} \right)_\rho$

$$\Gamma_3 - 1 \equiv \left(\frac{\partial \ln T}{\partial \ln \rho} \right)_S = \frac{P/\rho - \left(\frac{\partial E}{\partial \ln \rho} \right)_T}{c_v T}$$

Using $\left(\frac{\partial E}{\partial \ln P}\right)_T = E \left(\frac{\partial \ln E}{\partial \ln P}\right)_T = E \left[-\frac{P}{E} (\chi_T - 1)\right]$ we obtain

$$C_v = \frac{P}{\rho T} \frac{\chi_T}{\Gamma_3 - 1} \quad \text{or} \quad \underline{\Gamma_3 - 1 = \frac{P}{\rho T} \frac{\chi_T}{C_v}}$$

Now $d \ln P = \chi_T d \ln T + \chi_p d \ln \rho$ } Valid for any change
 or $\frac{d \ln P}{d \ln \rho} = \chi_p + \chi_T \frac{d \ln T}{d \ln \rho}$

For adiabatic change $\left(\frac{\partial \ln P}{\partial \ln \rho}\right)_s \equiv \Gamma_1$, $\left(\frac{\partial \ln T}{\partial \ln \rho}\right)_s \equiv \Gamma_3 - 1$

Hence $\underline{\Gamma_1 = \chi_p + \chi_T (\Gamma_3 - 1) = \chi_p + \frac{P}{\rho T} \frac{\chi_T^2}{C_v}}$

$$\frac{\Gamma_2}{\Gamma_2 - 1} = \frac{1}{1 - 1/\Gamma_2} = \frac{\Gamma_1}{\Gamma_3 - 1} \quad \text{or} \quad 1 - \frac{1}{\Gamma_2} = \frac{\Gamma_3 - 1}{\Gamma_1}$$

$$\text{or} \quad 1 - \frac{\Gamma_3 - 1}{\Gamma_1} = \frac{1}{\Gamma_2}$$

$$\Gamma_2 = \frac{1}{1 - \frac{\Gamma_3 - 1}{\Gamma_1}} = \frac{\Gamma_1}{\Gamma_1 - \Gamma_3 + 1} = \frac{\Gamma_1}{\Gamma_1 - (\Gamma_3 - 1)}$$

$$\underline{\Gamma_2 = \frac{\chi_p + \frac{P}{\rho T} \frac{\chi_T^2}{C_v}}{\chi_p + \frac{P}{\rho T} \frac{\chi_T^2}{C_v} - \frac{P}{\rho T} \frac{\chi_T}{C_v}} = \frac{\chi_p + \frac{P}{\rho T} \frac{\chi_T^2}{C_v}}{\chi_p + \frac{P}{\rho T} \frac{\chi_T}{C_v} (\chi_T - 1)}}$$

$$\frac{1}{\Gamma_2} = \frac{\Gamma_1 - (\Gamma_3 - 1)}{\Gamma_1} = 1 - \frac{\Gamma_3 - 1}{\Gamma_1} = 1 - \left(\frac{P}{\rho T} \frac{\chi_T}{C_v}\right) / \left(\chi_p + \frac{P}{\rho T} \frac{\chi_T^2}{C_v}\right)$$

$$\frac{\Gamma_3}{\Gamma_2 - 1} = \frac{1}{1 - 1/\Gamma_2} = \frac{\Gamma_1}{\Gamma_3 - 1} = \frac{\chi_p + \frac{P}{\rho T} \frac{\chi_T^2}{C_v}}{\frac{P}{\rho T} \frac{\chi_T}{C_v}} = \chi_T + \frac{\rho T}{P} C_v \frac{\chi_p}{\chi_T}$$

$$\gamma \equiv \frac{c_p}{c_v} = 1 + \frac{c_p - c_v}{c_v} = 1 + \left(\frac{P}{\rho T} \cdot \frac{\chi_T^2}{\chi_P} \right) / \left(\frac{P}{\rho T} \frac{\chi_T}{\Gamma_3 - 1} \right)$$

$$= 1 + \frac{\chi_T}{\chi_P} (\Gamma_3 - 1) = \frac{\Gamma_1}{\chi_P} = \frac{\Gamma_3 - 1}{\chi_P} \frac{\Gamma_2}{\Gamma_3 - 1}$$

Specific Heats

$$c_\alpha = (dQ/dT)_\alpha \quad dQ = dE + PdV = dE + Pd\left(\frac{1}{\rho}\right) = dE - \left(\frac{P}{\rho^2}\right)d\rho$$

$$c_v \equiv (dQ/dT)_v \quad c_p \equiv (dQ/dT)_p$$

$$c_v = (dQ/dT)_v = (\partial E/\partial T)_v = (dQ/dT)_p = (\partial E/\partial T)_p$$

$$E = E(P, T)$$

$$dQ = dE - \left(\frac{P}{\rho^2}\right)d\rho = \left(\frac{\partial E}{\partial P}\right)_T dP + \left(\frac{\partial E}{\partial T}\right)_P dT - \frac{P}{\rho^2} d\rho$$

$$\rho = \rho(P, T)$$

$$dQ = \left[\left(\frac{\partial E}{\partial P}\right)_T - \frac{P}{\rho^2} \left(\frac{\partial \rho}{\partial P}\right)_T \right] dP + \left[\left(\frac{\partial E}{\partial T}\right)_P - \frac{P}{\rho^2} \left(\frac{\partial \rho}{\partial T}\right)_P \right] dT$$

$$c_p = \left(\frac{dQ}{dT}\right)_p = \left(\frac{\partial E}{\partial T}\right)_P - \frac{P}{\rho^2} \left(\frac{\partial \rho}{\partial T}\right)_P$$

$$\text{Let } \chi_T \equiv \left(\frac{\partial \ln P}{\partial \ln T}\right)_\rho = \left(\frac{\partial \ln P}{\partial \ln T}\right)_v$$

$$\chi_P \equiv \left(\frac{\partial \ln P}{\partial \ln \rho}\right)_T = - \left(\frac{\partial \ln P}{\partial \ln v}\right)_T$$

$$\text{Now } dP = \left(\frac{\partial P}{\partial \rho}\right)_T d\rho + \left(\frac{\partial P}{\partial T}\right)_\rho dT$$

$$\text{For } dP = 0 \quad \left(\frac{\partial \rho}{\partial T}\right)_P = - \frac{\left(\frac{\partial P}{\partial T}\right)_P}{\left(\frac{\partial P}{\partial \rho}\right)_T} = - \left(\frac{P}{T} \chi_T\right) / \left(\frac{P}{\rho} \chi_P\right) = - \frac{P}{T} \frac{\chi_T}{\chi_P}$$

$$\begin{aligned} \text{Also } dE &= \left(\frac{\partial E}{\partial P}\right)_T dP + \left(\frac{\partial E}{\partial T}\right)_P dT \\ &= \left(\frac{\partial E}{\partial P}\right)_T \left[\left(\frac{\partial P}{\partial \rho}\right)_T d\rho + \left(\frac{\partial P}{\partial T}\right)_\rho dT \right] + \left(\frac{\partial E}{\partial T}\right)_P dT \end{aligned}$$

$$\text{so } \left(\frac{\partial E}{\partial T}\right)_P = \left(\frac{\partial E}{\partial P}\right)_T \left(\frac{\partial P}{\partial T}\right)_\rho + \left(\frac{\partial E}{\partial T}\right)_P$$

$$\text{or } \left(\frac{\partial E}{\partial T}\right)_P = \left(\frac{\partial E}{\partial T}\right)_P - \left(\frac{\partial E}{\partial P}\right)_T \left(\frac{\partial P}{\partial T}\right)_\rho$$

$$\begin{aligned} c_p &= c_v - \left(\frac{\partial E}{\partial P}\right)_T \left(\frac{\partial P}{\partial T}\right)_\rho + \frac{P}{\rho T} \frac{\chi_T}{\chi_\rho} \\ &= c_v - \left(\frac{\partial E}{\partial \rho}\right)_T \left(\frac{\partial \rho}{\partial P}\right)_T \left(\frac{\partial P}{\partial T}\right)_\rho + \frac{P}{\rho T} \frac{\chi_T}{\chi_\rho} \\ &= c_v - \frac{E}{T} \left(\frac{\partial \ln E}{\partial \ln \rho}\right)_T \frac{\chi_T}{\chi_\rho} + \frac{P}{\rho T} \frac{\chi_T}{\chi_\rho} \end{aligned}$$

$$\text{But } \left(\frac{\partial E}{\partial V}\right)_T = T \left(\frac{\partial P}{\partial T}\right)_V - P \quad \text{so } \left(\frac{\partial \ln E}{\partial \ln \rho}\right)_T = \frac{P}{E} \left(\frac{\partial E}{\partial P}\right)_T = -\frac{1}{\rho E} \left(\frac{\partial E}{\partial V}\right)_T$$

$$\text{i.e. } \left(\frac{\partial \ln E}{\partial \ln \rho}\right)_T = -\frac{1}{\rho E} \left[T \left(\frac{\partial P}{\partial T}\right)_V - P \right] = -\frac{P}{\rho E} [\chi_T - 1]$$

$$\text{Hence } c_p - c_v = \frac{\chi_T}{\chi_\rho} \left[\frac{P}{\rho T} + \frac{E}{T} \frac{P}{\rho E} (\chi_T - 1) \right] = \frac{P}{\rho T} \frac{\chi_T}{\chi_\rho} \cdot \chi_T = \frac{P}{\rho T} \frac{\chi_T^2}{\chi_\rho}$$

$$\text{where } c_v = \left(\frac{\partial E}{\partial T}\right)_V = \left(\frac{\partial E}{\partial T}\right)_P = \frac{E}{T} \left(\frac{\partial \ln E}{\partial \ln T}\right)_P$$

$$\underline{\gamma = c_p / c_v}$$

APPENDIX J

Abundances of Elements and Isotopes

All the calculations on statistical mechanics are based on the abundances obtained from Cameron (4), which are given here for those elements and isotopes used in this work.

In table (J.1), the relative abundance by number normalized to 10^6 for Si is given for each element summed over all its isotopic forms. For each individual isotope, the mass number and percentage abundance by number of that isotope making up that element are given.

Note that for H, He and K, Cameron (4) does not give the percentage abundance for the least abundant isotope of each of these elements, so we have recalculated the percentages of all the isotopes of these elements to four decimal places to show up the least abundant isotopes. Ar^{40} has a very small and uncertain abundance, so it is omitted and the remaining isotopic abundances are recalculated. Otherwise, all the figures in table (J.1) are exactly those obtained from Cameron, with all the isotopes of the 22 elements in the list being considered.

Table (J.1) of Abundances of Elements and Isotopes

<u>Z</u>	<u>Element</u>	<u>Abundance</u>	<u>A</u>	<u>Abundance in %</u>
1	H	3.18×10^{10}	1	99.9984
			2	0.0016
2	He	2.21×10^9	3	0.0167
			4	99.9833
6	C	1.18×10^7	12	98.89
			13	1.11
7	N	3.74×10^6	14	99.634
			15	0.366
8	O	2.15×10^7	16	99.759
			17	0.0374
			18	0.2039
9	F	2450	19	100.0
10	Ne	3.44×10^6	20	88.89
			21	0.27
			22	10.84
11	Na	6.0×10^4	23	100.0

<u>Z</u>	<u>Element</u>	<u>Abundance</u>	<u>A</u>	<u>Abundance in %</u>
12	Mg	1.061×10^6	24	78.70
			25	10.13
			26	11.17
13	Al	8.5×10^4	27	100.0
14	Si	1.00×10^6	28	92.21
			29	4.70
			30	3.09
15	P	9600	31	100.0
16	S	5.0×10^5	32	95.0
			33	0.760
			34	4.22
			36	0.0136
17	Cl	5700	35	75.529
			37	24.471
18	Ar	1.172×10^5	36	84.2150
			38	15.7850
19	K	4200	39	92.9899
			40	0.1370
			41	6.8732

<u>Z</u>	<u>Element</u>	<u>Abundance</u>	<u>A</u>	<u>Abundance in %</u>
20	Ca	7.21×10^4	40	96.97
			42	0.64
			43	0.145
			44	2.06
			46	0.0033
			48	0.185
22	Ti	2775	46	7.93
			47	7.28
			48	73.94
			49	5.51
			50	5.34
24	Cr	1.27×10^4	50	4.31
			52	83.7
			53	9.55
			54	2.38
25	Mn	9300	55	100.0
26	Fe	8.3×10^5	54	5.82
			56	91.66
			57	2.19
			58	0.33

<u>Z</u>	<u>Element</u>	<u>Abundance</u>	<u>A</u>	<u>Abundance in %</u>
28	Ni	4.80×10^4		
			58	67.88
			60	26.23
			61	1.19
			62	3.66
			64	1.08

REFERENCES

- (1). Cox J.P. & Giuli R.T., Principles of Stellar Structure, Gordon and Breach, (1968).
- (2). Cox A.N. Stewart J.N., Ap.J.Suppl., 19, 261, (1970).
- (3). Carson T.R., Private Communication.
- (4). Cameron A.G.W., Space Science Reviews, 15, 121, (1970).
- (5). Carson T.R., Ann.Rev.Astr.Ap., 14, 95, (1976).
- (6). Hack M., Proceedings of Trieste Colloquium, (1966).
- (7). Yamashita Y., Publ.Astr.Soc.Japan, 14, 390, (1962).
- (8). Cox A.N., J.Q.S.R.T., 4, 737, (1964).
- (9). Tsuji T., Publ.Astr.Soc.Japan, 18, 127, (1966).
- (10). Tsuji T., p.457 in Low Luminosity Stars, ed. S.S.Kumar, Gordon and Breach, (1969).
- (11). Tsuji T., Publ.Astr.Soc.Japan., 23, 553, (1971).
- (12). Vardya M.S., J.Q.S.R.T., 6, 539, (1966).
- (13). Golden S.A., J.Q.S.R.T., 9, 1067, (1969).
- (14). Tsuji T., Astr.Ap., 23, 411, (1973).
- (15). Auman Jr. J., Ap.J.Suppl., 14, 171, (1966).
- (16). Auman Jr. J. & Bodenheimer P., Ap.J., 149, 641, (1967).
- (17). Strom S.E. & Kurucz R.L., J.Q.S.R.T., 6, 591, (1966).
- (18). Mihalas D., Stellar Atmospheres, W.H. Freeman & Co., (1970).
- (19). Kunde V.G., Ap.J., 158, 1167, (1969).
- (20). Querci F., Querci M. & Kunde V.G., Astr.Ap., 15, 256, (1971).
- (21). Querci F., Querci M. & Tsuji T., Astr.Ap., 31 265, (1974).
- (22). Querci F. & Querci M., Astr.Ap., 39, 113, (1975).
- (23). Carbon D.F., Ap.J., 187, 135, (1974).
- (24). Mould J.R., Astr.Ap., 48, 443, (1976).

- (25). Gustafsson B., Eriksson K. & Nordlund Å., *Astr.Ap.*, 42, 407, (1975).
- (26). Bell R.A., Eriksson K., Gustafsson B. & Nordlund Å., *Astr.Ap.Suppl.*, 23, 37, (1975).
- (27). Sneden C., Johnson H.R. & Krupp B.M., *Ap.J.*, 204, 281, (1976).
- (28). Johnson H.R. & Krupp B.M., *Ap.J.*, 206, 201, (1976).
- (29). Herzberg G., *Molecular Spectra and Molecular Structure*,
I. Spectra of Diatomic Molecules,
D. Van Nostrand Co. Inc., Reprint (1957).
- (30). Herzberg G., *Molecular Spectra and Molecular Structure*,
II. Infrared and Raman Spectra of Polyatomic Molecules,
D. Van Nostrand Co. Inc., (1945).
- (31). Kovács I., *Rotational Structure in the Spectra of Diatomic Molecules*, Adam Hilger Ltd., (1969).
- (32). Allen C.W., *Astrophysical Quantities*, 3rd edition, (1973).
- (33). Moore C.E., *Atomic Energy Levels*, Circular 467 of the N.B.S.
- (34). Herzberg G., *Molecular Spectra and Molecular Structure*,
III. Electronic Spectra and Electronic Structure of Polyatomic Molecules, D. Van Nostrand Co. Inc., (1966).
- (35). Rosen B., *Spectroscopic Data Relative to Diatomic Molecules*, Pergamon Press (1970).
- (36). Mizushima M., *The Theory of Rotating Diatomic Molecules*, John Wiley & Sons (1975).
- (37). Kassel L.S., *J.Chem.Phys.*, 1, 576, (1933).
- (38). Kassel L.S., *Phys.Rev.*, 43, 364, (1933).
- (39). Tatum J.B., *Ap.J.Suppl.*, 14, 21, (1967).
- (40). Hirschfelder J.O., *J.Chem.Phys.*, 6, 795, (1938).
- (41). Lechner F., *Monatshefte f.Chemie*, 61, 385, (1932).

- (42). Carson T.R., Stellar Evolution p427, edited by Chiu H-Y. & Muriel A., M.I.T. Press, (1972).
- (43). Carson T.R., Stellar Opacity, Reprint from Progress in High Temperature Physics and Chemistry, Pergamon Press, (1971).
- (44). Tarafdar S.P. & Vardya M.S., M.N.R.A.S., 145, 171, (1969).
- (45). Vardya M.S., Ap.J., 135, 303, (1962).
- (46). Abramowitz M. & Stegun I.A., Handbook of Mathematical Functions, Dover Publications.
- (47). Tarafdar S.P. & Vardya M.S., M.N.R.A.S., 163, 261, (1973).
- (48). Dalgarno A. & Kingston A.E., Proc.Roy.Soc., A259, 424, (1960).
- (49). Dalgarno A., Adv.Phys., 11, 281, (1962).
- (50). Dalgarno A. & Williams D.A., Ap.J., 136, 690, (1962).
- (51). Somerville W.B., Ap.J., 141, 811, (1965).
- (52). John T.L. & Morgan D.J., M.N.R.A.S., 170, 1, (1975).
- (53). Myerscough V.P. & McDowell M.R.C., M.N.R.A.S., 132, 457, (1966).
- (54). John T.L., M.N.R.A.S., 172, 305, (1975).
- (55). Robinson E.J. & Geltman S., Phys.Rev., 153, 8, (1967).
- (56). Somerville W.B., Ap.J., 139, 192, (1964).
- (57). Tarafdar S.P. & Das P.K., M.N.R.A.S., 170, 559, (1975).
- (58). Solomon P.M., Ap.J., 139, 999, (1964).
- (59). Linsky J.L., Ap.J., 156, 989, (1969).
- (60). Born M. & Oppenheimer R., Ann.Physik, 84, 457, (1927).
- (61). Mulliken R.S., Rev.Mod.Phys., 2, 60, (1930).
- (62). Schadee A., B.A.N., 17, 311, (1963-64).
- (63). Budó A., Zeit.f.Phys., 98, 437, (1936).
Pitman & Sons Ltd., (1964).
- (64). Challacombe C.N. & Almy G.M., Phys.Rev., 51, 930, (1937).

- (65). Kovács I., *Can.J.Phys.*, 38, 955, (1960).
- (66). Tatum J.B. & Watson J.K.G., *Can.J.Phys.*, 49, 2693, (1971).
- (67). Manneback C., *Physica*, 17, 1001, (1951).
- (68). Hutchisson E., *Phys.Rev.*, 37, 45, (1931).
- (69). Hutchisson E., *Phys.Rev.*, 36, 410, (1930).
- (70). Bates D.R., *M.N.R.A.S.*, 112, 614, (1952).
- (71). Doktorov E.V., Malkin I.A. & Man'ko V.I., *J.Q.S.R.T.*, 16, 1021, (1976).
- (72). Bouanich J.B., *J.Q.S.R.T.*, 20, 419, (1978).
- (73). Fraser P.A., *Can.J.Phys.*, 32, 515, (1954).
- (74). Fraser P.A. & Jarmain W.R., *Proc.Phys.Soc.*, A66, 1145, (1953).
- (75). Jarmain W.R. & Fraser P.A., *Proc.Phys.Soc.*, A66, 1153, (1953).
- (76). Manneback C. & Rahman A., *Physica*, 20, 497, (1954).
- (77). Nicholls R.W. & Jarmain W.R., *Proc.Phys.Soc.*, A69, 253, (1956).
- (78). Nicholls R.W., *Proc.Phys.Soc.*, 85, 159, (1965).
- (79). Schamps J., *J.Q.S.R.T.*, 17, 685, (1977).
- (80). Shaffer W.H. & Krohn B.J., *J.Mol.Spec.*, 63, 323, (1976).
- (81). Whiting E.E. & Nicholls R.W., *Ap.J.Suppl.*, 27, 1, (1974).
- (82). Schadee A., *J.Q.S.R.T.*, 19, 451, (1978).
- (83). Doktorov E.V., Malkin I.A. & Man'ko V.I., *J.Mol.Spec.*, 56, 1, (1975).
- (84). Secroun C., Barbe A. & Jouve P., *J.Mol.Spec.*, 45, 1, (1973).
- (85). Dennison D.M., *Rev.Mod.Phys.*, 12, 175, (1940).
- (86). Penner S.S., *Quantitative Molecular Spectroscopy and Gas Emissivity*, Addison-Wesley Publishing Co. Inc., (1959).
- (87). Schrödinger E., *Ann.Phys.*, 80, 483, (1926).

- (88). McClatchey R.A., Benedict W.S., Clough S.A., Burch D.E.,
Calfee R.F., Fox K., Rothman L.S. & Garing J.S.,
AFCRL Atmospheric Absorption Line Parameters Compilation,
Project 7670, (1973).
- (89). Valero F.P.J., Suarez C.B. & Boese R.W., J.Q.S.R.T., 22, 93,
(1979).
- (90). Wang S.C., Phys.Rev., 34, 243, (1929).
- (91). King G.W., Hainer R.M. & Cross P.C., J.Chem.Phys., 11, 27,
(1943).
- (92). Cross P.C., Hainer R.M. & King G.W., J.Chem.Phys., 12, 210,
(1944).
- (93). Wacker P.F. & Pratto M.R., Microwave Spectral Tables, Line
Strengths of Asymmetric Rotors, N.B.S. Monograph 70, 2, (1964).
- (94). Mecke R., Zeit.f.Phys., 81, 313, (1933).
- (95). Badger R.M. & Zumwalt L.R., J.Chem.Phys., 6, 711, (1938).
- (96). Hinkle K.H. & Barnes T.G., Ap.J., 227, 923, (1979).
- (97). Ludwig C.B., Ferriso C.C., Malkmus W. & Boynton F.P.,
J.Q.S.R.T., 5, 697, (1965).
- (98). Dennison D.M., Rev.Mod.Phys., 3, 280, (1931).
- (99). Camy-Peyret C., Flaud J.M. & Toth R.A., J.Mol.Phys., 67, 117,
(1977).
- (100). Toth R.A., Camy-Peyret C. & Flaud J.M., J.Q.S.R.T., 18, 515,
(1977).
- (101). Luh W.T. & Lie G.C., J.Q.S.R.T., 21, 547, (1979).
- (102). Oka T., Phys.Rev.Lett., 45, 531, (1980).
- (103). Shy J.-T., Farley J.W., Lamb Jr. W.E. & Wing W.H.,
Phys.Rev.Lett., 45, 535, (1980).

- (104). Carney G.D. & Porter R.N., Phys.Rev.Lett., 45, 537, (1980).
- (105). Adams N.G. & Smith D., Ap.J., 248, 373, (1981).
- (106). Cody W.J. & Thacher B.M., Mathematics of Computation, 21, 30, (1967).
- (107). American Institute of Physics Handbook, Third Edition, McGraw-Hill Book Company.
- (108). Phillips J.G., J.Mol.Spec., 28, 233, (1968).
- (109). Cooper D.M., J.Q.S.R.T., 17, 543, (1977).
- (110). Jain D.C., J.Q.S.R.T., 4, 427, (1964).
- (111). Bouanich J.P., J.Q.S.R.T., 16, 1119, (1976).
- (112). Kaiser E.W., J.Mol.Spec., 77, 143, (1979).
- (113). Feinberg J. & Davis S.P., J.Mol.Spec., 69, 445, (1978).
- (114). Feinberg J. & Davis S.P., J.Mol.Spec., 65, 264, (1977).
- (115). Nordlund \AA ., Private Communication.
- (116). Massey H.S.W. & Kestelman H., Ancillary Mathematics, Pitman & Sons Ltd., (1964).
- (117). Kassel L.S., Chem.Rev., 18, 277, (1936).
- (118). Schadee A., J.Q.S.R.T., 7, 169, (1967).
- (119). Cooper D.M. & Nicholls R.W., J.Q.S.R.T., 15, 139, (1975).
- (120). Reis V.H., J.Q.S.R.T., 4, 783, (1964).
- (121). Stevens W.J., Das G., Wahl A.C., Krauss M. & Neumann D., J.Chem.Phys., 61, 3686, (1974).
- (122). Dimpfl W.L. & Kinsey J.L., J.Q.S.R.T., 21, 233, (1979).
- (123). Golden S.A., J.Q.S.R.T., 7, 225, (1967).
- (124). Hefferlin R., J.Q.S.R.T., 16, 1101, (1976).
- (125). Billingsley F.P., J.Mol.Phys., 61, 53, (1976).
- (126). Langhoff S.R. & Arnold J.O., J.Chem.Phys., 70, 852, (1979).

- (127). Demtröder W., Stetzenbach W., Stock M. & Witt J.,
J.Mol.Spec., 61, 382, (1976).
- (128). Meredith R.E. & Smith F.G., J.Q.S.R.T., 13, 89, (1973).
- (129). Arnold J.O., Whiting E.E. & Langhoff S.R.,
J.Chem.Phys., 66, 4459, (1977).